THE DEVELOPMENT AND UTILIZATION OF NOVEL ANTIBIOTIC ALTERNATIVES

EDITED BY: Wang Jiajun, Kianoush KHosravi-Darani and In Ho Kim
PUBLISHED IN: Frontiers in Microbiology

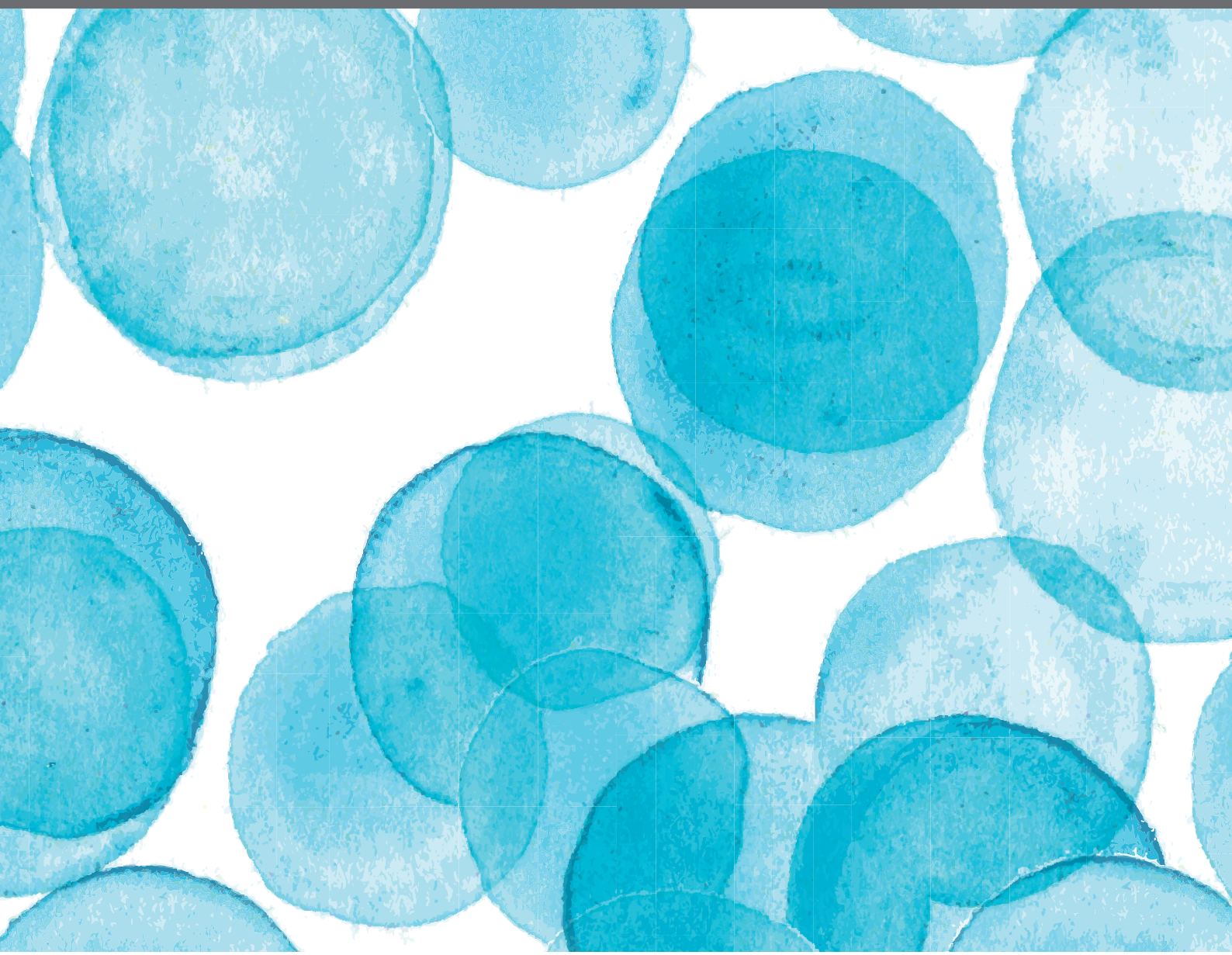

frontiers Research Topics

ISSN 1664-8714
ISBN 978-2-83250-205-1
DOI 10.3389/978-2-83250-205-1

About Frontiers

Frontiers is more than just an open-access publisher of scholarly articles: it is a pioneering approach to the world of academia, radically improving the way scholarly research is managed. The grand vision of Frontiers is a world where all people have an equal opportunity to seek, share and generate knowledge. Frontiers provides immediate and permanent online open access to all its publications, but this alone is not enough to realize our grand goals.

Frontiers Journal Series

The Frontiers Journal Series is a multi-tier and interdisciplinary set of open-access, online journals, promising a paradigm shift from the current review, selection and dissemination processes in academic publishing. All Frontiers journals are driven by researchers for researchers; therefore, they constitute a service to the scholarly community. At the same time, the Frontiers Journal Series operates on a revolutionary invention, the tiered publishing system, initially addressing specific communities of scholars, and gradually climbing up to broader public understanding, thus serving the interests of the lay society, too.

Dedication to Quality

Each Frontiers article is a landmark of the highest quality, thanks to genuinely collaborative interactions between authors and review editors, who include some of the world's best academicians. Research must be certified by peers before entering a stream of knowledge that may eventually reach the public - and shape society; therefore, Frontiers only applies the most rigorous and unbiased reviews.
Frontiers revolutionizes research publishing by freely delivering the most outstanding research, evaluated with no bias from both the academic and social point of view. By applying the most advanced information technologies, Frontiers is catapulting scholarly publishing into a new generation.

What are Frontiers Research Topics?

Frontiers Research Topics are very popular trademarks of the Frontiers Journals Series: they are collections of at least ten articles, all centered on a particular subject. With their unique mix of varied contributions from Original Research to Review Articles, Frontiers Research Topics unify the most influential researchers, the latest key findings and historical advances in a hot research area! Find out more on how to host your own Frontiers Research Topic or contribute to one as an author by contacting the Frontiers Editorial Office: frontiersin.org/about/contact

THE DEVELOPMENT AND UTILIZATION OF NOVEL ANTIBIOTIC ALTERNATIVES

Topic Editors:
Wang Jiajun, Northeast Agricultural University, China
Kianoush KHosravi-Darani, National Nutrition and Food Technology Research Institute, Iran
In Ho Kim, Dankook University, South Korea

Citation: Jiajun, W., KHosravi-Darani, K., Kim, I. H., eds. (2022). The Development and Utilization of Novel Antibiotic Alternatives. Lausanne: Frontiers Media SA. doi: 10.3389/978-2-83250-205-1

Table of Contents

frontiers | Frontiers in Microbiology

TYPE Editorial
PUBLISHED 31 August 2022
DOI 10.3389/fmicb.2022.1008850

OPEN ACCESS

EDITED AND REVIEWED BY
Jianhua Wang,
Chinese Academy of Agricultural Sciences (CAAS), China

*CORRESPONDENCE
Wang Jiajun
wjj1989@neau.edu.cn

SPECIALTY SECTION
This article was submitted to Antimicrobials, Resistance and Chemotherapy, a section of the journal Frontiers in Microbiology

RECEIVED 01 August 2022
ACCEPTED 15 August 2022
PUBLISHED 31 August 2022

CITATION
Jiajun W, Wenyu L, KHosravi-Darani K and Kim IH (2022) Editorial: The development and utilization of novel antibiotic alternatives.
Front. Microbiol. 13:1008850.
doi: 10.3389/fmicb.2022.1008850

Editorial: The development and utilization of novel antibiotic alternatives

Wang Jiajun[1]*, Li Wenyu[1], Kianoush KHosravi-Darani[2] and In Ho Kim[3]

[1]Department of Animal Nutrition, Institute of Animal Nutrition, Northeast Agricultural University, Harbin, China, [2]National Nutrition and Food Technology Research Institute, Faculty of Nutrition Sciences and Food Technology, Shahid Beheshti University of Medical Sciences, Tehran, Iran, [3]Department of Animal Resource & Science, Dankook University, Yongin, South Korea

KEYWORDS

antibiotic alternatives, antimicrobial peptides, endolysin, probiotics, phytochemicals

Editorial on the Research Topic
The development and utilization of novel antibiotic alternatives

The discovery of antibiotics is one of the greatest milestones in the history of human medical, meanwhile, that have promoted the rapid advancement in animal production. Statistics predict that up to 200,235 tons of antibiotics will be used in food animals to promote the growth of animals and to prevent bacterial infections in 2030, but most of them are not absorbed by animals and are excreted *via* feces and urine, which can directly contaminate and harm the surrounding environment (Xu et al., 2022; Li et al.). Even worse, the heavy misuse of antibiotics undoubtedly also contributes to the emergence of multidrug-resistant (MDR) bacteria, and results in a potential global health crisis. To tackle the resistance problems, countries have gradually restricted or banned the use of antibiotics in feed in recent years (Innes et al., 2020). Under this background, the development of antibiotic alternatives is a top priority to ensure the healthy development of animal production. In this Research Topic, a total of 14 excellent articles presenting different proposals of antibiotic alternatives are included.

Antimicrobial peptides

Antimicrobial peptides, as small molecule peptides produced by the host to resist the infections of external pathogens, are one of the most promising antibiotic alternatives based on their membrane disruption mechanisms and immunomodulatory effects (Wang et al., 2019a). Despite their potent activity as antimicrobials, AMPs still face significant challenges toward therapeutic applications, such as overall high toxicity and relatively poor metabolic stability, whilst the latter directly determines that most antimicrobial peptides are mainly administrated topically (Wang et al., 2019b; Nepal et al.).

Currently, numerous chemical modifications have been proposed to improve the metabolic stability of AMPs, among which, peptidomimetic approaches can reduce proteolytic susceptibility by removing the peptide-like characters of AMPs thereby resulting in the inability of proteases to recognize and degrade the resulting mimic molecules (Domalaon et al., 2016). Ramirez et al. designed a non-hemolytic peptidomimetic dUSTBβP 3, comprised of three β^3-homoarginine residues and two fatty acyl tails eight carbons long. In comparison to the α-amino acid-based counterpart, the compound 3 showed excellent *in vitro* plasma stability with an extrapolated half-life of 10.43 ± 3.70 h. Notably, dUSTBβP 3 could potentiate the activity of novobiocin and rifampicin against wild-type and multiple drug resistance (MDR) Gram-negative bacteria and reduce their minimum inhibitory concentrations below the interpretative susceptibility breakpoints.

In recent years, dietary modulation of endogenous AMPs synthesis has been continuously studied as a new antibiotic alternative approach to avoid the application problems of exogenous AMPs. Yang et al. investigated a potential synergy between sugars and butyrate in inducing HDP gene expression in chickens, and found that sugars differentially regulated HDP expression in both gene- and sugar-specific manners in chicken HD11 macrophage cells. Importantly, these sugars could synergize with butyrate to further enhance chicken HDP and barrier function gene expression to effectively control and prevent infectious diseases.

Endolysin

Bacteriophages, which are the natural predators of bacteria, have been reactivated for combating the continuing development of antibiotic resistance. In fact, bacteriophages-therapy has intrinsic disadvantages, one of which is that they cannot be administered intravenously since they are destroyed by the immune system (Bassetti et al., 2017). Thus, the endolysin itself has been proposed to instead of living phages as antibacterial agents. Vasina et al. provided a comprehensive study on the biological function of four Gram-negative bacteria-targeting endolysins LysAm24, LysAp22, LysECD7, and LysSi3. These endolysins possessed a wide antibacterial spectrum against planktonic bacteria and bacterial biofilms, and were effective in wound and burn skin infection animal models. In terms of safety, these endolysins did not contribute to the development of short-term resistance, with no cytotoxicity and no significantly effects on the normal intestinal microflora *in vivo*.

Probiotics

Probiotics, also known as live bacteria preparations or micro-ecological preparations, are increasingly popular as feed additives and alternatives to traditional antibiotics. Among numerous probiotics, the spore-forming *Bacillus* species are considered to be more suitable for application in the feed industry, in comparison to non-spore-forming probiotics (Bernardeau et al., 2017), but it is still unknown whether the probiotic functions of the *Bacillus* depend on the germination of spores *in vivo*. Addressing this issue, Lu et al. detected the germination response of 14 *Bacillus* spores in relation to different germinating agents, and revealed that the germination response was strain-specific and germinant-related, and demonstrated that the germination of spores initiated by L-alanine could result in an increased probiotic effects.

Metabolites are also one of underlying mechanisms by which probiotics exert antibacterial and immunomodulatory activities. Thus, Møller et al. utilized metabolomics analysis to explore the mechanisms by which *Lactobacillus* spp. Lb21 protected *C. elegans* against MRSA, and successfully identified a set of metabolites that potentially could lead to strategies for protection against MRSA.

Phytochemicals

Phytochemicals have been used for many years to treat various ailments (Li et al., 2021), which possess many unique advantages compared with the above several antibiotic alternatives, such as exceptionally rich sources, diverse chemical structures, and multiple biological functions (Porras et al., 2021). Therefore, phytochemicals are gaining significant attention as substitutes for antibiotics.

Plant polyphenolic compounds, as a large family of phytochemicals widely distributed in the plant kingdom, have won the favor of many researchers because of their variety of biological functions including anti-carcinogenic, anti-inflammatory, and anti-oxidant properties. Moreover, some phenolic compounds have been proven to be effective in inhibiting various pathogenic bacteria, such as *E. coli* (Bancirova, 2010), halitosis-related bacteria (Liu et al.) and so on. Currently, the exact antibacterial mechanisms of polyphenolic compounds are still unclear, but some studies have demonstrated that polyphenolic compounds can cause disruption in bacteria cell membranes, for instance, Zhang et al. confirmed that the compound phenolic acid (protocatechuic acid, hydrocinnamic acid, and chlorogenic acid) could cause bacterial flagellar abscission, cell membrane structure damage, and finally lead to the leakage of intracellular macromolecules, and bacterial death.

In addition to polyphenolic compounds, natural plant essential oils (EOs) also have been well-known as potential microbicides. However, bactericidal efficacies of EOs are controversial, mainly because the amount of active ingredients in individual EOs varies with sources and extraction process. Lu et al. comprehensively analyzed the main components of

oregano essential oil (OEO) and found carvacrol and thymol are the major ingredients responsible for its bactericidal activity. Moreover, carvacrol/thymol could synergize with 405 nm blue light (BL) to kill multidrug-resistant *Pseudomonas aeruginosa*, greatly improving their antibacterial potential. These findings offered a unique opportunity to standardize OEO products in the basis of the amount of carvacrol and thymol.

Due to their excellent properties as antibiotic alternatives, various phytochemicals have been used in animal production as feed additive to improve animal health and growth performance (Li et al., 2021; Ayalew et al., 2022), and some have been successfully commercialized. In this topic, Yin et al. demonstrated that dietary *Lycium barbarum* polysaccharides (LBPs) supplementation could improve growth performance, antioxidant capacity and immunity, and reduced diarrhea incidence in weaned piglets. Koorakula et al. systematically studied the impacts of a commercial phytogenic feed additives (PFAs) product on the gut microbiome and resistome of broiler chickens. The results revealed that PFA treatments increased the abundance of *Firmicutes* such as *Lactobacillus*, reduced the abundance of *Escherichia*, whilst resulted in a decrease in abundance of antibiotic resistance gene. Taken together, phytochemicals have very broad application prospects as feed additives to replace antibiotics in animal production.

Dihydropyrimidinones derivatives

DHPMs are nitrogen-containing heterocyclic substances with excellent pharmacological activities such as antitumor, antiviral, anti-inflammatory and so on. On this basis, Jara et al. further developed three DHPM derivatives with potent antibacterial activity against MDR bacteria and no significant cytotoxicity. It seems that the development of derivatives based on existing antibacterial substances is also an effective mean to expand the library of antibiotic alternatives.

In conclusion, in face of the increasing number of MDR bacteria, the development of new antibiotic alternatives, both for animal production and human health, is imperative. We hope that this Research Topic will be useful for further research in this field.

Author contributions

All authors listed have made a substantial, direct, and intellectual contribution to the work and approved it for publication.

Funding

This work was supported by the National Natural Science Foundation of China (32002215) and the Natural Science Foundation of Heilongjiang Province (YQ2020C009).

Acknowledgments

We would like to thank all the authors for their contributions in this Research Topic, and all the reviewers for their critical review of the manuscripts.

Conflict of interest

The authors declare that the research was conducted in the absence of any commercial or financial relationships that could be construed as a potential conflict of interest.

Publisher's note

References

Ayalew, H., Zhang, H. J., Wang, J., Wu, S. G., Qiu, K., Qi, G. H., et al. (2022). Potential feed additives as antibiotic alternatives in broiler production. *Front. Vet. Sci.* 9, 916473. doi: 10.3389/fvets.2022.916473

Bancirova, M. (2010). Comparison of the antioxidant capacity and the antimicrobial activity of black and green tea. *Food Res. Int.* 43, 1379–1382. doi: 10.1016/j.foodres.2010.04.020

Bassetti, M., Poulakou, G., Ruppe, E., Bouza, E., Van Hal, S. J., and Brink, A. (2017). Antimicrobial resistance in the next 30 years, humankind, bugs and drugs: a visionary approach. *Intensive Care Med.* 43, 1464–1475. doi: 10.1007/s00134-017-4878-x

Bernardeau, M., Lehtinen, M. J., Forssten, S. D., and Nurminen, P. (2017). Importance of the gastrointestinal life cycle of Bacillus for probiotic functionality. *J. Food Sci. Technol.* 54, 2570–2584. doi: 10.1007/s13197-017-2688-3

Domalaon, R., Zhanel, G. G., and Schweizer, F. (2016). Short antimicrobial peptides and peptide scaffolds as promising antibacterial agents. *Curr. Top. Med. Chem.* 16, 1217–1230. doi: 10.2174/1568026615666150915112459

Innes, G. K., Randad, P. R., Korinek, A., Davis, M. F., Price, L. B., So, A. D., et al. (2020). "External societal costs of antimicrobial resistance in humans attributable to antimicrobial use in livestock," in *Annual Review of Public Health*, Vol 41, ed J. E. Fielding (Palo Alto, CA: Annual Reviews) 141–157.

Li, L. X., Sun, X. Y., Zhao, D., and Dai, H. C. (2021). Pharmacological applications and action mechanisms of phytochemicals as alternatives

to antibiotics in pig production. *Front. Immunol.* 12, 798553. doi: 10.3389/fimmu.2021.798553

Porras, G., Chassagne, F., Lyles, J. T., Marquez, L., Dettweiler, M., Salam, A. M., et al. (2021). Ethnobotany and the role of plant natural products in antibiotic drug discovery. *Chem. Rev.* 121, 3495–3560. doi: 10.1021/acs.chemrev.0c00922

Wang, J., Dou, X., Song, J., Lyu, Y., Zhu, X., Xu, L., et al. (2019a). Antimicrobial peptides: promising alternatives in the post feeding antibiotic era. *Med. Res. Rev.* 39, 831–859. doi: 10.1002/med.21542

Wang, J., Song, J., Yang, Z., He, S., Yang, Y., Feng, X., et al. (2019b). Antimicrobial peptides with high proteolytic resistance for combating gram-negative bacteria. *J. Med. Chem.* 62, 2286–2304. doi: 10.1021/acs.jmedchem.8b01348

Xu, C. M., Kong, L. Q., Gao, H. F., Cheng, X. Y., and Wang, X. M. (2022). A review of current bacterial resistance to antibiotics in food animals. *Front. Microbiol.* 13, 822689. doi: 10.3389/fmicb.2022.822689

frontiers in Microbiology

ORIGINAL RESEARCH
published: 28 September 2021
doi: 10.3389/fmicb.2021.738282

Molecular Characterization of a Tolerant Saline-Alkali *Chlorella* Phosphatidate Phosphatase That Confers NaCl and Sorbitol Tolerance

Jingang Wang†, Qinghua Shan†, Ye Ran, Dexiang Sun, Haizhen Zhang, Jinzhu Zhang, Shufang Gong, Aimin Zhou and Kun Qiao**

College of Horticulture and Landscape Architecture, Northeast Agricultural University, Harbin, China

The gene encoding a putative *phosphatidate phosphatase* (*PAP*) from tolerant saline-alkali (TSA) *Chlorella*, *ChPAP*, was identified from a yeast cDNA library constructed from TSA *Chlorella* after a NaCl treatment. *ChPAP* expressed in yeast enhanced its tolerance to NaCl and sorbitol. The ChPAP protein from a GFP-tagged construct localized to the plasma membrane and the lumen of vacuoles. The relative transcript levels of *ChPAP* in *Chlorella* cells were strongly induced by NaCl and sorbitol as assessed by northern blot analyses. Thus, ChPAP may play important roles in promoting Na-ion movement into the cell and maintaining the cytoplasmic ion balance. In addition, ChPAP may catalyze diacylglycerol pyrophosphate to phosphatidate in vacuoles.

Keywords: tolerant saline-alkali *Chlorella*, NaCl, sorbitol, subcellular localization, gene expression

OPEN ACCESS

Edited by:
Kianoush KHosravi-Darani, National Nutrition and Food Technology Research Institute, Iran

Reviewed by:
Shiguo Li, Research Center for Eco-environmental Sciences (CAS), China
Quanyu Zhao, Nanjing Tech University, China
Swarnendu Roy, University of North Bengal, India
Santosh Kumar, Agriculture and Agri-Food Canada, Canada

****Correspondence:***
Aimin Zhou
aiminzhou@neau.edu.cn
Kun Qiao
kunqiao@neau.edu.cn

†These authors have contributed equally to this work

Specialty section:
This article was submitted to Antimicrobials, Resistance and Chemotherapy, a section of the journal Frontiers in Microbiology

Received: *08 July 2021*
Accepted: *27 August 2021*
Published: *28 September 2021*

Citation:
Wang J, Shan Q, Ran Y, Sun D, Zhang H, Zhang J, Gong S, Zhou A and Qiao K (2021) Molecular Characterization of a Tolerant Saline-Alkali Chlorella Phosphatidate Phosphatase That Confers NaCl and Sorbitol Tolerance. Front. Microbiol. 12:738282. doi: 10.3389/fmicb.2021.738282

INTRODUCTION

Phosphatidate phosphatase (PAP) has the effects of catalyzing the dephosphorylation of phosphatidate (PA), and generating diacylglycerol and inorganic phosphate (Smith et al., 1957). It is also an essential enzyme in lipid metabolism, plays important roles in lipid synthesis, and is involved in the generation or degradation of lipid signaling molecules (Brindley and Pilquil, 1984; Carman, 1997; Nanjundan and Possmayer, 2001). The PAP enzymes are divided into Mg^{2+}-dependent PAP1 or Mg^{2+}-independent PAP2 [also be called lipid phosphate phosphatase (LPP) or diacylglycerol pyrophosphate (DGPP) phosphatase] based on the cofactor requirement for catalytic activity (Jamal et al., 1991; Brindley et al., 2002). The PAP1 enzymes play roles in cell homeostasis and lipid synthesis (Han et al., 2006; Sherr et al., 2017; Hassaninasab et al., 2019), and PAP1 enzyme, PAH1, performs catalytic function to regulate phospholipid synthesis on the nuclear and endoplasmic reticulum (Eastmond et al., 2010; Hassaninasab et al., 2019). The absence of *Pahp1* (encoded PAH1) leads to the upregulated of *V-ATPase* (Sherr et al., 2017). The expression of *PAH1* is induced in the absence of Zn (Soto-Cardalda et al., 2012). The PAH1 protein of the fungal pathogen *Candida albicans* restricts viral replication by affecting phospholipid synthesis and plays significant roles in hyphal growth and environmental stress regulation (Mu et al., 2019). In this study, the PAP2 enzymes are highlighted. PAP2, encoded by DPP1 and LPP1, is a vacuole membrane-associated enzyme that catalyzes DGPP to form PA and then catalyzes PA to form diacylglycerol by removing the phosphate (Wu et al., 1996; Han et al., 2001). PAP2 enzymes contain a three-domain lipid phosphatase catalytic motif containing the conserved sequences

KxxxxxxRP (domain 1), PSGH (domain 2), and SRxxxxxHxxxD (domain 3). The conserved arginine residue in domain 1 and the conserved histidine residues in domains 2 and 3 are essential for the catalytic activities of PAP2 enzymes (Hemrika et al., 1997; Neuwald, 1997; Stukey and Carman, 1997; Toke et al., 1998, 1999a,b; Zhang et al., 2000; Han et al., 2004). The PAP2 enzymes are localized on the hydrophilic surfaces of the membrane (Stukey and Carman, 1997; Toke et al., 1998, 1999a,b; Zhang et al., 2000; Han et al., 2004), the vacuole (Han et al., 2001, 2004), and Golgi (Huh et al., 2003) and have broad substrate specificity levels and may function under stress conditions (Oshiro et al., 2003). In the early studies, PAP2 enzymes are found that are responsible for lipid signaling in yeast and mammals (Carman, 1997; Nanjundan and Possmayer, 2001; Brindley, 2004; Pyne et al., 2005). In plants, *Arabidopsis thaliana AtLPP1* appears to be more highly expressed in the leaves and roots compared with other tissues, and the expression level of *AtLPP1* increased in Arabidopsis after ionization and UV-B irradiation (Brindley, 2004; Pierrugues et al., 2011). In addition, the *AtLPP2* appears to be expressed at similar levels in all the plant's tissues, and *AtLPP2* is involved with abscisic acid signaling and regulation of stomatal movements (Paradis et al., 2011).

The *PAP2* gene has been also identified in microalgae (eukaryotic microbes), including *Chlorella variabilis* (Blanc et al., 2010), *Chlorella protothecoides* (Gao et al., 2014), *Chlamydomonas reinhardtii* (Deng et al., 2013), and *Coccomyxa subellipsoidea* (Blanc et al., 2010). However, there are limited reports on the cloning and functional analyses of *PAP2* genes of microalgae. Some studies indicated that the expression levels of citrate synthase and phosphoenolpyruvate carboxylase 1 in *Chlamydomonas reinhardtii* are decreased, but the *PAP2* has higher expression in the RNAi transgenic *Chlamydomonas* strains (Deng et al., 2013, 2014). In our previous study, we determined that tolerant saline-alkali (TSA) *Chlorella* can survive in an environment containing 600-mm NaCl, and the TSA *Chlorella PAP* gene was isolated from a TSA *Chlorella* full-length cDNA yeast library constructed under 1-M NaCl-stress conditions (Qiao et al., 2015). Here, we determined the growth rates of transgenic yeast on a solid medium under high salinity and drought conditions. The subcellular localization of the ChPAP protein in yeast cells was detected using confocal microscopy, and the effects of high salinity and drought conditions on *ChPAP* expression were investigated.

MATERIALS AND METHODS

Chlorella Source, Culture, and Gene

The TSA *Chlorella* was previously isolated from extreme saline-alkali soil on the Songnen Plain, Heilongjiang Province, China (Wang et al., 2011), which is rich in different salt types, including NaCl and $NaHCO_3$, and grown in liquid Bold's basal medium (BBM, Bold and Wynne, 1984). The culture conditions were 23°C under a 16-h light/8-h dark photoperiod. The illumination intensity was 40-mmol photons m^{-1} s^{-1}. The TSA *Chlorella* cells were maintained in solid BBM, and the sub-culturing and rapid propagation of TSA *Chlorella* was cultured in liquid BBM. A full-length cDNA yeast library of TSA *Chlorella* was constructed (Qiao et al., 2018). A sequence screened from the 1-M NaCl-treated TSA *Chlorella* library had close similarity levels to sequences of other species' *PAP* genes. Accordingly, it was named *ChPAP*.

Sequence Analysis

The full-length *ChPAP* sequence was analyzed using BlastX and ORFfinder on the NCBI Web site.[1] GeneDoc 3.0 software was used to align the sequences of the ChPAP protein and other species. The maximum-likelihood-based phylogenetic tree was constructed using MEGA 5.1 software. The transmembrane domains in the ChPAP sequence were predicted using the TMHMM server v. 2.0.[2]

Plasmid Construction, Yeast Transformation, and Stress-Tolerance Assays

The *ChPAP* cDNA fragment harboring the open reading frame was amplified from TSA *Chlorella* using PCR with the ChPAP-forward (5'-GGATCCATGTTGCACGCGATGGTGG-3'; BamHI restriction site) and -reverse (5'-GTCGACTCAAACAGGCACCATGCTGC-3'; KpnI restriction site) primers and Phanta Max Super-Fidelity DNA Polymerase (Vazyme Biotech Co., Ltd., Nanjing, China). For yeast transformation, *ChPAP* was ligated into the pYES2 vector (Invitrogen, United States) digested with BamHI and NotI restriction enzymes to construct the plasmid pYES2-*ChPAP*, which was transferred into InVSC1 yeast cells using the PEG/LiAC method (Gietz et al., 1992). First, to test the tolerance of transgenic yeast under different stress conditions, yeast cells containing, independently, the pYES2-*ChPAP* and empty pYES2 vectors were cultivated in liquid SD-Uracil (pH 5.8) medium at 30°C for 2 days. The concentration of the transgenic yeast cells was adjusted to an OD_{600} value of 0.5 and then diluted to 10^{-1}, 10^{-2}, 10^{-3}, and 10^{-4} with sterile H_2O. A total of 4.5 µl of each dilution series was placed into a solid yeast (1% yeast extract, 2% peptone, and 2% galactose) medium supplemented independently with 0.8-M NaCl, 1.0-M NaCl, and 1.6-M sorbitol. The empty pYES2 vector in yeast cells was used as a control, and the growth of yeast cells at 30°C was observed and photographed for 5–10 days.

Subcellular Localization of the ChPAP Protein in Yeast

To determine the subcellular localization of ChPAP, the expression plasmid pYES2-*ChPAP*-EGFP was constructed. The *ChPAP* full-length sequence with restriction sites was cloned using PCR with EGFP-specific forward GFP-F (5'-GGATCCATGTTGCACGCGATGGTGGAC-3') and reverse GFP-R (5'-GGTACCCCAACAGGCACCATGCTGCTTGC-3') primers. The PCR product was ligated into the pEGFP plasmid (Clontech) digested with the BamH1 and KpnI sites. The *ChPAP*-pEGFP fusion

[1]http://www.ncbi.nlm.nih.gov
[2]http://www.cbs.dtu.dk/services/TMHMM/

fragment was digested at the BamHI and NotI sites in the pEGFP plasmid to construct the empty pYES2 vector.

The pYES2-*ChPAP*-EGFP and pYES2-EGFP plasmids were transferred independently into yeast cells. The transgenic yeast cells were pre-cultured in liquid medium containing 1% yeast extract, 2% peptone, and 2% glucose at 30°C for 2 days. Afterward, they were washed three times to remove the remaining glucose. The EGFP and *ChPAP*-EGFP plasmids in yeast cells were induced to express in liquid yeast (1% yeast extract, 2% peptone, and 2% galactose) medium at 30°C for 6 h, and then, *ChPAP*-EGFP yeast cells were incubated at 30°C with 20-μm FM4-64 dye for 3 h. The remaining dye was removed by washing three times with sterile H_2O before samples were observed. The fluorescence was detected using laser-scanning confocal imaging system (Olympus Fluoview, FV500). The EGFP and FM4-64 signals were excited at 488 nm and 543 nm, respectively.

Expression Analysis of *ChPAP*

To investigate the *ChPAP* transcript levels under high salinity and drought stresses, the TSA *Chlorella* samples were grown on medium supplemented independently with 200-mm NaCl and 300-mm sorbitol. The samples were collected at 0, 3, 6, 12, 24, and 48 h and then ground with a mortar and pestle in liquid nitrogen for RNA isolation.

The total RNA of TSA *Chlorella* was extracted using RNAiso Plus reagent (TaKaRa, Japan). The ChPAP-specific forward (5'-ATGGGCCTCAAGGAAGAC-3') and reverse (5'-TCAAGCGTACTTCGCCTTCAG-3') primers were used to amplify the cDNA probes using a PCR Digoxigenin Probe Synthesis kit (Roche, Switzerland). The northern blot analysis was performed in accordance with a previously published protocol (Qiao et al., 2018).

RESULTS AND DISCUSSION

Characterization of *ChPAP* Gene

The *ChPAP* nucleic acid sequence contained an open reading frame of 1,002 nucleotides that translated into 333 amino acids. The ChPAP amino acid sequence shared close similarities with the previously reported PAP sequences of other species, such as 70% similarity with *C. variabilis* and 53% similarity with *Micractinium conductrix*. A comparison of the ChPAP domains with those in PAPs of other species revealed the presence of conserved domains 1, 2, and 3 (**Figure 1**), which contained two arginine, one histidine, and two histidine residues, respectively. These results were consistent with previously reported PAP2 protein structures (Hemrika et al., 1997; Neuwald, 1997; Stukey and Carman, 1997). The phylogenetic analysis showed that ChPAP was closely related to the PAP of *C. variabilis* (XP_005848979.1). The TSA *Chlorella* firstly clustered with unicellular microalgae, and then clustered with microbes,

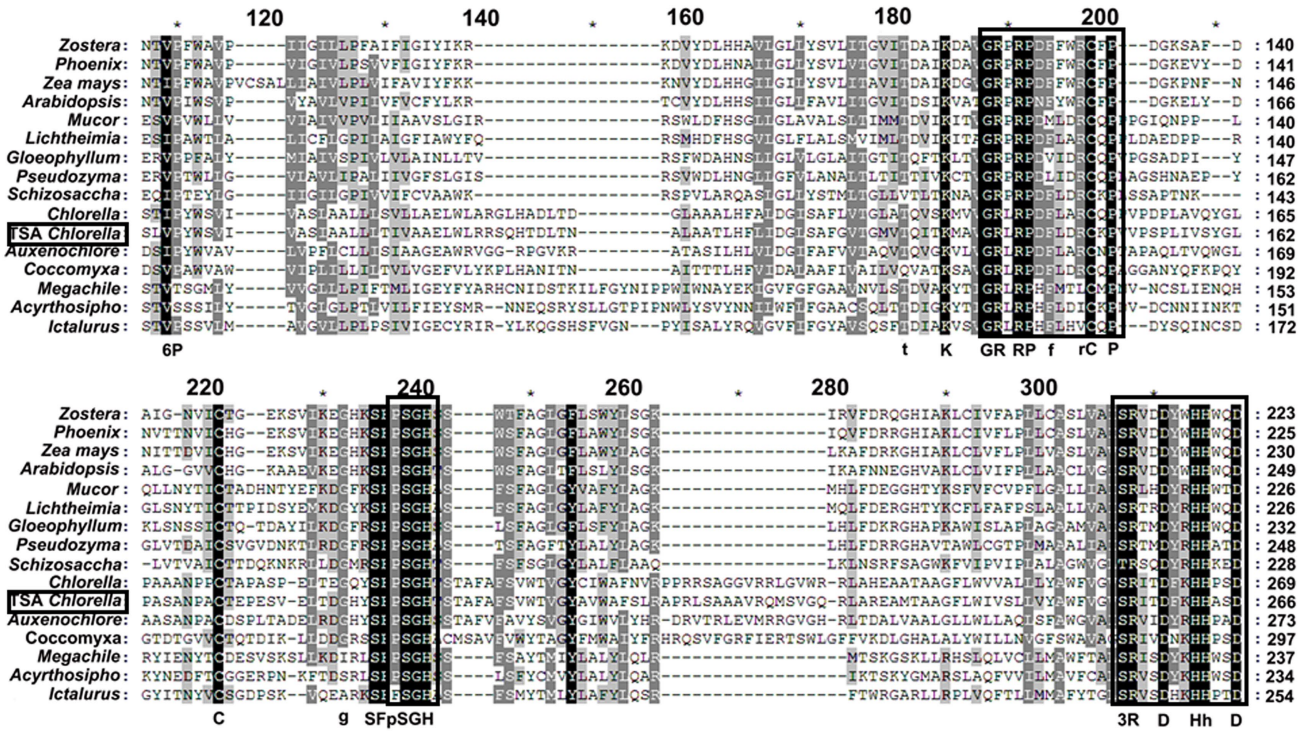

FIGURE 1 | Sequence alignment of the phosphatidate phosphatase (PAP) domains from tolerant saline-alkali (TSA) *Chlorella* ChPAP2 with those of other species. The conserved residues, including the KxxxxxxRP (domain 1), PSGH (domain 2), and SRxxxxxHxxxD (domain 3) motif, are indicated by boldface in boxes. The ChPAP2 sequence data have been deposited in the GenBank database and assigned accession no. KT750011. The other PAP protein sequences were downloaded from GenBank.

animals, and plants (**Figure 2**). Thus, *ChPAP2* is the *PAP* gene of TSA *Chlorella*.

Overexpression of *ChPAP2* in Yeast Enhanced Tolerance to NaCl and Sorbitol

The five serial dilutions of transgenic yeast cells were spotted into a solid yeast medium. The growth of yeast cells harboring the empty pYES2 vector was similar to that of the *ChPAP2* transgenic yeast in medium containing 1% yeast extract, 2% peptone, and 2% glucose without any stress. The *ChPAP2* transgenic yeast grew better than the controls in the presence of 0.8-M NaCl, 1-M NaCl, or 1.6-M sorbitol (**Figure 3**). Thus, the expression of *ChPAP2* in yeast cells improved the tolerance to NaCl and sorbitol, which indicated that ChPAP2 functions as lipid signaling molecule during abiotic stress (Munnik et al., 1996). *PAH1* encoded PAP1 was regulated to express under Zn deficiency and enhanced the activity of PAP enzyme (Soto-Cardalda et al., 2012). In addition, Arabidopsis PAP2 was found that was involved with ABA signaling and regulating the stomatal movements (Paradis et al., 2011). However, there was no relevant report on the investigation of PAP2 under abiotic stress.

The Expression of *ChPAP2* Was Inducible Under NaCl and Sorbitol Stresses

A northern blot analysis was used to detect *ChPAP2* expression patterns. Total RNA was used to analyze the effects of high salinity and drought stresses on *ChPAP2* expression. The TSA *Chlorella* cells were exposed independently to NaCl and sorbitol for 0, 3, 6, 12, 24, and 48 h. The *ChPAP2* mRNA expression dramatically increased with the 200-mm NaCl treatment from 6 to 48 h compared with the control (0 h), indicating that *ChPAP2* was upregulated (**Figure 4A**). Thus, in yeast, the increased *ChPAP2* expression level may increase NaCl resistance. The PA and DGPP levels also increase under hyperosmotic stress conditions (Munnik et al., 2000). The presence of NaCl in liquid media not only leads to high salinity stress, but also to hyperosmotic stress in plants. We hypothesized that the *ChPAP2* expression level may be upregulated, allowing it to catalyze the excess DGPP into PA.

In this study, a sorbitol solution was used as the drought agent (Bocchini et al., 2018; Lu et al., 2019). The *ChPAP2* expression levels did not differ significantly compared with those of the control after 3–6 h of exposure to 300-mm sorbitol.

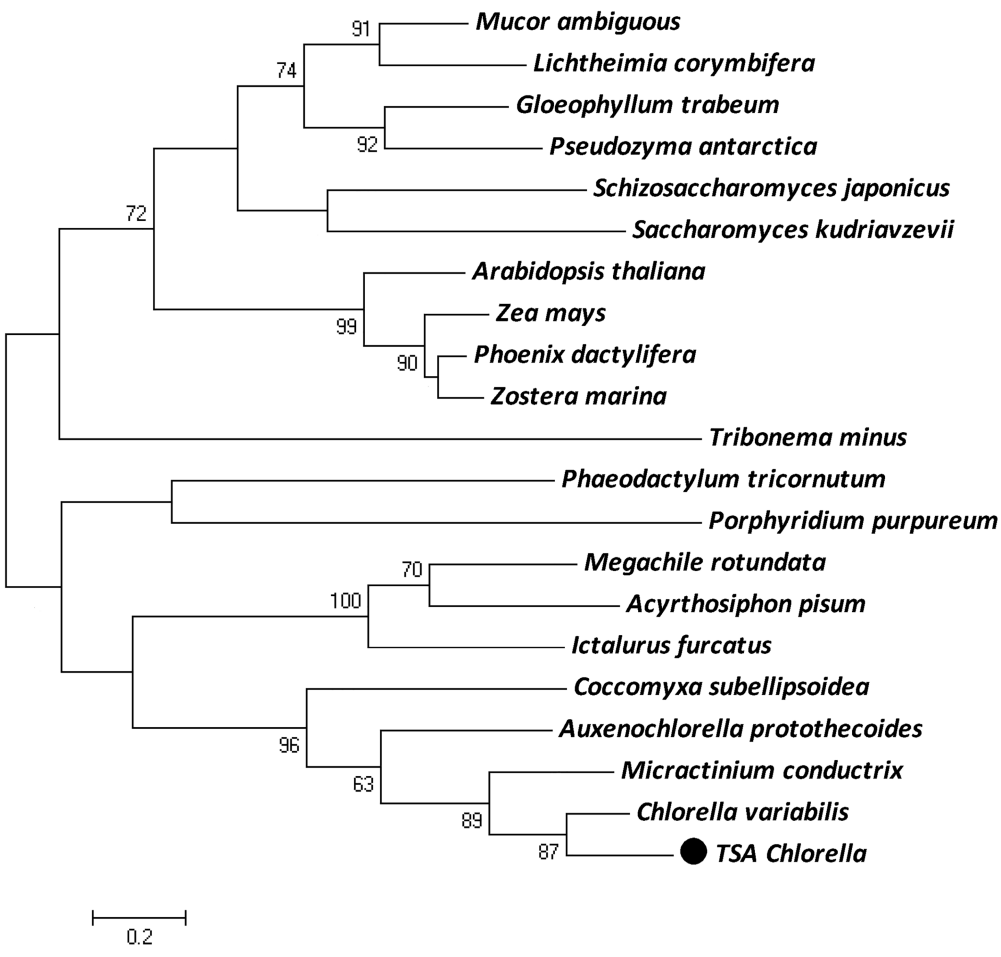

FIGURE 2 | The maximum-likelihood (ML) phylogenetic relationships of PAP proteins between TSA *Chlorella* sp. and those of other species. Bootstrap values were calculated 1,000 times, and values below 50% were not included. The TSA *Chlorella* sp. is indicated by boldface in a box.

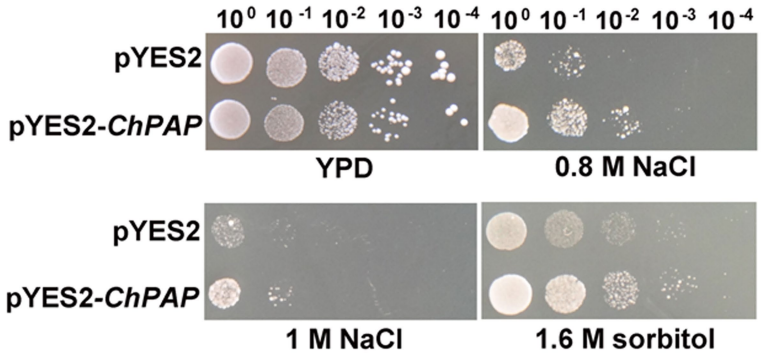

FIGURE 3 | *ChPAP2*-overexpressing yeast cells exposed to NaCl and sorbitol stresses. Serial dilutions of yeast cells containing the pYES2 empty vector or pYES2-*ChPAP2* were independently spotted into solid yeast (1% yeast extract, 2% peptone, and 2% galactose) medium containing plates supplemented independently with 0.8-M NaCl, 1.0-M NaCl, and 1.6-M sorbitol.

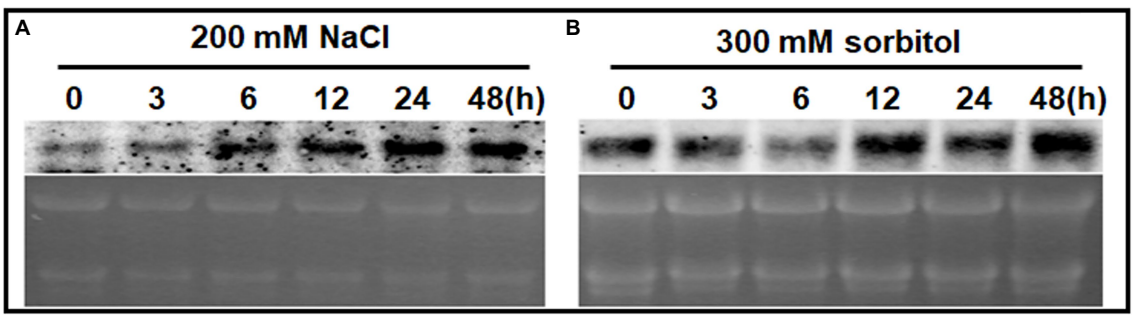

FIGURE 4 | The mRNA expression levels of *ChPAP2* at various time points after exposure to NaCl- and sorbitol-stress treatments. Northern blot analyses of the *ChPAP2* gene's expression levels in TSA *Chlorella* cells using a digoxigenin-labeled *ChPAP2* cDNA probe. The total RNA (5 μg) was extracted from *Chlorella* cells treated independently with 200-mm NaCl **(A)** and 300-mm sorbitol **(B)**.

The *ChPAP2* mRNA level began to rise at 12 h, and the level was the most significantly different from that of the control at 48 h after treatment (**Figure 4B**). In *Saccharomyces cerevisiae*, PAP accumulates during exposure to hyperosmotic and dehydration stresses (Munnik et al., 2000). Thus, the upregulated *ChPAP2* expression may enhance drought tolerance.

ChPAP2 Localized at the Plasma Membrane and in the Lumen of Vacuoles

The deduced ChPAP2 amino acid sequence was predicted to contain six transmembrane domains (**Figure 5A**). To determine its subcellular localization, GFP was fused to the C-terminus of ChPAP2 (ChPAP2-GFP). The green fluorescence of the GFP protein alone was almost evenly distributed throughout the yeast cells (**Figures 5B1,2**). FM4-64 stained the vacuole membrane, and its localization signal was consistent with the vacuolar membrane signal (red fluorescence area; **Figure 5B4**). Thus, the ChPAP2 protein appeared to localize on the plasma membrane and in the lumen of vacuoles in yeast cells (**Figures 5B3,5**). The results suggested that ChPAP2 might play important roles in transporting lipids through the plasma membrane and in catalyzing DGPP into PA in the vacuoles.

ChPAP2, as a catalytic enzyme, participates in lipid metabolism. ChPAP2 localized on the plasma membrane may function in maintaining cell membrane stability and the ion balance of the cytoplasm in response to abiotic stresses. The ChPAP2 protein also is localized in the lumen of vacuoles, where it may be involved with lipid translocation and DGPP catalysis to form PA. Therefore, we hypothesized that ChPAP2 participates in catalyzing DGPP in the lumen of vacuoles.

The PAP protein may function as a signaling molecule in planta under stress conditions, and its levels accumulate during hyperosmotic and dehydration stresses (Munnik et al., 1996). Therefore, the PAP enzyme may play a role in regulating specific cellular DGPP and PA pools under stress conditions (Oshiro et al., 2003).

In summary, the *ChPAP* in TSA *Chlorella* was upregulated expression in treated with high salinity and drought, and the *ChPAP* in yeasts could tolerate high salinity and drought stresses. Its protein was localized at the plasma membrane and in the lumen of vacuoles. The ChPAP might translocate excess NaCl and sorbitol from plasma membrane and then segregate them into vacuole to regulate ion balance in the cytoplasm. As a consequence, the PAP as a novel transporter can enhance high salinity tolerance and accumulate excess high salinity. These characteristics make ChPAP for the bioremediation of saline-alkali soil.

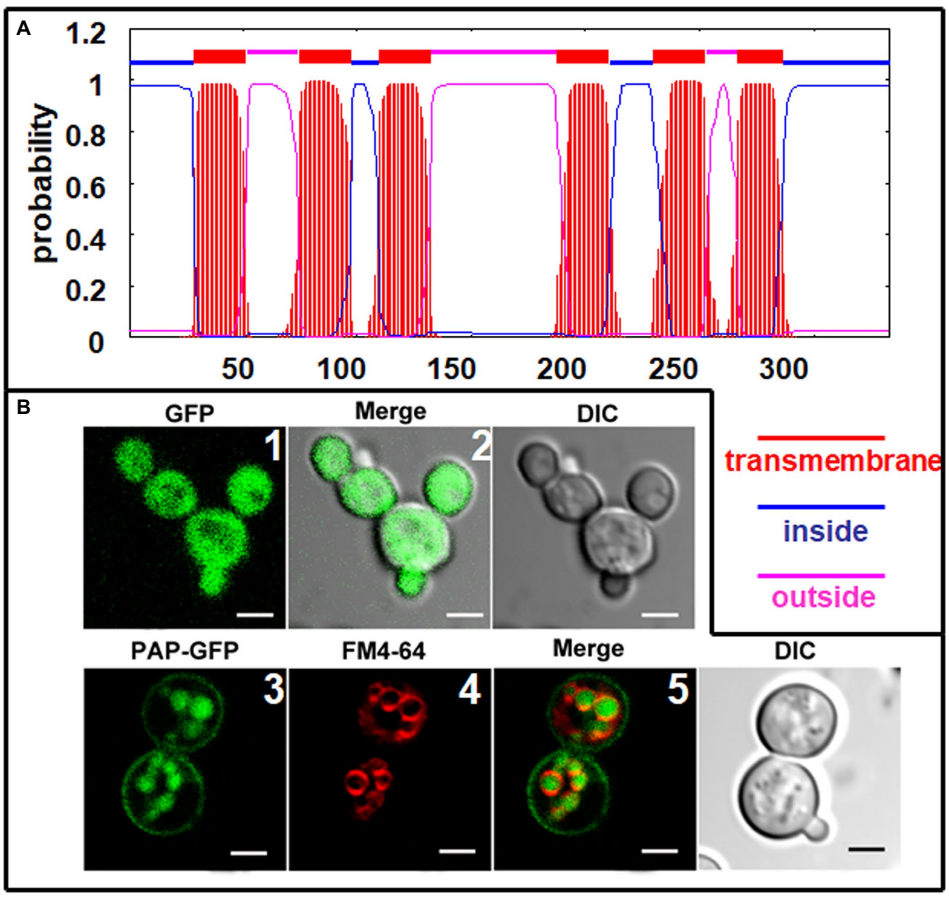

FIGURE 5 | Subcellular localization of ChPAP2 in yeast cells. **(A)** Transmembrane helices in ChPAP2 (GenBank no. KT750011) were predicted using the TMHMM server v. 2.0; **(B)** the green fluorescence was observed using a confocal microscope. Upper: GFP gene expressed in the pYES2 vector and in the yeast strain INVSc1. Left, middle, and right panels show fluorescence, merged, and bright-field (DIC) images. Lower: *ChPAP2*-EGFP fusion gene expressed in the pYES2 vector and in the yeast strain INVSc1. Live cells overexpressing *ChPAP2*-EGFP were incubated with FM4-64. Left, second, third, and right panels show fluorescence, FM4-64, merged, and bright-field (DIC) images. Bars = 5 μm.

DATA AVAILABILITY STATEMENT

The datasets presented in this study can be found in online repositories. The names of the repository/repositories and accession number(s) can be found in the article/supplementary material.

AUTHOR CONTRIBUTIONS

JW designed the research. QS, YR, and DS performed the experiments. HZ, JZ, and SG analyzed the data. KQ and AZ wrote the manuscript. All authors revised and approved the manuscript.

FUNDING

This study was supported by the National Natural Science Foundation of China (grant nos. 31800200, 31902052, and 31972450), the Natural Science Foundation of Heilongjiang Province of China (grant no. YQ2020C002), and the Postdoctoral Research Initiation Funding Project of Heilongjiang Province (grant no. LBH-Q19084).

REFERENCES

Blanc, G., Duncan, G., Agarkova, I., Borodovsky, M., Gurnon, J., Kuo, A., et al. (2010). The *Chlorella variabilis* NC64A genome reveals adaptation to photosymbiosis, coevolution with viruses, and cryptic sex. *Plant Cell* 22, 2943–2955. doi: 10.1105/tpc.110.076406

Bocchini, M., D'Amato, R., Ciancaleoni, S., Fontanella, M. C., Palmerini, C. A., Beone, G. M., et al. (2018). Soil selenium (se) biofortification changes the physiological, biochemical and epigenetic responses to water stress in *Zea mays* L. by inducing a higher drought tolerance. *Front. Plant Sci.* 9:389. doi: 10.3389/fpls.2018.00389

Bold, H. C., and Wynne, M. J. (1984). (Bold) introduction to the algae prentice hall. *Inc. New Jersey* 720, 573–574.

Brindley, D. N. (2004). Lipid phosphate phosphatases and related proteins: signaling functions in development, cell division, and cancer. *J. Cell. Biochem.* 92, 900–912.

Brindley, D. N., English, D., Pilquil, C., Buri, K., and Ling, Z. C. (2002). Lipid phosphate phosphatases regulate signal transduction through glycerolipids and sphingolipids. *Biochim. Biophys. Acta* 1582, 33–44. doi: 10.1016/s1388-1981(02)00135-x

Brindley, D. N., and Pilquil, C. (1984). Lipid phosphate phosphatases and signaling. *Prog. Lipid Res.* 23, 115–133.

Carman, G. M. (1997). Phosphatidate phosphatases and diacylglycerol pyrophosphate phosphatases in Saccharomyces cerevisiae and *Escherichia coli*. *Biochim. Biophys. Acta* 1348, 45–55. doi: 10.1016/s0005-2760(97)00095-7

Deng, X. D., Cai, J. J., and Fei, X. W. (2013). Effect of the expression and knockdown of citrate synthase gene on carbon flux during triacylglycerol biosynthesis by green algae *Chlamydomonas reinhardtii*. *BMC Biochem.* 14:38. doi: 10.1186/1471-2091-14-38

Deng, X. D., Cai, J. J., Li, Y. J., and Fei, X. W. (2014). Expression and knockdown of the *PEPC1* gene affect carbon flux in the biosynthesis of triacylglycerols by the green alga *Chlamydomonas reinhardtii*. *Biotechnol. Lett.* 36, 2199–2208. doi: 10.1007/s10529-014-1593-3

Eastmond, P. J., Quettier, A. L., Kroon, J. T. M., Craddock, C., Adams, N., and Slabasb, A. R. (2010). Phosphatidic acid phosphohydrolases 1 and 2 regulate phospholipid synthesis at the endoplasmic reticulum in *Arabidopsis*. *Plant Cell* 22, 2796–2811. doi: 10.1105/tpc.109.071423

Gao, C. F., Wang, Y., Shen, Y., Yan, D., He, X., Dai, J. B., et al. (2014). Oil accumulation mechanisms of the oleaginous microalga *Chlorella protothecoides* revealed through its genome, transcriptomes, and proteomes. *BMC Genomics* 15:582. doi: 10.1186/1471-2164-15-582

Gietz, D., Stjean, A., Woods, R. A., and Schiestl, R. H. (1992). Improved method for high efficiency transformation of intact yeast cells. *Nucleic Acids Res.* 20:1425. doi: 10.1093/nar/20.6.1425

Han, G. S., Johnston, C. N., and Carman, G. M. (2004). Vacuole membrane topography of the DPP1-encoded diacylglycerol pyrophosphate phosphatase catalytic site from *Saccharomyces cerevisiae*. *J. Biol. Chem.* 279, 5338–5345. doi: 10.1074/jbc.M311779200

Han, G. S., Johnston, C. N., Chen, X., Athenstaedt, K., Daum, G., and Carman, G. M. (2001). Regulation of the *Saccharomyces cerevisiae* DPP1-encoded diacylglycerol pyrophosphate phosphatase by zinc. *J. Biol. Chem.* 276, 10126–10133. doi: 10.1074/jbc.M011421200

Han, G. S., Wu, W. I., and Carman, G. M. (2006). The *Saccharomyces cerevisiae* lipin homolog is a Mg^{2+}-dependent phosphatidate phosphatase enzyme. *J. Biol. Chem.* 281, 9210–9218. doi: 10.1074/jbc.M600425200

Hassaninasab, A., Hsieh, L. S., Su, W. M., Han, G. S., and Carman, G. M. (2019). Yck1 casein kinase I regulates the activity and phosphorylation of Pah1 phosphatidate phosphatase from *Saccharomyces cerevisiae*. *J. Biol. Chem.* 294, 18256–18268. doi: 10.1074/jbc.RA119.011314

Hemrika, W., Renirie, R., Dekker, H. L., Barnett, P., and Wever, R. (1997). From phosphatases to vanadium peroxidases: a similar architecture of the active site. *Proc. Natl. Acad. Sci. U. S. A.* 94, 2145–2149. doi: 10.1073/pnas.94.6.2145

Huh, W. K., Falvo, J. V., Gerke, L. C., Carroll, A. S., Howson, R. W., Weissman, J. S., et al. (2003). Global analysis of protein localization in budding yeast. *Nature* 425, 686–691. doi: 10.1038/nature02026

Jamal, Z., Martin, A., Gomez-Muiioz, A., and Brindley, D. N. (1991). Plasma membrane fractions from rat liver contain a phosphatidate phosphohydrolase distinct from that in the endoplasmic reticulum and cytosol. *J. Biol. Chem.* 266, 2988–2996. doi: 10.1016/S0021-9258(18)49945-0

Lu, X. P., Gao, H. J., Zhang, L., Wang, Y. P., Shao, K. Z., Zhao, Q., et al. (2019). Dynamic responses of *Haloxylon ammodendron* to various degrees of simulated drought stress. *Plant Physiol. Biochem.* 139, 121–131. doi: 10.1016/j.plaphy.2019.03.019

Mu, C. H., Pan, C. Y., Han, Q., Liu, Q. Z., Wang, Y., and Sang, J. L. (2019). Phosphatidate phosphatase Pah1 has a role in the hyphal growth and virulence of *Candida albicans*. *Fungal Genet. Biol.* 124, 47–58. doi: 10.1016/j.fgb.2018.12.010

Munnik, T., deVrije, T., Irvine, R. F., and Musgrave, A. (1996). Identification of diacylglycerol pyrophosphate as a novel metabolic product of phosphatidic acid during G-protein activation in plants. *J. Biol. Chem.* 271, 15708–15715. doi: 10.1074/jbc.271.26.15708

Munnik, T., Meijer, H. J. G., Ter Riet, B., Hirt, H., Frank, W., Bartels, D., et al. (2000). Hyperosmotic stress stimulates phospholipase D activity and elevates the levels of phosphatidic acid and diacylglycerol pyrophosphate. *Plant J.* 22, 147–154. doi: 10.1046/j.1365-313x.2000.00725.x

Nanjundan, M., and Possmayer, F. (2001). Pulmonary lipid phosphate phosphohydrolase in plasma membrane signalling platforms. *Biochem. J.* 358, 637–646. doi: 10.1042/bj3580637

Neuwald, A. F. (1997). An unexpected structural relationship between integral membrane phosphatases and soluble haloperoxidases. *Protein Sci.* 6, 1764–1767. doi: 10.1002/pro.5560060817

Oshiro, J., Han, G. S., and Carman, G. M. (2003). Diacylglycerol pyrophosphate phosphatase in *Saccharomyces cerevisiae*. *Biochim. Biophys. Acta* 1635, 1–9. doi: 10.1016/j.bbalip.2003.10.002

Paradis, S., Villasuso, A. L., Aguayo, S. S., Maldiney, R., Habricot, Y., Zalejski, C., et al. (2011). *Arabidopsis thaliana* lipid phosphate phosphatase 2 is involved in abscisic acid signalling in leaves. *Plant Physiol. Biochem.* 49, 357–362. doi: 10.1016/j.plaphy.2011.01.010

Pierrugues, O., Brutesco, C., Oshiro, J., Gouy, M., Deveaux, Y., Carman, G. M., et al. (2001). Lipid phosphate phosphatases in Arabidopsis regulation of the *AtLPP1* gene in response to stress. *J. Biol. Chem.* 276, 20300–20308. doi: 10.1074/jbc.M009726200

Pyne, S., Long, J. S., Ktistakis, N. T., and Pyne, N. J. (2005). Lipid phosphate phosphatases and lipid phosphate signaling. *Biochem. Soc. Trans.* 33, 1370–1374. doi: 10.1042/BST0331370

Qiao, K., Takano, T., and Liu, S. K. (2015). Discovery of two novel highly tolerant $NaHCO_3$ Trebouxiophytes: identification and characterization of microalgae from extreme saline-alkali soil. *Algal Res.* 9, 245–253. doi: 10.1016/j.algal.2015.03.023

Qiao, K., Wang, M., Takano, T., and Liu, S. K. (2018). Overexpression of acyl-CoA-binding protein 1 (ChACBP1) from saline-alkali-tolerant *chlorella* sp. enhances stress tolerance in Arabidopsis. *Front. Plant Sci.* 9:1772. doi: 10.3389/fpls.2018.01772

Sherr, G. L., LaMassa, N., Li, E., Phillips, G., and Shen, C. H. (2017). Pah1p negatively regulates the expression of V-ATPase genes as well as vacuolar acidification. *Biochem. Bioph. Res. Co.* 491, 693–700. doi: 10.1016/j.bbrc.2017.07.127

Smith, S. W., Weiss, S. B., and Kennedy, E. P. (1957). The enzymatic dephosphorylation of phosphatidic acids. *J. Biol. Chem.* 228, 915–922. doi: 10.1016/S0021-9258(18)70670-4

Soto-Cardalda, A., Fakas, S., Pascual, F., Choi, H. S., and Carman, G. M. (2012). Phosphatidate phosphatase plays role in zinc-mediated regulation of phospholipid synthesis in yeast. *J. Biol. Chem.* 287, 968–977. doi: 10.1074/jbc.M111.313130

Stukey, J., and Carman, G. M. (1997). Identification of a novel phosphatase sequence motif. *Protein Sci.* 6, 469–472. doi: 10.1002/pro.5560060226

Toke, D. A., Bennett, W. L., Dillon, D. A., Wu, W. I., Chen, X. M., Ostrander, D. B., et al. (1998). Isolation and characterization of the *Saccharomyces cerevisiae* DPP1 gene encoding for diacylglycerol pyrophosphate phosphatase. *J. Biol. Chem.* 273, 3278–3284. doi: 10.1074/jbc.273.6.3278

Toke, D. A., Bennett, W. L., Oshiro, J., Wu, W. I., Voelker, D. R., and Carman, G. M. (1999a). Isolation and characterization of the *Saccharomyces cerevisiae* LPP1 gene encoding a Mg^{2+}-independent phosphatidate phosphatase. *J. Biol. Chem.* 273, 14331–14338. doi: 10.1074/jbc.273.23.14331

Toke, D. A., Mcclintick, M. L., and Carman, G. M. (1999b). Mutagenesis of the phosphatase sequence motif in diacylglycerol pyrophosphate phosphatase from *Saccharomyces cerevisiae*. *Biochemistry* 38, 14606–14613. doi: 10.1021/bi991472x

Wang, J., Shi, W., Takano, T., and Liu, S. K. (2011). Purification and resistance analysis of algae of soda soil in Northeast China. *Mol. Soil Biol.* 3, 1–4. doi: 10.5376/msb.2011.03.0001

Wu, W. I., Liu, Y. S., Riedel, B., Wissing, J. B., Fischl, A. S., and Carman, G. M. (1996). Purification and characterization of diacylglycerol pyrophosphate phosphatase from *Saccharomyces cerevisiae*. *J. Biol. Chem.* 271, 1868–1876. doi: 10.1074/jbc.271.4.1868

Zhang, Q. X., Pilquil, C. S., Dewald, J., Berthiaume, L. G., and Brindley, D. N. (2000). Identification of structurally important domains of lipid phosphate phosphatase-1: implications for its sites of action. *Biochem. J.* 345, 181–184. doi: 10.1042/bj3450181

Conflict of Interest: The authors declare that the research was conducted in the absence of any commercial or financial relationships that could be construed as a potential conflict of interest.

be evaluated in this article, or claim that may be made by its manufacturer, is not guaranteed or endorsed by the publisher.

frontiers in Microbiology

ORIGINAL RESEARCH
published: 13 October 2021
doi: 10.3389/fmicb.2021.748718

Discovering the Potentials of Four Phage Endolysins to Combat Gram-Negative Infections

Daria V. Vasina[1†], Nataliia P. Antonova[1†], Igor V. Grigoriev[2], Victoria S. Yakimakha[3], Anastasiya M. Lendel[1,3], Maria A. Nikiforova[1], Andrei A. Pochtovyi[1,3], Timofey A. Remizov[2], Evgeny V. Usachev[1], Natalia V. Shevlyagina[4], Vladimir G. Zhukhovitsky[4,5], Mikhail V. Fursov[6], Vasiliy D. Potapov[6], Aleksei M. Vorobev[7], Andrey V. Aleshkin[7] Aleksei I. Laishevtsev[8], Valentine V. Makarov[9], Sergey M. Yudin[9], Artem P. Tkachuk[2] and Vladimir A. Gushchin[1,3*]*

[1]Laboratory of Pathogen Population Variability Mechanisms, N. F. Gamaleya National Research Center for Epidemiology and Microbiology, Ministry of Health of the Russian Federation, Moscow, Russia, [2]Translational Biomedicine Laboratory, N. F. Gamaleya National Research Center for Epidemiology and Microbiology, Ministry of Health of the Russian Federation, Moscow, Russia, [3]Faculty of Biology, Lomonosov Moscow State University, Moscow, Russia, [4]Laboratory of Indication and Ultrastructural Analysis of Microorganisms, N. F. Gamaleya National Research Center for Epidemiology and Microbiology, Ministry of Health of the Russian Federation, Moscow, Russia, [5]Russian Medical Academy of Continuing Professional Education (RMANPO), Ministry of Public Health, Moscow, Russia, [6]Aerobiological Laboratory, State Research Center for Applied Microbiology and Biotechnology, Obolensk, Russia, [7]Laboratory of Clinical Microbiology and Biotechnology of Bacteriophages, G. N. Gabrichevsky Moscow Research Institute for Epidemiology and Microbiology, Moscow, Russia, [8]Laboratory for Diagnostics and Control of Antibiotic Resistance of the Most Clinically Significant Pathogens of Animals, Federal State Budget Scientific Institution "Federal Scientific Centre VIEV" (FSC VIEV), Moscow, Russia, [9]Center for Strategic Planning of the Ministry of Health of the Russian Federation, Moscow, Russia

Endolysin-based therapeutics are promising antibacterial agents and can successfully supplement the existing antibacterial drugs array. It is specifically important in the case of Gram-negative pathogens, e.g., ESKAPE group bacteria, which includes *Enterococcus faecium*, *Staphylococcus aureus*, *Klebsiella pneumoniae*, *Acinetobacter baumannii*, *Pseudomonas aeruginosa*, and *Enterobacter* species, and are highly inclined to gain multiple antibiotic resistance. Despite numerous works devoted to the screening of new lytic enzymes and investigations of their biochemical properties, there are significant breaches in some aspects of their operating characteristics, including safety issues of endolysin use. Here, we provide a comprehensive study of the antimicrobial efficacy aspects of four Gram-negative bacteria-targeting endolysins LysAm24, LysAp22, LysECD7, and LysSi3, their *in vitro* and *in vivo* activity, and their biological safety. These endolysins possess a wide spectrum of action, are active against planktonic bacteria and bacterial biofilms, and are effective in wound and burn skin infection animal models. In terms of safety, these enzymes do not contribute to the development of short-term resistance, are not cytotoxic, and do not significantly affect the normal intestinal microflora *in vivo*. Our results provide a confident base for the development of effective and safe candidate dosage forms for the treatment of local and systemic infections caused by Gram-negative bacterial species.

Keywords: endolysin, Gram-negative bacteria, antimicrobial agents, local infection, animal models, safety

OPEN ACCESS

Edited by:
Wang Jiajun,
Northeast Agricultural University, China

Reviewed by:
Jingmin Gu,
Jilin University, China
Heejoon Myung,
Hankuk University of Foreign Studies, South Korea

***Correspondence:**
Daria V. Vasina
d.v.vasina@gmail.com
Vladimir A. Gushchin
wowaniada@gmail.com

[†]These authors have contributed equally to this work and share first authorship

Specialty section:
This article was submitted to Antimicrobials, Resistance and Chemotherapy, a section of the journal Frontiers in Microbiology

Received: *28 July 2021*
Accepted: *17 September 2021*
Published: *13 October 2021*

Citation:
Vasina DV, Antonova NP, Grigoriev IV, Yakimakha VS, Lendel AM, Nikiforova MA, Pochtovyi AA, Remizov TA, Usachev EV, Shevlyagina NV, Zhukhovitsky VG, Fursov MV, Potapov VD, Vorobev AM, Aleshkin AV, Laishevtsev AI, Makarov VV, Yudin SM, Tkachuk AP and Gushchin VA (2021) Discovering the Potentials of Four Phage Endolysins to Combat Gram-Negative Infections. Front. Microbiol. 12:748718. doi: 10.3389/fmicb.2021.748718

INTRODUCTION

The rapid increase of the discovery of new antibiotics during the 1950–60s is now replaced with moderate development of these therapeutics because of the growing commercial risks associated with the emergence of bacterial resistance. This has resulted in a rising focus on the development of derivatives of known antibiotics rather than discovery of antimicrobials with fundamentally new mechanisms of action. However, a significant drawback of such an approach is concluded in its inability to withstand the increase of bacterial antibiotic resistance. Thus, an active search for nonconventional approaches to limit or eliminate the emergence of resistant infectious agents' burden is carried out (Theuretzbacher et al., 2020).

During the last decades, the pharmaceutical industry set sights on biotherapeutics and biotechnologically derived antimicrobials, primarily proteins, peptides, mABs, and their artificial derivatives (Theuretzbacher and Piddock, 2019). Among new treatment strategies is the use of peptides and enzymes, specifically lysins and endolysins, with bacterial cell wall disruptive activity from the outside (Grabowski et al., 2021). On the one hand, this resembles a classical and effective mechanism of action of several classes of antibiotic agents (glycopeptide antibiotics, β-lactams, and polymyxins); on the other hand, it is believed that the enzybiotic mechanism of action oriented toward specific conservative targets will lead to the less dramatic and slow emergence of bacterial resistance (Grishin et al., 2020).

Dozens of peptidoglycan-degrading molecules acting against different bacterial species, either Gram-positive or Gram-negative, are reported annually. However, very few of them reach the advanced preclinical and clinical phases of development, among which are recombinant lysins against *Staphylococcus aureus* SAL200 (tonabacase; Jun et al., 2017) and *CF*-301 (exebacase; Fowler et al., 2020) for systemic administration and topical endolysins for the treatment of atopic dermatitis infected with *S. aureus* (Gladskin; Totté et al., 2017) and for prevention of nasal MRSA colonization (GangaGen, ClinicalTrials.gov Identifier: NCT01746654). Endolysin-based formulations against Gram-positive bacteria (especially *S. aureus*) predominate in late preclinical or clinical experience despite the fact that recent studies have also shown effectiveness of endolysins against highly resistant Gram-negative bacteria-caused infections (Gutiérrez and Briers, 2021).

Such a gap is the result of specific hurdles accompanying the development of Gram-negative acting enzymes, among which are (i) troubles with the transition from *in vitro* antibacterial activity results to *in vivo* level. The antibacterial action *in vitro* is usually evaluated under controlled cell growth conditions or growth stage, and the experiments do not fully reflect the real or even model conditions (Oliveira et al., 2018). (ii) The potential for bacterial resistance to lysins is still under question, although it was not shown for any of endolysins previously using the serial passage experiments (Grishin et al., 2020). (iii) Safety profiles *in vitro* and *in vivo* as well as pharmacokinetics of endolysins are not yet well understood. The sizes and origin of proteins restrict their distribution in the body; however, their ability to affect cells and blood components has not been evaluated. (iv) The immunogenicity of reusable lysin-based preparations is also not clarified yet. The protein origin of lysins should induce immune response in mammals causing reduced activity of preparations with each subsequent application. Thus, the development of neutralizing antibodies is of concern for repeated use in humans (Murray et al., 2021). The success of further developments of lysin-based preparations is based on reliable data on their efficiency and safety, solving the raised questions.

Previously, we characterized the *in vitro* activity of *Myoviridae* bacteriophage endolysins LysAm24, LysECD7, and LysSi3 (Antonova et al., 2019), representing diverse domain organizations (single-domain vs. two-domain) and different predicted mechanisms of action (lysozyme vs. peptidase activities). Likewise, LysAp22 lysozyme-like endolysin was obtained and tested. All of the assayed molecules were capable of lysing Gram-negative clinical isolates – representatives of the ESKAPE pathogen group. About 5–50 μg/ml of individual endolysins was enough to eradicate growing cells over more than five orders of magnitude. Importantly, recombinant enzymes revealed bactericidal activity without any specialized OM penetration approach or additives, suggesting their potential in the development of medicines with reliable effectiveness. Here, we assess the potentials and risks of the application of these four Gram-negative bacteria-targeting endolysins with different structures and mechanisms of action in *in vitro* and *in vivo* experiments. We report the results of *in vitro* and *in vivo* efficacy studies against bacterial strains and biofilms, including skin and burn wound animal models. Also, we review the safety aspects of endolysin use, assessing the impact on intestinal microbiome, interaction with immune response, and the ability of bacteria to acquire resistance toward the enzymes.

MATERIALS AND METHODS

Bacterial Strains

The bacterial strains used in the study included laboratory strains and clinical isolates of Gram-negative representatives of the ESKAPE group of pathogens from the collection of the N.F. Gamaleya Federal Research Center for Epidemiology and Microbiology, Ministry of Health of the Russian Federation, from the State Collection of Pathogenic Microorganisms and Cell Cultures "SCPM-Obolensk" and the Collection of Gabrichevsky Moscow Research Institute of Epidemiology and Microbiology (**Supplementary Table S1**). All the strains were stored at −80°C and cultivated in the appropriate medium at 37°C, at 250 rpm overnight before performing the assays.

Ethics Statements

All animal experiments were conducted following the relevant guidelines for the care and use of laboratory animals. The Ethics Committee of the State Research Center for Applied Microbiology and Biotechnology (Obolensk, Russia) approved the *in vivo* studies (Veterinary Protocol No. VP-2019/9 of SRCAMB Bioethics Committee). The outbred female mice were

used for the *in vivo* assessment of endolysins' impact on the intestinal microbiome. The outbred female mice and male Wistar rats were used in effectiveness experiments for skin wound and burn wound models correspondingly. Two female Californian rabbits (4.5–5.0 kg) were used for the immunization. Animals were purchased from Andreevka Nursery (Russia). All animals were housed in separate cages with controlled temperature (20–24°C) and humidity (45–65%) and fed with a balanced diet and water *ad libitum*.

Recombinant Expression and Purification of Proteins

Recombinant endolysins LysAm24 (NCBI AN: APD20282.1), LysAp22 (NCBI AN: CCH57765.1), LysECD7 (NCBI AN: ASJ80195.1), and LysSi3 (NCBI AN: ARK07361.1) were obtained as described previously (Antonova et al., 2019). The initial coding sequences were artificially synthesized in a pAL-TA commercial vector (Evrogen, Moscow, Russia). Thereafter, endolysins' ORFs were amplified from pAL-TA clones and integrated into the expression vector pET-42b(+; Evrogen, Moscow, Russia), resulting in four pET42b-endolysin-8his plasmids. All constructs were checked for errors *via* Sanger sequencing. The expression vectors were introduced into the competent *Escherichia coli* cells, strain BL21(DE3) pLysS (chloramphenicol resistance), using a heat shock transformation protocol.

The *E. coli* exponential cultures were induced with 1 mM β-D-1-thiogalactopyranoside at 37°C for 3 h, centrifuged, and disrupted by sonication. The cells were harvested by centrifugation (6,000 × *g* for 10 min at 4°C) and resuspended in lysis buffer (20 mM Tris–HCl, 250 mM NaCl, and 0.1 mM EDTA, pH = 8.0), incubated with 100 μg/ml lysozyme at room temperature for 30 min, and disrupted by sonication. The cell debris was removed by centrifugation (10,000 × *g* for 30 min at 4°C), and the supernatant was filtered through a 0.2-μm filter. The proteins were purified on an NGC Discovery™ 10 FPLC system (Bio-Rad, Hercules, CA, United States) with HisTrap FF column (GE Healthcare, Munich, Germany) pre-charged with Ni^{2+} ions. The filtered lysate was mixed with 30 mM imidazole and 1 mM $MgCl_2$ and loaded on the column pre-equilibrated with binding buffer (20 mM Tris–HCl, 250 mM NaCl, and 30 mM imidazole, pH = 8.0). The fractions were eluted using a linear gradient to 100% elution buffer (20 mM Tris–HCl, 250 mM NaCl, and 500 mM imidazole pH 8.0). The protein fractions were dialyzed against 20 mM Tris–HCl (pH = 7.5).

The purity of the proteins was determined by 16% SDS-PAGE, and protein concentrations were measured using a spectrophotometer (Implen NanoPhotometer, Implen, München, Germany) at 280 nm and calculated using predicted extinction coefficients [0.840, 0.831, 1.4595, and 1.0289 $(mg/ml)^{-1}$ cm^{-1} for LysAm24, LysAp22, LysECD7, and LysSi3, respectively]. All proteins were lyophilized and stored at −80°C.

Endolysin Activity Assay

Overnight bacterial cultures were diluted in a Mueller–Hinton broth and grown to the exponential phase (OD_{600} = 0.6). Subsequently, the cells were harvested by centrifugation (3,000 × *g*, 10 min, RT) and resuspended in 20 mM Tris–HCl (pH = 7.5) buffer to a final density of approximately 10^5–10^6 cells/ml. Afterward, 100 μl of the bacterial suspension and 100 μl of the protein at the final 100-μg/ml concentration were mixed in 96-well plate wells, with a buffer without endolysins used as the negative control. The mixtures were incubated at 37°C for 5, 10, 30, 60, or 120 min with shaking at 200 rpm, diluted 10-fold in PBS (pH = 7.4), and plated onto Mueller–Hinton agar. The number of surviving bacterial colonies was counted after overnight incubation at 37°C. All experiments were performed in triplicate, and the antibacterial activity was expressed as follows: bactericidal activity (%) = 100% – (CFUexp/CFUcont) × 100%, where CFU_{exp} is the number of bacterial colonies in the experimental culture plates and CFU_{cont} is the number of bacterial colonies in the control culture plates. Antibacterial activity on the definite strain was regarded as meaningful when it was higher than 33%.

The spectrum of activity was studied as described above with a 30-min incubation period at the 100-μg/ml final protein concentration. Antibiotic susceptibility analysis of some bacterial strains was performed by the broth microdilution method using Mueller–Hinton broth, according to ISO recommendations (ISO 20776-1; Clinical laboratory testing and *in vitro* diagnostic test systems – Susceptibility testing of infectious agents and evaluation of the performance of antimicrobial susceptibility testing devices – part 1. Geneva, Switzerland: International Organization for Standardization, 2006). Results were interpreted according to The European Committee on Antimicrobial Susceptibility Testing (breakpoint tables for interpretation of MICs and zone diameters, Version 11.0, 2021).

Scanning Electron Microscopy of Planktonic Cells

An overnight *Acinetobacter baumannii* strain Ts 50-16 bacterial culture was diluted in LB broth, grown to an exponential phase (OD_{600} = 0.6), and harvested by centrifugation. Subsequently, the cell pellet was washed twice with distilled water and resuspended in water to a final density of approximately 10^8 cells/ml (McFarland 0.5). Afterward, 150 μl of the bacterial suspension was mixed with 150 μl of the protein diluted in water to the 50-μg/ml concentration and incubated at 37°C for 30 min with shaking at 200 rpm. Buffer without endolysins was used as the negative control. Mixtures were fixed by adding 600 μl of 10% formalin for 24 h. Next, 10 μl of mixtures was placed on a slide and dried at RT conditions. The samples were mounted to stubs and sputter-coated with a gold layer (5 nm) in an SPI-Module Sputter/Carbon Coater System (SPI Inc., West Chester, PA, United States). The sputtering samples were analyzed using a scanning Quanta 200 3D Dual Beam Electron Microscope (FEI Company, Hillsboro, OR, United States) using the high vacuum mode (10 kV).

Microscopy of Biofilms

Sterile glass coverslips (Hampton Research, Aliso Viejo, CA, United States) were plunged into overnight *A. baumannii* Ts

50-16 culture in tryptic soy broth (TSB) medium in Petri dishes and incubated at 37°C for 24 h without shaking for biofilm formation. Then, slides were washed with distilled water three times and air-dried. Three slides were left intact, three were submerged into 20 mM Tris–HCl (pH = 7.5) control buffer, other slides were submerged into 100 μg/ml LysAm24, LysAp22, LysECD7, or LysSi3 solutions, with three slides for each solution, respectively, for 2 h at RT. Afterward, all slides were again washed with distilled water three times and air-dried. One slide from each group was fixed in 10% formalin vapors for 24 h and analyzed using scanning electron microscopy after coating with a gold layer, as described above. Another slide from each group was imprinted on LB agar to assess bacterial viability. The remaining slides were stained with 0.1% aqueous solution of crystal violet for 20 min at RT, washed three times with water, and dried. These slides were analyzed using an Axiostar Plus Transmitted Light Microscope (Zeiss AG, Jena, Germany) at ×400 magnification.

Biofilm Reduction Assay

Endolysin antibiofilm activity was assessed on mature biofilms of *A. baumannii* Ts 50-16, *Klebsiella pneumoniae* Ts 104-14, and *Pseudomonas aeruginosa* Ts 38-16, as described before (Fursov et al., 2020) with modifications. Overnight bacterial cultures in TSB medium were diluted 1:50 in fresh TSB, with 100 μl added to wells of 96-well sterile polystyrene cell culture plates, and incubated for 24 h at 37°C, 250 rpm, to allow biofilm formation. After incubation, the wells' contents with planktonic cells were shaken off, and the plate was washed with 200 μl of PBS (pH = 7.4) three times and air-dried for approximately 10 min. Then, 100 μl of endolysin solutions in the concentration of 100 and 1 mg/ml or 20 mM Tris–HCl buffer (pH = 7.5) as negative control was added to the wells and incubated at 37°C, 250 rpm, for 2 h. After incubation, wells were twice washed with 200 μl of PBS (pH = 7.4) and air-dried. Washed biofilms were stained with 0.1% aqueous solution of crystal violet for 20 min at RT followed by triple rinsing with PBS. The remaining stain was re-solubilized in 200 μl of 33% acetic acid, and OD_{600} of the obtained solution was measured using SPECTROstar NANO (BMG LABTECH, Ortenberg, Germany). All experiments were performed in triplicate. Values were normalized by dividing by OD_{600} of untreated biofilm.

The interpretation of the level of biofilm formation was done according to Stepanović et al. (2007). Weak biofilm was defined at $ODc < ODbf \leq 2 \times ODc$, moderate biofilm at $2 \times ODc < ODbf \leq 4 \times ODc$, and strong biofilm at $4 \times ODc < ODbf$, where ODc is the cutoff value calculated as three SDs above the mean OD of the negative control and ODbf = the optical density of bacterial biofilm stained with crystal violet.

Determination of Bacterial Resistance

Resistance development was tested using repeated exposure of endolysins on bacterial cultures in plate lysis assay and antibacterial assay on initial and passed strains of *A. baumannii* Ts 50-16 and *K. pneumoniae* Ts 104-14.

Overnight bacterial cultures were diluted in LB broth and grown at 37°C, 250 rpm, to an exponential phase ($OD_{600} = 0.6$). Subsequently, 200 μl of the bacterial suspension was spread over a Petri dish with LB agar and air-dried at RT. Then, 10 μl of 1 mg/ml endolysin solutions or control 20 mM Tris–HCl buffer (pH = 7.5) were dropped onto the bacterial lawn, and the dish was treated for 16–18 h at 37°C. The next day, bacteria from the sublethal lysis zone with a not fully cleared lawn were scraped and incubated in LB broth to exponential phase at 37°C with constant shaking to generate a new bacterial lawn for the next passage. There were 20 passages of *A. baumannii* and *K. pneumoniae* cultures during the experiment. Afterward, cultures from initial and passed strains were used to assess the antibacterial activity of endolysins as described before in 50 μg/ml concentration. All experiments were performed in triplicate.

Cytotoxicity Assay

Cytotoxicity was measured for HEK293 (ATCC-CRL-1573) cells by MTT assay. Cells were seeded at 4.5×10^4 cells/well in 96-well plates and cultivated in 100 μl of DMEM medium supplemented with 10% fetal bovine serum, 2 mM glutamine, 50 U/ml penicillin, and 50 μg/ml streptomycin for 24 h in a humidified atmosphere of 5% CO_2 and 95% air at 37°C. Afterward, the medium was removed and 50 μl of endolysin serial dilutions in DMEM (from 2,000 to 31.1 μg/ml) was added into each well. DMEM was used as a negative control, and 0.1% Triton X-100 was used as a positive control. Mixtures were incubated for 1 h (37°C, 5% CO_2), and the cells were then stained with 10% MTT solution in DMEM (final stain concentration is 0.5 mg/ml) for 4 h (37°C, 5% CO_2). After incubation, the content of the wells was replaced with 100 μl of DMSO and the absorbance of the solutions at the wavelength of 570 nm was measured using SPECTROstar NANO (BMG LABTECH). All experiments were performed in triplicate, and the viability of the HEK293 cells was estimated as follows: $\text{Viability } (\%) = (OD_{exp} - OD_{min})/(OD_{max} - OD_{min}) \times 100\%$, where OD_{exp} is OD_{570} in the experimental culture wells, OD_{min} is OD_{570} in the positive control (0.1% Triton X-100) culture wells, and OD_{max} is OD_{570} in the negative control (DMEM) culture wells.

Hemolytic Assay

The hemolytic activity of endolysins was determined against human red blood cells (RBC). Fresh human blood was obtained in a heparin-containing tube and was centrifuged at 500 *g* for 10 min, 4°C. The pellet was washed three times with PBS buffer, and a solution of 10% RBC in PBS was prepared. An RBC solution was mixed in a ratio of 1:1 with endolysin solutions in concentrations of 100 and 1 mg/ml in 20 mM Tris–HCl buffer (pH = 7.5). PBS buffer was used as a negative control, and 0.1% Triton X-100 was used as a positive control. The reaction mixtures were incubated for 1 h at 37°C and harvested by centrifugation (500 *g*, 10 min, 4°C), and the absorbance at the wavelength of 405 nm of the supernatants was measured. All experiments were performed in triplicate, and the hemolysis rate was estimated as follows:

Hemolysis (%) = $(OD_{exp} - OD_{PBS})/(OD_{Triton} - OD_{PBS}) \times 100\%$, where OD_{exp} is OD_{405} in the experimental mixtures, OD_{PBS} is OD_{405} in the negative control (PBS) mixtures, and OD_{Triton} is OD_{405} in the positive control (0.1% Triton X-100) mixtures.

Neutralizing Antibody Effect Assessment

The neutralization effect of specific anti-LysAm24, LysAp22, LysECD7, and LysSi3 antibodies on enzymes antibacterial activity was tested in the presence of hyperimmune serum or purified antibodies.

To obtain hyperimmune serum, rabbits were immunized with 0.25 mg of each endolysin eight times with 10-day interval resulting in a 3-month immunization period. For the first immunization, the solutions of each antigen were emulsified with equal volumes of Freund's complete adjuvant (Sigma, St. Louis, MO, United States) and injected subcutaneously to 8–9 sites on the back, and re-immunizations were repeated with Freund's incomplete adjuvant (Sigma, United States). Rabbit sera were sampled 10 days after the last injection, and the titers of specific antibodies (>100,000) were determined using the ELISA method. Serum from rabbits without immunization was used as a control.

The neutralization effect of immunized serum was estimated by mixing 20 µl of 1 mg/ml of endolysin solutions with 80 µl of immunized or control rabbit serum, followed by incubation at 37°C for 10 min. Afterward, 100 µl of exponential *A. baumannii* Ts 50-16 culture in 20 mM Tris–HCl buffer (pH = 7.5) with a cell density of 10^5–10^6 CFU/ml was added to each 96-well plate well, with a buffer without endolysins as the negative control. Next, the mixtures were incubated at 37°C for 30 min with shaking at 200 rpm, diluted 10-fold in PBS (pH = 7.4), and plated onto an LB agar. The number of surviving bacterial colonies was counted after overnight incubation at 37°C. All of the experiments were performed in triplicate, and the antibacterial activity was expressed as described before.

The neutralization effect of specific antibodies was estimated after antibody purification from hyperimmune serum with affinity chromatography. Each endolysin in 0.05 M MES (pH = 5.5) and 0.15 M NaCl buffer was conjugated to aminoethyl-sepharose sorbent by overnight incubation with 200 µg/ml EDC [1-ethyl-3-(3-dimethylaminopropyl)carbodiimide] at RT with rotation at 15 rpm and equilibrated with PBS, 0.5 M NaCl, and 0.1% NaN_3. Then, hyperimmune rabbit serum was supplied with 0.5 M NaCl, centrifuged (30 min, 10,000 × *g*), loaded on the column, and washed with the same buffer. The specific antibody fractions were eluted using 0.1 M CH_3COOH and 0.5 M NaCl (pH = 2.5–2.8) buffer, and the pH was immediately adjusted to neutral by adding 1 M Tris–HCl pH 8.0. Afterward, the buffer was exchanged to PBS (pH = 7.4) using a PD-10 gel-filtration column (GE Healthcare, Chicago, IL, United States), and the solution was concentrated with Amicon® Ultra-15 Centrifugal Filter Units, 30-kDa MWCO (Millipore, Bedford, MA, United States). The antibody concentration was measured using a spectrophotometer (Implen NanoPhotometer, Implen, Germany) at 280 nm while antibody-specific activity was confirmed by indirect ELISA.

Endolysin solutions (50 µl) in 20 mM Tris–HCl buffer (pH = 7.5) were mixed with 50 µl of antibodies in PBS in mass ratios of 1:1, 1:2, and 1:5 (the PBS solution was used as a positive control) and incubated at 37°C for 10 min without agitation in a 96-well plate. Endolysin concentrations in wells were 25 µg/ml for LysAm24 and LysAp22, 50 µg/ml for LysECD7, and 100 µg/ml for LysSi3. Thereafter, 100 µl of exponential *A. baumannii* Ts 50-16 culture in 20 mM Tris–HCl buffer (pH = 7.5) was added to each 96-well plate well, with a 20 mM Tris–HCl buffer (pH = 7.5) without endolysins as the negative control. Further, the experiment was performed as described above.

Assessment of Impact of Endolysins on Intestinal Microbiome

In vitro Tests

Endolysins' effect on microbiota representatives was tested *in vitro* on eight strains of *Bifidobacterium* sp. and three strains of *Lactobacillus* sp. (**Supplementary Table S1**). These bacteria are representatives of normal microbial flora and are a form of probiotic drugs intended for correction of the microflora of three age groups of patients with dysbiosis of the gastrointestinal tract: children under the age of 3 years (patent RU 2491331), those from 3 to 14 years (patent RU 2491335), and people over 14 years old (patent RU 2491336).

Freeze-dried bacterial cultures were rehydrated in 1 ml specific for *Bifidobacterium* or *Lactobacillus* media (State Research Center for Applied Microbiology and Biotechnology, Russia), and their 10-fold dilutions in fresh liquid medium were cultivated at 37°C for 24 h in anaerobic conditions. Grown bacterial colonies were reinoculated in fresh medium twice and then plated onto agar in an anaerobic culture apparatus. Next, bacterial colonies were resuspended in normal saline to $OD_{600} = 0.6$ and diluted in 20 mM Tris–HCl (pH = 7.5) buffer to a final density of approximately 10^5–10^6 cells/ml. Endolysin solutions (1 ml) with a protein concentration of 1 mg/ml were mixed in glass tubes with bacterial suspension (9 ml), incubated for 30 min at 37°C, 10-fold diluted in a liquid medium, and incubated for 48 h at 37°C in anaerobic conditions. The final proteins concentration was 100 µg/ml. Afterward, the number of surviving bacterial colonies in tubes was counted. All of the experiments were performed in triplicate. The experimental workflow is shown in **Supplementary Figure S1**.

In vivo Evaluation

Endolysins' effect on bacterial intestinal microbiome was also assessed *in vivo* using a murine model of outbred female mice (22–27 g). Before the experiment, animals were randomized into experimental groups ($n = 5$ per group), which were intraperitoneally injected with 0.5 ml of endolysin in the concentration of 1 mg/ml (500 µg/mouse) every 24 h for 5 days and one control group ($n = 8$) that received 0.5 ml of 20 mM Tris–HCl (pH = 7.5) the same way. On the seventh day of the experiment (2 days after the last injection of LysAm24, LysECD7, LysAp22, and LysSi3), mice were sacrificed by CO_2 inhalation and the parietal microbiota was investigated using the 16S sequencing of samples containing intestine with excrements. All samples were stored at −80°C until the analysis.

16S rRNA Gene Sequencing of Parietal Microbiome

Frozen intestine samples from each of the animals were homogenized with TissueLyser II (Qiagen, Manchester, United Kingdom) in PBS buffer, and DNA isolation was performed using the DNeasy PowerSoil Kit (Qiagen, United Kingdom) according to the manufacturer's instructions. DNA quality was assessed using agarose gel, and the yield was measured with a Qubit 3 Fluorometer (Invitrogen, Carlsbad, CA, United States).

The hypervariable V3-V4 region of the bacterial 16S rRNA gene was amplified using the forward primer NR_16S_341F (5'-TCGTCGGCAGCGTCAGATGTGTATAAGAGACAGTGCC TACGGGN BGCASCAG-3') and reverse primer NR_16S_806R (5'-GTCTCGTGGGCTCGGAGATGTGTATAAGAGACAGCCG GACTACNV GGGTWTCTAATCC-3'). Primers were modified with forward overhang 5'-TCGTCGGCAGCGTCAGATG TGTATAAGAGACAG-3' and with reverse overhang 5'-GTCTC GTGGGCTCGGAGATGTGTATAAGAGACAG-3' (Nextera tag sequences) for dual index library preparation. Amplicons were pooled in equal concentrations and purified using magnetic bead extraction to remove unwanted products. The purified libraries were quantified with 2100 Bioanalyzer (Agilent, Santa Clara, CA, United States), diluted as recommended by Illumina MiSeq library preparation guide, and sequenced with a MiSeq Reagent Kit v3 (2×300 cycles).

Sequencing Data Analysis

Raw Illumina fastq files were demultiplexed and quality filtered (quality score not less Q30), chimeric reads were removed, and paired amplicon sequencing reads were joined using the QIIME pipeline (version 1.9.1). Operational taxonomic units (OTUs) were identified from the trimmed sequences at 97% identity level as implemented in QIIME with the Silva reference database (version 132). The OTUs to family and genus were then collapsed, and the relative abundance of each bacterium in every sample was calculated. The following statistical analyses were based on family- and genus-level data. The fold changes in microbial species after the endolysins administration in comparison to Tris-buffer injections samples were calculated for genus–taxa level.

Animal Efficacy Studies

Skin Wound Model

Skin infection was induced with a *K. pneumoniae* Ts 141-14 clinical isolate. The backs of outbred female mice (20–22 *g*) were shaved and infected subcutaneously with 100 µl of 2×10^8 CFU/ml bacterial suspension in PBS buffer. During the first day after the infection, the abscess was formed and ruptured spontaneously, resulting in an open wound in the place of injection. At 24 h post-infection (PI), the treatment had begun. The infected area was either treated epicutaneously with 100 µl of 20 mM Tris–HCl (pH = 7.5) control buffer ($n = 10$) or treated with 100 µl of each endolysin solution in the concentration of 500 µg/mouse ($n = 10$ mice in each group), left untreated ($n = 20$). Mice were treated every 24 h for 5 days.

To access the endolysins' therapeutic effect, the dynamics of wound healing and microbial contamination were measured after 1, 3, and 7 days PI. CFU counts of *K. pneumoniae* were estimated using the wound swabs with sterile cotton balls wetted with saline. Inoculations were serially diluted and plated on LB agar. After 7 days of the experiment, the mice were sacrificed by CO_2 inhalation, and the infected dermal grafts of the wound area and animal spleens were excised, weighted, and homogenized in PBS. The solutions were serially diluted and plated on LB agar, and bacterial CFU loads were assessed after overnight incubation at 37°C.

Burn Wound Model

For the burn wound model, the *P. aeruginosa* Ts 38-16 clinical isolate was used. The backs of 8–10-week-old male Wistar rats (180–210 *g*) were shaved with an electric razor. To induce burn injury, a copper plate with a surface area 150 mm^2 was heated to 300°C and then applied on the shaved backs for 30 s. To restore the water–electrolyte balance, 1 ml of PBS buffer was injected subcutaneously to the burned areas. Five minutes later, the burn was infected with 3.5×10^{10} CFU/ml of *P. aeruginosa* (100 µl in PBS). After 24 h PI, the infected burns were either left untreated ($n = 20$), treated with 100 µl of 20 mM Tris–HCl (pH = 7.5) control buffer ($n = 10$), or treated with 100 µl of endolysin solution in the concentration of 2,500 µg/rat ($n = 10$ in each group). The rats were treated epicutaneously every 24 h for 5 days.

To access the endolysins' therapeutic effect, the dynamics of wound size and microbial contamination were observed after 1, 3, and 7 days PI. CFU counts of *P. aeruginosa* were estimated using the wound swabs as mentioned above using the selective Pseudomonas Agar B Medium (for fluorescein; HiMedia, Mumbai, India). After 7 days of experiment, the rats were sacrificed by CO_2 inhalation. Infected dermal grafts of the burn area and animal spleens were excised, weighted, and homogenized in PBS. The solutions were serially diluted and plated on Agar B Medium, and bacterial CFU were counted after overnight incubation at 37°C.

Statistical Analysis

The data were analyzed using GraphPad Prism 7.0 software. A value of $p < 0.05$ was considered statistically significant. The methods used for comparison tests are indicated in figure and table captions.

RESULTS

In vitro Antimicrobial Activity of Endolysins

The enzymes' bactericidal activity was evaluated using the microplate assay measuring CFU counts after incubation of *A. baumannii* cell suspension with endolysins. All lysins exhibited rapid activity, capable of eliminating 100% of cells within 1 h except for LysSi3, which required 2 h for the total elimination of bacteria (**Figure 1A**). It was suggested to compare time required to kill 99.9% of *A. baumannii* planktonic cells by

endolysins in equal concentrations and, in fact, characterize its bactericidal activity (Pfaller et al., 2004; Balouiri et al., 2016). For LysAp22, LysECD7, LysAm24, and LysSi3 in concentration 100 μg/ml, it was 22.7, 23.3, 24.1, and 99.6 min, respectively. Cell lysis of the exponentially growing bacteria after the incubation with lysins was confirmed with scanning electron microscopy (**Figure 1B**). The formation of debris accompanying osmosis-mediated cell lysis resulted in cell disruption of bacteria due to the loss of peptidoglycan integrity under lysin action.

The spectrum of activity of LysAm24, LysAp22, LysECD7, and LysSi3 was estimated against 100 clinical isolates and strains of Gram-negative pathogens, including multidrug-resistant *K. pneumoniae*, *Salmonella* sp., *P. aeruginosa*, *Escherichia coli*, *A. baumannii*, and *Enterobacter* sp. (**Figure 1C**; **Supplementary Table S1**). For all endolysins, we observed similar results that indicated a broad range of sensitive bacterial species, with LysECD7 being the most active among enzymes with the highest rate of antimicrobial activity (99% of strains with activity above 33%). LysAm24 was active against 81% of strains, LysAp22 – 66%, LysSi3 – 54%. A concentration of 100 μg/ml was enough to eradicate growing bacteria up to five orders of magnitude. Among the investigated species, *A. baumannii* was the most sensitive to lysins.

The bacterial biofilms' disruptive activity was also investigated. The ability of endolysins to eliminate 24-h preformed strong biofilms of *A. baumannii* Ts 50-16, *K. pneumoniae* Ts 104-14, and *P. aeruginosa* Ts 38-16 in microtiter plates is shown in **Figure 2A**.

Two hours of exposure to 100 and 1 mg/ml of endolysins resulted in a dose-dependent decrease of optical density of biofilms. LysECD7 again had the most pronounced effect compared to LysAm24, LysAp22, and LysSi3 and was capable of eliminating biofilms. Also, it was noticed that *A. baumannii* biofilms were exposed to endolysin activity most significantly, which is consistent with data on planktonic cells. To directly observe the interactions of antimicrobial enzymes with bacterial films, a combination of light and scanning electron microscopy was applied (**Figure 2B**). The breakdown of the structural integrity of the bacterial film occurs under the action of lysins, while the film matrix is destroyed and only individual shapeless cells are indicated. Nondisrupted cells were also observed, and their viability was confirmed by glass slide imprinting on a solid medium after treatment with the endolysin solution. Growth of single CFUs was found after exposure to LysECD7, LysAp22, and LysSi3, and no bacterial growth in the case of LysAm24.

In vitro Safety of Recombinant Endolysins

Bacterial Resistance Development Toward Endolysins

The ability of bacteria to develop resistance after repeated exposure to sublethal endolysin concentrations was studied on *A. baumannii* Ts 50-16 and *K. pneumoniae* Ts 104-14 clinical isolates in a plate lysis assay. Antibacterial activity of lysins (50 μg/ml) against initial and passed strains after 20 passages did not differ in the case of *K. pneumoniae* Ts 104-14 or *A. baumannii* Ts 50-16. Thus, no resistance appearance to Gram-negative endolysins with different enzymatic activities accompanying the loss of antibacterial effect was estimated.

Cytotoxicity and Hemolysis

Safety of LysAm24, LysAp22, LysECD7, and LysSi3 endolysins was assessed in cytotoxicity and hemolytic assays. The impact on eukaryotic HEK293 cells in the concentration range from 2,000 to 31 μg/ml was not significant, and cell viability was approximately 100% in almost all proteins. Significant cell viability reduction was reported in the 2,000-μg/ml concentration of LysAm24 and LysSi3; it was 58.4 and 70.9%, respectively (**Supplementary Figure S2**). The percent of hemolysis of human blood cells did not exceed 0.5% in the 1-mg/ml concentration, which is very insufficient (**Supplementary Figure S3**).

Interaction With Specific IgG

The neutralization effect specific to LysAm24, LysAp22, LysECD7, and LysSi3 antibodies on their antibacterial activity was tested in the presence of hyperimmune serum and purified antibodies (**Figure 3**).

The presence of hyperimmune rabbit serum completely inhibited the antibacterial activity of all enzymes. However, the activity of 100 μg/ml of endolysins in nonimmunized serum was significantly lower than in PBS (73, 47, and 44% for LysAm24, LysECD7, and LysSi3, correspondingly) and LysAp22 did not kill bacterial cells at all. Apparently, this is due to the inhibitory effect of the serum itself.

Therefore, the neutralization effect of purified antibodies was investigated to eliminate the serum effect. The addition of specific antibodies in mass ratios of 1:1 and 1:2 to reaction significantly decreased the antibacterial effect of LysAm24, LysAp22, LysECD7, and LysSi3. Moreover, a 1:5 mass ratio that corresponds approximately to the 1:1 molar ratio completely inhibits endolysin activity.

Impact of Endolysins on the Normal Flora of the Gastrointestinal Tract

Interaction of Endolysins With Human Gut Microbiota *in vitro*

The *in vitro* impact on microbiota representatives was tested on strains of Gram-positive *Bifidobacterium* spp. and *Lactobacillus* spp. (**Supplementary Table S1**). Several strains were susceptible to endolysin LysAm24, LysAp22, and LysSi3 exposure (**Figure 4A**). LysAp22 was the most active against investigated strains and influenced the growth of five from 11 microbiota representatives. However, LysECD7 did not influence bacterial counts. The *Lactobacillus* genus was more susceptible to endolysin treatment *in vitro* and reached 98–99% of bacterial growth elimination for LysAm24 and LysSi3.

Interaction of Endolysins With Gut Microbiota in the Murine Model

Endolysins' impact on the normal flora was also assessed in a murine model. Endolysin solutions in the concentration of 500 μg/mouse were administered intraperitoneally every

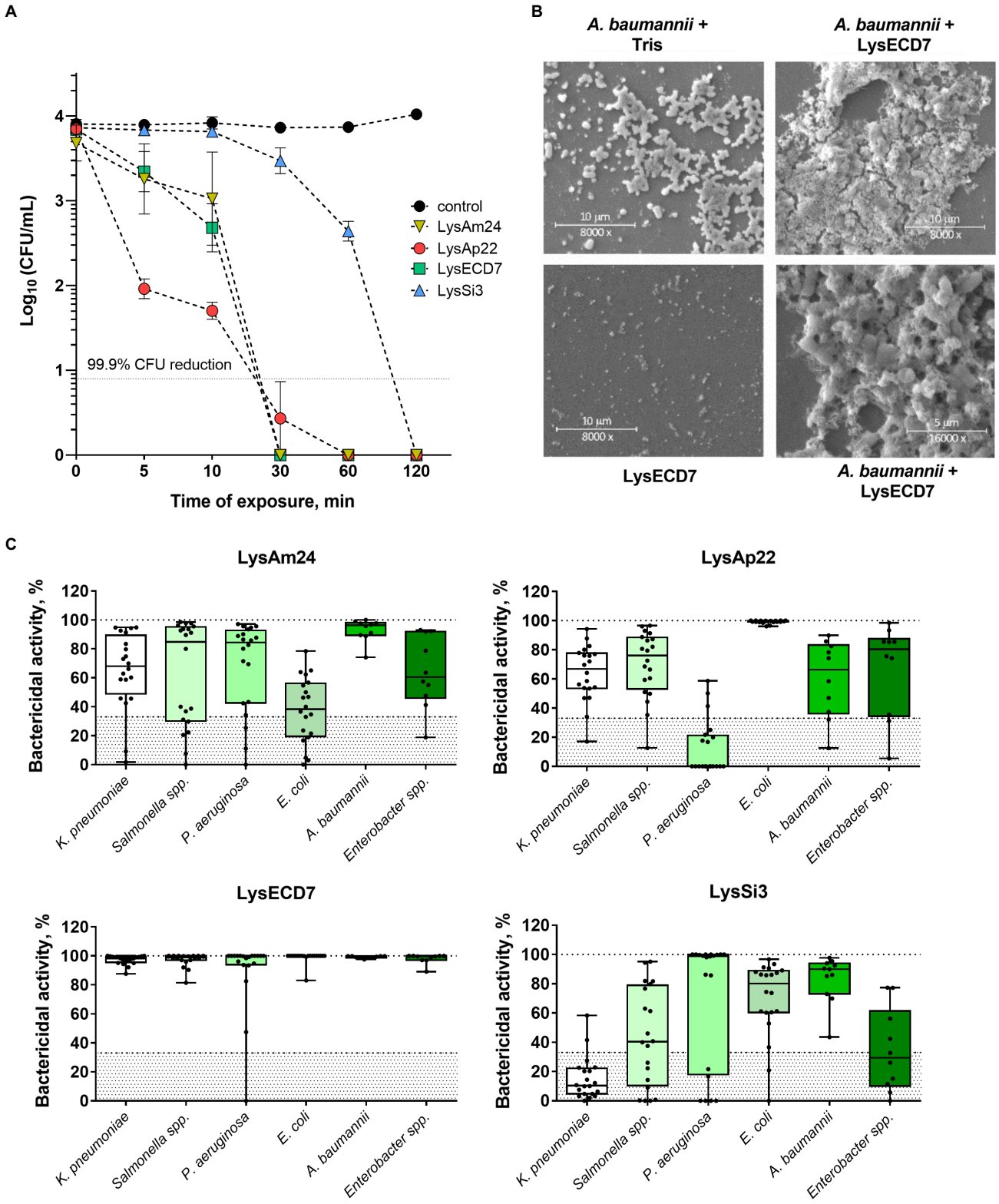

FIGURE 1 | *In vitro* efficacy of four endolysins. **(A)** Time-kill curve of endolysins activity in 100 µg/ml concentration against logarithmic-phase growing planktonic *Acinetobacter baumannii* Ts 50-16 cells. Data are shown as mean ± SEM. **(B)** Scanning electron microscopy of *A. baumannii* Ts 50-16 planktonic cells exposed to 50 µg/ml of LysECD7 or Tris–HCl buffer for 30 min, or protein in Tris–HCl buffer. **(C)** LysAm24, LysECD7, LysAp22, and LysSi3 (100 µg/ml) spectra of activity after a 30-min incubation with logarithmic-phase growing bacteria. Each dot represents a single strain within the species, lines, and

(Continued)

FIGURE 1 | medians; boxes, IQR whiskers, and min–max. The 33% activity cutoff is indicated with a dotted line.

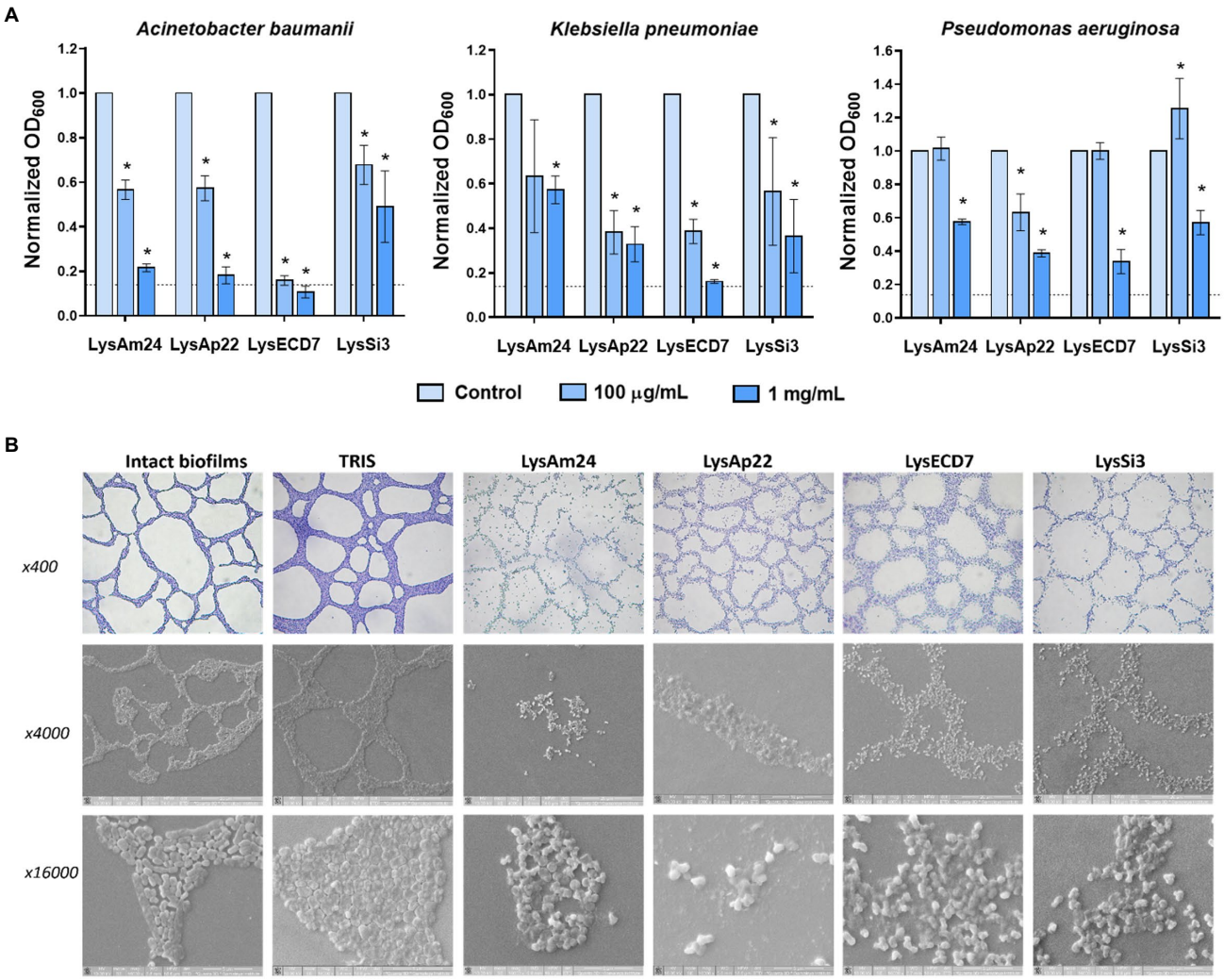

FIGURE 2 | Disruption of bacterial biofilms by endolysins. **(A)** Antibiofilm activity of endolysins against *Klebsiella pneumoniae* Ts 104-14, *A. baumannii* Ts 50-16, and *Pseudomonas aeruginosa* Ts 38-16 biofilms stained with crystal violet. OD_{600} was measured after 2 h of exposure to endolysins. Dash line indicates the cutoff value calculated as three SDs above the mean OD of the negative control. Data are shown as mean ± SD. Asterisk (*) indicates significant difference in optical density compared to control without the enzyme treatment of biofilm ($p < 0.05$, one-way ANOVA). **(B)** Light and scanning electron microscopy images of lysis of *A. baumannii* Ts 50-16 preformed biofilms on glass slides after a 2-h exposure to endolysins in 100 mg/ml concentration.

day for 5 days. The composition of the parietal microbiome was estimated on the seventh day of experiment (2 days after the last injection), and sequencing of intestinal fragments with feces was carried out, which showed changes in the microbiome from Tris–HCl buffer injections, illustrated in **Figure 4B**. In general, the identified bacteria of the gastrointestinal tract corresponded to those previously described in the literature as a healthy core gut microbiota (Wang et al., 2019). The main phyla that underwent quantitative changes under the endolysins administration were Proteobacteria and Bacteroidetes (Gram-negative) as well as Firmicutes (Gram-positive; **Figure 4B**). When comparing microflora profiles, mostly the increased growth of bacteria was observed, among which Lachnospiraceae, Lactobacillaceae, and Ruminococcaceae families were prevalent. While the most pronounced bacterial profile changes (both increase and decrease in 16S relative abundance) were shown under the administration of LysSi3, we detected a significant bacterial decrease for LysSi3 (Lachnospiraceae: *Acetatifactor*) and LysAp22 (Porphyromonadaceae, Caulobacteraceae, and Methylocystaceae families; **Supplementary Figure S4**). There was no decrease in *Bifidobacterium* genus *in vivo*, in contrast to *in vitro* data, while *Lactobacillus* tended to increase after the use of LysSi3 and LysECD7. Interestingly, no significant differences were found in opportunistic Gram-negative pathogens like *Escherichia* or *Klebsiella*. Thus, the experimental

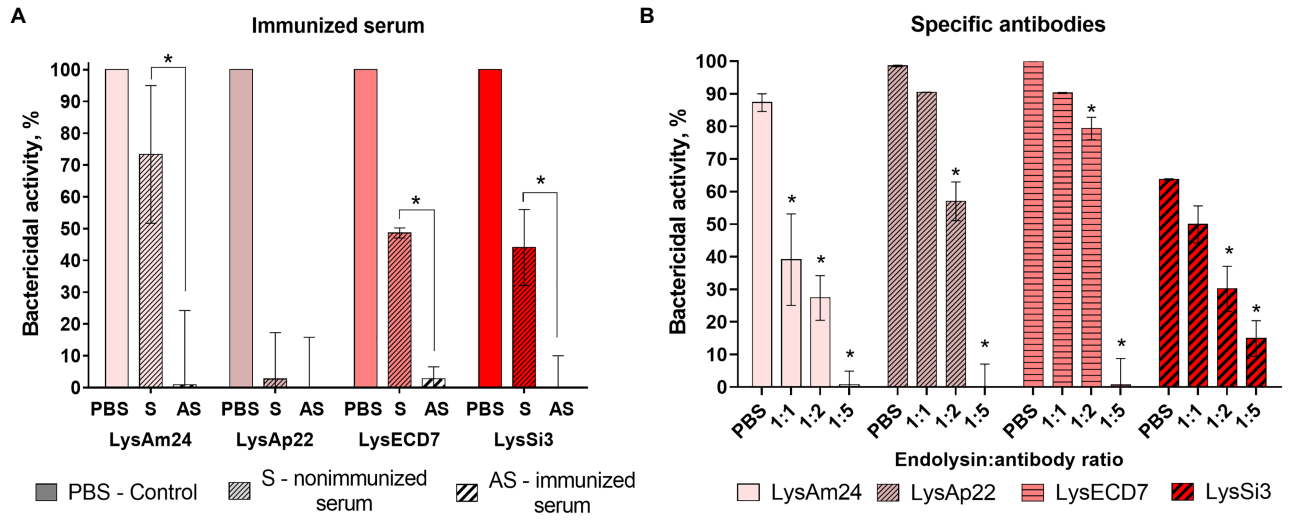

FIGURE 3 | The neutralization effects of immunized serum **(A)** and specific antibodies **(B)** toward four endolysins. LysAm24, LysECD7, LysAp22, and LysSi3 were preincubated with endolysin-immunized rabbit serum, nonimmunized serum, PBS solution, or affinity-purified antibodies for 10 min at 37°C. Each mixture was then added to the growing culture of *A. baumannii* Ts 50-16, and CFU count was estimated after 30-min incubation. Data are shown as mean ± SD (one-way ANOVA). Asterisk (*) indicates significant difference in activity compared to nonimmunized serum **(A)** or control in PBS **(B**; $p < 0.05$).

data confirm moderate endolysins' effect on microbiome when administered parenterally.

In vivo Efficacy of Endolysins

Skin Wound Model

Skin infection of outbred mice was induced with subcutaneous injection of *K. pneumoniae* Ts 141-14 suspension. The open wound was formed after the abscess rupture within 24 h PI. Then infected areas were either left untreated, treated with control buffer (20 mM Tris–HCl, pH 7.5), or treated with solutions of each investigated endolysin in the concentration of 500 μg/mouse. The mice were treated epicutaneously once a day for 5 days.

The wound sizes and their microbial contamination were assessed in dynamics as well as spleen and dermal graft bacterial load (**Figure 5**).

The mean wound sizes in untreated animals were 3.8, 5.0, and 3.8 mm in diameter on 1, 3, and 7 days, respectively (data not shown). Tris-treated animals showed 3.4-, 4.0-, and 3.5-mm wound sizes on 1, 3, and 7 days, respectively. Therefore, during the experiment, the size of the wounds in the control groups did not change significantly and no spontaneous wound healing was observed. At the same time, it was shown that administration of endolysin solutions results in a significant reduction of the wound size or ever-complete wound healing from the third day after the beginning of treatment. This reduction was 3.5 and 3.2 mm for LysAm24; 3.0 and 2.3 mm for LysECD7; 2.4 and 3.2 mm for LysSi3; and 2.7 and 3.2 mm for LysAp22 on 3 and 7 days, respectively, compared to untreated animals on the same day. So, the pronounced wound healing was observed in all experimental groups and it was 60.5% for LysECD7 and 84.2% for LysAm24, LysSi3, and LysAp22 on the seventh day of the experiment.

The bacterial count after inoculation of wound swabs is shown in **Figure 5A**. Wound contamination in untreated mice on 1, 3, and 7 days after infection was 1.2×10^3, 2.5×10^1, and 2.1×10^3 CFU/ml, respectively, which can be explained by nonsignificant infection healing and its further regression. Tris-treated mice showed a stable infectious process, and bacterial counts were 2.3×10^2, 6.3×10^1, and 2.7×10^2 CFU/ml on 1, 3, and 7 days, respectively. Endolysin administration resulted in different antibacterial effects. LysAp22 did not show any significant microbial reduction in swabs, although wound sizes in this group were significantly lower. LysAm24, LysECD7, and LysSi3 showed pronounced bacterial reduction dynamics; in all three groups, more than 50% of animals had sterile wound swabs at the last time point (60% for LysAm24, 50% for LysECD7, and 70% for LysSi3), having mean values of, in CFU/ml, 1.1, 12.1, and 0.4 for LysAm24, LysECD7 and LysSi3, respectively. In total, microbial contamination reduction was 2.2–3.7 $\log_{10}$ compared to the untreated group on the seventh day.

On the seventh day of the experiment, the mouse dermal grafts and spleens were also investigated for microbial contamination. It was shown that local wound infection was generalized as bacteria were found in animals' spleens (**Figure 5B**). Control groups showed a mean of 40 and 64 CFU/organ for untreated and buffer-treated mice. All endolysins groups had significantly reduced bacterial counts or absence of bacteria in the spleen. Treatment with LysAm24 reduced the CFU/organ to 3.5, LysECD7 to 0.3, LysSi3 to 4.0, and LysAp22 to 4.9. Thus, endolysins prevented infection systematization reducing the bacterial load in the spleen for 0.9–2.14 $\log_{10}$ CFU compared to untreated animals.

Dermal graft homogenates contained 2.4×10^6 CFU/graft in the untreated group and 1.8×10^6 CFU/graft in buffer-treated mice (**Figure 5C**). LysAm24, LysSi3, and LysAp22 administration

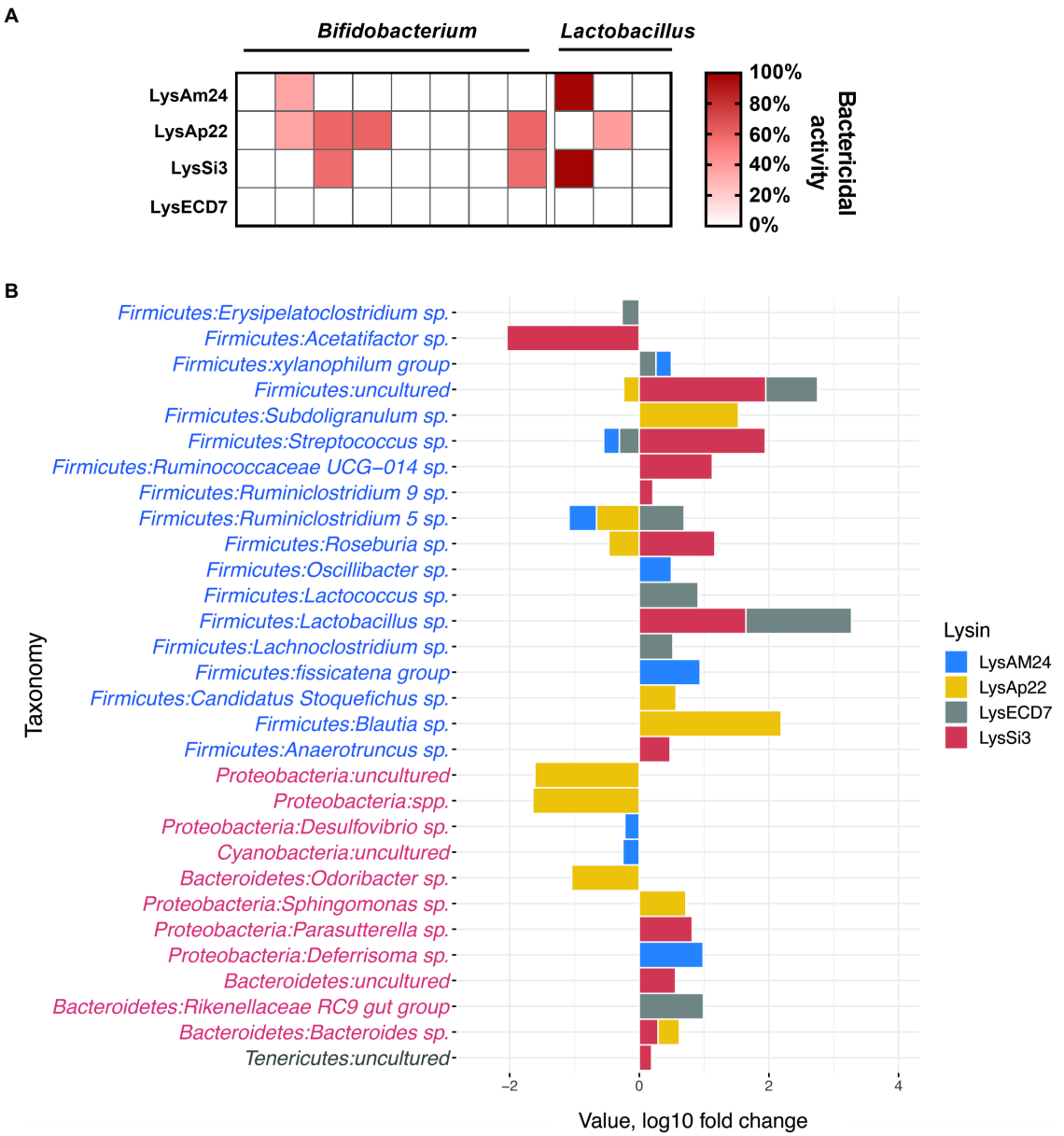

FIGURE 4 | Impact of endolysins on the normal bacterial flora. **(A)** *In vitro* activity of LysAm24, LysECD7, LysAp22, and LysSi3 against *Bifidobacterium* spp. and *Lactobacillus* spp. strains. Activity spectra were assessed at 100-μg/ml endolysin concentration after 30-min incubation with bacterial suspension in a liquid medium. **(B)** Intestine microflora changes in mice under endolysin administration compared to control buffer (Tris–HCl) injections on the seventh day of experiment. Blue and red taxa indicate Gram-positive and Gram-negative bacteria correspondingly.

did not significantly reduce contamination, and CFU/graft was 1.4×10^6, 1.5×10^6, and 9.9×10^5, respectively. Nevertheless, LysECD7 reduced bacterial count to 5.1×10^4 CFU/graft, which is a 1.7 $\log_{10}$ CFU reduction compared to untreated mice.

Burn Wound Model

Burn wound infection of Wistar rats was performed with a heated copper plate and infected with *P. aeruginosa* Ts 38-16 suspension. At 24 h, PI burns were either left untreated or treated with control buffer (20 mM Tris–HCl, pH 7.5) or treated with solutions of each investigated endolysin in the concentration of 2,500 μg/animal. The rats were treated epicutaneously once a day for 5 days.

Microbial contamination of infected areas of untreated animals was 7.7×10^6, 2.2×10^5, and 3.5×10^3, respectively, on 1, 3, and 7 days after infection (**Figure 6A**). Tris-treated rats showed 4.2×10^6, 2.5×10^5, and 3.1×10^3 CFU/ml bacterial load on 1, 3, and 7 days, respectively. The infectious process was stable in control groups; self-healing was not observed. Treatment with endolysin solutions resulted in positive dynamics of bacterial count reduction in all experimental groups, especially on the

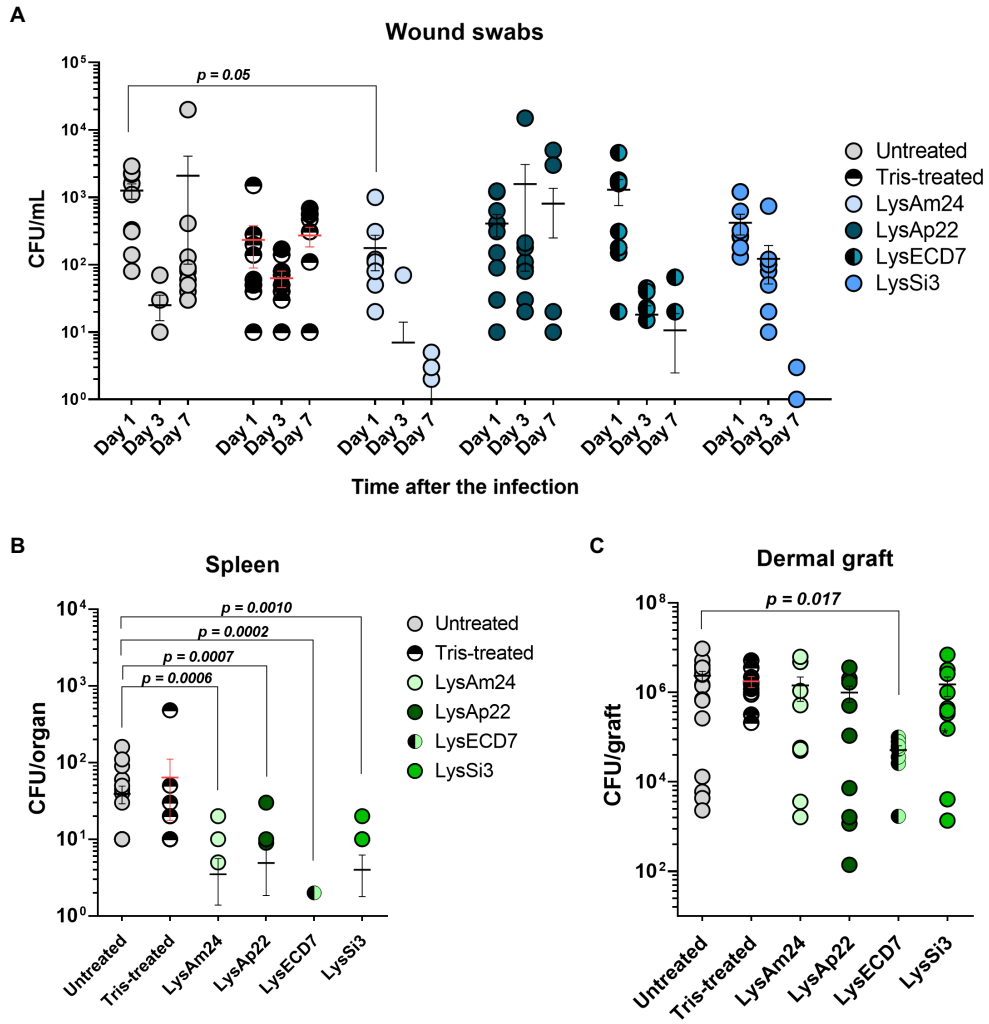

FIGURE 5 | Skin wound model of outbred mice infected with the *K. pneumoniae* Ts 141-14 strain and epicutaneously treated with control buffer or 500-μg/ml endolysins solutions. **(A)** Bacterial counts in the wounds resulting from swabs of the infected areas. Significant differences are shown as *p* values; otherwise, no statistical difference was found (two-way ANOVA with Sidak multiple-comparison test). Spleen **(B)** and dermal graft **(C)** microbial load on the seventh day of the experiment. Significant differences are shown as *p* values; otherwise, no statistical difference was found (Mann–Whitney test). The resulting CFU/mL, CFU/graft, or CFU/organ values from each animal are plotted as individual points. Data are shown as mean ± SEM.

seventh day, when more than 40% of animals had a sterile burn surface (40% for LysAm24, 50% for LysECD7, LysSi3, and LysAp22) with mean values of 79, 32, 19, and 30 CFU/ml for LysAm24, LysECD7, LysSi3, and LysAp22, respectively, which is a 1.6–2.3 $\log_{10}$ reduction.

Dermal grafts and spleen investigations were performed on the seventh day of the experiment. Spleens of infected animals were contaminated with *P. aeruginosa* so burn infection was generalized. Control groups showed means of 4.5×10^2 and 5.2×10^2 CFU/organ for untreated and buffer-treated rats, respectively (**Figure 6B**). All endolysin groups, except LysAm24-treated animals, had up to 100-fold reduced bacterial count or absence of bacteria in the spleen and, therefore, prevented systematization of an infectious process. Treatment with LysECD7 reduced CFU/organ to a mean value of 3.8, LysSi3 to 128, and LysAp22 to 39.

Dermal grafts in control groups contained 2.0×10^7 CFU/graft in untreated animals and 1.3×10^7 CFU/graft in Tris-treated animals (**Figure 6C**). All endolysins significantly reduced contamination; the CFUs/graft were 3.5×10^6, 1.4×10^6, 1.2×10^4, and 2.0×10^6 for LysAm24, LysECD7, LysSi3, and LysAp22, respectively. Therefore, LysECD7 reduced bacterial count most pronounced, a 3.2 $\log_{10}$ reduction compared to approximately 1.0 $\log_{10}$ reduction in case of other endolysins.

DISCUSSION

Numerous endolysin studies confirm the *in vitro* effectiveness of these enzymes and describe valuable advantages of their use to combat multiple Gram-positive or -negative bacterial pathogens. However, very few of the studies are devoted to

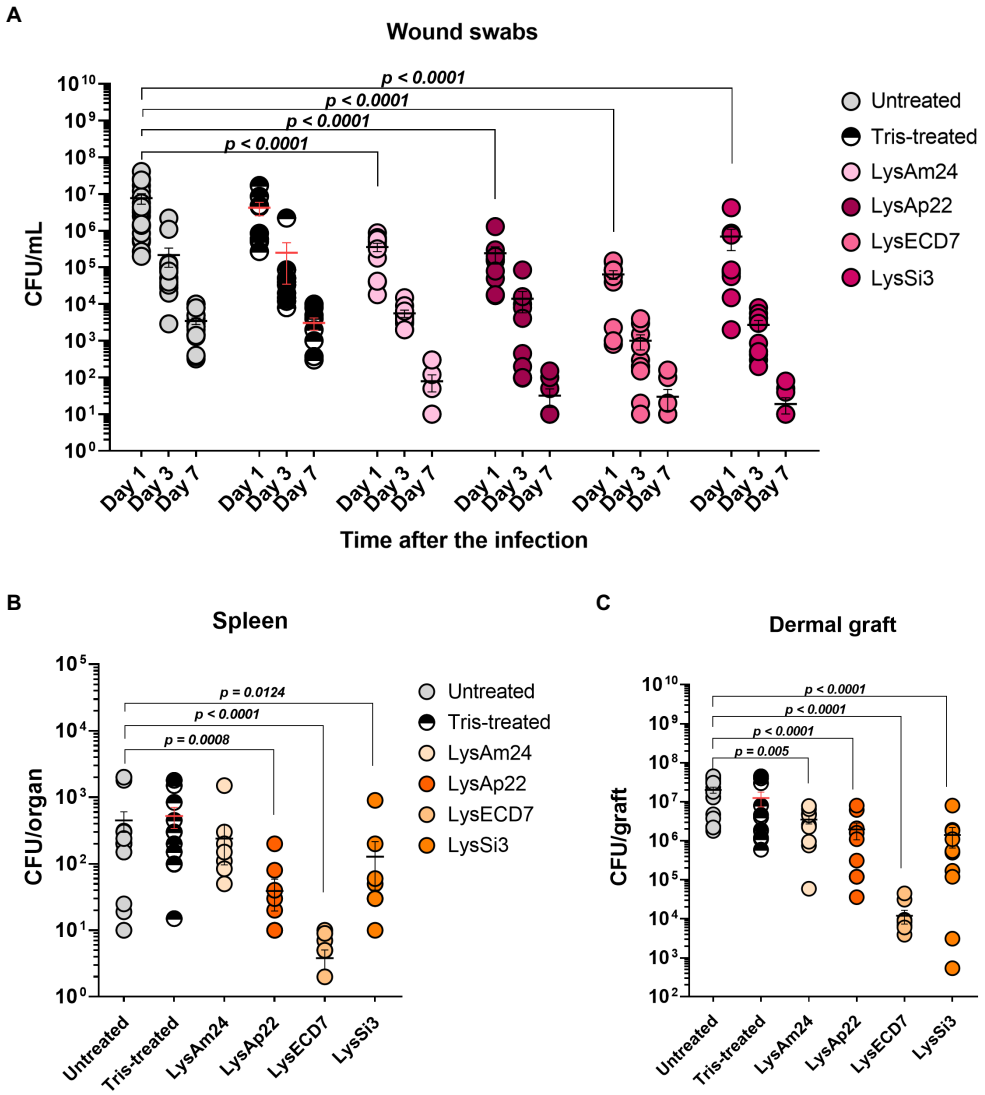

FIGURE 6 | Burn wound model of Wistar rats infected with the *P. aeruginosa* Ts 38-16 strain and epicutaneously treated with control buffer or 2,500-μg/ml endolysin solutions. **(A)** Count of culturable bacteria in the wound swabs of the infected areas. Significant differences are shown as *p* values; otherwise, no statistical difference was found (two-way ANOVA with the Sidak multiple-comparison test). Spleen **(B)** and dermal graft **(C)** microbial contamination (CFU/organ) on the seventh day of the experiment are shown. Significant differences are shown as *p* values; otherwise, no statistical difference was found (Mann–Whitney test). The resulting CFU/mL, CFU/graft, or CFU/organ values from each animal are plotted as individual points. Data are shown as mean ± SEM.

in vivo application and just several molecules are in clinical trials (Abdelrahman et al., 2021; Grabowski et al., 2021; Schmelcher and Loessner, 2021). Such a trend does not promote the acceleration of the development and implication of endolysin-based drugs into clinical practice. Moreover, it remains unclear what is the potential of using these molecules, especially for the treatment of drug-resistant Gram-negative bacteria-induced infections, which are the limitations and advantages of endolysin administration as individual antimicrobial therapy or in combination with antibiotics.

We provide a comprehensive study of four different unmodified Gram-negative bacteria-targeting endolysins, LysAm24, LysAp22, LysECD7, and LysSi3, devoted to their *in vitro* and *in vivo* potentials. The antibacterial activity kinetics showed that three out of four investigated molecules (LysAm24, LysAp22, and LysECD7) have similar dynamics of bacterial count reduction, although LysAp22 is more vigorous acting within the first 10 min of incubation. LysSi3 acted significantly more slowly, although finally all proteins killed 100% of bacterial cells. These results are in consistency with previously published data, where up to 10^8 CFU/ml of the Gram-negative bacterial species were completely eliminated within 5 min–1 h by different endolysins (Raz et al., 2019; Wang et al., 2020; Chen et al., 2021). Since endolysins are proteins and can be prone to proteolytic degradation within the organism, it is highly desirable that they can remain in an active state at the injection site for a time sufficient for the implementation of antibacterial activity. Pharmacokinetics of unmodified Gram-positive hosting endolysin

SAL200 shows the effective half-life $t_{1/2}$ within 15–25 min after a single intravenous infusion of 1–10 mg/kg dose (Jun et al., 2017). The time-killing curves of LysAm24, LysAp22, and LysECD7 show that although the complete elimination of bacteria occurs after an hour, the activity begins to manifest itself within the first 5–10 min. Dependent on the lysin concentration, this may be sufficient for a local bactericidal effect before the significant degradation of the enzyme.

Although topical treatment strategies are much more common for endolysins and other lytic enzymes, systemic use also seems to be possible and effective enough (Lood et al., 2015; Raz et al., 2019; Wu et al., 2019). The broad spectrum of the bactericidal activity of endolysins under the study against both planktonic cells and bacterial films supports the possibility of their use to treat deep soft tissue lesions and abscesses, as well as polymicrobial infections of implanted devices or wound surfaces, associated with bacterial film formation (Lebeaux et al., 2014; Vestby et al., 2020). Antibiofilm activity is widespread among the Gram-negative acting endolysins. Thus, the disruption of *A. baumannii* (Chen et al., 2021), *P. aeruginosa* (Guo et al., 2017), or other bacterial species (Yuan et al., 2021) biofilms in a concentration-dependent manner was previously shown. Our results indicated that significantly greater concentrations of enzymes are needed for pronounced antibiofilm activity, compared to planktonic cells, but the observed effectiveness of LysAm24, LysAp22, LysECD7, and LysSi3 was enough to eliminate the BF to the threshold level, regardless of the biofilm-forming species. Microscopic investigation of biofilms grown on glass slides and exposed to endolysins showed bacterial film integrity disruption and significant bacterial cell rupture although some non-disrupted cells were also observed. It was shown that in our case these bacteria were capable of growing on an agar medium, with exception of LysAm24, so complete disruption of biofilm integrity does not necessarily mean the bacteria's death. While the mechanisms of biofilm disruption by Gram-negative endolysins are not fully understood, it is unlikely that the effects are limited by the peptidoglycan interactions and the degradation could be associated with nonspecific interactions with matrix components.

During the safety experiments, we detected neither cytotoxic effect of endolysins on eukaryotic cells and red blood cells nor resistance development in bacteria toward LysAm24, LysAp22, LysECD7, and LysSi3. Earlier, no endolysin cytotoxicity against lung epithelial cells (Kim et al., 2020; Chen et al., 2021) or inhibitory effects on osteocyte-like cells were detected (Kuiper et al., 2021). Together with the previously published data (Briers et al., 2014; Zhang et al., 2016), this indicates that their application does not raise significant safety concerns, but should be approved in preclinical and clinical trials. At the same time, it is worth noting that we have shown the possibility of neutralizing antibody formation after animals' immunization, which was capable of significantly reducing the antibacterial activity of enzymes. All endolysin-specific antibodies purified out of hyperimmune sera completely inhibited *in vitro* bactericidal activity in a 1:5 mass ratio or 1:1 molar ratio. This finding is opposite to data existing for Gram-positive bacteria-targeting endolysins whose activity in hyperimmune serum did not change (Rashel et al., 2007; Zhang et al., 2016; Yang et al., 2017). It is suggested that due to the presence of the cell wall-binding domain (CBD) in the structure, Gram-positive bacteria-targeting endolysins bind to neutralizing antibodies with less affinity compared to bacterial cell wall binding (Murray et al., 2021). On the opposite, Gram-negative bacteria-targeting endolysins often contain a single catalytic domain without CBD and, therefore, cannot counteract with bacterial cell walls, masking it from antibody neutralization. Thus, the reversible lysin–antibody interactions predominate. These results pose some potential obstacles to systemic endolysin-based drug development especially for administration into the bloodstream with long repeated courses. It remains unclear how much of the antibodies of hyperimmune rabbit sera obtained with the use of an adjuvant can be comparable in their neutralizing qualities with antibodies formed with the repeated use of finished dosage forms containing endolysin. Nevertheless, our results show that the neutralizing effects should be studied in detail in the development of antibacterials based on endolysins at the stage of preclinical and clinical studies.

Another aspect of safety concern is the effect of endolysin-based drugs on nontarget microorganisms, including the normal microbiota of patients (Becattini et al., 2016). In the case of Gram-positive targeting endolysins, this is avoided due to the high specificity of the action of such enzymes, which is frequently limited by one species or even the strain of the microorganism (Murray et al., 2021). Broad spectra of action of Gram-negative-targeting endolysins suggest that they can cause dysbiotic complications affecting the commensal microbial consortium. Since the intestinal flora is most susceptible, representatives of normal microflora that are part of probiotic drugs intended for correction of microflora were used to study the effect of endolysins. LysAm24, LysAp22, and LysSi3 significantly affected the growth of several strains, especially *Lactobacillus* representatives. At the same time, LysECD7 did not show any antibacterial effect against microflora *in vitro*. In general, the activity of endolysins against *Bifidobacterium* spp. and *Lactobacillus* spp. was significantly lower than against the Gram-negative genus. The 5-fold parenteral injections of investigated endolysins in *mice* have also resulted in bacterial changes. The increased growth of both Gram-negative and Gram-positive species was mainly observed, as indicated with 16S sequencing data. Only two of the investigated endolysins significantly reduced the abundance of commensal bacterial species compared to control group animals: LysSi3 reduced gram-positive Lachnospiraceae and LysAp22 inhibited bacteria from three Gram-negative families (Porphyromonadaceae, Caulobacteraceae, and Methylocystaceae). Although the moderate effects were mostly shown for all enzymes under investigation, these results indicate that no general uniform rules are applicable for different endolysins, and during the preliminary studies of preparations, it is important to assess the spectra of their action both against the target microorganisms and against the most common commensal species.

The effectiveness of Gram-negative infection treatment with endolysins was confirmed in two animal models. It was shown that administration of multiple epicutaneous endolysins on the

wound and burn infections results in different degrees of antibacterial effect, but, in all cases, we observed a decreased microbial contamination, increased wound healing rates, and prevention of generalization of the infection. Different approaches for endolysin-based therapy applications were screened using the animal models. For example, the efficacy toward *P. aeruginosa* local lung and skin infection resulted in a more than 2-$\log_{10}$ CFU decrease by treatment with 100–300 μg of PlyPa91 endolysin (Raz et al., 2019), and LysAB2-KWK endolysin was effective against *A. baumannii* systemic infection of *Galleria mellonella* larva in a 5-μg dose (Chen et al., 2021). More extensive data could be found for Gram-positive bacteria-caused local wound or burn infections, where it was shown that significantly lower doses (5–100 μg of enzymes) are required to achieve the same or more pronounced therapeutic effect (Yang et al., 2017; Cheng et al., 2018; Wang et al., 2020).

Although these results are encouraging, now it is obvious that the effectiveness of unmodified Gram-negative bacteria-targeting enzybiotics is not enough to use them as self-therapy antibacterials. In the case of native, unmodified enzymes, their combination with antibiotics seems to be much more promising. For example, the synergistic effects of endolysins and antibiotics (colistin) *in vitro* and *in vivo* therapies were shown (Schirmeier et al., 2018; Abdelkader et al., 2020; Blasco et al., 2020). If developers succeed in defining an appropriate dosing schedule (beyond a single dose) as a basis for successful clinical studies for patients with confirmed infection due to drug-resistant pathogens or who experience recurrent or relapse infections, endolysins may provide an adjunctive therapy option. Another solution lies in the scope of endolysin bioengineering modifications and optimization to obtain specified properties or improve operational characteristics (Antonova et al., 2020; Gutiérrez and Briers, 2021).

To sum up, we have shown that LysAm24, LysAp22, LysECD7, and LysSi3 are capable of quickly eliminating Gram-negative bacteria *in vitro*, possess a wide spectrum of action, and are able to destroy the biofilms and significantly reduce contamination of the wound and burn skin surfaces, limiting the generalization of local infections. In terms of safety, these enzymes do not contribute to the development of short-term resistance, are not cytotoxic, and do not significantly affect the normal intestinal microflora *in vivo*. These properties provide a perspective basis for the development of preparations for the treatment of local infections, as well as for short-term use in systemic infections.

Endolysin-based drug development is an ambitious area of research, especially on account of raising bacterial resistance. However, insufficient information about their effectiveness in various animal models and clinical effectiveness complicates a decision-making process concerning the applicability of this alternative approach in antibacterial therapy. Studies of four different lysins show that, although they differ structurally, there are general patterns of their efficacy and safety, which means that the conclusions presented in this article can be applied and extended to some level to other lytic enzymes under investigation. An individual antibacterial therapy, especially systemic application, can be challenging due to their high molecular weight and proteinaceous nature, formation of neutralizing antibodies, rapid elimination, and pharmacokinetics. However, different studies and our data indicate that this class of antibacterial agents can increase the effectiveness of antibiotics, decrease therapeutic doses, and reduce the development and spread of antibiotic resistance.

DATA AVAILABILITY STATEMENT

The datasets presented in this study can be found in online repositories. The names of the repository/repositories and accession number(s) can be found at: https://www.ncbi.nlm.nih.gov/genbank/, APD20282.1, CCH57765.1, ASJ80195.1, and ARK07361.1.

ETHICS STATEMENT

The animal study was reviewed and approved by the Ethics Committee of the State Research Center for Applied Microbiology and Biotechnology, Obolensk, Russia.

AUTHOR CONTRIBUTIONS

DV, NA, and VG conceived of the study and wrote, reviewed, and edited the manuscript. DV, NA, VP, AA, and IG provided the methodology. NA, IG, VY, AL, MN, EU, NS, MF, AV, and AL contributed to the investigation process. NA and AP provided formal analysis. VZ, TR, SY, and AT contributed to the funding acquisition and provided resources. VG and VM supervised the work. DV, NA, and AP wrote the original draft of the manuscript. All authors contributed to the article and approved the submitted version.

FUNDING

This research study was supported by the Ministry of Health of the Russian Federation carried out in the frame of State Contract no. 0373100122119000013 of 15 May 2019 with the Center for Strategic Planning of the Ministry of Health of the Russian Federation.

ACKNOWLEDGMENTS

The content of this manuscript has been partly published as part of the thesis of NA (Antonova, 2021).

SUPPLEMENTARY MATERIAL

The Supplementary Material for this article can be found online at: https://www.frontiersin.org/articles/10.3389/fmicb.2021.748718/full#supplementary-material

REFERENCES

Abdelkader, K., Gutiérrez, D., Grimon, D., Ruas-Madiedo, P., Lood, C., Lavigne, R., et al. (2020). Lysin LysMK34 of *Acinetobacter baumannii* bacteriophage PMK34 has a turgor pressure-dependent intrinsic antibacterial activity and reverts colistin resistance. *Appl. Environ. Microbiol.* 86, e01311–e01320. doi: 10.1128/AEM.01311-20

Abdelrahman, F., Easwaran, M., Daramola, O. I., Ragab, S., Lynch, S., Oduselu, T. J., et al. (2021). Phage-encoded endolysins. *Antibiotics* 10:124. doi: 10.3390/antibiotics10020124

Antonova, N. P. (2021). Development, standardization and pharmacological study of the endolysin LysECD7-based substance. PhD Thesis. I. M. Sechenov First Moscow State Medical University, Moscow.

Antonova, N. P., Vasina, D. V., Lendel, A. M., Usachev, E. V., Makarov, V. V., Gintsburg, A. L., et al. (2019). Broad bactericidal activity of the myoviridae bacteriophage lysins LysAm24, LysECD7, and LysSi3 against gram-negative ESKAPE pathogens. *Viruses* 11:284. doi: 10.3390/v11030284

Antonova, N. P., Vasina, D. V., Rubalsky, E. O., Fursov, M. V., Savinova, A. S., Grigoriev, I. V., et al. (2020). Modulation of endolysin LysECD7 bactericidal activity by different peptide tag fusion. *Biomol. Ther.* 10:440. doi: 10.3390/biom10030440

Balouiri, M., Sadiki, M., and Ibnsouda, S. K. (2016). Methods for in vitro evaluating antimicrobial activity: A review. *J. Pharm. Anal.* 6, 71–79. doi: 10.1016/j.jpha.2015.11.005

Becattini, S., Taur, Y., and Pamer, E. G. (2016). Antibiotic-induced changes in the intestinal microbiota and disease. *Trends Mol. Med.* 22, 458–478. doi: 10.1016/j.molmed.2016.04.003

Blasco, L., Ambroa, A., Trastoy, R., Bleriot, I., Moscoso, M., Fernández-Garcia, L., et al. (2020). In vitro and in vivo efficacy of combinations of colistin and different endolysins against clinical strains of multi-drug resistant pathogens. *Sci. Rep.* 10:7163. doi: 10.1038/s41598-020-64145-7

Briers, Y., Walmagh, M., Grymonprez, B., Biebl, M., Pirnay, J. P., Defraine, V., et al. (2014). Art-175 is a highly efficient antibacterial against multidrug-resistant strains and persisters of *Pseudomonas aeruginosa*. *Antimicrob. Agents Chemother.* 58, 3774–3784. doi: 10.1128/AAC.02668-14

Chen, X., Liu, M., Zhang, P., Leung, S. S. Y., and Xia, J. (2021). Membrane-permeable antibacterial enzyme against multidrug-resistant *Acinetobacter baumannii*. *ACS Infect. Dis.* 7, 2192–2204. doi: 10.1021/acsinfecdis.1c00222

Cheng, M., Zhang, L., Zhang, H., Li, X., Wang, Y., Xia, F., et al. (2018). An ointment consisting of the phage lysin LysGH15 and apigenin for decolonization of methicillin-resistant *Staphylococcus aureus* from skin wounds. *Viruses* 10:244. doi: 10.3390/v10050244

Fowler, V. G. Jr., Das, A. F., Lipka-Diamond, J., Schuch, R., Pomerantz, R., Jáuregui-Peredo, L., et al. (2020). Exebacase for patients with *Staphylococcus aureus* bloodstream infection and endocarditis. *J. Clin. Invest.* 130, 3750–3760. doi: 10.1172/JCI136577

Fursov, M. V., Abdrakhmanova, R. O., Antonova, N. P., Vasina, D. V., Kolchanova, A. D., Bashkina, O. A., et al. (2020). Antibiofilm activity of a broad-range recombinant endolysin LysECD7: in vitro and in vivo study. *Viruses* 12:545. doi: 10.3390/v12050545

Grabowski, Ł., Łepek, K., Stasiłojć, M., Kosznik-Kwaśnicka, K., Zdrojewska, K., Maciąg-Dorszyńska, M., et al. (2021). Bacteriophage-encoded enzymes destroying bacterial cell membranes and walls, and their potential use as antimicrobial agents. *Microbiol. Res.* 248:126746. doi: 10.1016/j.micres.2021.126746

Grishin, A. V., Karyagina, A. S., Vasina, D. V., Vasina, I. V., Gushchin, V. A., and Lunin, V. G. (2020). Resistance to peptidoglycan-degrading enzymes. *Crit. Rev. Microbiol.* 46, 703–726. doi: 10.1080/1040841X.2020.1825333

Guo, M., Feng, C., Ren, J., Zhuang, X., Zhang, Y., Zhu, Y., et al. (2017). A novel antimicrobial endolysin, LysPA26, against *Pseudomonas aeruginosa*. *Front. Microbiol.* 8:293. doi: 10.3389/fmicb.2017.00293

Gutiérrez, D., and Briers, Y. (2021). Lysins breaking down the walls of gram-negative bacteria, no longer a no-go. *Curr. Opin. Biotechnol.* 68, 15–22. doi: 10.1016/j.copbio.2020.08.014

Jun, S. Y., Jang, I. J., Yoon, S., Jang, K., Yu, K. S., Cho, J. Y., et al. (2017). Pharmacokinetics and tolerance of the phage endolysin-based candidate drug SAL200 after a single intravenous administration among healthy volunteers. *Antimicrob. Agents Chemother.* 61, e02629–e02616. doi: 10.1128/AAC.02629-16

Kim, S., Lee, D. W., Jin, J. S., and Kim, J. (2020). Antimicrobial activity of LysSS, a novel phage endolysin, against *Acinetobacter baumannii* and *Pseudomonas aeruginosa*. *J. Glob. Antimicrob. Resist.* 22, 32–39. doi: 10.1016/j.jgar.2020.01.005

Kuiper, J. W. P., Hogervorst, J. M. A., Herpers, B. L., Bakker, A. D., Klein-Nulend, J., Nolte, P. A., et al. (2021). The novel endolysin XZ.700 effectively treats MRSA biofilms in two biofilm models without showing toxicity on human bone cells in vitro. *Biofouling* 37, 184–193. doi: 10.1080/08927014.2021.1887151

Lebeaux, D., Ghigo, J. M., and Beloin, C. (2014). Biofilm-related infections: bridging the gap between clinical management and fundamental aspects of recalcitrance toward antibiotics. *Microbiol. Mol. Biol. Rev.* 78, 510–543. doi: 10.1128/MMBR.00013-14

Lood, R., Winer, B. Y., Pelzek, A. J., Diez-Martinez, R., Thandar, M., Euler, C. W., et al. (2015). Novel phage Lysin capable of killing the multidrug resistant gram-negative bacterium *Acinetobacter Baumannii* in a mouse bacteremia model. *Antimicrob. Agents Chemother.* 59, 1983–1991. doi: 10.1128/AAC.04641-14

Murray, E., Draper, L. A., Ross, R. P., and Hill, C. (2021). The advantages and challenges of using endolysins in a clinical setting. *Viruses* 13:680. doi: 10.3390/v13040680

Oliveira, H., São-José, C., and Azeredo, J. (2018). Phage-derived peptidoglycan degrading enzymes: challenges and future prospects for in vivo therapy. *Viruses* 10:292. doi: 10.3390/v10060292

Pfaller, M. A., Sheehan, D. J., and Rex, J. H. (2004). Determination of fungicidal activities against yeasts and molds: lessons learned from bactericidal testing and the need for standardization. *Clin. Microbiol. Rev.* 17, 268–280. doi: 10.1128/CMR.17.2.268-280.2004

Rashel, M., Uchiyama, J., Ujihara, T., Uehara, Y., Kuramoto, S., Sugihara, S., et al. (2007). Efficient elimination of multidrug-resistant *Staphylococcus aureus* by cloned lysin derived from bacteriophage phi MR11. *J. Infect. Dis.* 196, 1237–1247. doi: 10.1086/521305

Raz, A., Serrano, A., Hernandez, A., Euler, C. W., and Fischetti, V. A. (2019). Isolation of phage lysins that effectively kill *Pseudomonas aeruginosa* in mouse models of lung and skin infection. *Antimicrob. Agents Chemother.* 63, e00024–e00019. doi: 10.1128/AAC.00024-19

Schirmeier, E., Zimmermann, P., Hofmann, V., Biebl, M., Gerstmans, H., Maervoet, V. E. T., et al. (2018). Inhibitory and bactericidal effect of Artilysin® Art-175 against colistin-resistant mcr-1-positive *Escherichia coli* isolates. *Int. J. Antimicrob. Agents* 51, 528–529. doi: 10.1016/j.ijantimicag.2017.08.027

Schmelcher, M., and Loessner, M. J. (2021). Bacteriophage endolysins—extending their application to tissues and the bloodstream. *Curr. Opin. Biotechnol.* 68, 51–59. doi: 10.1016/j.copbio.2020.09.012

Stepanović, S., Vuković, D., Hola, V., Di Bonaventura, G., Djukić, S., Cirković, I., et al. (2007). Quantification of biofilm in microtiter plates: overview of testing conditions and practical recommendations for assessment of biofilm production by staphylococci. *APMIS* 115, 891–899. doi: 10.1111/j.1600-0463.2007.apm_630.x

Theuretzbacher, U., Outterson, K., Engel, A., and Karlén, A. (2020). The global preclinical antibacterial pipeline. *Nat. Rev. Microbiol.* 18, 275–285. doi: 10.1038/s41579-019-0288-0

Theuretzbacher, U., and Piddock, L. J. V. (2019). Non-traditional antibacterial therapeutic options and challenges. *Cell Host Microbe* 26, 61–72. doi: 10.1016/j.chom.2019.06.004

Totté, J. E. E., van Doorn, M. B., and Pasmans, S. G. M. A. (2017). Successful treatment of chronic *Staphylococcus aureus*-related dermatoses with the topical endolysin staphefekt SA.100: a report of 3 cases. *Case Rep. Dermatol.* 9, 19–25. doi: 10.1159/000473872

Vestby, L. K., Grønseth, T., Simm, R., and Nesse, L. L. (2020). Bacterial biofilm and its role in the pathogenesis of disease. *Antibiotics* 9:59. doi: 10.3390/antibiotics9020059

Wang, F., Ji, X., Li, Q., Zhang, G., Peng, J., Hai, J., et al. (2020). TSPphg lysin from the extremophilic thermus bacteriophage TSP4 as a potential antimicrobial agent against both gram-negative and gram-positive pathogenic bacteria. *Viruses* 12:192. doi: 10.3390/v12020192

Wang, J., Lang, T., Shen, J., Dai, J., Tian, L., and Wang, X. (2019). Core gut bacteria analysis of healthy mice. *Front. Microbiol.* 10:887. doi: 10.3389/fmicb.2019.00887

Wu, M., Hu, K., Xie, Y., Liu, Y., Mu, D., Guo, H., et al. (2019). A novel phage PD-6A3, and its endolysin Ply6A3, with extended lytic activity against *Acinetobacter baumannii*. *Front. Microbiol.* 9:3302. doi: 10.3389/fmicb.2018.03302

Yang, H., Zhang, H., Wang, J., Yu, J., and Wei, H. (2017). A novel chimeric lysin with robust antibacterial activity against planktonic and biofilm methicillin-resistant *Staphylococcus aureus*. *Sci. Rep.* 7:40182. doi: 10.1038/srep40182

Yuan, Y., Li, X., Wang, L., Li, G., Cong, C., Li, R., et al. (2021). The endolysin of the *Acinetobacter baumannii* phage vB_AbaP_D2 shows broad antibacterial activity. *Microb. Biotechnol.* 14, 403–418. doi: 10.1111/1751-7915.13594

Zhang, L., Li, D., Li, X., Hu, L., Cheng, M., Xia, F., et al. (2016). LysGH15 kills *Staphylococcus aureus* without being affected by the humoral immune response or inducing inflammation. *SC Rep.* 6:29344. doi: 10.1038/srep29344

Conflict of Interest: NA, DV, AT, and VG are the authors but not the patent holders of the following patents issued according to the results of this work (RU): RU 2730613 C1 "Antibacterial composition (embodiments) and use of protein as antimicrobial agent directed against bacteria *Pseudomonas aeruginosa*, *Klebsiella pneumoniae*, *Escherichia coli*, *Salmonella typhi*, and *Staphylococcus haemolyticus* (embodiments)"; RU 2730614 C1 "Antibacterial composition (embodiments) and use of protein as antimicrobial agent directed against bacteria *P. aeruginosa*, *K. pneumoniae*, *Escherichia coli*, *Salmonella typhi*, and *Staphylococcus haemolyticus* (embodiments)"; RU 2730615 C1 "Antibacterial composition (embodiments) and use of protein as antimicrobial agent directed against Gram-negative bacteria: *P. aeruginosa*, *Acinetobacter baumannii*, *K. pneumoniae*, and *Salmonella typhi* (embodiments)"; and RU 2730616 C1 "Antibacterial composition (embodiments) and use of protein as an antimicrobial agent directed against *A. baumannii* bacteria (embodiments)."

The remaining authors declare that the research was conducted in the absence of any commercial or financial relationships that could be construed as a potential conflict of interest.

Publisher's Note: All claims expressed in this article are solely those of the authors and do not necessarily represent those of their affiliated organizations, or those of the publisher, the editors and the reviewers. Any product that may be evaluated in this article, or claim that may be made by its manufacturer, is not guaranteed or endorsed by the publisher.

frontiers in Microbiology

ORIGINAL RESEARCH
published: 26 November 2021
doi: 10.3389/fmicb.2021.764451

Broad-Spectrum Antibacterial Peptide Kills Extracellular and Intracellular Bacteria Without Affecting Epithelialization

*Anala Nepal[1], Synnøve Brandt Ræder[1], Caroline Krogh Søgaard[1], Maria Schei Haugan[2] and Marit Otterlei[1,2]**

[1] Department of Clinical and Molecular Medicine, Faculty of Medicine and Health Sciences, Norwegian University of Science and Technology (NTNU), Trondheim, Norway, [2] Department of Medical Microbiology, St. Olav's University Hospital, Trondheim, Norway

OPEN ACCESS

Edited by:
Wang Jiajun, Northeast Agricultural University, China

Reviewed by:
Yuan Liu, Yangzhou University, China
Xiao Wang, Ningbo University, China
Zhaofei Wang, Shanghai Jiao Tong University, China
Denise Mara Soares Bazzolli, Universidade Federal de Viçosa, Brazil

***Correspondence:**
Marit Otterlei
marit.otterlei@ntnu.no

Specialty section:
This article was submitted to Antimicrobials, Resistance and Chemotherapy, a section of the journal Frontiers in Microbiology

Received: *25 August 2021*
Accepted: *25 October 2021*
Published: *26 November 2021*

Citation:
Nepal A, Ræder SB, Søgaard CK, Haugan MS and Otterlei M (2021) Broad-Spectrum Antibacterial Peptide Kills Extracellular and Intracellular Bacteria Without Affecting Epithelialization. Front. Microbiol. 12:764451. doi: 10.3389/fmicb.2021.764451

New antibacterial drugs with novel modes of action are urgently needed as antibiotic resistance in bacteria is increasing and spreading throughout the world. In this study, we aimed to explore the possibility of using APIM-peptides targeting the bacterial β-clamp for treatment of skin infections. We selected a lead peptide, named betatide, from five APIM-peptide candidates based on their antibacterial and antimutagenic activities in both G^+ and G^- bacteria. Betatide was further tested in minimal inhibitory concentration (MIC) assays in ESKAPE pathogens, in *in vitro* infection models, and in a resistance development assay. We found that betatide is a broad-range antibacterial which obliterated extracellular bacterial growth of methicillin-resistant *Staphylococcus epidermidis* (MRSE) in cell co-cultures without affecting the epithelialization of HaCaT keratinocytes. Betatide also reduced the number of intracellular *Staphylococcus aureus* in infected HaCaT cells. Furthermore, long-time exposure to betatide at sub-MICs induced minimal or no increase in resistance development compared to ciprofloxacin and gentamicin or ampicillin in *S. aureus* and *Escherichia coli*. These properties support the potential of betatide for the treatment of topical skin infections.

Keywords: APIM, antimicrobial resistance, β-clamp, translesion synthesis, antibacterial peptide, antimutagenic, ESKAPE

INTRODUCTION

Antibiotic resistance is a global problem. Widespread misuse of antibiotics, not only in human medicine but also in animal husbandry, has led to the emergence and spread of bacteria conferring resistance to multiple antibiotics. The World Health Organization (2017, 2018) has published a list of highly virulent bacteria with increasing multidrug resistance (MDR) such as the ESKAPE pathogens (*Enterococcus faecium*, *Staphylococcus aureus*, *Klebsiella pneumoniae*, *Acinetobacter*

Abbreviations: AMP, Antimicrobial peptide; AMR, Antimicrobial resistance; APIM, AlkB homolog 2 PCNA-interacting motif; CFU, Colony-forming unit; CPP, Cell-penetrating peptide; ESKAPE, *Enterococcus faecium*, *Staphylococcus aureus*, *Klebsiella pneumoniae*, *Acinetobacter baumannii*, *Pseudomonas aeruginosa*, and *Enterobacter* species; MDR, Multidrug resistance; MIC, Minimal inhibitory concentration; MRSA, Methicillin-resistant *Staphylococcus aureus;* MRSE, Methicillin-resistant *Staphylococcus epidermidis;* PCNA, Proliferating cell nuclear antigen; TLS, Translesion synthesis.

baumannii, *Pseudomonas aeruginosa*, and *Enterobacter* species). New antibiotics are urgently needed to cope with the increasing antimicrobial resistance (AMR) emerging in these pathogens because this is expected to give high annual global mortality and a high economic burden (World Health Organization, 2015).

Bacteria can become antibiotic resistant by harboring mutations in endogenous genes, or by taking up genes. This lack or gain of gene product may give them a functional advantage to resist the antibiotic. Cellular stress, for example, induced by antibiotic treatments, can activate the SOS damage response system (Beaber et al., 2004) and thereby DNA translesion synthesis (TLS) in bacteria (Pham et al., 2001; Goodman, 2002). TLS increases the mutation frequency and is the main cause of increased levels of endogenous mutations (Merrikh and Kohli, 2020). Targeting the SOS response is therefore a potential strategy for inhibiting mutagenesis and development of antibiotic resistance (Yakimov et al., 2021).

Antimicrobial peptides (AMPs) are one of the drug classes emerging as an alternative to conventional antibiotics. They usually act by targeting the bacterial cell wall but can also have intracellular targets. The major hurdle for AMP drug development has been low serum stability and toxicity (Magana et al., 2020). Another concern with AMPs is the development of cross-resistance, as prolonged bacterial exposure to one AMP in sublethal doses is shown to lead to resistance development to a wide variety of other AMPs; however, this is dependent on the nature of the peptides and their target(s) (Andersson et al., 2016).

APIM-peptides are cell-penetrating peptides (CPPs) containing the proliferating cell nuclear antigen (PCNA) interaction motif APIM, which were originally developed as anticancer drugs (Gilljam et al., 2009; Muller et al., 2013; Søgaard et al., 2018). Interestingly, they were found to have antibacterial properties in selected gram-positive (G^+) and gram-negative (G^-) bacteria (Nedal et al., 2020). This antibacterial property was mainly due to their ability to bind to the bacterial β-clamp via their APIM sequence, thereby inhibiting bacterial DNA replication and TLS. This killed the bacteria or, at sublethal concentrations, reduced their ability to develop resistance against other antibiotics if used in combination treatments (Nedal et al., 2020; Raeder et al., 2021). The APIM-peptide variant ATX-101, which is under development as an anticancer drug, was shown to have a favorable toxicity profile in a recent Phase I study (Lemech et al., 2021). Therefore, the two main concerns with AMPs, i.e., development of resistance and toxicity, may not apply to APIM-peptides.

Skin is the main physical barrier against bacteria. A bruise or an open cut after surgery makes the underlying tissue vulnerable to infection, and accordingly, use of topical antibiotics is shown to prevent infections and accelerate healing. However, the rise and spread of MDR bacteria has led to severe chronic infections in hospitalized patients where current antibiotics are ineffective (Filius and Gyssens, 2002). MDR variants of staphylococci are examples of bacteria that cause recurring infections in hospitalized patients. *Staphylococcus epidermidis* is a bacterium in the normal skin microbiota (Kloos and Musselwhite, 1975) and *S. aureus*, which is more virulent (Massey et al., 2006; Otto, 2009), is more common in the microbiota of the upper respiratory tract (Tulloch, 1954). Both species can become opportunistic pathogens post surgery, especially in immunocompromised patients and those with medical implants. *S. aureus* can in addition thrive intracellularly, making it hard to treat with antibiotics (Tuchscherr et al., 2011).

In wound healing, keratinocytes migrate toward the open gap after 24 h and protect the underlying cells before dermal layers take over and close the gap (Rousselle et al., 2019). In order to develop a drug for topical application, it is important that the reepithelialization capacity of the keratinocytes surrounding the wound area is not severely affected (Pastar et al., 2014). In this study, we selected a lead APIM-peptide, betatide, and examined its antibacterial potential and its effects on epithelialization of keratinocytes in two different cell line-based *in vitro* infection assays. We also examined the ability of bacteria to develop resistance against betatide and betatide's activity on resistant and reference ESKAPE pathogens, alone and in combination with selected antibiotics.

MATERIALS AND METHODS

Bacterial Strains

All bacterial strains used in this study are listed in **Table 1**. The reference strains are indicated by their ATCC and CCUG numbers, while the clinical strains, which were obtained from the strain collection at the Department of Medical Microbiology, St. Olav's (SO) University Hospital, are indicated by their SO codes.

Antibiotic Resistance

For the clinical strains, this was essentially done as defined by EUCAST Clinical Breakpoints and guidance (EUCAST, 2021).

APIM-Peptides

APIM-peptides (Innovagen, SE) used in this study have the same N-termini but differ in the composition of linkers and/or CPPs as shown in **Table 2**. Peptides 1 (RWLVK) and 2 (RWLVK*) are previously used in Nedal et al. (2020). A C-terminus FAM-labeled betatide (Innovagen) was used to study intracellular import. All the concentrations of APIM-peptides given in the different figures are net peptide concentrations, and 4 μg/ml equals approximately 1 μM.

Cell Culture and Maintenance

HaCaT, a human spontaneous immortalized keratinocyte cell line, was cultured in Dulbecco's Modified Eagle Medium (DMEM; 4.5 g/L glucose; Sigma-Aldrich), supplemented with 10% fetal bovine serum (FBS; Sigma-Aldrich) and 1 mM L-glutamine (Sigma-Aldrich). HEK293, an immortalized embryonic kidney cell line, was grown in DMEM (BioWhittaker, Walkersville, MD, United States) with the same supplements as described above. In addition, Fungizone® amphotericin B (2.5 μg/ml; Gibco, Thermo Fisher Scientific, Waltham, MA, United States) and 1 mM antibiotic mixture containing 100 μg/ml penicillin and 100 μg/ml Streptomycin (Gibco) were added to the growth media. The cells were incubated at 37°C in a humidified incubator with 5% CO_2.

TABLE 1 | Bacterial strains used in this study.

Bacterial species	Strain	Antibiotic resistance	Used in experiment
Staphylococcus epidermidis	SO-SEP9-1	Erythromycin, penicillin, cloxacillin/dicloxacillin (MRSE)	Epithelialization assay
Staphylococcus aureus	ATCC 29213	None	Intracellular infection assay, resistance assay
	SO-SAU19-1 (MRSA), SO-SAU19-2, -3 and -4 (FR-MRSA)	*mecA*+	MIC (ESKAPE), resistance assay
Escherichia coli	K-12 MG1655	None	MIC (ESKAPE), growth inhibition, mutagenesis and resistance assays
	SO-ECO19-1	ESBL-CARB-A(CTX-M-24)/D (OXA-48)	MIC (ESKAPE)
Enterococcus faecium	CCUG 59167	*vanA*+ (VRE)	MIC (ESKAPE)
	SO-EFU19-1	*vanB*+ (VRE)	MIC (ESKAPE)
Enterococcus faecalis	ATCC 29212	None	MIC (ESKAPE)
	SO-EFA19-1	*optrA*+	MIC (ESKAPE)
Klebsiella pneumoniae	ATCC 13883	None	MIC (ESKAPE)
	SO-KPN19-1	ESBL-CARBA-D (OXA-48-like)	MIC (ESKAPE)
Pseudomonas aeruginosa	ATCC 27853	None	MIC (ESKAPE)
	SO-PAE19-1	Multidrug resistant	MIC (ESKAPE)
Acinetobacter baumannii	ATCC 19606	None	MIC (ESKAPE)
	SO-ABA19-1	ESBL-CARBA-D (OXA-24)	MIC (ESKAPE)
Enterobacter cloacae	SO-ECL18-1	ESBL-CARBA (NDM)	MIC (ESKAPE)

Minimal Inhibitory Concentration Assay

Minimal inhibitory concentration assay was conducted as recommended by the Clinical and Laboratory Standards Institute (CLSI) (Cockerill et al., 2012), similar to a previous report (Nedal et al., 2020). Briefly, bacterial colonies from blood agar plates were suspended and grown in Cation-Adjusted Mueller-Hinton Broth (CAMHB, 22.5 mg/ml Ca^{2+}, 11 mg/ml Mg^{2+}). The bacterial suspension was adjusted to 0.5 McFarland standard ($\sim 1 \times 10^8$ colony-forming units (CFU)/ml) and serial diluted 1:200 in CAMHB ($\sim 5 \times 10^5$ CFU/mL). This was subsequently added to polypropylene microtiter plates (Greiner, 100 μl/well, $\sim 5 \times 10^4$ CFU/well) already prepared with betatide and different antibiotics as single agents or in combinations (11 μl/well, twofold serial dilutions). The suspension was plated out on blood agar plates to confirm the CFU/ml. Both the microtiter plates and the blood agar plates were incubated at 37°C for 24 h. The lowest concentration of antibiotics and/or betatide capable of inhibiting visible bacterial growth was determined as the MIC.

The MICs of ampicillin (Sigma, A9518), cefoxitin (Sigma, C4786), cefotaxime (Sigma, 219504), ceftazidime (Sigma, C3809), ceftriaxone (Sigma, C5793), ciprofloxacin (Sigma, 17850), clindamycin (Sigma, C5269), ertapenem (Sigma, SML1238), gentamicin (Gibco, 1510049), linezolid (Sigma, PZ0014), meropenem (Sigma, M2574), methicillin (Sigma, 51454), and fusidic acid (MedChemExpress, HY-B1350A) were determined in addition to that of betatide.

Growth Inhibition Assay

An overnight culture of *Escherichia coli* was diluted 1:100 in Luria-Bertani (LB) medium and allowed to grow until an optical density (OD) at 600 nm (OD600) of 0.06–0.1. APIM-peptides were prepared by serial dilution in Milli-Q H_2O and kept at 4°C. Fresh LB medium (60 μl) was added to a flat-bottom microtiter plate. The bacterial suspension was diluted 1:100 in LB, and 75 μl of this suspension was added to the wells. Finally, 15 μl of APIM-peptide solution (to final concentrations 60, 120, and 240 μg/ml) or distilled water (positive control) was added to the wells, reaching a total volume of 150 μl per well. Data are presented only for the dose that separated the effect of the different peptides, i.e., 60 μg/ml. A blank sterile medium was used as negative control. The plates were incubated with shaking at 510 rpm at 37°C inside a plate reader (TECAN, Spark®), and OD was read every hour over a period of 24 h.

The MIC for *E. coli* in LB medium is higher than that in CAMHB; thus, concentrations higher than the MIC given in **Table 2** are used in the growth inhibition and mutagenesis assays.

Viability

HEK293 cells (6,000 cells/well) were seeded in 96-well microtiter plates. After 4 h, APIM-peptides (12–48 μg/ml) were added, and the cells were incubated without change of media for up to 4 days. Viability was measured using the 3-(4,5-dimethylthiazol-2-yl)-2,5-diphenyltetrazolium bromide (MTT) assay as described (Gilljam et al., 2009). Data show the percentage of viable cells relative to untreated cells for 24 μg/ml at 72 h.

Mutagenesis Assay

The rifampicin (Rif^R) mutagenesis assay was performed as described (Nedal et al., 2020). Briefly, an overnight culture of *E. coli* was diluted 1:1,000 and grown until an OD600 of 0.01. APIM-peptides (20 μg/ml) were added to LB media with glass beads (for uniform distribution of APIM-peptides) and incubated for 30 min at 37°C. The pellets were next collected, resuspended in 500 μl PBS, and exposed to UV-C (20 mJ/cm^2) in a six-well plate at 4°C. The unexposed bacteria (-UV) were

otherwise handled exactly like the UV-exposed bacteria. Next, the cells were resuspended in LB media and incubated in a rotary shaker at 37°C at 250 rpm for 2 h before being harvested, diluted, and plated on LB with soft agar with and without rifampicin (100 μg/ml). Mutation frequency, $Rif^R/10^8$, is obtained as follows: (number of colonies on the rifampicin plate (Rif^R)/(number of colonies on LB plates without antibiotics), per milliliter of bacterial suspension.

Epithelialization Assay

The epithelialization assay is a modified version of the scratch test (Longaker et al., 1989; Walter et al., 2010). Briefly, HaCaT cells (1×10^6 cells/well) were seeded in six-well plates with Steri-Strips™ (R1540, 3M Healthcare, United States) attached to the bottom. The cells were confluent in monolayer after 24 h (day 1), and the strips were then removed, creating even 3-mm gaps in the middle of the wells. The wells were washed 2× with PBS before fresh medium was added. The cells were next infected with 450 CFU/ml of an antibiotic-resistant *S. epidermidis* strain (MRSE, see **Table 1**) and treated with betatide (2–24 μg/ml). All treatments were done at day 1, and the epithelialization of the gaps was examined over a period of 7 days by taking pictures every 24 h in light microscopy (EVOS® FL, Life Technologies). Bacterial growth was examined by plating of supernatants. The effect of betatide on noninfected HaCaT cells with regard to viability and epithelization was examined in parallel wells without MRSE.

Epithelialization was calculated from the change in the area of the gaps over time using freehand or rectangular selections in the software Fiji ImageJ 1.52p (National Institutes of Health, United States).

$$\%\ \text{Epithelialization} = \frac{(\text{Area of gap in Day 1} - \text{Area of gap in each consecutive day})}{\text{Area of gap in Day 1}}$$

The MIC for MRSE in DMEM (0.25 μg/ml) is lower than the MIC given in **Table 2**; thus, concentrations lower than MIC were used.

Intracellular Infection Model

The intracellular infection model used was modified from Iqbal et al. (2016) by optimizing the number of multiplicity of infection (MOI: number of bacteria per cell) and time of infection. Briefly, HaCaT cells (6.5×10^4/well) were seeded in 24-well plates and incubated overnight in a medium without antibiotics. The next day, approximately 1.25×10^5 cells/well were infected with *S. aureus* at an MOI of 100 in antibiotic-free media. The plates were incubated for 3 h. Next, the cells were washed 2× with 500 μl PBS and treated with 100× MIC of gentamicin (100 μg/ml, MIC = 1 μg/ml) for 1 h, before further incubation in media with 10× MIC of gentamicin to kill the extracellular bacteria. Betatide (8–48 μg/ml) was added to the infected cells, and an equal amount of distilled water was added to the untreated control. After 16 h of incubation, the extracellular media (100 μl) from each well were plated to confirm the eradication of extracellular *S. aureus*. Next, the cells were washed 2× with 500 μl PBS before they were lysed with 0.2% Triton-X (500 μl) for 30 min at room temperature. The lysed samples were placed on ice, and 500 μl cold Tryptic Soy Broth was added before they were plated on blood agar plates. Data are presented for the dose that showed the best intracellular effects and low HaCaT cell toxicity, i.e., 24 μg/ml.

Imaging

Intracellular import of betatide in HaCaT cells was examined using a fluorescent-tagged betatide (betatide-FAM, ∼20 μg/ml). Vybrant® DyeCycle™ Ruby stain (VDR, 5 μM, V10273, Life Technologies™), which can penetrate plasma membranes, was used to stain DNA of live cells. Both betatide-FAM and VDR were added to live HaCaT cells immediately before (<2 min) examination in a Zeiss LSM 510 Meta laser scanning microscope equipped with a plan-apochromat × 63/1.4 oil immersion objective. FAM was excited at λ = 514 nm and detected above 515 nm, and VDR was excited at λ = 633 nm and detected above 650 nm. We used consecutive scans, and the optical slices were 1 μm.

Resistance Development Assay

Bacteria (*E. coli* K-12 MG1655 and *S. aureus* ATCC 29213 and SO-SAU19-1) were serial passaged in CAMHB as described by Silverman et al. (2001) with some small modifications. Briefly, bacteria were passaged for up to 32 days in a round-bottom polypropylene microtiter plate (Greiner) in media containing 0.25, 0.5, 1, and 2× MIC of betatide or other antibiotics. In *E. coli*, the MIC was 0.06 μg/ml for ciprofloxacin and 16 μg/ml for ampicillin. In *S. aureus*, the MIC was 1 μg/ml for gentamicin, 0.25 μg/ml for ciprofloxacin in ATCC 29213, and 0.5 μg/ml for SO-SAU19-1. For every passage (each day), the new MIC was determined, and bacterial cells from the 0.5× MIC culture were continued for passage by adjusting this culture to $\sim 0.5 \times 10^6$ CFU/ml in CAMHB. Fresh preparations of betatide/other antibiotics (0.25–2× MIC) were finally added to the diluted cultures, adjusted to the new MIC.

RESULTS

Selection of the Most Efficient Antibacterial and Antimutagenic APIM-Peptide

The antibacterial effect of APIM-peptides was previously shown to be partly caused by the CPP part, although MIC was 2×–3× higher for the CPP only than for the full-length APIM-peptide variants (Nedal et al., 2020). We have also previously found that an APIM sequence linked to a CPP containing 11 arginines (R11) had higher antibacterial activity than the same sequence linked to HIV-TAT, transportan, and penetratin CPPs (data not shown). Peptide 1, which is based on the sequence of the original anticancer peptide (Muller et al., 2013), is previously shown to have lower antibacterial efficacy (higher MIC) than the same peptide with a different linker, peptide 2 (Nedal et al., 2020),

TABLE 2 | Properties of APIM-peptide variants.

N-termini*	Linker	CPP*	MIC (μg/ml)		Reduction of viability		Reduction of mutation frequency
MDRWLVK			***S. epidermidis* MRSE**	***E. coli***	***E. coli* (60 μg/ml)**	**HEK293 (24 μg/ml)**	***E. coli* (20 μg/ml)**
#Peptide 1	W-KKKRK-I	R11	32	32	–	+	+
#Peptide 2/betatide	GILQ-WRK-I	R11	16	16	++++	+	++++
Peptide 3	GILQ-WRK-I	R10	16	32	ND	+	++
Peptide 4	GILQ-WRK-I	R9	16	32	++	ND	ND
Peptide 5	GILQ-WRK-I	R8	16	16	++	+	++

MIC, Minimum inhibitory concentration.
**All peptides were acetylated on the N-termini and amidated on the C-termini.*
#Peptides 1 and 2 are named RWLVK and RWLVK, respectively, in Nedal et al. (2020).*
"++" to "++++" denotes degree of reduced viability and mutation frequency relative to untreated control; "–" no effect; "+" tendency, but not a significant reduction; ND, not done. The raw data are shown in ***Supplementary Figures 1–3****.*

and this was verified here (**Table 2**). The number of arginines (Rs) required to facilitate uptake into the nucleus of mammalian cells has been found to be eight, while an increased proportion of the peptide was detected in the cell membrane when Rs were increased to 16 (Futaki et al., 2001). Here, we therefore explored if the number of Rs in the CPP domain of peptide 2 affected the growth of bacteria and human cells differently. **Table 2** includes comparison of performance of the peptides in more assays than previously reported (Nedal et al., 2020); therefore, we also included peptide 1 in these tests.

Reduction in the number of Rs from 11 to 8 (peptides 2–5) did not affect MIC in the MRSE strain, while peptides 2 and 5 had the lowest MIC in *E. coli* (K-12 MG1655) (**Table 2**). The MIC assay determines visual growth inhibition after 24 h; therefore, to explore potential differences in antibacterial efficacy in more detail, we examined these peptides' inhibitory effect on the growth of *E. coli* over 24 h (for growth curves, see **Supplementary Figure 1**). We found that peptide 2 inhibited bacterial growth more than peptide 5 did in this assay (**Table 2**, reduction of viability, *E. coli*); thus, the superior antibacterial efficacy based on these two assays was determined to be that of peptide 2.

One of the most important factors to consider when selecting and developing a drug is low toxicity for human cells. The ideal situation would be to develop an APIM-peptide variant with a lower effect on mammalian cells and a larger effect on bacteria, i.e., to increase the therapeutics window. However, when the viability of HEK293 cells was tested after treatment with the peptides using the MTT assay, the peptides reduced the viability of HEK293 cells similarly, with peptide 5 (R8) possibly inhibiting the viability slightly more than the other peptide variants did (**Table 2** and **Supplementary Figure 2**).

Peptides 1 and 2 are previously shown to inhibit TLS at sub-MICs via inhibition of polymerase V (Pol V) binding to the β-clamp (Nedal et al., 2020). Because inhibition of TLS is an important trait of these peptides, we compared these two peptides with the peptides with shorter CPPs for their ability to reduce the mutation frequency in *E. coli* using the Rif^R assay. We found that peptide 2 reduced the mutation frequency more efficiently than the other peptides did (**Table 2** and **Supplementary Figure 3**).

In summary, these results show that the peptide with the GILQ-WRK-I linker and the R11 CPP is superior to the peptide with the W-KKKRK-I linker and to peptides with shorter arginine chains, with regard to antibacterial and antimutagenic properties, while the toxic effects on human cells are similar in all the peptide variants tested. Based on the results summarized in **Table 2**, peptide 2 was selected as the lead antibacterial peptide candidate and hereafter named betatide (beta-clamp targeting peptide).

Betatide Has Low Minimal Inhibitory Concentration for *Enterococcus faecium*, *Staphylococcus aureus*, *Klebsiella pneumoniae*, *Acinetobacter baumannii*, *Pseudomonas aeruginosa*, and *Enterobacter cloacae* and Shows No Cross-Resistance With Other Antibiotics

Next, the activity of betatide against a wider selection of bacterial species from the ESKAPE list, i.e., MDR clinical isolates and corresponding reference strains, was examined (**Table 3A**). MICs for conventional antibiotics in the different MDR strains were determined in parallel with betatide, and this showed that the MDR strains had a 4× to >16,000× increase in MIC relative to their reference strains. However, betatide had an overall low MIC for all species (8–16 μg/ml) and was equally efficient against the reference strains as the clinical MDR isolates (except in one case: *Enterococcus faecalis*, 2× MIC). These results show that betatide has broad antibacterial activity and has no cross-resistance with the other antibiotics tested. This was expected as betatide has a ubiquitous bacterial target that is not shared by the other antibiotics. In some strains, a 2×–4× additive effect of the commercial antibiotic was detected when combined with 0.5× MIC of betatide, and an additive effect was observed more often for the MDR clinical isolates than for the reference strains (**Table 3**A).

TABLE 3 | MIC values and combination effects of betatide and commercial antibiotics in **(A)** ESKAPE strains and **(B)** *Staphylococcus aureus* fusidic acid sensitive (MRSA) and resistant (FR-MRSA).

A	Reference strain		Clinical isolate/resistant strain	
	MIC (μg/ml)	Combination effect with 0.5× MIC betatide	MIC (μg/ml)	Combination effect with 0.5× MIC betatide
E. faecium	CCUG 59167 (*vanA*+)		SO-EFU19-1 (*vanB*+)	
Betatide	8		8	
Ampicillin	1	None	2,048	None
S. aureus	ATCC 29213		SO-SAU19-1 (MRSA)	
Betatide	16		16	
Methicillin	1	Additive 2×	8	Additive 4×
Cefoxitin	4	None	32	Additive 2×
Clindamycin	0.25	Additive 2×	2,048	Additive 2×
K. pneumoniae	ATCC 13883		SO-KPN19-1 (ESBL-CARBA-D)	
Betatide	16		16	
Gentamicin	0.50	Additive 4×	64	Additive 4×
Ertapenem	0.03	Additive 4×	32	Additive 2×
Cefotaxime	0.13	Additive 2×	2,048	None
A. baumannii	ATCC 19606		SO-ABA19-1 (ESBL-CARBA-D)	
Betatide	8		8	
Gentamicin	8	None	>1,000	NA
Meropenem	4	None	512	None
Ciprofloxacin	1	None	512	Additive 2×
P. aeruginosa	ATCC 27853		SO-PAE19-1 (multidrug resistant)	
Betatide	16		16	
Gentamicin	2	None	16	None
Meropenem	0.5	None	64	Additive 2×
Ceftazidime	2	None	128	None
E. cloacae			SO-ECL18-1 [ESBL-CARBA (NDM)]	
Betatide			16	
Gentamicin			>1,000	NA
Cefotaxime			>1,024	NA
Ceftazidime			>1,000	NA
E. coli	MG1655		SO-ECO19-1 (ESBL-CARB-A(CTX-M-24)/D(OXA-48))	
Betatide	16		16	
Gentamicin	0.5	None	>500	NA
Ertapenem	0.06	None	64	Additive 2×
Ceftriaxone	0.06	None	1,024	Additive 4×
E. faecalis	ATCC 29212		SO-EFA19-1 (*optrA*+)	
Betatide	8		16	
Linezolid	2	None	8	None
B				
S. aureus	ATCC 29213		SO-SAU19-1 (MRSA)	
Betatide	16		16	
Fusidic acid	0.25	Additive, 2×	0.25	Additive 8×
			SO-SAU 19-2 (FR-MRSA)	
Betatide			32	
Fusidic acid			8	Additive 2×
			SO-SAU 19-3 (FR-MRSA)	
Betatide			32	
Fusidic acid			8	Additive 4×
			SO-SAU 19-4 (FR-MRSA)	
Betatide			32	
Fusidic acid			8	Additive 2×

NA, Not applicable; Combination effect = Additive effects, not (reduced MIC) of antibiotics when combining treatments with 0.5× MIC betatide. MIC values were confirmed in three independent experiments.

Because fusidic acid is commonly used in the treatment of wound infections, we examined if betatide enhanced the effect of fusidic acid against *S. aureus*. An 8× reduction in MIC of fusidic acid was observed when combined with 0.5× MIC betatide in a fusidic acid-sensitive MRSA strain (**Table 3B**). Further, a 2×–4× additive effect was detected in three fusidic acid-resistant MRSA strains (FR-MRSA).

Altogether, these results support the potential of betatide, both as a single antibacterial agent and in combination with commonly used antibiotics.

Betatide Eradicates Methicillin-Resistant *Staphylococcus epidermidis* Infections Without Affecting Epithelialization

In a mouse MRSA wound infection model, a gel containing a variant of the APIM-peptide significantly reduced the bacterial load with no visible toxicity on the skin (Nedal et al., 2020). As wound infections could be a suitable indication for these peptides and mouse skin may differ from human skin, we next more closely examined the efficacy of betatide and its effect on the epithelialization in an *in vitro* wound infection model. For this, we developed an epithelialization assay that is similar to the scratch test (Longaker et al., 1989; Walter et al., 2010), but where the gaps were made identical for accurate quantification by using strips. HaCaT cells infected with MRSE without treatment were all dead by day 2 after an exponential growth of the bacteria (**Figure 1A**, second panel). However, betatide (2 μg/ml) already eradicated MRSE from the culture wells at day 2 (**Figure 1A**, fourth panel). The epithelialization was completed at day 4, similar to the uninfected cells (**Figure 1A**, first and third panels). Thus, the epithelialization capacity of the cells was not affected at doses that completely abolished infection (epithelialization quantified in **Figure 1B**, CFU/ml depicted on the image in **Figure 1A**). The cells were cultured for up to 7 days without the infection re-emerging (**Figure 1A**, day 7, fourth and first panels).

When examining how epithelialization was affected by higher doses of betatide, a gradual decrease in percentage of epithelialization with increasing doses of betatide was observed (**Figure 1C**, quantified in **Figure 1D**). An approximately 70% decrease in epithelialization at day 4 was detected when using a betatide dose that was 12× higher than what is needed for a total eradication of the bacteria (24 μg/ml); however, the cells were not dying, and the epithelialization was re-established on day 7. Epithelialization was also re-established on day 7 after treatment with up to 40 μg/ml betatide (data not shown). Overall, these data indicate that doses that are more than 12× higher than the antibacterial dose could be used without severely affecting epithelialization.

Betatide Reduces Intracellular *S. aureus* Infections

Betatide is a variant of the APIM-peptide ATX-101, which is previously shown to be rapidly imported into multiple cells and to be distributed to all tissues upon intravenous infusion (Muller et al., 2013; Søgaard et al., 2018). Here, we show that fluorescent-labeled betatide (betatide-FAM, green) is rapidly taken up by live HaCaT cells (**Figure 2A**) and has similar subcellular localizations as ATX-101 (Muller et al., 2013); i.e., it is found in the cytosol, in the nuclei, and in the nucleoli. In addition, betatide-FAM in *S. aureus*-infected cells is found in small circular dots in the cytosol (highlighted by white arrows in **Figure 2A**, upper panel) that also are stained with live-cell DNA staining (magenta). These dots are not detected in uninfected HaCaT cells stained with live-cell DNA staining (lower panel), suggesting that these circular dots represent *S. aureus*.

To examine if betatide, which co-localizes with intracellular *S. aureus* (**Figure 2A**, merged image, white arrows), has antibacterial activity against intracellular *S. aureus*, we next measured intracellular bacterial counts in infected HaCaT cells treated with the peptide. Because *S. aureus* produces toxin that kills mammalian cells (Fraunholz and Sinha, 2012), optimization of the infection period and the number of infecting bacteria per cell was vital. We found that 100 MOI and infection for 3 h gave an intracellular infection without severe HaCaT cell cytotoxicity. The remaining extracellular bacteria were killed by gentamicin treatment prior to treatment of the infected cells with betatide (confirmed by plating at the time of harvest of the cells). A 4× reduction in intracellular bacterial load was found in betatide-treated cells (24 μg/ml), compared to untreated control (**Figure 2B**). Treatment with lower concentrations of betatide did not cause a significant reduction in CFU, while higher concentrations killed the infected HaCaT cells. Toxins from *S. aureus* likely sensitized the infected cells as uninfected HaCaT cells tolerated up to 40 μg/ml betatide. The maximum tolerated dose of betatide may therefore be different in different types of bacterial infections. In conclusion, these results show that betatide is rapidly taken up in mammalian cells where it retains its antibacterial activity.

Bacteria Have Low Capacity to Develop Resistance Against Betatide

Long-time exposure to sub-MIC levels of antibiotics are known to increase TLS and induce resistance development (Kreuzer, 2013; Raeder et al., 2021). To directly examine the resistance development against betatide, we exposed *E. coli* and *S. aureus* (both MDR and reference strain) to sub-MIC and 1×–2× MIC levels of betatide through serial passage and measured MIC over 20–30 days. Compared to bacteria exposed to gentamicin, ampicillin, and ciprofloxacin, those exposed to betatide had a much lower capacity to develop resistance (**Figure 3**). In *E. coli*, betatide showed only a temporary 2× increase in MIC during these 32 days, compared to up to a 64× stable increase in MIC for ciprofloxacin and ampicillin (**Figure 3A**). *S. aureus* developed a higher increase in MIC toward all the treatments compared to *E. coli*: up to a 256× increase in MIC for ciprofloxacin and gentamicin, while only an 8× increase in MIC for betatide was detected in the first experiment (**Figure 3B**, parallel 1). As mutations are stochastic events, we repeated this experiment and found no detectable resistance development with betatide after 30 days (**Figure 3B**, parallel 2), while ciprofloxacin was more similar to parallel 1). Furthermore, an MDR strain of *S. aureus* (MRSA) did not show any signs of resistance development against

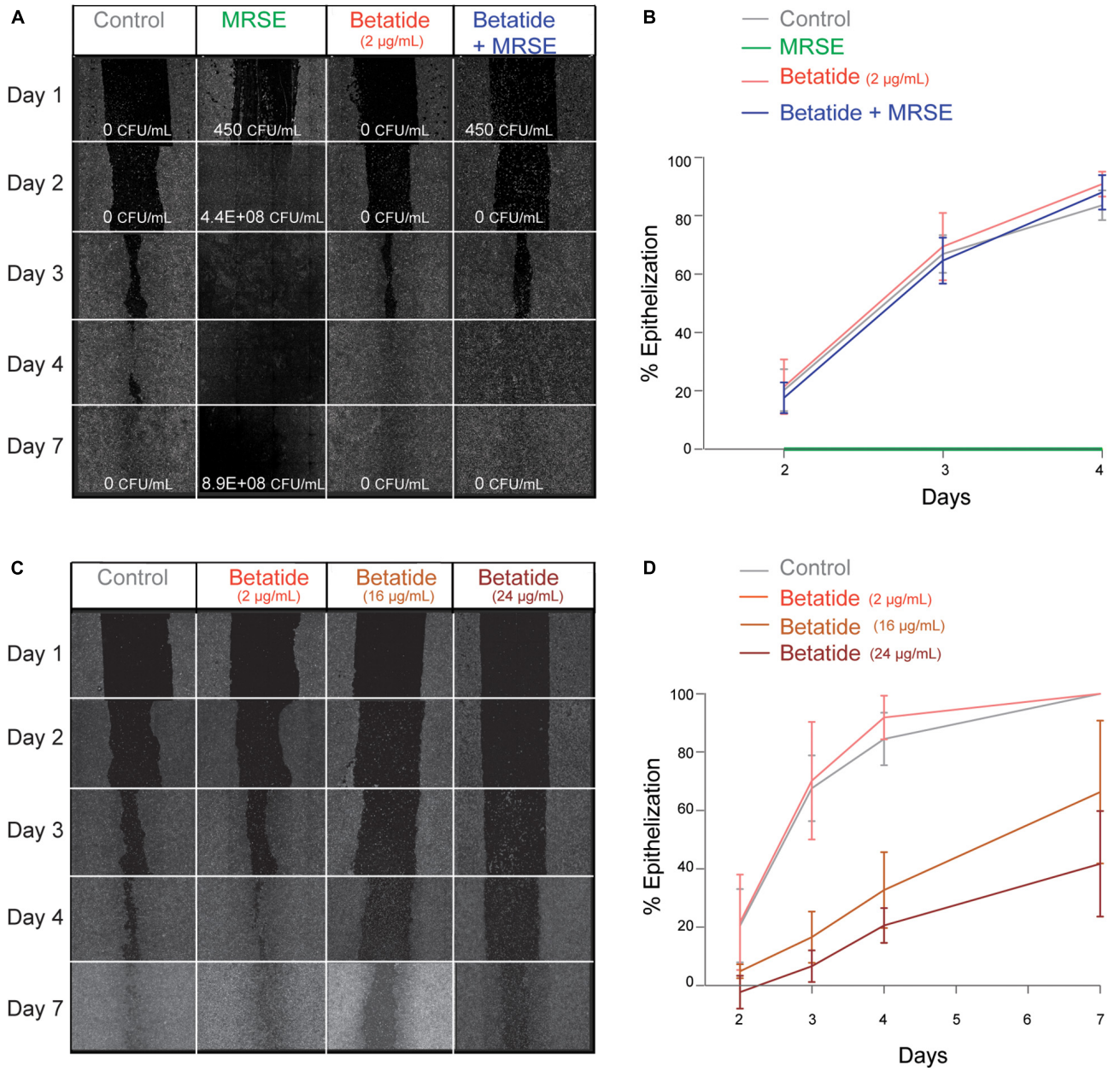

FIGURE 1 | Betatide kills methicillin-resistant *Staphylococcus epidermidis* SO-SEP9-1 (MRSE) *in vitro*, without affecting the epithelialization of HaCaT keratinocytes. **(A)** Images from one representative biological replicate showing epithelialization in gaps on days 1–7 (day 1 = day of infection, day 2 = 24 h after infection) in the individual treatment groups: untreated cells (control, gray, first panel); cells infected with MRSE (green, second panel); cells treated with betatide (2 μg/ml, red, third panel); and cells infected with MRSE but treated with betatide (2 μg/ml, blue, fourth panel). Number of bacteria added on day 1 and obtained after plating of the supernatants on day 2 and day 7 is given as CFU/ml in the images. **(B)** Quantification of percentage of epithelialization in the gaps relative to the original area of the gaps in **(A)** and in two additional biological replicates, on days 1–4. Mean ± SD. **(C)** Images from one representative biological replicate showing levels of epithelialization with increasing doses of betatide. Control (gray, first panel) and betatide 2 μg/ml (red), 16 μg/ml (orange), and 24 μg/ml (dark red) in the second to fourth panels, respectively. **(D)** Quantification of the percentage of epithelialization in the gaps relative to the original area of the gaps in **(C)** and in two additional biological replicates on days 1–7. Mean ± SD.

betatide during 20 passages even though 8× and 32× increases in MIC against gentamicin and ciprofloxacin, respectively, were detected (**Figure 3C**). These experiments show reduced ability of the bacteria to develop resistance against betatide compared to commonly used antibiotics.

DISCUSSION

In this study, we show that the lead antibacterial APIM-peptide candidate, betatide, kills ESKAPE MDR variants and their corresponding reference strains with low MIC. Betatide

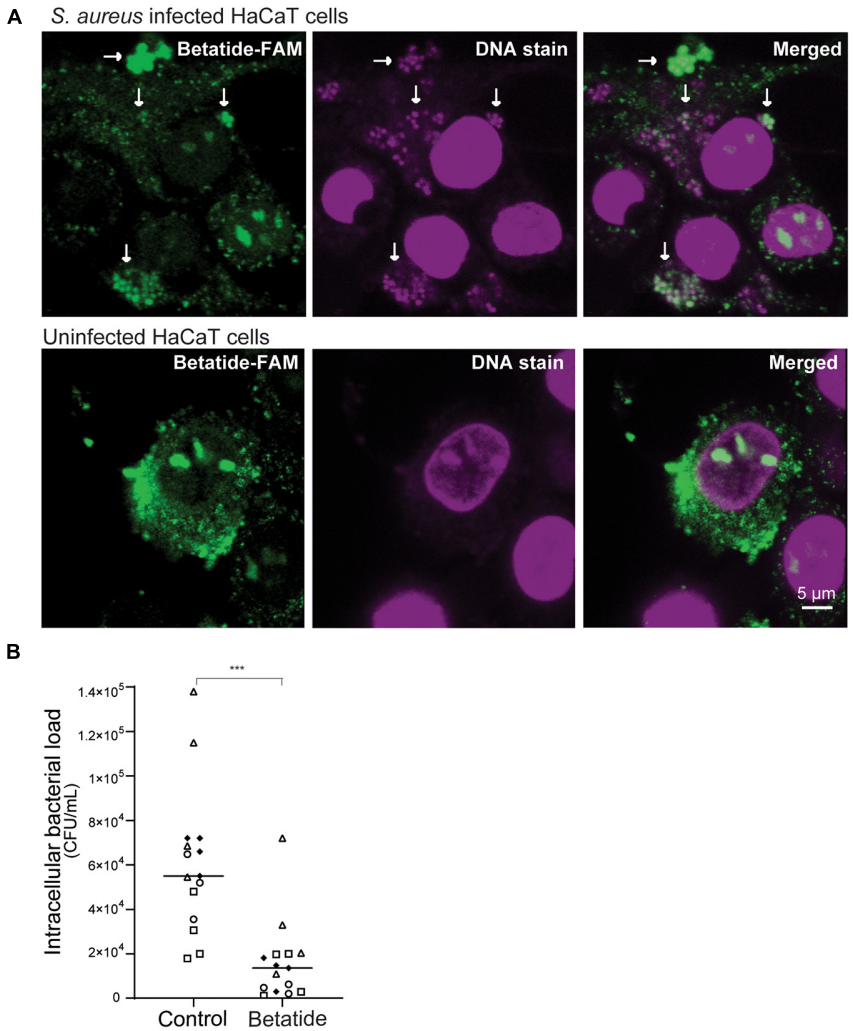

FIGURE 2 | Betatide reduces intracellular bacterial load in HaCaT cells infected with *Staphylococcus aureus*. **(A)** Images show import of fluorescently tagged betatide (betatide-FAM, 20 μg/ml, green) in *S. aureus* ATCC 29213-infected HaCaT cells (upper panels) and uninfected HaCaT cells (lower panels). DNA is stained with Vybrant® DyeCycle™ Ruby stain (VDR, 5 μM). Examples of small circular dots in the cytosol containing both betatide-FAM and DNA are marked with white arrows. **(B)** Intracellular bacterial load (CFU/ml) after *S. aureus* infection in HaCaT cells treated with betatide (24 μg/ml for 16 h) compared to untreated control. Extracellular *S. aureus* were eradicated by gentamicin treatment prior to this exposure in both the control and betatide-treated samples. Technical replicates from each biological replicate are shown with identical symbols (circles, triangles, squares, and diamonds). ***$p < 0.0001$ in unpaired two-tailed *t*-test with Welch's correction.

is not cytotoxic to mammalian cells, does not hinder the epithelialization capacity of a human keratinocyte cell line, and kills both extracellular MRSE and intracellular *S. aureus* in infected cell cultures. More than just killing already resistant bacterial strains, no/little endogenous resistance against betatide is detected after long-time exposure in *E. coli* and *S. aureus*.

Many AMPs have been and are under development, but a majority of them are failing in clinical phases due to low stability, undesired immune responses, resistance development, and high cytotoxicity (Andersson et al., 2016; Magana et al., 2020). How betatide behaves *in vivo* needs to be further tested; however, data from the Phase I study of the similar anticancer APIM-peptide ATX-101 are promising as this peptide has a favorable toxicity profile (Lemech et al., 2021). The arginine-rich CPPs in APIM-peptides enable rapid uptake in bacteria, yeast, and mammalian cells, and the peptides are detected in all tissues examined upon intravenous infusion, including the brain (Muller et al., 2013; Olaisen et al., 2018; Søgaard et al., 2018). The preference for bacteria over mammalian cells for betatide compared to ATX-101 is increased by amidation of the C-termini (reduced MIC by ∼4×, unpublished data) and changes in the linker region between the APIM sequence and the CPP (reduced MIC by ∼2×, **Table 2**). Therefore, MICs for betatide are much lower than doses that affect mammalian cells. APIM-peptides kill bacteria rapidly, i.e., 1× MIC leads to 97% killing within 5 min (Raeder et al., 2021); thus, the short serum half-life of 15–30 min in humans found for the similar anticancer APIM-peptide ATX-101 (Lemech et al., 2021) may therefore be sufficient

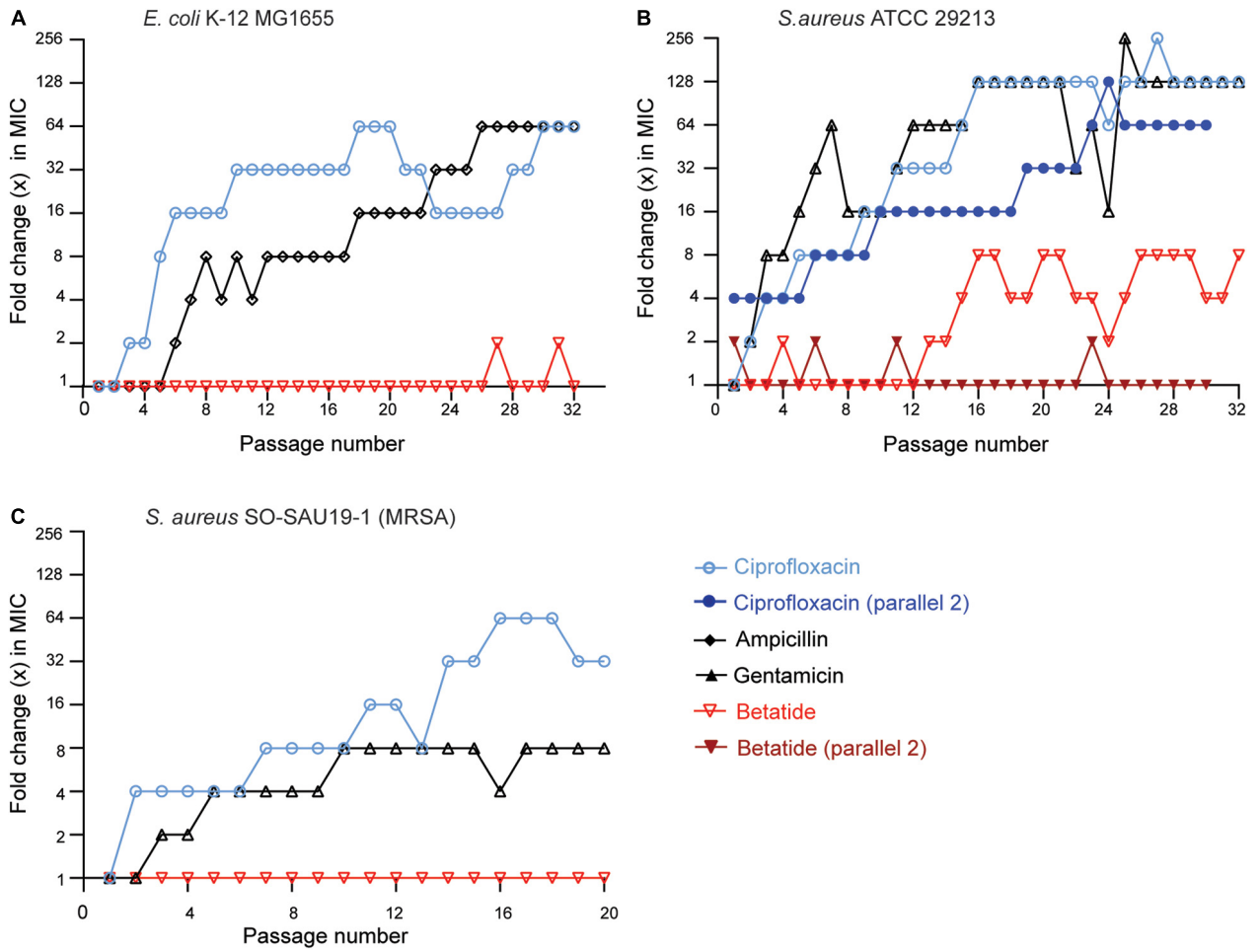

FIGURE 3 | Low ability for bacteria to develop resistance against betatide after serial passages in media containing sub-MIC levels of betatide. Increase in MIC relative to day 1 in **(A)** *E. coli* K-12 MG1655, **(B)** *S. aureus* ATCC 29213, and **(C)** *S. aureus* SO-SAU19-1 (MRSA) after exposure to sub-MIC-level (0.25× and 0.5×) betatide and two reference antibiotics over 20–32 days. The bacteria were serial passaged every day with fresh media and treated with new doses of ciprofloxacin (blue circles), ampicillin (black diamonds) or gentamicin (black upright triangles), and betatide (red inverted triangles) to determine new MICs. Two independent experiments are shown for ciprofloxacin and betatide for *S. aureus* ATCC 29213 where parallel 2 is shown as darker shades of filled blue circles and filled red inverted triangles, respectively.

for good antibacterial *in vivo* activity. Short serum half-life may rather be an advantage as this lowers the chances of developing immunogenicity and affecting the normal microbiota if given intravenously and/or topically.

The relative increase in antibacterial and antimutagenic activity of betatide (peptide 2, R11) versus peptide 5 (R8) could be due to slightly more efficient uptake of the peptide in bacteria and thereby more APIM being available for interaction with the β-clamp. The reason for the improved activity by the GILQ-WRK-I linker compared to the W-KKKRK-I linker, used in the anticancer peptide and which is based on viral SV40 nuclear localization signal, is elusive. However, it could, as previously discussed (Nedal et al., 2020), involve altered β-clamp binding capacities of residues flanking the APIM-motif in addition to increased uptake and/or stability.

The likelihood of resistance development against a new antibacterial drug is a critical feature to consider prior to antibacterial drug development. Betatide targets the β-clamp and reduces mutation frequency in bacteria via inhibition of Pol V–β-clamp interaction at sub-MICs, and this was shown to reduce the bacteria's ability to develop resistance against other antibiotics (Nedal et al., 2020). Here, we show that bacteria have a low ability to develop resistance against betatide. This, in combination with the low cytotoxicity of betatide in both HEK293 and HaCaT cells and the weak reduction of epithelization in HaCaT detected at concentrations more than 12× of what is required to abolish extracellular MRSE, warrants further examinations for topical use.

The resistance development to betatide is low, and we have so far not detected any cross-resistance with other antibiotics. One reason contributing to this could be that a mutation on the β-clamp that leads to reduced affinity for betatide is likely to also affect interactions with the polymerases and, thereby, affect both replication and TLS. This, in turn, can reduce the

fitness of the bacteria, similar to what has been shown for another peptide targeting the β-clamp called griselimycin. Griselimycin-resistant mutants with mutations in the β-clamp were found to have considerably lower fitness than the wild-type (WT) *Mycobacterium smegmatis* (Kling et al., 2015). However, other resistance mechanisms not affecting the target, but the import of the peptide and/or degradation of the peptide, could lead to higher tolerance to betatide. It has recently been shown that the activation of the Cpx-envelope stress response system in *E. coli* can increase the tolerance toward antibacterial peptides and peptide nucleic acids (PNAs) containing arginine-rich CPPs by inhibiting the uptake (Frimodt-Moller et al., 2021). Betatide showed a 2× increase in MIC in Cpx mutant *E. coli* cells which had a constitutive active Cpx response (Frimodt-Moller et al., 2021). This resulted in reduced membrane potential in the inner membrane and thereby reduced uptake of the peptide. This tolerance mechanism is common for arginine-rich CPPs and other AMPs, such as LL37 (Audrain et al., 2013), and are therefore likely not due to the APIM-motif in betatide itself.

Some increase in resistance against betatide was detected in the first serial passage in the *S. aureus* reference strain, while not in the second serial passage or in the MDR strain of *S. aureus* (MRSA). Mutations are stochastic events, and the outcome of the mutations thus vary each time, and only mutations that increase tolerance while not compromising fitness would be detected in these experiments. However, all the experiments in *S. aureus*, together with the low resistance development in *E. coli*, indicate a low tendency to develop resistance against betatide compared to several commonly used antibiotics.

Betatide showed a broad-spectrum activity against multiple bacterial strains independent of resistance patterns toward other antibiotics. Since wound infections are not likely to be monocultures, broad antibacterial activity is a favorable trait for topical antibacterial treatments. Fusidic acid, an inhibitor of the bacterial elongator factor, is a bacteriostatic antibiotic with a novel target. It is commonly used topically to treat skin infections caused by both sensitive and MDR *S. aureus*. Because single mutations in multiple genes (e.g., *fus* A-C) can cause resistance to fusidic acid, the drug is often used in combination with other drugs, most commonly rifampicin (also bacteriostatic) (Fernandes, 2016). The additive effect observed when betatide was combined with fusidic acid (2×–8×) suggests that betatide could be an alternative broad-spectrum antibacterial drug for use in combination with fusidic acid.

CONCLUSION

To summarize, betatide has antibacterial effects on both naive and resistant bacterial species (as the ESKAPE variants) without toxic effects on epithelialization. Its ability to impair resistance development toward other antibiotics and increase other antibiotics' efficacy, in combination with the low ability of bacteria to develop resistance against betatide, warrants further examinations for use in ointments, creams, or gels for topical application.

DATA AVAILABILITY STATEMENT

The original contributions presented in the study are included in the article/**Supplementary Material**, further inquiries can be directed to the corresponding author/s.

AUTHOR CONTRIBUTIONS

AN, SR, and MO planned and initiated the study. AN, SR, CS, and MH performed the laboratory experiments and/or interpreted the results. AN, SR, CS, and MO wrote the manuscript. All authors contributed to the article and approved the submitted version.

FUNDING

This work was supported by NTNU Discovery; the Joint Research Committee between St. Olav's University Hospital and Faculty of Medicine and Health Science, NTNU; the program NTNU Health at NTNU Norwegian University of Science and Technology; and Trond Mohn foundation. The funders had no role in the study design, data collection and analysis, decision to publish, or preparation of the manuscript.

SUPPLEMENTARY MATERIAL

The Supplementary Material for this article can be found online at: https://www.frontiersin.org/articles/10.3389/fmicb.2021.764451/full#supplementary-material

REFERENCES

Andersson, D. I., Hughes, D., and Kubicek-Sutherland, J. Z. (2016). Mechanisms and consequences of bacterial resistance to antimicrobial peptides. *Drug Resist. Updat.* 26, 43–57.

Audrain, B., Ferrières, L., Zairi, A., Soubigou, G., Dobson, C., Coppée, J. Y., et al. (2013). Induction of the Cpx envelope stress pathway contributes to *Escherichia coli* tolerance to antimicrobial peptides. *Appl. Environ. Microbiol.* 79, 7770–7779. doi: 10.1128/AEM.02593-13

Beaber, J. W., Hochhut, B., and Waldor, M. K. (2004). SOS response promotes horizontal dissemination of antibiotic resistance genes. *Nature* 427, 72–74. doi: 10.1038/nature02241

Cockerill, F. R., Wikler, M. A., Alder, J., Dudley, M. N., Eliopoulos, G. M., Ferraro, M. J., et al. (2012). *Methods For Dilution Antimicrobial Susceptibility Tests For Bacteria That Grow Aerobically: Approved Standard*. 9th ed. M07-A9. Wayne, PA: Clinical and Laboratory Standards Institute.

EUCAST (2021). *Breakpoint Tables For Interpretation Of Mics And Zone Diameters [Online]. The European Committee On Antimicrobial Susceptibility Testing*. Available online at: http://www.eucast.org [Accessed 11, 2021]

Fernandes, P. (2016). Fusidic acid: a bacterial elongation factor inhibitor for the oral treatment of acute and chronic staphylococcal infections. *Cold Spring Harb. Perspect. Med.* 6:a025437. doi: 10.1101/cshperspect.a025437

Filius, P. M., and Gyssens, I. C. (2002). Impact of increasing antimicrobial resistance on wound management. *Am. J. Clin. Dermatol.* 3, 1–7. doi: 10.2165/00128071-200203010-00001

Fraunholz, M., and Sinha, B. (2012). Intracellular staphylococcus aureus: live-in and let die. *Front. Cell. Infect. Microbiol.* 2:43. doi: 10.3389/fcimb.2012.00043

Frimodt-Moller, J., Koulouktsis, A., Charbon, G., Otterlei, M., Nielsen, P. E., and Lobner-Olesen, A. (2021). Activating the Cpx response induces tolerance to antisense PNA delivered by an arginine-rich peptide in *Escherichia coli*. *Mol. Ther. Nucleic Acids* 25, 444–454. doi: 10.1016/j.omtn.2021.06.009

Futaki, S., Suzuki, T., Ohashi, W., Yagami, T., Tanaka, S., Ueda, K., et al. (2001). Arginine-rich Peptides: an abundant source of membrane-permeable peptides having potential as carriers for intracellular protein delivery*. *J. Biol. Chem.* 276, 5836–5840.

Gilljam, K. M., Feyzi, E., Aas, P. A., Sousa, M. M., Muller, R., Vagbo, C. B., et al. (2009). Identification of a novel, widespread, and functionally important PCNA-binding motif. *J. Cell Biol.* 186, 645–654. doi: 10.1083/jcb.200903138

Goodman, M. F. (2002). Error-prone repair DNA polymerases in prokaryotes and eukaryotes. *Annu. Rev. Biochem.* 71, 17–50. doi: 10.1146/annurev.biochem.71.083101.124707

Iqbal, Z., Seleem, M. N., Hussain, H. I., Huang, L., Hao, H., and Yuan, Z. (2016). Comparative virulence studies and transcriptome analysis of *Staphylococcus aureus* strains isolated from animals. *Sci. Rep.* 6, 35442–35442. doi: 10.1038/srep35442

Kling, A., Lukat, P., Almeida, D. V., Bauer, A., Fontaine, E., Sordello, S., et al. (2015). Antibiotics: targeting DnaN for tuberculosis therapy using novel griselimycins. *Science* 348, 1106–1112. doi: 10.1126/science.aaa4690

Kloos, W. E., and Musselwhite, M. S. (1975). Distribution and persistence of *Staphylococcus* and *Micrococcus* species and other aerobic bacteria on human skin. *Appl. Microbiol.* 30, 381–385. doi: 10.1128/am.30.3.381-395.1975

Kreuzer, K. N. (2013). DNA damage responses in prokaryotes: regulating gene expression, modulating growth patterns, and manipulating replication forks. *Cold Spring Harb. Perspect. Biol.* 5:a012674. doi: 10.1101/cshperspect.a012674

Lemech, C. R., Kichenadasse, G., Marschner, J. P., Alevizopoulos, K., Otterlei, M., and Millward, M. (2021). *Safety Profile And Disease Stabilization In Late Stage, Heavily Pretreated, Solid Tumor Patients In A First-In-Human (FIH) Study of ATX-101, A Drug Targeting Proliferating Cell Nuclear Antigen (PCNA)*. Alexandria, VA: ASCO American Society of Clinical Oncology.

Longaker, M. T., Harrison, M. R., Langer, J. C., Crombleholme, T. M., Verrier, E. D., Spendlove, R., et al. (1989). Studies in fetal wound healing: II. A fetal environment accelerates fibroblast migration in vitro. *J. Pediatr. Surg.* 24, 793–798. doi: 10.1016/s0022-3468(89)80539-1

Magana, M., Pushpanathan, M., Santos, A. L., Leanse, L., Fernandez, M., Ioannidis, A., et al. (2020). The value of antimicrobial peptides in the age of resistance. *Lancet Infect. Dis.* 20, e216–e230.

Massey, R. C., Horsburgh, M. J., Lina, G., Höök, M., and Recker, M. (2006). The evolution and maintenance of virulence in *Staphylococcus aureus*: a role for host-to-host transmission? *Nat. Rev. Microbiol.* 4, 953–958. doi: 10.1038/nrmicro1551

Merrikh, H., and Kohli, R. M. (2020). Targeting evolution to inhibit antibiotic resistance. *FEBS J.* 287, 4341–4353. doi: 10.1111/febs.15370

Muller, R., Misund, K., Holien, T., Bachke, S., Gilljam, K. M., Vatsveen, T. K., et al. (2013). Targeting proliferating cell nuclear antigen and its protein interactions induces apoptosis in multiple myeloma cells. *PLoS One* 8:e70430. doi: 10.1371/journal.pone.0070430

Nedal, A., Raeder, S. B., Dalhus, B., Helgesen, E., Forstrom, R. J., Lindland, K., et al. (2020). Peptides containing the PCNA interacting motif APIM bind to the beta-clamp and inhibit bacterial growth and mutagenesis. *Nucleic Acids Res.* 48, 5540–5554. doi: 10.1093/nar/gkaa278

Olaisen, C., Kvitvang, H. F. N., Lee, S., Almaas, E., Bruheim, P., Drablos, F., et al. (2018). The role of PCNA as a scaffold protein in cellular signaling is functionally conserved between yeast and humans. *FEBS Open Bio* 8, 1135–1145. doi: 10.1002/2211-5463.12442

Otto, M. (2009). Staphylococcus epidermidis–the 'accidental' pathogen. *Nat. Rev. Microbiol.* 7, 555–567. doi: 10.1038/nrmicro2182

Pastar, I., Stojadinovic, O., Yin, N. C., Ramirez, H., Nusbaum, A. G., Sawaya, A., et al. (2014). Epithelialization in wound healing: a comprehensive review. *Adv. Wound Care (New Rochelle)* 3, 445–464. doi: 10.1089/wound.2013.0473

Pham, P., Rangarajan, S., Woodgate, R., and Goodman, M. F. (2001). Roles of DNA polymerases V and II in SOS-induced error-prone and error-free repair in *Escherichia coli*. *Proc. Natl. Acad. Sci. U.S.A.* 98, 8350–8354. doi: 10.1073/pnas.111007198

Raeder, S. B., Sandbakken, E. T., Nepal, A., Loseth, K., Bergh, K., Witso, E., et al. (2021). Novel peptides targeting the beta-clamp rapidly kill planktonic and biofilm staphylococcus epidermidis both in vitro and in vivo. *Front. Microbiol.* 12:631557. doi: 10.3389/fmicb.2021.631557

Rousselle, P., Braye, F., and Dayan, G. (2019). Re-epithelialization of adult skin wounds: cellular mechanisms and therapeutic strategies. *Adv. Drug Deliv. Rev.* 146, 344–365. doi: 10.1016/j.addr.2018.06.019

Silverman, J. A., Oliver, N., Andrew, T., and Li, T. (2001). Resistance studies with daptomycin. *Antimicrob. Agents Chemother.* 45, 1799–1802.

Søgaard, C. K., Blindheim, A., Røst, L. M., Petrović, V., Nepal, A., Bachke, S., et al. (2018). "Two hits – one stone"; increased efficacy of cisplatin-based therapies by targeting PCNA's role in both DNA repair and cellular signaling. *Oncotarget* 9, 32448–32465. doi: 10.18632/oncotarget.25963

Tuchscherr, L., Medina, E., Hussain, M., Völker, W., Heitmann, V., Niemann, S., et al. (2011). Staphylococcus aureus phenotype switching: an effective bacterial strategy to escape host immune response and establish a chronic infection. *EMBO Mol. Med.* 3, 129–141. doi: 10.1002/emmm.201000115

Tulloch, L. G. (1954). Nasal carriage in staphylococcal skin infections. *Br. Med. J.* 2, 912–913. doi: 10.1136/bmj.2.4893.912

Walter, M. N., Wright, K. T., Fuller, H. R., Macneil, S., and Johnson, W. E. (2010). Mesenchymal stem cell-conditioned medium accelerates skin wound healing: an in vitro study of fibroblast and keratinocyte scratch assays. *Exp. Cell Res.* 316, 1271–1281. doi: 10.1016/j.yexcr.2010.02.026

World Health Organization (2015). *Global Action Plan On Antimicrobial Resistance [Online]*. Geneva: World Health Organization.

World Health Organization (2017). *WHO Publishes List Of Bacteria For Which New Antibiotics Are Urgently Needed [Online]*. Geneva: World Health Organization.

World Health Organization (2018). *Antimicrobial Resistance [Online]*. Geneva: World Health Organization.

Yakimov, A., Bakhlanova, I., and Baitin, D. (2021). Targeting evolution of antibiotic resistance by SOS response inhibition. *Comput. Struct. Biotechnol. J.* 19, 777–783. doi: 10.1016/j.csbj.2021.01.003

Conflict of Interest: The authors declare that the research was conducted in the absence of any commercial or financial relationships that could be construed as a potential conflict of interest.

Publisher's Note: All claims expressed in this article are solely those of the authors and do not necessarily represent those of their affiliated organizations, or those of the publisher, the editors and the reviewers. Any product that may be evaluated in this article, or claim that may be made by its manufacturer, is not guaranteed or endorsed by the publisher.

frontiers in Microbiology

ORIGINAL RESEARCH
published: 29 November 2021
doi: 10.3389/fmicb.2021.738896

A Natural Antimicrobial Agent: Analysis of Antibacterial Effect and Mechanism of Compound Phenolic Acid on *Escherichia coli* Based on Tandem Mass Tag Proteomics

*Geyin Zhang[1†], Yunqiao Yang[1†], Fareed Uddin Memon[1†], Kaiyuan Hao[1], Baichang Xu[1], Shuaiyang Wang[1], Ying Wang[1], Enyun Wu[1], Xiaogang Chen[1], Wenguang Xiong[2] and Hongbin Si[1]**

[1] College of Animal Science and Technology, Guangxi University, Nanning, China, [2] College of Veterinary Medicine, South China Agricultural University, Guangzhou, China

OPEN ACCESS

Edited by:
Wang Jiajun,
Northeast Agricultural University, China

Reviewed by:
Ranjith Kumar Manoharan, Yeungnam University, South Korea
Erick Paul Gutiérrez-Grijalva, Centro de Investigación en Alimentación y Desarrollo, Consejo Nacional de Ciencia y Tecnología (CONACYT), Mexico

***Correspondence:**
Hongbin Si
shb2009@gxu.edu.cn

[†] These authors have contributed equally to this work and share first authorship

Specialty section:
This article was submitted to Antimicrobials, Resistance, and Chemotherapy, a section of the journal Frontiers in Microbiology

Received: 09 July 2021
Accepted: 01 November 2021
Published: 29 November 2021

Citation:
Zhang G, Yang Y, Memon FU, Hao K, Xu B, Wang S, Wang Y, Wu E, Chen X, Xiong W and Si H (2021) A Natural Antimicrobial Agent: Analysis of Antibacterial Effect and Mechanism of Compound Phenolic Acid on Escherichia coli Based on Tandem Mass Tag Proteomics. Front. Microbiol. 12:738896. doi: 10.3389/fmicb.2021.738896

The objective of this study was to evaluate the antibacterial mechanisms of phenolic acids as natural approaches against multi-drug resistant *Escherichia coli* (*E. coli*). For that purpose, five phenolic acids were combined with each other and 31 combinations were obtained in total. To select the most potent and effective combination, all of the obtained combinations were examined for minimum inhibitory concentration (MIC) and it was found that the compound phenolic acid (CPA) 19 (protocatechuic acid, hydrocinnamic acid, and chlorogenic acid at concentrations of 0.833, 0.208, and 1.677 mg/mL, respectively) showed better efficacy against *E. coli* compared to other combinations. Furthermore, based on tandem mass tag (TMT) proteomics, the treatment of CPA 19 significantly downregulated the proteins associated with resistance (Tsr, Tar, CheA, and CheW), OmpF, and FliC of multidrug-resistant *E. coli*. At the same time, we proved that CPA 19 improves the sensitivity of *E. coli* to antibiotics (ceftriaxone sodium, amoxicillin, fosfomycin, sulfamonomethoxine, gatifloxacin, lincomycin, florfenicol, cefotaxime sodium, and rifampicin), causes the flagellum to fall off, breaks the structure of the cell wall and cell membrane, and leads to macromolecules leaks from the cell. This evidence elaborated the potential therapeutic efficacy of CPA 19 and provided a significant contribution to the discovery of antibacterial agents.

Keywords: compound phenolic acids, *Escherichia coli*, TMT, antibacterial mechanism, new antimicrobial agent

INTRODUCTION

About 78 years ago, penicillin and other antibiotics were discovered as antimicrobial agents and introduced in various clinical treatments because of their positive influences in preventing bacterial infections (Paitan, 2018). However, Abraham and Chain (1988) reported the emergence of antimicrobial resistance.

Among these resistant bacterial strains, species of *E. coli* have emerged against the variety of antibiotic agents used in clinical practice, which not only damages the production of the animal industry, but also seriously affects the health of human beings. Therefore, there is an urgent need for the search of safe and effective approaches to overcome single as well as multidrug-resistant bacterial infections (Roth et al., 2019).

In recent years, more and more researchers have been devoted to the study of the inhibition of plant polyphenols because of their natural and broad antibacterial properties (Yun-Seok et al., 2010; Sidhu et al., 2014; Yang et al., 2020). Phenolic acids are major plant metabolites, which occur in all parts of the plant: shells, leaves, seeds, fruits, and wood parts (Efenberger et al., 2021). Previous studies have demonstrated that phenolic compounds possess a variety of biological functions including anti-carcinogenic, anti-inflammatory, and anti-oxidant properties. Moreover, some phenolic compounds have been proven to be effective in inhibiting various pathogenic bacteria such as *E. coli* (Cushnie and Lamb, 2005; Almajano et al., 2007; Martina, 2010), however, the antibacterial effect was not satisfactory, and their studies only assessed the level of the simple antibacterial mechanism. What is more, the components in plants are complex and diverse, it is impossible to determine effective specific antibacterial ingredients, and it is difficult to explain the mechanism of phenolic acids.

Therefore, in this study, five phenolic acids were combined with each other in order to obtain one of the most effective combinations against multidrug-resistant *E. coli*, which may provide a significant contribution to the field of antibiotic agent discovery.

MATERIALS AND METHODS

Bacterial Strains

Seven strains of *E. coli* (E1, E2, E3, E4, E5, E6, and E7) from poultry were stored in Guangxi University (Nanning, China), which were confirmed by the analysis of 16S rDNA sequencing (Kim et al., 2010). The resistance genes of the seven *E. coli* strains are shown in **Table 1** (identification by the 25 μL PCR reaction system).

TABLE 1 | Resistance genes of the seven strains of *E. coli*.

Number of *E. coli*	Resistance genes
E1	*rmtB*, *tetA*, *tetM*, *bla* $_{OXA-1}$, *bla* $_{CTX-m-u}$, *bla* $_{CTX-m-1}$, *sul1*, *sul2* *sul3*, *floR*, *oqxA*
E2	*rmtB*, *tetA*, *tetM*, *bla* $_{OXA-1}$, *bla*$_{CTX-m-u}$, *bla* $_{CTX-m-1}$, *sul1*, *sul2*, *oqxA*
E3	*armA*, *rmtA*, *rmtB*, *rmtC*, *tetA*, *bla* $_{OXA-2}$, *bla* $_{CTX-m-1}$, *qnrA, floR*, *oqxA*, *mcr-1*
E4	*rmtD*, *tetB*, *tetC*, *bla* $_{CTX-m-u}$, *bla* $_{CTX-m-1}$, *bla* $_{CTX-m-9}$, *sul2*, *floR*, *mcr-1*
E5	*rmtD*, *tetA*, *tetM*, *bla* $_{TEM}$, *bla* $_{OXA-10}$, *bla* $_{CTX-m-u}$, *bla* $_{CTX-m-9}$, *qrnB*, *floR*, *oqxA*, *sul2*, *sul3*
E6	*rmtD*, *tetA*, *bla* $_{OXA-10}$, *bla* $_{CTX-m-u}$, *bla* $_{CTX-m-9}$, *sul2*, *sul3*, *fosA3*, *mcr-1*
E7	*rmtA*, *rmtD*, *tetB*, *tetC*, *bla* $_{TEM}$, *bla* $_{CTX-m-u}$, *bla* $_{CTX-m-1}$, *bla* $_{CTX-m-9}$, *oqxA*, *sul1*, *sul2*

Preparation of Compound Phenolic Acids

The five phenolic acids were dissolved with maximum solubility (salicylic acid, CAS: 69-72-7, 0.22 g/100 g H_2O; protocatechuic acid, CAS: 99-50-3, 2 g/100 g H_2O; gallic acid, GAS: 149-91-7, 1.14 g/100 g H_2O; hydrocinnamic acid, GAS: 501-52-0, 0.5 g/100 g H_2O; chlorogenic acid, GAS: 327-97-9, 4 g/100 g H_2O), and 5% dimethyl sulfoxide (DMSO) was added to promote the solubility of phenolic acids. Finally, the phenolic acids were mixed with each other in equal volumes to obtain CPAs with different compositions.

Determination of Minimum Inhibitory Concentrations

The microdilution method (Smekalova et al., 2016) was used to detect the MIC of each CPA on *E. coli*, and the results were statistically analyzed. Mueller-Hinton Broth (MHB) was used as the incubation medium. The CPAs (100 μL) were serially diluted in a 96-well plate by 100 μL of *E. coli* inoculum (approximately 1.5×10^5 CFU/mL) for 12 times, and the final concentrations of CPAs were 50, 25, 12.5, 6.15, 3.125, 1.5625, 0.78125, 0.39065, 0.1953125, 0.09765625, 0.048828125, and 0.0244140625% of the initial concentration, respectively. After incubation at 37°C for 12–16 h, MICs were measured by visual inspection of the turbidity of broth in tubes. That is to say, if the test tube was still clear and transparent (un-cloudy) after incubation, the cells could not grow at that concentration and then the MIC value was obtained. Florfenicol (in China, florfenicol is an approved animal-specific antibiotic, but it is banned in laying hens) was used as a positive anti-*E. coli* control; MHB was used as a blank control.

Tandem Mass Tag Quantitative Proteomics

Cultivation and Pre-treatment of *Escherichia coli*

Escherichia coli were cultured at 37°C until the logarithmic growth phase at 220 r/min. The optical density value (OD_{600}) of the bacterial fluid was diluted to 0.6, and then evenly divided into two groups, each group was tested in triplicate. Group A was treated with CPA at the concentration of 1/2 MIC, while same amount of H_2O was added in group B and kept as the control group. The mixture was incubated at 37°C for 60 min at 220 r/min, centrifuged for 15 min (4°C, 5000 r/min), and the supernatant was discarded. After repeated washing with RNA-free PBS three times, the samples were immediately frozen in liquid nitrogen, and then stored at −80°C for further use.

Protein Extraction

The samples were lysed by ultrasound using four times the volume of lysis buffer (8 M urea, 1% protease inhibitor). Following centrifugation at 12000 g for 10 min (to remove the cell debris), the supernatant was collected to determine the protein

concentration using a BCA kit (A045-4-2, NanJing JianCheng Bioengineering Institute Co., Ltd., Nanjing, China).

Trypsin Digestion

For digestion, the protein solution was reduced with 5 mM of dithiothreitol for 30 min at 56 °C and alkylated with 11 mM of iodoacetamide for 15 min at room temperature in darkness. The protein sample was then diluted by adding 100 mM of TEAB to a urea concentration less than 2 M. Finally, trypsin was added at a 1:50 trypsin-to-protein mass ratio for the first digestion overnight and a 1:100 trypsin-to-protein mass ratio for a second 4-h digestion.

Tandem Mass Tag Labeling

After trypsin digestion, the peptide was desalted by a Strata X C18 SPE column (Phenomenex) and vacuum-dried. The peptide was reconstituted in 0.5 M of TEAB and processed according to the manufacturer's protocol for the TMT kit. Briefly, one unit of TMT reagent was thawed and reconstituted in acetonitrile. The peptide mixtures were then incubated for 2 h at room temperature and pooled, desalted, and dried by vacuum centrifugation.

HPLC Fractionation

The tryptic peptides were fractionated into fractions by high pH reverse-phase HPLC using a Thermo Betasil C18 column (5 μm particles, 10 mm ID, 250 mm length). Briefly, peptides were first separated with a gradient of 8 to 32% acetonitrile (pH 9.0) over 60 min into 60 fractions. Then, the peptides were combined into six fractions and dried by vacuum centrifuging. LC-MS/MS Analysis.

The tryptic peptides were dissolved in 0.1% formic acid (solvent A), directly loaded onto a homemade reversed-phase analytical column (15-cm length, 75 μm i.d.). The gradient was comprised of an increase from 6 to 23% solvent B (0.1% formic acid in 98% acetonitrile) over 26 min, 23 to 35% in 8 min and climbing to 80% in 3 min then holding at 80% for the last 3 min, all at a constant flow rate of 400 nL/min on an EASY-nLC 1000 UPLC system. The peptides were subjected to NSI source followed by tandem mass spectrometry (MS/MS) in Q Exactive TM Plus (Thermo Fisher Scientific) coupled online to the UPLC. The electrospray voltage applied was 2.0 kV. The m/z scan range was 350 to 1800 for full scan, and intact peptides were detected in the Orbitrap at a resolution of 70,000. Peptides were then selected for MS/MS using the NCE setting at 28 and the fragments were detected in the Orbitrap at a resolution of 17,500. A data-dependent procedure that alternated between one MS scan followed by 20 MS/MS scans with 15.0 s dynamic exclusion was used. Automatic gain control (AGC) was set at 5E4. The fixed first mass was set as 100 m/z.

Database Search

The resulting MS/MS data were processed using the Maxquant search engine (v.1.5.2.8). Tandem mass spectra were searched against the human uniprot database concatenated with a reverse decoy database. Trypsin/P was specified as the cleavage enzyme allowing up to four missing cleavages. The mass tolerance for precursor ions was set as 20 ppm in the first search and 5 ppm in the main search, and the mass tolerance for fragment ions was set as 0.02 Da. Carbamidomethyl on Cys was specified as the fixed modification, and acetylation modification and oxidation on Met were specified as variable modifications. FDR was adjusted to $< 1\%$ and the minimum score for modified peptides was set > 40.

Parallel Reaction Monitoring

Parallel reaction monitoring (PRM) mass spectrometric analysis was performed using tandem mass spectrometry (MS/MS) in Q ExactiveTM Plus (Thermo Fisher Scientific). The liquid chromatography parameters, electrospray voltage, scan range, and Orbitrap resolution were the same as the TMT methods. Automatic gain control (AGC) was set at 3×10^6 for full MS and 1×10^5 for MS/MS. The maximum IT was set at 20 ms for full MS and auto for MS/MS. The isolation window for MS/MS was set at 2.0 m/z. After the quantitative information was normalized by the heavy isotope-labeled peptide, a relative quantitative analysis (three biological replications) was performed on the target peptides.

Fractional Inhibition Concentration Index of Antibiotics and Compound Phenolic Acids

Modified Lorian (2005) method was used to determine the interaction between antibiotics and CPAs. The CPA was diluted vertically, and the antibiotic was diluted horizontally in a 96-well plate. The following formula was used to calculate FICI:

$$\mathrm{FICI} = \frac{\mathrm{MIC(antibiotic\ in\ combination)}}{\mathrm{MIC(antibiotic\ alone)}} + \frac{\mathrm{MIC(CPA\ in\ combination)}}{\mathrm{MIC(CPA\ alone)}}$$

The combined antimicrobial action of CPAs and antibiotics was determined according to FICI, the combined antibacterial effects were considered to be synergy, additivity, indifference, or oppositive when the FCIC was ≤ 0.5, > 0.5 to ≤ 1, > 1 to ≤ 2, and > 2, respectively (Kurek et al., 2012).

Determination of Extracellular Soluble Protein

The CPA was added in a bacterial suspension (10^6 CFU/mL) with a concentration of 1/2 MIC. The same volume of H_2O was used as the control group. The mixture was cultured at 37°C with shaking at 220 r/min. Samples were collected separately from 0 to 18 h every hour. The determination of extracellular soluble protein was measured by a protein quantitative test kit (A045-2, NanJing JianCheng Bioengineering Institute Co., Ltd., Nanjing, China). Each group test was repeated three times.

The Ultrastructure of Cells Was Observed by Transmission Electron Microscopy

The CPA was added to E6 at the logarithmic growth stage, and the final concentration was adjusted to 1/2 MIC, incubated at

37°C and 220 r/min for 4 h, and the same amount of H_2O was used as a blank control. After centrifugation of the mixture (3 000 r/min, 15 min), the precipitation was collected and washed twice with PBS. A total of 1 mL of 3% glutaraldehyde was added to the bacterial plate and kept at 4°C overnight. The liquid was centrifuged (3 000 r/min, 30 min) and the supernatant was collected. After separation, the supernatant was washed with PBS three times, fixed with 1% osmium tetroxide, and kept at 4°C for 2 h. After this, the supernatant was uninterruptedly dehydrated using 30, 50, 75, 95, and 100% ethanol for dehydration. Epoxy resin was embedded at 60°C for 48 h and sliced (with 50-nm thickness) (Ultra 45°, Daitome). The samples were placed on a 400-mesh copper network and stained with 2.0% uranium dioxane acetate and lead citrate for 30 min. After washing with distilled water, the samples were dried at 37°C. Finally, the ultrastructural changes were observed under TEM (TECNAI G2 20 TWIN, FEI).

TABLE 2 | Composition and concentration of 31 combinations of CPAs.

Number	Composition and concentration of CPAs
1	Salicylic acid 1.1 mg/mL,protocatechuic acid 10 mg/mL
2	Salicylic acid 1.1 mg/mL, gallic acid 5.7 mg/mL
3	Salicylic acid 1.1 mg/mL,hydrocinnamic acid 2.5 mg/mL
4	Salicylic acid 1.1 mg/mL,chlorogenic acid 20 mg/mL
5	Protocatechuic acid 10 mg/mL,gallic acid 5.7 mg/mL
6	Protocatechuic acid 10 mg/mL,hydrocinnamic acid 2.5 mg/mL
7	Protocatechuic acid 10 mg/mL,chlorogenic acid 20 mg/mL
8	Gallic acid 5.7 mg/mL,hydrocinnamic acid 2.5 mg/mL
9	Gallic acid 5.7 mg/mL,chlorogenic acid 20 mg/mL
10	Hydrocinnamic acid 2.5 mg/mL,chlorogenic acid 20 mg/mL
11	Salicylic acid 0.73 mg/mL,protocatechuic acid 6.67 mg/mL,gallic acid 3.8 mg/mL
12	Salicylic acid 0.73 mg/mL,protocatechuic acid 6.67 mg/mL,hydrocinnamic acid 1.67 mg/mL
13	Salicylic acid 0.73 mg/mL,protocatechuic acid 6.67 mg/mL,chlorogenic acid 13.33 mg/mL
14	Salicylic acid 0.73 mg/mL,gallic acid 3.8 mg/mL,hydrocinnamic acid 1.67 mg/mL
15	Salicylic acid 0.73 mg/mL,gallic acid 3.8 mg/mL,chlorogenic acid 13.33 mg/mL
16	Salicylic acid 0.73 mg/mL, hydrocinnamic acid1.67 mg/mL, chlorogenic acid 13.33 mg/mL
17	Protocatechuic acid 6.67 mg/mL, gallic acid 3.8 mg/mL, hydrocinnamic acid 1.67 mg/mL
18	Protocatechuic acid 6.67 mg/mL, gallic acid 3.8 mg/mL, chlorogenic acid 13.33 mg/mL
19	Protocatechuic acid 6.67 mg/mL, hydrocinnamic acid 1.67 mg/mL, chlorogenic acid 13.33 mg/mL
20	Gallic acid 3.8 mg/mL, hydrocinnamic acid 1.67 mg/mL, chlorogenic acid 13.33 mg/mL
21	Salicylic acid 0.55 mg/mL, protocatechuic acid 5 mg/mL, gallic acid 2.85 mg/mL, hydrocinnamic acid 1.25 mg/mL
22	Salicylic acid 0.55 mg/mL, protocatechuic acid 5 mg/mL, gallic acid 2.85 mg/mL, chlorogenic acid 10 mg/mL
23	Salicylic acid 0.55 mg/mL, protocatechuic acid 5 mg/mL, hydrocinnamic acid 1.25 mg/mL, chlorogenic acid 10 mg/mL
24	Salicylic acid 0.55 mg/mL, gallic acid 2.85 mg/mL, hydrocinnamic acid 1.25 mg/mL, chlorogenic acid 10 mg/mL
25	Protocatechuic acid 5 mg/mL, gallic acid 2.85 mg/mL, hydrocinnamic acid 1.25 mg/mL, chlorogenic acid 10 mg/mL
26	Salicylic acid 0.44 mg/mL, protocatechuic acid 4 mg/mL, gallic acid 2.28 mg/mL, hydrocinnamic acid 1 mg/mL, chlorogenic acid 8 mg/mL
27	Salicylic acid 2.2 mg/mL
28	Protocatechuic acid 20 mg/mL
29	Gallic acid 11.4 mg/mL
30	Hydrocinnamic acid 5 mg/mL
31	Chlorogenic acid 40 mg/mL

RESULTS

Composition and Concentration of 31 Compound Phenolic Acids

A total of 31 combinations of CPAs were obtained; all components and their concentrations in each CPA are presented in **Table 2**. In our subsequent study, the initial concentration of each CPA was recorded as 1, which was not only convenient

TABLE 3 | The MICs of 31 combinations of CPAs against the 7 strains of *E. coli*.

Agents	MICs of *E. coli*						
	E1 (%)	E2 (%)	E3 (%)	E4 (%)	E5 (%)	E6 (%)	E7 (%)
CPA 1	25	25	25	25	25	25	25
CPA 2	25	25	25	25	25	25	50
CPA 3	50	50	50	50	50	50	25
CPA 4	25	25	25	25	25	25	25
CPA 5	25	25	25	25	25	25	25
CPA 6	12.5	12.5	12.5	12.5	12.5	25	25
CPA 7	25	25	12.5	25	25	25	25
CPA 8	25	25	25	25	25	25	25
CPA 9	25	25	25	25	25	25	25
CPA 10	12.5	25	25	25	25	25	25
CPA 11	25	25	25	25	25	25	25
CPA 12	25	25	25	25	25	25	25
CPA 13	25	25	25	25	25	25	25
CPA 14	25	25	25	25	25	25	25
CPA 15	25	25	25	25	25	25	25
CPA 16	25	25	25	25	25	25	25
CPA 17	25	25	25	12.5	25	25	25
CPA 18	25	25	25	25	25	25	25
CPA 19	12.5	12.5	12.5	12.5	12.5	12.5	12.5
CPA 20	25	25	25	25	25	25	25
CPA 21	25	25	25	25	25	25	25
CPA 22	25	25	25	25	25	25	25
CPA 23	12.5	25	25	12.5	12.5	25	25
CPA 24	25	25	25	25	25	25	25
CPA 25	25	25	25	12.5	25	25	12.5
CPA 26	25	25	25	25	25	25	12.5
CPA 27	>50	>50	>50	50	50	50	50
CPA 28	25	25	25	25	25	25	50
CPA 29	50	50	50	50	25	50	25
CPA 30	50	50	25	25	25	25	25
CPA 31	25	50	25	25	25	25	25
Florfenicol	1280	640	640	640	640	2560	640

MICs were calculated with the initial concentration of CPA as 1, the unit of florfenicol was μg/mL.

for recording, but also more intuitive to reflect the antibacterial effect. The specific calculation method of actual MIC values of each CPA in subsequent experiments is described in the second sentence of the next section.

Determining the Compound Phenolic Acid With the Best Antibacterial Effect

Seven strains of *E. coli* were used to assess the antibacterial efficacy of all CPAs by the microdilution method. The results are shown in **Table 3**, taking E1 as an example, the MIC of CPA 1 on E1 was 25% of its initial concentration, at this time, the concentration of each component in CPA1 = 25%*1 (salicylic acid 1.1 mg/mL,protocatechuic acid 10 mg/mL), which meant 0.275 mg/mL of salicylic acid and 2.5 mg/mL of protocatechuic acid.

As shown in **Table 3**, all of the CPAs showed certain inhibitory effects on *E. coli*. The antibacterial effect of each combination was different due to different components and *E. coli* strains. However, compared to all other CPAs, CPA 19 showed better efficacy against all seven strains of *E. coli* and the MIC was reached at 12.5%. In other words, the concentrations of each component in the MIC (12.5% CPA 19) were 0.834 mg/mL (protocatechuic acid), 0.208 mg/mL (hydrocinnamic acid), and 1.67 mg/mL (chlorogenic acid). Therefore, CPA 19 was selected as a potential antimicrobial agent and its mechanisms were further explored against E6 *E. coli*.

General Features of Proteome After Compound Phenolic Acid 19 Treatment

After treatment with a subinhibitory concentration of CPA 19, 2688 proteins were detected and identified, and 2560 were quantified. The detailed data (the protein score, coverage percentage, number of peptides matching individual proteins, and accession number assigned to each identified protein) of related proteins are shown in **Supplementary Table 1**. The MS proteomic results reported in this paper have been deposited in the OMIX, China National Center for Bioinformation/Beijing Institute of Genomics, Chinese Academy of Sciences, under accession number OMIX382 which is accessible at https://ngdc.cncb.ac.cn/omix.

Differentially Expressed Proteins After Compound Phenolic Acid 19 Treatment

There were 268 differentially expressed proteins after treatment with a subinhibitory concentration of CPA 19, including 84 upregulated proteins and 184 downregulated proteins, when the fold change was defined as greater than 1.3 or lower than 1/1.3, and $P < 0.05$ (**Figure 1**). Among them, there were

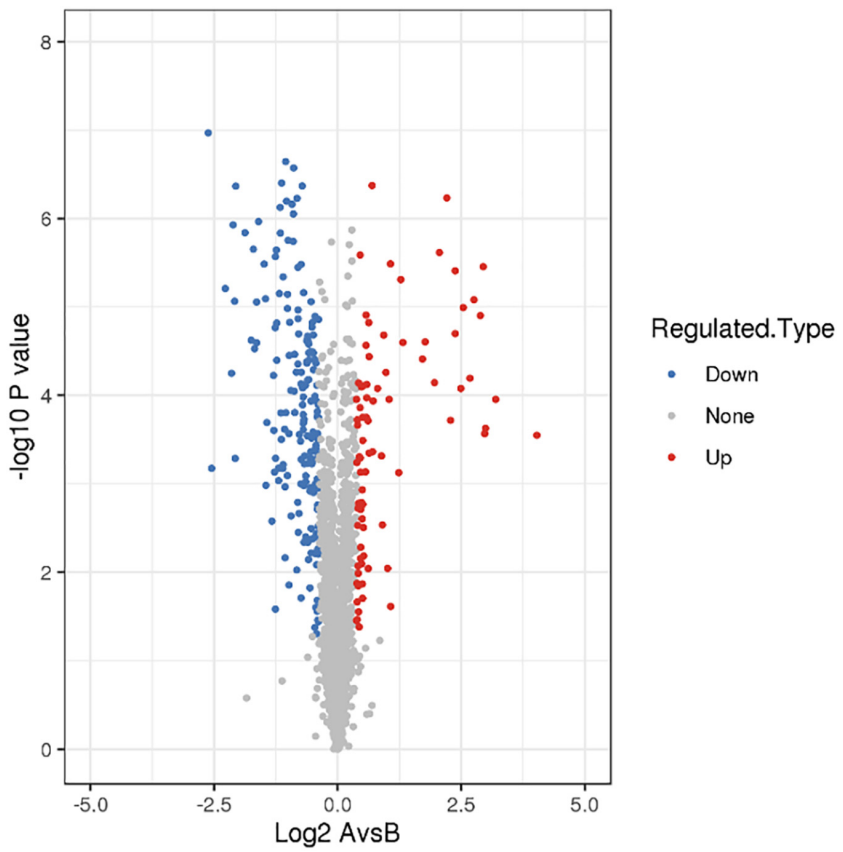

FIGURE 1 | Screening of differentially expressed proteins.

25/51 significantly up/downregulated proteins with more than two fold changes.

Gene Ontology Functional Enrichment Analysis

The 268 identified proteins were annotated by GO secondary classification, and the effect of the subinhibitory concentration of CPA 19 on multi-drug resistant *E. coli* was preliminarily analyzed (**Supplementary Table 2**). The distribution statistics of differentially expressed proteins in the three major categories of GO secondary annotations are shown in **Figure 2**. Biological process (**Figure 2A**) was mainly enriched with the proteins involved in cellular processes (29%), metabolic processes (27%), and response to stimulus (16%); in the classification of cell composition (**Figure 2B**), most of the differential proteins

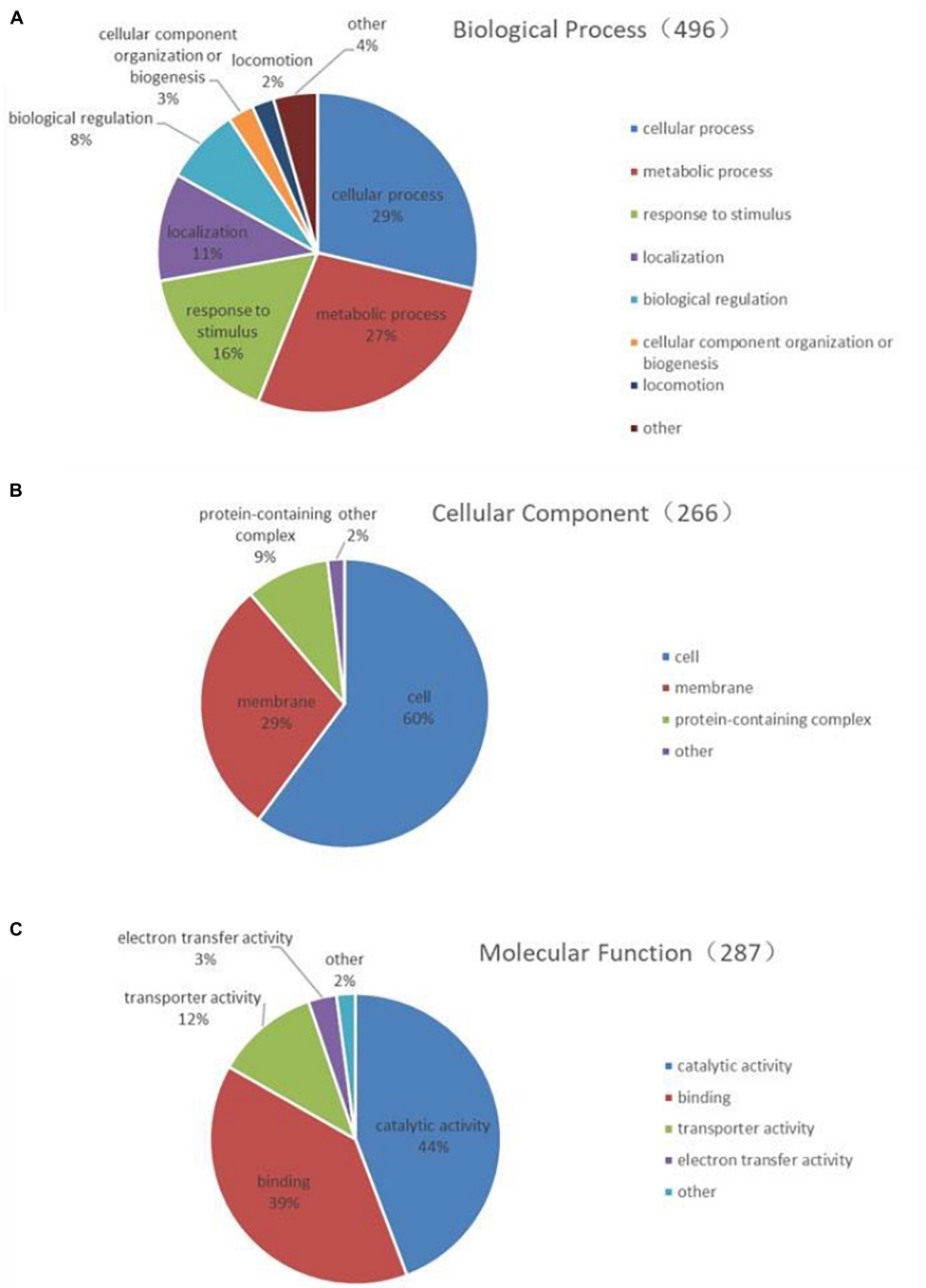

FIGURE 2 | Functional classification of differentially expressed proteins **(A)** biological process, **(B)** cell composition, and **(C)** molecular function.

were distributed in cells (60%), membranes (29%), and the protein-containing complex (9%); in the molecular function classification (**Figure 2C**), there were mainly differentially expressed proteins in catalytic activity (44%), binding (39%), and transport activity (12%).

Kyoto Encyclopedia of Genes and Genomes Pathway Enrichment Analysis

In order to further understand the effect of CPA 19 on multi-drug resistant *E. coli*, KEGG pathway enrichment analysis was performed on these 268 differentially expressed proteins (**Supplementary Table 3**). There were 11 significantly enriched ($P < 0.05$) KEGG upregulation pathways: Degradation of aromatic compounds, phenylalanine metabolism, sulfur metabolism, microbial metabolism in diverse environments, dioxin degradation, xylene degradation, monobactam biosynthesis, two-component system, selenocompound metabolism, benzoate degradation, and nitrotoluene degradation. And there were 18 significantly enriched ($P < 0.05$) KEGG downregulation pathways: Bacterial chemotaxis, arginine and proline metabolism, lysine metabolism, ABC transporter, propionate lipid metabolism, microbial metabolism in different environments, phenylalanine metabolism, beta-alanine metabolism, valine, leucine, and isoleucine degradation, fatty acid degradation, geraniol degradation, benzoic acid degradation, quorum sensing, limonene and pinene degradation, caprolactam degradation, tryptophan metabolism, two-component system, and methyl butyrate metabolism. The top 20 enriched pathways are shown in **Figure 3**.

As can be seen from **Figure 4**, the expression of some important enzymes (long-chain acyl-CoA synthetase [EC:6.2.1.3], enoyl-CoA hydratase [EC:4.2.1.17], 3-hydroxyacyl-CoA dehydrogenase [EC:1.1.1.35], acetyl-CoA acyltransferase [EC:2.3.1.16]) regulating β oxidation were significantly downregulated in the fatty acid degradation pathway, indicating that the fatty acid degradation of multidrug-resistant *E. coli* was inhibited after treatment with the subinhibitory concentration of CPA 19, and leading to blocked generation of acetyl-CoA. Similarly, in the pathway of phenylalanine metabolism (**Figure 5**) and lysine metabolism (**Figure 6**), the metabolic process of phenylalanine and lysine were also stressed by CPA 19, which led to the obstruction of the conversion of acetyl-CoA.

In the two-component system (**Figure 7**), the expression of outer membrane pore protein F (OmpF) and flagellin (FliC) in the OmpR family, as well as methyl-accepting chemotaxis protein (MCP), purine-binding chemotaxis protein CheW (CheW), sensor kinase (CheA), chemotaxis protein CheY (CheY), and glutaminase (CheB) in the chemotactic family were significantly downregulated. MCP, CheW, CheA, CheY, and CheB were also significantly enriched in the bacterial chemotaxis pathway (**Figure 8**). At the same time, the expression of serine sensor

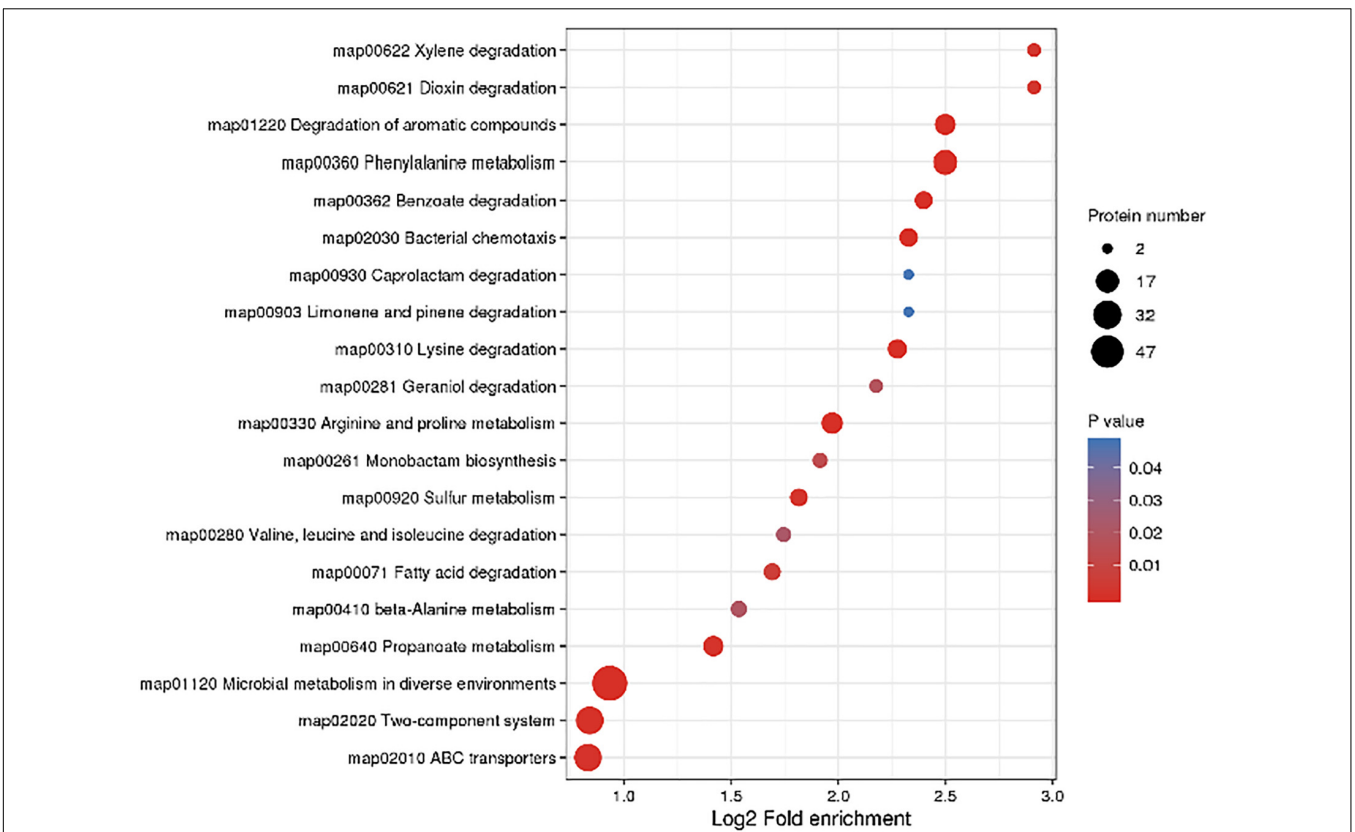

FIGURE 3 | Significantly enriched KEGG pathways.

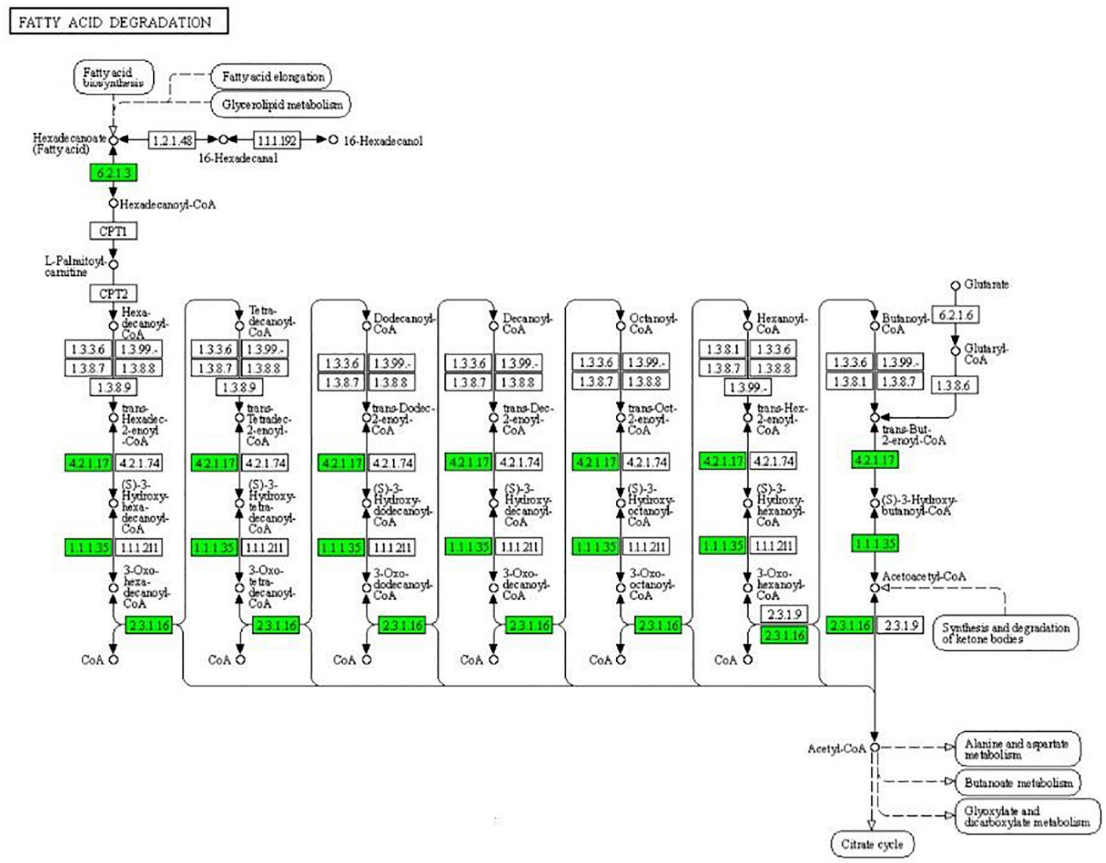

FIGURE 4 | Significantly enriched KEGG pathway: Fatty acid degradation (from the KEGG database, green frames represent downregulation, and red frames represent upregulation).

receptor (Tsr) and aspartate sensor receptor (Tar) in the bacterial chemotaxis pathway were significantly downregulated.

Parallel Reaction Monitoring Validation

We performed PRM verification on the significantly different expressed proteins in multi-drug resistant *E. coli* treated with the subinhibitory concentration of CPA 19. After evaluation of 50 differential proteins, 27 candidate proteins met the conditions, and 20 (10 upregulated, 10 downregulated) candidate proteins were selected for further verification. The results of PRM are shown in **Table 4** and prove that all 20 target proteins were quantitative and consistent with the change trend of proteomics results, which supports the credibility and reliability of proteomics.

The Results of the Interaction Between Antibiotics and Compound Phenolic Acid 19

It can be seen from **Table 5** that the FICI of CPA 19 and ceftiofur sodium was 1.5, which meant the interaction was indifferent, while the interaction of CPA 19 and azithromycin was oppositive. In addition, when combined with ceftriaxone sodium, amoxicillin, fosfomycin, sulfamonomethoxine, gatifloxacin, lincomycin, florfenicol, cefotaxime sodium, and rifampicin, additive effects were expressed. The MICs of several antibiotics (ceftriaxone sodium, amoxicillin, fosfomycin, sulfamonomethoxine, gatifloxacin, lincomycin, florfenicol, cefotaxime sodium, and rifampicin) after the combination with CPA 19 were all reduced by four times or more, which meant the antibacterial activities in vitro were significantly enhanced.

Effect of Compound Phenolic Acid 19 on Cell Membrane

As shown in **Figure 9**, the concentration of soluble protein in the culture medium of the 1/2 MIC-treated group was significantly higher than in the culture medium of control group for the previous 12 h. During 13–18 h of incubation, the extracellular soluble protein tended to decline, which might be due to the antibacterial components gradually losing their effects with the lengthening of time.

Effect of Compound Phenolic Acid 19 on Morphology

The morphological changes of *E. coli* cells are shown in **Figure 10**. The cell wall of the control group was compact, complete, smooth with uniform cytoplasm, and flagellated (**Figure 10A**). After the

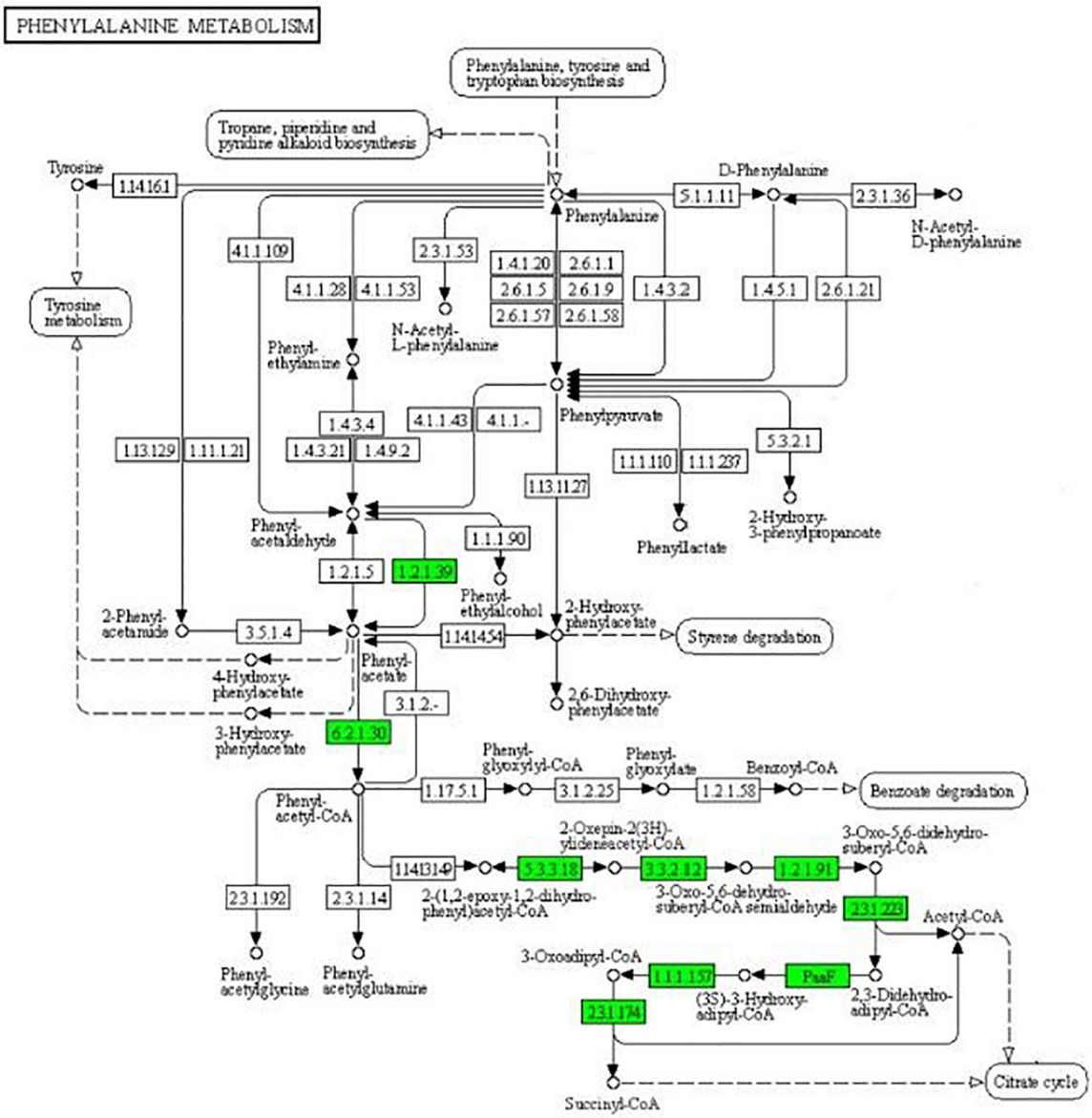

FIGURE 5 | Significantly enriched KEGG pathway: Phenylalanine metabolism (from the KEGG database, green frames represent downregulation, and red frames represent upregulation).

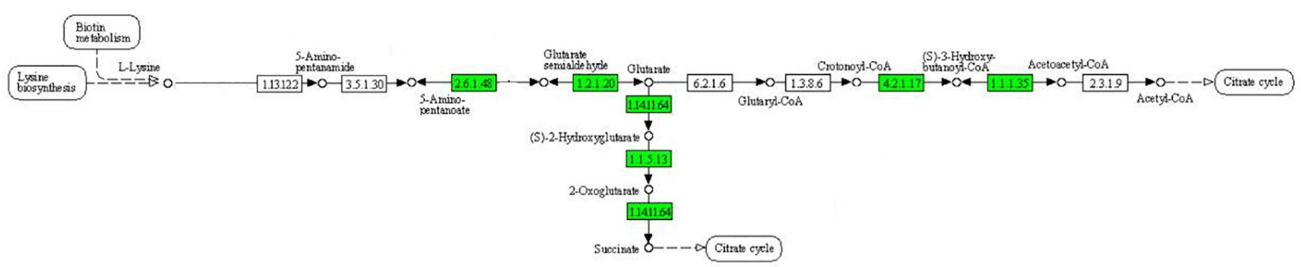

FIGURE 6 | Significantly enriched KEGG pathway: Lysine metabolism (from the KEGG database, green frames represent downregulation, and red frames represent upregulation).

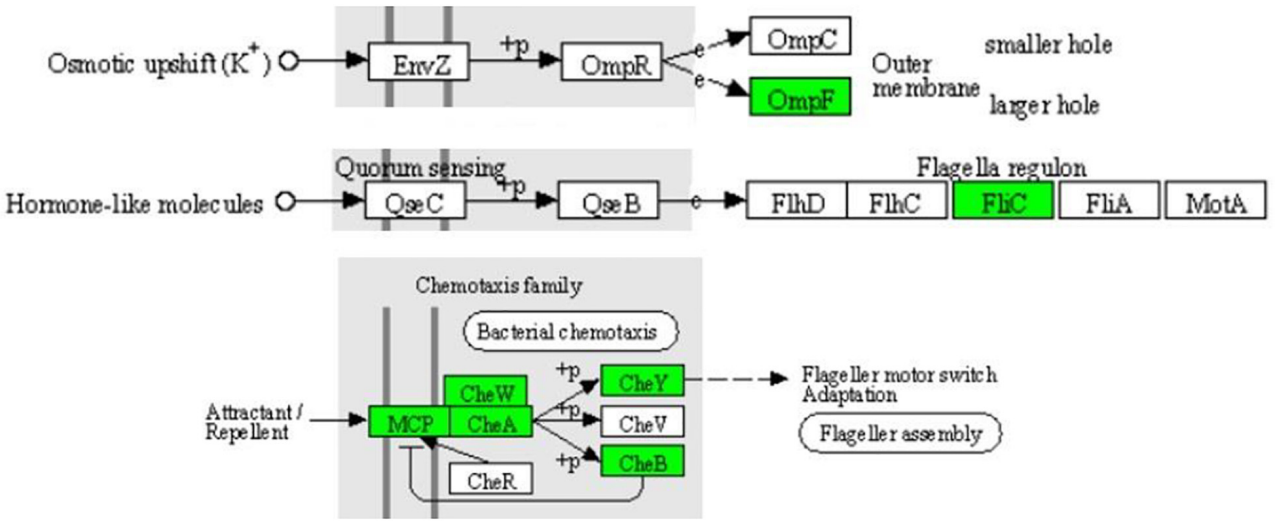

FIGURE 7 | Significantly enriched KEGG pathway: Two-component system (from the KEGG database, green frames represent downregulation, and red frames represent upregulation).

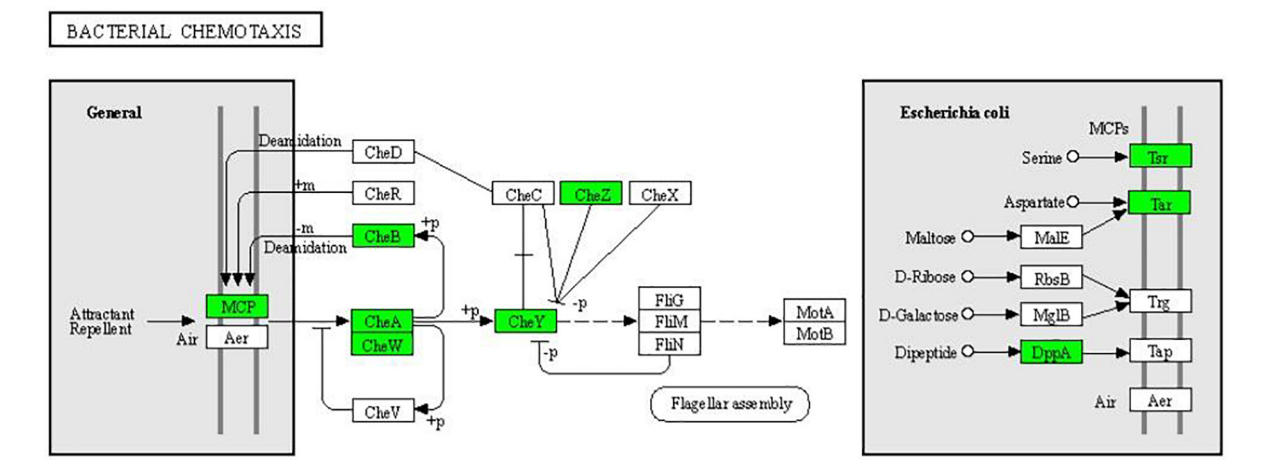

FIGURE 8 | Significantly enriched KEGG pathway: Bacterial chemotaxis (from the KEGG database, green frames represent downregulation, and red frames represent upregulation).

treatment of CPA 19 with 1/2 MIC, significant changes were observed in the bacterial cell wall, the surface area of the cell wall became rough and the boundary between the cell wall and cell membrane became fuzzy, in addition, there was no flagellum on the surface of the bacterial cell (**Figure 10B**).

DISCUSSION

Phenolic acids, a major component in plants, have been shown to have antioxidant and antimicrobial activity against Gram-positive and Gram-negative bacteria (Shen et al., 2020). In addition, the order of antibacterial activity of the active ingredients in plants is: phenol > aldehyde > ketone > alcohol > ether > hydrocarbon (Nguyen et al., 2018). In this study, 31 CPAs of five phenolic acids were used to explore new and natural antimicrobial agents against multi-resistant *E. coli*. Our results of the MICs revealed the antibacterial effects of each CPA. However, the inhibitory effect of each CPA was different against all examined strains of *E. coli*. A previous study reported that the better therapeutic action of phenolic acids can be achieved from the synergistic effect of complex plant phenolic acid mixtures rather than from individual phenolic acid compounds (Coman and Vodnar, 2020). Moreover, the composition of plants is too complex and diverse to explain its antibacterial mechanism, which greatly limits its further development in clinical applications. Therefore, five phenolic acids were selected to explore the new antimicrobial agents, which could not only make the composition clear, but also retain the better antibacterial effect

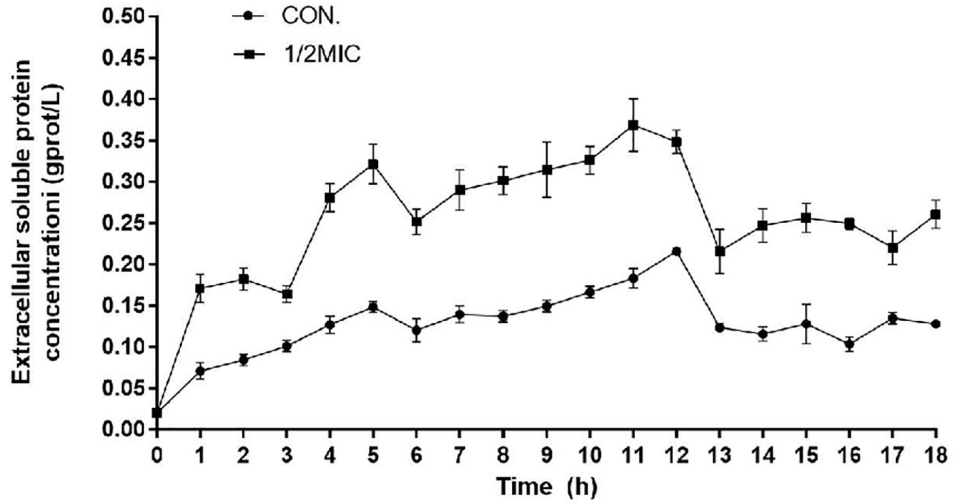

FIGURE 9 | Variation diagram of extracellular soluble protein concentrations.

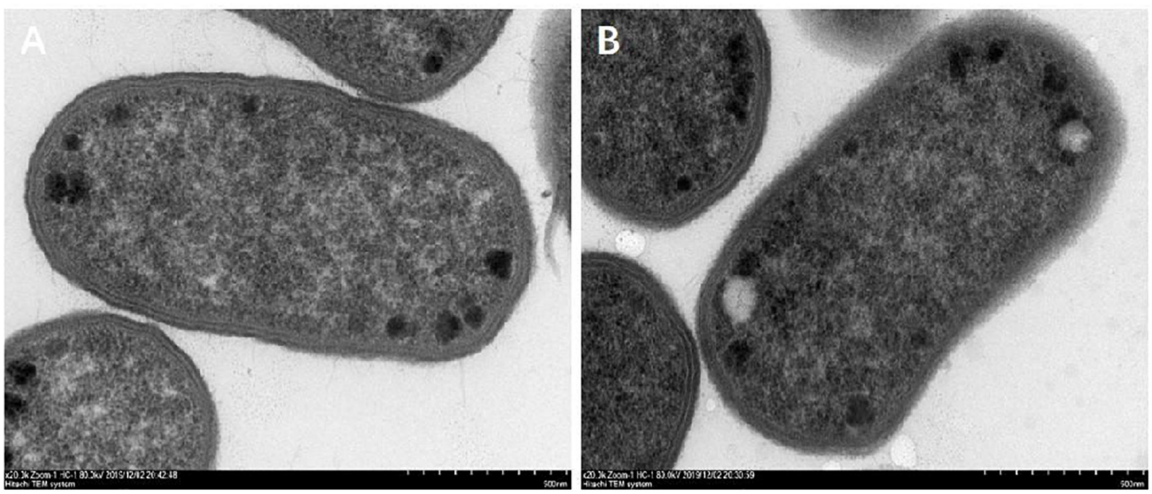

FIGURE 10 | Morphological changes after CPA treatment. **(A)** CON and **(B)** 1/2 MIC.

of plant phenolic acid mixtures when compared with single phenolic acids. Compared to all other CPAs, CPA 19 showed the best antibacterial efficacy. These findings implied that CPAs are better than individual compounds, and the best antibacterial effect of combination 19 not only elaborated the synergism of phenolic acids, but also represented its potential role against all examined multidrug-resistant *E. coli*.

The tricarboxylic acid cycle (TAC) is the final metabolic pathway through which the three nutrients (carbohydrates, lipids, and amino acids) provide and interconvert energy. These three nutrients can be metabolized to produce acetyl-CoA and then participate in TAC (Fan et al., 2021). Lipids are degraded by fatty acid degradation to generate acetyl-CoA followed by β-oxidation in the cytoplasm by activation of prokaryotic fatty acids. β-oxidation is a cyclic reaction of dehydrogenation, hydration, dehydrogenation, and thiolysis until the acyl-CoA is completely cleaved to acetyl-CoA (Yunqiao Yang et al., 2020). After CPA 19 treatment, the expression of some key enzymes in the β-oxidation process was downregulated, and the downregulation of these key proteins resulted in the decrease of acetyl-CoA. In the meanwhile, the conversion process of acetyl-CoA in the phenylalanine metabolism pathway and lysine metabolism pathway also could be impeded. These findings suggested that the CPA treatment may inhibit *E. coli* by perturbing the production of acetyl-CoA, and thus interrupt the material conversion and energy metabolism of *E. coli*.

Proteomic technology was used to analyze the differentially expressed proteins between multidrug-resistant *E. coli* and ATCC25922, which found that resistance of *E. coli* is associated with bacterial chemotaxis. Compared with ACCC25922, the expressions of Tsr, Tar, CheA, and CheW in resistant *E. coli* were significantly upregulated, indicating that these proteins are

TABLE 4 | PRM analysis of 20 candidate proteins.

Candidate proteins	A/B ratio	A/B *P* value	A/B ratio (TMT)
mhpB	331.32	0.000030	7.96
hcaB	206.09	0.000055	7.87
torA	209.67	0.000018	7.71
hcaD	82.12	0.000556	7.40
mhpC	339.84	0.000002	6.76
hcaE	202.34	0.000010	6.40
mhpD	190.85	0.000027	5.20
speF	1164.88	0.000001	4.87
mhpF	199.81	0.000028	3.42
mhpA	2.76	0.001827	2.36
CadA	0.31	0.000213	0.41
DUF1471 domain-containing protein	0.14	0.000012	0.37
yagU	0.15	0.000095	0.36
speC	0.09	0.000040	0.36
pdhR_2	0.14	0.000045	0.33
yeaW	0.10	0.000002	0.32
prpB	0.15	0.000001	0.31
cheM	0.13	0.000015	0.30
puuD	0.15	0.000031	0.27
tas	0.16	0.000005	0.23

TABLE 5 | The FICI of CPA 19 with antibiotics (E6).

Name of antibiotics	MIC (μg/mL)	Drug combination MIC		FICI	Effect
		Antibiotics (μg/mL)	CPA 19 (%)		
Ceftriaxone sodium	1600	<0.78125	6.25	0.5004	A
Amoxicillin	1600	<0.78125	6.25	0.5004	A
Fosfomycin	>3200	200	6.25	0.5625	A
Sulfamonomethoxine	>3200	<0.78125	6.25	0.5002	A
Gatifloxacin	100	6.25	6.25	0.5625	A
Lincomycin	3200	<0.78125	6.25	0.5002	A
Ceftiofur sodium	400	400	6.25	1.5	I
Florfenicol	2560	640	6.25	0.75	A
Azithromycin	100	200	6.25	2.5	O
Cefotaxime sodium	50	6.25	6.25	0.625	A
Rifampicin	1600	<0.78125	6.25	0.5004	A

MICs were calculated with the initial concentration of CPA as 1. S, synergy; A, additivity; I, indifference; O, oppositive.

involved in the resistance of multidrug-resistant *E. coli* (Xia et al., 2020). What is more, Tsr, CheA, CheW, and CheR have also been shown to be related to the resistance of *Bacillus* and *Aeromonas hydrophila* (Wada et al., 2016). In our experiment, after treatment with CPA 19, the expression of Tsr, Tar, CheA, and CheW was significantly downregulated, suggesting that treatment with CPA 19 may restore the sensitivity of multidrug-resistant *E. coli* to antibiotics.

Combination with antibiotics as a synergist is also an important direction for the development of new antimicrobial agents. Yan (2020) reported that the combination of honokiol and polymyxin showed synergistic effects on *Enterobacteriaceae*. Further investigation has shown that honokiol could directly bind to the active region of MCR-1 and had competition for the specific binding of MCR-1 to the substrate, thus restoring the sensitivity of MCR-1-positive strains to polymyxin. In our results, CPA 19 also showed additive effects when combined with ceftriaxone sodium, amoxicillin, and cefotaxime sodium, which suggested that treatment with CPA 19 can indeed enhance the sensitivity of multidrug-resistant *E. coli* to antibiotics.

There have been studies that reported that bacterial chemotaxis had a regulatory effect on bacterial flagella, especially CheA and CheY (Yuhai et al., 2008; Yuan et al., 2012). In this study, not only were CheA and CheY downregulated, but also FliC. The downregulation of these proteins was also corroborated by flagella shedding on the surface of *E. coli* treated with phenolic acid 19 which was observed via TEM.

Destruction of the cell membrane is the major target of various antimicrobial agents, including phenolic acids (Fang et al., 2018). The antibacterial effect of phenolic acids may be due to the mechanism of the phenol-membrane interaction, isolation of metal ions, and inhibition of enzyme activity (Mirjana et al., 2005; Kemperman et al., 2010; Wang et al., 2010). As an important component of the cell membrane, OmpF crosses the phospholipid bilayer which is closely related to bacterial resistance of *E. coli* and the entry and exit of intracellular molecules (Jo-Anne and Elizabeth, 1997). In the two-component system, the expression of OmpF was significantly downregulated by the treatment of CPA 19, suggesting that the integrity of the membrane of the *E. coli* may be damaged. Macromolecular proteins originally present in the cell membrane and cytoplasm, which can be used to evaluate the integrity of the cell membrane (Vivek et al., 2013; Yunbin et al., 2016). The determination of extracellular soluble protein after CPA 19 treatment confirmed the downregulation of OmpF and cell membrane damage. These findings were in great agreement with Chenjie (Chenjie et al., 2015), they reported that the treatment of lactic acid perforated cell membranes, leaked intracellular material, and changed the morphology of *E. coli*. Phenolic acids can alter the permeability of cell membranes, damage the integrity of cells, not only causing the leakage of macromolecular substances, but also making it easier for harmful substances outside the cell to enter, which will eventually lead to cell death (Moreno et al., 2006). It could be seen from the results of this study that the damage of CPA 19 to the cell membrane might be the reason for the increased sensitivity of multidrug-resistant *E. coli* to antibiotics, and the antibiotics found it easier to enter the cell interior to play a role. In short, the cell membrane was also one of the targets of CPA 19.

CONCLUSION

Compound phenolic acid 19, composed of protocatechuic acid, hydrocinnamic acid, and chlorogenic acid, had a good antibacterial effect against multi-drug resistant *E. coli*. When combined with antibiotics (ceftriaxone sodium, amoxicillin, fosfomycin, sulfamonomethoxine, gatifloxacin, lincomycin,

florfenicol, cefotaxime sodium, and rifampicin), CPA 19 increased the susceptibility of *E. coli* to antibiotics. CPA 19 could shed the flagellum of multidrug-resistant *E. coli*, break the structure of the cell membrane, and cause the macromolecules to leak out from the cell. These data suggested that the natural compounds represented by CPA 19 in this study can be further developed as novel antimicrobial agents, and the use of CPA 19 in combination with antibiotics can be further explored for expression patterns of proteins involved in *E. coli* resistance.

DATA AVAILABILITY STATEMENT

The datasets presented in this study can be found in online repositories. The names of the repository/repositories and accession number(s) can be found in the article/ **Supplementary Material**.

AUTHOR CONTRIBUTIONS

HS designed the work. All authors reviewed and approved the final manuscript.

FUNDING

This work was supported by the National Natural Science Foundation of China (31760746) and the Key Research and Development Plan of Guangxi, China (AB19245037).

SUPPLEMENTARY MATERIAL

The Supplementary Material for this article can be found online at: https://www.frontiersin.org/articles/10.3389/fmicb.2021.738896/full#supplementary-material

REFERENCES

Abraham, E. P., and Chain, E. (1988). An enzyme from bacteria able to destroy penicillin. 1940. *Rev. Infect. Dis.* 10, 677–678.

Almajano, M. P., Rosa, C., Jiménez, J. A. L., and Michael, H. G. (2007). Antioxidant and antimicrobial activities of tea infusions. *Food Chem.* 108, 55–63.

Chenjie, W., Tong, C., Hong, Y., and Min, C. (2015). Antibacterial mechanism of lactic acid on physiological and morphological properties of *Salmonella* Enteritidis, *Escherichia coli* and *Listeria monocytogenes*. *Food Control* 47, 231–236. doi: 10.1016/j.foodcont.2014.06.034

Coman, V., and Vodnar, D. C. (2020). Hydroxycinnamic acids and human health: recent advances. *J. Sci. Food Agric.* 100, 483–499. doi: 10.1002/jsfa.10010

Cushnie, T. P., and Lamb, A. J. (2005). Antimicrobial activity of flavonoids. *Int. J. Antimicrob. Agents* 26, 343–356. doi: 10.1016/j.ijantimicag.2005.09.002

Efenberger, S. M., Nowak, A., and Czyzowska, A. (2021). Plant extracts rich in polyphenols: antibacterial agents and natural preservatives for meat and meat products. *Crit. Rev. Food Sci. Nutr.* 61, 149–178.

Fan, J., Zhou, J., Su, S., Yu, Y., Chen, L., Le, Y., et al. (2021). Quantitative detection and metabolic profile analysis of metabolites of tricarboxylic acid cycle and amino acids in psoriasis serum before and after receiving monoclonal antibody treatment by one-pot GC-MS derivatization. *Int. J. Mass Spectrom.* 460:116478. doi: 10.1016/j.ijms.2020.116478

Fang, L., Fengting, W., Lihui, D., Tong, Z., Michael, P. D., Daoying, W., et al. (2018). Antibacterial and antibiofilm activity of phenyllactic acid against *Enterobacter cloacae*. *Food Control* 84, 442–448. doi: 10.1016/j.foodcont.2017.09.004

Jo-Anne, H., and Elizabeth, W. (1997). Molecular characterization of the *Serratia marcescens* OmpF porin, and analysis of *S. marcescens* OmpF and OmpC osmoregulation. *Microbiology* 143, 2797–2806. doi: 10.1099/00221287-143-8-2797

Kemperman, R. A., Bolca, S., Roger, L. C., and Vaughan, E. E. (2010). Novel approaches for analysing gut microbes and dietary polyphenols: challenges and opportunities. *Microbiology (Reading)* 156(Pt 11), 3224–3231. doi: 10.1099/mic.0.042127-0

Kim, T., Kim, Y., Kim, S., Lee, J., Park, C., and Kim, H. (2010). Identification and distribution of Bacillus species in doenjang by whole-cell protein patterns and 16S rRNA gene sequence analysis. *J. Microbiol. Biotechnol.* 20, 1210–1214.

Kurek, A., Nadkowska, P., Pliszka, S., and Wolska, K. I. (2012). Modulation of antibiotic resistance in bacterial pathogens by oleanolic acid and ursolic acid. *Phytomedicine* 19, 515–519. doi: 10.1016/j.phymed.2011.12.009

Lorian, V. (2005). *Antibiotics in Laboratory Medicine*. Philadelphia, PA: Lippincott Williams & Wilkins.

Martina, B. (2010). Comparison of the antioxidant capacity and the antimicrobial activity of black and green tea. *Food Res. Int.* 43, 1379–1382.

Mirjana, A., John, V. C., Bruno, D. M., Griet, D., Carmen, S., Marc, V., et al. (2005). Iron-chelation properties of phenolic acids bearing catechol and galloyl groups. *Food Chem.* 98, 23–31. doi: 10.1016/j.foodchem.2005.05.044

Moreno, S., Scheyer, T., Romano, C. S., and Vojnov, A. A. (2006). Antioxidant and antimicrobial activities of rosemary extracts linked to their polyphenol composition. *Free Radic. Res.* 40, 223–231. doi: 10.1080/10715760500473834

Nguyen, H. V., Meile, J. C., Lebrun, M., Caruso, D., Chu-Ky, S., and Sarter, S. (2018). Litsea cubeba leaf essential oil from Vietnam: chemical diversity and its impacts on antibacterial activity. *Lett. Appl. Microbiol.* 66, 207–214. doi: 10.1111/lam.12837

Paitan, Y. (2018). "Current trends in antimicrobial resistance of *Escherichia coli*," in *Escherichia coli, A Versatile Pathogen*, eds G. Frankel and E. Z. Ron (Cham: Springer International Publishing), 181–211.

Roth, N., Kasbohrer, A., Mayrhofer, S., Zitz, U., Hofacre, C., and Domig, K. J. (2019). The application of antibiotics in broiler production and the resulting antibiotic resistance in *Escherichia coli*: a global overview. *Poult. Sci.* 98, 1791–1804. doi: 10.3382/ps/pey539

Shen, H., Tong, X., Yang, J., Yu, L., Zhou, H., Wang, Y., et al. (2020). Biotransformation of natural hydroxycinnamic acids by gut microbiota from normal and cerebral ischemia-reperfusion injured rats: a comparative study. *Food Funct.* 11, 5389–5395. doi: 10.1039/d0fo00775g

Sidhu, N. S., Schreiber, K., Propper, K., Becker, S., Uson, I., Sheldrick, G. M., et al. (2014). Structure of sulfamidase provides insight into the molecular pathology of mucopolysaccharidosis IIIA. *Acta Crystallogr. D Biol. Crystallogr.* 70(Pt 5), 1321–1335. doi: 10.1107/S1399004714002739

Smekalova, M., Aragon, V., Panacek, A., Prucek, R., Zboril, R., and Kvitek, L. (2016). Enhanced antibacterial effect of antibiotics in combination with silver nanoparticles against animal pathogens. *Vet. J.* 209, 174–179. doi: 10.1016/j.tvjl.2015.10.032

Vivek, K. B., Ajay, S., and Kwang-Hyun, B. (2013). Antibacterial mode of action of *Cudrania tricuspidata* fruit essential oil, affecting membrane permeability and surface characteristics of food-borne pathogens. *Food Control* 32, 582–590. doi: 10.1016/j.foodcont.2013.01.032

Wada, K., Kobayashi, J., Furukawa, M., Doi, K., Ohshiro, T., and Suzuki, H. (2016). A thiostrepton resistance gene and its mutants serve as selectable markers in *Geobacillus kaustophilus* HTA426. *Biosci. Biotechnol. Biochem.* 80, 368–375. doi: 10.1080/09168451.2015.1079478

Wang, W., Du, Y., and Song, H. (2010). α-Glucosidase and α-amylase inhibitory activities of guava leaves. *Food Chem.* 123, 6–13. doi: 10.1016/j.foodchem.2010.03.088

Xia, Z., Rui, L., Haixia, G., Wenjing, W., Jun, X., Ruiliang, Z., et al. (2020). Proteomics difference between *Escherichia coli* multidrug resistant and susceptible strains. *J. Northwest. A F Univ. (Nat. Sci. Ed.)* 48, 40–48. doi: 10.13207/j.cnki.jnwafu.2020.01.006

Yan, G. (2020). *Extraction of Honokiol and Its Enhancement of the Antibacterial Activity of Polymyxin Against mcr-1-Positive Bacteria*. Master's thesis. Jilin: Jilin University.

Yang, Y., Chen, Y., Zhang, G., Sun, J., Guo, L., Jiang, M., et al. (2020). Transcriptomic analysis of *Staphylococcus aureus* under the stress condition caused by *Litsea cubeba* L. Essential oil via RNA sequencing. *Front. Microbiol.* 11:1693. doi: 10.3389/fmicb.2020.01693

Yuan, J., Branch, R. W., Hosu, B. G., and Berg, H. C. (2012). Adaptation at the output of the chemotaxis signalling pathway. *Nature* 484, 233–236. doi: 10.1038/nature10964

Yuhai, T., Thomas, S. S., and Howard, C. B. (2008). Modeling the chemotactic response of *Escherichia coli* to time-varying stimuli. *Proc. Natl. Acad. Sci. U.S.A.* 105, 14855–14860. doi: 10.1073/pnas.0807569105

Yunbin, Z., Xiaoyu, L., Yifei, W., Pingping, J., and SiewYoung, Q. (2016). Antibacterial activity and mechanism of cinnamon essential oil against *Escherichia coli* and *Staphylococcus aureus*. *Food Control* 59, 282–289. doi: 10.1016/j.foodcont.2015.05.032

Yun-Seok, C., Jay, J. O., and Kye-Heon, O. (2010). Antimicrobial activity and biofilm formation inhibition of green tea polyphenols on human teeth. *Biotechnol. Bioprocess Eng.* 15, 359–364. doi: 10.1007/s12257-009-0195-8

Conflict of Interest: The authors declare that the research was conducted in the absence of any commercial or financial relationships that could be construed as a potential conflict of interest.

Publisher's Note: All claims expressed in this article are solely those of the authors and do not necessarily represent those of their affiliated organizations, or those of the publisher, the editors and the reviewers. Any product that may be evaluated in this article, or claim that may be made by its manufacturer, is not guaranteed or endorsed by the publisher.

frontiers in Microbiology

ORIGINAL RESEARCH
published: 02 December 2021
doi: 10.3389/fmicb.2021.796158

Nutrient L-Alanine-Induced Germination of *Bacillus* Improves Proliferation of Spores and Exerts Probiotic Effects *in vitro* and *in vivo*

*Shuang Lu[1], Xianyin Liao[1], Li Zhang[1], Ying Fang[1], Meixian Xiang[2] and Xiaohua Guo[1]**

[1]College of Life Science, South-Central University for Nationalities, Wuhan, China, [2]School of Pharmaceutical Sciences, South-Central University for Nationalities, Wuhan, China

OPEN ACCESS

Edited by:
Wang Jiajun,
Northeast Agricultural University, China

Reviewed by:
Jin Wan,
Nanchang University, China
Xi Ma,
China Agricultural University, China
Xiao Yuncai,
Huazhong Agricultural University, China

***Correspondence:**
Xiaohua Guo
guo_xh@hotmail.com

Specialty section:
This article was submitted to Antimicrobials, Resistance and Chemotherapy, a section of the journal Frontiers in Microbiology

Received: 16 October 2021
Accepted: 10 November 2021
Published: 02 December 2021

Citation:
Lu S, Liao X, Zhang L, Fang Y, Xiang M and Guo X (2021) Nutrient L-Alanine-Induced Germination of Bacillus Improves Proliferation of Spores and Exerts Probiotic Effects in vitro and in vivo. Front. Microbiol. 12:796158. doi: 10.3389/fmicb.2021.796158

As alternatives to antibiotics in feed, probiotic *Bacillus* carries multiple advantages in animal production. Spores undergo strain-related germination in the gastrointestinal tract, but it is still unknown whether the probiotic function of the *Bacillus* depends on the germination of spores *in vivo*. In this study, based on 14 potential probiotic *Bacillus* strains from fermented food and feed, we detected the germination response of these *Bacillus* spores in relation to different germinating agents. The results showed the germination response was strain-specific and germinant-related, and nutrient germinant L-alanine significantly promoted the growth of strains with germination potential. Two strains of *Bacillus subtilis*, S-2 and 312, with or without a high spore germination response to L-alanine, were selected to study their morphological and genic differences induced by L-alanine through transmission electron microscopy and comparative transcriptomics analysis. Consequently, after L-alanine treatment, the gray phase was largely increased under microscopy, and the expression of the germination response genes was significantly up-regulated in the *B. subtilis* S-2 spores compared to the *B. subtilis* 312 spores ($p < 0.05$). The protective effect of L-alanine-induced spore germination of the two strains was comparatively investigated both in the IPEC-J2 cell model and a Sprague–Dawley (SD) rat model challenged by enterotoxigenic *Escherichia coli* K99. The result indicated that L-alanine helped *B. subtilis* S-2 spores, but not 312 spores, to decrease inflammatory factors (IL-6, IL-8, IL-1β, TNF-α; $p < 0.05$) and promote the expression of occludin in IPEC-J2 cells. Besides, supplement with L-alanine-treated *B. subtilis* S-2 spores significantly improved the growth of the SD rats, alleviated histopathological GIT lesions, and improved the ratio of jejunal villus length to crypt depth in comparison to the *B. subtilis* S-2 spores alone ($p < 0.05$). Improved species diversity and abundance of fecal microbiota were only observed in the group with L-alanine-treated S-2 spores ($p < 0.05$). The study demonstrates L-alanine works well as a probiotic *Bacillus* adjuvant in improving intestinal health, and it also provides a solution for the practical and accurate regulation of their use as antibiotic alternatives in animal production.

Keywords: *Bacillus*, probiotics, L-alanine, spores, germination

INTRODUCTION

Antimicrobial resistance has been recognized as one of the top three major threats to public health by The World Health Organization (Xiong et al., 2018). The antimicrobials applied in feed animals promote the emergence and spread of antimicrobial resistance (Gil-Gil et al., 2019). Several countries have restricted or banned the use of antimicrobials in feed. As alternatives to antibiotics, probiotics have been widely used in feed industries for preventing infections by alleviating antimicrobial-mediated resistance (Ouwehand et al., 2016; Mingmongkolchai and Panbangred, 2018; Abd El-Hack et al., 2020). Particularly, as one of the general sources of probiotics, the spore-forming *Bacillus* species offer several advantages, such as heat stability and resistance to adverse environments of low pH and bile salt toxicity, in comparison to non-spore-formers (Davies, 2010; Setlow, 2010). Spore formation increases the survival of living cells during the manufacture and storage processes, including freezing, drying, thawing, and granulation. Additionally, spores have a stronger ability to survive passage through the stomach and to proliferate in the digestive tract (Casula and Cutting, 2002). Therefore, the *Bacillus* probiotics seemed to be more suitable for application in the feed industry because of their processing and storage stabilities and low production costs.

The efficacy of *Bacillus* species as probiotics has been demonstrated in the control of pathogens (Zhang et al., 2017; Rajabi et al., 2020; Soto, 2021), improvement of intestinal homeostasis (Fujiya et al., 2007; Kang et al., 2021), and anti-oxidant and immune-modulatory abilities in animals (Du et al., 2018; Jing et al., 2018; Mirk et al., 2021). However, in comparison to non-spore-formers, *Bacillus* species as probiotics have been found to have a complexity in cell morphology, including spores and vegetative cells, which are modulated by sprouting and sporulation factors (Tam et al., 2006; Bernardeau et al., 2017). Due to the anaerobic or slightly aerobic environment of the gastrointestinal tract (GIT), the dynamics of germination and sporulation in the GIT and the corresponding mechanism of *Bacillus* spores on the intestinal homeostasis are not easily explored since various pathways are involved in the behaviors (Leser et al., 2010; Bernardeau et al., 2017).

Vegetative cells and spores might show a different effect on the protective activities *in vitro* and *in vivo*. Treatment with *Bacillus megaterium* SF185 spores has been found to prevent or reduce the damages caused by oxidative stress both at the level of Caco-2 cells and in a dextran sodium sulfate-induced mouse model (Mazzoli et al., 2019). *Bacillus* SC06 vegetative cells alleviated oxidative stress-induced disorders and apoptosis *via* p38-mediated autophagy in rat jejunum and IEC-6 cells (Wu et al., 2019). Bs 29784 vegetative cells were found to significantly reduce the upregulation of iNOS protein levels in Caco-2 cells (Rhayat et al., 2019). The vegetative variants of Bs PB6-PR induced higher levels of IL-10, TNF-α, and IFN-γ than prepared spore powder (Selvam et al., 2009). Huang et al. showed that the vegetative cells of *Bacillus subtilis* could stimulate expression of the Toll-like receptors (TLR) genes containing TLR2 and TLR4, whereas spores could not (Huang et al., 2008). In some comparative studies, the *Bacillus* strain of Bs 29784, but not Bs A and Bs B, was able to specifically decrease IL-8 production and increase the transepithelial electrical resistance of differentiated Caco-2 cells, and *Bacillus* SC06 showed more significant intestinal tissue repair and antioxidant properties than SC08 in a rat model (Rhayat et al., 2019; Wu et al., 2019). Therefore, the protective effect of *Bacillus* might be strain-specific and cell type-related.

Moreover, the activity of postbiotics is closely associated with the mode of action of probiotic *Bacillus*. The International Scientific Association of Probiotics and Prebiotics has defined postbiotics as the "preparation of inanimate microorganisms and/or their components that confers a health benefit on the host" (Salminen et al., 2021). Some antimicrobial substances produced by *Bacillus*, including subtilin, coagulin, surfactin, and bacilysin, were considered one of the main mechanisms of pathogen exclusion in the GIT (Urdaci et al., 2004). Piewngam et al. demonstrated that a *Bacillus* lipopeptide, fengycin, restricted intestinal *Staphylococcus aureus* colonization by inhibiting quorum sensing (Piewngam et al., 2018). The *B. subtilis*-derived competence and sporulation factor, as a quorum-sensing pentapeptide, activated the Akt and p38 MAPK pathways and protected epithelial cells from oxidant stress in the intestine (Di Luccia et al., 2016).

When living *Bacillus* cells are ingested into the intestine in the form of spores, the spores usually undergo a life cycle consisting of germination, growth, and re-sporulation, which is responsible for the metabolic and immunomodulatory mechanisms in *Bacillus* (Tam et al., 2006; Bernardeau et al., 2017). Studies on the *Bacillus* germination dynamics were largely conducted *in vitro,* and the germination of *Bacillus* spores was strain-specifically triggered by both nutrient and non-nutrient germinants (Real et al., 2005; Lovdal et al., 2012; Amon et al., 2020; Christie and Setlow, 2020). Moreover, *Bacillus* germination and sporulation processes in the GIT have also been observed in many studies in broilers, pigs, human beings, and mice (Jadamus et al., 2001; Casula and Cutting, 2002; Leser et al., 2010; Ghelardi et al., 2015). However, to the best of our knowledge, the association between the selection of *Bacillus* strains and germination potential *in vitro* and the corresponding protective effect *in vivo* has not yet been investigated. Nutrient germinants were hypothesized to induce the spore germination of a *Bacillus* strain in the GIT and improve the metabolic activity and the protective effect on intestinal homeostasis. Thus, the present study aimed to identify and characterize *Bacillus* spores with germination potential and to determine whether the germination was improved by L-alanine as a germinant to stimulate the protective efficacy in IPEC-J2 cells and rats challenged by *Escherichia coli* (ETEC) K99.

MATERIALS AND METHODS

Bacterial Strains

Fourteen wild-type *Bacillus* strains were originally isolated from fermented food and feed. They were screened for potential spore-forming probiotics based on the functionalities, safety,

and stress resistance reported by Mingmongkolchai and Panbangred (2018). All the strains were identified according to morphology, physiological and biochemical tests, and sequencing of 16S rDNA. *B. subtilis* 168 was used as the standard model strain from *Bacillus* species, and it is also used as a reference strain to compare the difference in germination response of *Bacillus* from other strains (Moir et al., 1991; Alzahrani and Moir, 2014). The evolutionary trees (**Supplementary Figure 1**) of the strains involved in the study were drawn according to the 16S rDNA sequences of each isolated strain. The ETEC K99 was purchased from the China Center of Veterinary Culture Collection (CVCC; C83529). The ETEC K99 was activated and cultured in nutrient broth. All the strains used in the study were stored in 20% sterile glycerol at −80°C until needed.

Preparation of the Spores

The *Bacillus* strains were grown and sporulated in Difco sporulation medium (DSM) from 48 h to 60 h at 37°C. The spores were harvested after a heat shock of 80°C for 15 min. The spores were washed twice and then resuspended in phosphate-buffered saline (PBS) buffer. Each spore suspension was sampled immediately to determine the number of colony-forming units (CFUs) per milliliter before use. The spore concentration was adjusted depending on the requirements of each experiment. The spores were freshly prepared for each experiment.

Bacillus Spore Germination Assay

Eight nutrient mediators that might be present in the intestine were used as the germination agents, including D-glucose, L-alanine, L-glutamine, L-aspartate, L-valine, L-lysine, L-glutamate, and complex sprouting agents AGFK (100 mm L-aspartate +10 mm D-glucose +10 mm D-fructose +10 mm KCl) based on the report of Yi and Setlow (2010). Each germination agent was dissolved in 50 mm Tris–HCl buffer (pH 8) and prepared to a concentration of 100 mm. Freshly prepared spore suspensions were diluted by Tris–HCl buffer to a concentration of approximately 10^7 CFU/ml. Then, the dilution was treated immediately to check the germination potential based on the release of dipicolinic acid (DPA) from the endospores. Two methods used were for heat shock and germinant–triggered germination based on the method of Liang et al. (2018). For the heat shock, the spore suspensions were autoclaved in screw-cap glass test tubes at 121°C for 10 min for the full release of DPA. After cooling, the supernatants containing the DPA were sampled after centrifugation (2,500 × *g* for 10 min) and tested for fluorescence intensity based on the method of Liang et al. (2018). Briefly, the supernatants were mixed with $EuCl_3$ (2 mm) and 1,2-cyclohexanediamine-N,N,N′N′-tetraacetic acid (CyDTA; 2 mm) in the proportion of 1:4.5:4.5 by a vortex oscillator. The fluorescence intensity of the complexes were quantified by a Hitachi F-7000 spectrofluorophotometer (Hitachi Ltd., Tokyo, Japan; 272 nm excitation and 619 nm emission) with the pre-set parameters of a 5 nm/10 nm slit and a photo-multiplier tube voltage of 700 V. The fluorescence intensity of the supernatants treated by heat shock was designated as AU1.

In the germinant–treated method, the freshly prepared spores were centrifuged and resuspended in 100 mm germinant solution buffered by 50 mm Tris–HCl. The fluorescence intensity of the germinant–treated supernatants were tested as AU2. The germination potential of each spore treated by different germinants was evaluated based on the relative fluorescence intensity expressed by AU2/AU1. The time and concentration effects on the germination of the spores treated by L-alanine as a universal germinant were studied by setting specific L-alanine concentration gradients and time sampling gradients, then testing the relative fluorescence intensity.

Spore Growth Assay

One strain from each *Bacillus* species (*B. subtilis*, *Bacillus cereus*, *Bacillus licheniformis*, and *Bacillus coagulans*) with significant germination potential was selected for the spore growth assay. One strain of *B. subtilis* without germination response to 100 mm L-alanine was included as the control. The synthetic medium (10 g/L glucose, 10 g/L urea, 5 g/L diamine citrate, 1.5 g/L KH_2PO_4, 1.5 g/L $NaNO_3$; pH 7.0) in a 50 ml/250 ml Erlenmeyer flask was used to exclude the possible interference of nutrient germinants. For each strain, two experimental treatments were set with three replications, including a spore-treated group and an L-alanine-pretreated group. In the spore-treated group, 200 µl of the spore suspensions with the initial concentration of 10^8 CFU/ml was directly inoculated into the 50 ml synthetic medium. In the L-alanine-pretreated group, the 10^8 CFU/ml spore suspensions were centrifuged at 12,000 rpm for 3 min, and the pellets were resuspended in Tris–HCl buffer containing 100 mm L-alanine. After 30 min of incubation at 37°C, the bacteria were collected, washed twice, and resuspended in PBS buffer in an equal volume. Then, 200 µl of the L-alanine pretreated-spore suspensions were inoculated into the 50 ml synthetic medium. The culture conditions were set on a rotating shaker at 37°C and 200 rpm. The samples were selected at 3 h intervals for the detection of cell optical density at 600 nm.

Transmission Electron Microscopy

To monitor the germination in the spores treated by L-alanine, purified spores were concentrated and then resuspended in Tris–HCl buffer or Tris–HCl buffer containing 100 mm L-alanine respectively, followed by incubation with agitation at 37°C for 30 min. The collected cells were fixed in 2.5% glutaraldehyde for 4 h at 4°C and post-fixed with 1% osmium tetroxide in PBS (pH 7.4) for 2 h at 20°C. The samples were washed three times with PBS and then dehydrated with graded series of alcohol (50, 70, 80, 90, 95, 100% for 15 min, respectively). Subsequently, the samples were embedded into Epon that were polymerized at 65°C for more than 48 h. Finally, the samples were cut into 60–80 nm sections and stained with uranyl acetate, and counterstained with lead citrate. The Transmission electron microscopy (TEM) images were captured using a transmission electron microscope (Hitachi, HT7800/HT7700).

TABLE 1 | Primers for RT-qPCR.

Primers	Sequence (5'→3')
GAPDH-F	TGGTGAAGGTCGGAGTGAAC
GAPDH-R	GGAAGATGGTGATGGGATTTC
IL-1β-F	GGCCATAGTACCTGAACCCG
IL-1β-R	CCAAGGTCCAGGTTTTGGGT
IL-6-F	TGGCAGAAAAAGACGGATGC
IL-6-R	TACTAATCTGCACGGCCTCG
IL-8-F	GCCTTCTTGGCAGTTTTCCTG
IL-8-R	TGGAAAGGTGTGGAATGCGTA
TNF-α-F	CAACGGCGTGAAGCTGAAAG
TNF-α-R	AGACCCCTCCCAGGTAGATG

Comparative Transcriptomics Analysis

Based on the results of the spore germination assay and growth assay, two strains of *B. subtilis*, S-2 and 312, were included in the comparative transcriptomics analysis. The spores of *B. subtilis* S-2 were selected because of their high germination potential to L-alanine. The spores of *B. subtilis* 312 without a response to L-alanine were used as the control. Similar to the treatments in the spore growth assay, the two strains were inoculated into the synthetic medium according to the spore-treated group and L-alanine-pretreated group, respectively. The cells with or without L-alanine pretreatment were cultured in the synthetic medium for 9 h, and then collected. The pellets were washed three times with PBS and resuspended in 100 μl of lysozyme (10 mg/ml) in a water bath at 37°C for 30 min. Then, 400 ml of TRIzol reagent (Invitrogen Life Technologies) was added, and total RNA was extracted according to the instructions provided by the manufacturer. The quality of the total RNA was assessed by NanoDrop 2000 (Thermo Scientific) and Bioanalyzer system (Agilent). Then ribosomal RNA was removed using the Zymo-Seq RiboFree Total RNA Library Kit (Irvine, CA, United States). The RNA was then fragmented to 200–300 bp, followed by random primers and reverse transcriptase to synthesize the first strand cDNA and then the second strand of cDNA. The fragments were purified using the AMPure XP beads (Beckman Coulter, Beverly, CA, United States) to enrich cDNA of 400–500 bp. The library was then quantified by the Agilent high sensitivity DNA assay and finally sequenced on Hiseq X ten platform (Illumina).

The raw data were filtered according to the following criteria: (1) Cutadapt (v1.15) is used to remove the adaptor sequence at the 3′ end; (2) the reads are removed if their average quality score is lower than Q20. Then, the filtered reads are mapped to the reference genomes[1] using the Bowtie2 tool (v2.2.6).[2] According to the sequence alignment results, the expression level of each gene was calculated, and the expression level was normalized by Fragments Per Kilo bases Per Million Fragments (FPKM). DESeq (version 1.18.0) was used to identify the differentially expressed genes (DEGs). The DEGs were selected with $|\log_2(\text{fold change})| > 1$ and a value of $p < 0.05$. All genes were mapped to terms in the Gene Ontology (GO) database and calculated the numbers of DEGs in each Term. Using topGO to perform GO enrichment analysis and ClusterProfiler (3.4.4) software carry out the enrichment analysis of the KEGG pathway on the differential genes. A value of $p < 0.05$ was considered statistically significant.

[1]https://www.ncbi.nlm.nih.gov/assembly/GCF_000009045.1/
[2]http://bowtie-bio.sourceforge.net/index.shtml

Co-culture of IPEC-J2 With Spores and ETEC Infection

The IPEC-J2 cells were purchased from the China Center for Type Culture Collection and were cultured in T25 flasks with Dulbecco's modified Eagle's medium (DMEM) with 10% fetal bovine serum (Gibco) and 1% penicillin–streptomycin solution at 37°C in 5% CO_2. The IPEC-J2 cells were plated on 24- or 6-well plates at a density of 10^5 cells/cm^2 before the experiments. Spores of *B. subtilis* S-2 and 312 were pretreated with PBS or PBS containing L-alanine (100 mm) for 2 h at 37°C, and then they were washed three times with PBS. The IPEC-J2 cells were incubated with PBS or L-alanine pretreated *B. subtilis* S-2 and 312 spores (10^7 CFU/ml) for 16 h. Then, the cells were infected with ETEC (10^6 CFU/ml) for another 12 h. Finally, the cells were harvested for quantitative reverse transcription polymerase chain reaction (RT-qPCR) and Western blot (WB) analysis.

RT-qPCR Analysis of the Inflammatory Cytokines

Total RNA of the IPEC-J2 cells was isolated with TRIzol reagent (Invitrogen), following the manufacturer's instructions. The mRNAs were reverse transcribed using reverse transcriptase (HiScript II Q Select RT SuperMix for qPCR, Vazyme, Nanjing, China). qPCR was performed with SYBR Green qPCR Master Mix (qPCR SYBR Green Master Mix, Vazyme). GAPDH was used as a housekeeping gene. The expression levels of the inflammatory cytokines, IL-6, IL-8, IL-1β, and TNF-α, were calculated based on the change-in-cycling-threshold ($2^{-\Delta\Delta Ct}$) method. The primers used in qPCR are shown in **Table 1**.

WB Analysis of the Tight Junction Proteins and IL-6

The IPEC-J2 cells were first lysed with RIPA lysis buffer (Servicebio, Wuhan, China, G2002) for 30 min on ice, and the supernatant was collected after centrifugation. The protein concentration was determined by bicinchoninic acid assay (Servicebio, Protein Quantification Kit G2026). A total of 40 μg of protein mixed with 5 × SDS loading buffer was electrophoresed in an 8–12% sodium dodecyl sulfate polyacrylamide gel electrophoresis and transferred to a polyvinylidene fluoride membrane. The membrane with protein blots was first blocked in tris-buffered saline with 0.1% Tween-20 containing 5% bull serum albumin, then incubated with the primary antibody at 4°C overnight, and finally incubated with horseradish peroxidase (HRP)-labeled secondary antibody at room temperature for 1 h, and later washed five times. Finally, the pictures were taken by a Gel Imager System (Bio-Rad, United States). The antibodies used in this study are listed in **Table 2**.

TABLE 2 | The antibodies used in WB and IFA analysis.

Antibodies	Source	Identifier
Claudin1 rabbit polyclonal antibody	protrintech	Cat#13050-1-AP
Occludin mouse polyclonal antibody	protrintech	Cat#66378-1-Ig
IL6 rabbit pAb	ABclonal technology	Cat#A0286
GAPDH mouse mAb	ABclonal technology	Cat#AC002
HRP goat anti-mouse IG(H + L)	ABclonal technology	Cat#AS003
Anti-rabbit IgG HRP-linked antibody	Cell signaling technology	Cat#7074S
DAPI	Beyotime	Cat#C1005

Animal Experiments

Thirty-six weaned male Sprague–Dawley (SD) rats were randomly divided into six treatment groups with six rats per treatment. After 3 days of acclimation, the rats underwent six experimental treatments as follows: (1) the CON group: daily oral administration of PBS; (2) the ETEC group: daily oral administration of PBS for 14 days, followed by ETEC K99 oral gavage challenge; (3) the S-2 + ETEC group: daily oral administration of *B. subtilis* S-2 spore suspensions for 14 days, followed by ETEC K99 gavage challenge; (4) the S-2 + L-alanine + ETEC group: daily oral administration of L-alanine-pretreated *B. subtilis* S-2 spore suspensions for 14 days, followed by ETEC K99 challenge; (5) the 312 + ETEC group: daily oral administration of *B. subtilis* 312 spore suspensions for 14 days, followed by ETEC K99 challenge; and (6) the 312 + L-alanine + ETEC group: daily oral administration of L-alanine-pretreated *B. subtilis* 312 spore suspensions for 14 days, followed by ETEC K99 challenge. The inoculation concentration of *Bacillus* was adjusted to 10^7 CFU/ml in the PBS drinking water. In the challenge groups, all the rats were intragastrically inoculated with 1 ml dose of PBS solution containing 10^8 CFU/ml of ETEC K99 on day 15. Individual body weight and water intake were recorded daily for the duration of the study. The rats were sacrificed by cervical vertebra dislocation on day 18 to collect the jejunum samples and fresh feces in the anus.

Hematoxylin & Eosin Staining

The rats' jejunum was fixed with 4% paraformaldehyde and embedded with paraffin. After cutting the tissues into 5-μm sections, they were mounted on a glass slide and deparaffinized in xylene, and rehydrated in a graded ethanol series. The tissue sections were washed in distilled water for 2 min, incubated with hematoxylin solution at 37°C for 5 min, immersed five times in a solution of 1% HCl and 70% ethanol, and subsequently washed with distilled water for 10 min. The sections were then incubated with eosin solution at 37°C for 2 min, dehydrated with alcohol, and immersed in xylene. Finally, the Hematoxylin & eosin (H&E)-stained slides were mounted with neutral gum and then covered with a coverslip for viewing with a microscope.

Immunofluorescence Assays

The rat jejunum sections underwent H&E staining, were incubated with EDTA solution (pH 9.0), and were heated in a microwave for antigen retrieval. After heat treatment, the slides were cooled to room temperature and washed three times in PBS. The sections were subsequently blocked with 3% BSA for 40 min at room temperature and incubated with mouse anti-occludin antibody at 4°C overnight. The sections were then washed three times with PBS, followed by incubation with Dylight 594-conjugated anti-mouse IgG (Abbkine) for 1 h at RT. After washing three times, the nuclei were stained with DAPI for 15 min, and the cells were imaged by fluorescence microscopy (Nikon Eclipse C1, Japan).

16S rRNA Sequencing of Microbiota and Data Analysis

Total genomic DNA of the feces was extracted using a PowerSoil® DNA Isolation kit (MoBio Laboratories, Carlsbad, CA, United States) following the manufacturer's instructions. DNA quantity and quality were evaluated by NanoDrop 2000 (Thermo Scientific, United States) and the A260/A280 ratio. Phusion (New England Biolabs) and primers MPRK341F (5'-ACTCCTACGGGAGGCAGCAG-3') and MPRK806R: (5'-GGACTACHVGGGT WTCTAAT-3') targeted the V3 + V4 region of the 16S rRNA gene and were used for PCR. The PCR products were purified using gel electrophoresis followed by the MinElute® PCR Purification Kit (QIAGEN, Hilden, Germany) and VAHTSTM DNA Clean Beads (Vazyme, Nanjing, China). The libraries were constructed using the TruSeq Nano DNA LT Library Prep Kit (Illumina) and sequenced using HiSeq2500 (Illumina). The raw reads were merged and filtered into clean reads using Quantitative Insights into Microbial Ecology (QIIME) version 1.9.1 (Caporaso et al., 2010). The operational taxonomic units (OTUs) with ≥97% sequence similarity were annotated using the SILVA database (bacteria, http://www.arb-silva.de; Quast et al., 2013). Each OTU was generally considered to be a microbial species. OTU analysis was used to calculate the microbial diversity and abundance of the different samples. The linear discriminate analysis (LDA) effect size (LEfSe) was performed to determine the differences in abundance; the threshold of the LDA score was 4.0.

Statistical Analyses

Statistical analysis was performed using GraphPad Prism software (version 7.0). Data were expressed as means ± standard deviation (SD), and statistical differences were determined using one-way ANOVA. The value of $p < 0.05$ was considered statistically significant. All the experiments were repeated at least three times.

RESULTS

Response of *Bacillus* Strains to Different Nutrient Germinants

In the 14 *Bacillus* strains isolated for the potential spore-former probiotics, plus the standard strain of *B. subtilis* 168, the result presented in **Figures 1A–D** showed that the germination response was strain-specific and germinant-related. Most of the spores from the different *Bacillus* species were

sensitive to L-alanine, L-valine, and L-glutamine. In the present study, L-alanine showed the potential to be a general germinating agent, which could induce the release of DPA and trigger the germination effect on most *Bacillus* spores. However, in the *B. subtilis* species, L-alanine greatly increased the release of DPA of *B. subtilis* S-2 (66.06%); and almost no release was seen in *B. subtilis* 312 (1.97%; **Figure 1D**). The strains from each species with higher germination potential were selected to study the time effect and concentration-effect exerted by L-alanine. As seen in **Figures 1E,F**, the germination of the spores was associated with the L-alanine concentration and treatment time. The spore germination was triggered by at least 100 μm of L-alanine, and the maximum release of DPA could be reached at 100 mm L-alanine treatment for at least 3 h.

The Effect of L-Alanine on the Growth of *Bacillus*

The strains in each *Bacillus* genus that were the most responsive to L-alanine were selected, and inactive *B. subtilis* 312 was used as the control. The growth curves show that L-alanine significantly promoted the growth of spores in all the *Bacillus* strains in the synthetic medium, except for *B. subtilis* 312, compared to the untreated spores (**Figures 2A–D**). In the same *Bacillus* genus, *B. subtilis* S-2 and *B. subtilis* 312 showed a great discrepancy in germination in response to L-alanine as well as differences in the growth-promoting effect (**Figure 2A**). Therefore, their biological characteristics and functions affected by L-alanine were further explored and compared in the subsequent experiments.

Different TEM-Based Morphology of *B. subtilis* S-2 and 312 Treated by L-Alanine

The differential morphological changes that occurred after L-alanine treatment were observed by TEM based on *B. subtilis* S-2 and 312 spores and their spores treated by L-alanine. As shown in **Figure 3**, the spores of *B. subtilis* S-2 and 312 appeared to be in a dormant state, and most of the cells showed bright circles under TEM. After treatment with L-alanine, most of the *B. subtilis* S-2 spores turned gray. However, the *B. subtilis* 312 spores remained in the dormant state, and bright cycles did not produce any change in comparison to the spores without L-alanine treatment.

Comparative Transcriptome Analysis of *B. subtilis* S-2 and 312 in Response to L-Alanine

The differences between the *B. subtilis* S-2 and 312 spores in response to L-alanine germination at the gene level were further studied based on the comparative transcriptome analysis. As seen in **Figure 4A**, a total of 1,438 genes were significantly changed in *B. subtilis* S-2 after L-alanine treatment (S-2 vs. S-2 + L-alanine), among which 716 genes were up-regulated and 722 genes were down-regulated. However, only 48 genes were up-regulated, and 11 genes were down-regulated in *B. subtilis*

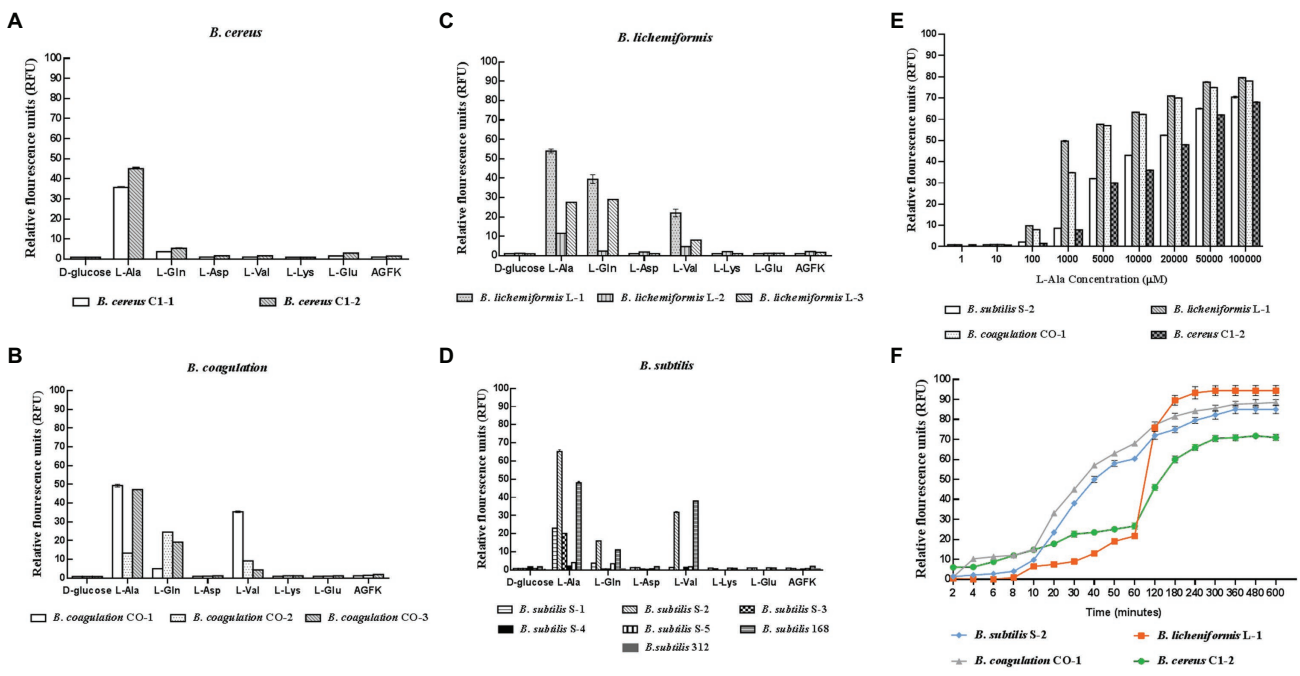

FIGURE 1 | Response of different probiotic *Bacillus* strains to different nutrient germinants. D-glucose, L-alanine (L-Ala), L-glutamine (L-Gln), L-aspartate (L-Asp), L-valine (L-Val), L-lysine (L-Lys), L-glutamate (L-Glu), and complex sprouting agents AGFK. **(A–D)** *Bacillus cereus*, *Bacillus coagulans*, *Bacillus lichemiformis*, *Bacillus subtilis*, respectively. **(E)** Concentration effect of L-alanine on DPA release of spores. **(F)** Time effect of L-alanine treatment on DPA release of spores.

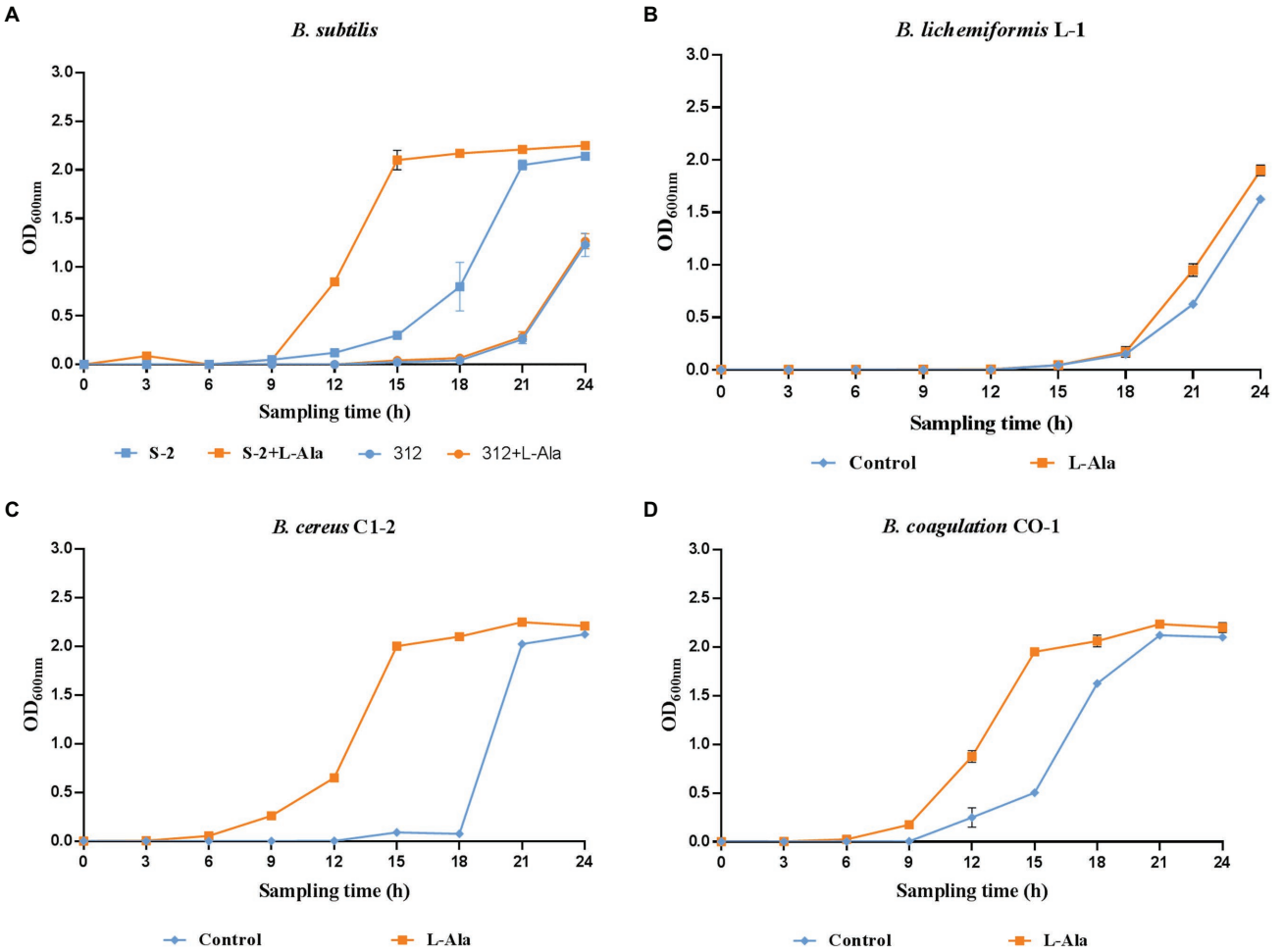

FIGURE 2 | The growth curves of **(A)** *B. subtilis* S-2/312, **(B)** *B. lichemiformis* L-1, **(C)** *B. cereus* C1-2, **(D)** *B. coagulans* CO-1 with or without L-alanine pre-treatment.

312 after L-alanine treatment (312 vs. 312 + L-alanine; **Figure 4B**). These results suggest that more genes are involved in the L-alanine response in *B. subtilis* S-2 in comparison to *B. subtilis* 312.

Figure 4C shows a Venn diagram of the number of DEGs among different groups. A total of 341 DEGs were found between *B. subtilis* 312 and *B. subtilis* S-2, most of which were overlapped to the DEGs in the L-alanine-treated *B. subtilis* S-2 vs. L-alanine-treated *B. subtilis* 312 group. Only 17 DEGs were the same between S-2 vs. S-2 + L-alanine group and 312 vs. 312+ L-alanine group. This indicates that there are significant differences in the DEGs responding to L-alanine between the two strains. However, the S-2 vs. S-2+ L-alanine group and the S-2+ L-alanine vs. 312+ L-alanine group shared the largest number (819) of DEGs.

The GO and KEGG pathway enrichment analyses for the DEGs in the S-2 strain before and after L-alanine treatment (S-2 vs. S-2 + L-alanine) were also conducted. The GO functional enrichment analysis found that the DEGs were mainly included in biological processes (**Figure 4D**). The *De Novo* IMP biosynthetic progress was the most enriched pathway. The secondary enrichment pathways also included flagellum formation, biosynthetic pathways, and enhanced nucleotide metabolism. These results indicate that the main function of L-alanine was to promote the biosynthesis and growth of *B. subtilis* S-2. The KEGG pathway analysis showed that the main enriched pathways of DEGs primarily included quorum sensing, flagellar assembly, and nonribosomal peptide structure (**Figure 4E**). **Figures 4F,G** showed the DEGs annotated to spore germination term (GO:0009847) between different groups. It was found that 20 germination-related genes were differentially expressed after L-alanine treatment in *B. subtilis* S-2; only one gene, *spoVAA*, was differentially expressed in *B. subtilis* 312 (data not shown). A total of 12 germination-related genes were differentially expressed in *B. subtilis* S-2 and *B. subtilis* 312, with four up-regulated genes and eight down-regulated genes (**Figure 4G**). The expression level of the L-alanine receptor gene, *gerAA*, in the two strains was verified by RT-qPCR. As seen in **Figure 4H**, the relative expression of *gerAA* gene was about 20,000-fold greater in *B. subtilis* S-2 than that in *B. subtilis* 312.

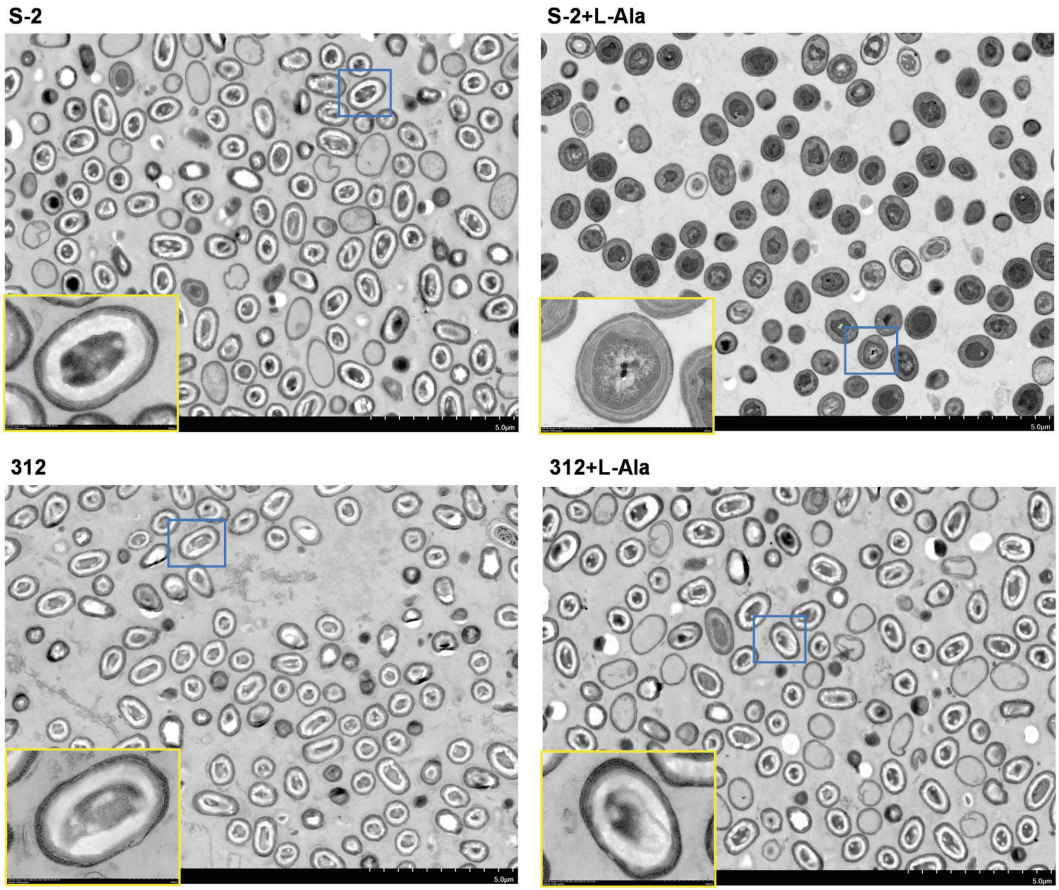

FIGURE 3 | Morphological changes of *B. subtilis* S-2 and 312 with L-alanine treatment. The cell morphology of *B. subtilis* S-2 spores, L-alanine treated *B. subtilis* S-2 spores, *B. subtilis* 312 spores, L-alanine treated *B. subtilis* 312 spores were displayed by transmission electron microscopy (TEM). The yellow frame is an enlarged version of the blue frame.

The Different Effects of *B. subtilis* S-2 and 312 Exerted by L-Alanine on the Inflammatory Cytokines and Intestinal Barrier in IPEC-J2 Cells

The protective effect of L-alanine-induced spore germination on the IPEC-J2 cells infected by ETEC K99 was compared. As shown in **Figures 5A–D**, ETEC K99 infection significantly increased the mRNA expression level of the inflammatory factors, IL-6, IL-8, IL-1β, and TNF-α, in the IPEC-J2 cells in comparison to the control ($p < 0.0001$). In contrast to the ETEC K99 infection group, the *B. subtilis* S-2 spores decreased the mRNA expression of the four inflammatory cytokines, and the levels of IL-8 and TNF-α were significant ($p < 0.01$ and $p < 0.001$, respectively). The *B. subtilis* 312 spores significantly decreased the mRNA expression level of IL-8 ($p < 0.0001$). Interestingly, the *B. subtilis* S-2 spores treated by L-alanine tended to further reduce the mRNA expression of IL-6, IL-8, IL-1β, and TNF-α in comparison to the *B. subtilis* S-2 spores alone, and the decrease in the level of IL-6 was significant ($p < 0.05$). However, there was no difference in the effect on inhibition of the inflammatory factors between the L-alanine-treated *B. subtilis* 312 spores and *B. subtilis* 312 spores alone.

The expression of tight junction proteins and IL-6 was further tested by WB, as shown in **Figure 5E**. It was found that ETEC K99 infection significantly increased the expression of IL-6 and decreased the expression of occludin and cluadin1 compared to the control. Compared to the untreated *B. subtilis* S-2 spores, the L-alanine-induced S-2 spores increased the expression of occludin and decreased the expression of IL-6. *B. subtilis* 312 spores and their L-alanine induced spores both up-regulated the expression of occludin and cluadin1. However, no difference was observed between the *B. subtilis* 312 spores treated with L-alanine and those not treated with L-alanine.

Promoting Effects of L-Alanine-Mediated Spore Germination on Rat Growth and the Intestinal Barrier

The effect of spore germination induced by L-alanine was investigated using a rat challenge model (**Figure 6A**). **Figure 6B** shows that the average daily gain (ADG) of the SD rats was significantly decreased after ETEC K99 infection in contrast

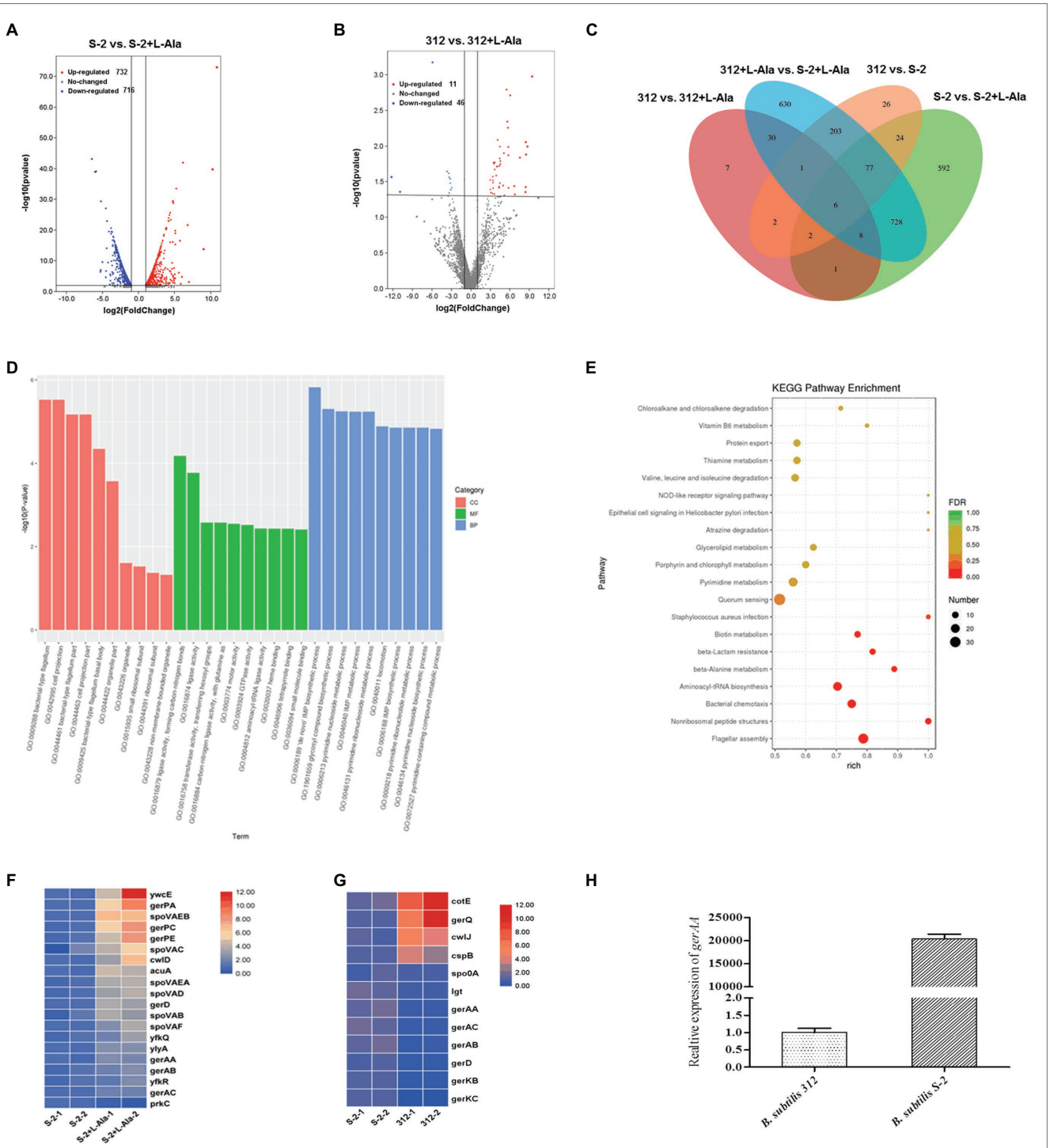

FIGURE 4 | Comparative transcriptome analysis of *B. subtilis* S-2 and 312 strains in response to L-alanine. **(A)** Volcano plot of differently expressed genes (DEGs) between *B. subtilis* S-2 spores and L-alanine pre-treated *B. subtilis* S-2 spores. **(B)** Volcano plot of DEGs in *B. subtilis* 312 spores and L-alanine pre-treated 312 spores. **(C)** Venn diagram of the numbers of DEGs between 4 groups. **(D)** GO analysis of the DEGs between *B. subtilis* S-2 spores and L-alanine pre-treated *B. subtilis* S-2 spores. **(E)** GO analysis of the DEGs between *B. subtilis* 312 spores and L-alanine pre-treated *B. subtilis* 312 spores. **(F)** DEGs enriched in spore germination pathway between *B. subtilis* S-2 spores and L-alanine pre-treated *B. subtilis* S-2 spores. Each row represents one gene, and each column represents one sample; Red indicates high expression, and blue represents low expression. **(G)** DEGs enriched in spore germination pathway between *B. subtilis* S-2 and *B. subtilis* 312. Each row represents one gene, and each column represents one sample; Red indicates high expression, and blue represents low expression. **(H)** The expression level of *gerAA* in *B. subtilis* S-2 and 312 spores.

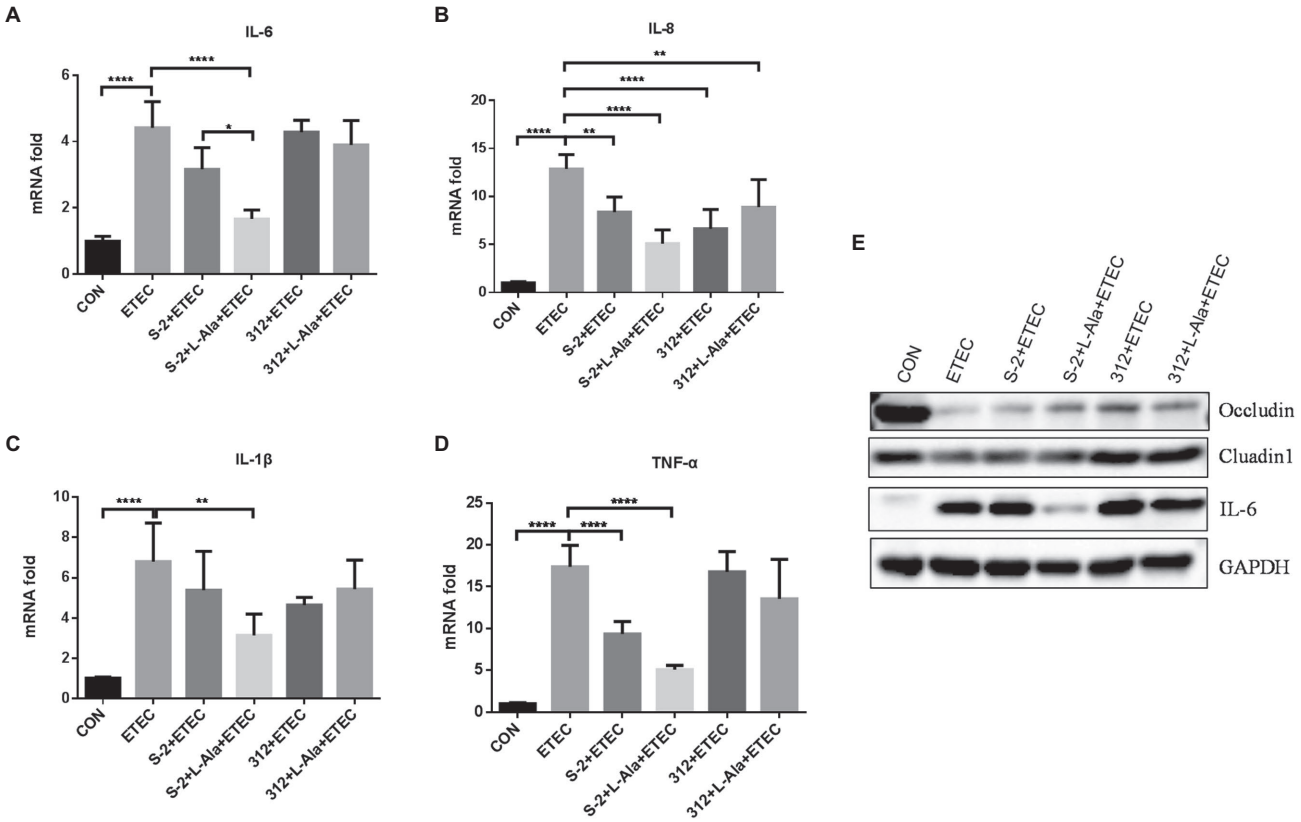

FIGURE 5 | The different effects of L-alanine mediated *B. subtilis* S-2 and 312 strains on inflammatory cytokines and tight junction proteins in IPEC-J2 cells. IPEC-J2 cells were incubated with *B. subtilis* S-2 and 312 spores (10^6 CFU/ml) with or without L-alanine pre-treated for 16 h. Then the cells were infected with ETEC-K99 (10^6 CFU/ml) for 12 h. The mRNA expression of IL-6 **(A)**, IL-8 **(B)**, IL-1β **(C)**, TNF-α **(D)** were detected by RT-qPCR; **(E)** The protein expression of occludin, claudin, and IL-6 were tested by WB. Values are expressed as the mean ± SD from three independent experiments. $^*p < 0.05$; $^{**}p < 0.01$; $^{****}p < 0.0001$, as calculated by one-way ANOVA with Tukey's multiple comparisons test. Groups with no significant difference were not marked.

to the control ($p < 0.05$). Administration of the spores from the untreated *B. subtilis* S-2 and *B. subtilis* 312 or their associated L-alanine-treated spores all significantly increased the ADG of the rats ($p < 0.05$) and the ADG level of the L-alanine-treated *B. subtilis* S-2 spores was the highest ($p < 0.0001$) in comparison to the ETEC K99 groups. The ETEC K99 infection increased the expression of the intestinal cytokines IL-6 and IL-8 (**Figures 6C,D**). However, administration of the L-alanine-treated *B. subtilis* S-2 spores significantly decreased IL-6 expression in the jejunum compared to the ETEC K99 group and the *B. subtilis* group ($p < 0.01$ and $p < 0.05$, respectively; **Figure 6C**).

The H&E staining results revealed that ETEC infection caused shortened villi, larger space among the villi, and loss of epithelial cells in the intestinal epithelium of the jejunal structure in the SD rats (**Figure 6H**). Administration of the L-alanine-treated *B. subtilis* S-2 spores attenuated the ETEC-induced jejunal mucosa lesions and improved the expression of occludin (**Figure 6H**). The length of the jejunal villi was significantly decreased ($p < 0.001$), and the crypt depth was increased ($p < 0.0001$) in the ETEC group in comparison to the control (**Figures 6E,F**). The crypt depths were decreased in all four of the *Bacillus* administration groups. However, only the L-alanine-induced *B. subtilis* S-2 spores significantly increased the villi length ($p < 0.05$) and the ratio of villus length to crypt depth ($p < 0.0001$; **Figures 6E,G**).

Regulating Effects of L-Alanine-Mediated Spore Germination on Gut Microbiota

The microbiome of the rat feces was explored to study the discrepancy resulting from the administration of spores treated by L-alanine. As seen in **Figures 7A,B**, the L-alanine-treated *B. subtilis* S-2 spores had the highest number of bacterial genus and species, and the increase in the genus level was significant ($p < 0.01$). Additionally, the L-alanine-treated *B. subtilis* S-2 spores tended to promote the abundance of *Lactobacillus*, *Bacteroides*, *Romboutsia,* and UCG-005 in the rat feces (**Figure 7C**).

The abundance of the taxa at the genus level was also analyzed. A total of 13 genera were found to have significant changes in taxa abundance between the S-2 and S-2 + L-alanine groups ($p < 0.05$; **Figure 7D**). In contrast, the taxa abundance of only 5 genera was significantly changed between the 312 and 312 + L-alanine groups ($p < 0.05$; **Figure 7E**). A total of

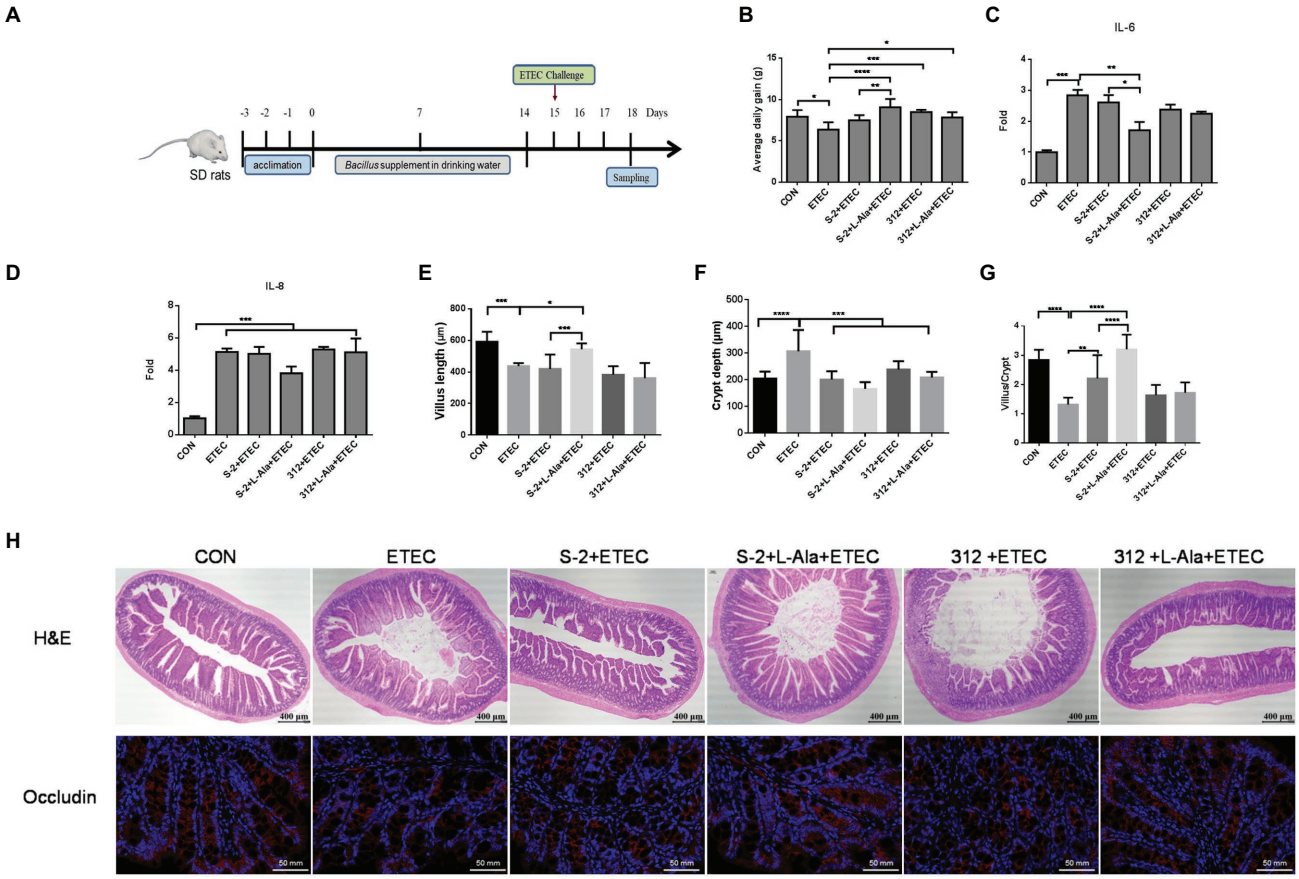

FIGURE 6 | Promoting effects of L-alanine-mediated spore germination on animal growth and intestinal barrier. **(A)** Diagram illustrating the ETEC-challenge model employed in this study. **(B)** Average daily gain of SD rats feeding *B. subtilis* S-2 and 312 spores with or without L-alanine treated from day 15 to day 18. **(C,D)** The mRNA fold of IL-6 and IL-8 in the jejunum of SD rats feeding different spores. **(H)** H&E stain (up line) and immunofluorescence analysis (IFA; bottom) of occludin in the jejunum of SD rats. Occludin was stained as red, and DAPI was stained as blue. **(E–G)** The villus length, crypt depth, and villus length/crypt depth ratio in jejunum of different groups, respectively. Values are expressed as the mean ± SD from at least 6 animals. $^{*}p < 0.05$; $^{**}p < 0.01$; $^{***}p < 0.001$; $^{****}p < 0.0001$, as calculated by one-way ANOVA with Tukey's multiple comparisons test. Groups without significant difference were not marked.

10 taxa were found to have significant differences in abundance at the genus level between the ETEC and S-2 + ETEC groups (**Supplementary Table 1**), and 20 taxa were found to have a significant difference in abundance at the genus level between the ETEC and S-2 + ETEC groups (**Supplementary Table 2**).

Next, LDA was performed to identify the biomarkers with a significant difference in taxa abundance in each group (**Figure 7F**). It was found that the L-alanine-pretreated *B. subtilis* S-2 had the largest number of species with a significantly different abundance in comparison to the other groups. The functional analysis of the samples showed that the gene functions of the six groups were mostly enriched in carbohydrate metabolism, amino acid metabolites, metabolism of cofactors, and the vitamin pathways (**Figure 7G**).

DISCUSSION

The massive use of antibiotics leads to the emergence of antimicrobial resistance, which poses a great threat to human health and animal production. Therefore, it is important to find suitable alternatives to antibiotics. Studies have shown that *Bacillus* species have been used as probiotics in medical supplements and livestock feeds for more than 60 years, and scientific interest has increased significantly in the last two decades (Hong et al., 2005; Cutting, 2011; Piewngam et al., 2018). The most attractive advantages of using *Bacillus* species as probiotics are their high stability and their significant capacity for metabolic activity, including the production of various enzymes, antimicrobial metabolites, pentapeptide, and lipopeptides, such as fengycin, coagulin, and surfactin (Piewngam et al., 2018). However, metabolic activity is highly associated with the germination process, which is dependent on the strain itself and the intestinal environmental conditions (Bernardeau et al., 2017). The complexity and dynamics in the GIT of *Bacillus* probiotics are largely unknown since the *Bacillus* species are ingested in the form of spores. Thus, it is crucial to explore the relationship between *Bacillus* strain-related germination and the influence of their protective effect in the gut.

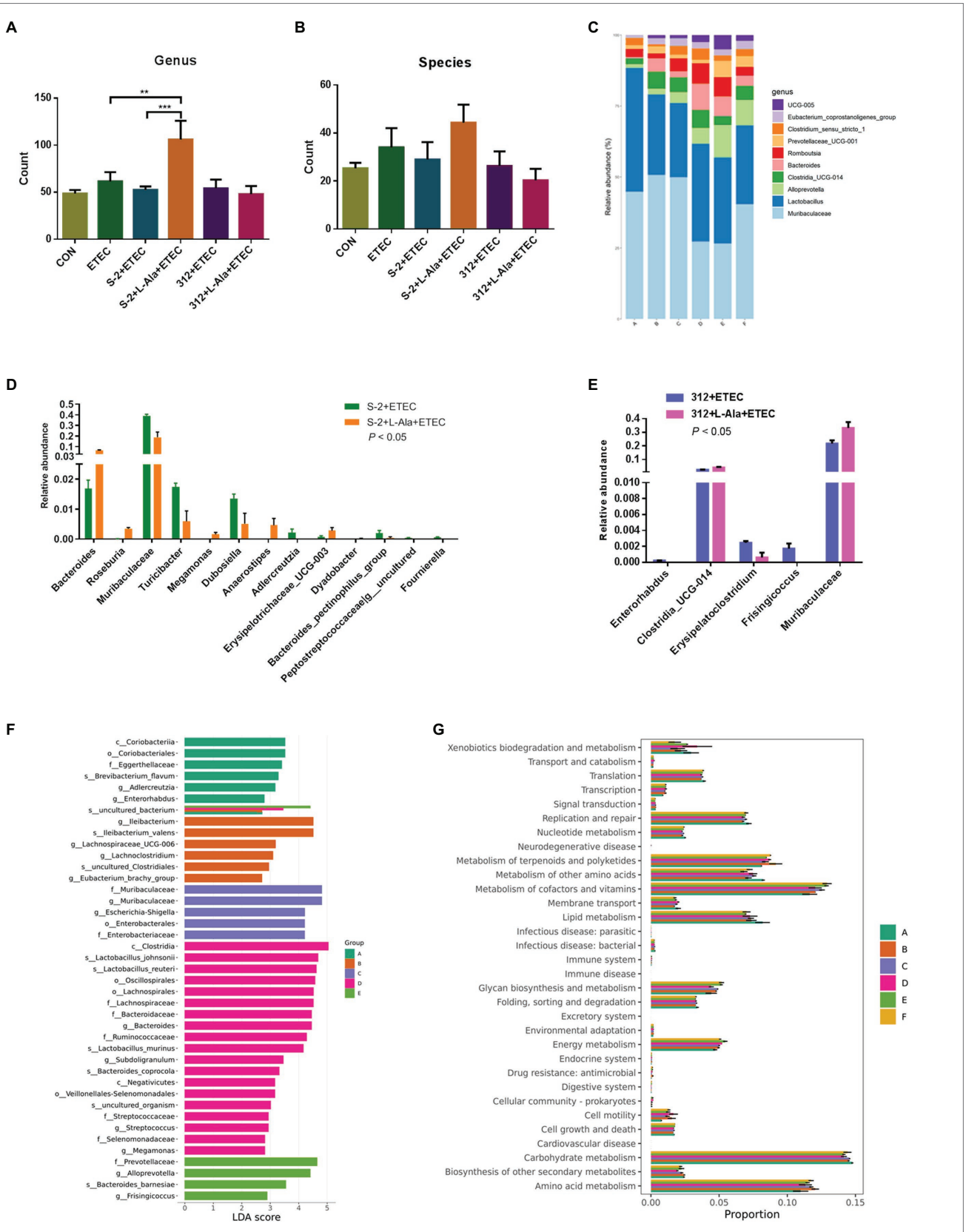

FIGURE 7 | Continued

FIGURE 7 | Regulating effects of L-alanine-mediated spore germination on gut microbiota. **(A)** Number of bacteria detected at genus level in different treatments. **(B)** Number of bacteria detected at species level in different treatments. **(C)** Histogram of the top 10 abundant genera in each group. **(D)** The taxa with significant differences ($p < 0.05$) in abundance at genus level between *B. subtilis* S-2 and S-2 + L-alanine groups. **(E)** The taxa with significant differences ($p < 0.05$) in abundance at genus level between 312 and 312 + L-alanine groups. **(F)** Histogram of LDA value distribution. **(G)** KEGG pathway analysis based on the abundance of marker gene sequences in the samples. There are 3 samples in each group. (Group A represents CON, Group B represents ETEC, Group C represents S-2 + ETEC, Group D represents S-2 + L-alanine+ETEC, Group E represents 312 + ETEC, Group F represents 312 + L-alanine+ETEC.) Values are expressed as the mean ± SD. $^{**}p < 0.01$; $^{***}p < 0.001$, as calculated by one-way ANOVA with Tukey's multiple comparisons test.

In the present study, we confirmed the strain-specific and germinant-related properties of spores in response to germination. As seen in **Figures 1A–D**, not all spores from the *Bacillus* species are responsible for the germination triggered by nutrients, including L-alanine. As a sole nutrient-germinant, L-alanine most often triggers the germination of spore-formers (Moir and Smith, 1990; Lovdal et al., 2012). The spore germination assay of the 15 *Bacillus* strains involved in this study also supports the view that L-alanine is an important nutrient-germinant for different *Bacillus* species.

The results shown in **Figure 2** further indicate that L-alanine-triggered gemination promotes the proliferation of spores in a restricted medium, which is similar to what occurs in the intestinal environment. When dormant spores sense an environment with specific nutrients conducive to vegetative growth, they can rapidly return to active growth through germination followed by outgrowth (Moir and Cooper, 2015; Christie and Setlow, 2020). The growth of vegetative *B. subtilis* under anaerobe conditions has been verified from the early report (Nakano and Zuber, 1998). Therefore, in the intestinal environments, the presence of potential nutrient agents, such as amino acids, sugars, ribosides, and some inorganic salts, could be provided to promote spore germination in the gut. Previous reports have verified that ingested *Bacillus* spores can germinate in varying proportions and have whole life cycles in the GIT of mice, pigs, and chickens (Tam et al., 2006; Bernardeau et al., 2017). However, the persistence of *Bacillus* strains in the GIT is species- and strain-specific. As seen in **Figure 2A**, the L-alanine growth-promoting effect was only observed in the L-alanine-induced *B. subtilis* S-2 strain. This result indicates that the germination-specific strain contributes to the germination and proliferation of spores, which enhances the persistence of *Bacillus* strains in the GIT.

The differential morphological changes of *B. subtilis* S-2 and *B. subtilis* 312 after L-alanine treatment were further verified by TEM. Because of the thick, multilayered structure of spores with low water content, they were highly refractive and difficult to stain. The spores often showed bright circles under TEM. However, after the release of DPA and the water uptake by the spores triggered by the germinants, the germinating spores changed from the transparent phase to the gray phase. The germination process could also be captured through phase contrast microscopy, in which the germinated and dormant spores appeared dark and white/bright, respectively (Lovdal et al., 2012; Amon et al., 2020). In the present study, TEM also clearly showed that *B. subtilis* S-2 germinated with L-alanine, and there was no apparent increase in the number of gray spores of *B. subtilis* 312 supplemented with L-alanine or the negative controls. The results of the differential TEM images of the two strains responding to L-alanine were also consistent with the results of the germination assay and growth assay.

The germination triggered by the nutrient germinants are closely associated with the specific receptors located in the spore's inner membrane, resulting in the release of DPA from the spore core and subsequent cortex degradation (Chirakkal et al., 2002; Christie and Setlow, 2020). Different *Bacillus* strains have different germinant receptors that recognize specific nutrient germinants. The comparative transcriptome results showed that the DEGs of *B. subtilis* S-2 responding to L-alanine was far greater than the DEGs of *B. subtilis* 312, and the spore germination-related genes (*ywcE*, *gerPA*, *spoVAEB*, *gerPC*, *gerPE*, *spoVAC*, *cwlD*, *acuA*, etc.; **Figure 4**). Moreover, the DEGs were principally enriched in metabolism, cellular processes, and biosynthetic pathways. To be specific, *ywcE* is important for proper spore morphogenesis (Real et al., 2005), and *GerPA*, *GerPC*, and *GerPE* are involved in the establishment of normal spore coat structure and permeability, which allows the germinants to access their receptors (Casula and Cutting, 2002; Chirakkal et al., 2002; Moir et al., 2002; Ghosh et al., 2018). The up-regulated *acuA* gene helped mediate the post-translational regulation during the 80 min to 100 min of spore germination and into the outgrowth phase (Gardner and Escalante-Semerena, 2008). The L-alanine-induced germinant receptor in *B. subtilis* is encoded by the *gerA* operon, *gerAA*, *gerAB*, and *gerAC* (Mongkolthanaruk et al., 2011). Consequently, the expression of the germinant receptors is much higher in the *B. subtilis* S-2 strain than the *B. subtilis* 312 (**Figure 4H**). These findings confirm that differences in gene expression between the *B. subtilis* S-2 and 312 strains are due to differences in the germination and growth responses to L-alanine. The higher expression of the germination receptors promoted the germination response in the *Bacillus* strains.

The anti-inflammatory and immunomodulatory functions of probiotic *B. subtilis* have been confirmed in other studies (Du et al., 2018; Gong et al., 2018; Luise et al., 2019). However, probiotic activities are often strain-related even in the same reports (Hu et al., 2018; Rhayat et al., 2019). When considering the specific germination of spores, in the present study, the effect of L-alanine-induced germination of *B. subtilis* S-2 and *B. subtilis* 312 spores on the protective activities was intensively investigated in ETEC challenged intestinal epithelial cells and SD rats *in vitro* and *in vivo*, respectively. The ETEC K99 challenge model was successful in both the cell model and animal model since the inflammatory cytokines were significantly up-regulated after the challenge (**Figures 5, 6**). Both the *B. subtilis* S-2 and *B. subtilis* 312 spores shared some anti-inflammatory activity by significantly decreasing the expression of some of the inflammatory cytokines at the IPEC-J2 cells (**Figure 5**). Moreover, after the challenge, the rat growth performance was improved

by administration of the spores from the two strains (**Figure 6**). The beneficial activities of the two spores might be associated with the immune effects of the spores, which was not strain-specific since the spores and vegetative cells exhibit differential functional properties (Foligne et al., 2012). However, from a living *Bacillus* perspective, the probiotic effect is the result of the complementary action of vegetative cells and spores (Bernardeau et al., 2017). The bacterial spores are metabolically dormant, and vegetative cells provide more health benefits because of their metabolic activity and growth potential. Importantly, our study showed that the spores of *B. subtilis* S-2 triggered by L-alanine can more effectively inhibit the expression of inflammatory factors, promote the expression of tight junction proteins, and help repair intestinal barrier injury. The probiotic function was significantly increased after L-alanine induced the alteration of *Bacillus* germination both in the IPEC-J2 cell model and in the rat model. To the best of our knowledge, this is the first report to show that L-alanine-induced *Bacillus* spore germination can improve the protective activity against ETEC K99-induced intestine injury.

Probiotic *Bacillus* species are beneficial for modulating the intestinal microflora and micro-ecological balance (Motlagh et al., 2012; Wang et al., 2017; Luo et al., 2020). In the present study, the increased intestinal microbiota barrier by the L-alanine-induced spores was further confirmed in the SD rats (**Figure 7**). The diversity of fecal microbiota was only significantly enhanced in the L-alanine-induced *B. subtilis* spores group ($p < 0.01$). Thus, an environment with more highly diverse gut microbiota could be more stable and healthier than an environment with gut microbiota that is less diverse (Li et al., 2018). The increased abundance of *Lactobacillus*, *Bacteroides*, *Romboutsia*, UCG-005 in the rats ingesting the L-alanine-induced spores contributed to creating a better intestinal environment. The increased microbiota function of the spores induced by L-alanine was in accordance with the results in the anti-inflammatory and growth-promoting effect shown in **Figures 5, 6**. The improved intestinal microbiota by *Bacillus* administration might be caused by the metabolic activity and biological oxygen-capturing potential (Yu et al., 2019), which are both closely related to the germination and proliferation of spores in the gut. Therefore, the results of the intestinal microbiota analyses also support the view that the germination of spores initiated by L-alanine could result in an increased probiotic effect.

In summary, we first described that L-alanine-induced *Bacillus* germination increased the protective effects by alleviating ETEC K99-induced intestine injury and enhancing the intestinal microbiota barrier. We propose that L-alanine works well as a probiotic *Bacillus* adjuvant based on the strain's germination potential in improving intestinal health. It also provides a solution for the accurate screening of *Bacillus* probiotics and the practical and accurate regulation of their use as antibiotic alternatives in animal production.

DATA AVAILABILITY STATEMENT

The datasets presented in this study can be found in online repositories. The names of the repository/repositories and accession number(s) can be found in the article/**Supplementary Material**.

ETHICS STATEMENT

The animal study was reviewed and approved by the Ethical Committee of South-Central University for Nationalities.

AUTHOR CONTRIBUTIONS

XG conceived and designed the experiments and revised the manuscript. SL, XL, LZ, YF, and MX performed the experiments. SL and XG analyzed the data and made the figures. SL wrote the original draft. All authors reviewed and approved the final manuscript.

FUNDING

This study was supported by the National Natural Science Foundation of China (Nos. 32072767 and 31672455), the Fundamental Research Funds for Central Universities South-Central University for Nationalities (No. CZZ21011), and the Fundamental Research Funds for Health Commission of Hubei Province (ZY2021M061).

SUPPLEMENTARY MATERIAL

The Supplementary Material for this article can be found online at: https://www.frontiersin.org/articles/10.3389/fmicb.2021.796158/full#supplementary-material

Supplementary Figure 1 | Phylogenetic tree based on the 16S ribosomal RNA sequences from 26 *Bacillus* strains. The tree was constructed using the neighbor-joining method with MEGA 5.0. Branch quality was assessed by the bootstrap test using 1,000 replications.

REFERENCES

Abd El-Hack, M. E., El-Saadony, M. T., Shafi, M. E., Qattan, S. Y. A., Batiha, G. E., Khafaga, A. F., et al. (2020). Probiotics in poultry feed: a comprehensive review. *J. Anim. Physiol. Anim. Nutr.* 104, 1835–1850. doi: 10.1111/jpn.13454

Alzahrani, O. M., and Moir, A. (2014). Spore germination and germinant receptor genes in wild strains of *Bacillus subtilis*. *J. Appl. Microbiol.* 117, 741–749. doi: 10.1111/jam.12566

Amon, J. D., Yadav, A. K., Ramirez-Guadiana, F. H., Meeske, A. J., Cava, F., and Rudner, D. Z. (2020). SwsB and safA are required for cwlj-dependent spore germination in *Bacillus subtilis*. *J. Bacteriol.* 202:e00668-19. doi: 10.1128/JB.00668-19

Bernardeau, M., Lehtinen, M. J., Forssten, S. D., and Nurminen, P. (2017). Importance of the gastrointestinal life cycle of *Bacillus* for probiotic functionality. *J. Food Sci. Technol.* 54, 2570–2584. doi: 10.1007/s13197-017-2688-3

Caporaso, J. G., Kuczynski, J., Stombaugh, J., Bittinger, K., Bushman, F. D., Costello, E. K., et al. (2010). QIIME allows analysis of high-throughput community sequencing data. *Nat. Methods* 7, 335–336. doi: 10.1038/nmeth.f.303

Casula, G., and Cutting, S. M. (2002). *Bacillus* probiotics: spore germination in the gastrointestinal tract. *Appl. Environ. Microbiol.* 68, 2344–2352. doi: 10.1128/AEM.68.5.2344-2352.2002

Chirakkal, H., O'Rourke, M., Atrih, A., Foster, S. J., and Moir, A. (2002). Analysis of spore cortex lytic enzymes and related proteins in *Bacillus subtilis* endospore germination. *Microbiology* 148, 2383–2392. doi: 10.1099/00221287-148-8-2383

Christie, G., and Setlow, P. (2020). *Bacillus* spore germination: knowns, unknowns and what we need to learn. *Cell. Signal.* 74:109729. doi: 10.1016/j.cellsig.2020.109729

Cutting, S. M. (2011). *Bacillus* probiotics. *Food Microbiol.* 28, 214–220. doi: 10.1016/j.fm.2010.03.007

Davies, F. L. (2010). Heat resistance of *Bacillus* species. *Int. J. Dairy Technol.* 28, 69–78. doi: 10.1111/j.1471-0307.1975.tb00683.x

Di Luccia, B., D'Apuzzo, E., Varriale, F., Baccigalupi, L., Ricca, E., and Pollice, A. (2016). *Bacillus megaterium* SF185 induces stress pathways and affects the cell cycle distribution of human intestinal epithelial cells. *Benef. Microbes* 7, 609–620. doi: 10.3920/BM2016.0020

Du, W., Xu, H., Mei, X., Cao, X., Gong, L., Wu, Y., et al. (2018). Probiotic *Bacillus* enhance the intestinal epithelial cell barrier and immune function of piglets. *Benef. Microbes* 9, 743–754. doi: 10.3920/BM2017.0142

Foligne, B., Peys, E., Vandenkerckhove, J., Van Hemel, J., Dewulf, J., Breton, J., et al. (2012). Spores from two distinct colony types of the strain *Bacillus subtilis* PB6 substantiate anti-inflammatory probiotic effects in mice. *Clin. Nutr.* 31, 987–994. doi: 10.1016/j.clnu.2012.05.016

Fujiya, M., Musch, M. W., Nakagawa, Y., Hu, S., Alverdy, J., Kohgo, Y., et al. (2007). The *Bacillus subtilis* quorum-sensing molecule CSF contributes to intestinal homeostasis via OCTN2, a host cell membrane transporter. *Cell Host Microbe* 1, 299–308. doi: 10.1016/j.chom.2007.05.004

Gardner, J. G., and Escalante-Semerena, J. C. (2008). Biochemical and mutational analyses of AcuA, the acetyltransferase enzyme that controls the activity of the acetyl coenzyme a synthetase (AcsA) in *Bacillus subtilis*. *J. Bacteriol.* 190, 5132–5136. doi: 10.1128/JB.00340-08

Ghelardi, E., Celandroni, F., Salvetti, S., Gueye, S. A., Lupetti, A., and Senesi, S. (2015). Survival and persistence of *Bacillus clausii* in the human gastrointestinal tract following oral administration as spore-based probiotic formulation. *J. Appl. Microbiol.* 119, 552–559. doi: 10.1111/jam.12848

Ghosh, A., Manton, J. D., Mustafa, A. R., Gupta, M., Ayuso-Garcia, A., Rees, E. J., et al. (2018). Proteins encoded by the gerP operon are localized to the inner coat in *Bacillus cereus* spores and are dependent on gerpa and safa for assembly. *Appl. Environ. Microbiol.* 84:e00760-18. doi: 10.1128/AEM.00760-18

Gil-Gil, T., Laborda, P., Sanz-García, F., Hernando-Amado, S., Blanco, P., and Martínez, J. L. (2019). Antimicrobial resistance: a multifaceted problem with multipronged solutions. *MicrobiologyOpen* 8:e945. doi: 10.1002/mbo3.945

Gong, L., Wang, B., Mei, X., Xu, H., Qin, Y., Li, W., et al. (2018). Effects of three probiotic *Bacillus* on growth performance, digestive enzyme activities, antioxidative capacity, serum immunity, and biochemical parameters in broilers. *Anim. Sci. J.* 89, 1561–1571. doi: 10.1111/asj.13089

Hong, H. A., Duc, L. H., and Cutting, S. M. (2005). The use of bacterial spore formers as probiotics. *FEMS Microbiol. Rev.* 29, 813–835. doi: 10.1016/j.femsre.2004.12.001

Hu, S., Cao, X., Wu, Y., Mei, X., Xu, H., Wang, Y., et al. (2018). Effects of probiotic *Bacillus* as an alternative of antibiotics on digestive enzymes activity and intestinal integrity of piglets. *Front. Microbiol.* 9:2427. doi: 10.3389/fmicb.2018.02427

Huang, J. M., La Ragione, R. M., Nunez, A., and Cutting, S. M. (2008). Immunostimulatory activity of *Bacillus* spores. *FEMS Immunol. Med. Microbiol.* 53, 195–203. doi: 10.1111/j.1574-695X.2008.00415.x

Jadamus, A., Vahjen, W., and Simon, O. (2001). Growth behaviour of a spore forming probiotic strain in the gastrointestinal tract of broiler chicken and piglets. *Arch. Tierernahr.* 54, 1–17. doi: 10.1080/17450390109381962

Jing, L., Yunbin, L., Li, M., Jing, S., Huang, Z., Lu, F., et al. (2018). Alleviating acute alcoholic liver injury in mice with *Bacillus subtilis* co-expressing alcohol dehydrogenase and acetaldehyde dehydrogenase. *J. Funct. Foods* 49, 342–350. doi: 10.1016/j.jff.2018.09.006ISBN: 1756-4646

Kang, S., Park, M. Y., Brooks, I., Lee, J., Kim, S. H., Kim, J. Y., et al. (2021). Spore-forming *Bacillus coagulans* SNZ 1969 improved intestinal motility and constipation perception mediated by microbial alterations in healthy adults with mild intermittent constipation: a randomized controlled trial. *Food Res. Int.* 146:110428. doi: 10.1016/j.foodres.2021.110428

Leser, T. D., Knarreborg, A., and Worm, J. (2010). Germination and outgrowth of *Bacillus subtilis* and *Bacillus licheniformis* spores in the gastrointestinal tract of pigs. *J. Appl. Microbiol.* 104, 1025–1033. doi: 10.1111/j.1365-2672.2007.03633.x

Li, C. L., Wang, J., Zhang, H. J., Wu, S. G., Hui, Q. R., Yang, C. B., et al. (2018). Intestinal morphologic and microbiota responses to dietary *Bacillus* spp. in a broiler chicken model. *Front. Physiol.* 9:1968. doi: 10.3389/fphys.2018.01968

Liang, X. S., Liu, C., Long, Z., and Guo, X. H. (2018). Rapid and simple detection of endospore counts in probiotic *Bacillus* cultures using dipicolinic acid (DPA) as a marker. *AMB Express* 8:101. doi: 10.1186/s13568-018-0633-0

Lovdal, I. S., From, C., Madslien, E. H., Romundset, K. C., Klufterud, E., Rosnes, J. T., et al. (2012). Role of the gerA operon in L-alanine germination of *Bacillus licheniformis* spores. *BMC Microbiol.* 12:34. doi: 10.1186/1471-2180-12-34

Luise, D., Bertocchi, M., Motta, V., Salvarani, C., Bosi, P., Luppi, A., et al. (2019). *Bacillus* sp. probiotic supplementation diminish the *Escherichia coli* F4ac infection in susceptible weaned pigs by influencing the intestinal immune response, intestinal microbiota and blood metabolomics. *J. Anim. Sci. Biotechnol.* 10:74. doi: 10.1186/s40104-019-0380-3

Luo, R., Zhang, J., Zhang, X., Zhou, Z., and Peng, G. (2020). *Bacillus subtilis* HH2 ameliorates TNBS-induced colitis by modulating gut microbiota composition and improving intestinal barrier function in rabbit model. *J. Funct. Foods* 74:104167. doi: 10.1016/j.jff.2020.104167

Mazzoli, A., Donadio, G., Lanzilli, M., Saggese, A., and Isticato, R. (2019). *Bacillus megaterium* SF185 spores exert protective effects against oxidative stress in vivo and in vitro. *Sci. Rep.* 9:12082. doi: 10.1038/s41598-019-48531-4

Mingmongkolchai, S., and Panbangred, W. (2018). *Bacillus* probiotics: an alternative to antibiotics for livestock production. *J. Appl. Microbiol.* 124, 1334–1346. doi: 10.1111/jam.13690

Mirk, A., Dk, A., Tgc, A., and Gr, B. (2021). Dietary administration of a host-gut derived probiotic *Bacillus amyloliquefaciens* COFCAU_P1 modulates immune-biochemical response, immune-related gene expression, and resistance of *Labeo rohita* to *Aeromonas hydrophila* infection. *J. Aquacult.* 546:737390. doi: 10.1016/j.aquaculture.2021.737390

Moir, A., and Cooper, G. (2015). Spore germination. *Microbiol. Spectr.* 3:TBS-0014-2012. doi: 10.1128/microbiolspec.TBS-0014-2012

Moir, A., Corfe, B. M., and Behravan, J. (2002). Spore germination. *Cell. Mol. Life Sci.* 59, 403–409. doi: 10.1007/s00018-002-8432-8

Moir, A., and Smith, D. A. (1990). The genetics of bacterial spore germination. *Annu. Rev. Microbiol.* 44, 531–553. doi: 10.1146/annurev.mi.44.100190.002531

Moir, A., Yazdi, M. A., and Kemp, E. H. (1991). Spore germination genes of *Bacillus subtilis* 168. *Res. Microbiol.* 142, 847–850. doi: 10.1016/0923-2508(91)90064-H

Mongkolthanaruk, W., Cooper, G. R., Mawer, J. S., Allan, R. N., and Moir, A. (2011). Effect of amino acid substitutions in the GerAA protein on the function of the alanine-responsive germinant receptor of *Bacillus subtilis* spores. *J. Bacteriol.* 193, 2268–2275. doi: 10.1128/JB.01398-10

Motlagh, H., Farhangi, M., Rafiee, G., and Noori, F. (2012). Modulating gut microbiota and digestive enzyme activities of *Artemia urmiana* by administration of different levels of *Bacillus subtilis* and *Bacillus licheniformis*. *J. Aquacult. Int.* 20, 693–705. doi: 10.1007/s10499-012-9497-5

Nakano, M. M., and Zuber, P. (1998). Anaerobic growth of a "strict aerobe" (*Bacillus subtilis*). *Annu. Rev. Microbiol.* 52, 165–190. doi: 10.1146/annurev.micro.52.1.165

Ouwehand, A. C., Forssten, S., Hibberd, A. A., Lyra, A., and Stahl, B. (2016). Probiotic approach to prevent antibiotic resistance. *Ann. Med.* 48, 246–255. doi: 10.3109/07853890.2016.1161232

Piewngam, P., Zheng, Y., Nguyen, T. H., Dickey, S. W., Joo, H. S., Villaruz, A. E., et al. (2018). Pathogen elimination by probiotic *Bacillus* via signalling interference. *Nature* 562, 532–537. doi: 10.1038/s41586-018-0616-y

Quast, C., Pruesse, E., Yilmaz, P., Gerken, J., Schweer, T., Yarza, P., et al. (2013). The SILVA ribosomal RNA gene database project: improved data processing and web-based tools. *Nucleic Acids Res.* 41, D590–D596. doi: 10.1093/nar/gks1219

Rajabi, S., Darban, D., Tabatabaei, R. R., and Hosseini, F. (2020). Antimicrobial effect of spore-forming probiotics *Bacillus laterosporus* and *Bacillus megaterium*

against *Listeria monocytogenes*. *Arch. Microbiol.* 202, 2791–2797. doi: 10.1007/s00203-020-02004-9

Real, G., Pinto, S. M., Schyns, G., Costa, T., Henriques, A. O., and Moran, C. P. Jr. (2005). A gene encoding a holin-like protein involved in spore morphogenesis and spore germination in *Bacillus subtilis*. *J. Bacteriol.* 187, 6443–6453. doi: 10.1128/JB.187.18.6443-6453.2005

Rhayat, L., Maresca, M., Nicoletti, C., Perrier, J., Brinch, K. S., Christian, S., et al. (2019). Effect of *Bacillus subtilis* strains on intestinal barrier function and inflammatory response. *Front. Immunol.* 10:564. doi: 10.3389/fimmu.2019.00564

Salminen, S., Collado, M. C., Endo, A., Hill, C., Lebeer, S., Quigley, E. M. M., et al. (2021). The international scientific association of probiotics and prebiotics (ISAPP) consensus statement on the definition and scope of postbiotics. *Nat. Rev. Gastroenterol. Hepatol.* 18, 649–667. doi: 10.1038/s41575-021-00440-6

Selvam, R., Maheswari, P., Kavitha, P., Ravichandran, M., Sas, B., and Ramchand, C. N. (2009). Effect of *Bacillus subtilis* PB6, a natural probiotic on colon mucosal inflammation and plasma cytokines levels in inflammatory bowel disease. *Indian J. Biochem. Biophys.* 46, 79–85. doi: 10.1007/s00249-008-0372-2

Setlow, P. (2010). Spores of *Bacillus subtilis*: their resistance to and killing by radiation, heat and chemicals. *J. Appl. Microbiol.* 101, 514–525. doi: 10.1111/j.1365-2672.2005.02736.x

Soto, J. O. (2021). Feed intake improvement, gut microbiota modulation and pathogens control by using *Bacillus* species in shrimp aquaculture. *World J. Microbiol. Biotechnol.* 37:28. doi: 10.1007/s11274-020-02987-z

Tam, N. K., Uyen, N. Q., Hong, H. A., Duc le, H., Hoa, T. T., Serra, C. R., et al. (2006). The intestinal life cycle of *Bacillus subtilis* and close relatives. *J. Bacteriol.* 188, 2692–2700. doi: 10.1128/JB.188.7.2692-2700.2006

Urdaci, M. C., Bressollier, P., and Pinchuk, I. (2004). *Bacillus clausii* probiotic strains: antimicrobial and immunomodulatory activities. *J. Clin. Gastroenterol.* 38, S86–S90. doi: 10.1097/01.mcg.0000128925.06662.69

Wang, Y., Sun, J., Zhong, H., Li, N., Xu, H., Zhu, Q., et al. (2017). Effect of probiotics on the meat flavour and gut microbiota of chicken. *Sci. Rep.* 7:6400. doi: 10.1038/s41598-017-06677-z

Wu, Y., Wang, B., Xu, H., Tang, L., Li, Y., Gong, L., et al. (2019). Probiotic *Bacillus* attenuates oxidative stress-induced intestinal injury via p38-mediated autophagy. *Front. Microbiol.* 10:2185. doi: 10.3389/fmicb.2019.02185

Xiong, W., Sun, Y., and Zeng, Z. (2018). Antimicrobial use and antimicrobial resistance in food animals. *Environ. Sci. Pollut. R.* 25, 18377–18384. doi: 10.1007/s11356-018-1852-2

Yi, X., and Setlow, P. (2010). Studies of the commitment step in the germination of spores of *Bacillus* species. *J. Bacteriol.* 192, 3424–3433. doi: 10.1128/JB.00326-10

Yu, T., Kong, J., Zhang, L., Gu, X., Wang, M., and Guo, T. (2019). New crosstalk between probiotics *Lactobacillus plantarum* and *Bacillus subtilis*. *Sci. Rep.* 9:13151. doi: 10.1038/s41598-019-49688-8

Zhang, W., Zhu, Y. H., Zhou, D., Wu, Q., Song, D., Dicksved, J., et al. (2017). Oral administration of a select mixture of *Bacillus* probiotics affects the gut microbiota and goblet cell function following *Escherichia coli* challenge in newly weaned pigs of genotype *MUC4* that are supposed to be enterotoxigenic *E. coli* f4ab/ac receptor negative. *Appl. Environ. Microbiol.* 83:e02747-16. doi: 10.1128/AEM.02747-16

Conflict of Interest: The authors declare that the research was conducted in the absence of any commercial or financial relationships that could be construed as a potential conflict of interest.

Publisher's Note: All claims expressed in this article are solely those of the authors and do not necessarily represent those of their affiliated organizations, or those of the publisher, the editors and the reviewers. Any product that may be evaluated in this article, or claim that may be made by its manufacturer, is not guaranteed or endorsed by the publisher.

frontiers in Microbiology

ORIGINAL RESEARCH
published: 09 December 2021
doi: 10.3389/fmicb.2021.781649

Synergistic Induction of Chicken Antimicrobial Host Defense Peptide Gene Expression by Butyrate and Sugars

Qing Yang[1†], Li-An Fong[1†], Wentao Lyu[1,2], Lakshmi T. Sunkara[1,3], Kan Xiao[1,4] and Guolong Zhang[1]*

[1]*Department of Animal and Food Sciences, Oklahoma State University, Stillwater, OK, United States,* [2]*State Key Laboratory for Managing Biotic and Chemical Threats to the Quality and Safety of Agro-Products, Institute of Agro-Product Safety and Nutrition, Zhejiang Academy of Agricultural Sciences, Hangzhou, China,* [3]*Veterinary Diagnostic Center, Clemson University, Clemson, SC, United States,* [4]*Hubei Key Laboratory of Animal Nutrition and Feed Science, Hubei Collaborative Innovation Center for Animal Nutrition and Feed Safety, Wuhan Polytechnic University, Wuhan, China*

OPEN ACCESS

Edited by:
Wang Jiajun,
Northeast Agricultural University, China

Reviewed by:
Chanisa Kiatsurayanon, Ministry of Public Health, Thailand
Corwin D. Nelson, University of Florida, United States
Xiangbing Mao, Sichuan Agricultural University, China

***Correspondence:**
Guolong Zhang
zguolon@okstate.edu

†These authors have contributed equally to this work

Specialty section:
This article was submitted to Antimicrobials, Resistance and Chemotherapy, a section of the journal Frontiers in Microbiology

Received: *23 September 2021*
Accepted: *12 November 2021*
Published: *09 December 2021*

Citation:
Yang Q, Fong L-A, Lyu W, Sunkara LT, Xiao K and Zhang G (2021) Synergistic Induction of Chicken Antimicrobial Host Defense Peptide Gene Expression by Butyrate and Sugars. Front. Microbiol. 12:781649. doi: 10.3389/fmicb.2021.781649

Antimicrobial resistance is a major concern to public health demanding effective alternative strategies to disease control and prevention. Modulation of endogenous host defense peptide (HDP) synthesis has emerged as a promising antibiotic alternative approach. This study investigated a potential synergy between sugars and butyrate in inducing HDP gene expression in chickens. Our results revealed that sugars differentially regulated HDP expression in both gene- and sugar-specific manners in chicken HD11 macrophage cells. Among eight mono- and disaccharides tested, all were potent inducers of avian β-defensin 9 (*AvBD9*) gene ($p < 0.05$), but only galactose, trehalose, and lactose obviously upregulated cathelicidin-B1 (*CATHB1*) gene expression. The expression of *AvBD14* gene, on the other hand, was minimally influenced by sugars. Moreover, all sugars exhibited a strong synergy with butyrate in enhancing *AvBD9* expression, while only galactose, trehalose, and lactose were synergistic with butyrate in *CATHB1* induction. No synergy in *AvBD14* induction was observed between sugars and butyrate. Although lactose augmented the expression of nearly all HDP genes, its synergy with butyrate was only seen with several, but not all, HDP genes. Mucin-2 gene was also synergistically induced by a combination of lactose and butyrate. Furthermore, lactose synergized with butyrate to induce *AvBD9* expression in chicken jejunal explants ($p < 0.05$). Mechanistically, hyper-acetylation of histones was observed in response to both butyrate and lactose, relative to individual compounds. Mitogen-activated protein kinase, NF-κB, and cyclic adenosine monophosphate signaling pathways were also found to be involved in butyrate- and lactose-mediated synergy in *AvBD9* induction. Collectively, a combination of butyrate and a sugar with both HDP-inducing and barrier protective activities holds the promise to be developed as an alternative to antibiotics for disease control and prevention.

Keywords: antimicrobial resistance, antibiotic alternatives, host defense peptides, antimicrobial peptides, sugar, monosaccharide, lactose, butyrate

INTRODUCTION

Routine use of antibiotics at subtherapeutic levels in feed for animal growth promotion and disease prophylaxis has been linked to the emergence of antibiotic-resistant bacteria in humans (Manyi-Loh et al., 2018; Mcewen and Collignon, 2018). It is a global trend to phase out in-feed antibiotics, necessitating the development of alternatives to antibiotics to maintain the productivity and health of food-producing animals. Host defense peptides (HDPs), also known as antimicrobial peptides, constitute an essential component of the innate immunity system (Robinson et al., 2015; Hancock et al., 2016; Ting et al., 2020). Dietary modulation of endogenous HDP synthesis has the potential to be developed as a novel antibiotic-free approach to disease control with a minimum risk of triggering antimicrobial resistance (Lyu et al., 2015; Robinson et al., 2018; Bergman et al., 2020; Rodriguez-Carlos et al., 2021).

In vertebrate animals, defensins and cathelicidins represent two major families of HDPs (Zhang and Sunkara, 2014; Rodriguez-Carlos et al., 2021). A total of 14 β-defensins known as AvBD1-14 and four cathelicidins (CATH1-3 and CATHB1) have been reported in chickens (Zhang and Sunkara, 2014). HDPs are produced in myeloid and/or epithelial cells lining the digestive, respiratory, and urogenital tracts (Zhang and Sunkara, 2014; Hancock et al., 2016). HDPs exert direct antimicrobial activities against Gram-negative and Gram-positive bacteria, fungi, and enveloped viruses with a minimum of risk triggering resistance. HDPs also play a range of immunomodulatory roles such as chemotaxis, activation of immune cells, and modulation of inflammation and autophagy (Hancock et al., 2016; Robinson et al., 2018). Additionally, HDPs contribute to maintaining epithelial homeostasis by inducing mucins and tight junction proteins (Robinson et al., 2015). Down-regulation of HDPs is employed by certain pathogens to evade host defense and establish infections, while stimulation of endogenous HDP synthesis has shown potential for antimicrobial therapy (Hancock et al., 2016; Robinson et al., 2018; Bergman et al., 2020; Rodriguez-Carlos et al., 2021). Several classes of compounds such as histone deacetylase inhibitors (HDACi), short-chain fatty acids, and vitamin D_3 have been shown to promote HDP synthesis without triggering inflammation (Lyu et al., 2015; Bergman et al., 2020; Rodriguez-Carlos et al., 2021).

Butyrate is a major species of short-chain fatty acids produced by bacterial fermentation of undigested dietary fibers (Liu et al., 2018). Butyrate induces HDPs in humans, chickens, cattle, and pigs (Robinson et al., 2018; Rodriguez-Carlos et al., 2021) and confers protection against infections (Sunkara et al., 2011; Xiong et al., 2016). Butyrate induces HDPs by acting mainly as an HDACi to increase acetylation of core histones and relaxation of the target gene promoter (Kida et al., 2006; Robinson et al., 2018), and mitogen-activated protein kinase (MAPK) signaling pathways are also involved (Schauber et al., 2003). Sugars are represented by a group of dietary carbohydrates containing 1–2 monomeric sugar units and include monosaccharides, disaccharides, and sugar alcohols (Cummings and Stephen, 2007). Glucose has been found to enhance human β-defensin 1 (*DEFB1*) gene expression in keratinocytes (Cruz Diaz et al., 2015) and renal cells (Malik and Al-Kafaji, 2007), but decrease *DEFB3* and *DEFB4* in keratinocytes (Lan et al., 2011, 2012) and human cathelicidin antimicrobial peptide (*CAMP*) gene in monocyte-derived macrophages (Montoya-Rosales et al., 2016). However, lactose, a disaccharide derived from condensation of galactose and glucose, is capable of inducing the *CAMP* gene in human intestinal epithelial cells that involves MAPK, but not cyclic adenosine 3,5-monophosphate (cAMP) signaling (Cederlund et al., 2013). The induction of *CAMP* expression is also observed with several other mono- and disaccharides in the same study (Cederlund et al., 2013). Moreover, lactose is synergistic with butyrate in *CAMP* induction (Cederlund et al., 2013). The impact of lactose and its potential synergy with butyrate in HDP synthesis in other animal species and particularly non-mammalian species such as poultry remains unknown. Species-specific induction of HDPs in fact exists. For example, vitamin D_3 is a potent inducer for human *CAMP* gene (Wang et al., 2004), but has a minimum ability to induce HDP expression in chickens (Zhang et al., 2016) and loses its activity completely in mice (Gombart et al., 2005).

To evaluate whether lactose can activate HDP gene expression and whether the synergy exists between lactose and butyrate in chickens, we studied the expression of three representative chicken HDP genes including *AvBD9*, *AvBD14*, and *CATHB1* in chicken HD11 macrophage cells in response to lactose and butyrate individually and in combination. We further extended our study to a panel of eight different mono- and disaccharides for their HDP-inducing ability and their synergy with butyrate in chicken cells. Additionally, the mechanisms by which butyrate and lactose induce *AvBD9* gene expression were examined.

MATERIALS AND METHODS

Culture and Stimulation of Chicken HD11 Cells

Chicken HD11 macrophage cells (Sunkara et al., 2011, 2014) were maintained in complete RPMI 1640 medium (HyClone, Logan, UT, United States) containing 10% fetal bovine serum (Atlanta Biologicals, Flowery Branch, GA, United States), 100 U/ml penicillin, and 100 μg/ml streptomycin (Lonza, Walkersville, MD, United States). After overnight seeding at 2×10^6 cells/well in 6-well cell culture plates, cells were stimulated with 0.1 M or 0.2 M of various sugars in the presence or absence of 2 mM sodium butyrate (all from MilliporeSigma, St. Louis, MO, United States) for 3, 6, 12, 24, or 48 h, followed by RNA isolation and gene expression analysis as described below. To study the role of different signaling pathways in HDP induction, 50 μM PD98059, 20 μM SP600125, 25 μM SB203580, 0.1 μM QNZ, or 1 mm SQ22536 were incubated with cells 1 h prior to treatment with 2 mM butyrate and/or 0.2 M lactose for 24 h. To further probe the involvement of the Ras-Raf-MEK-ERK-RSK pathway, HD11 cells were pretreated with specific inhibitors including BAY43 (10, 20, and 40 μM), U0126 (5, 10, 20, and 40 μM), PD98059 (25, 50, 100, and 200 μM), AG126 (25, 50, and 100 μM), or SL0101 (10, 20, and 40 μM) for 1 h prior to

stimulation with 2 mM butyrate for 24 h. All inhibitors were purchased from Santa Cruz Biotechnology (Dallas, TX, United States) or Cayman Chemical (Ann Arbor, Michigan, United States) and dissolved in dimethyl sulfoxide (DMSO).

Preparation, Culture, and Stimulation of Chicken Jejunal Explants

The jejunal segments were harvested from 1- to 2-week-old broiler chickens, washed, cut into a series of 0.5-cm-long segments, and then cultured individually in 6-well plates as we previously described (Sunkara et al., 2014; Lyu et al., 2018). Each segment was stimulated with 0.1 M lactose with or without 2 mM butyrate and incubated in a Hypoxia Chamber (StemCell Technologies, Vancouver, BC, Canada) filled with 95% O_2 and 5% CO_2 at 37°C for 24 h. Jejunal segments were then centrifuged and homogenized in RNAzol RT for RNA extraction.

Quantitative Reverse Transcription-PCR

HD11 cells were lysed, and jejunal explants were homogenized in RNAzol RT (Molecular Research Center, Cincinnati, OH, United States) for extraction of total RNA. The first-strand cDNA was synthesized from 300 ng of total RNA using Maxima® First Strand cDNA Synthesis Kit (Thermo Fisher Scientific, Pittsburgh, PA, United States) in 4 μl. Real-time PCR was then performed using QuantiTech® SYBR Green I PCR kit (Qiagen, Valencia, CA, United States) and MyiQ Real-Time PCR Detection System (Bio-Rad, Hercules, CA, United States) in 10-μl reactions containing 1/10 of the first-strand cDNA and gene-specific primers for *AvBD1–10*, *AvBD14*, *CATHB1*, mucin-2 (*MUC2*), or claudin 1 (*CLDN1*). PCR cycling conditions were 95°C for 10 min, followed by 40 cycles of 94°C for 15 s, 55°C for 20 s, and 72°C for 30 s. The specificity of PCR reactions was confirmed by the melting curve analysis. The gene expression levels were quantified using the comparative ΔΔCt method with the glyceraldehyde-3-phosphate dehydrogenase (*GAPDH*) gene as a reference for data normalization as described (Sunkara et al., 2011, 2014). Primers for chicken HDP genes and *GAPDH* used in the current study were as previously described (Sunkara et al., 2011). The primers for *MUC2* were TCTGGAGAGAGTTGTCCTGAC (forward) and TCCTTGCAGCAGGAACAACT (reverse), while TTCCAACCAGGCTTTATGATG (forward) and TGCAGAGTCAGGTCAAACAGA (reverse) were used for *CLDN1*.

Western Blot Analysis

Chicken HD11 cells were stimulated with 0.2 M lactose in the presence or absence of 2 mM butyrate for 6, 12, or 24 h, followed by wash with phosphate buffered saline and lysis in the radioimmunoprecipitation (RIPA) lysis buffer (Santa Cruz Biotechnology). Protein concentration was measured using the Bradford Assay (Bio-Rad). To determine the levels of histone H4 acetylation, 20 μg proteins were separated in 12.5% SDS-PAGE gels and then transferred to polyvinylidene difluoride (PVDF) membranes. After overnight blocking in the blocking buffer containing 5% dry skim milk in TTBS (0.05% Tween 20, 20 mm Tris-HCl, 150 mm NaCl, pH 7.5) at 4°C, the membranes were incubated with a primary rabbit antibody against acetyl-histone H4 (Cell Signaling, Danvers, MA, United States) or a rabbit antibody against β-actin (MilliporeSigma) in the blocking buffer for 1 h at room temperature. After three washes in TTBS, the membrane was incubated with an alkaline phosphatase-conjugated goat anti-rabbit IgG antibody (MilliporeSigma) for 45 min at room temperature. Western blots were visualized with Western Blotting Luminol Reagent (Santa Cruz Biotechnology).

Statistical Analysis

Statistical analysis and data visualization were implemented in GraphPad Prism (GraphPad Software, La Jolla, CA, United States). The results were expressed as means ± standard error of the mean (SEM) from 2 to 3 independent experiments. Statistics was performed with one-way ANOVA and *post hoc* Tukey's test. The results were considered statistically significant if $p < 0.05$.

RESULTS

Time- and Concentration-Dependent Induction of HDP Genes by Sugars

To determine whether chicken HDP genes are induced by sugars, chicken HD11 macrophages were treated with three monosaccharides (glucose, galactose, and fructose), four disaccharides (lactose, maltose, sucrose, and trehalose), and a sugar alcohol (mannitol; **Figure 1**). All sugars at 0.2 M clearly stimulated *AvBD9* gene expression in a time-dependent manner. *AvBD9* was readily induced as early as 3 h, peaked at 6 h, and then gradually declined to nearly basal levels at 24 and 48 h (**Figure 2A**). All five sugars including mannitol showed a comparable efficacy in *AvBD9* induction, each with a peak response of an approximately 50- to 100-fold increase. Apparently, sugar-mediated HDP induction was gene-specific. Although the kinetics of the *CATHB1* mRNA expression was similar to that of *AvBD9* with a peak response at 6 h, different sugars showed a dramatic variation in their potency to induce *CATHB1*. Galactose led to a greater than 200-fold maximum increase in *CATHB1* expression at 6 h, whereas lactose gave only approximately 20-fold induction, with glucose, fructose, and mannitol showing a minimum two-fold to five-fold peak induction (**Figure 2B**). In the case of *AvBD14*, a peak induction occurred as early as 3 h for lactose, glucose, and fructose, while galactose had a maximum induction at 6 h (**Figure 2C**). However, only a maximum of five-fold to eight-fold change was observed with lactose, galactose, glucose, and mannitol, with essentially no induction seen with fructose (**Figure 2C**).

Sugar-triggered *AvBD9* induction was also in a strong dose-dependent manner. All sugars at 0.1 M showed a marginal effect on *AvBD9* induction at 6 h, while 0.2 M gave a substantial induction in HD11 cells (**Figure 3A**). As for *CATHB1*, only galactose, trehalose, and lactose triggered an obvious dose-dependent induction at 6 h, with 0.2 M galactose giving an approximately 150-fold increase, 0.2 M trehalose giving an approximately 40-fold increase, and 0.2 M lactose leading to a 20-fold induction (**Figure 3B**). Other sugars including

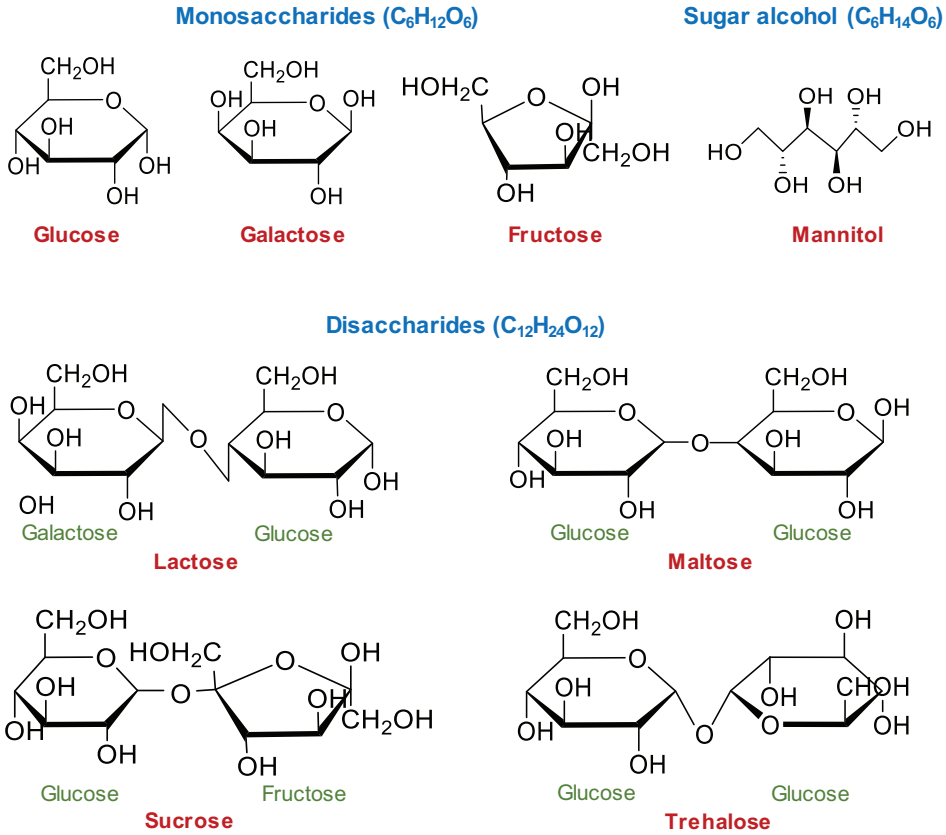

FIGURE 1 | Chemical structure of mono- and disaccharide sugars and sugar alcohol tested in this study. Haworth projections of the chemical structures were drawn using ChemDraw JS (https://chemdrawdirect.perkinelmer.cloud/js/sample/index.html).

maltose, glucose, sucrose, fructose, and mannitol had no or a negligible impact on *CATHB1* induction. *AvBD14* mRNA expression was minimally induced by most sugars, except for galactose causing an approximately five-fold increase at 0.2 M (**Figure 3C**).

Synergistic Induction of HDP and *MUC2* Gene Expression by Butyrate and Lactose

To further explore a potential synergy between sugars and butyrate in HDP induction, we treated chicken HD11 cells with 2 mM butyrate and 0.2 M lactose individually or in combination for various lengths of time. As expected, butyrate triggered a peak response with an approximately 1,750-fold *AvBD9* induction at 24 h, whereas lactose gave a maximum 350-fold *AvBD9* induction at 6 h (**Figure 4A**). Desirably, a combination of butyrate and lactose resulted in synergistic enhancement of *AvBD9* expression at nearly all time points except for 3 h. A peak response was seen at 12 h with a nearly 70,000-fold increase, and the synergistic induction was sustained for at least 48 h (**Figure 4A**). Butyrate and lactose also synergistically improved *CATHB1* transcription, peaking at 24 h with a 2,000-fold induction (**Figure 4B**). Although butyrate and lactose enhanced *AvBD14* expression individually albeit at much lower magnitudes, no obvious synergy was observed when they were used together (**Figure 4C**), reinforcing the notion of differential regulation of HDP genes by lactose and butyrate.

In addition, several other HDP genes such as *AvBD3*, *AvBD8,* and *AvBD10* were synergistically induced by a combination of butyrate and lactose (**Figure 5A**). For example, lactose alone strongly increased *AvBD10* expression and further synergized with butyrate to strengthen *AvBD10* transcription. A synergistic enhancement of *AvBD3* and *AvBD8* expressions was also observed at 12 h or 24 h. However, the remaining HDP genes were moderately affected by lactose and butyrate with no obvious synergy observed (**Figure 5A**). It is important to note that most HDP genes were induced by butyrate with a peak induction at 24 h, but lactose induced HDP genes rather quickly peaking at 6 h in many cases with a notable exception being *AvBD10*, which exhibited a time-depending increase with a maximum induction at 24 h (**Figure 5A**). The strongest synergy occurred at 12 or 24 h for most HDP genes.

Because of our interest in mucosal immunity and barrier integrity, two major genes involved in barrier function, namely *MUC2* and *CLDN1,* were also evaluated. Interestingly, lactose induced *MUC2* quickly showing a maximum induction in

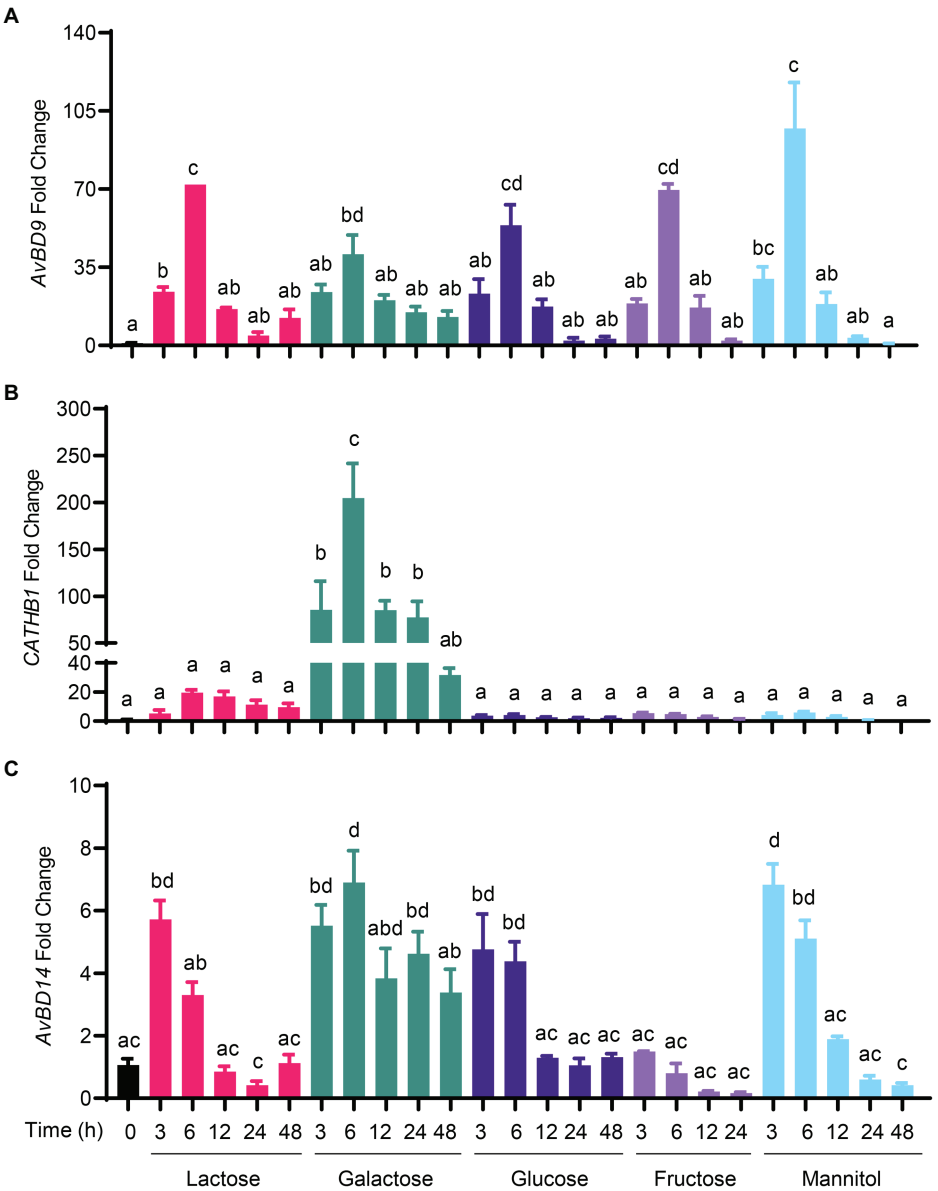

FIGURE 2 | Time-dependent induction of host defense peptide (HDP) expression by sugars. Chicken HD11 macrophages were stimulated in duplicate with 0.2 M of indicated sugars for 3, 6, 12, 24, or 48 h. Cells were then subjected to RNA isolation and RT-qPCR analysis of gene expressions of avian β-defensin 9 (*AvBD9*) **(A)**, cathelicidin-B1 (*CATHB1*) **(B)**, and *AvBD14* **(C)**. Results are expressed as means ± SEM of 2–3 independent experiments. The bars without common superscript letters denote statistical significance ($p < 0.05$) as determined by one-way ANOVA and *post hoc* Tukey's test.

HD11 cells at 6 h (**Figure 5B**). A clear synergy was also observed between butyrate and lactose in *MUC2* induction particularly at 12 and 24 h (**Figure 5B**). On the other hand, *CLDN1* was prominently induced by butyrate, but not by lactose, and no obvious synergy was observed (**Figure 5C**).

To evaluate whether other mono- and disaccharides could also synergize with butyrate in improving HDP expression, HD11 cells were treated with butyrate and different sugars individually or in combination for 12 h. Similarly, galactose, glucose, and trehalose showed a dramatic synergy in *AvBD9* induction (**Figure 6A**). Moreover, galactose and trehalose synergized with butyrate more strongly than lactose in *CATHB1* induction, whereas glucose and mannitol failed to induce *CATHB1* expression showing no synergy with butyrate (**Figure 6B**). In the case of *AvBD14*, none of the sugars investigated exhibited synergy with butyrate (**Figure 6C**).

To confirm whether the HDP-inducing synergy between butyrate and sugars also occurs in other cell types, chicken jejunal explants were prepared and treated with butyrate and lactose separately or together. Butyrate (2 mM) and lactose (0.1 M) gave an approximately 120- and 20-fold induction of *AvBD9*, respectively, but more importantly, a marked synergy was observed,

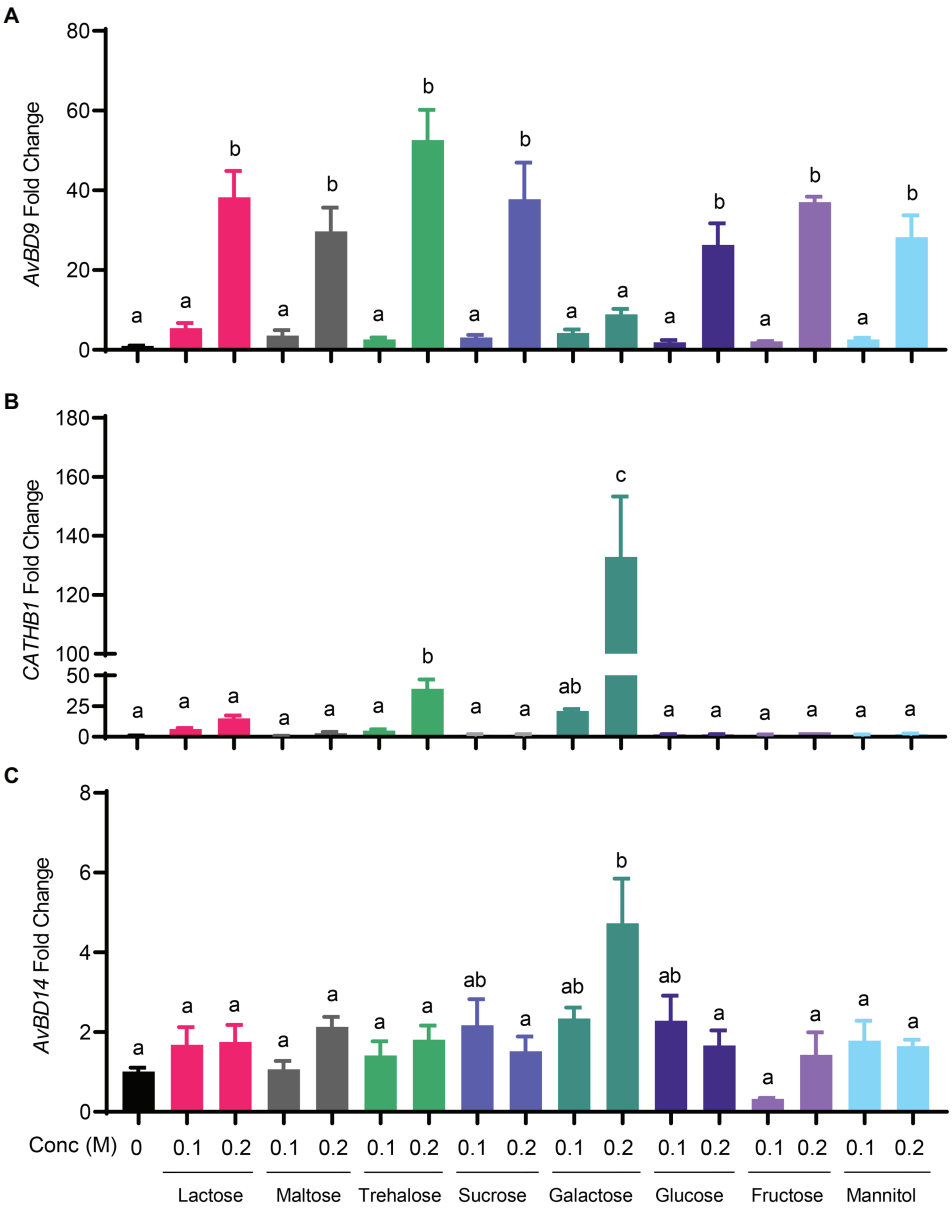

FIGURE 3 | Dose-dependent induction of chicken HDP expression by sugars. Chicken HD11 macrophage cells were stimulated in duplicate with 0.1 or 0.2 M of indicated sugars for 6 h, followed by RNA isolation and RT-qPCR analysis of the gene expressions of *AvBD9* **(A)**, *CATHB1* **(B)**, and *AvBD14* **(C)**. Results are expressed as means ± SEM of 2–3 independent experiments. The bars without common superscript letters denote statistical significance ($p < 0.05$) as determined by one-way ANOVA and *post hoc* Tukey's test.

showing an approximately 550-fold increase in response to both compounds (**Figure 7**). To further examine how inflammatory response is affected by butyrate and lactose, HD11 cells were treated with butyrate or lactose individually or in combination in the presence or absence of bacterial lipopolysaccharide (LPS). As expected, butyrate was anti-inflammatory without altering interleukin-1β (*IL-1β*) expression; however, lactose caused a minimum induction of *IL-1β* expression (**Figure 8**). Importantly, lactose, butyrate, and the combination significantly reduced LPS-induced IL-1β expression, although no synergistic suppression was observed (**Figure 8**), suggesting an overall anti-inflammatory effect of the butyrate/lactose combination.

Role of Histone Acetylation and MAPK, NF-κB, and cAMP Signaling in HDP Gene Expression Induced by Butyrate and Lactose

Butyrate induces HDP expression in chickens and humans mainly by acting as a HDACi (Kida et al., 2006; Robinson

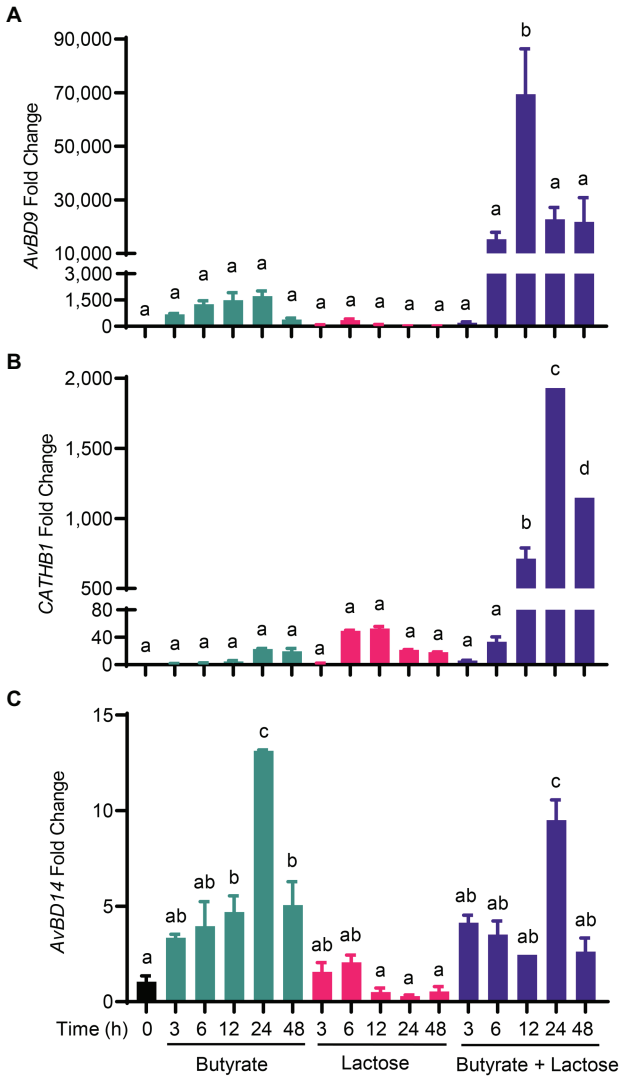

FIGURE 4 | Synergistic induction of HDP expression by butyrate and lactose. Chicken HD11 macrophage cells were stimulated in duplicate with 2 mM sodium butyrate and 0.2 M lactose individually or in combination for 3, 6, 12, 24, or 48 h, followed by RNA isolation and RT-qPCR analysis of the mRNA expression levels of *AvBD9* **(A)**, *CATHB1* **(B)**, and *AvBD14* **(C)**. Results are expressed as means ± SEM of 2–3 independent experiments. The bars without common superscript letters denote statistical significance ($p < 0.05$) as determined by one-way ANOVA and *post hoc* Tukey's test.

et al., 2018). To examine the impact of butyrate and lactose on histone acetylation, chicken HD11 cells were treated with butyrate and lactose individually or in combination for 6, 12, and 24 h, followed by evaluation of the acetylation status of histone 4 (H4) using immunoblotting. As expected, butyrate triggered obvious H4 acetylation at 12 h and the acetylation become more pronounced at 24 h, while lactose had no impact on histone acetylation at any time point (**Figure 9**). A combination of both butyrate and lactose apparently accelerated and intensified histone acetylation, with H4 acetylation occurring evidently as early as 6 h, peaking at 12 h, and sustained at 24 h.

To examine the role of MAPK, NF-κB, and cAMP signaling pathways in butyrate- and lactose-mediated synergy in *AvBD9* induction, chicken HD11 cells were treated with butyrate and/or lactose for 24 h in the presence or absence of specific inhibitors for each pathway. As expected, all inhibitors alone had a minimum influence on *AvBD9* gene expression, and inhibition of p38 MAPK (with SB203580), NF-κB (with QNZ), and cAMP pathways (with SQ22536) also had no influence on lactose-induced *AvBD9* expression (**Figure 10A**). On the other hand, inhibition of p38 MAPK, JNK (with SP600125), NF-κB, and cAMP pathways partially blocked butyrate-induced *AvBD9* expression, and the same four signaling pathways were similarly involved in *AvBD9* induction by a combination of butyrate and lactose (**Figure 10A**). Surprisingly, blocking the MAPK kinase 1/2 (MEK1/2) pathway by PD98059 significantly potentiated *AvBD9* gene expression induced by lactose, butyrate, or the combination (**Figure 10A**).

To further probe the involvement of the Ras-Raf-MEK1/2-ERK1/2-RSK pathway, inhibitors specific for kinases at different steps (**Figure 10B**) were employed. Consistently, inhibition of MEK1/2 with low concentrations of PD98059 and U0126 enhanced *AvBD9* gene expression, while increasing the concentrations of PD98059 and U0126 significantly suppressed *AvBD9* expression (**Figure 10C**). Inhibition of Raf with BAY43 also dose-dependently reduced *AvBD9* expression. The *AvBD9*-suppressing effect of blocking ERK1/2 and ribosomal S6 kinase (RSK) with AG126 and SL0101 was much more pronounced (**Figure 10C**). Collectively, these results suggested that, similar to the p38 MAPK and JNK pathways, the MEK-ERK pathway is also involved in butyrate-mediated HDP induction.

DISCUSSION

Sugars include mono- and disaccharides and constitute a group of dietary carbohydrates consisting of 1–2 simple sugar units, while oligosaccharides contain 3–9 sugar units, and polysaccharides contain >9 sugar units (Cummings and Stephen, 2007). All carbohydrates need to be broken down into monosaccharides to be utilized by animal hosts. Glucose and galactose are transported and taken up by the intestinal epithelial cells similarly through the involvement of sodium/glucose cotransporter 1 (SGLT1) and glucose transporter 2 (GLUT2), while GLUT2 and GLUT5 are involved in fructose transportation and absorption (Elferink et al., 2020). Disaccharides such as lactose, maltose, and trehalose lack the mechanism to be transported directed into intestinal epithelial cells and have to be broken down into two units of monosaccharides by different enzymes in the GI tract. Extended from an earlier study in humans (Cederlund et al., 2013), we have confirmed the conservation of the HDP-inducing activity of sugars in the chicken, a non-mammalian species, and further revealed a pronounced synergy between sugars and butyrate in augmenting chicken HDP expression. All eight most common sugars examined in this study including three monosaccharides, four

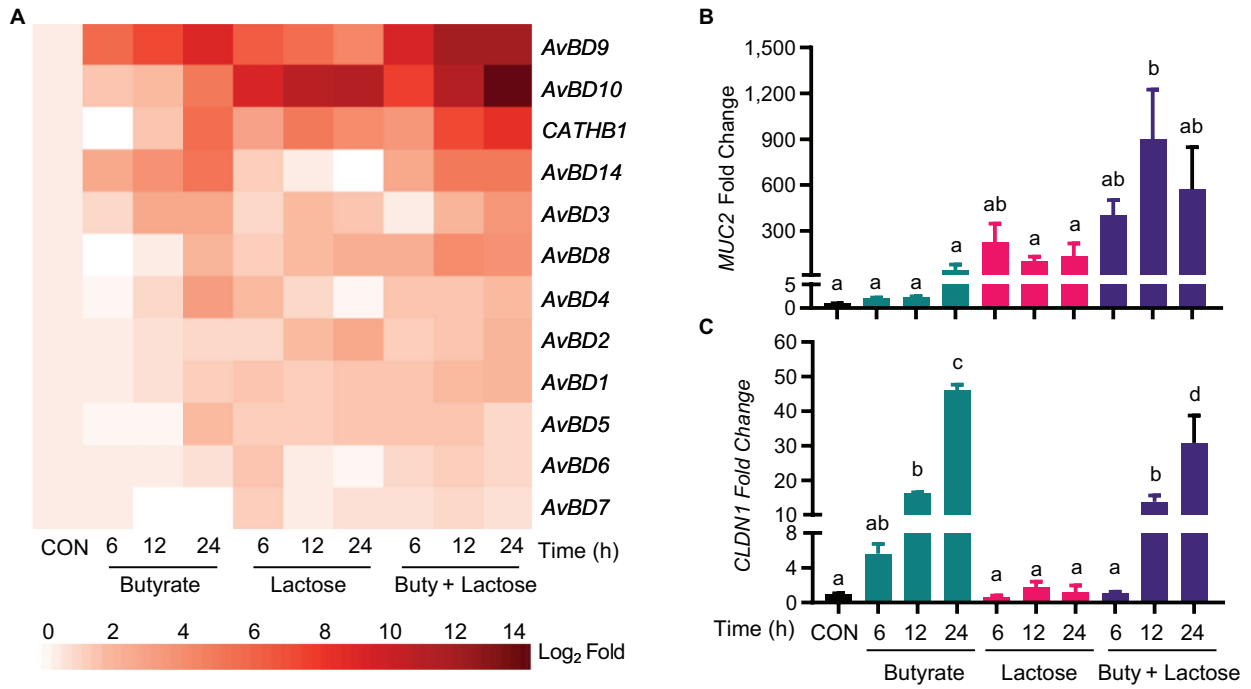

FIGURE 5 | Synergistic induction of HDP and barrier function gene expression by butyrate and lactose. Chicken HD11 cells were stimulated in duplicate with 2 mM sodium butyrate and 0.2 M lactose individually or in combination for 6, 12, or 24 h, followed by RNA isolation and RT-qPCR analysis of the mRNA expression levels of multiple HDP genes **(A)**, mucin 2 (*MUC2*) **(B)**, and claudin 1 (*CLDN1*) **(C)**. Results are expressed as means ± SEM of two independent experiments. The bars without common superscript letters denote statistical significance ($p < 0.05$) as determined by one-way ANOVA and *post hoc* Tukey's test.

disaccharides, and a sugar alcohol have the ability to induce the expression of certain HDP genes.

We have found that sugar-induced HDP expression is both gene- and sugar-specific. Among all chicken HDP genes, *AvBD9* and *AvBD10* are most readily inducible by lactose, while other genes are moderately or minimally induced. Among all sugars, *AvBD9* is uniformly induced, but other HDP genes exhibit a clear preference. For example, galactose is a potent inducer of *CATHB1* gene expression, while trehalose and lactose have a modest activity, and many other sugars are minimally active in *CATHB1* induction. On the other hand, *AvBD14* is minimally regulated by virtually all mono- and disaccharides tested. These results are consistent with an earlier study in humans, where trehalose is the most active in human *CAMP* gene induction in human HT-29 epithelial cells, with the potency gradually decreased in the order of maltose, lactose, glucose, and galactose (Cederlund et al., 2013). Gene-specific induction of HDPs was also observed with other small-molecule compounds such as butyrate (Sunkara et al., 2011, 2012; Zeng et al., 2013) and vitamin D_3 (Zhang et al., 2016). For example, approximately a half number of chicken HDP genes are induced by butyrate, with *AvBD9* being the most inducible in chicken HD11 cells (Sunkara et al., 2012).

The synergy between butyrate and sugars also shows similar gene- and sugar-specific patterns of HDP regulation. All sugars synergize with butyrate in *AvBD9* induction with a similar potency; however, only galactose, trehalose, and lactose show a synergistic effect with butyrate in *CATHB1* induction, with galactose and trehalose giving much stronger synergy than lactose. It is noted that the kinetics of HDP induction by sugars or the sugar/butyrate combination is much different from most other HDP-inducing compounds. While it takes 24–48 h for butyrate, fatty acids, HDACi, and vitamin D_3 to achieve maximum HDP induction (Wang et al., 2004; Sunkara et al., 2011, 2012; Jiang et al., 2013; Zeng et al., 2013; Deng et al., 2018; Lyu et al., 2018), peak HDP expression occurs as early as 3–6 h with a sugar.

All sugars tested in this study are capable of inducing *AvBD9* gene expression; however, the underlying mechanism remains largely unknown. An earlier human study revealed a partial involvement of the JNK and p38 MAPK pathways in lactose-induced human *CAMP* gene expression in HT-29 cells (Cederlund et al., 2013). However, neither MAPK pathway plays a critical role in lactose-mediated *AvBD9* induction. Such a discrepancy might be due to a difference in species, cell type, or HDP gene examined in the two studies. However, we have confirmed that all three canonical MAPK signaling pathways (JNK, p38 MAPK, and ERK1/2) are involved in the synergy in *AvBD9* gene induction by the lactose/butyrate combination. Although they are dispensable for lactose-induced *AvBD9* expression, NF-κB and cAMP signaling are partially responsible for the lactose/butyrate synergy, which is perhaps unsurprising, given the fact that sugars such as glucose are known to activate cAMP (Tengholm and Gylfe, 2017) and NF-κB (Kracht et al., 2020).

Butyrate is well known to induce HDP expression mainly by acting as an HDACi (Xiong et al., 2016; Rodriguez-Carlos et al., 2021). In this study, we have further revealed that although

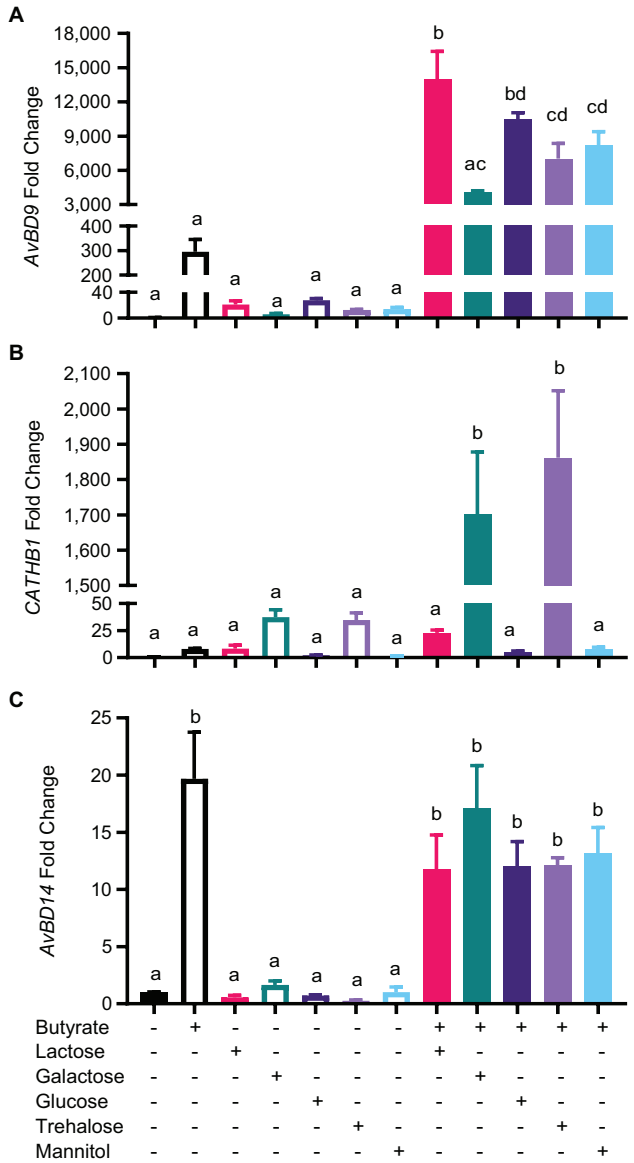

FIGURE 6 | Synergistic induction of HDP expression by butyrate and sugars. Chicken HD11 cells were stimulated in duplicate with 2 mM butyrate and 0.2 M of indicated sugars separately or in combination for 12 h, followed by RNA isolation and RT-qPCR analysis of the mRNA expression levels of *AvBD9* **(A)**, *CATHB1* **(B)**, and *AvBD14* **(C)**. Results are expressed as means ± SEM of 2–3 independent experiments. The bars without common superscript letters denote statistical significance ($p < 0.05$) as determined by one-way ANOVA and *post hoc* Tukey's test.

lactose has no direct impact on histone acetylation, histones are hyper-acetylated in response to a combination of lactose and butyrate. The exact mechanism is unknown, but it is tempting to speculate that lactose may act similarly as glucose, which has been extensively studied and shown to regulate gene expression through p300, also known as EP300 (Chen et al., 2010), a central transcriptional coactivator with histone acetyltransferase activity to enhance histone acetylation, chromatin relaxation, and gene transcription (Dancy and Cole, 2015). Glucose-mediated enhancement of p300 phosphorylation was recently shown to mediate through activation of 5′ adenosine monophosphate-activated protein kinase (AMPK) in a metabolic context-dependent manner (Gutierrez-Salmeron et al., 2020). AMPK is normally activated during glucose deprivation, but can also be activated in response to high glucose if glucose is blocked for glycogen synthesis inside a cell (Gutierrez-Salmeron et al., 2020).

It is worth noting that 25–50 mM glucose was mostly used in the literature to activate AMPK or induce phosphorylation of p300. Much higher concentrations (0.1–0.2 M) of glucose and other sugars have to be used in order to achieve optimal HDP induction in this study. The reason is unclear, but unlikely due to osmotic stress, because of the facts that: (1) up to 0.4 M NaCl or KCl fails to induce human *CAMP* gene in HT-29 cells, whereas different sugars do so readily (Cederlund et al., 2013); (2) certain HDP genes such as *AvBD14* are barely induced by any sugar even at 0.2 M (**Figure 3**); and (3) HDP genes such as *CATHB1* are only induced by few, but not all, sugars (**Figures 2, 3**). Mannitol, a non-metabolizable and membrane-impermeable sugar alcohol (Chen et al., 2020) induces chicken *AvBD9* gene and also synergizes with butyrate in *AvBD9* induction, similar to most other sugars, which is consistent with its ability to induce human *CAMP* gene (Cederlund et al., 2013). Additionally, chickens produce maltase and sucrase to break down sucrose and maltose, respectively, but appear to lack lactase to break down and take up lactose (Siddons, 1969; Siddons and Coates, 1972). Lactose is nevertheless still capable of inducing most HDP genes in chicken cells. These observations collectively suggest a presence of transmembrane receptors to mediate sugar-induced HDP expression. In fact, sugars and sweeteners can bind to ubiquitously expressed sweet taste receptors T1R2 and T1R3 to activate multiple complex signaling pathways in mammals (Lee and Owyang, 2017; Von Molitor et al., 2021) and also in avian species (Niknafs and Roura, 2018; Roura and Foster, 2018). It will be important to examine the involvement of taste receptors or other receptors in sugar-mediated HDP induction.

In addition to upregulating HDP expression, lactose and likely other sugars also strongly augment the gene expression of *MUC2*, which is in turn translated to the predominant mucin protein in the intestinal epithelium (Vancamelbeke and Vermeire, 2017; Liu et al., 2020). Butyrate is also well-known to induce *MUC2* (Bach Knudsen et al., 2018). The synergy between butyrate and lactose in inducing *MUC2* may potentiate their protection of the epithelial barrier. With an additional ability to suppress LPS-induced inflammatory response (**Figure 8**), butyrate and lactose have the potential to enhance gut health and alleviate infections. In fact, butyrate and 2.5% lactose have been separately used in chickens with a beneficial effect on alleviating infections such as necrotic enteritis (Mcreynolds et al., 2007; Liu et al., 2019). Although the mechanism of action was not studied earlier, augmenting HDP gene expression and barrier function while suppressing inflammation may be at least partially responsible for enhanced disease resistance in chickens fed butyrate or lactose. Although a combination of butyrate and lactose is yet to be tested, we recently found chickens supplemented with a mixture of 0.1% encapsulated sodium butyrate, 1% lactose, and 5–10 ppm forskolin-containing plant extract to

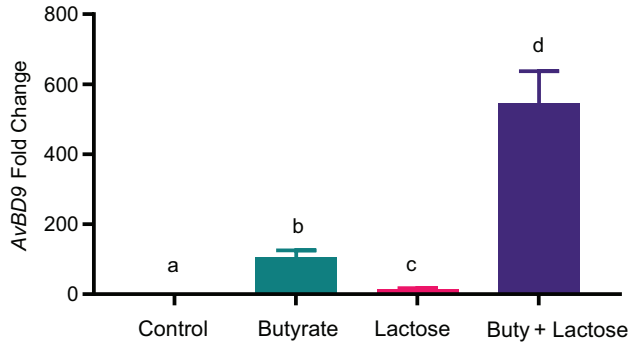

FIGURE 7 | Synergistic induction of *AvBD9* gene expression in chicken jejunal explants by butyrate and lactose. Chicken jejunal explants were treated in duplicate with 2 mM sodium butyrate and 0.1 M lactose individually or in combination for 24 h, followed by RNA isolation and RT-qPCR analysis of *AvBD9* expression. Results are shown as means ± SEM of three independent experiments. The bars without common superscript letters denote statistical significance ($p < 0.05$) as determined by one-way ANOVA and *post hoc* Tukey's test.

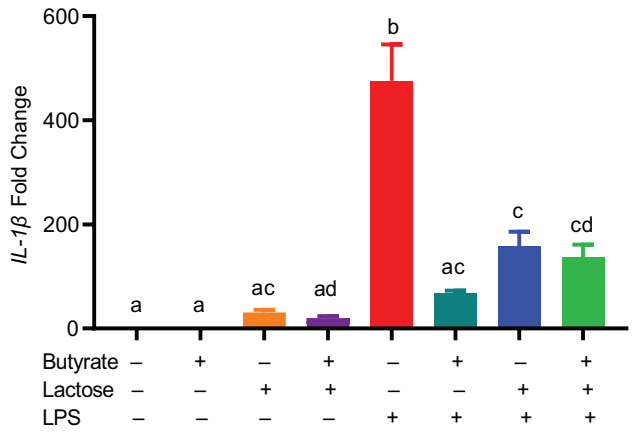

FIGURE 8 | Suppression of lipopolysaccharide (LPS)-induced interleukin 1β (*IL-1β*) by butyrate and lactose. Chicken HD11 cells were treated in duplicate with 2 mM butyrate, 0.1 M lactose, or in combination for 1 h, followed by stimulation with 10 ng/ml LPS for another 3 h and RT-qPCR measurement of *IL-1β* gene expression. The results presented means ± SEM of two independent experiments. The bars without common superscript letters denote statistical significance ($p < 0.05$) as determined by one-way ANOVA and *post hoc* Tukey's test.

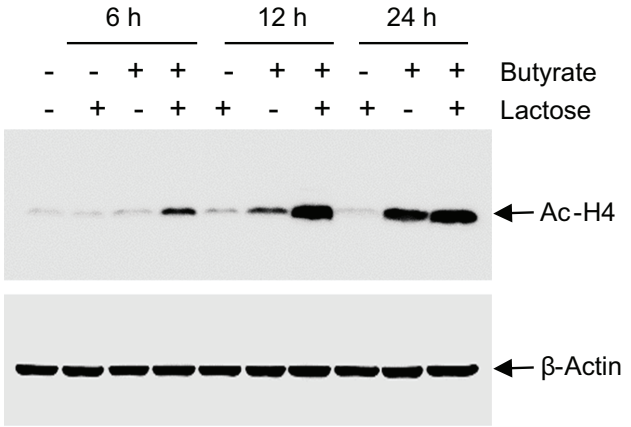

FIGURE 9 | Acetylation of histone H4 in response to butyrate and lactose. Chicken HD11 cells were treated with 0.2 M lactose with or without 2 mM sodium butyrate for 6, 12, or 24 h, followed by Western blot analysis for acetylation of histone H4. β-actin was also probed to show an equal amount of protein loading in each lane. The results are a representative of two independent experiments.

be protected from both necrotic enteritis and coccidiosis (Yang et al., 2021). Butyrate/forskolin-mediated protection of chickens from necrotic enteritis is also mediated through enhancing HDP expression and barrier function (Robinson et al., 2021).

This study is focused on mono- and disaccharides. The role of dietary oligosaccharides and polysaccharides in regulating HDP gene expression is largely unknown, except that two human milk oligosaccharides were recently found to increase human β-defensin 2 protein synthesis, but not other HDPs or inflammatory cytokines (Gursoy et al., 2021). It will be interesting to explore possible HDP-inducing and other immunomodulatory roles of commonly used dietary oligosaccharides and polysaccharides such as fructo-oligosaccharides, galacto-oligosaccharides, xylo-oligosaccharides, mannan-oligosaccharides, and inulin, all of which are being actively explored as prebiotics to manage the gut microbiome, gut health, and diseases (Zhu et al., 2019).

CONCLUSION

Mono- and disaccharide sugars are capable of inducing the expressions of HDP genes in chicken HD11 macrophages and jejunal explants in gene- and sugar-specific manners. Moreover, these sugars synergize with butyrate to further enhance chicken HDP expression. Additionally, lactose is synergistic with butyrate in upregulating *MUC2* expression. Promoting histone hyper-acetylation is at least partially responsible for lactose- and butyrate-mediated synergy in *AvBD9* induction. MAPK, NF-κB, and cAMP signaling pathways are all involved in *AvBD9* expression induced by lactose and butyrate. Our results suggest a prospect for the development of a combination of sugars and butyrate as an antibiotic-alternative approach to infectious disease control and prevention.

DATA AVAILABILITY STATEMENT

The original contributions presented in the study are included in the article/supplementary material, further inquiries can be directed to the corresponding author.

AUTHOR CONTRIBUTIONS

QY, L-AF, WL, LTS, and KX conducted the experiments. QY, L-AF, and GZ performed data analysis. QY and L-AF drafted the

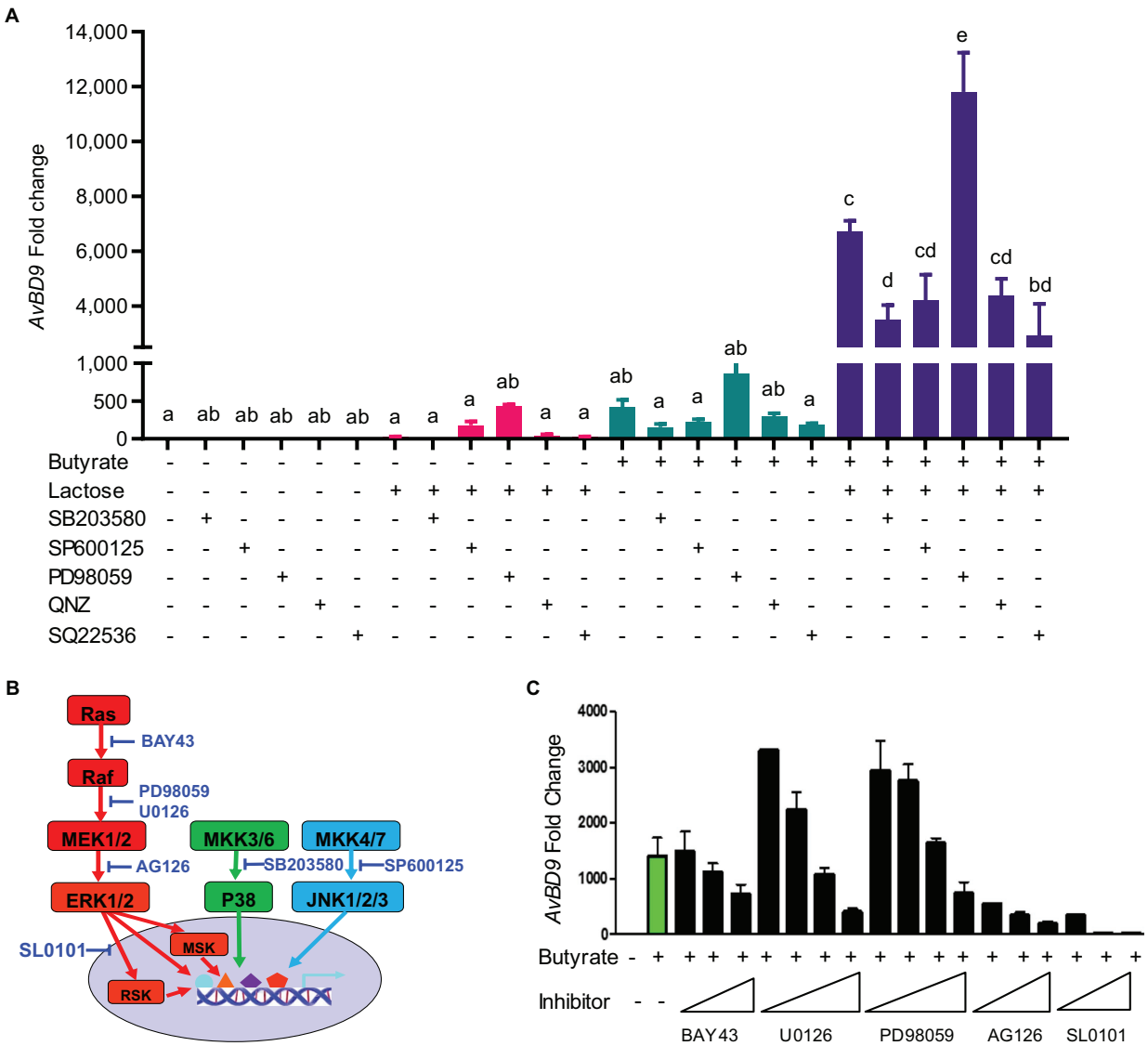

FIGURE 10 | Involvement of mitogen-activated protein kinase (MAPK), NF-κB, and cAMP signaling pathways in *AvBD9* induction mediated by butyrate and lactose. **(A)** Chicken HD11 cells were pretreated for 1 h with or without a specific inhibitor for p38 MAPK (SB203580), JNK (SP600125), MEK1/2 (PD98059), NF-κB (QNZ), or cAMP signaling (SQ22536), followed by stimulation with 2 mM sodium butyrate and 0.2 M lactose separately or in combination for another 24 h. **(B)** A schematic drawing of three canonical MAPK pathways showing the steps where specific inhibitors act. **(C)** HD11 cells were pretreated for 1 h with or without an indicated inhibitor for the Ras-Raf-MEK-ERK-RSK pathway, followed by stimulation with 2 mM sodium butyrate for another 24 h. RT-qPCR analysis of *AvBD9* expression was performed. Results are shown as means ± SEM of 2–3 independent experiments. The bars without common superscript letters denote statistical significance ($p < 0.05$) as determined by one-way ANOVA and *post hoc* Tukey's test.

manuscript. GZ conceived the study and revised the manuscript. All authors contributed to the article and approved the submitted version.

FUNDING

This research was funded by the USDA National Institute of Food and Agriculture (grant nos. 2018-68003-27462 and 2020-67016-31619), Oklahoma Center for the Advancement of Science and Technology (grant no. AR19-027), the Ralph F. and Leila W. Boulware Endowment Fund, and Oklahoma Agricultural Experiment Station Project H-3112.

ACKNOWLEDGMENTS

The authors appreciate Hyun Lillehoj at the USDA-Agricultural Research Services for kindly providing HD11, a chicken macrophage cell line.

REFERENCES

Bach Knudsen, K. E., Laerke, H. N., Hedemann, M. S., Nielsen, T. S., Ingerslev, A. K., Gundelund Nielsen, D. S., et al. (2018). Impact of diet-modulated butyrate production on intestinal barrier function and inflammation. *Nutrients* 10:1499. doi: 10.3390/nu10101499

Bergman, P., Raqib, R., Rekha, R. S., Agerberth, B., and Gudmundsson, G. H. (2020). Host directed therapy against infection by boosting innate immunity. *Front. Immunol.* 11:1209. doi: 10.3389/fimmu.2020.01209

Cederlund, A., Kai-Larsen, Y., Printz, G., Yoshio, H., Alvelius, G., Lagercrantz, H., et al. (2013). Lactose in human breast milk an inducer of innate immunity with implications for a role in intestinal homeostasis. *PLoS One* 8:e53876. doi: 10.1371/journal.pone.0053876

Chen, S., Feng, B., George, B., Chakrabarti, R., Chen, M., and Chakrabarti, S. (2010). Transcriptional coactivator p300 regulates glucose-induced gene expression in endothelial cells. *Am. J. Physiol. Endocrinol. Metab.* 298, E127–E137. doi: 10.1152/ajpendo.00432.2009

Chen, M., Zhang, W., Wu, H., Guang, C., and Mu, W. (2020). Mannitol: physiological functionalities, determination methods, biotechnological production, and applications. *Appl. Microbiol. Biotechnol.* 104, 6941–6951. doi: 10.1007/s00253-020-10757-y

Cruz Diaz, L. A., Flores Miramontes, M. G., Chavez Hurtado, P., Allen, K., Gonzalez Avila, M., and Prado Montes De Oca, E. (2015). Ascorbic acid, ultraviolet C rays, and glucose but not hyperthermia are elicitors of human beta-defensin 1 mRNA in normal keratinocytes. *Biomed. Res. Int.* 2015:714580. doi: 10.1155/2015/714580

Cummings, J. H., and Stephen, A. M. (2007). Carbohydrate terminology and classification. *Eur. J. Clin. Nutr.* 61(Suppl. 1), S5–S18. doi: 10.1038/sj.ejcn.1602936

Dancy, B. M., and Cole, P. A. (2015). Protein lysine acetylation by p300/CBP. *Chem. Rev.* 115, 2419–2452. doi: 10.1021/cr500452k

Deng, Z., Wang, J., Lyu, W., Wieneke, X., Matts, R., Ma, X., et al. (2018). Development of a cell-based high-throughput screening assay to identify porcine host defense peptide-inducing compounds. *J Immunol Res* 2018:5492941. doi: 10.1155/2018/5492941

Elferink, H., Bruekers, J. P. J., Veeneman, G. H., and Boltje, T. J. (2020). A comprehensive overview of substrate specificity of glycoside hydrolases and transporters in the small intestine: "a gut feeling". *Cell. Mol. Life Sci.* 77, 4799–4826. doi: 10.1007/s00018-020-03564-1

Gombart, A. F., Borregaard, N., and Koeffler, H. P. (2005). Human cathelicidin antimicrobial peptide (CAMP) gene is a direct target of the vitamin D receptor and is strongly up-regulated in myeloid cells by 1,25-dihydroxyvitamin D3. *FASEB J.* 19, 1067–1077. doi: 10.1096/fj.04-3284com

Gursoy, U. K., Salli, K., Soderling, E., Gursoy, M., Hirvonen, J., and Ouwehand, A. C. (2021). Regulation of hBD-2, hBD-3, hCAP18/LL37, and proinflammatory cytokine secretion by human milk oligosaccharides in an organotypic oral mucosal model. *Pathogens* 10:739. doi: 10.3390/pathogens10060739

Gutierrez-Salmeron, M., Garcia-Martinez, J. M., Martinez-Useros, J., Fernandez-Acenero, M. J., Viollet, B., Olivier, S., et al. (2020). Paradoxical activation of AMPK by glucose drives selective EP300 activity in colorectal cancer. *PLoS Biol.* 18:e3000732. doi: 10.1371/journal.pbio.3000732

Hancock, R. E., Haney, E. F., and Gill, E. E. (2016). The immunology of host defence peptides: beyond antimicrobial activity. *Nat. Rev. Immunol.* 16, 321–334. doi: 10.1038/nri.2016.29

Jiang, W., Sunkara, L. T., Zeng, X., Deng, Z., Myers, S. M., and Zhang, G. (2013). Differential regulation of human cathelicidin LL-37 by free fatty acids and their analogs. *Peptides* 50, 129–138. doi: 10.1016/j.peptides.2013.10.008

Kida, Y., Shimizu, T., and Kuwano, K. (2006). Sodium butyrate up-regulates cathelicidin gene expression via activator protein-1 and histone acetylation at the promoter region in a human lung epithelial cell line, EBC-1. *Mol. Immunol.* 43, 1972–1981. doi: 10.1016/j.molimm.2005.11.014

Kracht, M., Muller-Ladner, U., and Schmitz, M. L. (2020). Mutual regulation of metabolic processes and proinflammatory NF-kappaB signaling. *J. Allergy Clin. Immunol.* 146, 694–705. doi: 10.1016/j.jaci.2020.07.027

Lan, C. C., Wu, C. S., Huang, S. M., Kuo, H. Y., Wu, I. H., Liang, C. W., et al. (2012). High-glucose environment reduces human beta-defensin-2 expression in human keratinocytes: implications for poor diabetic wound healing. *Br. J. Dermatol.* 166, 1221–1229. doi: 10.1111/j.1365-2133.2012.10847.x

Lan, C. C., Wu, C. S., Huang, S. M., Kuo, H. Y., Wu, I. H., Wen, C. H., et al. (2011). High-glucose environment inhibits p38MAPK signaling and reduces human beta-defensin-3 expression [corrected] in keratinocytes. *Mol. Med.* 17, 771–779. doi: 10.2119/molmed.2010.00091

Lee, A. A., and Owyang, C. (2017). Sugars, sweet taste receptors, and brain responses. *Nutrients* 9:653. doi: 10.3390/nu9070653

Liu, J. D., Lumpkins, B., Mathis, G., Williams, S. M., and Fowler, J. (2019). Evaluation of encapsulated sodium butyrate with varying releasing times on growth performance and necrotic enteritis mitigation in broilers. *Poult. Sci.* 98, 3240–3245. doi: 10.3382/ps/pez049

Liu, H., Wang, J., He, T., Becker, S., Zhang, G., Li, D., et al. (2018). Butyrate: a double-edged sword for health? *Adv. Nutr.* 9, 21–29. doi: 10.1093/advances/nmx009

Liu, Y., Yu, X., Zhao, J., Zhang, H., Zhai, Q., and Chen, W. (2020). The role of MUC2 mucin in intestinal homeostasis and the impact of dietary components on MUC2 expression. *Int. J. Biol. Macromol.* 164, 884–891. doi: 10.1016/j.ijbiomac.2020.07.191

Lyu, W., Curtis, A. R., Sunkara, L. T., and Zhang, G. (2015). Transcriptional regulation of antimicrobial host defense peptides. *Curr. Protein Pept. Sci.* 16, 672–679. doi: 10.2174/1389203716666150630133432

Lyu, W., Deng, Z., Sunkara, L. T., Becker, S., Robinson, K., Matts, R., et al. (2018). High throughput screening for natural host defense peptide-inducing compounds as novel alternatives to antibiotics. *Front. Cell. Infect. Microbiol.* 8:191. doi: 10.3389/fcimb.2018.00191

Malik, A. N., and Al-Kafaji, G. (2007). Glucose regulation of beta-defensin-1 mRNA in human renal cells. *Biochem. Biophys. Res. Commun.* 353, 318–323. doi: 10.1016/j.bbrc.2006.12.037

Manyi-Loh, C., Mamphweli, S., Meyer, E., and Okoh, A. (2018). Antibiotic use in agriculture and its consequential resistance in environmental sources: potential public health implications. *Molecules* 23:795. doi: 10.3390/molecules23040795

Mcewen, S. A., and Collignon, P. J. (2018). Antimicrobial resistance: a one health perspective. *Microbiol. Spectr.* 6:ARBA-0009-2017. doi: 10.1128/microbiolspec.ARBA-0009-2017

Mcreynolds, J. L., Byrd, J. A., Genovese, K. J., Poole, T. L., Duke, S. E., Farnell, M. B., et al. (2007). Dietary lactose and its effect on the disease condition of necrotic enteritis. *Poult. Sci.* 86, 1656–1661. doi: 10.1093/ps/86.8.1656

Montoya-Rosales, A., Castro-Garcia, P., Torres-Juarez, F., Enciso-Moreno, J. A., and Rivas-Santiago, B. (2016). Glucose levels affect LL-37 expression in monocyte-derived macrophages altering the *Mycobacterium tuberculosis* intracellular growth control. *Microb. Pathog.* 97, 148–153. doi: 10.1016/j.micpath.2016.06.002

Niknafs, S., and Roura, E. (2018). Nutrient sensing, taste and feed intake in avian species. *Nutr. Res. Rev.* 31, 256–266. doi: 10.1017/S0954422418000100

Robinson, K., Deng, Z., Hou, Y., and Zhang, G. (2015). Regulation of the intestinal barrier function by host defense peptides. *Front. Vet. Sci.* 2:57. doi: 10.3389/fvets.2015.00057

Robinson, K., Ma, X., Liu, Y., Qiao, S., Hou, Y., and Zhang, G. (2018). Dietary modulation of endogenous host defense peptide synthesis as an alternative approach to in-feed antibiotics. *Anim. Nutr.* 4, 160–169. doi: 10.1016/j.aninu.2018.01.003

Robinson, K., Yang, Q., Li, H., Zhang, L., Aylward, B., Arsenault, R. J., et al. (2021). Butyrate and forskolin augment host defense, barrier function, and disease resistance without eliciting inflammation. *Front. Nutr.* 8:778424. doi: 10.3389/fnut.2021.778424

Rodriguez-Carlos, A., Jacobo-Delgado, Y. M., Santos-Mena, A. O., and Rivas-Santiago, B. (2021). Modulation of cathelicidin and defensins by histone deacetylase inhibitors: a potential treatment for multi-drug resistant infectious diseases. *Peptides* 140:170527. doi: 10.1016/j.peptides.2021.170527

Roura, E., and Foster, S. R. (2018). Nutrient-sensing biology in mammals and birds. *Annu. Rev. Anim. Biosci.* 6, 197–225. doi: 10.1146/annurev-animal-030117-014740

Schauber, J., Svanholm, C., Termen, S., Iffland, K., Menzel, T., Scheppach, W., et al. (2003). Expression of the cathelicidin LL-37 is modulated by short chain fatty acids in colonocytes: relevance of signalling pathways. *Gut* 52, 735–741. doi: 10.1136/gut.52.5.735

Siddons, R. C. (1969). Intestinal disaccharidase activities in the chick. *Biochem. J.* 112, 51–59. doi: 10.1042/bj1120051

Siddons, R. C., and Coates, M. E. (1972). The influence of the intestinal microflora on disaccharidase activities in the chick. *Br. J. Nutr.* 27 101–112. doi: 10.1079/bjn19720074

Sunkara, L. T., Achanta, M., Schreiber, N. B., Bommineni, Y. R., Dai, G., Jiang, W., et al. (2011). Butyrate enhances disease resistance of chickens by inducing antimicrobial host defense peptide gene expression. *PLoS One* 6:e27225. doi: 10.1371/journal.pone.0027225

Sunkara, L. T., Jiang, W., and Zhang, G. (2012). Modulation of antimicrobial host defense peptide gene expression by free fatty acids. *PLoS One* 7:e49558. doi: 10.1371/journal.pone.0049558

Sunkara, L. T., Zeng, X., Curtis, A. R., and Zhang, G. (2014). Cyclic AMP synergizes with butyrate in promoting beta-defensin 9 expression in chickens. *Mol. Immunol.* 57, 171–180. doi: 10.1016/j.molimm.2013.09.003

Tengholm, A., and Gylfe, E. (2017). cAMP signalling in insulin and glucagon secretion. *Diabetes Obes. Metab.* 19(Suppl. 1), 42–53. doi: 10.1111/dom.12993

Ting, D. S. J., Beuerman, R. W., Dua, H. S., Lakshminarayanan, R., and Mohammed, I. (2020). Strategies in translating the therapeutic potentials of host defense peptides. *Front. Immunol.* 11:983. doi: 10.3389/fimmu.2020.00983

Vancamelbeke, M., and Vermeire, S. (2017). The intestinal barrier: a fundamental role in health and disease. *Expert Rev. Gastroenterol. Hepatol.* 11, 821–834. doi: 10.1080/17474124.2017.1343143

Von Molitor, E., Riedel, K., Krohn, M., Hafner, M., Rudolf, R., and Cesetti, T. (2021). Sweet taste is complex: signaling cascades and circuits involved in sweet sensation. *Front. Hum. Neurosci.* 15:667709. doi: 10.3389/fnhum.2021.667709

Wang, T. T., Nestel, F. P., Bourdeau, V., Nagai, Y., Wang, Q., Liao, J., et al. (2004). Cutting edge: 1,25-dihydroxyvitamin D3 is a direct inducer of antimicrobial peptide gene expression. *J. Immunol.* 173, 2909–2912. doi: 10.4049/jimmunol.173.5.2909

Xiong, H., Guo, B., Gan, Z., Song, D., Lu, Z., Yi, H., et al. (2016). Butyrate upregulates endogenous host defense peptides to enhance disease resistance in piglets via histone deacetylase inhibition. *Sci. Rep.* 6:27070. doi: 10.1038/srep27070

Yang, Q., Whitmore, M. A., Robinson, K., Lyu, W., and Zhang, G. (2021). Butyrate, forskolin, and lactose synergistically enhance disease resistance by inducing the expression of the genes involved in innate host defense and barrier function. *Antibiotics* 10:1175. doi: 10.3390/antibiotics10101175

Zeng, X., Sunkara, L. T., Jiang, W., Bible, M., Carter, S., Ma, X., et al. (2013). Induction of porcine host defense peptide gene expression by short-chain fatty acids and their analogs. *PLoS One* 8:e72922. doi: 10.1371/journal.pone.0083753

Zhang, L., Lu, L., Li, S., Zhang, G., Ouyang, L., Robinson, K., et al. (2016). 1,25-dihydroxyvitamin-D3 induces avian beta-defensin gene expression in chickens. *PLoS One* 11:e0154546. doi: 10.1371/journal.pone.0168928

Zhang, G., and Sunkara, L. T. (2014). Avian antimicrobial host defense peptides: from biology to therapeutic applications. *Pharmaceuticals* 7, 220–247. doi: 10.3390/ph7030220

Zhu, D., Yan, Q., Liu, J., Wu, X., and Jiang, Z. (2019). Can functional oligosaccharides reduce the risk of diabetes mellitus? *FASEB J.* 33, 11655–11667. doi: 10.1096/fj.201802802RRR

Conflict of Interest: The authors declare that the research was conducted in the absence of any commercial or financial relationships that could be construed as a potential conflict of interest.

Publisher's Note: All claims expressed in this article are solely those of the authors and do not necessarily represent those of their affiliated organizations, or those of the publisher, the editors and the reviewers. Any product that may be evaluated in this article, or claim that may be made by its manufacturer, is not guaranteed or endorsed by the publisher.

frontiers in Microbiology

ORIGINAL RESEARCH
published: 23 December 2021
doi: 10.3389/fmicb.2021.803309

Dioctanoyl Ultrashort Tetrabasic β-Peptides Sensitize Multidrug-Resistant Gram-Negative Bacteria to Novobiocin and Rifampicin

*Danyel Ramirez[1], Liam Berry[1], Ronald Domalaon[1], Yanqi Li[2], Gilbert Arthur[3], Ayush Kumar[2] and Frank Schweizer[1,4]**

[1]Department of Chemistry, University of Manitoba, Winnipeg, MB, Canada, [2]Department of Microbiology, University of Manitoba, Winnipeg, MB, Canada, [3]Department of Biochemistry and Medical Genetics, University of Manitoba, Winnipeg, MB, Canada, [4]Department of Medical Microbiology and Infectious Diseases, University of Manitoba, Winnipeg, MB, Canada

Recently reported peptidomimetics with increased resistance to trypsin were shown to sensitize priority multidrug-resistant (MDR) Gram-negative bacteria to novobiocin and rifampicin. To further optimize proteolytic stability, β-amino acid-containing derivatives of these compounds were prepared, resulting in three dioctanoyl ultrashort tetrabasic β-peptides (dUSTBβPs). The nonhemolytic dUSTBβP 3, comprised of three β^3-homoarginine residues and two fatty acyl tails eight carbons long, enhanced the antibacterial activity of various antibiotics from different classes. Notably, compound 3 retained the ability to potentiate novobiocin and rifampicin in wild-type Gram-negative bacteria against MDR clinical isolates of *Pseudomonas aeruginosa*, *Acinetobacter baumannii*, *Escherichia coli*, *Klebsiella pneumoniae*, and *Enterobacter cloacae*. dUSTBβP 3 reduced the minimum inhibitory concentration of novobiocin and rifampicin below their interpretative susceptibility breakpoints. Furthermore, compound 3 exhibited improved *in vitro* stability (86.8 ± 3.7% remaining) relative to its α-amino acid-based counterpart (39.5 ± 7.4% remaining) after a 2 h incubation in human plasma.

Keywords: antibiotic adjuvant, novobiocin, rifampicin, peptidomimetic, β-amino acid, *Pseudomonas aeruginosa*, *Acinetobacter baumannii*, *Escherichia coli*

OPEN ACCESS

Edited by:
Wang Jiajun,
Northeast Agricultural University, China

Reviewed by:
Henrik Franzyk,
University of Copenhagen, Denmark
Kevin Bicker,
Middle Tennessee State University, United States

***Correspondence:**
Frank Schweizer
schweize@cc.umanitoba.ca

Specialty section:
This article was submitted to Antimicrobials, Resistance and Chemotherapy, a section of the journal Frontiers in Microbiology

Received: *27 October 2021*
Accepted: *29 November 2021*
Published: *23 December 2021*

Citation:
Ramirez D, Berry L, Domalaon R, Li Y, Arthur G, Kumar A and Schweizer F (2021) Dioctanoyl Ultrashort Tetrabasic β-Peptides Sensitize Multidrug-Resistant Gram-Negative Bacteria to Novobiocin and Rifampicin. Front. Microbiol. 12:803309. doi: 10.3389/fmicb.2021.803309

INTRODUCTION

Antimicrobial resistance is a major threat to the global healthcare system that has caused a lack of treatment options for challenging bacterial infections (Prestinaci et al., 2015). The relative decrease in successful antibiotic development in the past decades in addition to the rising transmission of resistance genes has accelerated the problem and new therapies are urgently needed (O'Neill, 2016). Antimicrobial resistance can occur through several distinct mechanisms, including efflux, reduced antibiotic membrane penetration, modification of antibiotic targets, and the production of enzymes to degrade antibiotics (Reygaert, 2018). Of special concern are Gram-negative bacteria due to their highly restrictive outer membrane (OM), which prevents entry of many antibiotics (Zgurskaya and Rybenkov, 2019). Recent advancements have shown the successful development of a number of new antibiotics, as well as increased

interest in the use of antibiotic adjuvants to overcome antimicrobial resistance (Årdal et al., 2020).

Adjuvants are molecules that enhance the efficacy of partner antibiotics in combination therapy (Wright, 2016). Adjuvants work primarily by disabling either innate or adaptive bacterial resistance mechanisms. Examples include β-lactamase inhibitors that prevent the enzymatic degradation of β-lactam antibiotics (Drawz and Bonomo, 2010), bacterial efflux pump inhibitors (Lamers et al., 2013), and OM-permeabilizing agents derived from cationic antimicrobial peptides (AMPs). Currently, the only adjuvants approved for clinical use are β-lactamase inhibitors, including clavulanic acid (combined with amoxicillin), vaborbactam (combined with meropenem), and others (Carcione et al., 2021). Membrane-permeabilizing adjuvants derived from the polymyxin family of AMPs have also seen some pre-clinical success. One example is polymyxin B nonapeptide (PMBN), which lacks the fatty acyl tail and the Dab_1 amino acid characteristic of polymyxins (Ofek et al., 1994). Despite a reduction in antibacterial activity, PMBN is able to permeabilize the OM of Gram-negative bacteria and allow other antibiotics to enter the cell at increased rates (Vaara, 1992). Spero Therapeutics is also presently developing SPR741, an adjuvant derived from PMBN, which has reduced toxicity and improved pharmacokinetics (Eckburg et al., 2019; Vaara, 2019). SPR741 was assessed for safety, tolerability, and in combination with partner antibiotics in Phase 1 clinical trials (Eckburg et al., 2019; Vaara, 2019). Various short cationic lipopeptide adjuvants have also been reported that display similar membrane permeabilizing properties (Domalaon et al., 2018a,b, 2019a; Ramirez et al., 2020).

A common feature of the activity of AMPs against Gram-negative bacteria is the presence of basic sidechains, which can be protonated at physiological pH (Velkov et al., 2010). These confer an overall positive charge to the peptide, which can electrostatically interact with negatively charged phosphate groups embedded in the lipid A component of the lipopolysaccharide of the OM. This interaction results in the displacement of divalent cations such as Ca^{2+} and Mg^{2+} which normally stabilize the negatively charged lipopolysaccharide (Hancock, 1984). After OM integrity has been disrupted, the fatty acyl tail of polymyxin inserts into the phospholipid bilayer causing lipid rearrangement that consequently results in cell lysis and cell death (Moubareck, 2020). Although PMBN lacks this fatty acyl tail and thus is unable to lyse the cell, localized perturbation of the membrane still occurs (Tsubery et al., 2000). Despite their potent activity as both antibiotics and adjuvants (Melander and Melander, 2017; Hollmann et al., 2018; Marquette and Bechinger, 2018; Sheard et al., 2019; Vaara, 2019), AMPs face significant challenges toward clinical use. Notable challenges include high production cost, relatively poor metabolic stability, and overall high toxicity due to hemolysis and nephrotoxicity (Chen and Lu, 2020).

Various approaches to improve the drug-likeness of AMPs have been reported. For instance, the above-mentioned PMBN and SPR741 have reduced toxicity (Vaara, 2019). We have previously reported dilipid ultrashort cationic lipopeptides (dUSCLs) containing two shorter instead of one longer fatty acyl tail that resulted to reduced hemolysis (Domalaon et al., 2019a). Metabolic instability due to protease activity remains a significant challenge for AMPs. Peptidomimetic approaches can mitigate proteolytic susceptibility by removing the peptide-like character of AMPs thereby resulting in the inability of proteases to recognize and degrade the resulting mimic molecule (Domalaon et al., 2016). Several peptidomimetic strategies can be enacted in lead AMP candidates including isosteric replacement of the peptide backbone, replacing naturally occurring L-amino acids with D-amino acids, and the use of β-amino acids and peptoid building blocks (Rink et al., 2010; Molchanova et al., 2017; Baker et al., 2019; Mood et al., 2021). For instance, dilipid ultrashort tetrabasic peptidomimetics (dUSTBPs) were previously developed from dUSCL lead candidates by introducing the branched molecular scaffold, *N*,*N*-bis(3-aminopropyl)glycine (*N*bap), into the structure to interrupt the peptide backbone (Ramirez et al., 2020). The nonhemolytic dUSTBP di(C_8-Arg)-*N*bap-Arg-NH_2 (**Figure 1**) enhanced the antibacterial activity of novobiocin and rifampicin, and was shown to have increased resistance to trypsin relative to dUSCL di-C_9-KKKK-NH_2 (**Figure 1**; Ramirez et al., 2020). Although improved peptide stability was observed in dUSTBPs, our continued effort in optimizing our lead candidates by incorporating further peptidomimetic structural features is reported herein.

Replacement of traditional α-amino acids in dUSTBPs with β-amino acid analogues resulted in dioctanoyl ultrashort tetrabasic β-peptides (dUSTBβPs). Three dUSTBβPs were prepared by incorporating fatty acids eight carbons (C_8) long and β-amino acids including β^3-homoornithine (β^3hOrn), β^3-homolysine (β^3hLys), or β^3-homoarginine (β^3hArg; **Figure 1**). The dUSTBβPs were all nonhemolytic and potentiated novobiocin and rifampicin against wild-type Gram-negative bacteria. Peptidomimetic 3, consisting of three β^3hArg residues, enhanced the antibacterial activity of various antibiotics from different classes, as well as retained novobiocin and rifampicin potentiation against multidrug-resistant (MDR) clinical isolates. Moreover, compound 3 was shown to possess enhanced plasma stability relative to its α-amino acid-based counterpart di(C_8-Arg)-*N*bap-Arg-NH_2. These results indicate that multiple peptidomimetic approaches can serve to further improve proteolytic resistance of AMPs without compromising adjuvant activity.

MATERIALS AND METHODS

Preparation of dUSTBβPs

The Rink amide 4-methylbenzyhydrylamine (MBHA) resin was obtained from Sigma-Aldrich (United States), Fmoc-β^3-hOrn(Boc)-OH was obtained from A2B Chem (United States), and Fmoc-β^3-hArg(Pbf)-OH was obtained from 1Click Chemistry (United States). Fmoc-β^3-hLys(Boc)-OH and *N*,*N*-bis(N′-Fmoc-3-aminopropyl)glycine potassium hemisulfate were purchased from Chem-Impex (United States). All other reagents and solvents were obtained from Sigma-Aldrich (United States) and used without further purification.

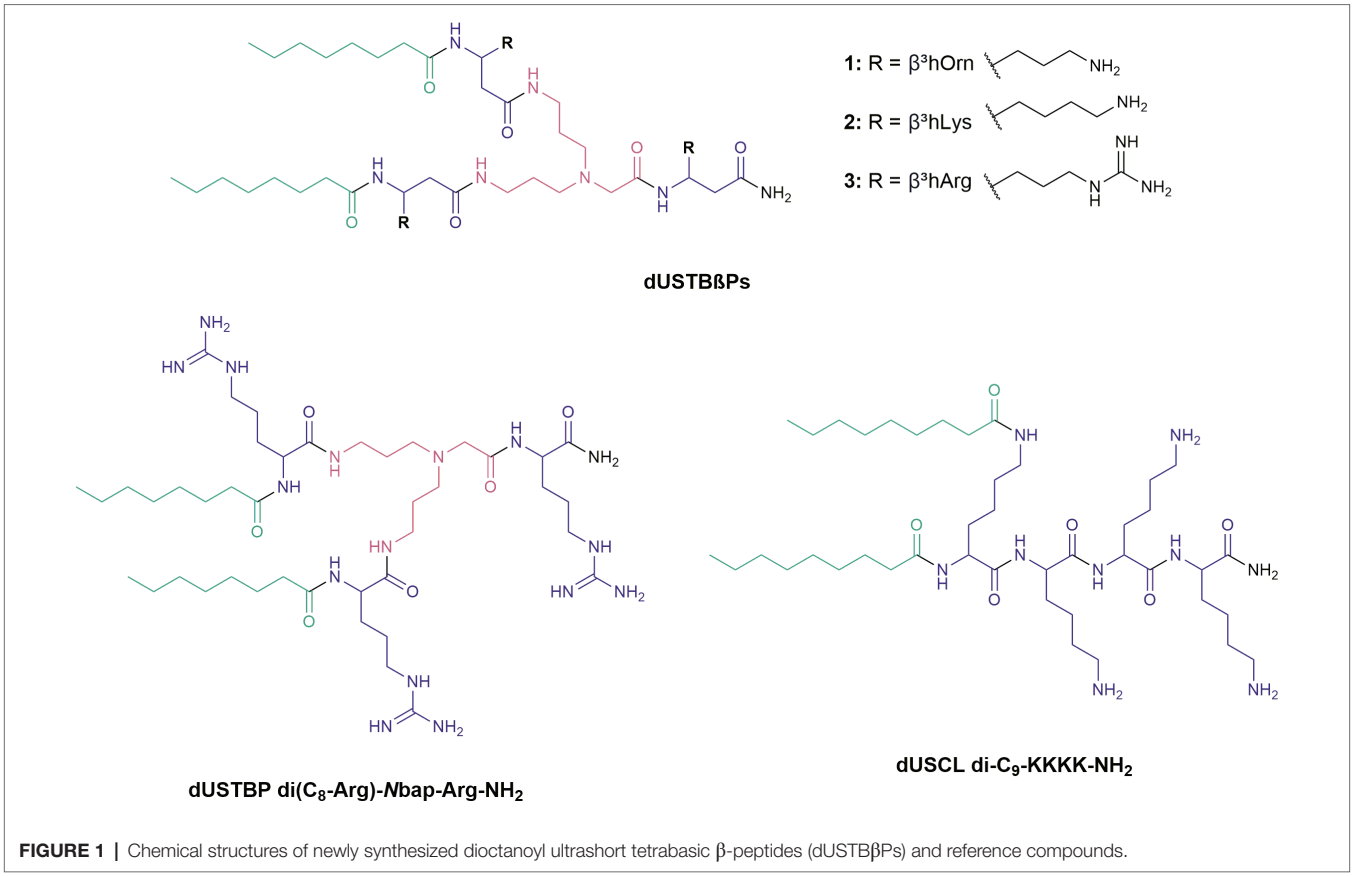

FIGURE 1 | Chemical structures of newly synthesized dioctanoyl ultrashort tetrabasic β-peptides (dUSTBβPs) and reference compounds.

All dUSTBβPs were prepared by following a standard fluorenylmethyloxycarbonyl (Fmoc) solid-phase peptide synthesis (SPPS) protocol using Rink amide MBHA resin (Chan and White, 2000). N-terminus of the amino acids was protected with Fmoc. The ϖ- and ω-amine sidechains of β³hOrn and β³hLys, and the ω-amine sidechain of β³hArg were protected with *tert*-butyloxycarbonyl and 2,2,4,6,7-pentamethyldihydrobenzofuran-5-sulfonyl, respectively. Fmoc deprotection was carried out using 20% piperidine in dimethylformamide (DMF; v/v). Peptide and fatty acid coupling were done *via* addition of a preactivated coupling solution to the resin and subsequent constant gentle agitation with nitrogen gas for 45 min. The coupling solution which consists of 3 molar equivalents (mol. eq.) of protected amino acid or lipid, 3 mol. eq. of *O*-(benzotriazol-1-yl)-*N*,*N*,*N*′,*N*′-tetramethyluronium tetrafluoroborate, and 8 mol. eq. of *N*-methylmorpholine in DMF was preactivated for 5 min. Following both Fmoc deprotection and coupling steps, the resin was washed with DMF (3×), dichloromethane (DCM; 3×), and DMF (3×) to remove traces of piperidine from the reaction vessel. The chloranil test (2% chloranil in DMF) was performed on a small amount of resin to verify the completion of the reaction. Deprotection of the amino acid sidechains and cleavage of the peptide from the resin were done using 95:5 trifluoroacetic acid (TFA)/water (v/v) for 30 min. The resin was washed with DCM (3×), and the solvent was removed *in vacuo* to afford the solid compounds as TFA salts. Molecular weights of the dUSTBβPs in TFA salt form are shown in **Supplementary Table 1**.

The dUSTBβPs were purified *via* reverse-phase flash chromatography using C_{18} silica gel (40–63 μm) purchased from Silicycle (United States). The solvent system used consisted of methanol and water containing 0.1% TFA. Purity of the compounds was determined to be ≥95% using high-performance liquid chromatography (HPLC) on a Thermo Scientific Vanquish UHPLC (United States) equipped with Phenomenex Kinetex (100 mm × 4.6 mm) 2.6 μm XB-C18 reverse-phase column and VF-D40 variable wavelength detector. The HPLC gradient used for purity analysis is shown in **Supplementary Table 8**. Chemical characterization of each dUSTBβP was assessed by one- and two-dimensional nuclear magnetic resonance experiments, such as ^{1}H, ^{13}C, COSY, HSQC, and HMBC on a Bruker AMX-500 (500 MHz) instrument (Germany). Matrix-assisted laser desorption ionization-time of flight mass spectrometry experiments were carried out on a Bruker Ultraflextreme (Germany) in positive ion mode with 2,5-dihydroxybenzoic acid as the matrix.

Bacterial Strains and Growth Conditions

Bacterial isolates were obtained from the American Type Culture Collection (ATCC), the Canadian National Intensive Care Unit (CAN-ICU) surveillance study (Zhanel et al., 2008), and the Canadian Ward (CAN-WARD) surveillance study (Hoban and Zhanel, 2013). CAN-ICU and CAN-WARD bacterial isolates

were collected from patients diagnosed with presumed infectious diseases admitted in participating medical centers across Canada. All pharmaceutical-grade antibiotics and reagents were purchased from commercial sources.

Hemolysis Assay

The degree of hemolysis induced by dUSTBβPs was determined by the amount of hemoglobin released from human erythrocytes upon incubation. Fresh human blood supplied by a commercial vendor was obtained from normal healthy volunteers following informed consent. The agent of interest was serially diluted in vehicle consisting of phosphate-buffered saline (PBS), saline, 5% glucose, or equivalents. The samples were incubated with gentle mixing at 37°C for 45 min and were subsequently centrifuged. The supernatant (plasma layer) was removed and centrifuged once more to completely pellet the cells. The plasma layer was diluted with Drabkin's reagent and analyzed at a wavelength of 540 nm. Experiments were conducted in triplicates, and a calibration curve prepared by diluting blood (after addition of vehicle) was used to quantitate heme release. The vehicle or Triton X-100 were used as negative or positive controls, respectively.

Antimicrobial Susceptibility Assay

The *in vitro* antibacterial activities of dUSTBβPs were evaluated using microbroth dilution susceptibility test, in accordance with the Clinical and Laboratory Standards Institute (CLSI) guidelines (Clinical and Laboratory Standards Institute, 2019). Overnight-grown bacterial culture diluted in saline to 0.5 McFarland turbidity was successively diluted 1:50 in Mueller-Hinton broth (MHB) to achieve a final concentration of 5×10^5 colony forming units (CFU)/mL for inoculation. The agents were serially diluted 2-fold in MHB on a 96-well plate; mixed with bacterial inoculum of equal volumes, and incubated at 37°C for 18 h. Antibacterial activity was determined by the minimum inhibitory concentration (MIC), which is the lowest concentration of agent required for inhibition of visible bacterial growth in the form of turbidity. Confirmation of turbidity was done using an EMax Plus microplate reader (Molecular Devices, United States) at a wavelength of 590 nm. Wells comprising MHB alone or MHB inoculated with bacteria were used as negative or positive controls, respectively.

Checkerboard Assay

The adjuvant activities of dUSTBβPs were evaluated using checkerboard assay as previously described (Berry et al., 2019). Overnight-grown bacterial culture diluted in saline to 0.5 McFarland turbidity was successively diluted 1:50 in MHB to achieve a final concentration of 5×10^5 CFU/mL for inoculation. The antibiotic and adjuvant were serially diluted 2-fold along the *x*-axis and *y*-axis, respectively, resulting in varying concentrations of both agents in each well. Subsequently, the 96-well plate was incubated with equal volumes of bacterial inoculum at 37°C for 18 h. Confirmation of turbidity was done using an EMax Plus microplate reader (Molecular Devices, United States) at a wavelength of 590 nm. Wells comprising MHB alone or in the presence of bacterial cells were used as negative or positive controls, respectively. Fractional inhibitory concentration index (FICI) is determined by adding the FICs of both antibiotic and adjuvant. The FIC of the antibiotic is calculated by dividing the MIC of the antibiotic in the presence of the adjuvant by the MIC of the antibiotic alone. Similarly, the FIC of the adjuvant is calculated by dividing the MIC of the adjuvant in the presence of the antibiotic by the MIC of the adjuvant alone. FICI ≤ 0.5, $0.5 < x \leq 4$, and >4 were deemed synergistic, additive, and antagonistic, respectively (Meletiadis et al., 2010).

Time-Kill Assay

The concentration-dependent killing kinetics of the combinations of dUSTBβP 3 and novobiocin or rifampicin was studied using time-kill assay as previously described (Domalaon et al., 2019b). Overnight-grown bacterial culture diluted in PBS to 0.5 McFarland turbidity was successively diluted 1:50 in lysogeny broth (LB). Cell cultures in the presence of dUSTBβP 3, novobiocin, or rifampicin, or combinations of adjuvant and antibiotic were incubated at 37°C. At designated intervals, 100 µL aliquots acquired from each culture tube were serially diluted in PBS and plated on LB agar plates. After incubation of the plates at 37°C for 18 h, the bacterial colonies were counted.

OM Permeabilization Assay

The ability of dUSTBβP 3 to permeabilize the OM of *Acinetobacter baumannii* ATCC 17978 and *Escherichia coli* ATCC 25922 was assessed using 1-*N*-phenylnaphthylamine (NPN) as previously described with minor modifications (Yang et al., 2017; Akhoundsadegh et al., 2019). Overnight grown culture was subcultured (1 in 100) in fresh LB broth and grown to a mid-logarithmic phase ($OD_{600} = 0.4–0.6$). The cells were pelleted by centrifugation for 10 min at $1{,}200 \times g$ at room temperature, washed, and resuspended in half volume of 5 mM 4-(2-hydroxyethyl)-1-piperazineethanesulfonic acid (HEPES; pH 7.2) with 5 mM glucose. NPN (10 µM final concentration) was added to a black 96-well plate containing the cell culture and incubated in 5 mM HEPES (pH 7.2) supplemented with 5 mM glucose and 5 µM carbonyl cyanide 3-chlorophenylhydrazone at room temperature for 30 min in darkness. Varying concentrations of compound were added onto the suspension, and the resulting change in NPN fluorescence was measured continuously (every 30 s) on a SpectraMax M2 microplate reader (Molecular Devices, United States) at an excitation wavelength of 350 nm and an emission wavelength of 420 nm. Cells with NPN and the OM permeabilizer PMBN served as a positive control, while cells with NPN alone served as a negative control. Three replicates were conducted, and the data were corrected for any background fluorescence.

Tryptic Digest Assay

Proteolytic resistance of dUSTBβP 3 and previously reported dUSCL di-C_9-KKKK-NH_2 was evaluated with tryptic digest assay as previously described (Ramirez et al., 2020). The compounds were diluted with 50 mM ammonium bicarbonate (pH 7.8) and were incubated with sequencing-grade modified trypsin from Promega (United States) at a molar ratio of

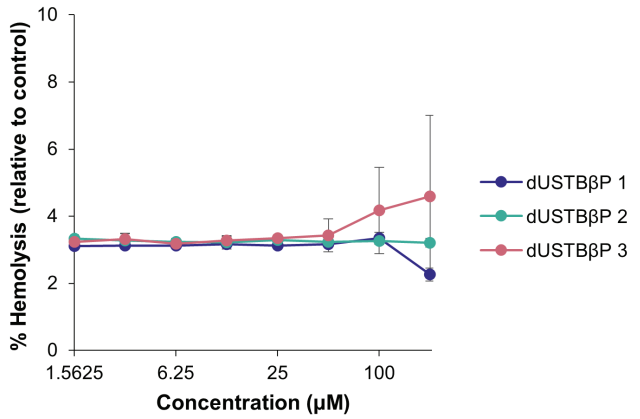

FIGURE 2 | Concentration-dependent hemolytic activity of dUSTBβPs against human erythrocytes. Control used was 1% Triton X-100. Results were an average of triplicates ($n = 3$) ± SD. See **Supplementary Tables 2**, **3** for exact values of % hemolysis and SDs.

TABLE 1 | Antibacterial activity of dUSTBβPs against wild-type Gram-negative bacteria.

Organism	MIC (μg/mL)			
	1	2	3	*P. aeruginosa* PAO1
>128	>128	128	*A. baumannii* ATCC 17978	>128
>128	>128	*E. coli* ATCC 25922	>128	>128
128				

1:5,000 (enzyme/compound) at 37°C for 2 h. Termination of the reaction was done by overnight freezing at −18°C, and the samples were purified and concentrated by using Pierce C_{18} tips (10 μL) from Thermo Scientific (United States). Stability toward trypsin was assessed by mass fragmentation analysis in positive ion mode on a Varian 500-MS ion trap mass spectrometer (United States).

Plasma Stability Assay

Stability of dUSTBβP 3 was evaluated in human plasma. Compound 3 was incubated at 37°C in prewarmed plasma for a final compound concentration of 1 μM. At designated time points (0, 0.5, 1, 1.5, and 2 h), aliquots of the mixture were diluted with acetonitrile, and centrifuged at 1,000 × *g* for 15 min at 4°C. The supernatant was analyzed by HPLC-tandem mass spectrometry using selected reaction monitoring. The % compound remaining was determined by comparing peak areas at different time points to time zero. Assuming first-order kinetics, the half-life was extrapolated from the slope of the initial linear range of the logarithmic curve of compound remaining over time. Experiments were performed in duplicates, and the reference compounds include propantheline and propoxycaine.

Cell Viability Assay

Cell viability assay was performed essentially as previously described (Ammeter et al., 2019). Human embryonic kidney cells (HEK293) and human liver carcinoma cells (HepG2) were grown in Dulbecco's modified eagle's medium with 10% fetal bovine serum at 37°C using a humidified 5% CO_2 incubator in 75 mm tissue culture flasks. The cells were detached with trypsin and equal numbers of cells (8,000 cells in 50 μL) were dispersed into five rows of each column in 96-well plate; the remaining three rows of each column, designated as blanks, received 50 μL of the media without cells. After 24 h incubation, aliquots of 50 μL of dUSTBβP 3 at varying concentrations were added to each well and incubated for 48 h. Thereafter, cell viability was measured using PrestoBlue Cell Viability reagent from Invitrogen (United States) according to manufacturer's protocol and fluorescence (540/590 nm) was measured with a SpectraMax M2 plate reader (Molecular Devices, United States). Values from the wells without cells (blank wells) were subtracted from the corresponding sample wells and cell viability values of the treated samples relative to the vehicle controls set to 100% was determined. Thus, relative cell viability of 0% indicates that there are no viable cells. The results represent the mean ± SD of two independent experiments with five samples per experiment. The concentration that causes 50% cytotoxicity (CC_{50}) was also estimated by using non-linear regression analysis. Colistin was used as a negative control and doxorubicin, an anticancer drug, was used as a positive control.

RESULTS

Hemolytic and Susceptibility Screening of dUSTBβPs

The ability of the compounds to cause lysis of red blood cells was determined by measuring the amount of hemoglobin released in plasma upon treatment (**Figure 2**). The β-amino acid-containing derivatives elicited low levels of hemolysis at all concentrations examined. At 200 μM, compounds 1, 2, and 3 only resulted in 2.26 ± 0.19, 3.21 ± 0.13, and 4.59 ± 2.42% hemolysis, respectively. To examine the susceptibility of wild-type Gram-negative bacteria to dUSTBβPs, MICs of the synthesized compounds were determined (**Table 1**). Limited activity of ≥128 μg/mL was observed for all the compounds against all tested strains.

dUSTBβPs Potentiated Novobiocin and Rifampicin Against Wild-Type Gram-Negative Bacteria

The capability of dUSTBβPs to potentiate novobiocin and rifampicin was assessed against wild-type *Pseudomonas aeruginosa* (**Table 2**), *A. baumannii* (**Table 3**), and *E. coli* (**Table 4**) by means of a checkerboard assay. The FICI was used to evaluate interactions between the two agents. FICI of ≤ 0.5, $0.5 < x \leq 4$, and >4 were interpreted as synergy, additive, and antagonistic, respectively (Meletiadis et al., 2010). All interactions of dUSTBβPs with novobiocin and rifampicin were synergistic against all tested strains. The combinations were most effective against

TABLE 2 | Synergy evaluation of combinations consisting of dUSTBβPs and novobiocin or rifampicin against wild-type *P. aeruginosa* PAO1.

dUSTBβP	Antibiotic	$MIC_{dUSTBβP}$ [MIC_{combo}] (μg/mL)	$MIC_{antibiotic}$ [MIC_{combo}] (μg/mL)	FICI	Interpretation	Absolute $MIC^{a}_{antibiotic}$ (μg/mL)	Potentiation[b]
1	Novobiocin	>128 [8]	1,024 [128]	$0.125 < x < 0.188$	Synergy	128	8-fold
	Rifampicin	>128 [16]	16 [4]	$0.25 < x < 0.375$	Synergy	8	2-fold
2	Novobiocin	>128 [8]	1,024 [128]	$0.125 < x < 0.188$	Synergy	128	8-fold
	Rifampicin	>128 [16]	16 [4]	$0.25 < x < 0.375$	Synergy	8	2-fold
3	Novobiocin	128 [8]	1,024 [32]	0.094	Synergy	32	32-fold
	Rifampicin	128 [8]	16 [0.25]	0.078	Synergy	0.25	64-fold

[a]*MIC of antibiotic in the presence of 8 μg/mL (6 μM) dUSTBβP.*
[b]*Degree of antibiotic potentiation in the presence 8 μg/mL (6 μM) dUSTBβP.*

TABLE 3 | Synergy evaluation of combinations consisting of dUSTBβPs and novobiocin or rifampicin against wild-type *A. baumannii* ATCC 17978.

dUSTBβP	Antibiotic	$MIC_{dUSTBβP}$ [MIC_{combo}] (μg/mL)	$MIC_{antibiotic}$ [MIC_{combo}] (μg/mL)	FICI	Interpretation	Absolute $MIC^{a}_{antibiotic}$ (μg/mL)	Potentiation[b]
1	Novobiocin	>128 [8]	16 [2]	$0.125 < x < 0.188$	Synergy	2	8-fold
	Rifampicin	>128 [8]	2 [0.125]	$0.063 < x < 0.125$	Synergy	0.125	16-fold
2	Novobiocin	>128 [8]	16 [2]	$0.125 < x < 0.188$	Synergy	2	8-fold
	Rifampicin	>128 [8]	2 [0.125]	$0.063 < x < 0.125$	Synergy	0.125	16-fold
3	Novobiocin	>128 [8]	16 [0.25]	$0.016 < x < 0.078$	Synergy	0.25	64-fold
	Rifampicin	>128 [8]	2 [0.008]	$0.004 < x < 0.066$	Synergy	0.008	256-fold

[a]*MIC of antibiotic in the presence of 8 μg/mL (6 μM) dUSTBβP.*
[b]*Degree of antibiotic potentiation in the presence 8 μg/mL (6 μM) dUSTBβP.*

TABLE 4 | Synergy evaluation of combinations consisting of dUSTBβPs and novobiocin or rifampicin against wild-type *E. coli* ATCC 25922.

dUSTBβP	Antibiotic	$MIC_{dUSTBβP}$ [MIC_{combo}] (μg/mL)	$MIC_{antibiotic}$ [MIC_{combo}] (μg/mL)	FICI	Interpretation	Absolute $MIC^{a}_{antibiotic}$ (μg/m1)	Potentiation[b]
1	Novobiocin	>128 [4]	64 [2]	$0.031 < x < 0.063$	Synergy	2	32-fold
	Rifampicin	>128 [8]	4 [0.25]	$0.063 < x < 0.125$	Synergy	0.25	16-fold
2	Novobiocin	>128 [8]	64 [1]	$0.016 < x < 0.078$	Synergy	1	64-fold
	Rifampicin	>128 [8]	4 [0.125]	$0.031 < x < 0.094$	Synergy	0.125	32-fold
3	Novobiocin	128 [8]	64 [0.125]	0.064	Synergy	0.125	512-fold
	Rifampicin	128 [8]	4 [0.008]	0.064	Synergy	0.008	512-fold

[a]*MIC of antibiotic in the presence of 8 μg/mL (6 μM) dUSTBβP.*
[b]*Degree of antibiotic potentiation in the presence 8 μg/mL (6 μM) dUSTBβP.*

E. coli (FICI of 0.016–0.125) and *A. baumannii* (FICI of 0.004–0.188), and least effective against PAO1 (FICI of 0.078–0.375).

dUSTBβP 3 Retains Novobiocin and Rifampicin Potentiation Against MDR Gram-Negative Bacteria

Potentiation of novobiocin (**Table 5**) and rifampicin (**Table 6**) by dUSTBβP 3 was also examined against MDR clinical isolates of *P. aeruginosa*, *A. baumannii*, and *Enterobacteriaceae*. **Supplementary Tables 4-6** contain the full data. MDR is characterized by nonsusceptibility to at least one agent in ≥3 different antibiotic categories (Magiorakos et al., 2012). The antibiotic susceptibility profile of the tested strains can be found in **Supplementary Table 9**. Testing of the α-amino acid-based counterpart di(C_8-Arg)-*N*bap-Arg-NH_2 (**Figure 1**) was included for comparison. Compound 3 synergized with both antibiotics against all clinical isolates tested. Similar to the trend found for the dUSTBP, the combinations of 8 μg/mL (6 μM) compound 3 and novobiocin or rifampicin were most potent against *A. baumannii* (absolute MIC values of 0.002–0.125 μg/mL) and *Enterobacteriaceae* (absolute MIC values of 0.004–32 μg/mL). Moreover, novobiocin or rifampicin in the presence of dUSTBβP 3 was least active against *P. aeruginosa* (absolute MIC values of 0.5–1,024 μg/mL).

Time-Kill Kinetics of dUSTBβP 3 and Novobiocin or Rifampicin in Wild-Type and MDR *A. baumannii*

The ability of the combinations of dUSTBβP 3 and novobiocin (**Figure 3**) or rifampicin (**Figure 4**) to enhance the bacterial killing of wild-type *A. baumannii* ATCC 17978 and MDR

TABLE 5 | Potentiation of novobiocin by dUSTBP di(C_8-Arg)-*N*bap-Arg-NH_2 or dUSTBβP 3 at a fixed concentration of 8 μg/mL (6 μM) against MDR *P. aeruginosa*, *A. baumannii*, and *Enterobacteriaceae*.

Organism	$MIC_{novobiocin}$ (μg/mL)		
	Alone	+ di(C_8-Arg)-*N*bap-Arg-NH_2[a]	+ dUSTBβP 3[a]
P. aeruginosa PA259-96196	1,024	16	32
P. aeruginosa PA262-101856	1,024	32	1,024
P. aeruginosa PA264-104354	1,024	4	512
P. aeruginosa PA91433	1,024	32	1,024
P. aeruginosa PA114228	1,024	256	256
A. baumannii AB027	8	0.031	0.063
A. baumannii AB031	4	0.031	0.031
A. baumannii LAC-4	1	0.008	0.002
A. baumannii 92247	4	0.063	0.063
A. baumannii 110193	128	0.25	0.125
E. coli 94393	64	0.5	0.125
E. coli 94474	256	0.5	0.5
E. coli 107115	128	0.25	0.5
K. pneumoniae 113250	128	2	2
K. pneumoniae 113254	256	2	4
K. pneumoniae 116381	256	1	1
E. cloacae 117029	512	0.5	0.25
E. cloacae 118564	256	0.5	0.5
E. cloacae 121187	32	2	2

[a]*MIC of novobiocin in the presence of 8 μg/mL (6 μM) compound. MIC of dUSTBP di(C_8-Arg)-Nbap-Arg-NH_2 and dUSTBβP 3 is ≥64 μg/mL against all strains tested, with the exception of A. baumannii LAC-4 (MIC of 16 μg/mL).*

A. baumannii 110193 was determined. Bactericidal and bacteriostatic activity is defined by $a \geq 3 \log_{10}$ and $a < 3 \log_{10}$ decrease in CFU/mL from the original inoculum after 24 h, respectively (Clinical and Laboratory Standards Institute, 1999). Treatment of both strains with 8 μg/mL (6 μM) dUSTBβP 3 alone resulted in growth curves similar to the negative controls, indicating that compound 3 does not have intrinsic antibacterial activity. Bacteriostatic activity was exhibited by 32 μg/mL novobiocin or 0.5 μg/mL rifampicin in both wild-type and MDR *A. baumannii* strains. Combinations of 8 μg/mL (6 μM) compound 3 with either 8 or 32 μg/mL novobiocin lowered the bacterial load of both *A. baumannii* strains below the detection limit after 24 h. The addition of 8 μg/mL (6 μM) dUSTBβP 3 to either 0.125 or 0.5 μg/mL rifampicin sterilized *A. baumannii* 110193 after 24 h. While the combination of 8 μg/mL (6 μM) compound 3 and 0.125 μg/mL rifampicin was not able to suppress regrowth of *A. baumannii* ATCC 17978 after 4 h, increasing the rifampicin concentration to 0.5 μg/mL resulted in bactericidal effects after 24 h.

dUSTBβP 3 Potentiated Multiple Classes of Antibiotics

In addition to novobiocin and rifampicin, synergy between dUSTBβP 3 and 19 other antibiotics were also screened against wild-type *P. aeruginosa*, *A. baumannii*, and *E. coli* (**Figure 5**). Synergy is defined by at least a 4-fold reduction in MIC of an antibiotic in combination with 8 μg/mL (6 μM) (>¼ × MIC of dUSTBβP 3) compound 3. dUSTBβP 3 potentiated multiple classes of antibiotics, including the aminocoumarins, ansamycins, antifolates, fluoroquinolones, lincosamides, macrolides, oxazolidinones, penicillins, pleuromutilins, and tetracyclines.

dUSTBβP 3 Permeabilizes the OM

To determine whether dUSTBβP 3 increases the intracellular concentration of novobiocin or rifampicin by permeabilizing the OM, the ability of the compound to increase the uptake of the nonpolar membrane-impermeable fluorescent probe NPN was measured in wild-type *A. baumannii* ATCC 17978 and *E. coli* ATCC 25922 (**Figure 6**). NPN uptake is normally prevented when the OM is intact (Idowu et al., 2019). Moreover, NPN fluoresces strongly and weakly in phospholipid and aqueous environments, respectively (Idowu et al., 2019). Since increasing concentrations of the OM permeabilizer PMBN or compound 3 resulted in increased fluorescence of NPN, this suggests that dUSTBβP 3 dose-dependently permeabilizes the OM.

dUSTBβP 3 Displayed Enhanced Resistance to Proteases

Previously reported dUSTBP di(C_8-Arg)-*N*bap-Arg-NH_2 remained intact after incubation with trypsin for 2 h (Ramirez et al., 2020). Therefore, the ability of dUSTBβP 3 to resist tryptic degradation was also examined as an initial study of stability toward proteases. Compound 3 was incubated in the presence of trypsin for 2 h, and the resulting degradation mixture was subsequently assessed by electrospray ionization mass spectrometry molecular fragmentation analysis. To verify trypsin cleavage, dUSCL di-C_9-KKKK-NH_2 (**Figure 1**) was selected as a positive control. Solutions consisting of trypsin alone and peptide alone were chosen as negative controls. Complete degradation of the dUSCL occurred, as indicated by the loss of parent mass ions characteristic to untruncated di-C_9-KKKK-NH_2 (**Supplementary Figure 1**). However, resistance to trypsin was observed with the dUSTBβP, as parent mass ions corresponding to untruncated compound 3 were still present after 2 h (**Supplementary Figure 2**). Proteolytic stability was further evaluated by incubating dUSTBβP 3 in human plasma (**Figure 7**). Compound 3 (86.8 ± 3.7% remaining) was found to be stable for 2 h in plasma, unlike the α-amino acid-based derivative di(C_8-Arg)-*N*bap-Arg-NH_2 (39.5 ± 7.4% remaining).

dUSTBβP 3 Is Noncytotoxic to Eukaryotic Cells

Toxicity of dUSTBβP 3 was evaluated against the eukaryotic HEK293 and HepG2 cell lines (**Supplementary Figure 3**). Testing of the anticancer drug doxorubicin was included as a positive control. Compound 3 at 125 μM and doxorubicin at 1 μM were noncytotoxic (86.4 ± 8.7% cell viability) and toxic (16.6 ± 2.3% cell viability) to HEK293 cells, respectively. Similarly, dUSTBβP 3 and doxorubicin exhibited limited activity (CC_{50} of 100.9 μM) and potent activity (CC_{50} of 0.032 μM) against HepG2 cells, respectively.

TABLE 6 | Potentiation of rifampicin by dUSTBP di(C_8-Arg)-*N*bap-Arg-NH_2 or dUSTBβP 3 at a fixed concentration of 8 μg/mL (6 μM) against MDR *P. aeruginosa*, *A. baumannii*, and *Enterobacteriaceae*.

Organism	$MIC_{rifampicin}$ (μg/mL)		
	Alone	+ di(C_8-Arg)-*N*bap-Arg-NH_2[a]	+ dUSTBβP 3[a]
P. aeruginosa PA259-96196	16	0.5	0.5
P. aeruginosa PA262-101856	1,024	32	64
P. aeruginosa PA264-104354	16	0.063	0.5
P. aeruginosa PA91433	16	1	8
P. aeruginosa PA114228	16	2	8
A. baumannii AB027	1	0.031	0.008
A. baumannii AB031	1	0.016	0.002
A. baumannii LAC-4	0.5	0.016	0.004
A. baumannii 92,247	2	0.031	0.016
A. baumannii 110,193	1	0.031	0.008
E. coli 94393	8	0.031	0.016
E. coli 94474	8	0.031	0.008
E. coli 107115	32	0.002	0.004
K. pneumoniae 113250	32	0.5	1
K. pneumoniae 113254	16	2	0.5
K. pneumoniae 116381	512	32	32
E. cloacae 117029	8	0.016	0.004
E. cloacae 118564	8	0.25	0.125
E. cloacae 121187	4	2	0.25

[a]*MIC of rifampicin in the presence of 8 μg/mL (6 μM) compound. MIC of dUSTBP di(C_8-Arg)-Nbap-Arg-NH_2 and dUSTBβP 3 is ≥64 μg/mL against all strains tested, with the exception of A. baumannii LAC-4 (MIC of 16 μg/mL).*

DISCUSSION

dUSTBβPs were designed based on our previously reported dUSTBPs (**Figure 1**). Basic amino acids were incorporated into the dUSTBP structure to achieve selective interaction with the anionic bacterial surface, two short hydrophobic fatty acyl tails for bacterial membrane destabilization, and the molecular scaffold *N*bap to improve proteolytic stability. Improved resistance to trypsin was observed with dUSTBP di(C_8-Arg)-*N*bap-Arg-NH_2 (**Figure 1**) in comparison to dUSCL di-C_9-KKKK-NH_2 (**Figure 1**; Ramirez et al., 2020). To further increase the resistance of dUSTBPs to proteases, β-amino acid-containing derivatives were produced. Particularly, $β^3$-amino acids were used in which the sidechains are adjacent to the amine (Cabrele et al., 2014). Since β-amino acids contain an additional methylene in the backbone, interaction with protease active sites may be impeded, potentially resulting in decreased enzymatic degradation (Godballe et al., 2011).

All dUSTBβPs were produced by using SPPS on a Rink amide MBHA resin following an Fmoc protection strategy. Due to the nature of the MBHA resin, all synthesized compounds have an amidated C-terminus. The basic amino acids $β^3$hOrn, $β^3$hLys, or $β^3$hArg were attached at three points on *N*bap. The N-terminus of both terminal amino acids was also acylated with C_8 fatty acids, yielding three dUSTBβPs. Structural activity relationships studies revealed that C_8 fatty acyl tails were relatively nonhemolytic and exhibited promising adjuvant potency by sensitizing Gram-negative bacteria to several antibiotics (Ramirez et al., 2020). However, fatty acyl tails four carbons long resulted to no potentiation possibly due to insufficient membrane interaction, and fatty acyl tails 12 carbons long exhibited hemolysis (Ramirez et al., 2020).

Selectivity of dUSTBβPs to bacterial cells rather than eukaryotic cells is a significant aspect to consider for clinical application. We previously reported di-C_8 dUSTBPs to be nonhemolytic against porcine erythrocytes (Ramirez et al., 2020). Thus, we evaluated the propensity for hemolysis of the prepared compounds on human erythrocytes (**Figure 2**). Red blood cells were subjected to dUSTBβPs at concentrations ranging from 1.5625 to 200 μM. Even at the highest concentration tested, the compounds were found to be nonhemolytic (<5% hemolysis).

Susceptibility of wild-type *P. aeruginosa*, *A. baumannii*, and *E. coli* to dUSTBβPs was also assessed (**Table 1**). Similar to the di-C_8 α-amino acid-based derivatives, the compounds did not display intrinsic antibacterial activity (Ramirez et al., 2020). While previous studies have shown that C_8 fatty acyl tails were not sufficient to confer inherent activity, they displayed potent synergy with novobiocin and rifampicin against wild-type and MDR clinical isolates of Gram-negative bacteria (Ramirez et al., 2020). Therefore, the adjuvant properties of dUSTBβPs were also investigated.

The di-C_8 dUSTBPs acted as adjuvants that consistently enhanced the antibacterial activity of novobiocin and rifampicin against wild-type Gram-negative bacteria (Ramirez et al., 2020). Hence, the ability of dUSTBβPs to also potentiate these two antibiotics against *P. aeruginosa* PAO1 (**Table 2**), *A. baumannii* ATCC 17978 (**Table 3**), and *E. coli* ATCC 25922 (**Table 4**) was studied. In general, the synthesized compounds displayed similar novobiocin and rifampicin potentiation in comparison with their α-amino acid-based counterparts. Out of the three compounds, dUSTBβP 3 (with $β^3$hArg residues) proved most promising. For instance, compound 3 reduced the MIC of novobiocin and rifampicin 4- to 32-fold better than the $β^3$hOrn and $β^3$hLys derivatives. This matches previous structural activity relationship studies that have shown that guanidino functions may confer preferential membrane activity compared to primary amines (Nakase et al., 2012; Andreev et al., 2014; Ramirez et al., 2020). As such, the adjuvant activity of compound 3 with novobiocin and rifampicin was further explored against MDR Gram-negative bacteria.

Potentiation of novobiocin (**Table 5**) or rifampicin (**Table 6**) by dUSTBβP 3 was examined against MDR clinical isolates of *P. aeruginosa*, *A. baumannii*, *E. coli*, *Klebsiella pneumoniae*, and *Enterobacter cloacae*. Relative to the α-amino acid-based derivative di(C_8-Arg)-*N*bap-Arg-NH_2, a slight reduction in antibiotic potentiation was observed with compound 3 against *P. aeruginosa* while an increase in rifampicin potentiation was observed against *A. baumannii* and *E. coli*. For instance, 8 μg/mL (6 μM) compound 3 potentiated rifampicin 8-fold less in PA264-104354 and PA91433. Moreover, 8 μg/mL (6 μM) dUSTBβP 3 potentiated rifampicin between 2- and 8-fold

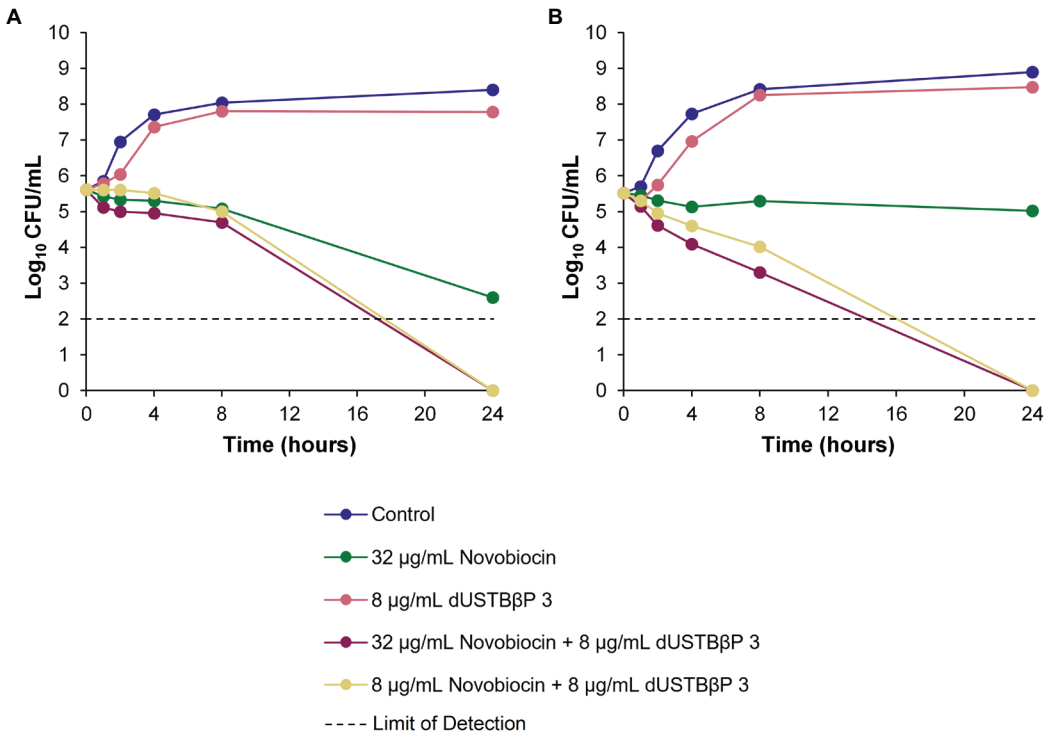

FIGURE 3 | Time-kill kinetics of novobiocin alone and in combination with a fixed concentration of 8 μg/mL (6 μM) dUSTBβP 3 against **(A)** wild-type *A. baumannii* ATCC 17978 and **(B)** MDR *A. baumannii* 110193.

more than di(C_8-Arg)-*N*bap-Arg-NH_2 against *A. baumannii* and *E. coli*, except against *E. coli* strain 107115.

The ability of dUSTBβP 3 to reduce absolute MICs of novobiocin and rifampicin below their clinical breakpoints was evaluated. Currently, both the CLSI and the European Committee on Antimicrobial Susceptibility Testing have no breakpoint values listed for these two antibiotics against *P. aeruginosa*, *A. baumannii*, and *Enterobacteriaceae*. Thus, established breakpoints for other organisms were cautiously selected as reference. For rifampicin, a CLSI susceptibility breakpoint of ≤1 μg/mL for *Staphylococcus* spp. was used (Clinical and Laboratory Standards Institute, 2019). For novobiocin, an interpretative susceptibility breakpoint of 4 μg/mL based on bovine mastitis pathogens was used (Thornsberry et al., 1997). It has also been previously reported that novobiocin and colistin combination therapy which potentiates novobiocin to below the steady-state serum concentration of 5 μg/mL may have clinical potential (MacNair et al., 2018). In combination with 8 μg/mL (6 μM) compound 3, the MIC of novobiocin was reduced below the susceptibility breakpoint in all *A. baumannii*, *E. coli*, *K. pneumoniae*, and *E. cloacae* strains (**Table 5**). Moreover, MICs of rifampicin below the clinical breakpoint were achieved in two of the five *P. aeruginosa* strains, all *A. baumannii* strains tested, and eight of the nine *Enterobacteriaceae* strains (**Table 6**). Indeed, these results indicate that dUSTBβP 3 is a potent adjuvant for novobiocin and rifampicin against MDR Gram-negative bacteria. The drastic potentiation of rifampicin in *A. baumannii* is of particular note. A concentration of 8 μg/mL SPR741 has previously been shown to reduce the MIC of rifampicin against *A. baumannii* to between 0.002 and 0.03 μg/mL against 25 clinical isolates (Corbett et al., 2017). All observed MIC values for rifampicin in combination with compound 3 fall within the same range, indicating that dUSTBβP 3 displays comparable potentiation with SPR741 (Corbett et al., 2017). To study the bacteriostatic or bactericidal activity of the combinations of compound 3 and the two antibiotics, time-kill kinetics against *A. baumannii* were conducted.

The combinations of dUSTBP di(C_8-Arg)-*N*bap-Arg-NH_2 and novobiocin or rifampicin were previously described to enhance the bacterial killing of wild-type *A. baumannii* ATCC 17978 and MDR *A. baumannii* 110193 (Ramirez et al., 2020). To determine whether this effect is conserved with dUSTBβP 3, time-kill assays were performed against the same strains (**Figures 3, 4**). Interestingly, the combination of 0.5 μg/mL rifampicin with 8 μg/mL (6 μM) di(C_8-Arg)-*N*bap-Arg-NH_2 resulted in complete eradication of the wild-type strain in just 8 h (Ramirez et al., 2020). Whereas the combination of 0.5 μg/mL rifampicin with 8 μg/mL (6 μM) compound 3 only reached the same effect past 8 h. This suggests that the β-amino acid-containing derivative possibly exhibits slower killing kinetics than its α-amino acid-based counterpart. Overall, our data indicate that enhanced bacterial

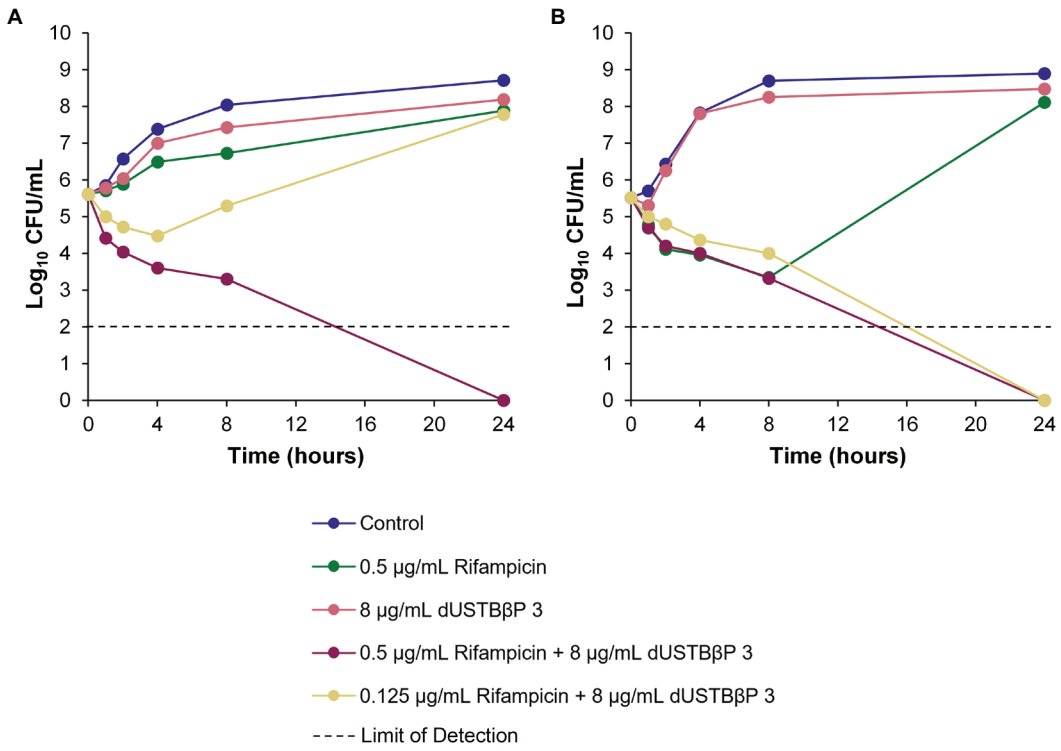

FIGURE 4 | Time-kill kinetics of rifampicin alone and in combination with a fixed concentration of 8 μg/mL (6 μM) dUSTBβP 3 against **(A)** wild-type *A. baumannii* ATCC 17978 and **(B)** MDR *A. baumannii* 110193.

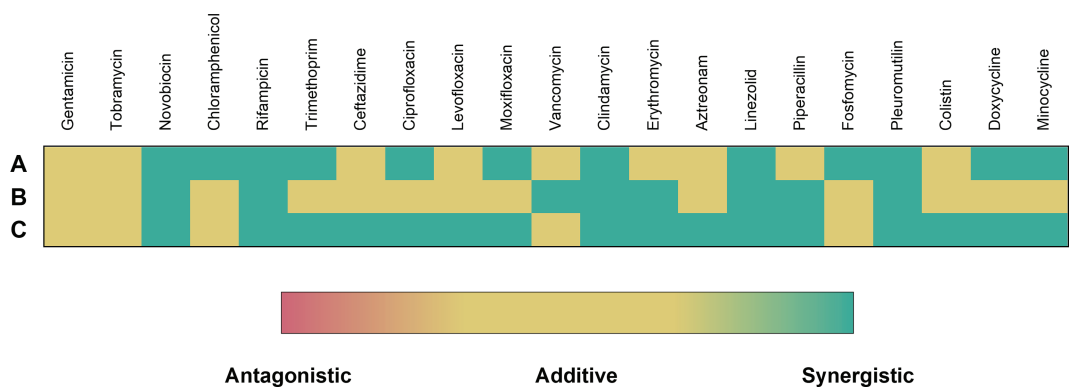

FIGURE 5 | Interactions of dUSTBβP 3 at a fixed concentration of 8 μg/mL (6 μM) with different antibiotics against wild-type **(A)** *P. aeruginosa* PAO1, **(B)** *A. baumannii* ATCC 17978, and **(C)** *E. coli* ATCC 25922. FICI (FIC) ≤ 0.5 = Green; FICI > 0.5 but ≤4.0 = Yellow; and FICI > 4.0 = Red. See **Supplementary Table 7** for MIC values of each combination.

killing of both *A. baumannii* strains can be achieved with combination therapy consisting of dUSTBβP 3 and novobiocin or rifampicin.

Potential for synergy between dUSTBβP 3 and other clinically relevant antibiotics was also examined in wild-type Gram-negative bacteria (**Figure 5**). Tested antibiotics include, but are not limited to, those that have minimal activity against Gram-negative bacteria but are potent against Gram-positive bacteria. Thus, dUSTBβP 3 synergized with antibiotics considered OM-impermeable (novobiocin, rifampicin, vancomycin, clindamycin, erythromycin, and linezolid) and efflux-susceptible (chloramphenicol, trimethoprim, ceftazidime, ciprofloxacin, levofloxacin, moxifloxacin, clindamycin, aztreonam, linezolid, piperacillin, fosfomycin, pleuromutilin, doxycycline, and minocycline). Of the 21 tested antibiotics, compound 3 potentiated 12,

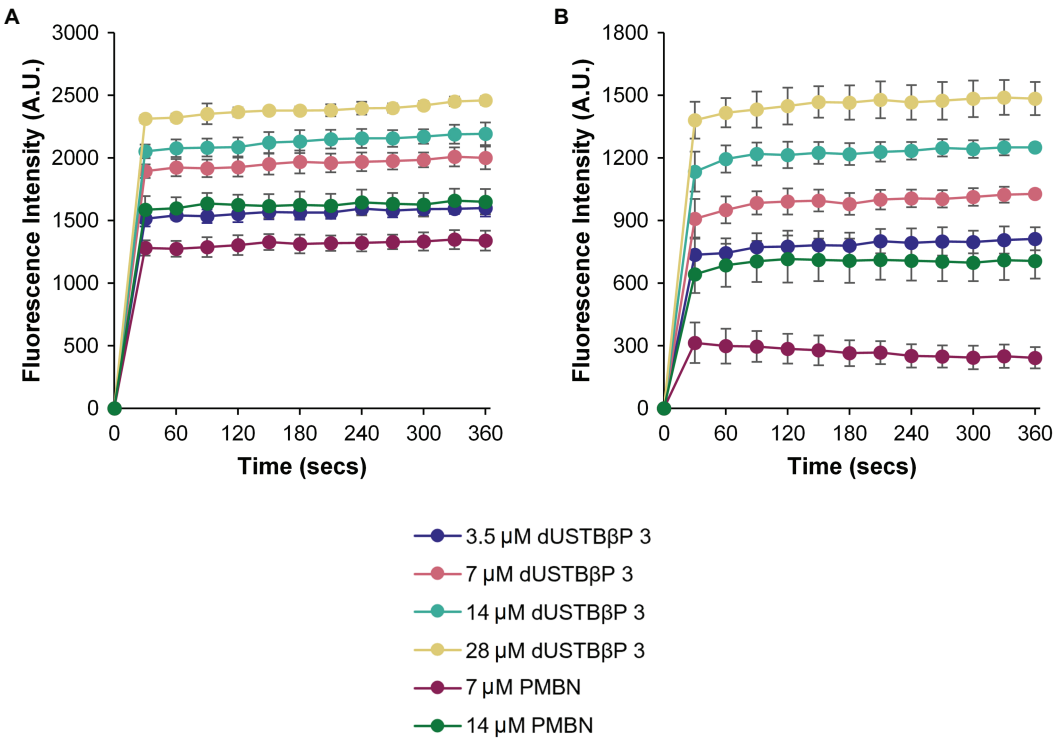

FIGURE 6 | Measurement of OM permeabilization by dUSTBβP 3 through the accumulation of NPN in **(A)** *A. baumannii* ATCC 17978 and **(B)** *E. coli* ATCC 25922 cells. Control used was PMBN. Results were an average of triplicates ($n = 3$) ± SD.

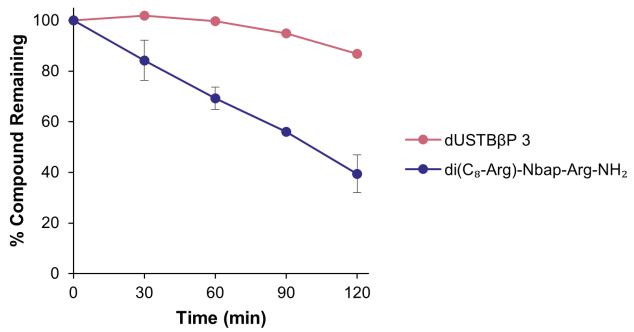

FIGURE 7 | Stability profile of dUSTBβP 3 and di(C_8-Arg)-*N*bap-Arg-NH_2 in human plasma. Results were an average of duplicates ($n = 2$) ± SD.

eight, and 16 in PAO1, *A. baumannii* ATCC 17978, and *E. coli* ATCC 25922, respectively. Besides novobiocin and rifampicin, clindamycin and pleuromutilin were also consistently potentiated against all tested wild-type strains. These initial results suggest that dUSTBβPs increase the uptake of antibiotics by permeabilizing the OM, as well as by potentially suppressing efflux. Future investigation will explore the precise mode of action to confirm these results.

To elucidate the mechanism of antibiotic potentiation, the ability of dUSTBβP 3 to permeabilize the OM was initially studied in *A. baumannii* ATCC 17978 and *E. coli* ATCC 25922 (**Figure 6**). The two wild-type strains were selected since the combinations of compound 3 with novobiocin or rifampicin were most active against these organisms. NPN assay was performed using compound 3 at concentrations ranging from 3.5 to 28 μM. Testing of the known OM permeabilizer PMBN was included as a positive control. The data confirm the synergy displayed in the checkerboard studies, and that compound 3 permeabilizes the OM of both strains in a concentration-dependent manner. Moreover, at equimolar concentrations (7 and 14 μM), dUSTBβP 3 caused higher NPN fluorescence than PMBN.

The systemic usage of peptide therapeutics has been limited due to the poor bioavailability and proteolytic susceptibility associated with these molecules (Latham, 1999). To overcome these challenges, peptidomimetic strategies such as backbone modifications and the integration of unnatural amino acids can be employed (Avan et al., 2014). We have formerly shown that the incorporation of the *N*-substituted glycine *N*bap to the dUSTBP design resulted in increased stability toward trypsin (Ramirez et al., 2020). β^3-amino acids were introduced herein into the lead dUSTBP structure to improve resistance to nonspecific proteolysis. To assess the proteolytic stability of dUSTBβP 3, the ability of the compound to resist degradation by trypsin and in human plasma was assessed (**Figure 7**; **Supplementary Figure 2**). After 2 h incubation in both conditions, it was found that

compound 3 was stable. In addition, compound 3 has an extrapolated *in vitro* plasma half-life (10.43 ± 3.70 h) comparable with the *in vivo* elimination half-lives of three of the seven AMPs approved by the Food and Drug Administration: colistin (5 h), daptomycin (8–9 h), and the lypoglycopeptide telavancin (8 h; Chen and Lu, 2020). These results indicate that employing multiple peptidomimetic strategies into one molecule can result in enhanced resistance to proteases.

The effect of dUSTBβPs on eukaryotic cells was initially screened against human erythrocytes (**Figure 2**). dUSTBβP 3, which was found to be nonhemolytic, showed the greatest adjuvant potency out of the three derivatives. Therefore, the probability of dUSTBβP 3 to induce cytotoxicity to HEK293 and HepG2 human cells was further examined (**Supplementary Figure 3**). Cell viability assay was performed at concentrations ranging from 1 to 125 μM. At the highest concentration tested, dUSTBβP 3 was noncytotoxic to HEK293 cells (86.4% ± 8.7% cell viability). In contrast, dUSTBβP 3 has a CC_{50} (100.9 μM) against HepG2 cells 17-fold higher than the effective adjuvant concentration (6 μM) used in the synergistic studies.

To improve resistance to nonspecific proteolytic degradation, three β-amino acid-containing derivatives of dUSTBPs were prepared. In comparison to the α-amino acid-based counterpart, novobiocin and rifampicin potentiation by compound 3 were conserved against wild-type and MDR clinical isolates of *P. aeruginosa*, *A. baumannii*, and *Enterobacteriaceae*. The nonhemolytic dUSTBβP 3, consisting of β^3hArg residues, lowered the MICs of novobiocin and rifampicin below their interpretative susceptibility breakpoints. Furthermore, compound 3 showed excellent *in vitro* plasma stability with an extrapolated half-life of 10.43 ± 3.70 h.

DATA AVAILABILITY STATEMENT

The original contributions presented in the study are included in the article/**Supplementary Material**; further inquiries can be directed to the corresponding author.

AUTHOR CONTRIBUTIONS

DR and FS conceived the study. DR prepared the compounds and performed the antimicrobial susceptibility, checkerboard, time-kill, and tryptic digest assays. DR and LB characterized the compounds. YL and DR performed the NPN assays. GA performed the cell viability assays. FS and AK supervised the microbiological and biochemical assays. DR, LB, RD, and FS wrote the manuscript. All authors contributed to the article and approved the submitted version.

FUNDING

This work was supported by the Canadian Institutes of Health Research (CIHR) in the form of a pilot project (162159) and the Natural Sciences and Engineering Research Council of Canada (NSERC) in the form of a discovery grant (2018-06047).

SUPPLEMENTARY MATERIAL

The Supplementary Material for this article can be found online at: https://www.frontiersin.org/articles/10.3389/fmicb.2021.803309/full#supplementary-material

REFERENCES

Akhoundsadegh, N., Belanger, C. R., and Hancock, R. E. W. (2019). Outer membrane interaction kinetics of new polymyxin B analogs in Gram-negative bacilli. *Antimicrob. Agents Chemother.* 63, e00935–e00919. doi: 10.1128/AAC.00935-19

Ammeter, D., Idowu, T., Zhanel, G. G., and Schweizer, F. (2019). Development of a nebramine-cyclam conjugate as an antibacterial adjuvant to potentiate β-lactam antibiotics against multidrug-resistant *P. aeruginosa*. *J. Antibiot.* 72, 816–826. doi: 10.1038/s41429-019-0221-9

Andreev, K., Bianchi, C., Laursen, J. S., Citterio, L., Hein-Kristensen, L., Gram, L., et al. (2014). Guanidino groups greatly enhance the action of antimicrobial peptidomimetics against bacterial cytoplasmic membranes. *Biochim. Biophys. Acta Biomembr.* 1838, 2492–2502. doi: 10.1016/j.bbamem.2014.05.022

Årdal, C., Balasegaram, M., Laxminarayan, R., McAdams, D., Outterson, K., Rex, J. H., et al. (2020). Antibiotic development—economic, regulatory and societal challenges. *Nat. Rev. Microbiol.* 18, 267–274. doi: 10.1038/s41579-019-0293-3

Avan, I., Dennis Hall, C., and Katritzky, A. R. (2014). Peptidomimetics via modifications of amino acids and peptide bonds. *Chem. Soc. Rev.* 43, 3575–3594. doi: 10.1039/c3cs60384a

Baker, K. R., Jana, B., Hansen, A. M., Nielsen, H. M., Franzyk, H., and Guardabassi, L. (2019). Repurposing azithromycin and rifampicin against gram-negative pathogens by combination with peptidomimetics. *Front. Cell. Infect. Microbiol.* 9:236. doi: 10.3389/fcimb.2019.00236

Berry, L., Domalaon, R., Brizuela, M., Zhanel, G. G., and Schweizer, F. (2019). Polybasic peptide-levofloxacin conjugates potentiate fluoroquinolones and other classes of antibiotics against multidrug-resistant Gram-negative bacteria. *Med. Chem. Commun.* 10, 517–527. doi: 10.1039/C9MD00051H

Cabrele, C., Martinek, T. A., Reiser, O., and Berlicki, Ł. (2014). Peptides containing β-amino acid patterns: challenges and successes in medicinal chemistry. *J. Med. Chem.* 57, 9718–9739. doi: 10.1021/jm5010896

Carcione, D., Siracusa, C., Sulejmani, A., Leoni, V., and Intra, J. (2021). Old and new beta-lactamase inhibitors: molecular structure, mechanism of action and clinical use. *Antibiotics* 10:995. doi: 10.3390/antibiotics10080995

Chan, W. C., and White, P. D. (2000). *Fmoc Solid Phase Peptide Synthesis: A Practical Approach. 1st Edn*. New York: Oxford University Press Inc.

Chen, C. H., and Lu, T. K. (2020). Development and challenges of antimicrobial peptides for therapeutic applications. *Antibiotics* 9:24. doi: 10.3390/antibiotics9010024

Clinical and Laboratory Standards Institute (1999). *Methods for Determining Bactericidal Activity of Antimicrobial Agents; Approved Guideline, CLSI document M26-A. 29th Edn.* Wayne, PA: Clinical and Laboratory Standards Institute.

Clinical and Laboratory Standards Institute (2019). *Performance standards for antimicrobial susceptibility testing, CLSI supplement M100. 29th Edn.* Wayne, PA: Clinical and Laboratory Standards Institute.

Corbett, D., Wise, A., Langley, T., Skinner, K., Trimby, E., Birchall, S., et al. (2017). Potentiation of antibiotic activity by a novel cationic peptide: potency and spectrum of activity of SPR741. *Antimicrob. Agents Chemother.* 61, e00200–e00217. doi: 10.1128/AAC.00200-17

Domalaon, R., Berry, L., Tays, Q., Zhanel, G. G., and Schweizer, F. (2018a). Development of dilipid polymyxins: investigation on the effect of hydrophobicity

through its fatty acyl component. *Bioorg. Chem.* 80, 639–648. doi: 10.1016/j.bioorg.2018.07.018

Domalaon, R., Brizuela, M., Eisner, B., Findlay, B., Zhanel, G. G., and Schweizer, F. (2019a). Dilipid ultrashort cationic lipopeptides as adjuvants for chloramphenicol and other conventional antibiotics against Gram-negative bacteria. *Amino Acids* 51, 383–393. doi: 10.1007/s00726-018-2673-9

Domalaon, R., Malaka De Silva, P., Kumar, A., Zhanel, G. G., and Schweizer, F. (2019b). The anthelmintic drug niclosamide synergizes with colistin and reverses colistin resistance in Gram-negative bacilli. *Antimicrob. Agents Chemother.* 63, e02574–e02518. doi: 10.1128/AAC.02574-18

Domalaon, R., Sanchak, Y., Cherono Koskei, L., Lyu, Y., Zhanel, G. G., Arthur, G., et al. (2018b). Short proline-rich lipopeptide potentiates minocycline and rifampin against multidrug- and extensively drug-resistant *Pseudomonas aeruginosa*. *Antimicrob. Agents Chemother.* 62, e02374–e02317. doi: 10.1128/AAC.02374-17

Domalaon, R., Zhanel, G. G., and Schweizer, F. (2016). Short antimicrobial peptides and peptide scaffolds as promising antibacterial agents. *Curr. Top. Med. Chem.* 16, 1217–1230. doi: 10.2174/1568026615666150915112459

Drawz, S. M., and Bonomo, R. A. (2010). Three decades of β-lactamase inhibitors. *Clin. Microbiol. Rev.* 23, 160–201. doi: 10.1128/CMR.00037-09

Eckburg, P. B., Lister, T., Walpole, S., Keutzer, T., Utley, L., Tomayko, J., et al. (2019). Safety, tolerability, pharmacokinetics, and drug interaction potential of SPR741, an intravenous potentiator, after single and multiple ascending doses and when combined with β-lactam antibiotics in healthy subjects. *Antimicrob. Agents Chemother.* 63, e00892–e00819. doi: 10.1128/AAC.00892-19

Godballe, T., Nilsson, L. L., Petersen, P. D., and Jenssen, H. (2011). Antimicrobial β-peptides and α-Peptoids. *Chem. Biol. Drug Des.* 77, 107–116. doi: 10.1111/j.1747-0285.2010.01067.x

Hancock, R. E. (1984). Alterations in outer membrane permeability. *Annu. Rev. Microbiol.* 38, 237–264. doi: 10.1146/annurev.mi.38.100184.001321

Hoban, D. J., and Zhanel, G. G. (2013). Introduction to the CANWARD study (2007-11). *J. Antimicrob. Chemother.* 68, i3–i5. doi: 10.1093/jac/dkt021

Hollmann, A., Martinez, M., Maturana, P., Semorile, L. C., and Maffia, P. C. (2018). Antimicrobial peptides: interaction with model and biological membranes and synergism with chemical antibiotics. *Front. Chem.* 6:204. doi: 10.3389/fchem.2018.00204

Idowu, T., Ammeter, D., Rossong, H., Zhanel, G. G., and Schweizer, F. (2019). Homodimeric tobramycin adjuvant repurposes novobiocin as an effective antibacterial agent against gram-negative bacteria. *J. Med. Chem.* 62, 9103–9115. doi: 10.1021/acs.jmedchem.9b00876

Lamers, R. P., Cavallari, J. F., and Burrows, L. L. (2013). The efflux inhibitor phenylalanine-arginine Beta-Naphthylamide (PAβN) Permeabilizes the outer membrane of Gram-negative bacteria. *PLoS One* 8:e60666. doi: 10.1371/journal.pone.0060666

Latham, P. W. (1999). Therapeutic peptides revisited. *Nat. Biotechnol.* 17, 755–757. doi: 10.1038/11686

MacNair, C. R., Stokes, J. M., Carfrae, L. A., Fiebig-Comyn, A. A., Coombes, B. K., Mulvey, M. R., et al. (2018). Overcoming mcr-1 mediated colistin resistance with colistin in combination with other antibiotics. *Nat. Commun.* 9:458. doi: 10.1038/s41467-018-02875-z

Magiorakos, A. P., Srinivasan, A., Carey, R. B., Carmeli, Y., Falagas, M. E., Giske, C. G., et al. (2012). Multidrug-resistant, extensively drug-resistant and pandrug-resistant bacteria: an international expert proposal for interim standard definitions for acquired resistance. *Clin. Microbiol. Infect.* 18, 268–281. doi: 10.1111/j.1469-0691.2011.03570.x

Marquette, A., and Bechinger, B. (2018). Biophysical investigations elucidating the mechanisms of action of antimicrobial peptides and their synergism. *Biomol. Ther.* 8:18. doi: 10.3390/biom8020018

Melander, R. J., and Melander, C. (2017). The challenge of overcoming antibiotic resistance: an adjuvant approach? *ACS Infect Dis.* 3, 559–563. doi: 10.1021/acsinfecdis.7b00071

Meletiadis, J., Pournaras, S., Roilides, E., and Walsh, T. J. (2010). Defining fractional inhibitory concentration index cutoffs for additive interactions based on self-drug additive combinations, Monte Carlo simulation analysis, and in vitro-in vivo correlation data for antifungal drug combinations against aspergillus fumigatus. *Antimicrob. Agents Chemother.* 54, 602–609. doi: 10.1128/AAC.00999-09

Molchanova, N., Hansen, P. R., and Franzyk, H. (2017). Advances in development of antimicrobial peptidomimetics as potential drugs. *Molecules* 22:1430. doi: 10.3390/molecules22091430

Mood, E. H., Goltermann, L., Brolin, C., Cavaco, L. M., Nejad, A. J., Yavari, N., et al. (2021). Antibiotic potentiation in multidrug-resistant Gram-negative pathogenic bacteria by a synthetic Peptidomimetic. *ACS Infect. Dis.* 7, 2152–2163. doi: 10.1021/acsinfecdis.1c00147

Moubareck, C. A. (2020). Polymyxins and bacterial membranes: A review of antibacterial activity and mechanisms of resistance. *Membranes* 10:181. doi: 10.3390/membranes10080181

Nakase, I., Okumura, S., Katayama, S., Hirose, H., Pujals, S., Yamaguchi, H., et al. (2012). Transformation of an antimicrobial peptide into a plasma membrane-permeable, mitochondria-targeted peptide via the substitution of lysine with arginine. *Chem. Commun.* 48, 11097–11099. doi: 10.1039/c2cc35872g

O'Neill, J. (2016). Tackling Drug-Resistant Infections Globally: Final Report and Recommendations. Available at: https://amr-review.org/sites/default/files/160518_Final%20paper_with%20cover.pdf (Accessed October 25, 2021).

Ofek, I., Cohen, S., Rahmani, R., Kabha, K., Tamarkin, D., Herzig, Y., et al. (1994). Antibacterial synergism of polymyxin B nonapeptide and hydrophobic antibiotics in experimental gram-negative infections in mice. *Antimicrob. Agents Chemother.* 38, 374–377. doi: 10.1128/AAC.38.2.374

Prestinaci, F., Pezzotti, P., and Pantosti, A. (2015). Antimicrobial resistance: A global multifaceted phenomenon. *Pathog. Glob. Health* 109, 309–318. doi: 10.1179/2047773215Y.0000000030

Ramirez, D., Berry, L., Domalaon, R., Brizuela, M., and Schweizer, F. (2020). Dilipid ultrashort tetrabasic Peptidomimetics potentiate Novobiocin and rifampicin against multidrug-resistant Gram-negative bacteria. *ACS Infect. Dis.* 6, 1413–1426. doi: 10.1021/acsinfecdis.0c00017

Reygaert, W. C. (2018). An overview of the antimicrobial resistance mechanisms of bacteria. *AIMS Microbiol.* 4, 482–501. doi: 10.3934/microbiol.2018.3.482

Rink, R., Arkema-Meter, A., Baudoin, I., Post, E., Kuipers, A., Nelemans, S. A., et al. (2010). To protect peptide pharmaceuticals against peptidases. *J. Pharmacol. Toxicol. Methods* 61, 210–218. doi: 10.1016/j.vascn.2010.02.010

Sheard, D. E., O'Brien-Simpson, N. M., Wade, J. D., and Separovic, F. (2019). Combating bacterial resistance by combination of antibiotics with antimicrobial peptides. *Pure Appl. Chem.* 91, 199–209. doi: 10.1515/pac-2018-0707

Thornsberry, C., Burton, P. J., Yee, Y. C., Watts, J. L., and Yancey, R. J. (1997). The activity of a combination of penicillin and Novobiocin Against bovine mastitis pathogens: development of a disk diffusion test. *J. Dairy Sci.* 80, 413–421. doi: 10.3168/jds.S0022-0302(97)75952-6

Tsubery, H., Ofek, I., Cohen, S., and Fridkin, M. (2000). Structure-function studies of Polymyxin B nonapeptide: implications to sensitization of Gram-negative bacteria. *J. Med. Chem.* 43, 3085–3092. doi: 10.1021/jm0000057

Vaara, M. (1992). Agents that increase the permeability of the outer membrane. *Microbiol. Rev.* 56, 395–411. doi: 10.1128/mr.56.3.395-411.1992

Vaara, M. (2019). Polymyxin derivatives that sensitize Gram-negative bacteria to other antibiotics. *Molecules* 24:249. doi: 10.3390/molecules24020249

Velkov, T., Thompson, P. E., Nation, R. L., and Li, J. (2010). Structure-activity relationships of polymyxin antibiotics. *J. Med. Chem.* 53, 1898–1916. doi: 10.1021/jm900999h

Wright, G. D. (2016). Antibiotic adjuvants: rescuing antibiotics from resistance. *Trends Microbiol.* 24, 862–871. doi: 10.1016/j.tim.2016.06.009

Yang, X., Goswami, S., Gorityala, B. K., Domalaon, R., Lyu, Y., Kumar, A., et al. (2017). A tobramycin vector enhances synergy and efficacy of efflux pump inhibitors against multidrug-resistant gram-negative bacteria. *J. Med. Chem.* 60, 3913–3932. doi: 10.1021/acs.jmedchem.7b00156

Zgurskaya, H. I., and Rybenkov, V. V. (2019). Permeability barriers of Gram-negative pathogens. *Ann. N. Y. Acad. Sci.* 1459, 5–18. doi: 10.1111/nyas.14134

Zhanel, G. G., DeCorby, M., Laing, N., Weshnoweski, B., Vashisht, R., Tailor, F., et al. (2008). Antimicrobial-resistant pathogens in intensive care units in Canada: results of the Canadian National Intensive Care Unit (CAN-ICU) study, 2005-2006. *Antimicrob. Agents Chemother.* 52, 1430–1437. doi: 10.1128/AAC.01538-07

Conflict of Interest: The authors declare that the research was conducted in the absence of any commercial or financial relationships that could be construed as a potential conflict of interest.

Publisher's Note: All claims expressed in this article are solely those of the authors and do not necessarily represent those of their affiliated organizations, or those of the publisher, the editors and the reviewers. Any product that may

be evaluated in this article, or claim that may be made by its manufacturer, is not guaranteed or endorsed by the publisher.

frontiers in Microbiology

ORIGINAL RESEARCH
published: 23 February 2022
doi: 10.3389/fmicb.2021.745100

Thinned-Young Apple Polyphenols Inhibit Halitosis-Related Bacteria Through Damage to the Cell Membrane

Ting Liu[1,2†], Hailiang Shen[3,4†], Furong Wang[1,2], Xueru Zhou[1,2], Pengtao Zhao[1,2], Yali Yang[1,2*] and Yurong Guo[1,2]*

[1] College of Food Engineering and Nutritional Science, Shaanxi Normal University, Xi'an, China, [2] National Research and Development Center of Apple Processing Technology, Xi'an, China, [3] Citrus Research Institute, Southwest University, Chongqing, China, [4] Citrus Research Institute, Chinese Academy of Agricultural Sciences, Chongqing, China

The thinned young apple is a by-product and is generally discarded in the orchard during fruit thinning. The polyphenol content of thinned young apples is about 10 times more than that of ripe apples. In our study, the antibacterial effect of thinned young apple polyphenols (YAP) on the halitosis-related bacteria including *Porphyromonas gingivalis*, *Prevotella intermedius*, and *Fusobacterium nucleatum* was investigated. The minimum inhibitory concentrations of YAP against *P. gingivalis*, *P. intermedia*, and *F. nucleatum* were 8.0, 8.0, and 12.0 mg/ml, while the minimum bactericidal concentrations were 10.0, 10.0, and 14.0 mg/ml, respectively. The scanning electron microscopy and transmission electron microscopy analyses showed that after YAP treatment, the membrane surface of halitosis-related bacterial cells was coarse and the cell wall and membrane were separated and eventually ruptured. The integrity of the cell membrane was determined by flow cytometry, indicating that the cells with the integrity membrane significantly reduced as the YAP concentration treatment increased. The release of proteins and nucleic acids into the cell suspension significantly increased, and the membrane potential reduced after the YAP treatment. This research illustrated the antibacterial mechanism of YAP against halitosis-related bacteria and provided a scientific basis of utilizing the polyphenols from the discarded thinned young apples.

Keywords: Thinned-young apple polyphenols, halitosis, antibacterial mechanism, cell membrane, membrane potential

OPEN ACCESS

Edited by:
Kianoush KHosravi-Darani, National Nutrition and Food Technology Research Institute, Iran

Reviewed by:
Zaixiang Lou, Jiangnan University, China
Lijun Sun, Northwest A&F University, China

***Correspondence:**
Pengtao Zhao
zhaopengtao@snnu.edu.cn
Yali Yang
yangyali@snnu.edu.cn

[†]These authors share first authorship

Specialty section:
This article was submitted to Antimicrobials, Resistance and Chemotherapy, a section of the journal Frontiers in Microbiology

Received: *21 July 2021*
Accepted: *27 December 2021*
Published: *23 February 2022*

Citation:
Liu T, Shen H, Wang F, Zhou X, Zhao P, Yang Y and Guo Y (2022) Thinned-Young Apple Polyphenols Inhibit Halitosis-Related Bacteria Through Damage to the Cell Membrane. Front. Microbiol. 12:745100. doi: 10.3389/fmicb.2021.745100

INTRODUCTION

Apples are rich in lots of nutrients, such as vitamin, fiber, pectin, and polyphenol which are good for the health. The major apple producers around the world are China, Italy, France, and United States (Nicolas et al., 1994). The total apple yield all over the world in 2014 was 84.56×10^6 and 40.92×10^6 tons in China, accounting for 48.39% of the total yield (Li et al., 2018). However,

Abbreviations: YAP, thinned-young apple polyphenols; *F. nucleatum*, *Fusobacterium nucleatum*; *P. gingivalis*, *Porphyromonas gingivalis*; *P. intermedius*, *Prevotella intermedius*; SEM, scanning electron microscopy; TEM, transmission electron microscope; MIC, minimum inhibitory concentration; MBC, minimum bactericidal concentration; CFU/mL, colony-forming unit per milliliter; PI, propidium iodide; MFI, mean fluorescence intensity; PCA, principal component; $OD_{260\ nm}$, optimal density at 260 nm; MP, membrane potential; PC1, the first component; PC2, the second component.

in order to improve the color, size, and quality of apples at harvest, the extra small thinned young apples should be removed from the apple tree after flowering (Miller and Rice-Evans, 1997). In China, about 1.9 million tons of thinned young apples are abandoned every year (Dou et al., 2015). These thinned young apples are usually directly discarded on the orchard grounds and may become a good energy source for the growth of microorganisms, which could increase the risk of fruit diseases and result in a significant reduction in the quality and yield of fruits (Hou et al., 2019). In recent years, some research has focused on the functional properties of thinned young apples (Chen W. et al., 2015; Yuan et al., 2016; Chen et al., 2017). Zhang et al. (2017) found that the polyphenols of thinned young apples have significant antibacterial activity against *Staphylococcus* and *Bacillus anthracis*. Nisar et al. (2019) reported that pectin films incorporated with young apple polyphenols could efficiently inhibit the growth of *Staphylococcus aureus*, *Escherichia coli*, and *Listeria monocytogenes*.

Halitosis is defined as an unpleasant odor caused by the catabolism of bacterial coverage of the tongue, periodontal disease, and other systemic diseases (Joda and Olukoju, 2013), but in halitosis, an incidence of 80–90% are caused by bacteria in the oral cavity (Sanz et al., 2001; Armstrong et al., 2010). *Porphyromonas gingivalis*, *Prevotella intermedius*, and *Fusobacterium nucleatum* are considered to be the main bacteria inducing halitosis (Wang et al., 2002; Lau et al., 2019). The sulfur volatiles such as hydrogen sulfide (H_2S) are mainly in the halitosis odor, which are generated by sulfur amino acids such as cystine, cysteine, and methionine. The chemical solutions including chlorhexidine, triclosan, and cetylpyridinium chloride are usually used to inhibit the halitosis odor, but they may induce side effects such as bacterial resistance and urticaria (Peruzzo et al., 2007; Cortelli et al., 2008). In recent years, many studies pay attention to identifying the safe and natural antibiotic properties such as essential oil, saponin, and phenolic compounds of fruits and vegetables for inhibiting the bacteria-related halitosis odor (Nijole et al., 2018; Sun et al., 2019; Lagha et al., 2020). However, there are rare studies about the antibacterial activity of phenolic compounds of thinned young apples against the bacteria-related halitosis.

In this study, the antibacterial effect and mechanism of young apple polyphenols (YAP) against *P. gingivalis*, *P. intermedius*, and *F. nucleatum* were investigated. This study aimed to identify the natural and safe phenolic compounds of thinned young apples for the suppression of bacteria-related halitosis, which provided a new environmental way of using thinned young apples.

MATERIALS AND METHODS

Materials and Chemicals

The apple cultivar 'Fuji' was obtained at the Baishui Apple Test Station of Northwest Agriculture and Forestry University in Shaanxi province (China). The thinned young apples were collected 35 days after blossom and stored at −80°C. All polyphenol standards used for high-performance liquid chromatography (HPLC) analysis were purchased from Yuanye Biotechnology (Shanghai, China). *P. intermedia*, *P. gingivalis*, and *F. nucleatum* were obtained from Bena Culture Collection (BNCC) (Beijing, China).

Extraction, Purification, and Determination of Thinned Young Apple Polyphenols

The YAP were extracted and purification according to our previous method (Gong et al., 2020). Briefly, the thinned young apples were crashed into 3–4-mm particles. The crude polyphenols were extracted with 70% alcohol at 65°C for 3 h. The extract was filtered with a Buchner funnel and concentrated in a rotary evaporator (OSB-2100, Shanghai Ailang Instrument Factory, China). Then, the solution was centrifuged at 3,500 × *g* for 20 min and the supernatant was collected and eluted by an X-5 macroporous resin. Subsequently, the polyphenol extract was concentrated and lyophilized to obtain the polyphenol powder of 'Fuji' thinned young apples. According to the Folin–Ciocalteu method, the total polyphenol content in YAP was determined and expressed as gallic acid equivalent (mg GAE/g) (Chen L. Y. et al., 2015). The individual phenol compounds were analyzed by HPLC according to our previous method (Wang et al., 2019).

Antibacterial Activity

Porphyromonas gingivalis, *F. nucleatum*, and *P. intermedia* were used in this experiment. The minimum inhibitory concentration (MIC) and the minimum bactericidal concentration (MBC) of YAP were determined according to the methods reported by Wang et al. (2013). Briefly, bacterial cells were cultured in BHI liquid medium which was added with Vitamin K_3, yeast extracted, and Hemin. The bacterial cell concentration was adjusted at 1×10^5 colony-forming units per ml (CFU/ml). Then, the different concentrations of YPA (16, 14, 12, 10, 8, 4, and 2 mg/ml) were added in the test samples with agent-free broth as the blank. All the samples were incubated at 37°C for 48 h. MIC was defined as the lowest antibacterial concentration that inhibited bacterial growth, as shown by the absence of turbidity. The MBC was analyzed by inoculating 10 μl of medium from each of the MIC test that showed no turbidity onto BHI agar plates and incubation at 37°C for 48 h. The MBC values were defined as the lowest concentrations of antibacterial agents where there was no bacterial growth on the plates.

Microstructure Analysis

Bacteria in this study were cultured in BHI liquid medium with different concentrations of YPA (control, MIC, and MBC) and incubated at 37°C for 24 h. Then each culture was harvested by centrifugation at 3,000 × *g* for 10 min. The samples were prepared according to the method of Wang et al. (2018) and then were observed and photographed by scanning electron microscopy (SEM; Quanta 200, FEI Co., Hillsboro, OR, United States).

The intracellular microstructure was observed and photographed by transmission electron microscope (TEM; H-7650, Hitachi Co., Tokyo, Japan). The preparation of TEM samples was performed according to the method of

Wang et al. (2018). The pellets were fixed in 2.5% (v/v) glutaraldehyde for 90 min and washed three times by 0.1 M phosphate buffer (pH 7.2). The cells of each group were fixed in 1% osmic acid for 2 h at room temperature. Then, the bacterial cells were dehydrated and infiltrated into acetone and epoxy resin. The samples were embedded, polymerized, and sectioned.

Cell Membrane Integrity Analysis

According to the previously reported method (Zhou et al., 2020), the bacterial cells stained by dye propidium iodide (PI) were used to evaluate the cell membrane integrity of *P. gingivalis*, *F. nucleatum*, and *P. intermedia via* flow cytometry. The cells used for cell membrane integrity analysis was prepared by the same method as the SEM analysis. After incubation and centrifugation, the bacterial cells were washed three times by 0.1 M phosphate buffer (pH 7.2) and the pellets were resuspended in 0.1 M phosphate buffer. 1 ml of cell suspension was stained with 3 μl of PI (5 mM) for 20 min at 37°C in the dark. The fluorescence intensity was detected by the BD Accuri C6 flow cytometer (Becton Dickinson, United States), and the NovoExpress software was used for data analysis.

The Release of Proteins and Nucleic Acids

The changes in DNA content outside the cell membrane were graphed with the optical density and the corresponding time as the ordinate and abscissa, respectively. Specifically, bacterial cells were cultured in BHI liquid medium combined with different concentrations of YPA (control, MIC, and MBC) at 37°C for 24 h. Every 4 h, the suspensions were collected and centrifuged at 5,000 × *g* for 10 min; the supernatants were collected and diluted with 0.1 M phosphate buffer. Then, the optical density was determined with a microplate reader (Multiskan GO, Molecular Devices, Sunnyvale, CA, United States) at 260 nm. The corrections were carried out for the optical density at 260 nm of suspensions with PBS (0.1 M, pH 7.4) containing the same concentrations of YAP. In addition, the suspension was collected to determine the protein concentration according to Bradford's method (Bradford, 1976).

Membrane Potential Determination

The cell suspensions (approximately 1×10^7 CFU/ml) were combined with different concentrations of YPA (control, MIC, and MBC) and incubated at 37°C for 8 h. The suspensions were washed three times with 0.1 M phosphate buffer (pH 7.2) and mixed with 2 μg/ml of rhodamine 123. Then, the samples were washed three times again, and the pellets were resuspended in PBS for 30 min in the dark. The cell suspensions were a 96-well microplate and detected by a microplate reader (Multiskan Go, Molecular Devices, Sunnyvale, CA, United States) (Comas and Vives-Rego, 1997). The data were expressed as median fluorescent intensity (MFI).

Statistical Analysis

All experiments were done in triplicate. The data were analyzed by using Origin 8.0 (OriginLab Co., Northampton, MA, United States) and SPSS software 24.0 (SPSS Inc., Chicago, IL, United States) and expressed as the average ± standard deviations. Duncan's multiple-range test with 95% confidential level was used to access the difference between the average values. $p < 0.05$ indicated the significant difference between variables. Principle component analysis (PCA) determined the relationships among the variables by the STAT-ITCF Statistical software (Bordeaux, France).

RESULTS

Chemical Characteristics of YAP

As **Figure 1** shows, the main individual phenols in thinned young apples are chlorogenic acid, L-epicatechin, catechin, quercetin, hyperin, rutin, and phlorizin. Their contents were 37, 5.28, 4.37, 6.02, 2.59, 6, and 29%, respectively. The contents of phlorizin and chlorogenic acid were the highest, accounting for 66% of the total phenolic content.

Antibacterial Activity of YAP

The antibacterial activity of YAP was evaluated by MIC and MBC. The MIC values of *P. gingivalis*, *F. nucleatum*, and *P. intermedia* were 8.0, 8.0, and 12.0 mg/ml, respectively, while the MBC values were 10.0, 10.0, and 14.0 mg/ml, respectively. Among the three bacteria, *P. gingivalis* and *F. nucleatum* were similarly susceptible to the YAP, with the lower MIC and MBC.

Effect of YAP on the Microstructure of Bacterial Cells

In order to investigate the effects of YAP on the outer wall structure of bacterial cells, SEM was used to analyze the wall structure changes of bacterial cells after the different concentrations of YAP (control, MIC, and MBC) treatment. As shown in **Figure 2**, untreated *P. intermedia* cells (**Figure 2A1**) showed the typical globe-shaped morphology, while *P. gingivalis* (**Figure 2B1**) and *F. nucleatum* (**Figure 2C1**) cells showed the typical rod-shaped morphology. After treatment with YAP at the MIC level, the bacterial cells (**Figures 2A2,B2,C2**) showed severe outer wall morphological changes. Additionally, the surface of bacterial cells treated with YAP at the MBC level (**Figures 2A3,B3,C3**) showed serious wrinkles and pores, and some cells were even broken, which indicated that the outer wall morphological changes were more serious compared to the bacterial cells treated with YAP at the MIC level. The observations of SEM suggested that the cell surface of *P. intermedia*, *P. gingivalis*, and *F. nucleatum* could be damaged by the YAP, which could affect the proliferation of bacterial cells and may lead to cell death. However, it was unclear whether the morphological changes of bacterial cells induced by YAP could lead to the penetration of the bacterial envelope, which was due to the fact that the YAP may pierce through the bacterial envelope and damage the cell barrier between the cytosol and extracellular environment. Thus, TEM analysis was further used to analyze this phenomenon.

Transmission electron microscopic analysis was performed on the bacterial cells treated with different concentrations

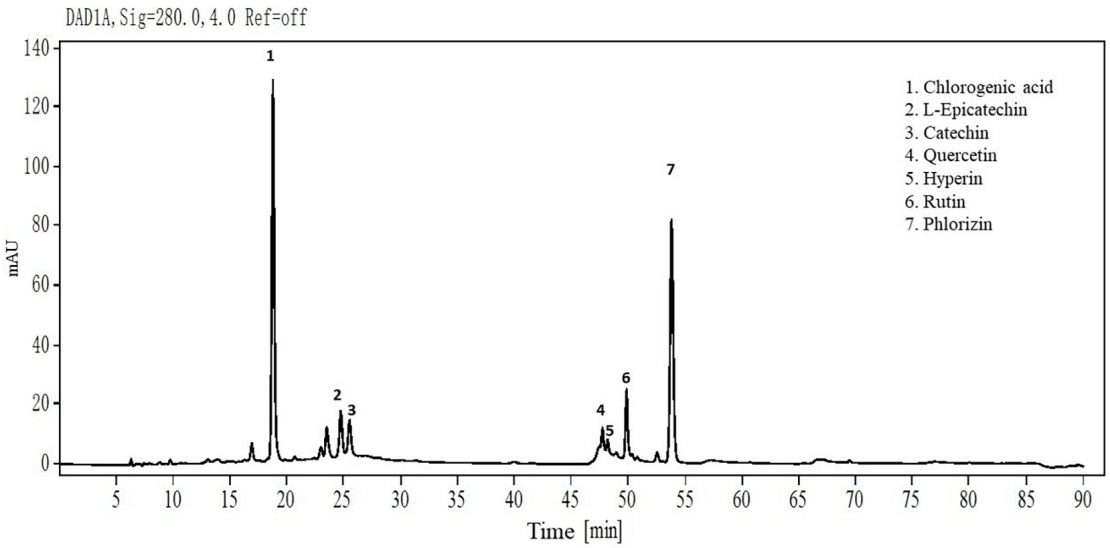

FIGURE 1 | HPLC chromatograms of YAP. YAP was 70% ethanol-eluted fractions from thinned young apples.

of YAP (control, MIC, and MBC). As shown in **Figure 3**, untreated bacterial cells (**Figures 3A1,B1,C1**) showed that the cells have complete cell walls and membranes, and homogeneous intracellular constituents. After treatment, the TEM images in **Figures 3A2,B2,C2** showed the surface of bacterial cells treated with YAP at the MIC level. Some part of the cell wall became blurred. The cell walls and membranes were separated, and the intracellular constituents were inhomogeneous. Furthermore, the cells treated with YAP at the MBC level (**Figures 3A3,B3,C3**) exhibited that the cell wall was ruptured and the cytoplasmic content was leaked from the cell. These observations of TEM further confirmed that YAP could damage the cell walls and membranes and alter the cell intracellular microstructure.

Effect of YAP on Cell Membrane Integrity

The integrity of cell membranes was analyzed by flow cytometry with the fluorescent probe PI (**Figure 4**). When the integrity of the cell membranes was damaged, the fluorescence intensity of the bacterial cells may increase. The percentages of *F. nucleatum*, *P. gingivalis*, and *P. intermedia* cells with PI fluorescence in the MIC group were 53.47, 52.91, and 57.14%, respectively, while the percentages of bacterial cells with PI fluorescence in the MBC group were 76.92, 94.51, and 78.77%, respectively. The flow cytometry results showed that the cells with the integrity membrane dramatically reduced with the increase in YAP concentrations ($p < 0.05$).

Effect of YAP on the Release of Proteins and Nucleic Acids

The release of proteins and nucleic acids into the cell suspension was studied to further explore the effect of YAP on the bacterial cells. The $OD_{260\ nm}$ values showed the release of nucleic acids into the suspension of the bacterial cells with different YAP concentration treatments, as shown in **Figure 5**. The $OD_{260\ nm}$ values of the three bacteria after YAP treatment at the MBC level were higher than those after the MIC treatment, which suggested that the release of nucleic acids significantly increased with the increase in YAP concentrations ($p < 0.05$). Compared to the untreated group, the $OD_{260\ nm}$ values of the three bacteria treated with YAP at both MIC and MBC levels significantly increased from 0 to 4 h ($p < 0.05$). However, the $OD_{260\ nm}$ values of the three bacteria treated with MIC and MBC of YAP steadily increased for the next tested hours, and its increasing rate was obviously lower than that for the first 4 h. **Figure 6** shows the release of protein content of three bacterial cells from 0 to 32 h. When the three bacterial cells were treated with YAP at the MBC level, the released protein content of three bacterial cells was significantly higher than that at the MIC level. Additionally, compared to the untreated group, the release of protein content remarkably increased from 0 to 4 h for three bacterial cells after YAP treatment with MBC and MIC levels, while the release of protein content of three bacterial cells after YAP treatment also increased from 4 to 24 h, but the increasing rate was lower than that from 0 to 4 h. For the last 8 h, the release of protein content of three bacterial cells remained stable, especially for *P. gingivalis* and *P. intermedia.*

Effect of YAP on Membrane Potential

Figure 7 shows the changes in membrane potential (MP) of three bacterial cells after YAP treatment. Compared with the untreated group, the MFI values of *P. intermedia*, *P. gingivalis*, and *F. nucleatum* decreased by 32.48, 34.74, and 48.47%, respectively, after YAP treatment at the MIC level, while the MFI values reduced by 52.97, 56.04, and 75.57%, respectively, after YAP treatment at the MBC level. The results indicated that the MP of three bacterial cells significantly reduced with the increase in YAP concentration ($p < 0.05$). The decrease in the cell MP means the depolarization of the cell membrane, which could

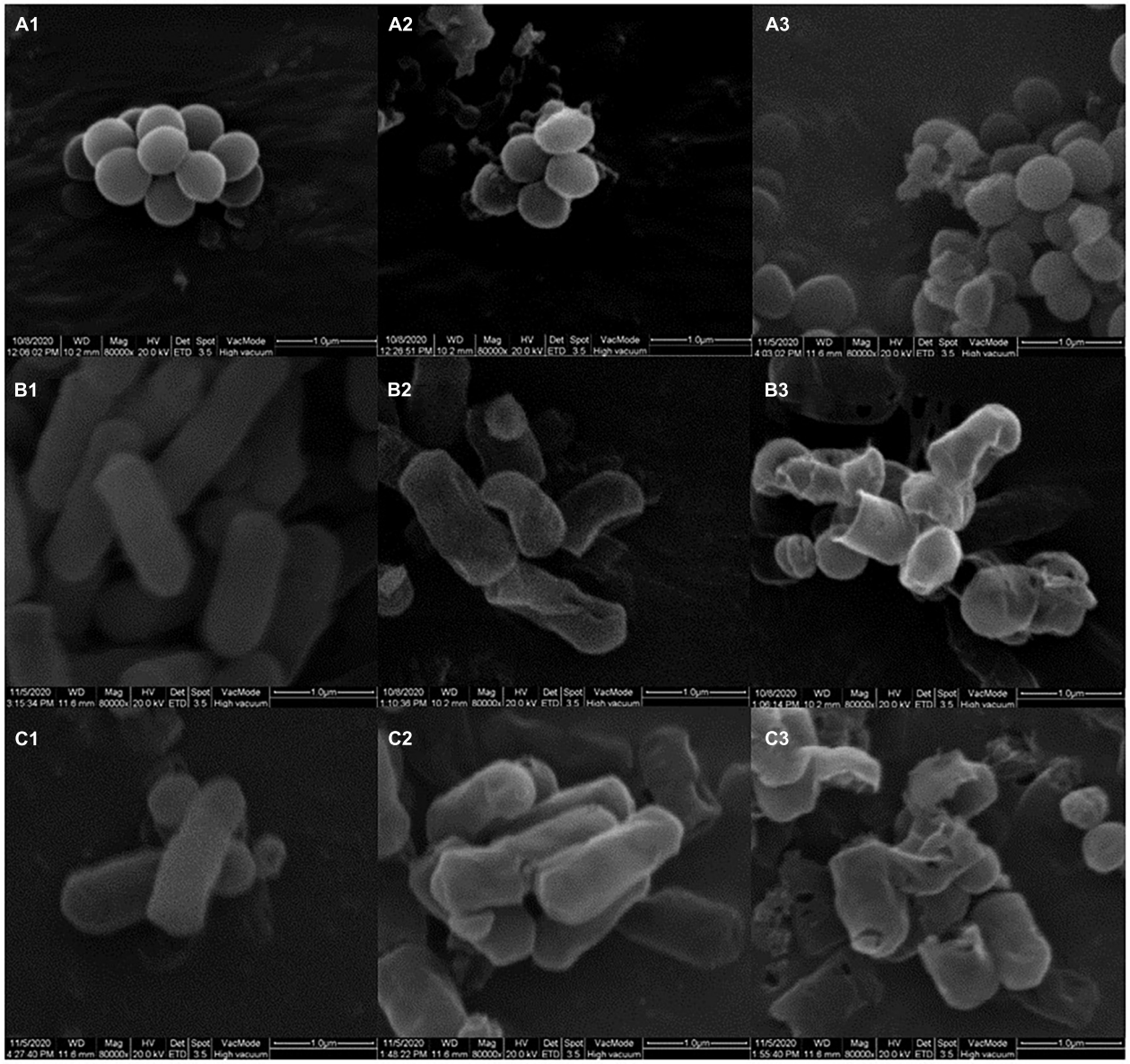

FIGURE 2 | The outer wall structure changes of bacterial cells treated with different concentrations of YAP. **(A1)** *P. intermedia* with untreated, as control; **(A2)** *P. intermedia* treated with MIC; **(A3)** *P. intermedia* treated with MBC; **(B1)** *P. gingivalis* with untreated, as control; **(B2)** *P. gingivalis* treated with MIC; **(B3)** *P. gingivalis* treated with MBC; **(C1)** *F. nucleatum* with untreated, as control; **(C2)** *F. nucleatum* treated with MIC; **(C3)** *F. nucleatum* treated with MBC. MIC, minimum inhibition concentration; MBC, minimum bactericide concentration.

eventually lead to irregular cell metabolism and cause cell death (Hamilton et al., 2021).

Principal Component Analysis

The relationships between the release of proteins and nucleic acids and MP of halitosis-related bacteria treated with different concentrations of YAP were analyzed by principal component analysis (**Figure 8**) (PCA) (Pu et al., 2020). The first component (PC1) and the second component (PC2) accounted for 99.15% of the total variance, which indicated that the first two principal components could distinguish the bacteria treated with different concentrations of YAP. Along with the direction of PC1, the control group is mainly distributed in the negative half axis of PC1, while the group treated with MIC and MBC is mainly distributed on the positive half axis, indicating that there is a significant difference between the groups treated with YAP and the control group. Surprisingly, according to the PC1 direction, the bacterial groups treated with YAP at the MIC level plotted was between the control and bacterial groups treated with YAP at the MBC level; this may be because under the treatment of MIC and MBC, the MP of bacterial cells was significantly reduced, and the release of proteins and nucleic acids was significantly

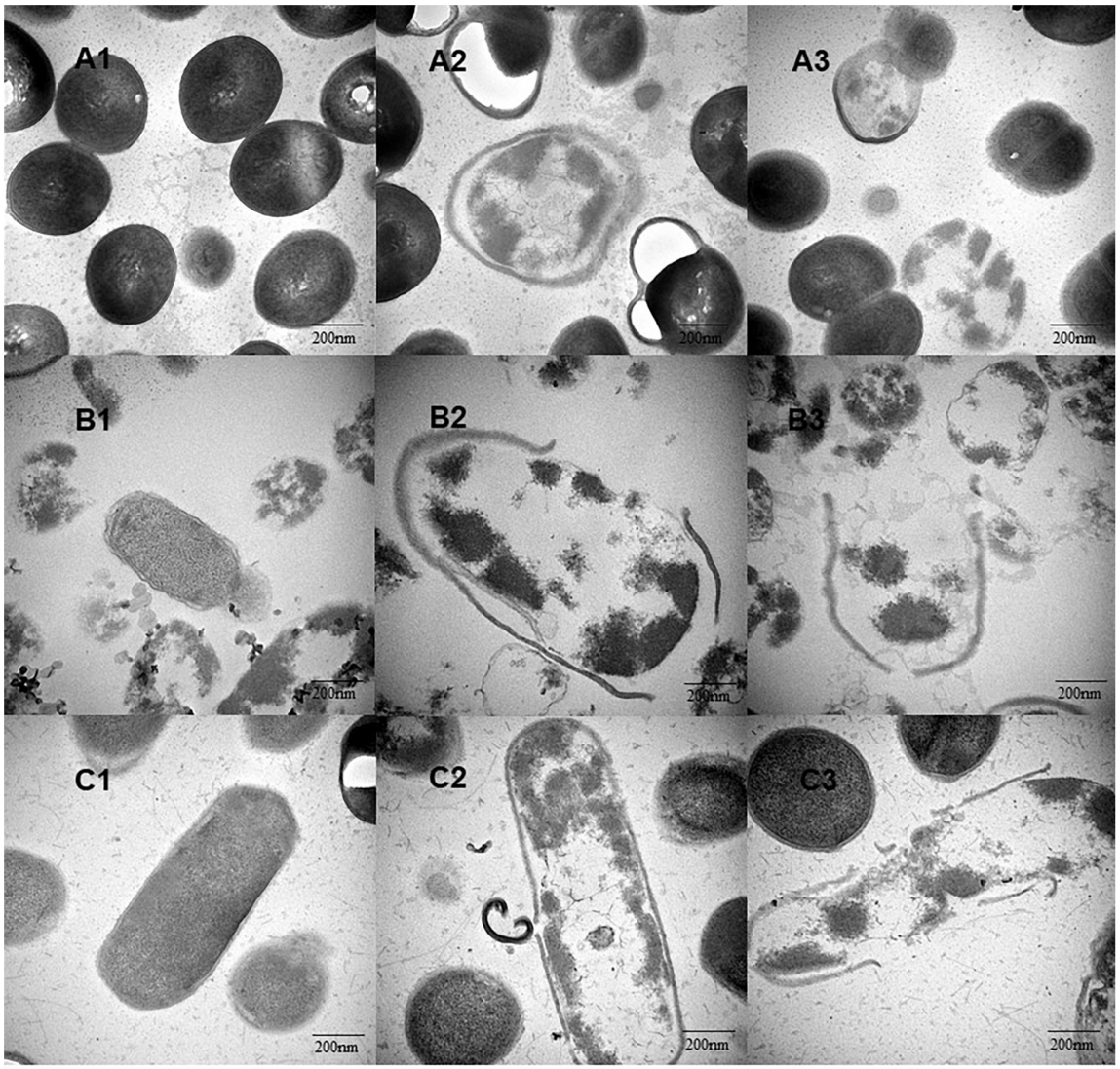

FIGURE 3 | The intracellular microstructure changes of bacterial cells treated with different concentrations of YAP. **(A1)** *P. intermedia* with untreated, as control; **(A2)** *P. intermedia* treated with MIC; **(A3)** *P. intermedia* treated with MBC; **(B1)** *P. gingivalis* with untreated, as control; **(B2)** *P. gingivalis* treated with MIC; **(B3)** *P. gingivalis* treated with MBC; **(C1)** *F. nucleatum* with untreated, as control; **(C2)** *F. nucleatum* treated with MIC; **(C3)** *F. nucleatum* treated with MBC. MIC, minimum inhibition concentration; MBC, minimum bactericide concentration.

increased. It also indicates that the effect of YAP content on the bacteria-related halitosis was significant. Along with the direction of PC2, the groups of *P. gingivalis* treated with different YAP concentrations were distributed at the positive half axis of PC2, while the groups of *F. nucleatum* were distributed at the negative half axis of PC2, which may be due to the different sensitivities to the pH of culture medium (Takahashl et al., 2010).

DISCUSSION

Although many literatures are focused on the antibacterial effects of apple polyphenols, there are few literatures on thinned young apple polyphenols. We extracted and purified polyphenols from 'Fuji' thinned young apples according to the methods of our previous publication (Gong et al., 2020) and analyzed the extracted YAP by HPLC. The higher contents of individual phenols in thinned young apples were chlorogenic acid and phlorizin. It was found that chlorogenic acid and phloretin/phlorizin, as natural antibacterial agents, are widely used in pharmaceutical products (Li et al., 2014; Zhang et al., 2016). However, the phenol extract from Golden Delicious apples by ethyl acetate had a lower antibacterial activity against *Staphylococcus aureus* and *Escherichia coli* than the phlorizin and phloretin standards (Zhang et al., 2016), which may be due to the fact that the polyphenols from apples were usually conjugated with glycosides and reduced the antibacterial activity (Cao et al., 2009). The relative position of the hydroxyl group

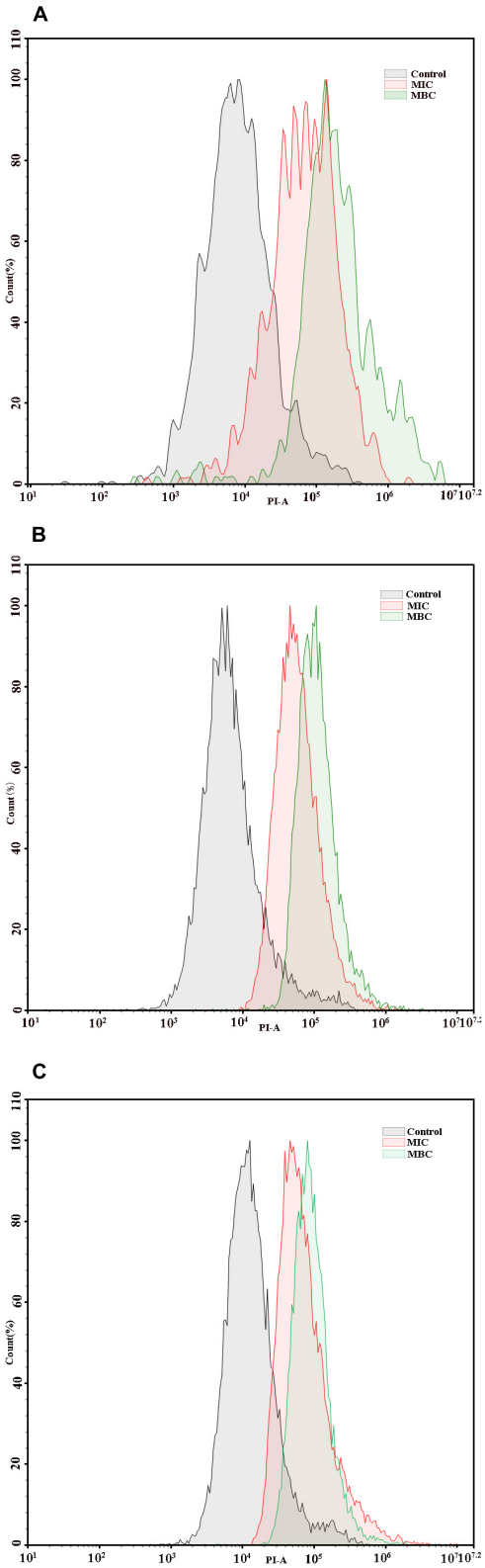

FIGURE 4 | Flow cytometric analysis. Data acquisition was set to 30 μl for each experiment. **(A)** *F. nucleatum*; **(B)** *P. gingivalis*; **(C)** *P. intermedia*. MIC, minimum inhibition concentration; MBC, minimum bactericide concentration.

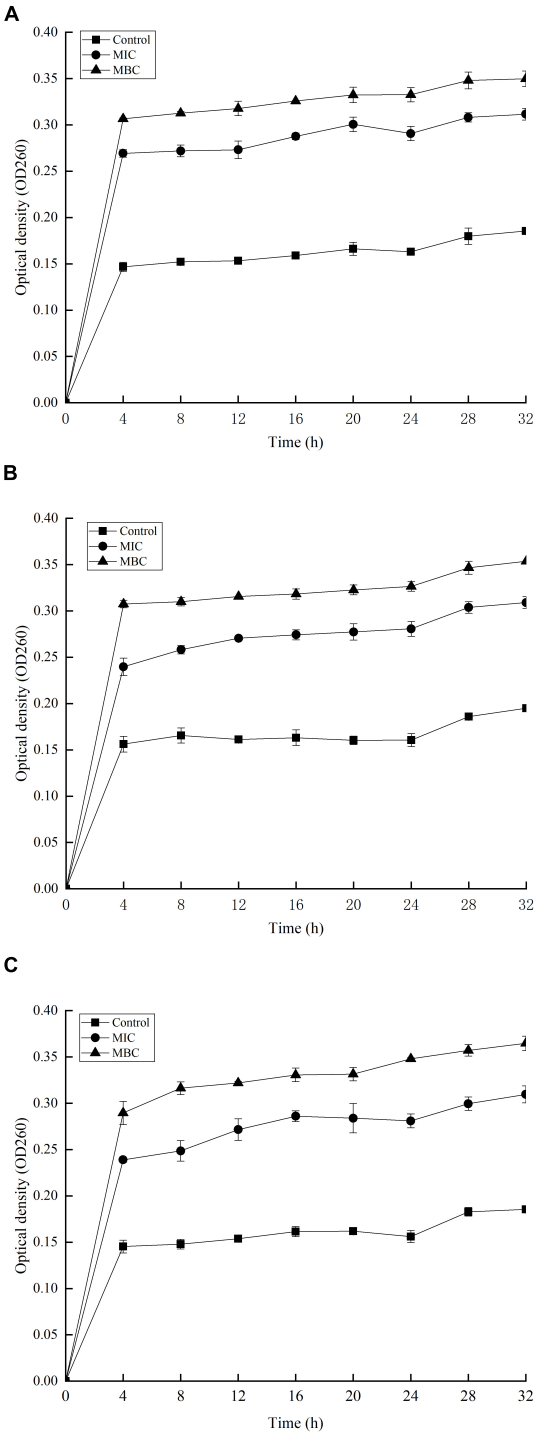

FIGURE 5 | Release of 260 nm absorbing material from **(A)** *F. nucleatum*; **(B)** *P. gingivalis*; and **(C)** *P. intermedia* treated with YAP for 32 h. MIC, minimum inhibition concentration; MBC, minimum bactericide concentration.

in the phenolic compounds and the types of alkyl substituents incorporated into the non-phenolic ring structure could also affect the antibacterial activity (Dorman and Deans, 2000). In

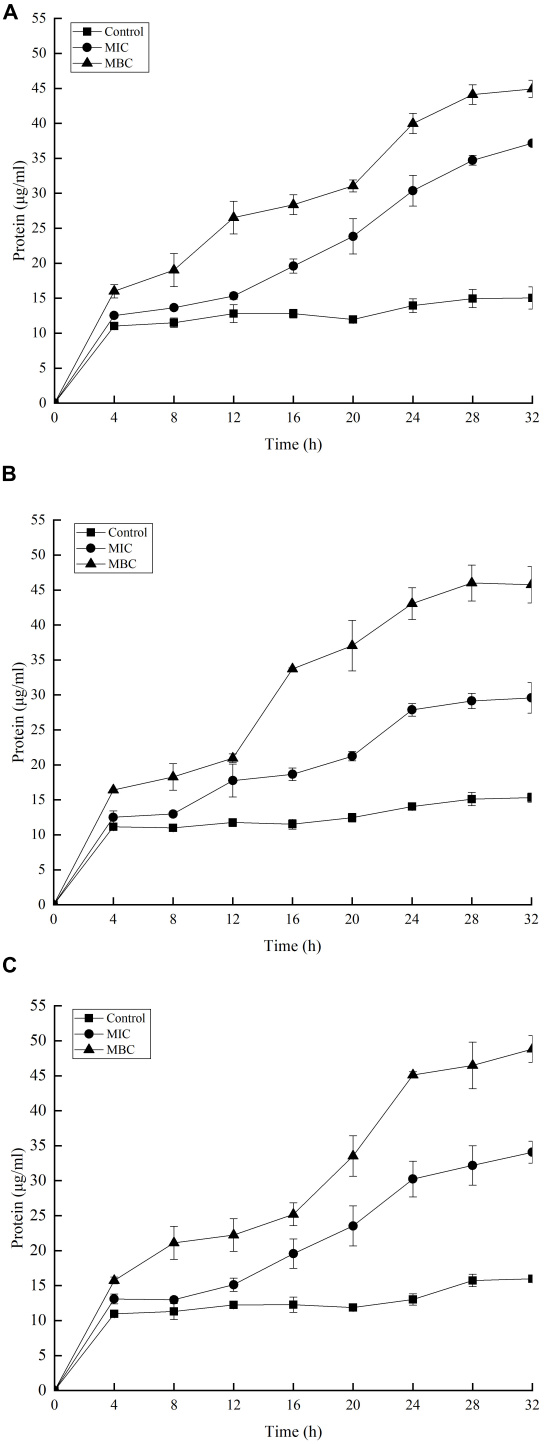

FIGURE 6 | Release of protein-absorbing material from **(A)** *F. nucleatum*; **(B)** *P. gingivalis*; and **(C)** *P. intermedia* treated with YAP for 32 h. MIC, minimum inhibition concentration; MBC, minimum bactericide concentration.

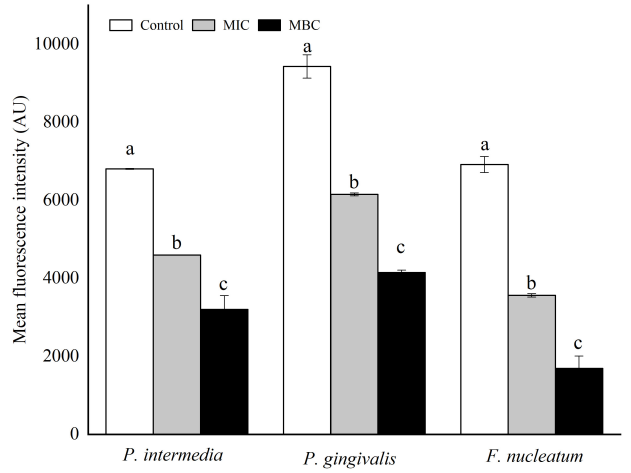

FIGURE 7 | Membrane potentials of *P. intermedia*, *P. gingivalis*, and *F. nucleatum* treated with different concentrations of YAP. MIC, minimum inhibition concentration; MBC, minimum bactericide concentration.

our study, the YAP showed a certain antibacterial activity, but the antibacterial activity was lower than other natural phenolic extracts, such as tea polyphenols and tart cherry phenolic extract (Lagha et al., 2017, 2021). In order to improve the antibacterial activity of YAP, the structure of YAP should be further studied and modified in the future.

Fusobacterium nucleatum, *P. gingivalis*, and *P. intermedius* have been strongly associated with periodontal lesions as well as halitosis (Awano et al., 2002; Tonetti et al., 2013). Morphological alterations could intuitively reflect the antibacterial effects of YAP against the halitosis-related bacteria. In the present study, we investigated the influence of different concentrations of YAP (control, MIC, and MBC) on morphological alterations in bacterial cells through SEM and TEM analyses. After YAP treatment, the SEM analyses observed that the membrane surface was coarse and wrinkles and pores occurred, which was consistent with other research about the extracted phenols of fruits, such as hawthorn and wild blueberry (Ben et al., 2015; Zhang et al., 2020). The TEM analyses observed that the cell walls and membranes were separated and eventually ruptured and the cell contents were leaked, which were irreversible. The morphological alterations of bacteria cells may be because the phenolic acid could change the hydrophobicity of the cell membrane, resulting in irreversible changes in intracellular components (Borges et al., 2013; Alshuniaber et al., 2020).

In prokaryotes, the cell membrane is not only related to the energy conversion but also related to nutrient processing, the synthesis of structural macromolecules, and the secretion of many enzymes required for life (Yuroff et al., 2003; Silhavy, 2016). Thus, the integrity of the cell membrane is essential for cell growth. The flow cytometer is used to determine the integrity of the cell membrane (Cao et al., 2009), and the release of large molecules including nucleic acids and proteins into the cell suspension could be further evaluated to determine whether the cell membrane integrity is damaged (Diao et al., 2014; Zhou et al., 2020). Our results indicated that the integrity of the cell membrane was destroyed and the leakage of proteins and nucleic acids into the cell suspension increased after YAP

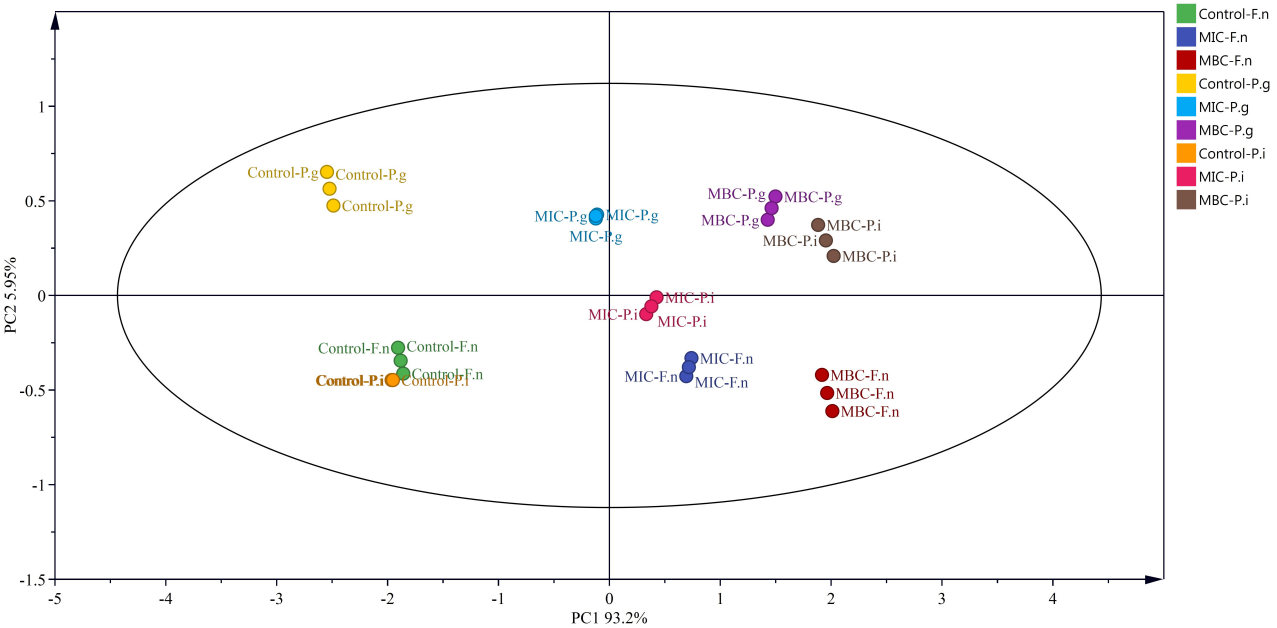

FIGURE 8 | Loadings of *P. intermedia*, *P. gingivalis*, and *F. nucleatum* treated with different concentrations of YAP on the first and second principal components. F.n, *F. nucleatum*; P.g, *P. gingivalis*; P.i, *P. intermedia*; MIC, minimum inhibition concentration; MBC, minimum bactericide concentration.

treatment. These phenomena provided evidence that the bacterial cell membranes are damaged, which agreed with the antibacterial activity of tea polyphenols (Yi et al., 2010). Lou et al. (2011) found that the negatively charged phenol compounds may be attached to the outer membrane of bacteria by the electrostatic interaction and destroy the outer membrane. Additionally, the study has shown that the electronegative phenol compounds could interfere with the biological process by the electron transfer and react with the nitrogen components such as nucleic acids and proteins (Dorman and Deans, 2000).

The MP is one of the most important parameters of bacterial cells. It is related to cellular antibiotic intake and bactericidal effect (Bajpai et al., 2013). A lot of information could be obtained by monitoring the MP of a cell. When the cell membrane is damaged, depolarization and hyperpolarization will be shown (Comas and Vives-Rego, 1997). Depolarization and hyperpolarization were mainly caused by the changing of the ion concentration in cells, which could damage the functions of the cell membrane (Eisenberg et al., 1982). Therefore, the MP could be used to determine whether the cell membrane of bacteria is damaged. In our study, the MP of bacteria-related halitosis significantly reduced after YAP treatment. These results suggested that YAP could effectively induce the depolarization of the bacterial cell membrane and damage the cell membrane, resulting in abnormal metabolism of bacterial cells. Studies found that the halitosis-related bacteria could be depolarized by quinoa saponins, which is consistent with our research results (Sun et al., 2019). Lou et al. (2011) reported that a large amount of K^+ was released to the cell suspension of *Shigella dysenteriae* and *Streptococcus pneumoniae* after chlorogenic acid treatment, which was due to the fact that chlorogenic acid changed the MP and damaged the cell membrane. However, the effect of YAP on the ions released from halitosis-related bacterial cells still needs to be further studied in the future.

The content of polyphenols of thinned young apples is about 10 times compared with ripe apples (Hiroshi et al., 2005). In our study, we explored the antibacterial effect and antibacterial mechanism of YAP on halitosis-related bacterial. The results indicated that YAP could inhibit *P. gingivalis*, *P. intermedius*, and *F. nucleatum* and alter the morphology of bacterial cells and the integrity of cell membranes. YAP had potential roles for curing oral odor induced by bacteria. However, the polyphenol was always attached with other large molecules such as protein and polysaccharide in food systems. Our future work should aim at investigating the influence of the protein, organic acid, and polysaccharide combined with the YAP, especially chlorogenic acid and phlorizin, on the antibacterial activity against halitosis-related bacteria and clarifying the antibacterial mechanism.

CONCLUSION

This study clearly showed that the phenolic extract from 'Fuji' has an inhibitory effect on halitosis-related bacteria, including *P. gingivalis*, *P. intermedius*, and *F. nucleatum*. The outer wall of the bacterial cells treated with YAP showed obvious wrinkles and holes, while in the internal microstructure, the cell wall and cell membrane were separated, blurred, and even disappeared. The release of proteins and nucleic acids into the cell suspension significantly increased with the increase in YAP concentration treatment. The MP of three bacterial cells treated with YAP significantly reduced. These results revealed that YAP could

destroy the integrity and permeability of the cell membrane, resulting in the cell death of bacteria related with halitosis. This research could open up new areas for the application of thinned young apples and provided new antibacterial agents for halitosis.

DATA AVAILABILITY STATEMENT

The original contributions presented in the study are included in the article/supplementary material, further inquiries can be directed to the corresponding authors.

AUTHOR CONTRIBUTIONS

TL: conceptualization, methodology, validation, formal analysis, investigation, data curation, writing—original draft, and visualization. HS: visualization and investigation. FW: methodology and software. XZ and PZ: methodology. YY: funding acquisition, supervision, resources, and writing—review and editing. YG: funding acquisition and resources. All authors contributed to the article and approved the submitted version.

FUNDING

This work was supported by the opening topic project by the Engineering Research Center of High Value Utilization of Western China Fruit Resources, the National Natural Science Foundation of China (No. 31701563), the Ministry of Education (XGZX2021G08), the Key Research and Development Program of Shaanxi province (No. 2019NY-124), and the Fundamental Research Funds for the Central Universities at Shaanxi Normal University (1301031057).

REFERENCES

Alshuniaber, M. A., Krishnamoorthy, R., and Alqhtani, W. H. (2020). Antimicrobial activity of polyphenolic compounds from Spirulina against food-borne bacterial pathogens. *Saudi. J. Biol. Sci.* 28, 459–464. doi: 10.1016/j.sjbs.2020.10.029

Armstrong, B. L., Sensat, M. L., and Stoltenberg, J. L. (2010). Halitosis: a review of current literature. *Int. J. Dent. Hyg.* 84, 65–74. doi: 10.4274/meandros.68077

Awano, S., Gohara, K., Kurihara, E., Ansai, T., and Takehara, T. (2002). The relationship between the presence of periodontopathogenic bacteria in saliva and halitosis. *Int. Dent. J.* 52, 212–216. doi: 10.1002/j.1875-595X.2002.tb00927.x

Bajpai, V. K., Sharma, A., and Baek, K. H. (2013). Antibacterial mode of action of Cudrania tricuspidata fruit essential oil, affecting membrane permeability and surface characteristics of food-borne pathogens. *Food Control* 32, 582–590. doi: 10.1016/j.foodcont.2013.01.032

Ben, L. A., Dudonné, S., Desjardins, Y., and Grenier, D. (2015). Wild Blueberry (Vaccinium angustifolium Ait.) Polyphenols Target *Fusobacterium nucleatum* and the Host Inflammatory Response: potential Innovative Molecules for Treating Periodontal Diseases. *J. Agric. Food. Chem.* 63, 6999–7008. doi: 10.1021/acs.jafc.5b01525

Borges, A., Ferreira, C., Saavedra, M. J., and Simes, M. (2013). Antibacterial Activity and Mode of Action of Ferulic and Gallic Acids Against Pathogenic Bacteria. *Larchmont. N.Y.* 19, 256–265. doi: 10.1089/mdr.2012.0244

Bradford, M. M. (1976). A rapid and sensitive method for the quantitation of microgram quantities of protein utilizing the principle of protein-dye binding. *Anal. Biochem.* 72, 248–254. doi: 10.1016/0003-2697(76)90527-90523

Cao, X. L., Wang, C., Pei, H. R., and Sun, B. G. (2009). Separation and identification of polyphenols in apple pomace by high-speed counter-current chromatography and high-performance liquid chromatography coupled with mass spectrometry. *J. Chromatogr A*. 1216, 4268–4274. doi: 10.1016/j.chroma.2009.01.046

Chen, L., Yang, X., Liu, R., Liu, L., Zhao, D., Liu, J., et al. (2017). Thinned young apple polysaccharide improves hepatic metabolic disorder in high-fat diet-induced obese mice by activating mitochondrial respiratory functions. *J. Funct. Foods* 33, 396–407. doi: 10.1016/j.jff.2017.03.055

Chen, L. Y., Cheng, C. W., and Liang, J. Y. (2015). Effect of esterification condensation on the folin-ciocalteu method for the quantitative measurement of total phenols. *Food Chem.* 170, 10–15. doi: 10.1016/j.foodchem.2014.08.038

Chen, W., Guo, Y., Zhang, J., Zhang, X., and Meng, Y. (2015). Effect of Different Drying Processes on the Physicochemical and Antioxidant Properties of Thinned Young Apple. *Int. J. Food. Eng.* 11, 207–219. doi: 10.1515/ijfe-2014-0211

Comas, J., and Vives-Rego, J. (1997). Assessement of the effects of gramicidin, formaldehyde, andsurfactants on *Escherichia coli* by flow cytometry using nucleic acid and membrane potential dyes. *Cytometry* 29, 58–64. doi: 10.1002/(sici)1097-0320(19970901)29:1<58::aid-cyto6<3.0.co;2-9

Cortelli, J. R., Silva, B. M. D., and Westphal, M. A. (2008). Halitosis: a review of associated factors and therapeutic approach. *Braz. Oral. Res.* 22, 44–54. doi: 10.1590/S1806-83242008000500007

Diao, W. R., Hu, Q. P., Zhang, H., and Xu, J. G. (2014). Chemical composition, antibacterial activity and mechanism of action of essential oil from seeds of fennel (Foeniculum vulgare mill.). *Food Control* 35, 109–116. doi: 10.1016/j.foodcont

Dorman, H. J., and Deans, S. G. (2000). Antimicrobial agents from plants: antibacterial activity of plant volatile oils. *J. Appl. Microbiol.* 88, 308–316. doi: 10.1046/j.1365-2672.2000.00969.x

Dou, J., Meng, Y., Liu, L., Li, J., Ren, D., and Guo, Y. (2015). Purification, characterization and antioxidant activities of polysaccharides from thinned-young apple. *Int. J. Biol. Macromol.* 72, 31–40. doi: 10.1016/j.ijbiomac.2014.07.053

Eisenberg, E. S., Mandel, L. J., Kaback, H. R., and Miller, M. H. (1982). Membrane potential and gentamicin uptake in *Staphylococcus aureus*. *P. Natl. Acad. Sci. U.S.A.* 79, 6693–6697. doi: 10.1073/pnas.79.21.6693

Gong, T., Yang, X., Bai, F. T., Li, D., Zhao, P. T., Sun, L. J., et al. (2020). Young apple polyphenols as natural α-glucosidase inhibitors: in vitro and in silico studies. *Bioorg. Chem.* 96:103625. doi: 10.1016/j.bioorg.2020.103625

Hamilton, J., Brustovetsky, T., and Brustovetsky, N. (2021). The effect of mitochondrial calcium uniporter and cyclophilin D knockout on resistance of brain mitochondria to Ca^{2+} -induced damage. *J. Biol. Chem.* 296:100669. doi: 10.1016/j.jbc.2021.100669

Hiroshi, A., Yuji, S., Takahiro, W., Megumi, H. N., Yasuo, Y., Toshihiko, S., et al. (2005). Dietary unripe apple polyphenol inhibits the development of food allergies in murine models. *Febs. Lett.* 579, 4485–4491. doi: 10.1016/j.febslet.2005.07.019

Hou, Y., Gong, T., Zhang, J., Yang, X., and Guo, Y. (2019). Structural characterization and emulsifying properties of thinned-young apples polysaccharides. *Biochem. Bioph. Res. Co.* 516, 1175–1182. doi: 10.1016/j.bbrc.2019.07.019

Joda, J., and Olukoju, O. (2013). Halitosis amongst students in tertiary institutions in lagos state. *Afr. Health. Sci.* 12, 473–478. doi: 10.4314/ahs.v12i4.12

Lagha, A. B., Haas, B., and Grenier, D. (2017). Tea polyphenols inhibit the growth and virulence properties of *Fusobacterium nucleatum*. *Sci. Rep.* 7:44815. doi: 10.1038/srep44815

Lagha, A. B., Lebel, G., and Grenier, D. (2020). Tart cherry (Prunus cerasus L.) fractions inhibit biofilm formation and adherence properties of oral pathogens and enhance oral epithelial barrier function. *Phytother. Res.* 34, 886–895. doi: 10.1002/ptr.6574

Lagha, A. B., Pellerin, G., Vaillancourt, K., and Grenier, D. (2021). Effects of a tart cherry (Prunus cerasus L.) phenolic extract on *Porphyromonas gingivalis*

and its ability to impair the oral epithelial barrier. *PLoS One* 16:e0246194. doi: 10.1371/journal.pone.0246194

Lau, P., Meethal, C., Middleton, M., Clark, M., and Darby, I. (2019). 'Say Ahhh': what do dentists, general medical practitioners and community pharmacists do about halitosis? *Int. Dent. J.* 69, 311–320. doi: 10.1111/idj.12458

Li, G., Qiao, M., Guo, Y., Wang, X., and Xia, X. (2014). Effect of subinhibitory concentrations of chlorogenic acid on reducing the virulence factor production by *Staphylococcus aureus*. *Foodborne Pathog. Dis.* 11, 677–683. doi: 10.1089/fpd.2013.1731

Li, M., Guo, J., Xu, C., Lei, Y., and Li, J. (2018). Identifying climatic factors and circulation indices related to apple yield variation in main production areas of china. *Glob. Ecol. Conserv*. 16:e00478. doi: 10.1016/j.gecco.2018.e00478

Lou, Z., Wang, H., Song, Z., Ma, C., and Wang, Z. (2011). Antibacterial Activity and Mechanism of Action of Chlorogenic Acid. *J. Food Sci.* 76, M398–M403. doi: 10.1111/j.1750-3841.2011.02213.x

Miller, N. J., and Rice-Evans, C. A. (1997). The relative contributions of ascorbic acid and phenolic antioxidants to the total antioxidant activity of orange and apple fruit juices and blackcurrant drink. *Food Chem*. 60, 331–337. doi: 10.1016/S0308-8146(96)00339-1

Nicolas, J. J., Richard-Forget, F. C., Goupy, P. M., Amiot, M. J., and Aubert, S. Y. (1994). Enzymatic browning reactions in apple and apple products. *Crit. Rev. Food Sci*. 34, 109–157. doi: 10.1080/10408399409527653

Nijole, S., Aiste, J., Lina, R., Asmaa, A., Andrea, C., Lia, R., et al. (2018). Efficacy of proanthocyanidins from pelargonium sidoides root extract in reducing *p. gingivalis* viability while preserving oral commensal *s. salivarius*. *Materials* 11:1499. doi: 10.3390/ma11091499

Nisar, T., Wang, Z. C., Alim, A., Iqbal, M., Yang, X., Sun, L. J., et al. (2019). Citrus pectin films enriched with thinned young apple polyphenols for potential use as bio-based active packaging. *CyTA J. Food* 17, 695–705. doi: 10.1080/19476337.2019.1640798

Peruzzo, D. C., Jandiroba, P. F. C. B., and Filho, G. D. R. N. (2007). Use of 0.1% chlorine dioxide to inhibit the formation of morning volatile sulphur compounds (VSC). *Braz. Oral. Res.* 21, 70–74. doi: 10.1590/S1806-83242007000100012

Pu, D., Duan, W., Huang, Y., Zhang, Y., Sun, B., Ren, F., et al. (2020). Characterization of the key odorants contributing to retronasal olfaction during bread consumption. *Food Chem*. 318:126520. doi: 10.1016/j.foodchem.2020.126520

Sanz, M., Roldán, S., and Herrera, D. (2001). Fundamentals of breath malodour. *J. Contemp. Dent. Pract*. 2, 1–17. doi: 10.5005/jcdp-2-4-22

Silhavy, T. J. (2016). Classic Spotlight: gram-Negative Bacteria Have Two Membranes. *J. Bacteriol.* 198:201. doi: 10.1128/JB.00599-15

Sun, X. Y., Yang, X. S., Xue, P., Zhang, Z. G., and Ren, G. X. (2019). Improved antibacterial effects of alkali-transformed saponin from quinoa husks against halitosis-related bacteria. *BMC. Complem. Altern. M*. 19:46. doi: 10.1186/s12906-019-2455-2

Takahashl, N., Saito, K., Schachtele, C. F., and Yamada, T. (2010). Acid tolerance and acid—neutralizing activity of *Porphyromonas gingivalis*, *Prevotella intermedia* and *Fusobacterium nucleatum*. *Mol. Oral. Microbiol.* 12, 323–328. doi: 10.1111/j.1399-302X.1997.tb00733.x

Tonetti, M. S., Van Dyke T. E; Working group 1 of the joint EFP/AAP workshop (2013). Periodontitis and atherosclerotic cardiovascular disease: consensus report of the Joint EFP/AAP Workshop on Periodontitis and Systemic Diseases. *J. Clin. Periodontol.* 40, S24–S29. doi: 10.1111/jcpe.12089

Wang, J. Y., Zhang, W. J., Tang, C. E., Xiao, J., Xie, B. J., and Sun, Z. D. (2018). Synergistic effect of B-type oligomeric procyanidins from lotus seedpod in combination with water-soluble Poria cocos polysaccharides against *E. coli* and mechanism. *J. Funct. Foods* 48, 134–143. doi: 10.1016/j.jff.2018.07.015

Wang, L., Yang, X., Yu, X., Yao, Y., and Ren, G. (2013). Evaluation of antibacterial and anti-inflammatory activities of less polar ginsenosides produced from polar ginsenosides by heat-transformation. *J. Agr. Food Chem.* 61, 12274–12282. doi: 10.1021/jf404461q

Wang, L., Yang, X. Z., and Hu, D. Y. (2002). Anti-halitosis effect of radix scutellariae and tea polyphenol. *Int. Dent. J.* 52, 212–216. doi: 10.1016/S1005-8885(07)60038-7

Wang, X., Wang, J., Wei, L., Hu, C. Y., and Meng, Y. H. (2019). Apple phlorizin oxidation product 2 inhibits proliferation and differentiation of 3t3-l1 preadipocytes. *J. Funct. Food*. 62:103525. doi: 10.1016/j.jff.2019.103525

Yi, S. M., Zhu, J. L., Fu, L. L., and Li, J. R. (2010). Tea polyphenols inhibit *Pseudomonas aeruginosa* through damage to the cell membrane. *Int. J. Food Microbiol.* 144, 111–117. doi: 10.1016/j.ijfoodmicro

Yuan, L., Lijun, S., Chen, W. Q., Meng, Y. H., and Guo, Y. R. (2016). ctions between polyphenols in thinned young apples and porcine pancreatic alpha-amylase: inhibition, detailed kinetics and fluorescence quenching. *Food Chem*. 208, 51–60. doi: 10.1016/j.foodchem.2016.03.093

Yuroff, A. S., Sabat, G., and Hickey, W. J. (2003). Transporter-Mediated Uptake of 2-Chloro- and 2-Hydroxybenzoate by *Pseudomonas* huttiensis Strain D1. *Appl. Environ. Microb.* 69, 7401–7408. doi: 10.1128/AEM

Zhang, J., Chen, W., Shuai, L., Xue, Z., and Guo, Y. (2017). Antibacterial activity and preservative properties of thinned young apples extracts for fish flesh. *J. Food Process Pres.* 42:e13435. doi: 10.1111/jfpp.13435

Zhang, L. L., Zhang, L. F., and Xu, J. G. (2020). Chemical composition, antibacterial activity and action mechanism of different extracts from hawthorn (Crataegus pinnatifida Bge.). *Sci. Rep. U.K.* 10:8876. doi: 10.1038/s41598-020-65802-7

Zhang, T., Wei, X., Miao, Z., Hassan, H., Song, Y., and Fan, M. (2016). Screening for antioxidant and antibacterial activities of phenolics from Golden Delicious apple pomace. *Chem. Cent. J.* 10:47. doi: 10.1186/s13065-016-0195-7

Zhou, Y., Yao, Q., Zhang, T., Chen, X., and Cheng, Y. (2020). Antibacterial activity and mechanism of green tea polysaccharide conjugates against *Escherichia coli*. *Ind. Crop Prod.* 152:112464. doi: 10.1016/j.indcrop.2020.112464

Conflict of Interest: The authors declare that the research was conducted in the absence of any commercial or financial relationships that could be construed as a potential conflict of interest.

Publisher's Note: All claims expressed in this article are solely those of the authors and do not necessarily represent those of their affiliated organizations, or those of the publisher, the editors and the reviewers. Any product that may be evaluated in this article, or claim that may be made by its manufacturer, is not guaranteed or endorsed by the publisher.

frontiers in Microbiology

ORIGINAL RESEARCH
published: 25 February 2022
doi: 10.3389/fmicb.2021.819993

Lycium barbarum Polysaccharides as Antibiotic Substitutes Improve Growth Performance, Serum Immunity, Antioxidant Status, and Intestinal Health for Weaned Piglets

Yexin Yin[1], Fang Wang[1], Mei Yang[1], Bie Tan[1], Yulong Yin[1,2], Jiashun Chen[1,2] and Zhe Yang[1]**

[1] *Animal Nutritional Genome and Germplasm Innovation Research Center, College of Animal Science and Technology, Hunan Agricultural University, Changsha, China,* [2] *Key Laboratory of Agro-ecological Processes in Subtropical Region, Scientific Observing and Experimental Station of Animal Nutrition and Feed Science in South-Central, Ministry of Agriculture, Hunan Provincial Engineering Research Center of Healthy Livestock, Institute of Subtropical Agriculture, Chinese Academy of Sciences, Changsha, China*

OPEN ACCESS

Edited by:
Wang Jiajun,
Northeast Agricultural University, China

Reviewed by:
Tarique Hussain,
Nuclear Institute for Agriculture and Biology, Pakistan
Dandan Han,
China Agricultural University, China
Yaoyao Xia,
South China Agricultural University, China

***Correspondence:**
Zhe Yang
zheyang@hunau.edu.cn
Jiashun Chen
jschen@hunau.edu.cn

Specialty section:
This article was submitted to Antimicrobials, Resistance and Chemotherapy, a section of the journal Frontiers in Microbiology

Received: *22 November 2021*
Accepted: *30 December 2021*
Published: *25 February 2022*

Citation:
Yin Y, Wang F, Yang M, Tan B, Yin Y, Chen J and Yang Z (2022) Lycium barbarum Polysaccharides as Antibiotic Substitutes Improve Growth Performance, Serum Immunity, Antioxidant Status, and Intestinal Health for Weaned Piglets. Front. Microbiol. 12:819993. doi: 10.3389/fmicb.2021.819993

The aim of the present study is to investigate the effects of dietary *Lycium barbarum* polysaccharides (LBPs) supplementation on the growth performance, immune response, serum antioxidant status, and intestinal health of weaned piglets. In total, 24 crossed healthy weaned piglets [Duroc × (Yorkshire × Landrace)], of similar body weight (7.47 ± 0.22 kg), were randomly allocated to three treatment groups: CON (basal diet); LBPs (basal diet plus 4,000 mg/kg LBPs); and antibiotic (ABO, basal diet plus 20 mg/kg flavomycin and 50 mg/kg quinocetone). There were eight pigs per group. The study lasted 28 days. When compared with CON, LBPs or ABO dietary supplementation increased average daily gain ($P < 0.05$), decreased the ratio of feed to gain and the diarrhea ratio ($P < 0.05$). Similarly, when compared with CON, LBPs dietary supplementation increased serum immunoglobulin G, immunoglobulin M, interleukin-10, interleukin-2, and tumor necrosis factor-α levels ($P < 0.05$). Dietary LBPs enhanced the activity of serum total antioxidant capacity and glutathione peroxidase, and decreased malondialdehyde levels ($P < 0.05$). Principal component analysis showed a distinct separation between CON and LBPs groups, but no differences between ABO and LBPs groups. LBPs addition increased *Lactobacillus* and *Faecalibacterium* ($P < 0.05$) levels, while it decreased *Enterococcaceae* and *Enterobacteriaceae* ($P < 0.05$) levels. Furthermore, when compared with the CON group, LBPs increased villus height ($P < 0.05$) and the villus height to crypt depth ratio in the duodenum and jejunum ($P < 0.05$). Thus, dietary supplementation with LBPs improved growth performance, antioxidant capacity and immunity, regulated intestinal microbial composition, and may be used as an efficient antibiotic alternative in weaned piglet feed.

Keywords: antioxidant, growth performance, immune, intestinal health, *Lycium barbarum* polysaccharides, weaned piglets

INTRODUCTION

Early weaning increases intestinal permeability and reduces antioxidant capacity and immunity, which reduces feed intake, and increases diarrhea incidence, morbidity, and mortality (Hu et al., 2013; Yin et al., 2014). Diarrhea after weaning is mainly associated with gut microbiome disturbances which may lead to fever and slow growth (Campbell et al., 2013). Antibiotics are widely used in animal feeds to regulate intestinal microorganisms, prevent infection, and improve growth performance (Cook, 2004; Wang W. et al., 2018). However, antibiotics over-dependence has facilitated the emergence of antimicrobial resistance and antimicrobial residues, which affect human health (Li, 2017). In the European Union, antibiotics in feed additives were banned in 2006, whereas, in China, their use ceased in July 2020, therefore, a healthy and pollution-free alternative to antibiotics is required.

Many plant extracts can be used as alternatives to antibiotics (Lu et al., 2010; Pourhossein et al., 2015). *Lycium barbarum*, as a food and medicine, has been used in Asian countries for thousands of years to induce various health benefits (Donno et al., 2015; Zhao J. et al., 2016). *L. barbarum* polysaccharides (LBPs) are major bioactive components of *L. barbarum* and possess distinct bioactivities, including anti-oxidant (Wang et al., 2020; Zhang et al., 2021), anti-tumor (Gong et al., 2020), anti-diabetic (Shimato et al., 2020), immunomodulatory (Feng et al., 2020; Kim et al., 2020), liver protective (Jia et al., 2016), neuroprotective (Zhao Z. et al., 2016), renal protective (Wu et al., 2020), and improved eyesight activities (Zhu et al., 2016). Liu et al. (2021a) demonstrated that variations in the molecular weight of LBPs exerted antioxidant effects on different free radical. Yang et al. (2013) indicated that LBPs treatment may protect intestinal damage by inhibiting oxidative stress and inflammation in rats. Long et al. (2020) reported that dietary supplementation of LBPs could improve the growth performance, immune function, antioxidant capacity, and digestive enzyme activities in broilers. Our previous studies demonstrated that 4,000 mg/kg LBPs dietary supplementation enhanced growth performance, immune status and antioxidant capacity, and improved intestinal microbial populations in weaned piglets (Chen et al., 2020). Based on these favorable effects, we hypothesized that dietary LBPs supplementation could effectively replace antibiotics by improving performance, gastrointestinal tract health, and function in weaned piglets. Therefore, the objective of the current study was to investigate the effects of a 4,000 mg/kg LBPs supplementation on growth performance, diarrhea incidence, serum immunity and antioxidant capacity, intestinal morphology, short-chain fatty acids (SCFAs) levels, and cecum intestinal microflora in weaned pigs.

MATERIALS AND METHODS

Experiments were conducted in accordance with Chinese guidelines for animal welfare and experimental protocols. All animal procedures were approved by the Committee of Animal Care at Hunan Agricultural University (Changsha, China) (permit number: CACAHU 2020-00156).

Experimental Design

We included 24 crossed healthy weaned piglets [Duroc × (Yorkshire × Landrace)] of similar body weight (BW = 7.47 ± 0.22 kg). Animals were randomly allocated to three treatment groups: CON (basal diet); LBPs (basal diet plus 4,000 mg/kg LBPs); and antibiotic (ABO, basal diet plus 20 mg/kg flavomycin & 50 mg/kg quinocetone). There were eight pigs per group. The basal diet was formulated to satisfy or outstrip National Research Council (National Research Council, 2012) nutrient requirements. Basal diet nutrient levels and ingredients are shown (**Table 1**).

All pigs were housed in a room with slatted floors. They were fed in individual metabolism cages with a side feeder and a stainless-steel nipple which provided full access to feed and water, respectively. The scale of feeding and feed surplus for each piglet was recorded throughout the study. At study beginning and end, body weights were measured; these data were used to calculate the average daily gain (ADG), average daily feed intake (ADFI),

TABLE 1 | Ingredients and chemical composition of experimental diets (as-fed basis).

Items	Content (%)
Ingredients	
Corn	55.00
Soybean meal	19.00
Full-fat soybean powder	10.00
Fish meal	5.00
Whey powder	6.15
Soybean oil	1.50
Dicalcium phosphate	0.90
L-Lysine-HCl	0.48
L-Threonine	0.05
DL-Methionine	0.10
L-Tryptophan	0.02
Salt	0.30
Limestone	0.50
Premix[a]	1.00
Total	100.00
Calculated nutrients	
Digestible energy (MJ/kg)	14.64
Crude protein	20.15
Lysine	1.38
Methionine	0.82
Methionine + cysteine	1.01
Threonine	0.97
Tryptophan	0.25
Calcium	0.80
Total phosphorus	0.73

[a]*The premix provided the following (per kilogram of compound feed): Vitamin A, 12,000 IU; Vitamin D, 2,500 IU; Vitamin E, 30 IU; Vitamin B12, 12 μg; Vitamin K, 3 mg; d-pantothenic acid, 15 mg; nicotinic acid, 40 mg; choline chloride, 400 mg; Mn, 40 mg; Zn, 100 mg; Fe, 90 mg; Cu, 8.8 mg; I, 0.35 mg; Se, 0.3 mg.*

and ratio of feed to gain (F/G). The study lasted for 28 days and diarrhea ratio was monitored daily. Diarrhea ratio (%) was calculated as the number of pigs with diarrhea × the number of days with diarrhea/(the total number of pigs × the number of study days) (Hung et al., 2019).

Sample Collection and Preparation

On the 27th day, blood was collected by anterior vena cava puncture before morning feeding. Blood was centrifuged at 3,000 × *g* for 15 min at 4°C to isolate serum which was stored at −80°C. All piglets were humanely killed by injection of pentobarbital sodium at study end and the gut, liver, and kidney immediately removed from the abdominal cavity. The intestinal segment and mucosa from the duodenum, jejunum, and ileum were collected and stored at −80°C. An intestinal segment (comprising duodenum, jejunum, and ileum) was fixed in 4% paraformaldehyde-phosphate buffered saline buffer to analyze intestinal morphological structures. Chyme from the ileum, cecum, and colon was collected and stored at −80°C.

Immune Responses

Serum immunoglobulins (Ig)A, IgM; IgG, the interleukins, (IL)-2, IL-6, IL-10, IL-1α, and IL-1β; and tumor necrosis factor-α (TNF-α) were measured by using pig-specific ELISA kits (Cusabio Biotechnology Co., Ltd., Wuhan, China).

Antioxidant Capacity

The activity levels of total antioxidant capacity (T-AOC), superoxide dismutase (SOD), glutathione peroxidase (GSH-Px), and malondialdehyde (MDA) in serum were determined using respective reagent kits (Nanjing Jiancheng Bioengineering Institute, Nanjing, China).

Intestinal Morphology

Sections of the duodenum, jejunum, and ileum in each pig were harvested and immediately fixed in 10% formalin, dehydrated in 50% ethanol, embedded paraffin, and sectioned 5 μm for hematoxylin and eosin staining. The sections were scanned using an optical binocular microscope connected to a digital camera (Nikon ECLIPSE 80i). Villus length, crypt depth, and the villus length vs. crypt depth (V/C) ratios were measured from 10 well-oriented villi × 3 sections of each pigs.

Gut Microbiota Analysis

According to the manufacturer's instructions, total genomic DNA was extracted from the chyme of cecum samples using the QIAamp Fast DNA stool mini kit (Qiagen, Hilden, Germany). DNA was checked on 1% agarose gels and concentration and purity were determined using a NanoDrop 2000 UV–vis spectrophotometer (Thermo Fisher Scientific, Wilmington, United States). The V3–V4 hypervariable region of the bacterial 16S rRNA gene was amplified using the following primers; 338 F (5′- ACTCCTACGGGAGGCAGCAG-3′) and 806 R (5′-GGACTACHVGGGTWTCTAAT-3′) on an ABI GeneAmp® 9700 PCR thermocycler (ABI, CA, United States) (Xu et al., 2016). The PCR amplification system and conditions have been previously described (Yang J. et al., 2020). PCR products were extracted from 2% agarose gel and purified using the AxyPrep DNA gel extraction kit (Axygen Biosciences, Union City, CA, United States) according to manufacturer's instructions and quantified using a Quantus™ Fluorometer (Promega, United States).

Purified amplicons were pooled in equimolar quantities and paired-end sequenced on an Illumina MiSeq PE300 platform/NovaSeq PE250 platform (Illumina, San Diego, CA, United States) according to standard protocols of Majorbio Bio-Pharm Technology Co., Ltd. (Shanghai, China). Raw reads were deposited into the National Center for Biotechnology Information Sequence Read Archive database (Accession Number: SRP342805).

Raw 16S rRNA gene sequencing reads were demultiplexed, quality-filtered by fastp version 0.20.0 (Chen et al., 2018), and merged by FLASH version 1.2.7 (Magoc and Salzberg, 2011) using the following criteria: (1) the 300 base pair (bp) reads were truncated at any site receiving an average quality score < 20 over a 50 bp sliding window. Truncated reads < 50 bp and reads containing ambiguous characters were also discarded; (2) only overlapping sequences longer than 10 bp were assembled according to their overlapped sequences. The maximum mismatch ratio of the overlap region was 0.2. Reads that could not be assembled were discarded; and (3) samples were distinguished according to the barcode and primers, and the sequence direction was adjusted, exact barcode matching, 2 nucleotide mismatch in primer matching.

Species diversity was evaluated using ACE and Chao richness estimators and Shannon and Simpson diversity indices (Lemieux-labonte et al., 2017). Operational taxonomic units (OTUs), with 97% similarity cutoff (Stackebrandt and Goebel, 1994; Edgar, 2013), were clustered using UPARSE version 7.1 (Edgar, 2013), with chimeric sequences identified and removed. Beta diversity was evaluated using Principal Component Analysis (PCA). Significant differences between samples were evaluated by analysis of similarities (ANOSIM).

Determination of Intestinal Short-Chain Fatty Acid Levels

We performed gas chromatography (GC) to determine the main SCFAs in intestinal chyme, as described previously (Franklin et al., 2002). Briefly, to isolate supernatants, digesta samples were weighed, vortexed in distilled water, and centrifuged at 12,000 × *g* for 15 min at 4°C. Supernatants were mixed with 25% metaphosphoric acid at a 9:1 volume ratio, statically reacted for 3–4 h, centrifuged, and filtered. A GC system (GC2014, Shimadzu Corporation, Kyoto, Japan) was used to measure filtered fluids.

Statistical Analysis

Experimental data were analyzed by one-way ANOVA using the General Linear Model procedure of the SPSS software v. 20.0 (SPSS Inc., Chicago, IL, United States). Differences between treatment means were tested using Tukey's multiple comparison test. Microbe abundance, with significant differences between groups, was assessed by the Kruskal–Wallis test. Results were

presented as the mean ± standard error of the mean. $P < 0.05$ was considered statistically significant.

RESULTS

Growth Performance and Diarrhea Incidence

As shown in **Table 2**, when compared with the CON group, both LBPs and ABO dietary supplementation significantly increased ADG ($P < 0.05$) and decreased the F/G ($P < 0.05$). However, neither dietary LBPs or ABO supplementation had significant effects on initial weight, final weight, or ADFI in weaned piglets ($P > 0.05$).

As shown (**Figure 1**), when compared with the CON group, both LBPs and ABO dietary supplementation decreased diarrhea ratios in weaned piglets ($P < 0.05$), but no significant differences were observed between the LBPs and ABO groups ($P > 0.05$).

Serum Immune Indices

As shown in **Table 3**, weaned piglets in the LBPs and ABO groups displayed higher IgG and IgM levels than the CON group ($P < 0.05$), but no significant differences were observed for IgA levels among the groups ($P > 0.05$). When compared with the CON group, LBPs dietary supplementation significantly increased serum IL-10, IL-2, and TNF-α ($P < 0.05$) levels, but no significant IL-6, IL-1α, and IL-1β differences were observed between the groups ($P > 0.05$) (**Table 4**).

Antioxidant Capacity

Table 5 presents the differences in serum antioxidant indicators between the treatment groups. Dietary LBPs effectively enhanced serum T-AOC and GSH-Px activities but decreased MDA levels ($P < 0.05$). No significant differences in SOD activities were observed between the groups ($P > 0.05$).

Intestinal Morphology

The effects of LBPs dietary supplementation on intestinal morphology in piglets at day 28 are shown in **Table 6**. When compared with the CON group, LBPs increased villus height in the duodenum and ileum ($P < 0.05$). A distinct decrease in crypt depth in the duodenum of piglets fed ABO was observed when compared with the CON group ($P < 0.05$). In addition, both LBPs and ABO dietary supplementation increased the V/C in the duodenum and jejunum when compared with the CON group ($P < 0.05$).

TABLE 2 | Effects of dietary LBPs supplementation on growth performance of weaned piglets.

Items[1]	Treatments[2]			SEM[3]	*P*-value
	CON	ABO	LBPs		
Initial weight, kg	7.47	7.48	7.47	0.204	1.000
Final weight, kg	16.5	17.3	17.6	0.297	0.317
ADG, g	323[b]	351[a]	362[a]	4.38	0.004
ADFI, g	563	584	572	7.28	0.492
F/G	1.75[a]	1.66[b]	1.58[b]	0.006	<0.001

[1]ADFI, average daily feed intake; ADG, average daily gain; F/G, Feed/gain.
[2]Treatments consisted of (1) CON; basal diet, (2) LBPs; basal diet + 4,000 mg/kg LBPs and (3) ABO; basal diet + 20 mg/kg flavomycin + 50 mg/kg quinocetone.
[3]SEM, pooled standard error of mean (n = 8).
[a,b]Means within each row with different superscripts differ significantly (P < 0.05).

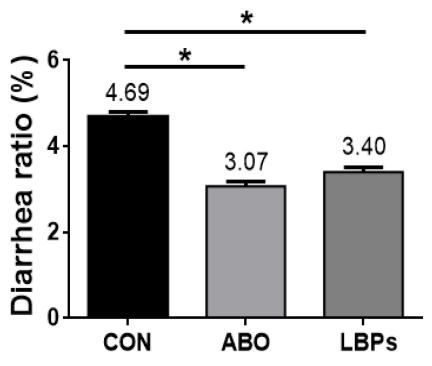

FIGURE 1 | Diarrhea rate of weaned piglets fed MB dietary treatments (%) ($n = 8$). CON, basal diet; LBPs, basal diet + 4,000 mg/kg LBPs; ABO, basal diet + 20 mg/kg flavomycin + 50 mg/kg quinocetone. Asterisks express statistical differences between different groups: *$P < 0.05$.

TABLE 3 | Effects of dietary LBPs supplementation on immune response in serum of weaned piglets.

Items[1]	Treatments[2]			SEM[3]	*P*-value
	CON	ABO	LBPs		
IgA, g/L	2.73	2.88	2.68	0.056	0.386
IgG, g/L	8.98[b]	11.2[a]	10.6[a]	0.302	0.018
IgM, g/L	0.09[b]	0.12[a]	0.11[a]	0.003	0.013

[1]IgA, Immunoglobulin A; IgG, Immunoglobulin G; IgM,: Immunoglobulin M.
[2]Treatments consisted of (1) CON; basal diet, (2) LBPs; basal diet + 4,000 mg/kg LBPs and (3) ABO; basal diet + 20 mg/kg flavomycin + 50 mg/kg quinocetone.
[3]SEM, pooled standard error of mean (n = 8).
[a,b]Means within each row with different superscripts differ significantly (P < 0.05).

TABLE 4 | Effects of dietary LBPs supplementation on immunologic factors levels in serum of weaned piglets.

Items[1]	Treatments[2]			SEM[3]	*P*-value
	CON	ABO	LBPs		
IL-2, pg/ml	90.9[b]	98.4[b]	112[a]	2.53	0.010
IL-6, pg/ml	6.36	5.15	5.39	0.274	0.187
IL-10, pg/ml	11.7[b]	13.8[a]	13.5[a]	0.317	0.036
IL-1α, pg/ml	255	263	256	6.57	0.857
IL-1β, pg/ml	24.5	23.4	21.8	0.953	0.512
TNF-α, pg/ml	0.29[b]	0.30[b]	0.35[a]	0.006	0.004

[1]IL, Interleukin; TNF-α, Tumor necrosis factor-α.
[2]Treatments consisted of (1) CON; basal diet, (2) LBPs; basal diet + 4,000 mg/kg LBPs and (3) ABO; basal diet + 20 mg/kg flavomycin + 50 mg/kg quinocetone.
[3]SEM, pooled standard error of mean (n = 8).
[a,b]Means within each row with different superscripts differ significantly (P < 0.05).

TABLE 5 | Effects of dietary LBPs supplementation on serum antioxidant activity of weaned piglets.

Items[1]	Treatments[2]			SEM[3]	*P*-value
	CON	ABO	LBPs		
T-AOC, U/mL	2.91[b]	3.31[a]	3.24[a]	0.045	0.004
GSH-Px, U/mL	319[b]	347[a]	338[a]	2.49	0.001
SOD, U/mL	189	184	197	3.81	0.403
MDA, nmol/mL	7.08[a]	4.81[b]	5.41[b]	0.224	0.001

[1] *T-AOC, Total antioxidant capacity; GSH-Px, Glutathione peroxidase; SOD, Superoxide dismutase; MDA, Malondialdehyde.*
[2] *Treatments consisted of (1) CON; basal diet, (2) LBPs; basal diet + 4,000 mg/kg LBPs and (3) ABO; basal diet + 20 mg/kg flavomycin + 50 mg/kg quinocetone.*
[3] *SEM, pooled standard error of mean (n = 8).*
[a,b] *Means within each row with different superscripts differ significantly (P < 0.05).*

TABLE 6 | Effects of dietary LBPs supplementation on intestinal morphology of weaned piglets.

Items[1]	Treatments[2]			SEM[3]	*P*-value
	CON	ABO	LBPs		
Villus height, μm					
Duodenum	289[b]	336[a]	362[a]	6.649	0.001
Jejunum	286	304	327	8.925	0.198
Ileum	234[b]	242[b]	289[a]	7.768	0.017
Crypt depth, μm					
Duodenum	268[a]	224[b]	264[a]	5.448	0.005
Jejunum	207	169	177	7.714	0.138
Ileum	149	150	142	5.361	0.807
V/C, μm: μm					
Duodenum	1.08[b]	1.52[a]	1.38[a]	0.034	<0.001
Jejunum	1.41[b]	1.83[a]	1.92[a]	0069	0.014
Ileum	1.60	2.08	1.69	0.086	0.076

[1] *V/C, the Villus height to Crypt depth rate.*
[2] *Treatments consisted of (1) Control; basal diet, (2) LBPs; basal diet + 4,000 mg/kg LBPs and (3) ABO; basal diet + 20 mg/kg flavomycin + 50 mg/kg quinones.*
[3] *SEM, pooled standard error of mean (n = 8).*
[a,b] *Means within each row with different superscripts differ significantly (P < 0.05).*

Intestinal Microflora

In total, 1,216,334 high-quality sequences were obtained from samples. After clustering at the 97% similarity level, sequences were assigned to 905 OTUs. Firmicutes were the most abundant phylum across all samples, followed by Proteobacteria, Actinobacteriota, Bacteroidota, Spirochaetota, Desulfobacterota, and Patescibacteria (**Figure 2**). When compared with the CON group, the relative abundance of Firmicutes was significantly increased ($P < 0.05$) in the ABO and LBPs groups (**Figure 3**). Alpha diversity analyses indicated that LBPs increased Chao and ACE indices when compared with the CON group ($P < 0.05$), but no significant differences were observed for Shannon and Simpson indices among the groups (**Supplementary Figure 1**). PCA showed a distinct separation between the CON and LBPs groups, but no differences between the ABO and LBPs groups (**Figure 4A**). Hierarchical clustering tree analyses showed that CON microbial composition had mostly gathered in another branch (**Figure 4B**). From ANOSIM analyses, significant differences were identified in the microbial composition of the study groups; $r = 0.2702$, $P < 0.01$ in the CON, LBPs, and ABO groups; $r = 0.2907$, $P < 0.05$ for the ABO vs. CON groups; $r = 0.4827$, $P < 0.01$ for the LBPs vs. CON groups; and $r = 0.0558$, $P = 0.185$ for the ABO vs. LBPs groups). Additionally, *Lactobacillus* and *Faecalibacterium* were enriched (**Figure 3**) in the LBPs group at the genus level ($P < 0.05$), while *Enterobacteriaceae* (**Figure 3**), *Enterococcaceae*, and *Escherichia-Shigella* (**Supplementary Figure 2**) were enriched in the CON group ($P < 0.05$).

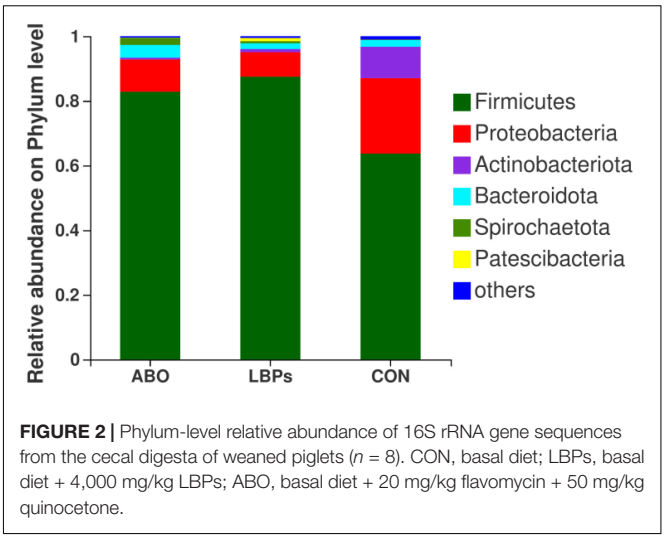

FIGURE 2 | Phylum-level relative abundance of 16S rRNA gene sequences from the cecal digesta of weaned piglets ($n = 8$). CON, basal diet; LBPs, basal diet + 4,000 mg/kg LBPs; ABO, basal diet + 20 mg/kg flavomycin + 50 mg/kg quinocetone.

Short-Chain Fatty Acids Levels

Total SCFAs, as well as acetic, propionic, isobutyric, butyric, isopentoic, and valeric acid levels in the cecum, ileum, and colon are shown in **Table 7**. When compared with the CON group, dietary both LBPs and ABO supplementation increased acetic, propionic and butyric acid levels, and total SCFAs, in the cecum ($P < 0.05$). However, no significant differences were observed in total ileum SCFAs or each SCFAs across groups ($P > 0.05$). Piglets fed the LBPs diet showed increased isobutyric and isopentoic acid levels in the colon when compared with the other groups ($P < 0.05$).

DISCUSSION

Weaning stress causes intestinal and immune system dysfunction and reduces pig growth and health (Campbell et al., 2013). Numerous studies have reported that plant-derived polysaccharides (e.g., *Achyranthes bidentata* and *Ganoderma lucidum* polysaccharides) improve immune responses, maintain intestinal structure integrity, balance intestinal microbiota, and reduce diarrhea, which promote pig growth (Li et al., 2015; Hou et al., 2021). In this study, dietary supplementation with either LBPs or ABO increased ADG and decreased the F/G, which may have been attributed to immune response stimulation by LBPs (Zhu et al., 2020). Tan et al. (2019) reported that

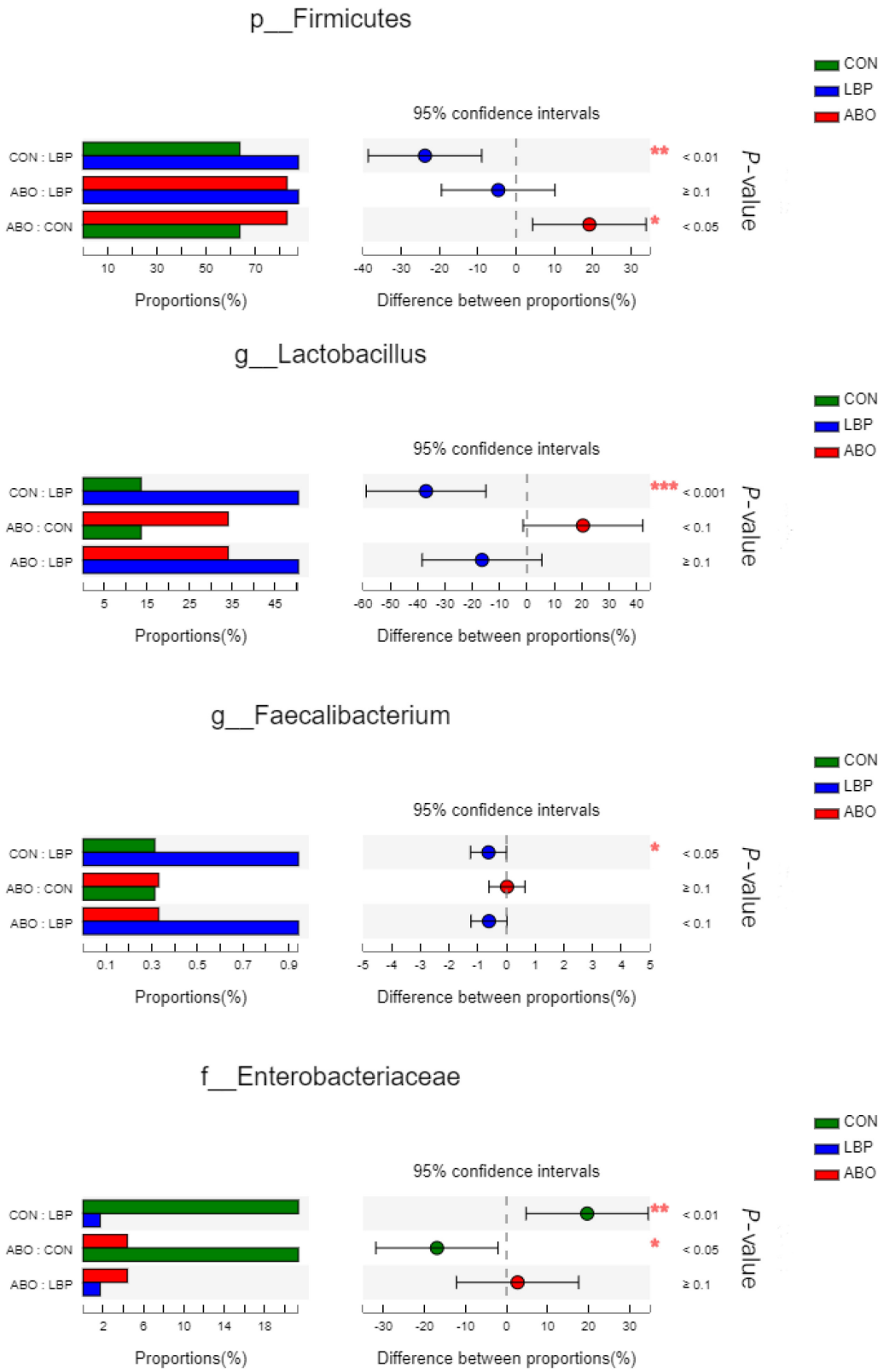

FIGURE 3 | Comparative analysis of 3 most relative abundances of gut microbiota (n = 8). Kruskal–Wallis test followed by Tukey test was used to evaluate the statistical significance. Asterisks express statistical differences between different groups: *0.01 < $P \leq 0.05$, **0.001 < $P \leq 0.01$, ***$P \leq 0.001$. CON, basal diet; LBP, basal diet + 4,000 mg/kg LBPs; ABO, basal diet + 20 mg/kg flavomycin + 50 mg/kg quinocetone.

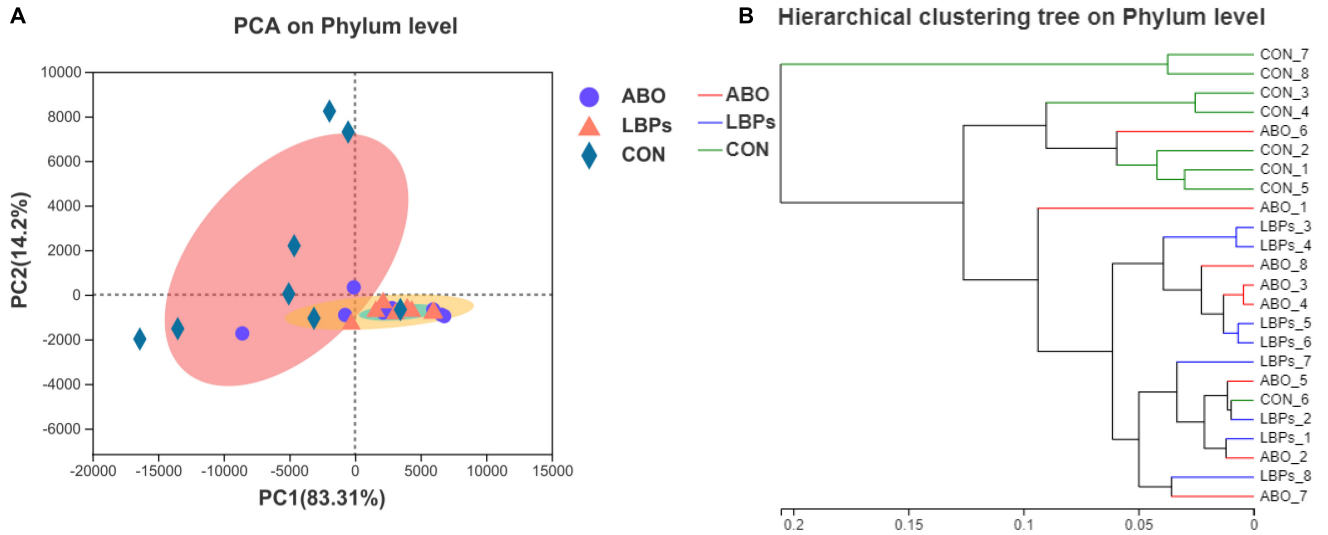

FIGURE 4 | (A) Principal Component Analysis (PCA) of bacterial communities in the cecal digesta of weaned piglets (based on the Bray–Curtis distance) (n = 8). **(B)** Analysis of hierarchical clustering tree on Phylun level showed that the microbial composition of CON was almost entirely gathered in another branch. CON, basal diet; LBPs, basal diet + 4,000 mg/kg LBPs; ABO, basal diet + 20 mg/kg flavomycin + 50 mg/kg quinocetone.

LBPs, when added to hybrid grouper (*Epinephelus lanceolatus* ♂ × *E. fuscoguttatus* ♀) diets, inhibited hepatic inflammatory responses, increased antioxidant enzyme activity, and improved growth performance and feed efficiency. The intestine has crucial roles in nutrient absorption and defenses against external pathogens (Halas et al., 2010). Wang et al. (2019) reported that dietary LBPs improved intestinal morphology and nutrient absorption in young rats. In addition, Hsieh et al. (2021) indicated that dietary LBPs improved gastric microbiota by increasing gastric *Bifdobacterium* levels in rats. Therefore, these and our evidence may be mediated by the promotional effects of LBPs on growth performance.

Diarrhea incidence has been used as an index to reflect gut health, with a lower diarrheal incidence beneficial for gut health (Pierce et al., 2005). Qiao et al. (2013) reported that diarrheal incidence in piglets was decreased by supplementing medicinal *Aloe vera* polysaccharides. In our study, dietary LBPs or ABO supplementation reduced diarrheal incidence in weaned piglets. Nagy et al. (1992) reported piglet diarrhea after weaning is related to some pathogen levels in the intestine. We previously demonstrated that weaned piglets fed 4,000 mg/kg LBPs had a decreased relative abundance of *Escherichia coli* and *Firmicutes* in the ileum and cecum (Chen et al., 2020). Also, intestinal pH is associated with the proliferation of probiotic microbes, preventing post weaning diarrhea, and maintaining gut enzyme activity (Beuria et al., 2005; Guggenbuhl et al., 2007). Furthermore, Xia et al. (2020) found that dietary LBPs supplementation increased the abundance of *Roseburia faecis, Prevotella* spp., *Butyricicoccus pullicaecorum*, and *Eubacterium uniforme* in mice, which generated particular SCFAs. Thus, LBPs appear to reduce diarrhea incidence in weaned piglets by modulating gut microbiota composition.

Immunoglobulins reflect the immune status of the animal (Yuan et al., 2015; Wang Y. et al., 2018). Hao et al. (2015) reported that the major serum Igs, IgA, IgG, and IgM, were key humoral immunity components in all mammals; they enhance monocyte macrophage phagocytosis and inhibit pathogenic virus and microorganism reproduction (Heidebrecht and Kulozik, 2019; Planchais and Mouquet, 2020). In our study, dietary LBPs supplementation increased serum IgG and IgM levels in weaned piglets. Similarly, Long et al. (2020) reported that broilers fed 2,000 mg/kg LBPs increased serum IgA and IgG levels. Furthermore, the immunoenhancing effects of LBPs may stimulate IL-2 and TNF-α gene expression in human monocytes (Lu and Zhang, 2002). In our study, LBPs dietary supplementation enhanced serum IL-2, IL-10, and TNF-α production in agreement with Ding et al. (2019a), who reported that LBPs administration increased IL-2, IL-6, IL-1, TNF-α, and interferon-γ levels in mice. Littringer et al. (2018) reported that IL-2 and TNF-α were secreted mainly through T helper cells. Wang et al. (2021) found that polysaccharides from traditional Chinese medicines, such as *Artemisia rupestris L., Astragalus, L. barbarum,* and *G. lucidum* regulated immune cell functions and metabolism by activating macrophages and T/B lymphocyte signal pathways. Thus, dietary LBPs appeared to improve the health status of piglets by activating the immune system.

Weaning decreases antioxidation capacity by increasing free radical levels and disrupting oxidative balance (Burke et al., 2009; Yin et al., 2014). Antioxidant parameters such as SOD, GSH-Px, T-AOC, and MDA are routinely used to evaluate antioxidation properties (Hao et al., 2015). SOD degrades superoxide radicals and thus functions as an antioxidant (Urso and Clarkson, 2003). The reduction reaction of lipid peroxides is catalyzed by GSH-Px, and total antioxidative capacity is reflected by T-AOC levels (Aleryani et al., 1998; Tao et al., 2006). MDA is

TABLE 7 | Effects of dietary LBPs supplementation on short-chain fatty acids in intestinal contents of weaned piglets (μg/kg).

Items[1]	Treatments[2]			SEM[3]	*P*-value
	CON	ABO	LBPs		
Cecum					
Acetic acid	3.32^{b}	6.00^{a}	7.77^{a}	0.336	<0.001
Propionic acid	2.84^{b}	4.27^{a}	4.30^{a}	0.215	0.017
Isobutyric acid	0.871	0.771	0.719	0.006	0.549
Butyric acid	2.40^{b}	3.75^{ab}	4.57^{a}	0.320	0.035
Isopentoic acid	0.149^{a}	0.090^{b}	0.083^{b}	0.007	0.001
Valeric acid	0.606^{a}	0.324^{b}	0.471^{ab}	0.038	0.022
Total SCFAs	9.40^{b}	14.5^{a}	17.3^{a}	0.865	0.004
Ileum					
Acetic acid	0.546	0.623	0.647	0.044	0.622
Propionic acid	0.114	0.103	0.106	0.002	0.186
Isobutyric acid	0.019	0.017	0.016	0.001	0.609
Butyric acid	0.083	0.068	0.059	0.006	0.324
Isopentoic acid	0.007	0.010	0.007	0.001	0.398
Valeric acid	0.009	0.008	0.008	0.001	0.133
Total SCFAs	0.777	0.829	0.844	0.052	0.864
Colon					
Acetic acid	2.46	2.95	2.75	0.115	0.246
Propionic acid	1.89	1.50	1.12	0.138	0.145
Isobutyric acid	0.114^{b}	0.090^{b}	0.167^{a}	0.009	0.005
Butyric acid	1.15	1.62	1.47	0.097	0160
Isopentoic acid	0.218^{ab}	0.136^{b}	0.280^{a}	0.017	0.010
Valeric acid	0.286	0.188	0.245	0.017	0.086
Total SCFAs	6.13	6.48	6.11	0.337	0.883

[1] *SCFAs, short-chain fatty acids.*
[2] *Treatments consisted of (1) CON; basal diet, (2) LBPs; basal diet + 4,000 mg/kg LBPs and (3) ABO; basal diet + 20 mg/kg flavomycin + 50 mg/kg quinocetone.*
[3] *SEM, pooled standard error of mean (n = 8).*
[a,b] *Means within each row with different superscripts differ significantly (P < 0.05).*

an indicator of lipid peroxidation and reflects the severity of free radical attack on cells (Jiang et al., 2016). It was reported that plant polysaccharides could alleviate this oxidative stress (Liu et al., 2018; Chen and Huang, 2019). In our study, LBPs dietary supplementation increased T-AOC and GSH-Px levels but decreased MDA production. Yang F. et al. (2020) reported that LBPs dietary supplementation relieved oxidative stress in high fat diet-induced obese mice. Liu et al. (2021b) found that LBPs supplementation reduced myocardial oxidative stress via activation of the nuclear factor erythroid-2 antioxidant signal pathway. Furthermore, plants containing flavonoids, phenolic compounds, ascorbic acid, and tocopherol were shown to exhibit antioxidant effects (Wang et al., 2008). It is documented that LBPs were rich in these abovementioned agents (Peng and Tian, 2001). Therefore, we speculated that the antioxidant effects of LBPs may be associated with these components, however, more research is required in this area.

A healthy mucosal structure is key for digestion, physiological function, and growth (Pluske et al., 1996). After weaning, significant changes occur in villus height, crypt depth, and V/C ratios (Cheng et al., 2017). A large V/C ratio represents a greater absorptive efficiency in the small intestine for nutrients, and increased resistance toward disease (Pu et al., 2018). Wang et al. (2019) reported that compound polysaccharide supplementation increased villus height and V/C ratios in the duodenum of young rats. In our study, LBPs dietary supplementation increased villus height and V/C ratios in the duodenum of weaned piglets. Thus, LBPs improved intestinal morphology, maintained intestinal integrity, and promoted intestinal absorption.

A balanced intestinal microbiota is critical for good gut health and nutrition. We observed that some changes had occurred in intestinal microbial composition and metabolism of cecal digesta across groups. PCA revealed that microbial composition and structures were distinct between the CON and LBPs groups, but no differences were determined between the ABO and LBPs groups. Some polysaccharides selectively stimulate the growth and metabolic activity of particular intestinal bacteria associated with health and well-being (Wang et al., 2019). We previously showed that LBPs dietary supplementation decreased the relative abundance of *E. coli* and *Firmicutes* in the ileum and cecum of pigs (Chen et al., 2020). Similar observations by Zhu et al. (2015) showed that polymannuronate addition to broiler diets increased lactic acid bacteria and decreased cecal *E. coli* levels. Furthermore, increased *E. coli* levels may be associated with an increased rate of diarrhea (Zhao et al., 2015). Interestingly, in our study, LBPs dietary supplementation reduced the relative abundance of *Escherichia-Shigella*, *Enterococcaceae*, and *Enterobacteriaceae* in the cecum, and also decreased the diarrhea ratio index. A previous study demonstrated that *Lactobacillus* could protect the intestine by producing antimicrobial agents that suppressed pathogen colonization (Yu et al., 2018). In the current study, dietary supplemental LBPs promoted *Faecalibacterium* and *Lactobacillus* levels. Similarly, Zhao et al. (2015) reported that *mulberry leaf* polysaccharide dietary supplementation reduced the relative abundance of *E. coli* and promoted *Lactobacilli* and *Bifidobacteria* abundance in weaned piglets. Furthermore, Zhu et al. (2020) also reported that LBPs dietary supplementation increased Proteobacteria and Firmicutes abundance, while reducing Bacteroidetes ratios in mice. These results indicated that LBPs could modulate gut microbiota composition and maintain the health of intestinal communities, which may underlie increased growth performance in animal models.

The intestinal digesta contains considerable microbial metabolites and fermentation products that reflect microbial activity and intestinal health (Diao et al., 2014). SCFAs are key metabolites that gut microbiota use to limit inflammation and maintain intestinal integrity to promote gut health (Liu et al., 2020). Thorburn et al. (2015) showed that acetic acid inhibited the histone deacetylase HDAC9.39 to promote regulatory T cell differentiation, with propionic acid enhancing the generation of macrophage. Cresci et al. (2010) reported that butyric acid promoted gut immune responses and preserved intestinal barrier integrity. In addition, intestinal pH was associated with the proliferation of probiotic microbes, the prevention of post weaning diarrhea, and the maintenance of gut enzyme activity (Beuria et al., 2005; Guggenbuhl et al., 2007). Furthermore, LBPs increased SCFAs production which reduced gut environment pH and inhibited *E. coli* levels *in vivo* and *in vitro* studies

(Knudsen et al., 2012; Ding et al., 2019b). In our study, LBPs enhanced acetic, propionic, and butyric acid production, and total SCFAs in the cecum, and also promoted *Faecalibacterium* which produced butyrate and generated anti-inflammatory properties (Wan et al., 2019). Therefore, LBPs may have active roles in host immunity and health by modulating gut microbiota and promoting SCFAs production.

CONCLUSION

The present research demonstrated that dietary LBPs supplementation improved growth performance, antioxidant capacity and immunity, and reduced diarrhea incidence in weaned piglets. These LBPs effects were associated with a regulatory input on intestinal microbial composition, microbial metabolite production, and intestinal morphology integrity. Thus, LBPs may be used as efficient antibiotic alternatives in weaned piglet feed.

DATA AVAILABILITY STATEMENT

The datasets presented in this study can be found in online repositories. The names of the repository/repositories and accession number(s) can be found in the article/ **Supplementary Material**.

ETHICS STATEMENT

The animal study was reviewed and approved by the Committee of Animal Care at Hunan Agricultural University (Changsha, China) (permit number: CACAHU 2020-00156).

AUTHOR CONTRIBUTIONS

YXY: conceptualization, formal analysis, and writing—original draft. JC: methodology, validation, and resources. FW: data curation. MY: software. BT: funding acquisition. YLY: investigation and supervision. ZY: methodology, project administration, and writing—review and editing. All authors have read and approved the final manuscript.

FUNDING

This work was supported by the National Natural Science Foundation of China (U20A2054 and 32072745), the Earmarked Fund for China Agriculture Research System (CARS-35), the Hunan Provincial Key Research and Development Project (2020NK2031), the Tianjin Synthetic Biotechnology Innovation Capacity Improvement Project (TSBICIP-CXRC-038), the Youth Science Foundation Project of Hunan Agricultural University (19QN01), and the Open Foundation of CAS Key Laboratory of Agro-ecological Processes in Subtropical Region, Institute of Subtropical Agriculture (ISA2020101).

ACKNOWLEDGMENTS

We thank International Science Editing (http://www.internationalscienceediting.com) for editing this manuscript.

SUPPLEMENTARY MATERIAL

The Supplementary Material for this article can be found online at: https://www.frontiersin.org/articles/10.3389/fmicb.2021.819993/full#supplementary-material

REFERENCES

Aleryani, S., Milo, E., Rose, Y., and Kostka, P. (1998). Superoxide-mediated decomposition of biological S-nitrosothiols. *J. Biol. Chem.* 273, 6041–6045. doi: 10.1074/jbc.273.11.6041

Beuria, T. K., Santra, M. K., and Panda, D. (2005). Sanguinarine blocks cytokinesis in bacteria by inhibiting FtsZ assembly and bundling. *Biochemistry* 44, 16584–16593. doi: 10.1021/bi050767

Burke, N. C., Scaglia, G., Boland, H. T., and Swecker, W. S. (2009). Influence of two-stage weaning with subsequent transport on body weight, plasma lipid peroxidation, plasma selenium, and on leukocyte glutathione peroxidase and glutathione reductase activity in beef calves. *Vet. Immunol. Immunopathol.* 127, 365–370. doi: 10.1016/j.vetimm.2008.11.017

Campbell, J. M., Crenshaw, J. D., and Polo, J. (2013). The biological stress of early weaned piglets. *J. Anim. Sci. Biotechnol* 4, 124–127. doi: 10.1186/2049-1891-4-19

Chen, F., and Huang, G. (2019). Antioxidant activity of polysaccharides from different sources of ginseng. *Int. J. Biol. Macromol.* 125, 906–908. doi: 10.1016/j.ijbiomac.2018.12.134

Chen, J., Long, L., Jiang, Q., Kang, B., Li, Y., and Yin, J. (2020). Effects of dietary supplementation of *Lycium barbarum* polysaccharides on growth performance, immune status, antioxidant capacity and selected microbial populations of weaned piglets. *J. Anim. Physiol. Anim. Nutr.* 104, 1106–1115. doi: 10.1111/jpn.13247

Chen, S., Zhou, Y., Chen, Y., and Gu, J. (2018). Fastp: an ultra-fast all-in-one FASTQ preprocessor. *Bioinformatics* 34, 884–890. doi: 10.1093/bioinformatics/bty560

Cheng, W., Lu, J., Li, B., Lin, W., Zhang, Z., Wei, X., et al. (2017). Effect of functional oligosaccharides and ordinary dietary fiber on intestinal microbiota diversity. *Front. Microbiol.* 8:1750. doi: 10.3389/fmicb.2017.01750

Cook, M. E. (2004). Antibodies: alternatives to antibiotics in improving growth and feed efficiency. *J. Appl. Poult. Res* 13, 106–119. doi: 10.1093/japr/13.1.106

Cresci, G. A., Thangaraju, M., Mellinger, J. D., Liu, K., and Ganapathy, V. (2010). Colonic gene expression in conventional and germ-free mice with a focus on the butyrate receptor GPR109A and the butyrate transporter SLC5A8. *J Gastrointest. Surg.* 14, 449–461. doi: 10.1007/s11605-009-1045-x

Diao, H., Zheng, P., Yu, B., He, J., Mao, X., Yu, J., et al. (2014). Effects of dietary supplementation with benzoic acid on intestinal morphological structure and microflora in weaned piglets. *Livest. Sci.* 167, 249–256. doi: 10.1016/j.livsci.2014.05.029

Ding, Y., Yan, Y., Chen, D., Ran, L., Mi, J., Lu, L., et al. (2019a). Modulating effects of polysaccharides from the fruits of *Lycium barbarum* on the immune response and gut microbiota in cyclophosphamide-treated mice. *Food Funct.* 10, 3671–3683. doi: 10.1039/c9fo00638a

Ding, Y., Yan, Y., Peng, Y., Chen, D., Mi, J., Lu, L., et al. (2019b). In vitro digestion under simulated saliva, gastric and small intestinal conditions and fermentation by human gut microbiota of polysaccharides from the fruits of

Lycium barbarum. *Int. J. Biol. Macromol.* 125, 751–760. doi: 10.1016/j.ijbiomac.2018.12.081

Donno, D., Beccaro, G. L., Mellano, M. G., Cerutti, A. K., and Bounous, G. (2015). Goji berry fruit (*Lycium* spp.): antioxidant compound fingerprint and bioactivity evaluation. *J. Funct. Foods* 18, 1070–1085. doi: 10.1016/j.jff.2014.05.020

Edgar, R. C. (2013). UPARSE: highly accurate OTU sequences from microbial amplicon reads. *Nat. Methods* 10, 996–998. doi: 10.1038/NMETH.2604

Feng, L., Xiao, X., Liu, J., Wang, J., Zhang, N., Bing, T., et al. (2020). Immunomodulatory effects of *Lycium barbarum* polysaccharide extract and its uptake behaviors at the cellular level. *Molecules* 25:1351. doi: 10.3390/molecules25061351

Franklin, M. A., Mathew, A. G., Vickers, J. R., and Clift, R. A. (2002). Characterization of microbial populations and volatile fatty acid concentrations in the jejunum, ileum, and cecum of pigs weaned at 17 vs 24 days of age. *J. Anim. Sci.* 80, 2904–2910. doi: 10.2527/2002.80112904x

Gong, G., Liu, Q., Deng, Y., Dang, T., Dai, W., Liu, T., et al. (2020). Arabinogalactan derived from *Lycium barbarum* fruit inhibits cancer cell growth via cell cycle arrest and apoptosis. *Int. J. Biol. Macromol.* 149, 639–650. doi: 10.1016/j.ijbiomac.2020.01.251

Guggenbuhl, P., Seon, A., Quintana, A. P., and Nunes, C. S. (2007). Effects of dietary supplementation with benzoic acid (VeVo Vitall®) on the zootechnical performance, the gastrointestinal microflora and the ileal digestibility of the young pig. *Livest. Sci.* 108, 218–221. doi: 10.1016/j.livsci.2007.01.068

Halas, D., Hansen, C. F., Hampson, D. J., Mullan, B. P., Kim, J. C., Wilson, R. H., et al. (2010). Dietary supplementation with benzoic acid improves apparent ileal digestibility of total nitrogen and increases villous height and caecal microbial diversity in weaner pigs. *Anim. Feed Sci. Technol.* 160, 137–147. doi: 10.1016/j.anifeedsci.2010.07.001

Hao, R., Li, Q., Zhao, J., Li, H., Wang, W., and Gao, J. (2015). Effects of grape seed procyanidins on growth performance, immune function and antioxidant capacity in weaned piglets. *Livest. Sci.* 178, 237–242. doi: 10.1016/j.livsci.2015.06.004

Heidebrecht, H., and Kulozik, U. (2019). Fractionation of casein micelles and minor proteins by microfiltration in diafiltration mode. study of the transmission and yield of the immunoglobulins IgG, IgA and IgM. *Int. Dairy J.* 93, 1–10. doi: 10.1016/j.idairyj.2019.01.009

Hou, G., Peng, W., Wei, L., Li, R., Huang, X., and Yin, Y. (2021). Probiotics and *Achyranthes bidentata* polysaccharides improve growth performance via promoting intestinal nutrient utilization and enhancing immune function of weaned pigs. *Animals* 11:2617. doi: 10.3390/ani11092617

Hsieh, S., Lian, Y., Lin, I., Yang, Y., Tinkov, A. A., Skalny, A. V., et al. (2021). Combined *Lycium babarum* polysaccharides and C-phycocyanin increase gastric *Bifidobacterium* relative abundance and protect against gastric ulcer caused by aspirin in rats. *Nutr. Metab.* 18:4. doi: 10.1186/s12986-020-00538-9

Hu, C., Xiao, K., Luan, Z., and Song, J. (2013). Early weaning increases intestinal permeability, alters expression of cytokine and tight junction proteins, and activates mitogen-activated protein kinases in pigs. *J. Anim. Sci.* 91, 1094–1101. doi: 10.2527/jas.2012-5796

Hung, D., Cheng, Y., Chen, W., Hua, K., Pietruszka, A., Dybus, A., et al. (2019). *Bacillus licheniformis*-fermented products reduce diarrhea incidence and alter the fecal microbiota community in weaning piglets. *Animals* 9:1145. doi: 10.3390/ani9121145

Jia, L., Li, W., Li, J., Li, Y., Song, H., Luan, Y., et al. (2016). *Lycium barbarum* polysaccharide attenuates high-fat diet-induced hepatic steatosis by up-regulating SIRT1 expression and deacetylase activity. *Sci. Rep.* 6, 1–11. doi: 10.1038/srep36209

Jiang, W., Wen, H., Liu, Y., Jiang, J., Wu, P., Zhao, J., et al. (2016). Enhanced muscle nutrient content and flesh quality, resulting from tryptophan, is associated with anti-oxidative damage referred to the Nrf2 and TOR signalling factors in young grass carp (*Ctenopharyngodon idella*): avoid tryptophan deficiency or excess. *Food Chem.* 199, 210–219. doi: 10.1016/j.foodchem.2015.12.003

Kim, H. J., Lee, J., Kim, S. C., Seo, J. Y., Hong, S. B., and Park, Y. I. (2020). Immunostimulating activity of *Lycium chinense* miller root extract through enhancing cytokine and chemokine production and phagocytic capacity of macrophages. *J. Food Biochem.* 44:e13215. doi: 10.1111/jfbc.13215

Knudsen, K. E., Hedemann, M. S., and Lærke, H. N. (2012). The role of carbohydrates in intestinal health of pigs. *Anim. Feed Sci. Technol.* 173, 41–53. doi: 10.1016/j.anifeedsci.2011.12.020

Lemieux-labonte, V., Simard, A., Willis, C. K., and Lapointe, F. (2017). Enrichment of beneficial bacteria in the skin microbiota of bats persisting with white-nose syndrome. *Microbiome* 5:115. doi: 10.1186/s40168-017-0334-y

Li, J. (2017). Current status and prospects for in-feed antibiotics in the different stages of pork production - a review. *Asian Austral. J. Anim.* 30, 1667–1673. doi: 10.5713/ajas.17.0418

Li, X., He, L., Yang, Y., Liu, F., Cao, Y., and Zuo, J. (2015). Effects of extracellular polysaccharides of *Ganoderma lucidum* supplementation on the growth performance, blood profile, and meat quality in finisher pigs. *Livest. Sci.* 178, 187–194. doi: 10.1016/j.livsci.2015.04.001

Littringer, K., Moresi, C., Rakebrandt, N., Zhou, X., Schorer, M., Dolowschiak, T., et al. (2018). Common features of regulatory T cell specialization during Th1 responses. *Front. Immunol.* 9:1344. doi: 10.3389/fimmu.2018.01344

Liu, J., Pu, Q., Qiu, H., Di, D., Liu, J., Pu, Q., et al. (2021a). Polysaccharides isolated from *Lycium barbarum L.* by integrated tandem hybrid membrane technology exert antioxidant activities in mitochondria. *Ind. Crops Prod.* 168:113547. doi: 10.1016/j.indcrop.2021.113547

Liu, J., Zhao, G., He, L., Wang, Z., Zibrila, A. I., Niu, B., et al. (2021b). *Lycium barbarum* polysaccharides inhibit ischemia/reperfusion-induced myocardial injury via the Nrf2 antioxidant pathway. *Toxicol. Rep.* 8, 657–667. doi: 10.1016/j.toxrep.2021.03.019

Liu, Y., Sun, Y., Huang, G., Liu, Y., Sun, Y., and Huang, G. (2018). Preparation and antioxidant activities of important traditional plant polysaccharides. *Int. J. Biol. Macromol.* 111, 780–786. doi: 10.1016/j.ijbiomac.2018.01.086

Liu, Y., Wang, X., Chen, Q., Luo, L., Ma, M., Xiao, B., et al. (2020). *Camellia sinensis* and *Litsea coreana* ameliorate intestinal inflammation and modulate gut microbiota in dextran sulfate sodium-induced colitis mice. *Mol. Nutr. Food Res.* 64:1900943. doi: 10.1002/mnfr.201900943

Long, L., Kang, B., Jiang, Q., and Chen, J. (2020). Effects of dietary *Lycium barbarum* polysaccharides on growth performance, digestive enzyme activities, antioxidant status, and immunity of broiler chickens. *Poultry. Sci.* 99, 744–751. doi: 10.1016/j.psj.2019.10.043

Lu, G., and Zhang, S. (2002). Effects of *Lycium barbarum* polysaccharide on cytokine expression in human monocytes. *Acta Nutr. Sin.* 24, 67–69. doi: 10.1038/sj.cr.7290131

Lu, T., Piao, X., Zhang, Q., Wang, D., Piao, X., and Kim, S. (2010). Protective effects of *Forsythia suspensa* extract against oxidative stress induced by diquat in rats. *Food Chem. Toxicol.* 48, 764–770. doi: 10.1016/j.fct.2009.12.018

Magoc, T., and Salzberg, S. L. (2011). Flash: fast length adjustment of short reads to improve genome assemblies. *Bioinformatics* 27, 2957–2963. doi: 10.1093/bioinformatics/btr507

Nagy, B., Arp, L. H., Moon, H. W., and Casey, T. A. (1992). Colonization of the small intestine of weaned pigs by enterotoxigenic *Escherichia coli* that lack known colonization factors. *Vet. Pathol.* 29, 239–246. doi: 10.1177/030098589202900308

National Research Council (2012). *Nutrient Requirements of Swine*, 11th Edn. Washington, DC: National Academy Press.

Peng, X., and Tian, G. (2001). Structural characterization of the glycan part of glycoconjugate LbGp2 from *Lycium barbarum L. Carbohydr. Res.* 331, 95–99. doi: 10.1016/S0008-6215(00)00321-9

Pierce, M., Callan, J., Mccarthy, P., and O'doherty, V. (2005). Performance of weanling pigs offered low or high lactose diets supplemented with avilamycin or inulin. *Anim. Sci.* 80, 313–318. doi: 10.1079/asc40900313

Planchais, C., and Mouquet, H. (2020). Easy pan-detection of human IgA immunoglobulins. *J. Immunol. Methods* 484:112833. doi: 10.1016/j.jim.2020.112833

Pluske, J., Williams, I., and Aherne, F. (1996). Maintenance of villous height and crypt depth in piglets by providing continuous nutrition after weaning. *Anim. Sci.* 62, 131–144.

Pourhossein, Z., Qotbi, A. A., Seidavi, A., Laudadio, V., Centoducati, G., and Tufarelli, V. (2015). Effect of different levels of dietary sweet orange (*Citrus sinensis*) peel extract on humoral immune system responses in broiler chickens. *Anim. Sci. J.* 86, 105–110. doi: 10.1111/asj.12250

Pu, J., Chen, D., Tian, G., He, J., Zheng, P., Mao, X., et al. (2018). Protective effects of benzoic acid, *Bacillus coagulans*, and oregano oil on intestinal injury

caused by enterotoxigenic *Escherichia coli* in weaned piglets. *Biomed. Res. Int.* 2018:1829632. doi: 10.1155/2018/1829632

Qiao, J., Li, H., Zheng, C., Feng, Z., and Wang, W. (2013). Dietary supplementation with *Aloe vera* polysaccharide enhances the growth performance and immune function of weaned piglets. *J. Anim. Feed Sci.* 22, 329–334. doi: 10.22358/jafs/65921/2013

Shimato, Y., Hattori, T., and Ohno, T. (2020). Hypoglycemic activity and the mechanisms of Lycium bark extract in *db/db* mice. *Biol. Pharm. Bull.* 43, 946–950. doi: 10.1248/bpb.b19-00814

Stackebrandt, E., and Goebel, B. (1994). Taxonomic note: a place for DNA-DNA reassociation and 16s rRNA sequence analysis in the present species definition in bacteriology. *Int. J. Syst. Evol. Micr.* 44, 846–849. doi: 10.1099/00207713-44-4-846

Tan, X., Sun, Z., Ye, C., Lin, H., Tan, X., Sun, Z., et al. (2019). The effects of dietary *Lycium barbarum* extract on growth performance, liver health and immune related genes expression in hybrid grouper (*Epinephelus lanceolatus*♂× *E. fuscoguttatus*♀) fed high lipid diets. *Fish Shellf. Immun.* 87, 847–852. doi: 10.1016/j.fsi.2019.02.016

Tao, X., Xu, Z., and Wang, Y. (2006). Effects of dietary fluoride levels on growth, serum indexes and antioxidant systems in growing pigs. *Turk. J. Vet. Anim. Sci.* 30, 65–70.

Thorburn, A. N., Mckenzie, C. I., Shen, S., Stanley, D., Macia, L., Mason, L. J., et al. (2015). Evidence that asthma is a developmental origin disease influenced by maternal diet and bacterial metabolites. *Nat. Commun.* 6:7320. doi: 10.1038/ncomms8320

Urso, M. L., and Clarkson, P. M. (2003). Oxidative stress, exercise, and antioxidant supplementation. *Toxicology* 189, 41–54. doi: 10.1016/S0300-483X(03)00151-3

Wan, Y., Wang, F., Yuan, J., Li, J., Jiang, D., Zhang, J., et al. (2019). Effects of dietary fat on gut microbiota and faecal metabolites, and their relationship with cardiometabolic risk factors: a 6-month randomised controlled-feeding trial. *Gut* 68, 1417–1429. doi: 10.1136/gutjnl-2018-317609

Wang, D., Liu, Y., and Zhao, W. (2021). The adjuvant effects on vaccine and the immunomodulatory mechanisms of polysaccharides from traditional Chinese medicine. *Front. Mol. Biosci.* 8:655570. doi: 10.3389/fmolb.2021.655570

Wang, H., Li, Y., Liu, J., Di, D., Liu, Y., and Wei, J. (2020). Hepatoprotective effect of crude polysaccharide isolated from *Lycium barbarum L.* against alcohol-induced oxidative damage involves Nrf2 signaling. *Food Sci. Nutr.* 8, 6528–6538. doi: 10.1002/fsn3.1942

Wang, L., Piao, X., Kim, S., Piao, X., Shen, Y., and Lee, H. (2008). Effects of *Forsythia suspensa* extract on growth performance, nutrient digestibility, and antioxidant activities in broiler chickens under high ambient temperature. *Poult. Sci.* 87, 1287–1294. doi: 10.3382/ps.2008-00023

Wang, M., Xie, Z., Li, L., Chen, Y., Li, Y., Wang, Y., et al. (2019). Supplementation with compound polysaccharides contributes to the development and metabolic activity of young rat intestinal microbiota. *Food Funct.* 10, 2658–2675. doi: 10.1039/c8fo02565g

Wang, W., Chen, J., Zhou, H., Wang, L., Ding, S., Wang, Y., et al. (2018). Effects of microencapsulated *Lactobacillus plantarum* and fructooligosaccharide on growth performance, blood immune parameters, and intestinal morphology in weaned piglets. *Food Aag. Immunol.* 29, 84–94. doi: 10.1080/09540105.2017.1360254

Wang, Y., Dong, Z., Song, D., Zhou, H., Wang, W., Miao, H., et al. (2018). Effects of microencapsulated probiotics and prebiotics on growth performance, antioxidative abilities, immune functions, and caecal microflora in broiler chickens. *Food Aag. Immunol.* 29, 859–869. doi: 10.1080/09540105.2018.1463972

Wu, Q., Liu, L., Wang, X., Lang, Z., Meng, X., Guo, S., et al. (2020). *Lycium barbarum* polysaccharides attenuate kidney injury in septic rats by regulating Keap1-Nrf2/are pathway. *Life Sci.* 242:117240. doi: 10.1016/j.lfs.2019.117240

Xia, W., Li, X., Khan, I., Yin, L., Su, L., Leong, W. K., et al. (2020). *Lycium berry* polysaccharides strengthen gut microenvironment and modulate gut microbiota of the mice. *Evid-Based Compl. Alt.* 2020:809702. doi: 10.1155/2020/8097021

Xu, N., Tan, G., Wang, H., and Gai, X. (2016). Effect of biochar additions to soil on nitrogen leaching, microbial biomass and bacterial community structure. *Eur. J. Soil Biol.* 74, 1–8. doi: 10.1016/j.ejsobi.2016.02.004

Yang, F., Wei, Y., Liao, B., Wei, G., Qin, H., Pang, X., et al. (2020). Effects of *Lycium barbarum* polysaccharide on endoplasmic reticulum stress and oxidative stress in obese mice. *Front. Pharmacol.* 11:742. doi: 10.3389/fphar.2020.00742

Yang, J., Wang, C., Huang, K., Zhang, M., Wang, J., and Pan, X. (2020). Compound *Lactobacillus* sp. administration ameliorates stress and body growth through gut microbiota optimization on weaning piglets. *App. Microbiol. Biot.* 104, 6749–6765. doi: 10.1007/s00253-020-10727-4

Yang, X., Bai, H., Cai, W., Li, J., Zhou, Q., Wang, Y., et al. (2013). *Lycium barbarum* polysaccharides reduce intestinal ischemia/reperfusion injuries in rats. *Chem-Biol. Interact.* 204, 166–172. doi: 10.1016/j.cbi.2013.05.010

Yin, J., Wu, M., Xiao, H., Ren, W., Duan, J., Yang, G., et al. (2014). Development of an antioxidant system after early weaning in piglets. *J. Anim. Sci.* 92, 612–619. doi: 10.2527/jas.2013-6986

Yu, M., Mu, C., Zhang, C., Yang, Y., Su, Y., and Zhu, W. (2018). Marked response in microbial community and metabolism in the ileum and cecum of suckling piglets after early antibiotics exposure. *Front. Microbiol.* 9:1166. doi: 10.3389/fmicb.2018.01166

Yuan, W., Jin, H., Ren, Z., Deng, J., Zuo, Z., Wang, Y., et al. (2015). Effects of antibacterial peptide on humoral immunity in weaned piglets. *Food Agr. Immunol.* 26, 682–689. doi: 10.1080/09540105.2015.1007448

Zhang, F., Zhang, X., Gu, Y., Wang, M., Guo, S., Liu, J., et al. (2021). Hepatoprotection of *Lycii fructus* polysaccharide against oxidative stress in hepatocytes and larval zebrafish. *Oxid. Med. Cell Longev.* 2021:3923625. doi: 10.1155/2021/3923625

Zhao, J., Ge, L., Xiong, W., Leong, F., Huang, L., and Li, S. (2016). Advanced development in phytochemicals analysis of medicine and food dual purposes plants used in China (2011-2014). *J. Chromatogr.* 1428, 39–54. doi: 10.1016/j.chroma.2015.09.006

Zhao, X., Li, L., Luo, Q., Ye, M., Luo, G., and Kuang, Z. (2015). Effects of mulberry (*Morus alba L.*) leaf polysaccharides on growth performance, diarrhea, blood parameters, and gut microbiota of early-weanling pigs. *Livest. Sci.* 177, 88–94. doi: 10.1016/j.livsci.2015.03.001

Zhao, Z., Yu, H., Liu, B., Wang, H., Luo, Q., and Ding, X. (2016). Antioxidative mechanism of *Lycium barbarum* polysaccharides promotes repair and regeneration following cavernous nerve injury. *Neural. Regen. Res.* 11, 1312–1321. doi: 10.4103/1673-5374.189197

Zhu, W., Li, D., Wang, J., Wu, H., Xia, X., Bi, W., et al. (2015). Effects of polymannuronate on performance, antioxidant capacity, immune status, cecal microflora, and volatile fatty acids in broiler chickens. *Poult. Sci.* 94, 345–352. doi: 10.3382/ps/pev006

Zhu, W., Zhou, S., Liu, J., Mclean, R. J., and Chu, W. (2020). Prebiotic, immuno-stimulating and gut microbiota-modulating effects of *Lycium barbarum* polysaccharide. *Biomed. Pharmacother.* 121:109591. doi: 10.1016/j.biopha.2019.109591

Zhu, Y., Zhao, Q., Gao, H., Peng, X., Wen, Y., and Dai, G. (2016). *Lycium barbarum* polysaccharides attenuates N-methy-N-nitrosourea-induced photoreceptor cell apoptosis in rats through regulation of poly (ADP-ribose) polymerase and caspase expression. *J. Ethnopharmacol.* 191, 125–134. doi: 10.1016/j.jep.2016.05.037

Conflict of Interest: The authors declare that the research was conducted in the absence of any commercial or financial relationships that could be construed as a potential conflict of interest.

Publisher's Note: All claims expressed in this article are solely those of the authors and do not necessarily represent those of their affiliated organizations, or those of the publisher, the editors and the reviewers. Any product that may be evaluated in this article, or claim that may be made by its manufacturer, is not guaranteed or endorsed by the publisher.

frontiers in Microbiology

ORIGINAL RESEARCH
published: 10 March 2022
doi: 10.3389/fmicb.2022.810746

Oregano Oil and Harmless Blue Light to Synergistically Inactivate Multidrug-Resistant *Pseudomonas aeruginosa*

Min Lu[1†], Ka Ioi Wong[2†], Xin Li[3†], Fei Wang[1], Li Wei[1], Shen Wang[2] and Mei X. Wu[4]*

[1] Shanghai Key Laboratory for Prevention and Treatment of Bone and Joint Diseases, Department of Orthopaedics, Ruijin Hospital, Shanghai Institute of Traumatology and Orthopaedics, Shanghai Jiao Tong University School of Medicine, Shanghai, China, [2] Department of Plastic and Reconstructive Surgery, Shanghai Ninth People's Hospital, Shanghai Jiao Tong University School of Medicine, Shanghai, China, [3] Instrumental Analysis Center, Shanghai Jiao Tong University, Shanghai, China, [4] Department of Dermatology, Wellman Center for Photomedicine, Harvard Medical School, Massachusetts General Hospital, Boston, MA, United States

OPEN ACCESS

Edited by:
Kianoush Khosravi-Darani,
National Nutrition and Food Technology Research Institute, Iran

Reviewed by:
Tim Maisch,
University of Regensburg, Germany
Nagendran Tharmalingam,
Rhode Island Hospital, United States

***Correspondence:**
Mei X. Wu
mwu5@mgh.harvard.edu

[†] These authors have contributed equally to this work and share first authorship

Specialty section:
This article was submitted to Antimicrobials, Resistance and Chemotherapy, a section of the journal Frontiers in Microbiology

Received: 07 November 2021
Accepted: 25 January 2022
Published: 10 March 2022

Citation:
Lu M, Wong KI, Li X, Wang F, Wei L, Wang S and Wu MX (2022) Oregano Oil and Harmless Blue Light to Synergistically Inactivate Multidrug-Resistant Pseudomonas aeruginosa. Front. Microbiol. 13:810746. doi: 10.3389/fmicb.2022.810746

Blue light (BL) at 405 nm and oregano essential oil (OEO) have shown bactericidal activity by its own. Here, we demonstrated that the two synergistically killed multidrug-resistant (MDR) *Pseudomonas aeruginosa* (*Pa*). *Pa* ATCC19660 and HS0065 planktonic cells and mature biofilms were reduced by more than 7 $\log_{10}$ after treatment by BL combined with OEO, in sharp contrast to no significant bacterial reduction with the monotreatment. The duo also sufficiently eliminated acute or biofilm-associated infection of open burn wounds in murine without incurring any harmful events in the skin. The synergic bactericide was attributed mainly to the ability of OEO to magnify cytotoxic reactive oxygen species (ROS) production initiated by BL that excited endogenous tetrapyrrole macrocycles in bacteria while completely sparing the surrounding tissues from the phototoxic action. OEO ingredient analysis in combination with microbial assays identified carvacrol and its isomer thymol to be the major phytochemicals that cooperated with BL executing synergic killing. The finding argues persuasively for valuable references of carvacrol and thymol in assessing and standardizing the bactericidal potential of various OEO products.

Keywords: blue light, oregano oil, synergistic effects, acute infections, biofilm-associated infections

INTRODUCTION

Pseudomonas aeruginosa (*Pa*) infections have become significant challenges in control of hospital-acquired infections, particularly in patients with severe burns, immunocompromised conditions, and cancers (El Zowalaty et al., 2015; Bassetti et al., 2018). The emergence of multidrug-resistant (MDR) *Pa* results in high rates of mortality either directly or indirectly, since some of these MDR bacteria fail to respond to almost all antibiotics designated to treat them (Obolski et al., 2015). Even last resort of colistin with a relatively low prescription rate confers less and less effectiveness in the control of *Pa* infections owing to increased resistance to the antibiotics (Leeb, 2004; Levy and Marshall, 2004). Apparently, there is an urgent need to research and develop for alternatives

in management of MDR *Pa*, especially non-antibiotics and combinatory modalities in fighting against MDR pathogens.

Among non-antibiotic alternatives, essential oils (EOs) have attracted increasing attentions and are considered promising strategies for treating MDR bacteria (Pandey et al., 2017). Natural EOs have been well-known for their enormous potentials as microbicides in ancient China and Egypt. We previously investigated antimicrobial activities of 42 EOs extracted from Chinese endemic aromatic herbs and spices against a panel of bacteria and fungi (Lu et al., 2013a,b,c). Among these EOs tested, 11 of them showed a superior antimicrobial activity against clinical and agricultural pathogens (Lu et al., 2013a,b,c). For instance, oregano essential oil (OEO) safely and substantially reduced bacterial loads after topical application onto the infected murine burns without development of any resistance to the treatment even after repeated treatments (Lu et al., 2018).

Another innovative sterile technique is antimicrobial blue light (BL) and has been extensively studied for the treatments of MDR microbes (Wang et al., 2016, 2019). The mechanism underlying BL-mediated bactericide is proven to specifically stimulate the excessive production of reactive oxygen species (ROS) by its ability to excite endogenous non-metallated tetrapyrrole macrocycles that are produced abundantly within most of bacteria but not in mammalian cells (Surdel et al., 2017; Wang et al., 2017). BL confers significant advantages as an alternative to antibiotics due to its faster action and great effectiveness irrespective of antibiotic susceptibility (Wang et al., 2017).

BL and EOs both possess multi-target features, i.e., targeting different organelles of bacterial cells, which would greatly shield the development of resistance to the modalities. In view of this, we investigated the bactericidal efficacy by combining BL and OEO against a standard strain of *Pa* ATCC19660 and a clinical isolate of *Pa* HS0065 *in vitro* and *in vivo*. We found that a combination of OEO with BL substantially and safely reduced bacterial loads in acute and biofilm-associated burn infections as compared to either alone, which was mainly attributed to its key ingredients carvacrol and its isomer thymol. This synergistic and non-antibiotic approach holds great promise to effectively and safely manage pathogenic *Pa* infections.

MATERIALS AND METHODS

Phytochemicals, Light Source, *Pseudomonas aeruginosa* Strains, and Human Cells

OEO and seven phytochemicals (>98% purity) were bought from Sigma-Aldrich. A light-emitting diode (LED) of BL, which had a peak width of 405 ± 12.5 nm, and a soft white LED bulb (3W, A15) were purchased from Thorlabs and General Electric, respectively. The irradiation was fixed to 55 mW/cm^2 for all experiments and measured on a PM100D power/energy meter (Thorlabs). *Pa* strains used in this study were verified MDR *via* conventional microbiology tests. *Pa* HS0065 was isolated from a burn-infected patient in Huashan Hospital in Shanghai, and a luminescent *Pa* ATCC19660 was employed for monitoring infection in alive mice by a Lumina *in vivo* image system (IVIS) (PerkinElmer) (Dai et al., 2013b). The human fibroblasts (ATCC PCS-201-012) were cultured for 2–3 days at 37°C, 5% CO_2 in Dulbecco's modified Eagle's medium (DMEM) containing 10% fatal bovine serum (FBS), 100 U/ml penicillin, and 100 μg/ml streptomycin.

Oregano Essential Oil Components Identified by Gas Chromatography/Mass Spectrometry

OEO constituents were analyzed by a gas chromatography (GC) (Agilent 6980) coupled to mass spectrometry (MS) (Agilent 5973N) *via* a fused-silica capillary column (HP-5MS: 30 m × 0.25 mm i.d.). The operating procedures were as follows: initial oven temperature, 60°C for 10 min; gradually increased to 220°C at 3°C/min; maintained at 220°C for additional 10 min; then elevated to 240°C with an increment of 1°C/min. The temperature of the injector port and ionization source was 250°C. The carrier gas was helium at 0.8 ml/min. Ionization voltage of MS in the EI mode was 70 eV. OEO constituents were identified and confirmed by comparing the retention index (RI) in reference to n-alkanes and the mass spectra of authentic compounds in NIST, Wiley databases, and Adams library.

Synergistic Effects of Blue Light and Oregano Essential Oil/Compounds Against *Pseudomonas aeruginosa* Planktonic Cells

OEO or seven compounds each were dissolved at 40 mg/ml in N,N-dimethylformamide (DMF) as stock solutions. To assess synergistic effects, 2,970 μl of *Pa* planktonic cells in phosphate-buffered saline (PBS) at 7.0 log CFU/ml was mixed with 30 μl of OEO or an indicated compound at varying concentrations in a 35-mm Petri dish and then irradiated immediately with BL at 55 mW/cm^2 while stirring at 60 rpm. Before or at indicated times after treatments, 50 μl aliquot was collected and assayed on brain heart infusion (BHI) agar plates to determine colony-forming units (CFU) (Jett et al., 1997). For comparisons, BL alone or OEO/compounds alone was also assayed in parallel. The synergistic degrees between BL and OEO/compounds against the two *Pa* strains were determined by *S*-values obtained through the following formula or the Bliss independence model:

$\underline{S}$-values = (logCFU/ml$_{BL}$/logCFU/ml$_{Control}$) (logCFU/ml$_{OEO\,(or\ carvacrol\ or\ thymol)}$/logCFU/ml$_{Control}$) − (logCFU/ml$_{BL+OEO(or\ carvacrol\ or\ thymol)}$/ logCFU/ ml$_{Control}$) (Courtney et al., 2017; Lu et al., 2021b). LogCFU/ml$_{BL}$, logCFU/ml$_{OEO\,(or\ carvacrol\ or\ thymol)}$, logCFU/ml$_{BL+OEO(or\ carvacrol\ or\ thymol)}$, and logCFU/ml$_{Control}$ numbers were viable bacteria left after an indicated treatment.

Verification of Any Possible Resistance to the Combined Therapy

The two *Pa* strains were evaluated for possible resistance to the combined therapy by repeated treatments per a published

protocol with some modifications (Lu et al., 2021b). In brief, *Pa* suspensions were exposed severally to a sublethal dose of the combined therapy, which could inactivate 3 log CFU/ml of bacterial growth. The initial sublethal dose was 60 J/cm^2 BL combined with 0.2 mg/ml OEO for *Pa* ATCC 19660 or 30 J/cm^2 BL and 0.2 mg/ml OEO for *Pa* HS0065. After first treatment cycle, bacteria that survived the treatment were re-cultured for the next suppressive growth cycle with a newly defined sublethal dose of the combined therapy, if necessary. The procedure was repeated for 20 successive cycles. Resistance was estimated by any significant rise in sublethal doses or CFU with increasing passages up to 20 cycles.

For comparison, ampicillin (AMP) resistance was assessed in parallel. Briefly, *Pa* suspension was added into 96-well plate at 200 μl/well containing serial dilutions of AMP as described (de Breij et al., 2018). After 24 h incubation, the lowest AMP concentration that could completely inactivate bacterial growth was defined as a minimum inhibitory concentration (MIC). Then, 10 μl of *Pa* suspension grown in BHI broth containing 1/2 MIC AMP was added into a fresh BHI broth. The bacteria were cultured and determined for its MIC again as above. AMP resistance was determined if any significant rise in MIC was found within 20 consecutive passages.

Synergistic Effects of Blue Light and Oregano Essential Oil/Compounds Against *Pseudomonas aeruginosa* Mature Biofilms

Pa grown in trypticase soy broth (TSB) was transferred into a 96-well plate at 100 μl/well and cultured for 3 days to establish biofilms. The biofilms were washed twice with PBS, soaked in 200 μl of OEO, carvacrol, or thymol each at 0.8 mg/ml, and immediately illuminated with BL at 100 J/cm^2. Antibacterial efficacy of BL alone at 100 J/cm^2 or OEO, carvacrol, or thymol alone each at 0.8 mg/ml against the biofilms was assayed side-by-side as controls. Bacteria left in the biofilms were enumerated *via* CFU assay after dislodging them in 200 μl PBS by 5-min ultrasonic vibration as described (Jett et al., 1997). The synergy between BL and OEO/compound (carvacrol or thymol) against the two *Pa* mature biofilms was verified by *S*-values calculated with the Bliss Independence model above (Courtney et al., 2017; Lu et al., 2021b).

Therapy of Acute Burn Infections

All animal studies were approved by the Shanghai Jiao Tong University Animal Study Committee. The lower dorsal skin of 8-week-old BALB/C mice were hair removed. A brass block at a size of 1 cm^2 was heated in 100°C boiling water before being applied onto the hairless skin for 5–8 s so that a full-thickness third-degree burn could be generated. For acute burn infection, approximately 6.5 log CFU luminescent *Pa* ATCC19660 in 50 μl PBS were inoculated, after 10 min of the burn, onto the burns for 30 min. The infected burns were spread uniformly with 50 μl OEO (10 mg/ml) prior to BL exposure for varying lengths. Likewise, the antibacterial activity was determined with BL, OEO, or PBS combined with sham light as controls. Bacterial luminescence images in burns were acquired by a Lumina IVIS (PerkinElmer) (Lu et al., 2021b). Bacterial luminescence intensity was measured with the Living Image software (Xenogen). All mice were sacrificed on day 8 after bacterial inoculation to determine viable bacteria remaining on wounds or in blood. Serial dilutions of wound homogenates and blood were cultivated on BHI agar plates with the supplements of Skirrow for bacterial enumeration.

Management of Biofilm-Associated Burns

Full-thickness murine burns were created as above and covered evenly with 50 μl of *Pa* HS0065 containing 7.5 log CFU in PBS (Wang et al., 2016), 3 days after which 20 μl of OEO at 20 mg/ml was distributed to the wounds, along with 60 or 120 J/cm^2 BL irradiation. The therapeutic effect of OEO, BL irradiation, or PBS together with sham light (control) was also evaluated simultaneously as controls. On day 15 after various treatments, all mice were euthanized and perfused with PBS through the heart. The wounds and vital organs such as lungs, livers, and spleens were dissected and processed by a homogenizer in 2 ml of PBS for bacterial CFU determination as above (Jett et al., 1997).

Measurements of H_2O_2 and HO in the Absence or Presence of Bacteria or Protoporphyrin IX

OEO, carvacrol, or thymol solution each at 0.1 mg/ml with or without 10^7 CFU/ml of *Pa* HS0065 was aliquoted to a 35-mm Petri dish at 3 ml/dish and then exposed to 30 J/cm^2 BL or sham light. After the treatment, 50 μl solution was collected from each dish, mixed with an equal amount of Amplex Red reagent/HRP working solution, and reacted at room temperature for 20 min. The amount of H_2O_2 was estimated by a microplate spectrophotometer at an excitation/emission wavelength of 571/585 nm (Zhao et al., 2012). To measure ·HO production, the solution was collected similarly and mixed for 15 min with the molecular probe 3′-(p-hydroxyphenyl) fluorescein (HPF) at a final concentration of 5 μM. A yield of HO was quantified by a microplate spectrophotometer at excitation/emission wavelength of 505/525 nm (Morones-Ramirez et al., 2013). Similar measurements of H_2O_2 and ·HO production were also carried out in the presence of 10 μM protoporphyrin IX (PPIX) in place of bacteria whereby PPIX provided an exogenous photosensitizer to simulate photochemical reaction in bacteria.

Cell Viability

Human fibroblasts were treated by 0, 0.1, 0.2, 0.4, or 0.8 mg/ml OEO along with 100 J/cm^2 BL. Cell viability was estimated with CCK-8 kit (Beyotime) based on the absorbance values at 450 nm. Moreover, human fibroblasts and bacteria were mixed and cultured together at an 1:10 ratio, and the co-culture was exposed to a lethal dose of the duo (50 J/cm^2 BL and 0.6 mg/ml of OEO). Then, 10 μM calcein-AM and propidium iodide (PI) solutions were added to the co-cultures to mark viable cells and dead cells, respectively, according to the manufacturer's

instruction. The images of cells were captured by the green/red fluorescence channel in the FluoView FV1000-MPE confocal microscope (Olympus).

Toxicity Assessment of the Combinatory Treatment *in vivo*

Mice were anesthetized, hair removed on the lower dorsal skin, and treated by 50 mg/ml of OEO (50 μl) alongside 150 J/cm^2 BL irradiation as above. The treatment was repeated daily for consecutive 3 days. Blood samples, skin biopsies, and vital organs of liver and kidney were taken 24 h after the final treatment. The index of alanine aminotransferase (ALT), aspartate aminotransferase (AST), alkaline phosphatase (ALP), creatinine (Cr), and blood urea nitrogen (BUN) were measured by automatic analytical instruments (Abbott AxSYM) through standard methods. The skin, liver, and kidney biopsies were immersed in 10% phosphate-buffered formalin to fix the tissue and processed for hematoxylin and eosin (H&E) staining for histological observation and visualization in Nanozoomer 2.0 HT (Hamamatsu). The resultant images were analyzed by using NDP viewer software (Hamamatsu). Possible DNA damage for skin biopsies was evaluated by the DeadEnd Fluorometric TUNEL staining per the manufacturer's instructions (Promega). DNA fragmentation was also induced in some tissue sections with 10 U/ml RQ1 RNase-free DNase I as positive controls. Fluorescence images were captured in a FluoView FV1000-MPE confocal microscope (Olympus).

Statistical Analyses

All data are mean ± standard deviations (SDs). Two tailed Student's *t*-test or one-way ANOVA analysis was performed to determine statistical significance between two groups or multiple groups. The survival curves were compared by Kaplan–Meier method. GraphPad Prism 7.0 (GraphPad software) was used for all statistical analyses, and $p < 0.05$ indicated statistically significant.

RESULTS

The Antibacterial Activity of Oregano Essential Oil and Its Synergy With Blue Light Are Ascribed Primarily to Carvacrol and Thymol

OEO was found to kill a standard strain *Pa* ATCC19660 and a clinical isolate *Pa* HS0065 in planktonic cultures equivalently with an MIC of 0.8 mg/ml, i.e., the minimal concentration of OEO needed to completely suppress the growth of 10^7 CFU/ml of the bacteria after 24 h treatment in a standard MIC assay (**Table 1**). Strikingly, the same concentration of OEO exterminated 7.0 log CFU/ml of *Pa* ATCC19660 (left panel) or *Pa* HS0065 (right panel) in 5 min, rather than 24 h, should OEO be combined with 15 J/cm^2 of BL (**Figure 1A**). The quick and efficacious bactericidal action of the duo therapy was unparalleled to any of monotherapies (**Figure 1A**). As can be seen in **Figure 1A**, 15 J/cm^2 of BL alone or 0.8 mg/ml OEO alone failed to significantly suppress growth of the bacteria under similar conditions. Reduction in the OEO concentration by half (0.4 mg/ml) could still eliminate 2.9 CFU/ml of *Pa* ATCC19660 or 3.8 CFU/ml of *Pa* HS0065 in the presence of 15 J/cm^2 of BL, highly significant compared with either BL or OEO alone ($p < 0.0001$) (**Figure 1A**). We next assessed whether *Pa* ATCC19660 and *Pa* HS0065 were susceptible to development of resistance to the duo therapy as previously described (Lu et al., 2021b). The two bacterial strains appeared not to develop any resistance to the combinatory therapy after 20 consecutive cycles of sublethal treatments (**Figure 1B**). In contrast, the MICs of *Pa* ATCC 19660 and *Pa* HS0065 to ampicillin (AMP) arose by 50- and 40-fold, respectively, after 20 passages (**Figure 1C**).

To determine specific ingredients responsible for the bactericidal activity and its synergy with BL, chemical constituents of OEO were analyzed by GC-MS. Twenty compounds were accounted for 98.29% of the total ingredients of OEO, among which a monoterpenoid phenol carvacrol and its isomer thymol along with α-pinene, myrcene, p-cymene, γ-terpinene, and linalool were the predominant ingredients of OEO (**Table 1**). Interestingly, among the seven compounds tested, thymol, and carvacrol showed the most sterilization activity with the same MIC as OEO (0.8 mg/ml), while other five compounds all had an MIC ≥ 1 mg/ml for both *Pa* strains (**Table 1**). The results suggest that thymol and carvacrol are the primary ingredients responsible for the bactericidal activity of OEO. Similar to OEO, carvacrol or thymol at 0.4 mg/ml did not exhibit significant bactericidal activity by its own but eliminated 4.5 or 3.2 log CFU/ml of *Pa* ATCC19660 and 4.9 or 1.5 log CFU/ml of *Pa* HS0065, respectively, when combined with 15 J/cm^2 BL (**Table 1**). Notably, the bactericidal activity mediated by carvacrol and BL was greater than that of OEO plus BL for both strains. In contrast to carvacrol and thymol, other five ingredients, namely, α-pinene, myrcene, p-cymene, γ-terpinene, and linalool, did not show any enhanced bactericidal activity when paired with BL under similar conditions (**Table 1**). The study concludes that active bactericidal ingredients of OEO, especially its synergy with BL, are composed primarily of carvacrol and thymol.

Blue Light and Oregano Essential Oil/Compounds Synergically Killed *Pseudomonas aeruginosa* Planktonic Cells and Mature Biofilms

The bactericidal effect mediated by BL combined with carvacrol or thymol resembled that of OEO exhibiting synergism in both BL- and phytochemical-dose-dependent fashions. As shown in **Figure 2**, with an increasing length of BL irradiation from 0 to 80 min, which corresponded to a fluence rise from 0 to 240 J/cm^2, 7.0 log CFU/ml of *Pa* ATCC19660 (left panel) or *Pa* HS0065 (right panel) was completely exterminated after 4 min BL irradiation in the presence of 1 × MIC or 0.8 mg/ml of carvacrol (middle) or thymol (bottom), comparable to that of OEO (upper). Similar bactericidal effectiveness was also obtained by reducing the concentration of OEO, carvacrol, or thymol to 0.2 or 0.4 mg/ml from 0.8 mg/ml, while extending the irradiation time to 80 or

TABLE 1 | Bactericidal activity and synergy with BL of OEO or its major ingredients.

No	Constituents	RI[a]	RI[b]	Peak area (%)[c]	*Pa* ATCC 19660	*Pa* HS0065	*Pa* ATCC 19660				*Pa* HS0065			
							BL 15J/cm^2	Com 0.4 mg/ml	BL + Com	S-value	BL 15 J/cm^2	Com 0.4 mg/ml	BL + Com	S-value
					MIC (mg/mL)		Log reduction of CFU/mL				Log reduction of CFU/mL			
1	α-thujene	926	924	0.25										
2	***α -pinene***	***939***	***932***	***1.42***	***>1***	***>1***	***0***	***0***	***0^{ns}***	***0***	***0***	***0***	***0^{ns}***	***0***
3	Camphene	953	946	0.17										
4	1-octen-3-ol	982	974	0.14										
5	***Myrcene***	***991***	***988***	***2.23***	***>1***	***>1***	***0***	***0***	***0^{ns}***	***0***	***0***	***0***	***0^{ns}***	***0***
6	α-phellandrene	1,002	1,002	0.82										
7	α-terpinene	1,018	1,014	0.71										
8	***p-cymene***	***1,026***	***1,020***	***4.82***	***>1***	***>1***	***0***	***0***	***0^{ns}***	***0***	***0***	***0***	***0^{ns}***	***0***
9	Limonene	1031	1024	0.27										
10	***γ -terpinene***	***1,060***	***1,054***	***3.89***	***1***	***1***	***0***	***0***	***0^{ns}***	***0***	***0***	***0***	***0^{ns}***	***0***
11	Terpinolene	1,092	1,086	0.21										
12	***Linalool***	***1,100***	***1,095***	***1.38***	***1***	***1***	***0***	***0***	***0^{ns}***	***0***	***0***	***0***	***0^{ns}***	***0***
13	Borneol	1,165	1,165	0.32										
14	Terpinen-4-ol	1,178	1,174	0.51										
15	***Thymol***	***1,295***	***1,289***	***7.02***	***0.8***	***0.8***	***0***	***0***	***3.2******	***0.46***	***0***	***0***	***1.5****	***0.21***
16	***Carvacrol***	***1,315***	***1,298***	***71.93***	***0.8***	***0.8***	***0***	***0***	***4.5*******	***0.64***	***0***	***0***	***4.9*******	***0.70***
17	Caryophyllene	1,426	1,417	0.82										
18	α-humulene	1,456	1,452	0.27										
19	β-bisabolene	1,509	1,505	0.35										
20	Isocaryophyllene oxide	1,585	1,582	0.76										
	Total			98.29										
	OEO				***0.8***	***0.8***	***0***	***0***	***2.9******	***0.41***	***0***	***0***	***3.8*******	***0.54***

The chemical compounds (Com) of OEO were identified by GC-MS. Seven main compounds > 1% of peak area were marked in bold and their MIC values evaluated against Pa ATCC19660 and Pa HS0065, alongside OEO. The antibacterial activities of BL alone at 15 J/cm^2, OEO/main compounds each at 0.4 mg/ml, or when combined with BL were assessed against Pa ATCC19660 and Pa HS0065.

[a]Retention index (RI) was calculated based on the C6–C28 n-alkanes reserved on the HP-5MS capillary column.

[b]Retention index (RI) was obtained from Kovat's retention index.

[c]Expressed as percentage of the total peak area of unadjusted chromatograms.

Synergistic bactericidal activities between BL and OEO, carvacrol or thymol were marked in red. 0 < S-value < 1 implicates that synergic effect happened; in the meantime, S-value < 0 implicates antagonistic interaction between BL and OEO/compound.

*(****p < 0.0001; ***p < 0.001; *p < 0.05; and ns, no significance.*

20 min, respectively (**Figure 2**). The inversed doses between the two varied with bacterial strains and individual compounds with *Pa* HS0065 (right) more sensitive than *Pa* ATCC19660 (left) and carvacrol more potent than OEO or thymol for both pathogens (**Figure 2**). It should be emphasized that the killing was not ascribed to heat because BL irradiation for 80 min alone or at a fluence as high as 240 J/cm^2 killed < 0.5 log CFU/ml of *Pa* ATCC19660 or 1.0 log CFU/ml of *Pa* HS0065 (**Figure 2**). The synergy of the combined therapies was verified by the Bliss Independence model, and synergistic degrees were established by *S*-values in the corresponding checkerboards on right (**Figure 2**); 0 < *S*-value < 1 indicates synergy, while *S*-value < 0 indicates antagonism. Apparently, the synergy was strengthened with an increasing BL intensity or a rising concentration of OEO, carvacrol, or thymol. The strongest synergy was seen at the upper right corner and the lowest at the lower left corner of the checkerboards.

We then extended the treatment to 3-day-old mature biofilms formed by *Pa* ATCC19660 and *Pa* HS0065. A combination of BL at 100 J/cm^2 and OEO/compounds each at 0.8 mg/ml efficaciously reduced 7 log CFU per well, whereas only < 0.5 log CFU per well were eliminated by the monotherapy under similar conditions (**Figures 3A,C,E**). The synergy in eradication of *Pa* biofilms between BL and OEO/compounds was once again proven by the Bliss Independence model (**Figures 3B,D,F**). All *S*-values were > 0.7, on average, indicating excellent synergism of the combined therapy against *Pa* mature biofilms.

Antibacterial Efficacy of Blue Light Paired With Oregano Essential Oil in the Treatment of Acute and Biofilm-Inflicted Wounds

The third-degree full thickness burns were infected with luminescent *Pa* ATCC19660 for 30 min as acute infection model. The wounds were treated with sham (control), monotherapies, or duo therapy (BL + OEO) (**Figure 4**). Bacterial luminescence on the wounds vanished 16 min after 50 J/cm^2 BL and OEO treatment and did not recrudesce within 8 days (**Figure 4A**). On the contrary, the bioluminescent signal remained unaltered in the

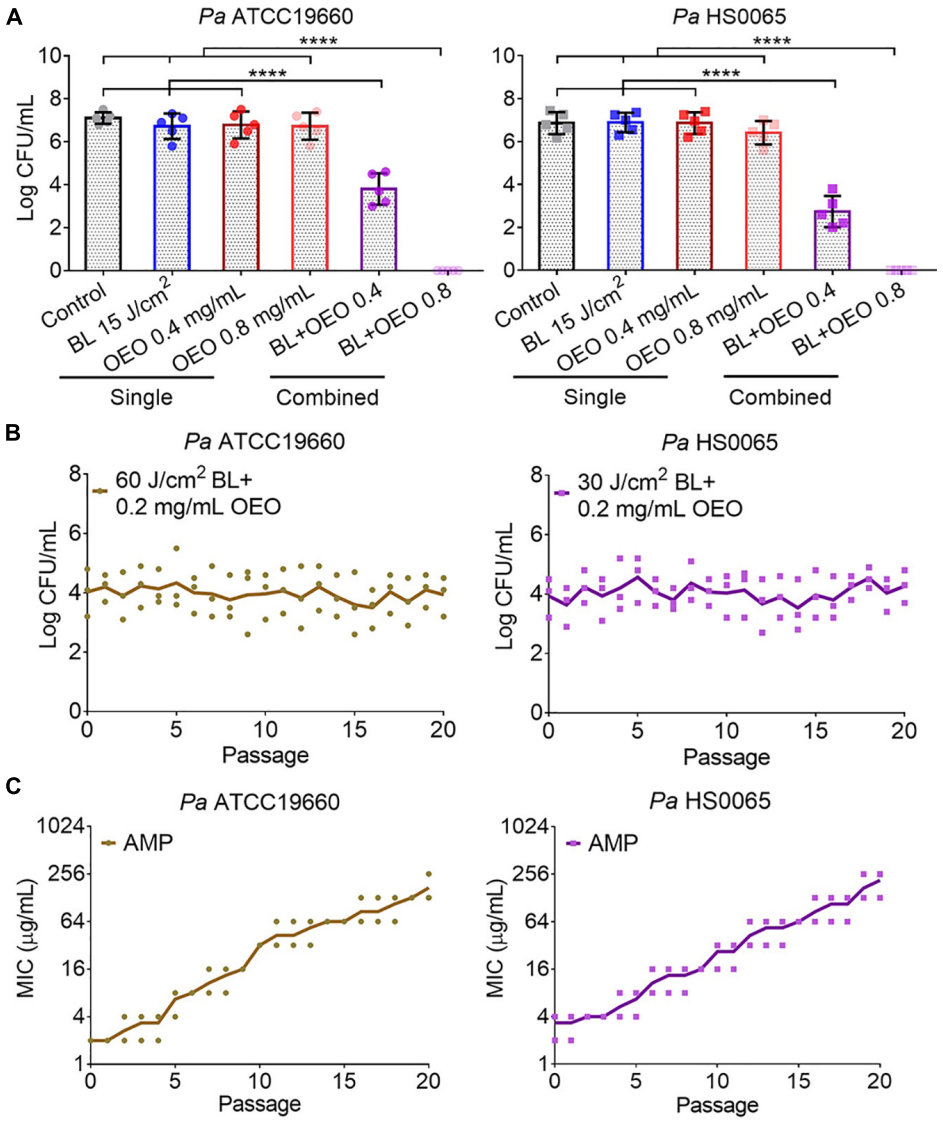

FIGURE 1 | Synergistic bactericidal activity of BL and OEO and no resistance development. **(A)** Synergy between OEO and BL. OEO was evaluated for its antibacterial activity at 0.8 or 0.4 mg/ml against planktonic *Pa* ATCC19660 (left) and *Pa* HS0065 (right), respectively, in the presence or absence of 15 J/cm^2 BL. The bacteria were sham treated (control) or treated with BL at 15 J/cm^2 alone as controls. **(B)** Resistance of *Pa* ATCC19660 (left) and *Pa* HS0065 (right) to 60 and 30 J/cm^2 BL combined with 0.2 mg/ml OEO, respectively. **(C)** Resistance of the two bacterial strains to ampicillin (AMP). Data represent the result of two independent experiments each performed in triplicate ($n = 6$) **(A)** or triplicate assays **(B,C)** ****$p < 0.0001$; and ns, no significance.

controls, while there was only a limited reduction in the animals receiving monotherapy over 8 days (**Figure 4A**). On average, 7.6 log RLU per model was exterminated directly by the combined therapy, whereas only < 2.0 log RLU per model was eliminated following the monotherapy (**Figure 4B**), a representative of more than 5.0 log more efficient killing of the combined therapy over the monotherapy (**Figure 4B**; $p < 0.0001$). The synergistic effect of the duo therapy was ascertained with the Bliss Independence model in a BL-dose-dependent manner (**Figure 4C**).

The bacterial luminescence on the wounds was also tracked every other day till day 8 after individual therapies (**Figure 4D**). No bacterial regrowth was found at the wounds in mice treated with the combined therapy (**Figures 4D,E**). On day 8 of the experiment, all mice were sacrificed to examine bacteria loads on wounds (**Figure 4F**) or in blood (**Figure 4G**). Only in the group receiving the combinatory therapy were bacteria detected neither on the wound nor in blood, in sharp contrast to a high CFU number in both wound and blood in mice sham treated or treated by a monotherapy. The results underscore the importance of effective controlling skin wound infections in the prevention of systemic infection that could cause sepsis or death.

To grow biofilms on wounds, 7.5 log CFU of *Pa* HS0065 was inoculated onto the third-degree burns and incubated for 3 days.

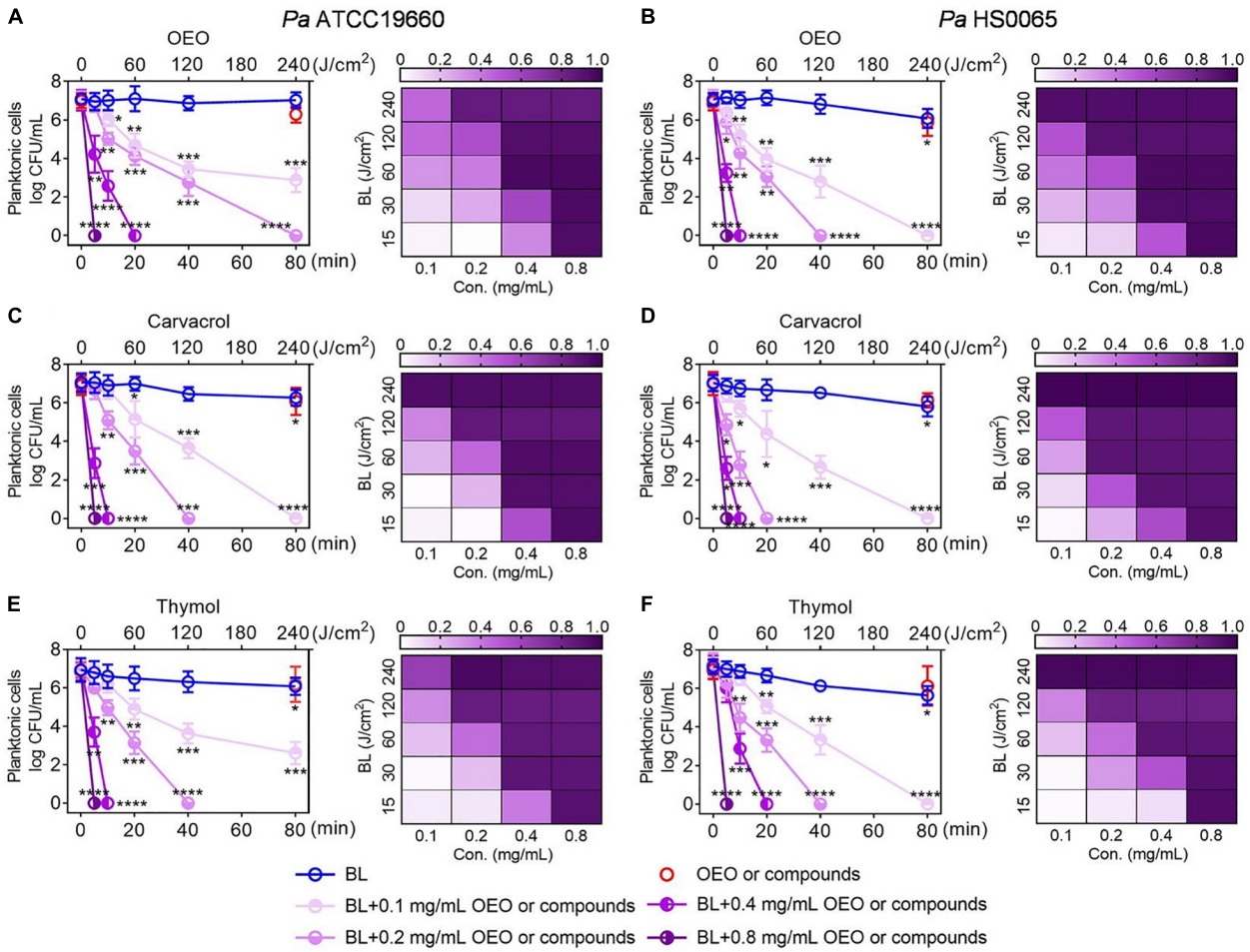

FIGURE 2 | Combination of BL with OEO **(A,B)**, carvacrol **(C,D)**, or thymol **(E,F)** synergistically inactivates *Pa* planktonic cells. *Pa* ATCC19660 (left) and *Pa* HS0065 (right) were treated with increasing lengths of BL irradiation in combination with indicated concentrations of OEO, carvacrol, or thymol. Killing curves (left) were shown on the left, and the corresponding checkerboards were on the right in which S-values (0–1.0) for indicated treatments were assessed by the Bliss Independence model as detailed in section "Materials and Methods". Results are expressed as mean ± SD of three independent experiments each run in triplicate. ****$p < 0.0001$; ***$p < 0.001$; **$p < 0.01$; and *$p < 0.05$.

The burns were treated with sham, 20 mg/ml of OEO in 50 μl PBS alone, 60 or 120 J/cm^2 of BL alone, or both, respectively (**Figure 5**). On day 1 after an indicated treatment, 50% of mice receiving the combined 120 J/cm^2 BL and OEO treatment gave rise to a sterile wound (**Figure 5A**). The synergy between OEO and BL became stronger as BL or OEO increased (**Figures 5A,B**). A fluence of 60 or 120 J/cm^2 BL in the presence of OEO both prevented the mice from death significantly during a course of 15-day infection, with 67 and 100% survival rates, respectively. On the contrary, the survival rates were much lower, only 0, 17, 17, and 34% in sham or monotherapy of OEO, 60 J/cm^2 BL, and 120 J/cm^2 BL, respectively (**Figure 5C**).

On day 15 after various treatments, all mice were sacrificed to determine the bacterial loads in wounds (**Figure 5D**), blood (**Figure 5E**), and vital organs (**Figure 5F**) of the lung, spleen, and liver. As expected, the combined therapy showed the most potent therapeutic effect than any of the monotherapies. Especially after treatment of 120 J/cm^2 BL combined with OEO, the percentages of mice with a sterile wound, blood, lung, spleen, and liver were 83, 100, 100, 100, and 100%, respectively (**Figures 5D–F**). The results indicate that the combined therapy effectively prevents system infection and holds back the bacteria from wound into the blood. Compared with *in vitro* experiment (**Figure 3A**), the bactericidal effect *in vivo* might be contributing to two reasons, first the different growth phases to bacteria and second the innate immune response that was aroused to increase phagocytosis or oxidative, which led to more effective treatment although using similar dose of BL.

Intracellular Reactive Oxygen Species Generated Exclusively in Bacteria Are Responsible for Bactericidal Action

It was found that in comparison with any monotherapy, the yields of H_2O_2 and ·HO were robustly enhanced by BL combined with OEO, carvacrol, or thymol in a range from 8- to more

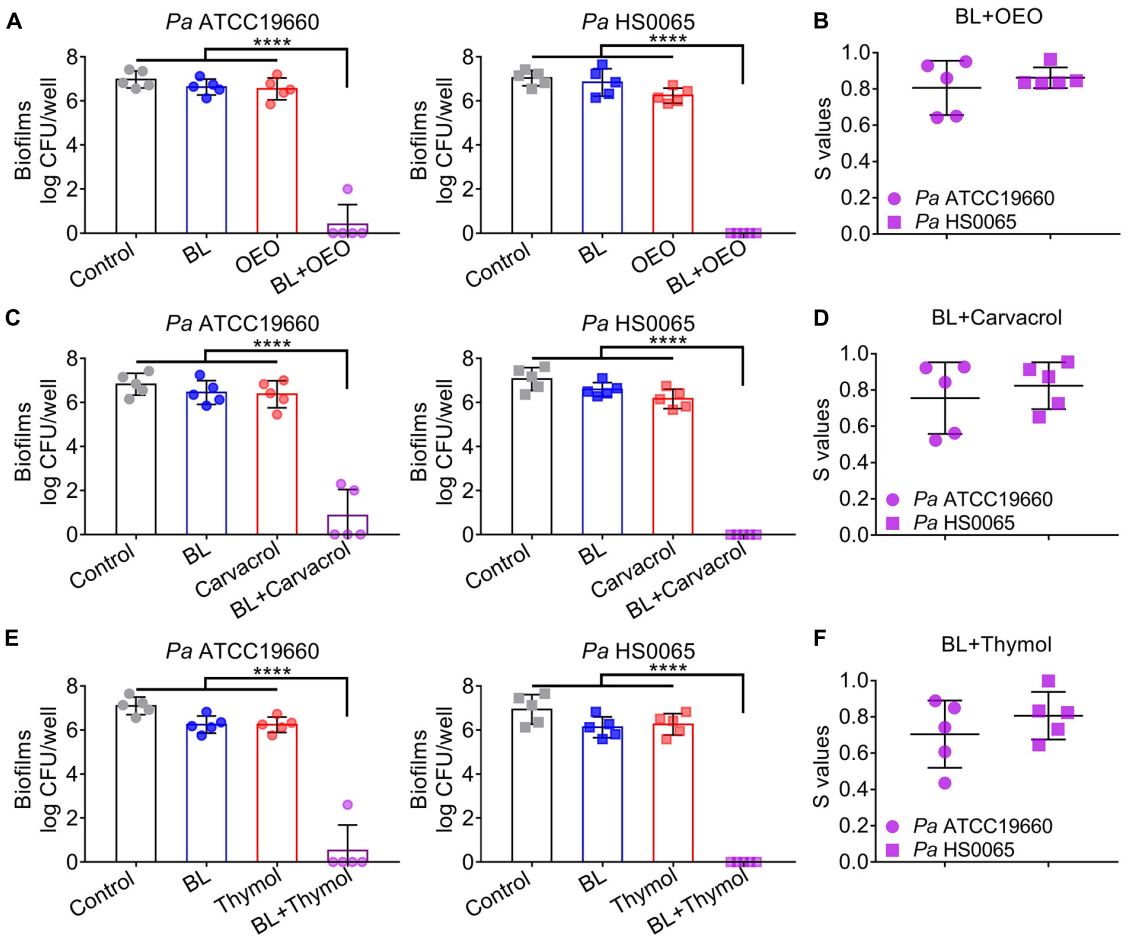

FIGURE 3 | A combination of BL and OEO (upper), carvacrol (middle), or thymol (bottom) synergistically eradicates Pa mature biofilms. **(A,C,E)** Anti-biofilm efficacies of BL at 100 J/cm^2, OEO/compounds each at 0.8 mg/ml, or both against established biofilms formed by *Pa* ATCC19660 (left) and *Pa* HS0065 (right). **(B,D,F)** Synergistic degrees (*S*-values) of the combinatory treatment for killing *Pa* biofilms were evaluated by Bliss Independence model as **Figure 2**. Data are presented as mean ± *SD* of five independent experiments each run in triplicate. ****$p < 0.0001$.

than 20-fold, which, however, occurred only in the presence of *Pa* HS0065 (**Figure 6A**, $p < 0.001$). When the bacteria were replaced with PPIX, a photosensitizer commonly found in bacteria including *Pa* (Hamblin et al., 2005; Wang et al., 2016, 2017), similar enhancements of H_2O_2 and HO formation were also noticed (**Figure 6B**). On the other hand, the bactericidal activities were significantly impeded by supplement of NaN_3, a specific quencher for the singlet oxygen ($^1O_2$), in the parallel study (**Figure 6C**, $p < 0.01$). Killing of the bacteria resulting mainly from HO was affirmed by perfect merging between HPF$^+$ green and PI$^+$ red in the bacteria (**Figure 6D**).

To ascertain that ROS were formed specifically in bacteria and not in mammalian cells, human fibroblasts were treated with a bacteria-lethal dose of BL and OEO. The viability of fibroblasts showed no significant change between control and treated groups (**Figure 6E**). Besides, fibroblasts were co-cultured with *Pa* ATCC19660 or *Pa* HS0065 and treated with the lethal dose of BL and OEO as above. Most fibroblasts remained viable, evidenced by positive staining of a vital dye calcein-AM and only background levels of PI$^+$ cells observed. On the contrary, bacteria were stained chiefly with PI, indicating selective inactivation of bacteria by the combined therapy (**Figures 6F,G**). The safety was also verified *in vivo*, as manifested by full preservation of dermal tissue structural integrity after irradiation with 150 J/cm^2 BL in the presence of OEO at 50 mg/ml (BL + OEO) daily for 3 consecutive days (**Figure 7A**). The doses of BL and OEO were higher than those lethal doses used in the bactericidal assay. Despite a high level of ROS production, we detected no DNA damage or apoptotic cells in the treated tissues, revealed by the TUNEL assay that detected broken DNA or apoptotic cells, consistent with ROS generation primarily within bacteria (**Figure 7B**). The structure of the liver and kidney remained completely intact (**Figure 7C**) in the treated group indistinguishable from controls. The index of ALT/AST/ALP and BUN/Cr showed no significant difference between treated and control mice (**Figure 7D**), in agreement with the histological results (**Figures 7A,C**). In conclusion, the combined therapy shows harmless to fibroblasts and skin tissues.

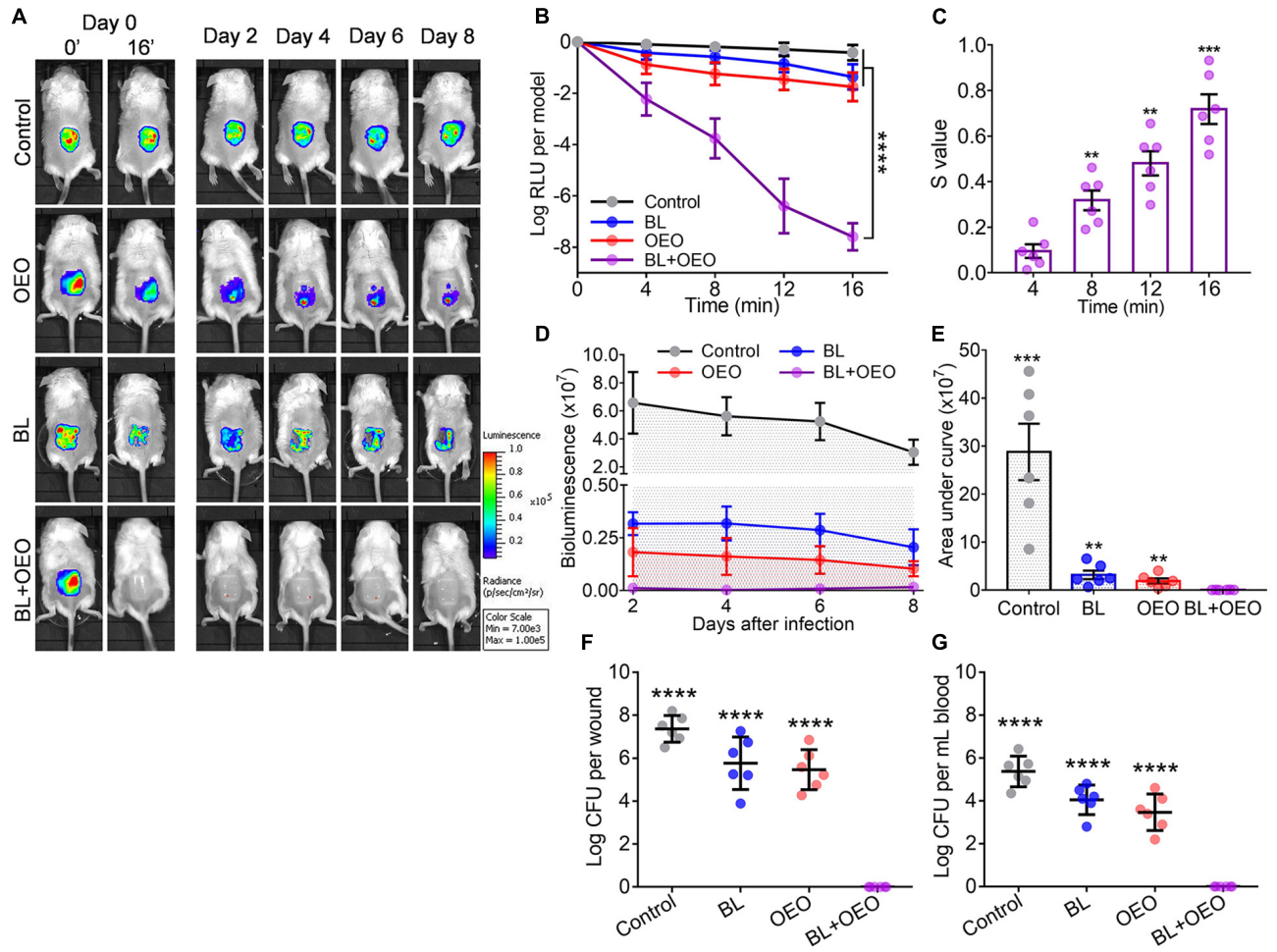

FIGURE 4 | Efficacies of BL plus OEO in the local treatment of burn wounds acutely infected with *Pa* ATCC19660. Murine third-degree burns were acutely infected with 6.5 log CFU of bioluminescent *Pa* ATCC19660 in 50 μl for 30 min. The wounds were subjected to treatment of PBS alongside sham light (control), an indicated dose of BL, 50 μl of OEO at 10 mg/ml, or both. **(A)** Luminescent images of the representative wounds were obtained at specific times. **(B)** Averaged logarithmic relative luminescence units (log RLU) were attained to define the bactericidal efficacy of various treatments. **(C)** Synergistic degrees between BL and OEO were assessed as **Figure 2**. **(D)** Mean bacterial luminescence of murine burns were real-time recorded at days 2, 4, 6, and 8 after the aforementioned treatments. **(E)** Average areas under the bacterial luminescent curve are shown in **(D)**, which encompasses an entire bacterial load over an 8-day infectious period. **(F,G)** The bacterial load was examined on wound **(F)** and in blood **(G)** on day 8 of the infection. The minimal detection of the infection is 40 CFU on the wound and 20 CFU/ml in blood. Data are presented as mean ± *SD* of six biological replicates. ****$p < 0.0001$; ***$p < 0.001$; and **$p < 0.01$.

DISCUSSION

Open wound infections of *Pa* can lead to bacterial bloodstream infections, bacteremia, and septicemia (Pont et al., 2020), in association with a high death rate. Should the infection not be kept under check in a timely fashion, the fatality rate can be as high as 45% (Aydın et al., 2018). BL combined with OEO may be a vital alternative to control open wound infections effectively and quickly as it disinfects the wound in < 10 min or about 30 min for biofilms. The modality can be used repeatedly without resistant development. The alternative may be particularly valuable for chronic wound infections. In this regard, patients with chronic, open wounds usually receive a significantly high number of antibiotics, both topically and systemically, and require prolonged hospital stay or frequent doctor visits, during which the patients can acquire additional MDR microbial infections, making even more difficult to treat. Moreover, the MDR bacteria are freely open to the atmosphere and readily spread in the healthcare setting, which presents a great risk to vulnerable patients (such as immunocompromised) in the hospitals. It is thus essential to quickly and efficaciously eliminate bacteria on the wound surface so that nosocomial infections can be minimized, and sepsis prevented in a timely fashion. Apparently, the combined therapy presented in this study represents such a long sought-after approach.

Essential oils are volatile, natural, and fragrant liquids that are extracted from leaves and flowers. More and more these essential oils are found able to kill microbes including MDR ones, such as mustard, thyme, oregano, Chinese cinnamon, etc. Cooperation between two of essential oils were also reported

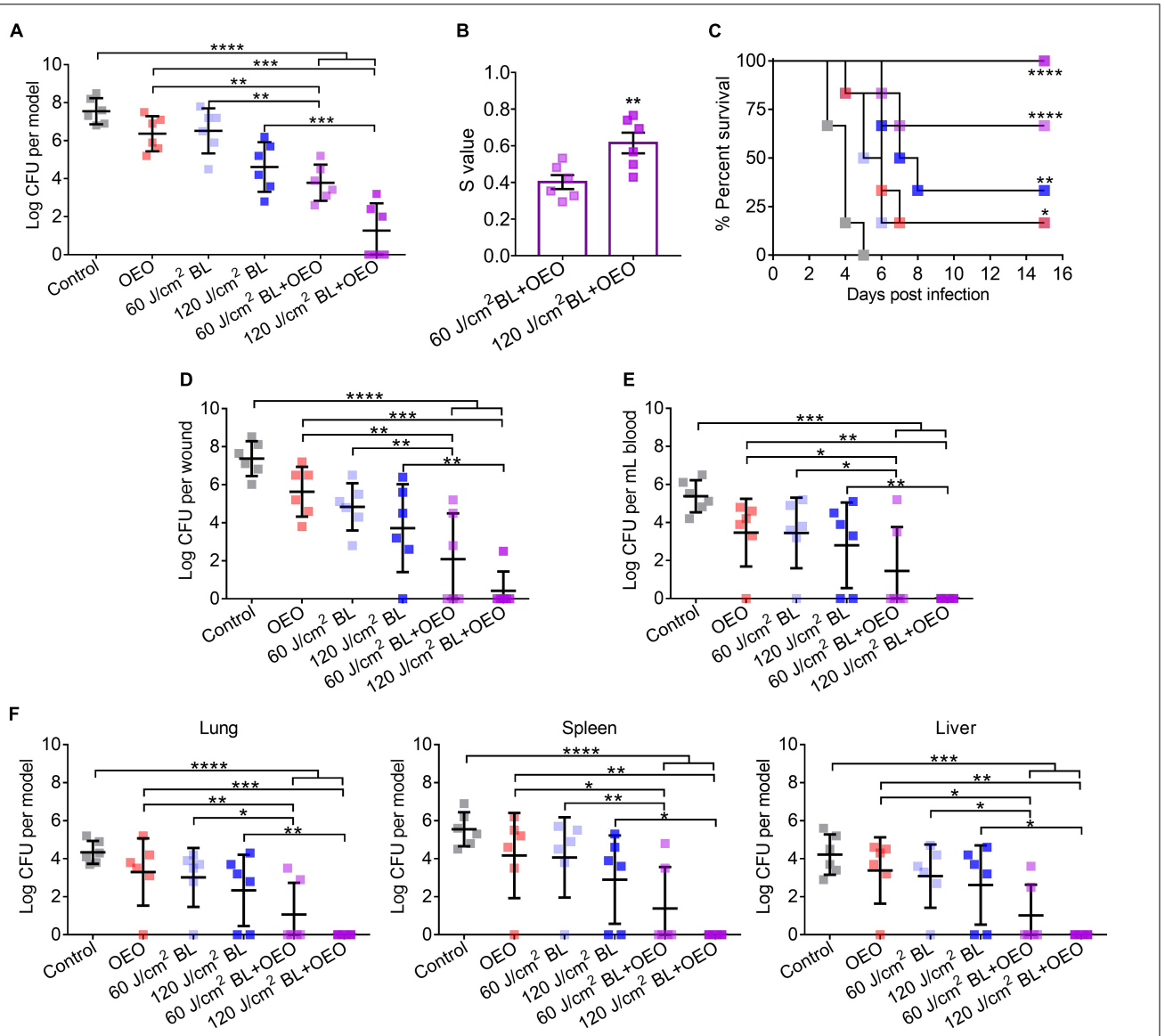

FIGURE 5 | Efficacies of BL and OEO in prevention of fatal biofilm-associated burn infections. The third-degree burns were infected with 7.5 log CFU of *Pa* HS0065. Three days after the infection, the wounds were exposed to sham (control), 50 μl of OEO at 20 mg/ml alone, BL alone at a dose of 60 or 120 J/cm^2, or both, respectively. **(A)** The infection was treated by indicated treatments. **(B)** Synergistic degrees between BL (60 or 120 J/cm^2) and OEO for biofilm damage were established as **Figure 2**. **(C)** Kaplan–Meier survival curves of biofilm-associated infection following various treatments. **(D–F)** Mice were sacrificed on day 15 after treatments to determine the bacterial loads on wounds **(D)** and in blood **(E)**. In addition, bacterial burdens in the vital organs of the lung, spleen, and liver were quantified after dissection and homogenate **(F)**. Data are expressed as mean ± *SD* from six biological replicates. Detection limitations are 40 CFU for wounds or organs and 20 CFU/ml for blood. ****$p < 0.0001$; ***$p < 0.001$; **$p < 0.01$; *$p < 0.05$.

to additively kill bacteria (Ji et al., 2021). However, bactericidal efficacies of these EOs are controversial, mainly because the amount of active ingredients in individual EOs varies with subspecies of the plant/herbs and/or various non-standardized procedures for refinement and fractional distillation of the EOs, giving rise to varying sometime contradict effects. For instance, OEO prepared from *Origanum vulgare* subspecies *hirtum* plants consists of more than 90% of carvacrol, while OEO prepared from *Origanum majorana* contains only 40–50% carvacrol (Daferera et al., 2000; Kokkini et al., 2003; Misharina et al., 2003). The finding that carvacrol and thymol are the major ingredients responsible for the bactericidal activity of OEO, and its synergy with BL offers a unique opportunity to standardize OEO products for their antimicrobial potentials in the basis of the amount of carvacrol and thymol and may also help to identify other EOs for their ability to treat infections. In addition to OEO, carvacrol is also present in the EOs prepared from thyme, pepperwort, and wild bergamot at a concentration ranging from 5 and 75% depending on the plant species and where the plants are grown (De Vincenzi et al., 2004).

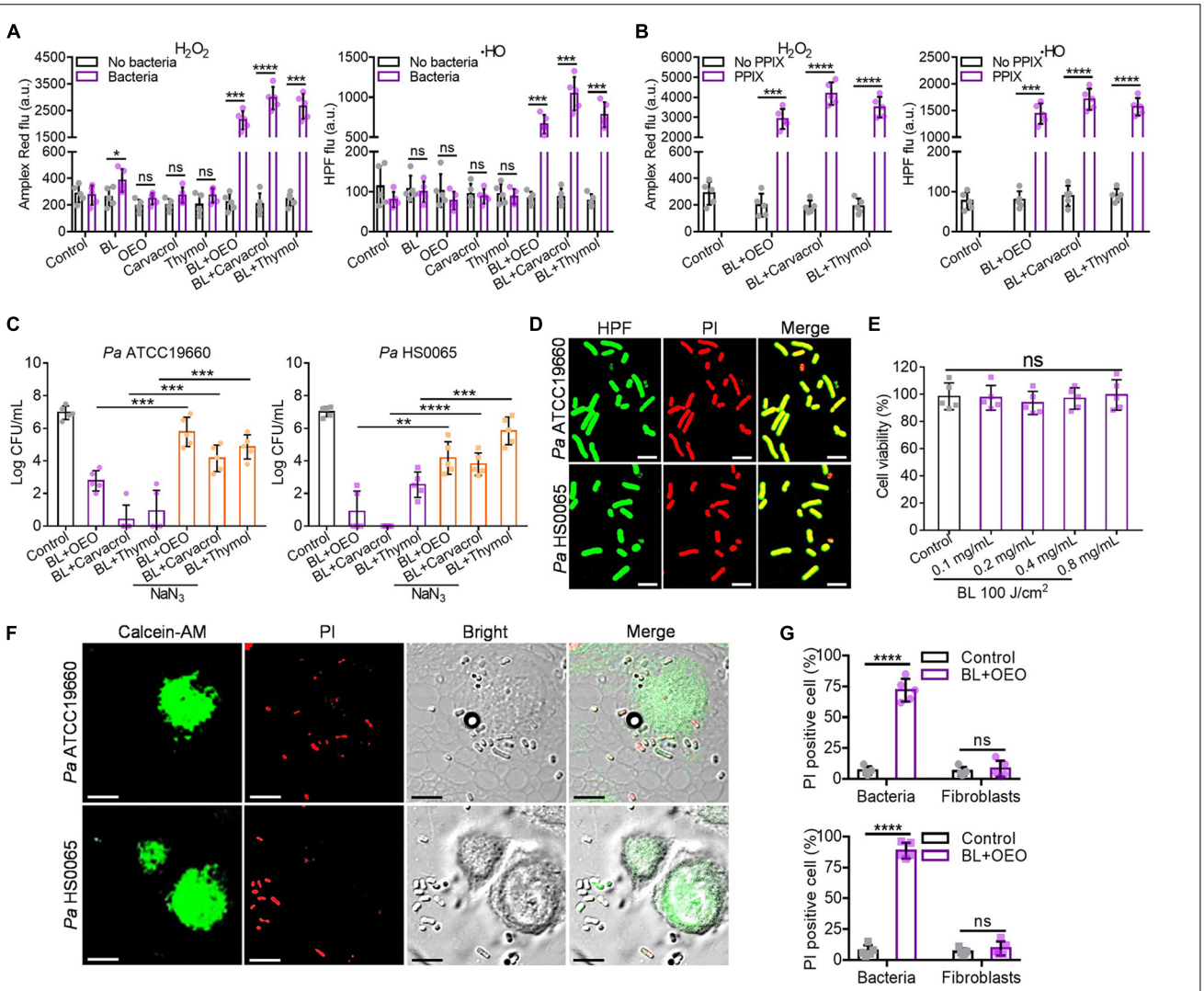

FIGURE 6 | Intracellular ROS are generated specifically in bacteria and play an essential role for the bactericidal action. **(A)** The yields of H_2O_2 and HO in the absence or presence of *Pa* HS0065 after corresponding treatments. The dose of OEO, carvacrol, or thymol was the same each at 0.1 mg/ml, and BL was 30 J/cm^2. **(B)** The generations of H_2O_2 and ·HO in the absence or presence of 10 μM PPIX under similar treatments as **(A)**. **(C)** Antibacterial efficacy of a combination of BL with OEO, carvacrol, or thymol in a compound dose and fluence as **(A)** against *Pa* ATCC19660 (left) and *Pa* HS0065 (right) in the absence or presence of 10 μM NaN_3. **(D)** Fluorescence images of *Pa* ATCC19660 and *Pa* HS0065 treated with a duo therapy: 60 J/cm^2 BL and 0.4 mg/ml OEO for *Pa* ATCC19660 and 30 J/cm^2 BL and 0.4 mg/ml OEO for *Pa* HS0065. **(E)** The viability of fibroblasts treated by different concentrations of OEO along with 100 J/cm^2 BL was analyzed by CCK-8 test. **(F)** Fluorescence images of *Pa* ATCC 19660 and *Pa* HS0065 co-cultured with fibroblasts and treated with 50 J/cm^2 BL and 0.6 mg/ml OEO. PI$^+$ cells (red) were dead cells, and calcein-AM$^+$ (green) cells were alive cells. Scale bars, 10 μm. **(G)** Co-cultures of PI$^+$ bacteria and fibroblasts were counted manually and converted to percentages relative to a total number of the cells. All data are presented as mean ± *SD* of five biological replicates. **(D,F)** Represent as five independent experiments. ****$p < 0.0001$; ***$p < 0.001$; **$p < 0.01$. ns, no significance.

The study unravels for the first time that OEO and BL can synergistically eradicate *Pa* owing to the pro-photosensitive characteristics of carvacrol and thymol. Our early investigation showed that BL excited endogenous porphyrins-like molecules, generating singlet oxygen ($^1O_2$) and the superoxide anion radical (O_2^-). The $^1O_2$ and/or O_2^- consequently oxidizes carvacrol and thymol into thymoquinone and thymohydroquinone via endoperoxide (Lu et al., 2021a,b). Thymoquinone and, to a lesser extent, thymohydroquinone act as a photosensitizer generating abundant O_2^- and $^1O_2$ that in turn oxidize additional carvacrol and thymol, forming more thymoquinone and thymohydroquinone. Thymohydroquinone can be also photo-oxidized into thymoquinone, which is then photo-hydrolyzed into thymohydroquinone while producing H_2O_2 and ·OH as long as BL is present. These two auto autoxidation cycles are likely to be the underlying mechanism for the synergy between OEO and BL, resembling that of BL plus carvacrol or thymol previously demonstrated (Lu et al., 2021a,b). It is worthwhile to mention that OEO, carvacrol, and thymol are not photosensitizers themselves as they cannot be excited by BL, producing little ROS irrespective

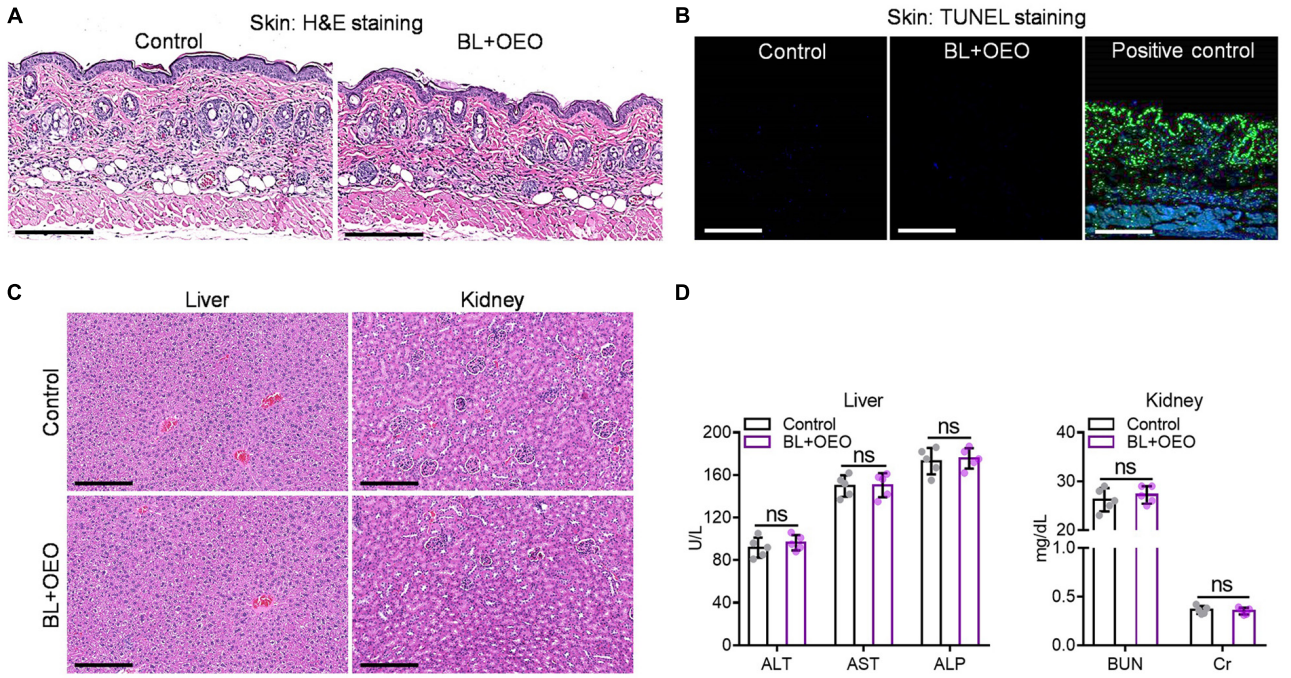

FIGURE 7 | The toxicity of combined BL and OEO *in vivo*. H&E histological examination **(A)** and TUNEL assay **(B)** of the dorsal skin with or without the duo therapy. The dorsal skin was exposed locally to PBS plus sham light (control) or 150 J/cm^2 BL plus 50 μl of OEO at 50 mg/ml (BL + OEO) daily for 3 consecutive days followed next day by skin biopsy for pathological examinations. Some skin sections were also DNase I treated prior to TUNEL staining as positive control in **(B)**. H&E histological examination **(C)** and related index detections **(D)** of liver and kidney functions from the mice. All data are presented as mean ± *SD* of five biological replicates. Images in **(A–D)** represent as five independent experiments. ns, no significance.

of BL's presence. However, carvacrol, thymol, and OEO function as non-toxic "pro-photosensitizers" that are activated exclusively in bacteria upon BL stimulation (Lu et al., 2021a,b). The super safe profiles of these bacteria-specific pro-photosensitizers are in sharp contrast to conventional photosensitizers used in photodynamic therapy (PDT), wherein the photosensitizers can enter both mammalian cells and bacteria and generate ROS within in response to a specific light, with relatively narrow selectivity.

BL has been broadly employed to treat jaundice in newborns for four decades or acne vulgaris for a decade worldwide (Liebmann et al., 2010; Dai et al., 2012). In contrast to UV, it does not directly interact with DNA and has little risk of carcinogenesis (Liebmann et al., 2010; Dai et al., 2012). It is very safe as long as it does not generate significant heat. We found that the skin temperature remained unaltered up to 200 J/cm^2 BL exposure and increased 3–5°C after treatment with 300 J/cm^2. Within the safety range (< 200 J/cm^2), BL at 405 nm alone has been shown able to sufficiently treat wound infections caused by a number of MDR microbes (Dai et al., 2013a,b; Zhang et al., 2014, 2016; Wang et al., 2016, 2017). The antimicrobial activity of BL relies on the level of non-metallated tetrapyrrole macrocycle production in microbes (Hamblin et al., 2005; Dai et al., 2013a). About 70% of bacterial pathogens generate these porphyrins-like molecules at much higher levels (10–100 ×) than mammalian cells, permitting selective killing of pathogens over mammalian cells (Zhang et al., 2014; Wang et al., 2016, 2017). Another limit of the modality is associated with BL poor tissue penetration, and it is effective mainly on the management of body surface infections.

CONCLUSION

In light of a widespread use of OEO for various medical remedy worldwide, this research expands the potential of OEO to disinfection of open wounds or skin infections by its combination with BL. Conceivably, OEO may be combined with sunlight to disinfect the chronic, open wounds in low-income regions, since the intensity of the light used is so low that can be readily obtained *via* sunlight that emits > 50 mW/cm^2 at a midday of a sunny day or *via* a longer exposure time in a less sunny day. Apart from sunlight, BL LED source is very cheap and can be fabricated as low as one dollar for disinfection. The combined modality is applicable at home to control infections preventing sepsis, which can potentially save many lives in underdeveloped countries.

DATA AVAILABILITY STATEMENT

The original contributions presented in the study are included in the article/supplementary material, further inquiries can be directed to the corresponding author/s.

ETHICS STATEMENT

The animal study was reviewed and approved by Shanghai Jiao Tong University Animal Study Committee.

AUTHOR CONTRIBUTIONS

ML, KW, XL, FW, LW, and SW designed and did all experiments, analyzed the data, and wrote the manuscript. MW supervised the study, analyzed the data, and wrote the manuscript. All authors have read and agreed to the published version of the manuscript.

FUNDING

This work was funded by the National Natural Science Foundation of China (82002188) to ML and the Defense/Air Force Office of Scientific Research Military Photomedicine Program (FA9550-17-1-0277 and FA9550-20-1-0063) to MW.

ACKNOWLEDGMENTS

We thank Prof. Fupin Hu at Huashan Hospital in Shanghai, China, for providing the clinical isolate of *Pa* HS0065.

REFERENCES

Aydın, M., Ergönül, Ö, Azap, A., Bilgin, H., Aydın, G., Çavuş, S. A., et al. (2018). Rapid emergence of colistin resistance and its impact on fatality among healthcare-associated infections. *J. Hosp. Infect.* 98, 260–263. doi: 10.1016/j.jhin.2017.11.014

Bassetti, M., Vena, A., Croxatto, A., Righi, E., and Guery, B. (2018). How to manage *Pseudomonas aeruginosa* infections. *Drugs Context* 7:212527.

Courtney, C. M., Goodman, S. M., Nagy, T. A., Levy, M., Bhusal, P., Madinger, N. E., et al. (2017). Potentiating antibiotics in drug-resistant clinical isolates via stimuli-activated superoxide generation. *Sci. Adv.* 3, 1–10. doi: 10.1126/sciadv.1701776

Daferera, D. J., Ziogas, B. N., and Polissiou, M. G. (2000). GC-MS of Essential oils from some greek aromatic plants and their fungitoxicity on *Penicillium digitatum*. *J. Agric. Food Chem.* 48, 2576–2581. doi: 10.1021/jf990835x

Dai, T., Gupta, A., Huang, Y. Y., Sherwood, M. E., Murray, C. K., Vrahas, M. S., et al. (2013a). Blue light eliminates community-acquired methicillin-resistant *Staphylococcus aureus* in infected mouse skin abrasions. *Photomed. Laser Surg.* 31, 531–538. doi: 10.1089/pho.2012.3365

Dai, T., Gupta, A., Huang, Y. Y., Yin, R., Murray, C. K., Vrahas, M. S., et al. (2013b). Blue light rescues mice from potentially fatal *Pseudomonas aeruginosa* burn infection: efficacy, safety, and mechanism of action. *Antimicrob. Agents Chemother.* 57, 1238–1245. doi: 10.1128/AAC.01652-12

Dai, T., Gupta, A., Murray, C. K., Vrahas, M. S., Tegos, G. P., and Hamblin, M. R. (2012). Blue light for infectious diseases: *Propionibacterium acnes*, *Helicobacter* pylori, and beyond? *Drug Resist. Updat.* 15, 223–236.

de Breij, A., Riool, M., Cordfunke, R. A., Malanovic, N., de Boer, L., Koning, R. I., et al. (2018). The antimicrobial peptide SAAP-148 combats drug-resistant bacteria and biofilms. *Sci. Transl. Med.* 10:eaan4044.

De Vincenzi, M., Stammati, A., De Vincenzi, A., and Silano, M. (2004). Constituents of aromatic plants: carvacrol. *Fitoterapia* 75, 801–804. doi: 10.1016/j.fitote.2004.05.002

El Zowalaty, M. E., Al Thani, A. A., Webster, T. J., El Zowalaty, A. E., Schweizer, H. P., Nasrallah, G. K., et al. (2015). *Pseudomonas aeruginosa*: arsenal of resistance mechanisms, decades of changing resistance profiles, and future antimicrobial therapies. *Future Microbiol.* 10, 1683–1706. doi: 10.2217/fmb.15.48

Hamblin, M. R., Viveiros, J., Yang, C., Ahmadi, A., Ganz, R. A., and Tolkoff, M. J. (2005). *Helicobacter* pylori accumulates photoactive porphyrins and is killed by visible light. *Antimicrob. Agents Chemother.* 49, 2822–2827. doi: 10.1128/AAC.49.7.2822-2827.2005

Jett, B. D., Fau, H. K. L., Fau, H. M. M., and Gilmore, M. S. (1997). Simplified agar plate method for quantifying viable bacteria. *Biotechniques* 23, 648–650. doi: 10.2144/97234bm22

Ji, J., Shankar, S., Fernandez, J., Juillet, E., Salmieri, S., and Lacroix, M. (2021). A rapid way of formulation development revealing potential synergic effects on numerous antimicrobial combinations against foodborne pathogens. *Microb. Pathog.* 158:105047. doi: 10.1016/j.micpath.2021.105047

Kokkini, S., Karousou, R., and Hanlidou, E. (2003). "HERBS | herbs of the labiatae," in *Encyclopedia of Food Sciences and Nutrition*, Second Edn, ed. B. Caballero (Oxford: Academic Press), 3082–3090. doi: 10.1016/b0-12-227055-x/00593-9

Leeb, M. (2004). Antibiotics: a shot in the arm. *Nature* 431, 892–893.

Levy, S. B., and Marshall, B. (2004). Antibacterial resistance worldwide: causes, challenges and responses. *Nat. Med.* 10, S122–S129. doi: 10.1038/nm1145

Liebmann, J., Born, M., and Kolb-Bachofen, V. (2010). Blue-light irradiation regulates proliferation and differentiation in human skin cells. *J. Invest. Dermatol.* 130, 259–269. doi: 10.1038/jid.2009.194

Lu, M., Dai, T., Murray, C. K., and Wu, M. X. (2018). Bactericidal property of oregano oil against multidrug-resistant clinical isolates. *Front. Microbiol.* 9:2329. doi: 10.3389/fmicb.2018.02329

Lu, M., Han, Z., Xu, Y., and Yao, L. (2013a). Effects of essential oils from Chinese indigenous aromatic plants on mycelial growth and morphogenesis of three phytopathogens. *Flavour Frag. J.* 28, 84–92. doi: 10.1002/ffj.3132

Lu, M., Han, Z., Xu, Y., and Yao, L. (2013b). In vitro and in vivo anti-tobacco mosaic virus activities of essential oils and individual compounds. *J. Microbiol. Biotechnol.* 23, 771–778. doi: 10.4014/jmb.1210.10078

Lu, M., Han, Z., and Yao, L. (2013c). In vitro and in vivo antimicrobial efficacy of essential oils and individual compounds against Phytophthora parasitica var. nicotianae. *J. Appl. Microbiol.* 115, 187–198. doi: 10.1111/jam.12208

Lu, M., Li, Y., and Wu, M. X. (2021a). Bacteria-specific pro-photosensitizer kills multidrug-resistant *Staphylococcus aureus* and *Pseudomonas aeruginosa*. *Commun. Biol.* 4:408. doi: 10.1038/s42003-021-01956-y

Lu, M., Wang, S., Wang, T., Hu, S., Bhayana, B., Ishii, M., et al. (2021b). Bacteria-specific phototoxic reactions triggered by blue light and phytochemical carvacrol. *Sci. Transl. Med.* 13:eaba3571. doi: 10.1126/scitranslmed.aba3571

Misharina, T. A., Polshkov, A. N., Ruchkina, E. L., and Medvedeva, I. B. (2003). Changes in the composition of the essential oil of marjoram during storage. *Appl. Biochem. Microbiol.* 39, 311–316.

Morones-Ramirez, J. R., Winkler, J. A., Spina, C. S., and Collins, J. J. (2013). Silver enhances antibiotic activity against gram-negative bacteria. *Sci. Transl. Med.* 5, 1–12. doi: 10.1126/scitranslmed.3006276

Obolski, U., Stein, G. Y., and Hadany, L. (2015). Antibiotic restriction might facilitate the emergence of multi-drug resistance. *PLoS Comput. Biol.* 11:e1004340. doi: 10.1371/journal.pcbi.1004340

Pandey, A. K., Kumar, P., Singh, P., Tripathi, N. N., and Bajpai, V. K. (2017). Essential oils: sources of antimicrobials and food preservatives. *Front. Microbiol.* 16:2161. doi: 10.3389/fmicb.2016.02161

Pont, S., Fraikin, N., Caspar, Y., Van Melderen, L., Attrée, I., and Cretin, F. (2020). Bacterial behavior in human blood reveals complement evaders with some persister-like features. *PLoS Pathog.* 16:e1008893. doi: 10.1371/journal.ppat.1008893

Surdel, M. C., Horvath, D. J. Jr., Lojek, L. J., Fullen, A. R., Simpson, J., Dutter, B. F., et al. (2017). Antibacterial photosensitization through activation of coproporphyrinogen oxidase. *Proc. Natl Acad. Sci. U.S.A.* 114, 6652–6659. doi: 10.1073/pnas.1700469114

Wang, Y., Ferrer-Espada, R., Baglo, Y., Goh, X. S., Held, K. D., Grad, Y. H., et al. (2019). Photoinactivation of *Neisseria gonorrhoeae*: a paradigm-changing approach for combating antibiotic-resistant gonococcal infection. *J. Infect. Dis.* 220, 873–881. doi: 10.1093/infdis/jiz018

Wang, Y., Wang, Y., Wang, Y., Murray, C. K., Hamblin, M. R., Hooper, D. C., et al. (2017). Antimicrobial blue light inactivation of pathogenic microbes: state of the art. *Drug Resist. Updat.* 33-35, 1–22. doi: 10.1016/j.drup.2017.10.002

Wang, Y., Wu, X., Chen, J., Amin, R., Lu, M., Bhayana, B., et al. (2016). Antimicrobial blue light inactivation of Gram-negative pathogens in biofilms: in vitro and in vivo studies. *J. Infect. Dis.* 213, 1380–1387. doi: 10.1093/infdis/jiw070

Zhang, Y., Zhu, Y., Chen, J., Wang, Y., Sherwood, M. E., Murray, C. K., et al. (2016). Antimicrobial blue light inactivation of *Candida albicans*: in vitro and in vivo studies. *Virulence* 7, 536–545.

Zhang, Y., Zhu, Y., Gupta, A., Huang, Y., Murray, C. K., Vrahas, M. S., et al. (2014). Antimicrobial blue light therapy for multidrug-resistant *Acinetobacter baumannii* infection in a mouse burn model: implications for prophylaxis and treatment of combat-related wound infections. *J. Infect. Dis.* 209, 1963–1971. doi: 10.1093/infdis/jit842

Zhao, B., Summers, F. A., and Mason, R. P. (2012). Photooxidation of Amplex Red to resorufin: implications of exposing the Amplex Red assay to light. *Free Radic. Biol. Med.* 53, 1080–1087. doi: 10.1016/j.freeradbiomed.2012.06.034

Conflict of Interest: The authors declare that the research was conducted in the absence of any commercial or financial relationships that could be construed as a potential conflict of interest.

Publisher's Note: All claims expressed in this article are solely those of the authors and do not necessarily represent those of their affiliated organizations, or those of the publisher, the editors and the reviewers. Any product that may be evaluated in this article, or claim that may be made by its manufacturer, is not guaranteed or endorsed by the publisher.

frontiers in Microbiology

ORIGINAL RESEARCH
published: 18 March 2022
doi: 10.3389/fmicb.2022.743213

Dihydropyrimidinones Against Multiresistant Bacteria

Marisa Castro Jara[1,2], Allison Carlos Assunção Silva[3], Marina Ritter[3], Adriana Fernandes da Silva[4], Carolina Lambrecht Gonçalves[2], Pedro Rassier dos Santos[2], Luciano Sisconetto Borja[3], Cláudio Martin Pereira de Pereira[3] and Patrícia da Silva Nascente[1,2]*

[1]Postgraduate Program in Biochemistry and Bioprospecting, Federal University of Pelotas, Pelotas, Brazil, [2]Department of Microbiology and Parasitology, Institute of Biology, Federal University of Pelotas, Pelotas, Brazil, [3]Lipidomics and Bioorganics Laboratory, Center for Chemical, Pharmaceutical and Food Sciences, Federal University of Pelotas, Pelotas, Brazil, [4]Cell Culture and Molecular Biology Laboratory, Federal University of Pelotas, Pelotas, Brazil

The increase in bacterial resistance to antimicrobials has led to high morbidity and mortality rates, posing a major public health problem, requiring the discovery of novel antimicrobial substances. The biological samples were identified as the Gram-negative bacilli *Acinetobacter baumannii*, *Escherichia coli*, *Enterobacter cloacae*, *Klebsiella pneumoniae*, *Morganella morgannii*, *Pseudomonas aeruginosa* and *Serratia marcescens* and the Gram-positive cocci *Enterococcus faecium*, and *Staphylococcus aureus*, all of them resistant to at least three classes of antimicrobials. The antibacterial activity of the compounds was checked *in vitro* by determining the minimum inhibitory concentration (MIC) and minimum bactericidal concentration (MBC) by the broth microdilution method and plating in brain heart infusion (BHI) agar, respectively. The chemical characterization of the compounds was performed by measuring the melting point and gas chromatography coupled with mass spectrometry (GC–MS) on a Shimadzu GC–MS-QP system 2010SE. Synthetic compounds showed antimicrobial activity against Gram-positive cocci at MIC concentrations 0.16–80 μg/ml and Gram-negative bacilli at MIC concentrations 23.2–80 μg/ml. *Enterococcus faecium* and *S. aureus* had the best MIC values. The results of the cytotoxicity test indicated that the synthetic compounds showed no significant difference in three concentrations tested (5, 20, and 80 μg/ml), allowing cell viability not different from that assigned to the control, without the tested compounds. In this context, the development of DHPM derivatives brings an alternative and perspective on effectiveness of drugs as potential future antimicrobial agents.

Keywords: antibacterial activity, biginelli compounds, cytotoxicity, DHPM, dihydropyrimidinones, hospital infection

OPEN ACCESS

Edited by:
Wang Jiajun,
Northeast Agricultural University, China

Reviewed by:
Bahman Mirzaei,
Zanjan University of Medical Sciences, Iran
Leticia Barrientos,
University of La Frontera, Chile

****Correspondence:***
Marisa Castro Jara
jaramarisa@hotmail.com

Specialty section:
This article was submitted to Antimicrobials, Resistance and Chemotherapy, a section of the journal Frontiers in Microbiology

Received: *17 July 2021*
Accepted: *14 February 2022*
Published: *18 March 2022*

Citation:
Castro Jara M, Assunção Silva AC, Ritter M, Fernandes da Silva A, Lambrecht Gonçalves C, Rassier dos Santos P, Sisconetto Borja L, Martin Pereira de Pereira C and da Silva Nascente P (2022) Dihydropyrimidinones Against Multiresistant Bacteria. Front. Microbiol. 13:743213. doi: 10.3389/fmicb.2022.743213

INTRODUCTION

Bacterial multidrug resistance is a serious and rapidly growing threat worldwide, leading to high morbidity and mortality rates (Tegos and Hamblin, 2014; Esposito and De Simone, 2017). Combating the advance of bacterial resistance to current antimicrobials should be a global priority.

It is estimated that in 2050, antimicrobial resistance will become one of the leading causes of death (Leung et al., 2011; O'Neill, 2016). It is thus crucial to discover new antimicrobials (Tacconelli et al., 2018).

This has increased the scientific interest in bioactive nitrogen-containing heterocyclic substances such as 3,4-dihydropyrimidin-2 (1H)-ones, or just dihydropyrimidinones (DHPMs). These compounds were first synthesized by the Italian chemist Pietro Biginelli in 1893 (Godoi et al., 2005; Mansouri et al., 2012; Venugopala et al., 2016). A pyrimidine ring integrates the molecular composition of various alkaloids (Prasad et al., 2016) and numerous nucleic acids (Kappe, 2000; Sharma et al., 2014).

There are reports of several pharmacological activities of analogues and derivatives of DHPMs, such as antitumor, antiviral, anti-inflammatory, antidepressant, antimalarial and anticancer (Ramachandran et al., 2016), antioxidant, antibacterial (Stefani et al., 2006; de Vasconcelos et al., 2012; Niemirowicz-Laskowska et al., 2018), insecticidal and larvicidal (Venugopala et al., 2016), and calcium channel modulation (Kappe, 2000; Fathima et al., 2013). Recent studies indicate effective action of pyrimidine analogs in the treatment of diabetes, by reducing the enzyme α-glucosidase and delaying the absorption of glucose (Bekircan et al., 2015; Peytam et al., 2021).

This present study evaluated *in vitro* the antimicrobial activity of three DHPM analogues against multiple drug resistant isolates from hospital patients.

MATERIALS AND METHODS

General Procedure for the Synthesis of Compounds (4a–c)

The DHPMs were obtained in the Laboratory of Lipidomics and Bioorganics of Federal University of Pelotas, located in the state of Rio Grande do Sul, Brazil. The desired compounds were synthesized by mixing ethyl acetoacetate (1; 5 mmol), the appropriate aldehyde (2a–c; 5 mmoL), urea (3; 8 mmol), and citric acid (5 mmol) in 10 ml of absolute ethanol. The mixture was stirred under reflux for 4 h, according to de Vasconcelos et al. (2012), and the reaction's progress was monitored by thin-layer chromatography (TLC) and gas chromatography (GC). The organic phase was extracted with ethyl acetate (2 × 10 ml), washed with cold water (2 × 20 ml), and dried with magnesium sulfate, and the solvent was removed under reduced pressure. The product obtained was purified by recrystallization with hexane and ethanol (**Figure 1**).

The chemical characterization of the compounds was performed by melting point measurement and gas chromatography coupled to mass spectrometry (GC–MS) in a Shimadzu GC–MS-QP 2010SE system.

Multidrug-Resistant Bacterial Isolates

The bacterial isolates were provided by two hospitals in the city of Pelotas (here called Hospital A and Hospital B), collected from patients admitted between October 2018 and January 2019, consisting of samples of lung tissue, body fluids, skin, blood, and urine. The bacteria were previously identified as to species, and their resistance profiles were determined with the bioMerrieux VITEK 2 (Hospital A) and BD Phoenix (Hospital B) systems, according to the recommendations of the Clinical and Laboratory Standards Institute (CLSI), 2012. The effectiveness of DHPM was tested against three multi-resistant bacteria of each species, selected from the study by Jara et al. (2021).

Three previously identified isolates of each bacterial species were evaluated, namely seven Gram-negative bacilli (GNB): *Acinetobacter baumannii*, *Escherichia coli*, *Enterobacter cloacae*, *Klebsiella pneumoniae*, *Morganella morgannii*, *Pseudomonas aeruginosa* and *Serratia marcescens*; and two Gram-positive cocci (GPC): *E. faecium* and *S. aureus*, all of which showed resistance to at least three classes of antimicrobials. The bacterial resistance was tested previously by the hospitals against the following classes and antimicrobials: aminoglycosides (amikacin, gentamicin, and streptomycin); association with β-lactamase inhibitors (ampicillin/sulbactam, ampicillin/clavulanic acid, and piperacillin/tazobactam); carbapenems (ertapenem, imipenem, and meropenem); cephalosporins (cephalin, cefoxitin, cefuroxime, ceftriaxone, cefepime, cefotaxime, cefazolin, ceftazidime, and ceftaroline); glucopeptides (teicoplanin and vancomycin); glycylcyclines (tigecycline); lincosamides (clindamycin); macrolides (erythromycin); nitrofurans (nitrofurantoin); oxazolidinones (linezolid); penicillins (ampicillin, penicillin, and oxacillin); polypeptides (colistin); quinolones (nalidixic acid, ciprofloxacin, levofloxacin, moxifloxacin, and norfloxacin); rifampicin (rifampicin); and tetracyclines (minocycline).

This study was approved by the university's research ethics committee under numbers 2,961,379 and 2,985,372 and by the National Ethics Committee on Research (CONEP) under number 2,880,831 (Brazilian Approval Platform). The experiments were carried out following biosafety standards and good laboratory practice (BRASIL, 2006).

Minimum Inhibitory Concentration

The minimum inhibitory concentration (MIC) assay was carried out according to the guidelines of document M07-A9 from the Clinical and Laboratory Standards Institute (CLSI), 2012. A concentration of 1,600 μg/ml was obtained by weighing 4,800 μg of the DHPMs diluted in 3 ml of P.A. dimethylsulfoxide (DMSO). Then, a 1:10 dilution [0.5 ml of the DHPM compound solution with 4.5 ml of Müller-Hinton broth (MHB)] was obtained at the final concentration of 160 μg/ml. A 96-well sterile microplate was pre-filled with 100 μl of MHB in all wells, the first column was used as a negative control (with 100 μl of MHB), the second column was added 100 μl of the test compound dilution in the concentration of 160 μg/ml, obtaining a concentration of 80 μg/ml in this well, followed by 10 microdilutions in series until the penultimate well (column 11) reaching a concentration of 0.16 μg/ml, in the latter, 100 μl was removed and discarded. The last well (column 12) was used as a positive control (MHB added to the inoculum containing the microorganism of interest). To prepare

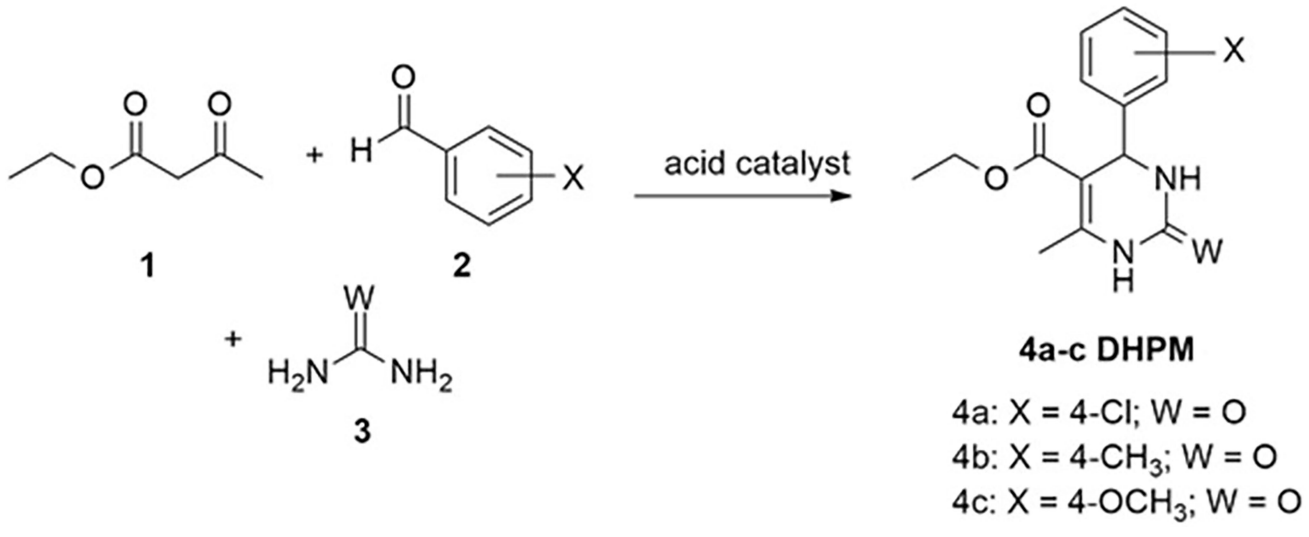

FIGURE 1 | Biginelli reaction and formation of the compounds of interest.

the inoculum solution, the microorganism was seeded on blood agar plates for 24 h prior to testing in an oven at 37°C. A small part of the colony was removed and diluted in 3 ml of saline solution, until turbidity equivalent to the MacFarland scale 0.5 (1×10^8 CFU/ml). Of this inoculum solution, 5 µl was added to each well from the second to the last well. Then, the plates were incubated at 37°C in an oven for 24 h. After this step, the MIC was evaluated by the colorimetric method with addition of 40 µl/well of the dye 2, 3, 5-triphenyltetrazolium chloride (TTC) at 0.015%. The plates were incubated in an oven at 37°C for 30 min. The visual reading involved the presence or absence of pink staining, which identified, respectively, metabolically active or inactive bacteria against the presence of the compound. The assays for each isolate were performed in duplicate and with three replicates on different dates.

Minimum Bactericidal Concentration

After reading the MIC values, a test was performed to determine the minimum bactericidal concentration (MBC), through plating in brain heart infusion (BHI) agar. Aliquots of 5 µl from the well corresponding to the positive MIC (active bacteria) and the next well were collected. After plating in BHI, the plate was incubated at 37°C for 24 h to determine whether the concentrations were bactericidal or bacteriostatic. The method consists of observing the bacterial growth of the inoculum of the active bacteria of the respective MICs; where the growth of bacterial colonies defines in compounds with bacteriostatic action and non-bacterial growth defines the bactericidal action of the DHPM test compound.

Cytotoxicity Assay

The cytotoxicity assay was performed in the Laboratory for Cell Biology and Tissue Center (NCT-BIO) of the School of Dentistry of Federal University of Pelotas. The cell viability assay was performed according to ISO 10993-5:2009 [International Organization for Standardization (ISO), 2009]. Mouse fibroblasts of the 3T3 immortalized cell line (2×10^{-4}/well) were cultured in Dulbecco's Modified Eagle Medium (DMEM) supplemented with 10% fetal bovine serum (FBS), 2% L-glutamine, penicillin (100 U/ml) and streptomycin (100 mg/ml). Cells were incubated at 37°C in a humidified atmosphere of 5% CO_2. The 3-(4,5-dimethylthiazol-2-yl)-2,5-diphenyltetrazolium bromide (MTT) assay (Sigma Chemical Company, St. Louis, MO, United States) was used to assess cell metabolic function by observing mitochondrial dehydrogenase activity.

The compounds were solubilized in DMSO and added to the DMEM medium, to obtain concentrations in the wells of 80, 20, and 5 µg/ml solubilized in 1.6% DMSO.

For evaluation of cell viability of the different DHPM analogues, the compounds diluted in 200 µl of DMEM were placed in the wells of 96-well plates containing mouse fibroblasts of the 3T3 immortalized cell line (2×10^{-4}/well). As a control, a group containing only fibroblast cells in DMEM was used. The plates were incubated for 24 h in a humidified atmosphere of 5% CO_2. After incubation, the DMEM was removed and a MTT solution was placed in each well. After 4 h of incubation at 37°C in darkness, the blue formazan precipitate was extracted from the mitochondria using 200 µl/well of DMSO in a shaker for 5 min at 150 rpm. The absorption was determined using a spectrophotometer at a wavelength of 540 nm.

Statistical Analysis

Statistical analysis of bacterial activity concentrations was obtained by the average of the samples tested. While one-way ANOVA was used to evaluate the difference between the treated groups. To confirm the significance of the differences between the concentrations of the compounds tested in relation to the control group (a group containing only fibroblast cells in DMEM), the Tukey *post hoc* test was used. The differences that presented $p < 0.05$ were considered as statistically significant.

RESULTS

Chemical Data

The synthesized DMPM compounds 4a, 4b, and 4c have the following chemical characteristics.

4a. Ethyl 4-(4-chlorophenyl)-6-methyl-2-oxo-1, 2, 3, 4-tetrahydropyrimidine-5-carboxylate. Yield 90%; melting point 215°C; temperature: 215°C (Puri et al., 2009); GC–MS m/z, (%), observed: 295.05 [M + 1] (2.48%), 294.00 (14.65%), 265.00 (68.48%), 221.00 (43.70%), 183.10 (100.00%), 155.10 (53.68%), 137.05 (45.35%), 42.10 (43.11%). C14H15ClN2O3 [M] + required: 294.00.

4b. Ethyl 6-methyl-2-oxo-4-(p-tolyl)-1, 2, 3, 4-tetrahydropyrimidine-5-carboxylate. Yield 75%; melting point 216°C; temperature: 216–217°C (Debache et al., 2008) GC–MS m/z, (%), observed: 274.10 (16.08%), 245.10 (70.02%), 201.10 (53.35%), 183.10 (100.00%), 155.05 (51.91%), 137.05 (42.42%), 91.05 (26.01%), 42.05 (33.05%). C15H18N2O3 [M] + required: 274.13.

4c. Ethyl 4-(4-methoxyphenyl)-6-methyl-2-oxo-1, 2, 3, 4-tetrahydropyrimidine-5-carboxylate. Yield 91%; melting point 205°C; temperature: 204–205°C (Ranjith et al., 2010); GC–MS m/z, (%), observed: 290.10 (20.72%), 261.05 (100.00%), 217.10 (69.51%), 183.10 (55.24%), 155.05 (39.75%), 137.10 (36.14%), 42.05 (30.29%). C15H18N2O4 [M] + required: 290.13.

Multidrug Resistant Bacterial Isolates

The bacterial isolates showed resistance to at least three classes of antibiotics, as shown by the susceptibility of the 15 classes tested (**Table 1**).

Minimum Inhibitory Concentration

DHPMs demonstrated inhibitory potential against all bacterial species tested, inhibiting the growth of at least one isolate of each species. For BGN only bacteriostatic (inhibitory) activity was observed (concentrations from 23.3 to 80 μg/ml).

The MIC values were in the range of 0.16–80 μg/ml, with the lowest values referring to GPC, reaching 0.16 μg/ml, while attaining lower inhibitory activities for all multiresistant species of GNB, with MIC values from 23.2 to 80 μg/ml. Bacteriostatic activity was observed in *E. faecium* and *S. aureus* at DHPM concentrations ranging from 80 μg/ml to 0.16 μg/ml. The MIC values observed according to each bacterial species are described in **Table 2** with the mean of the MICs.

The MIC values of the three compounds that showed simultaneous bacteriostatic activity for the same hospital bacterial isolate were submitted to ANOVA. In this analysis, only the isolate *S. aureus*[2] was sensitive to the compounds, with no statistically significant difference between the values, similar to the finding described for *E. coli*[3], which was not sensitive to any of the synthetic antimicrobials. *Morganella morganii*[3] showed a statistically significant difference in relation to compound 4c, which presented the best result for this species. For *S. marcescens*, compounds 4b and 4c showed a statistically significant difference in relation to compound 4a, so these two compounds were considered best for this species. In *E. faecium*[2], DHPM 4a, followed by compound 4b, presented the best results.

Comparison of all the MIC values for the same species with the values according to the compounds, in order to obtain a value for each species, indicated that compound 4c had a statistically significant difference in relation to the others, thus being the compound with the best activity for *M. morgannii* when compared to *A. baumannii*, *K. pneumoniae*, *M. morgannii*, *P. aeruginosa*, and *E. faecium*. The results obtained in the present study were published in patent application number BR1020200216538 (Jara et al., 2021).

Minimum Bactericidal Concentration

All DHPM analogues tested showed bactericidal activity in the GPC at concentrations that varied from 0.16 to 80 μg/ml. For GNB there was no bactericidal activity in any sample.

Toxicity of the Synthetic Compounds

The three compounds were found to be non-cytotoxic to the cell lines at the concentration tested (80 μg/ml), as shown in **Figure 1**. The three compounds presented cell viability above 80% in the three concentrations tested (**Figure 2**).

The results of the cytotoxicity test indicated that the synthetic compounds showed no significant difference at the three concentrations tested (5, 20, and 80 μg/ml), allowing cell viability not different from that attributed to the control, without the presence of the tested compounds.

LIMITATIONS

Our study had some limitations in testing the compounds with a small number of bacterial samples from each species, and it was relevant to analyze the cytotoxicity in other types of cells.

DISCUSSION

The problem of bacterial resistance to antimicrobials is multifaceted, from inappropriate drug management to a lack of investment in the discovery of new antimicrobials (Hughes and Karlén, 2014). Based on the definition by Magiorakos et al. (2012), the isolates used here are classified as multidrug-resistant, as they are resistant to three or more classes of antibiotics.

In the literature there are few reports of antibacterial activity in relation to the DHPM analogues described here, and we did not find any studies involving multidrug-resistant bacteria from hospitals. Chitra and Devanathan (2012) described analogues of DHPM with chlorine, nitrogen and fluorine at the 4-position of the aromatic aldehyde. These compounds showed *in vitro* antibacterial activity against *S. aureus*, *E. coli*, *K. pneumoniae*, *P. aeruginosa*, and *Salmonella typhi*.

Attri et al. (2017) and Medyouni et al. (2016) observed promising antibacterial activity of two of the same compounds

TABLE 1 | Bacterial susceptibility profile of each class of antimicrobials tested in two hospitals in the city of Pelotas, Brazil, 2018–2019.

Bacteria/Isolates		Classes of antimicrobials*														
		Aminoglycosides	β-Lactamase inhibitors**	Carbapenems	Cephalosporins	Glucopeptides	Glycylcyclines	Lincosamides	Macrolides	Nitrofurans	Oxazolidinones	Penicillins	Polypeptides	Quinolones	Rifampicines	Tetracyclines
Acinetobacter baumannii	1	R	R	R	R	99	88	99	99	99	99	R	S	R	99	99
Acinetobacter baumannii	2	R	R	R	R	99	S	99	99	99	99	R	S	R	99	99
Acinetobacter baumannii	3	R	R	R	R	99	I	99	99	99	99	R	S	R	99	99
Enterobacter cloacae	1	R	R	R	R	99	R	99	99	99	99	R	S	R	99	99
Enterobacter cloacae	2	S	R	R	R	99	S	99	99	99	99	R	S	R	99	99
Enterobacter cloacae	3	R	R	S	R	99	88	99	99	99	99	R	88	R	99	99
Escherichia coli	1	S	S	S	R	99	88	99	99	S	99	R	88	R	99	99
Escherichia coli	2	R	R	S	R	99	S	99	99	99	99	R	S	88	99	99
Escherichia coli	3	R	S	S	R	99	88	99	99	99	99	R	88	R	99	99
Klebsiella pneumoniae	1	S	R	R	R	99	88	99	99	R	99	R	88	R	99	99
Klebsiella pneumoniae	2	S	R	S	R	99	88	99	99	R	99	R	88	R	99	99
Klebsiella pneumoniae	3	R	R	S	R	99	88	99	99	R	99	R	88	R	99	99
Morganella morganii	1	S	R	R	R	99	R	99	99	99	99	R	R	R	99	99
Morganella morganii	2	S	R	S	R	99	R	99	99	99	99	R	R	R	99	99
Morganella morganii	3	R	S	S	R	99	88	99	99	99	99	R	88	R	99	99
Pseudomonas aeruginosa	1	S	R	R	R	99	R	99	99	99	99	R	S	S	99	99
Pseudomonas aeruginosa	2	R	R	R	R	99	88	99	99	99	99	R	88	R	99	99
Pseudomonas aeruginosa	3	R	R	R	R	99	R	99	99	99	99	R	S	R	99	99
Serratia marcescens	1	S	R	R	R	99	R	99	99	99	99	R	R	R	99	99
Serratia marcescens	2	S	R	R	R	99	R	99	99	99	99	R	R	R	99	99
Serratia marcescens	3	S	R	S	R	99	88	99	99	R	99	R	88	S	99	99
Enterococcus faecium	1	S	88	99	88	R	R	R	R	99	S	R	99	R	88	88
Enterococcus faecium	2	88	88	99	88	R	88	88	88	S	S	R	99	R	88	S
Enterococcus faecium	3	88	88	99	88	R	88	88	88	S	S	R	99	88	88	R
Staphylococcus aureus	1	R	88	99	88	R	88	R	88	88	88	R	99	R	S	88
Staphylococcus aureus	2	88	88	99	88	S	88	S	R	88	S	R	99	88	S	R
Staphylococcus aureus	3	S	88	99	8	S	S	S	S	88	S	R	99	R	S	R

*R: resistant; I: intermediate; S: sensitive; 88: not tested; 99: not applicable.

**β-Lactamase inhibitors: association with β-lactamase inhibitors.

TABLE 2 | Mean of the minimum inhibitory concentration (MIC) of DHPM against multiresistant bacteria of hospital origin.

Bacterial species	*Compounds (μg/ml)								
	4a			4b			4c		
	Number of bacterial isolates			Number of bacterial isolates			Number of bacterial isolates		
	1	2	3	1	2	3	1	2	3
A. baumannii	40.00	40.00	80.00	64.00	60.00	50.00	70.00	66.70	60.00
E. coli	80.00	-	-	60.00	80.00	-	66.70	-	-
E. cloacae	80.00	80.00	53.30	80.00	80.00	60.00	66.70	80.00	-
K. pneumoniae	80.00	60.00	80.00	70.00	73.30	80.00	60.00	80.00	80.00
M. morgannii	80.00	80.00	60.00	60.0	80.00	66.70	56.00	70.00	23.30**
P. aeruginosa	60.00	70.00	56.00	80.00	60.00	80.00	80.00	53.30	60.0
S. marcescens	66.70	70.00	60.00	30.00**	-	-	30.00**	-	73.30
E. faecium	70.00	0.16**	0.16	80.00	33.40*	20.00	60.00	80.00	0.16
S. aureus	-	0.16	-	-	0.16	-	-	0.16	-

**4a: 4-chlorophenyl; 4b: p-toluyl; 4c: 4-methoxyphenyl; (–) inconclusive MIC values.*
***Values with statistically significant differences.*

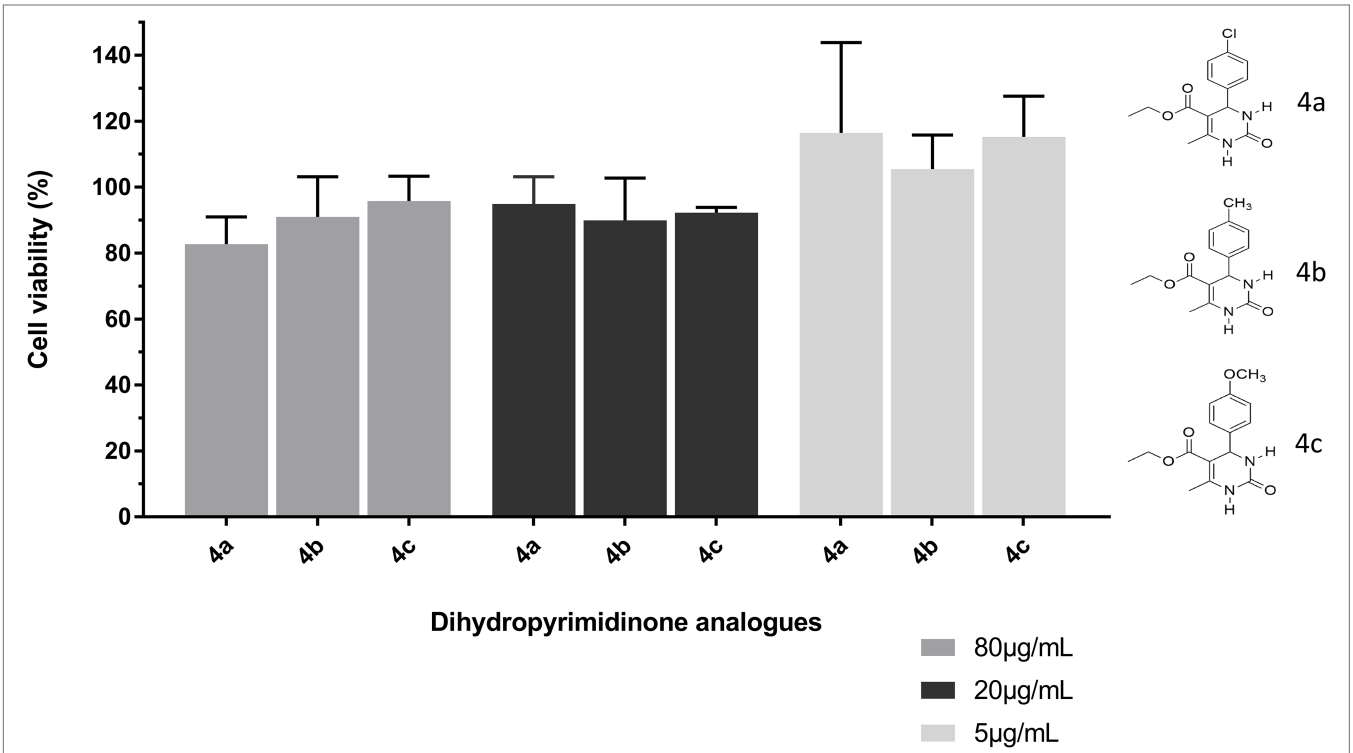

FIGURE 2 | Cytotoxicity of dihydropyrimidinone analogs 4a (4-chlorophenyl), 4b (p-toluyl), and 4c (4-methoxyphenyl) using the MTT assay. The compounds were tested at concentrations of 80, 20, and 5 μg/ml and incubated for 24 h. The cell viability/proliferation using mouse fibroblasts of the 3T3 cell line (control = negative group representing cell viability of 100%) showed no difference among the groups ($p > 0.05$).

analyzed by us (4a and 4b), but Attri et al. (2017) analyzed the compounds with the culture collection and gene bank of the Institute of Microbial Technology (Chandigarh, India) and Medyouni et al. (2016) analyzed standard bacterial strains. While in our study, we tested these compounds against multidrug-resistant hospital bacteria.

Attri et al. (2017) tested the DHPM compounds against the bacterial strains *E. coli* (MTCC 443), *S. aureus* (MTCC 3160), *P. aeruginosa* (MTCC 2581), and *K. pneumoniae* (MTCC 7028). Their results indicated that compound 4a showed inhibitory activity against all strains tested, while 4b did not show antibacterial activity against the *E. coli* and *K. pneumoniae* strains.

In our study, we used concentrations in μg/mL and Attri et al. (2017) used units in ppm, with equivalent concentrations (1 ppm = 1 μg/ml). According to Attri et al. (2017), compound 4a showed results against *E. coli* between 31.250 and 15.625 ppm, showing higher inhibitory activity in relation to our findings, which ranged from 60 to 80 ppm. (μg/ml). Regarding *S. aureus*, the authors reported moderate activity, with MICs of 62.5–125.0 ppm of compounds 4a and 4b, while the MIC was 0.155 ppm (μg/ml), indicating excellent antibacterial activity. Against *P. aeruginosa*, compounds 4a and 4b showed good antibacterial activity, with MIC values in the range of 15.625–31.250 ppm (μg/ml), while our tests of compound 4b showed 60 to 80 ppm (μg/ml), and of compound 4a resulted in 56 to 70 ppm (μg/ml). Therefore, Attri et al. (2017) obtained more promising results than our study. For compound 4a, Attri et al. (2017) reported activity against *K. pneumoniae* bacteria only with MICs of 31.25–62.50 ppm (μg/ml), while we found MICs between 60 and 80 ppm (μg/ml), Both studies showed very similar results at this point.

Medyouni et al. (2016) tested the efficacy of compound 4b *in vitro* by the plate diffusion method against standard GPC strains (*Agrobacterium tumefaciens*, *Listeria monocytogenes* ATCC 19117, *Micrococcus luteus* LB 14110 and *S. aureus* ATCC 6538), and GNB (*Salmonella Typhimurium* ATCC 14028 and *P. aeruginosa* ATCC 49189). The authors observed MIC values of 2.5 mg/ml (2,500 μg/ml) and 0.016 mg/ml (16 μg/ml) for *S. aureus* and *P. aeruginosa*. However, it is not possible to compare their results with our experimental application due to the different techniques used by those authors.

Ramachandran et al. (2016) evaluated *in silico* the antimicrobial activity of DHPM analogues and suggested that this class of compounds may be important to overcome the problem of bacterial resistance to antimicrobials.

Bacteriostatic agents include tigecycline, linezolid, macrolides, sulfonamides, tetracyclines and streptogramins, while bactericidal agents include β-lactams, glycopeptides, fluoroquinolones and aminoglycosides (Nemeth et al., 2015). Although it seems preferable for an antibiotic to kill bacteria rather than just inhibiting them, there are few reports that the clinical importance of a bactericidal action observed *in vitro* is better than a bacteriostatic action (Rhee and Gardiner, 2004). Studies suggest that combinations of bactericidal and bacteriostatic agents may lead to better clinical outcomes compared to single use. However, there are diseases such as endocarditis and meningitis where clinical experience favors the use of bactericidal agents (Finberg et al., 2004). Clindamycin and chloramphenicol are bacteriostatic antibiotics that slow bacterial growth, usually by inhibiting protein synthesis or reducing cellular respiration. As a result, the infectious agent is more easily eliminated by the immune system (Bernatová et al., 2013; Lobritz et al., 2015).

In the context of the emerging need to discover new products with antifungal and antibacterial properties, the development of DHPM derivatives is an alternative for more effective future antimicrobial agents. The results of *in vitro* antibacterial activity suggest that compounds A, B and C have potent *in vitro* antibacterial activity against multidrug-resistant hospitals bacteria. Furthermore, the cytotoxicity study revealed that all compounds did not show significant cytotoxicity against mouse fibroblast cell lines at the highest concentration evaluated, indicating the selectivity of their antimicrobial action. All three compounds showed antibacterial activity against both GNB and GPC.

Thus, it is necessary to continue research into the antimicrobial potential of these compounds, as well as to elucidate the mechanism of action attributed to them.

CONCLUSION

In the context of the emerging need to discover new products with antifungal and antibacterial properties, the development of DHPM derivatives brings an interesting alternative and perspective on the efficacy of drugs as future antimicrobial agents. The results of *in vitro* antibacterial activity suggest that compounds A, B, and C have potent *in vitro* antibacterial activity in multiresistant bacteria of hospital origin. In addition, the cytotoxicity study revealed that all compounds did not show significant cytotoxicity against mouse fibroblast cell lines at the maximal concentration assessed, indicating the selectivity of their antimicrobial action. All three compounds showed antibacterial activity in both BGN and CGP. Thus, it is necessary to invest in the continuity of research concerning these compounds.

DATA AVAILABILITY STATEMENT

The raw data supporting the conclusions of this article will be made available by the authors, without undue reservation.

AUTHOR CONTRIBUTIONS

MC conceived and designed the study and was responsible for the data curation and analysis of the experiments. MC and AA performed the statistical analysis. MR and LS wrote and reviewed different sections of the manuscript. AS was responsible for the formal analysis of the cytotoxicology section and performed the statistical analysis. CL and PS contributed to the laboratory analysis of the experiments. CM was responsible for the resources material and the synthesis and supply of compounds. PN managed the project, its resources, and validation. All authors contributed to and commented on the manuscript text and approved its final version.

FUNDING

This study was partially financed by the Coordination for the Improvement of Higher Education Personnel (CAPES – Brazil), financial code 001. PS received a grant from CAPES (no. 88887.502085/2020-00). LS received a grant from the Fundação

de Amparo à Pesquisa do Estado do Rio Grande do Sul (FAPERGS), no. 124733/2019-0. This study was also funded by the National Program for Quality Control (PNCq), no. 03/2018, and the Institutional Scientific Initiation Scholarship Program (PIBIC).

ACKNOWLEDGMENTS

The authors are grateful to Federal University of Pelotas (UFPel), CAPES, FAPERGS, PNCq, PIBIC, and National Council for Scientific and Technological Development (CNPq).

REFERENCES

Attri, P., Bhatia, R., Gaur, J., Arora, B., Gupta, A., Kumar, N., et al. (2017). Triethylammonium acetate ionic liquid assisted one-pot synthesis of dihydropyrimidinones and evaluation of their antioxidant and antibacterial activities. *Arab. J. Chem.* 10, 206–214. doi: 10.1016/j.arabjc.2014.05.007

Bekircan, O., Ülker, S., and Menteşe, E. (2015). Synthesis of some novel heterocylic compounds derived from 2-[3-(4-chlorophenyl)-5-(4-methoxybenzyl)-4H-1,2,4-triazol-4-yl]acetohydrazide and investigation of their lipase and α-glucosidase inhibition. *J. Enzyme Inhib. Med. Chem.* 30, 1002–1009. doi: 10.3109/14756366.2014.1003213. PMID: 25640970

Bernatová, S., Samek, O., Pilát, Z., Serý, M., Ježek, J., Jákl, P., et al. (2013). Following the mechanisms of bacteriostatic versus bactericidal action using raman spectroscopy. *Molecules* 18, 13188–13199. doi: 10.3390/molecules181113188

BRASIL (2006). Ministério da Saúde. Diretrizes gerais para o trabalho em contenção com Agentes Biológicos Brasília: Editora MS.

Chitra, S., and Devanathan, D. (2012). In-vitro microbiological evaluation of 5-ethoxycarbonyl-4-aryl-6-methyl-3, 4- dihydropyrimidin-2(1h)-ones. *Int. Res. J. Pharmaceut. Appl. Sci.* 2, 56–58.

Clinical and Laboratory Standards Institute (CLSI) (2012). Reference method of Broth. Methods for dilution antimicrobial susceptibility tests of or bacteria that grow aerobically. Approved Standard — Ninth Edition, NCCLS Document M07-A9, CLSI, Wayne, PA.

de Vasconcelos, A., Oliveira, P. S., Ritter, M., Freitag, R. A., Romano, R. L., Quina, F. H., et al. (2012). Antioxidant capacity and environmentally friendly synthesis of dihydropyrimidin-(2H)-ones promoted by naturally occurring organic acids. *J. Biochem. Mol. Toxicol.* 26, 155–161. doi: 10.1002/jbt.20424

Debache, A., Amimour, M., Belfaitah, A., Rhouati, S., and Carboni, B. (2008). A one-pot Biginelli synthesis of 3, 4-dihydropyrimidin-2-(1H)-ones/thiones catalyzed by triphenylphosphine as Lewis base. *Tetrahedron Lett.* 49, 6119–6121. doi: 10.1016/j.tetlet.2008.08.016

Esposito, S., and De Simone, G. (2017). Update on the Main MDR pathogens: prevalence and treatment options. *Infez. Med.* 25, 301–310.

Fathima, N., Nagarajaiah, H., and Begum, N. S. (2013). Methyl 5-(4-Acetoxyphenyl)-2-(2-Bromobenzylidine)-7-Methyl-3-Oxo-2,3-Di-hydro-5H-1,3-Thiazolo[3,2-a]Pyrimidine-6-carboxylate. *Acta Crystallogr. Sect. E Struct. Rep. Online* 69:o1262. doi: 10.1107/S1600536813019132

Finberg, R. W., Moellering, R. C., Tally, F. P., Craig, W. A., Pankey, G. A., Dellinger, E. P., et al. (2004). The importance of bactericidal drugs: future directions in infectious disease. *Clin. Infect. Dis.* 39, 1314–1320. doi: 10.1086/425009

Godoi, M. N., Costenaro, H. S., Kramer, E., Machado, P. S., Montes, M. G. D., and Russowsky, D. (2005). Síntese do Monastrol e Novos Compostos de Biginelli Promovida por In(OTf)3 [synthesis of monastrol and of new Biginelli compounds promoted by In(OTf)3]. *Quim Nova* 28, 1010–1013. doi: 10.1590/S0100-40422005000600015

Hughes, D., and Karlén, A. (2014). Discovery and preclinical development of new antibiotics. *Ups. J. Med. Sci.* 119, 162–169. doi: 10.3109/03009734.2014.896437

International Organization for Standardization (ISO) (2009). ISO 10993-5:2009 Biological evaluation of medical devices—Part 5: Tests for *in vitro* cytotoxicity. 2009.

Jara, M. C., Frediani, A. V., Zehetmeyer, F. K., Bruhn, F. R. P., Müller, M. R., Miller, R. G., et al. (2021). Multidrug-resistant hospital bacteria: epidemiological factors and susceptibility profile. *Microb. Drug Resist.* 27, 433–440. doi: 10.1089/mdr.2019.0209

Jara, M. C., Silva, A. C. A., Goncalves, C., Pereira, C. M. P., Santos, P. R., Biajoli, A. F., et al. (2021). Compostos De Bignelli Frente A Bactérias Multirresistentes A Antibiótico. Depositante: Universidade Federal De Pelotas (BR/RS). Titular: Universidade Estadual de Campinas. Procurador: Marisa Castro Jara. BR n. 10 2020 021653 8. Depósito: 22 out. 2020. Concessão: 12 abr. 2021.

Kappe, C. O. (2000). Review biologically active Dihydropyrimidones of the Biginelli-type: a literature survey. *Eur. J. Med. Chem.* 35, 1043–1052. doi: 10.1016/s0223-5234(00)01189-2

Leung, E., Weil, D. E., Raviglione, M., and Nakatani, H.World Health Organization World Health Day Antimicrobial Resistance Technical Working Group (2011). The WHO policy package to combat antimicrobial resistance. *Bull World Health Organ.* 89, 390–392. doi: 10.2471/BLT.11.088435

Lobritz, M. A., Belenky, P., Porter, C. B. M., Gutierrez, A., Yang, J. H., Schwarz, E. G., et al. (2015). Antibiotic efficacy is linked to bacterial cellular respiration. *Proc. Natl. Acad. Sci. U. S. A.* 112, 8173–8180. doi: 10.1073/pnas.1509743112

Magiorakos, A. P., Srinivasan, A., Carey, R. B., Carmeli, Y., Falagas, M. E., Giske, C. G., et al. (2012). Multidrug-resistant, extensively drug-resistant and pandrug-resistant bacteria: an international expert proposal for interim standard definitions for acquired resistance. *Clin. Microbiol. Infect.* 18, 268–281. doi: 10.1111/j.1469-0691.2011.03570.x

Mansouri, M., Movahedian, A., Rostami, M., and Fassihi, A. (2012). Synthesis and antioxidant evaluation of 4-(Furan-2-Yl)-6-methyl-2-thioxo-1,2,3,4-tetrahydropyrimidine-5-carboxylate esters. *Res. Pharm. Sci.* 7, 257–264.

Medyouni, R., Elgabsi, W., Naouali, O., Romerosa, A., Al-Ayed, A. S., Baklouti, L., et al. (2016). One-pot three-component Biginelli-type reaction to synthesize 3,4-Dihydropyrimidine-2-(1H)-ones catalyzed by co Phthalocyanines: synthesis, characterization, aggregation behavior and antibacterial activity Rawdha. *Spectrochim. Acta A Mol. Biomol. Spectrosc.* 167, 165–174. doi: 10.1016/j.saa.2016.04.045

Nemeth, J., Oesch, G., and Kuster, S. P. (2015). Bacteriostatic versus bactericidal antibiotics for patients with serious bacterial infections: systematic review and meta-analysis. *J. Antimicrob. Chemother.* 70, 382–395. doi: 10.1093/jac/dku379

Niemirowicz-Laskowska, K., Głuszek, K., Piktel, E., Pajuste, K., Durnaś, B., Król, G., et al. (2018). Bactericidal and immunomodulatory properties of magnetic nanoparticles functionalized by 1,4-dihydropyridines. *Int. J. Nanomedicine* 13, 3411–3424. doi: 10.2147/IJN.S157564

O'Neill, J. (2016). "Tackling drug-resistant infections globally: final report and recommendations," in *Review on Antimicrobial Resistance*. Government of the United Kingdom.

Peytam, F., Takalloobanafshi, G., Saadattalab, T., Norouzbahari, M., Emamgholipour, Z., Moghimi, S., et al. (2021). Design, synthesis, molecular docking, and in vitro α-glucosidase inhibitory activities of novel 3-amino-2,4-diarylbenzo[4,5]imidazo[1,2-a]pyrimidines against yeast and rat α-glucosidase. *Sci. Rep.* 11:11911. doi: 10.1038/s41598-021-91473-z

Prasad, B. D., Sastry, V. G., Ramana, H., Devilal, J., and Rao, A. S. (2016). Multicomponent Biginelli's synthesis, antimycobacterial activity and molecular docking studies of dihydropyrimidine derivatives as thymidylate kinase protein targets. *Pharmacologia* 7, 256–263. doi: 10.5567/pharmacologia.2016.256.263

Puri, S., Parmar, A., Kaur, B., and Kumar, H. (2009). Ultrasound promoted cu(clo4)2 catalyzed rapid synthesis of substituted l,2,3,4-tetrahydropyrimidine-2-ones & hantzsch 1,4-dihydropyridines in dry media Saurabh. *Heterocycl. Comm.* 15, 51–56. doi: 10.1515/HC.2009.15.1.51

Ramachandran, V., Arumugasamy, K., and Singh, S.-K. (2016). Synthesis, antibacterial studies, and molecular modeling studies of 3, 4-dihydropyrimidinone compounds. *J. Chem. Biol.* 9, 31–40. doi: 10.1007/s12154-015-0142-4

Ranjith, C., Srinivasan, G. V., and Vijayan, K. K. (2010). Tributyl borate mediated Biginelli reaction: A facile microwave-assisted green synthetic strategy toward Dihydropyrimidinones. *Bull. Chem. Soc. Jpn.* 83, 288–290. doi: 10.1246/bcsj.20090275

Rhee, K. Y., and Gardiner, D. F. (2004). Clinical relevance of bacteriostatic versus bactericidal activity in the treatment of gram-positive bacterial infections. *Clin. Infect. Dis.* 39, 755–756. doi: 10.1086/422881

Sharma, V., Chitranshi, N., and Agarwal, A. K. (2014). Significance and biological importance of pyrimidine in the microbial world. *Int. J. Med. Chem.* 2014:202784. doi: 10.1155/2014/202784

Stefani, H. A., Oliveira, C. B., Almeida, R. B., Pereira, C. M. P., Braga, R. C., Cella, R., et al. (2006). Dihydropyrimidin-(2H)-ones obtained by ultrasound irradiation: A new class of potential antioxidant agents. *Eur. J. Med. Chem.* 41, 513–518. doi: 10.1016/j.ejmech.2006.01.007

Tacconelli, E., Carrara, E., Savoldi, A., Harbarth, S., Mendelson, M., Monnet, D. L., et al. (2018). Discovery, research, and development of new antibiotics: the WHO priority list of antibiotic-resistant bacteria and tuberculosis. *Lancet Infect. Dis.* 18, 318–327. doi: 10.1016/S1473-3099(17)30753-3

Tegos, G. P., and Hamblin, M. R. (2014). Disruptive innovations: new anti-Infectives in the age of resistance. *Curr. Opin. Pharmacol.* 13, 673–677. doi: 10.1016/j.coph.2013.08.012

Venugopala, K. N., Dharma Rao, G. B., Bhandary, S., Pillay, M., Chopra, D., Aldhubiab, B. E., et al. (2016). Design, synthesis, and characterization of (1-(4-Aryl)-1H-1,2,3-triazol-4-Yl) methyl, substituted phenyl-6-methyl-2-oxo-1, 2, 3, 4-tetrahydropyrimidine-5-carboxylates against *Mycobacterium tuberculosis*. *Drug Des. Devel. Ther.* 10, 2681–2690. doi: 10.2147/DDDT.S109760

Conflict of Interest: The authors declare that the research was conducted in the absence of any commercial or financial relationships that could be construed as a potential conflict of interest.

Publisher's Note: All claims expressed in this article are solely those of the authors and do not necessarily represent those of their affiliated organizations, or those of the publisher, the editors and the reviewers. Any product that may be evaluated in this article, or claim that may be made by its manufacturer, is not guaranteed or endorsed by the publisher.

frontiers | Frontiers in Microbiology

ORIGINAL RESEARCH
published: 14 April 2022
doi: 10.3389/fmicb.2022.833790

Metatranscriptomic Analysis of the Chicken Gut Resistome Response to In-Feed Antibiotics and Natural Feed Additives

Raju Koorakula[1,2†], Matteo Schiavinato[3†], Mahdi Ghanbari[4], Gertrude Wegl[4], Nikolaus Grabner[4], Andreas Koestelbauer[4], Viviana Klose[4], Juliane C. Dohm[3] and Konrad J. Domig[1]*

[1] Department of Food Science and Technology, Institute of Food Science, University of Natural Resources and Life Sciences, Vienna, Austria, [2] Competence Centre for Feed and Food Quality, Safety and Innovation (FFoQSI), Tulln, Austria, [3] Department of Biotechnology, Institute of Computational Biology, University of Natural Resources and Life Sciences, Vienna, Austria, [4] DSM – BIOMIN Research Center, Tulln, Austria

OPEN ACCESS

Edited by:
Wang Jiajun, Northeast Agricultural University, China

Reviewed by:
Min Yue, Zhejiang University, China
Xiang Yang, University of California, Davis, United States

***Correspondence:**
Raju Koorakula
raju.koorakula@ffoqsi.at

† These authors have contributed equally to this work and share first authorship

Specialty section:
This article was submitted to Antimicrobials, Resistance and Chemotherapy, a section of the journal Frontiers in Microbiology

Received: *12 December 2021*
Accepted: *08 March 2022*
Published: *14 April 2022*

Citation:
Koorakula R, Schiavinato M, Ghanbari M, Wegl G, Grabner N, Koestelbauer A, Klose V, Dohm JC and Domig KJ (2022) Metatranscriptomic Analysis of the Chicken Gut Resistome Response to In-Feed Antibiotics and Natural Feed Additives. Front. Microbiol. 13:833790. doi: 10.3389/fmicb.2022.833790

The emergence of resistance against common antibiotics in the gut microbiota is a major issue for both human and livestock health. This highlights the need for understanding the impact of such application on the reservoir of antibiotic resistance genes in poultry gut and devising means to circumvent the potential resistome expansion. Phytogenic feed additives (PFAs) are potential natural alternative to antibiotic to improve animal health and performance, supposedly *via* positively affecting the gut microbial ecosystem, but there is little systematic information available. In this time-course study, we applied a shotgun meta-transcriptomics approach to investigate the impact of a PFA product as well as the commonly used antibiotic, zinc bacitracin either at AGP concentration or therapeutic concentration on the gut microbiome and resistome of broiler chickens raised for 35 days. Over the course of the trial, PFA treatments increased the abundance of *Firmicutes* such as *Lactobacillus* and resulted in a lower abundance of *Escherichia*, while the latter group increased significantly in the feces of chickens that received either AGP or AB doses of bacitracin. Tetracycline resistance and aminoglycoside resistance were the predominant antibiotic resistance gene (ARG) classes found, regardless of the treatment. PFA application resulted in a decrease in abundance of ARGs compared to those in the control group and other antibiotic treatment groups. In summary, the findings from this study demonstrate the potential of phytogenic feed additives could be an alternative to antibiotics in poultry farming, with the added benefit of counteracting antimicrobial resistance development.

Keywords: metatranscriptomics, gut microbiome, resistome, chicken, antibiotic resistance genes, phytogenic feed additives

INTRODUCTION

Antibiotic resistance is one of the most serious global threats to human health, so immediate action is needed to tackle the current situation and reduce its spread (Sabino et al., 2019). Antibiotics have been used for decades in livestock, both at subtherapeutic (low-dose) levels to promote growth and at therapeutic (high-dose) levels against diseases (Castanon, 2007; Looft et al., 2014;

Van Boeckel et al., 2015; Mehdi et al., 2018; Sun et al., 2018; Ghanbari et al., 2019). In poultry farming, low-dose antibiotics (antibiotic growth promoters, "AGPs") have been used for many years to increase nutrient uptake efficiency, for growth performance, to maintain bird health (Butaye et al., 2003; Danzeisen et al., 2011; Page and Gautier, 2012; Costa et al., 2017; Kumar et al., 2018) and to prevent enteric diseases (Butaye et al., 2003; Miles et al., 2006; Wei et al., 2013). However, recent studies suggest that this practice can contribute to the emergence of antimicrobial-resistant bacteria (ARBs), accelerating the antibiotic resistance problem in animal and human pathogens (Butaye et al., 2003; Diarra and Malouin, 2014; Costa et al., 2017; Ghanbari et al., 2019). Moreover, therapeutic dose administration of antibiotics may be subinhibitory for some host-associated bacteria, enhancing the selection for antibiotic resistance genes and their horizontal transfer (von Wintersdorff et al., 2016). Hence, poultry farmers are facing the challenge of finding alternatives to antibiotic growth promoters (Inglis et al., 2005; Doyle and Erickson, 2012; Lawley et al., 2013; Looft et al., 2014). However, zinc-bacitracin is still one of the most commonly used AGP in poultry farming (Sarmah et al., 2006; Crisol-Martínez et al., 2017) and is usually included in feed at non-therapeutic doses of <55 mg/kg body weight (KBW) to improve growth performance and reduce early mortality (Diarra and Malouin, 2014). Treatment with a higher dosage of 55–110 mg/kg body weight (KBW) is used to prevent and treat necrotic enteritis caused by *Clostridium perfringens,* which has a high mortality rate and is one of the most economically significant gut diseases in broiler chickens (Butaye et al., 2003). Bacitracin, a polypeptide antibiotic obtained from *Bacillus licheniformis*, is a mixture of high molecular weight cyclic peptides (bacitracins A, B, C and other minor compounds) that have antibacterial action against gram-positive microorganisms by interfering with cell wall development and the synthesis of peptidoglycan (Phillips, 1999; Marshall and Levy, 2011; Díaz Carrasco et al., 2018).

Due to their ability to mimic the bioactive properties of antibiotics, phytogenic feed additives (PFAs) are a possible alternative to AGPs (Murugesan et al., 2015; Salaheen et al., 2017). Phytogenics are plant-derived natural substances (herbs, spices, oils or extracts) that contain sensory and flavoring compounds. They are added to animal diets to improve animal health and feed acceptance (Wang J. et al., 2021) and have been linked to improved gut health, better nutrient digestibility, and increased growth performance (Murugesan et al., 2015; Kaschubek et al., 2018; Bampidis et al., 2019; Wang J. et al., 2021). There is, however, paucity of research on the effect of the PFAs application on gut microbiome of livestock species such as broiler chickens. By applying a shotgun meta-transcriptomics approach, in this study we systematically studied the impact of a PFA product as well as the commonly used antibiotic, zinc bacitracin at two different concentration (either as low dose AGP or high dose treatment) on the gut microbiome and resistome of broiler chickens. The findings of this study have important implications for broiler production and public health, since such analysis provided a deeper insight on the effect of the AGP and therapeutic doses of antibiotics on the antibiotic resistome. In addition, the analysis demonstrated the potential of using the natural alternative to antibiotics in poultry farming on mitigating antimicrobial resistance development.

MATERIALS AND METHODS

Animals and Experimental Design

The animal trial was carried out at the Center of Animal Nutrition (Tulln, Austria) under a protocol approved by the office of the Lower Austrian Region Government, Group of Agriculture and Forestry, Department of Agricultural Law (approval code LF1-TVG-57/005-2018) according to relevant guidelines and regulations. Two hundred forty-old male broiler chickens (Ross 308) were randomly assigned to 24 pens with 10 birds per pen, and then the pens were randomly assigned to one of six treatment groups, each with four replicating pens. The chickens were fed a standard broiler diet for 35 days *ad libitum*. Treatments were started after 3 days of adaptation, and the six groups received the following: (1) a standard diet of basal chicken feed [Control (CON), (2) supplementation with a phytogenic feed additive (Digestarom® DC Power, Biomin Holding GmbH, Austria; 150 mg/kg feed) throughout the trial (PFA), (3) supplementation with zinc-bacitracin (ALBAC, Huvepharma, Belgium) as an antibiotic growth promotor at 20 mg/kg throughout the trial (AGP), (4) supplementation of both the PFA and AGP groups throughout the trial (AGP + PFA), (5) a basal diet with an antibiotic intervention with zinc-bacitracin (200 mg/kg)] administered from Day 15 to Day 21 (AB), and (6) phytogenic supplementation as in the PFA group with the additional antibiotic intervention of the AB group.

Feces Sampling

On Day 3, before the switch to supplemented feed, one bird per pen was euthanized by asphyxiation, and following dissection, chicken digesta samples from the distal part of the colon (herein referred to as feces) were collected. Due to the low amount of digesta in such young animals, the four replicates of each treatment were pooled. As all birds still received the same diet at Day 3, the pooled samples from chickens were considered six replicates of the same condition and were used as Day 3 samples for all the treatments. On later sample Days 14, 21, and 35, two birds per pen were euthanized for sampling, and their combined homogenized digesta were counted as one sample. Samples were snap-frozen on dry ice and stored at −80°C for later processing (Peimbert and Alcaraz, 2016; Song et al., 2016). RNA was extracted from samples within 1 week. A total of 78 samples were collected (6 treatments × 3 sampling points × 4 replicates + 6 Day 3 pool samples).

RNA Extraction and Quantification

Extraction of total RNA was performed using the RNeasy Power Microbiome kit, QIAGEN GmbH, Hilden, Germany) following the manufacturer's instructions with some minor modifications: the input material was reduced to 150 mg fecal biomass, and RNA was finally eluted in 80 μL of RNAse-free water. After RNA isolation, RNA was quantified using the Qubit RNA XR Assay Kit on a Qubit 4.0 fluorometer (Invitrogen^{TM}, United States), while

the RIN was determined using the Bioanalyzer RNA 6000 Nano assay (Agilent) on the Bioanalyzer 21000 system (Agilent, Santa Clara, CA, United States). Extracted RNA was stored at −80°C until further use.

Library Construction and RNA Sequencing

All samples of chickens were sent for RNA sequencing to the Vienna Biocenter Core Facilities (VBCF-NGS, Vienna, Austria). Single-end sequencing cDNA libraries were prepared from the extracted RNA from chicken samples using standard Illumina library preparation with the NEBNext® Ultra™ RNA Library Prep Kit (Illumina Inc., San Diego, CA, United States), and rRNA was removed with the Ribo-Zero Magnetic Gold (Epidemiology) Kit (Epicentre Biotechnologies), followed by sequencing on an Illumina NovaSeq 6000 S1 FlowCell 100 cycle platform using high-output chemistry (1 × 100 bp) according to the manufacturer's protocol.

Filtering of Raw Reads

Raw sequencing reads from each of the 78 samples were quality-filtered with Trimmomatic (Bolger et al., 2014) (ILLUMINACLIP:TruSeq2-SE.fa:2:30:10, LEADING:20, TRAILING:20, SLIDINGWINDOW: 4:26, MINLEN:50). Bowtie2.4.2 (Langmead and Salzberg, 2012) was used to map the reads against the chicken reference genome (*Gallus gallus* release 90, downloaded from Ensembl) and the Phix174 bacteriophage genome to filter out host and contaminating reads. Ribosomal RNA was removed with SortMeRNA (Kopylova et al., 2012) based on the 16S, 18S, 23S, 28S, 83 5S, and 5.8S rRNA databases.

Resistome Annotation

Filtered reads were then assigned to antibiotic resistance genes (ARGs) based on sequence identity to known resistance genes contained in the MegaRES2 database with the AMR + + pipeline (Doster et al., 2019) using the "with RGI_Kraken" workflow adjusted to run with single-end reads. Each read was assigned uniquely to the ARG with which it had the highest sequence identity.

Assigned reads were also screened for the presence or absence of single nucleotide polymorphisms (SNPs) that could remove the resistance power of a certain ARG. For this, we adapted the workflow of this pipeline to work with single-end short reads and to properly perform SNP confirmation on them. In fact, certain ARGs are present in different alleles, and only some of them produce antibiotic resistance. Hence, AMR + + also performs a SNP confirmation step whereby it removes those reads that do not show any SNPs associated with antibiotic resistance, despite having been assigned to an ARG (Doster et al., 2019). A table containing the number of reads assigned to each ARG was obtained for each sample. The counts relative to each gene in this table refer to non-deduplicated reads that passed the SNP confirmation step (performed within AMR + +). The results of each of the 78 samples were merged in a single table with a custom Python script.

Gene Expression

A comprehensive table of non-deduplicated, SNP-confirmed counts was used to detect differentially expressed ARGs at each timepoint (D3, D14, D21, D35) between each feeding program. To extract differentially expressed ARGs, DESeq2 was used (Love et al., 2014). On D14, D21 and D35, four replicates per treatment were included. ARGs with low average read counts (<10) across all samples were filtered out since they are known to produce background noise in false discovery rate estimations (Stephens, 2016). The statistical significance of each differentially expressed gene was assessed using the "results()" function of DESeq2, calculating two-tailed *p*-values (altHypothesis = "greaterAbs") and using the Benjamini-Hochberg correction (pAdjustMethod = "BH"). Only significant ($p < 0.05$) differentially expressed ARGs were considered. Log2FoldChange values were shrunken using the "lfcShrink" DESeq2 function, as suggested by the DESeq2 guidelines, using the "ashr" method (Love et al., 2014).

DESeq2 was also used to produce a table of fragments per kilobase per million mapped reads (FPKM). The FPKM values were then converted to transcripts per million (TPM) values using a conversion formula (Pachter, 2011). A TPM table was then used to extract ARGs that were uniquely expressed in certain feeding programs and timepoints. TPM values were averaged among replicates of the same condition (i.e., feeding program + timepoint). A custom Python script based on the pandas and numpy modules was used to extract the unique ARGs, considering as expressed only those genes with an average TPM ≥ 1.

Taxonomy

Quality-trimmed reads were assigned to taxa using Kraken2 (Wood et al., 2019) (–minimum-hit-groups 2 –confidence 0.0). Taxa counts were then normalized and combined at the genus level with Bracken (Lu et al., 2017) (−r 100 −l G). The Bracken database was built with "bracken-build" using a read length of 100 and a k-mer size of 50 (−k 50 −l 100). Read counts per taxon were used as raw counts to assess differential taxa presence between each condition (i.e., timepoint + treatment) and the untreated D3 samples. The same was also done when comparing the treatments PFA (Digestarom®), AGP (low-dose bacitracin), AGP + PFA (low-dose bacitracin + digestarom), AB (high-dose bacitracin) and AB + PFA (high-dose bacitracin + digestarom) against the CON (control) at each timepoint. The same pipeline used for differential gene expression was used (see above), using genera as entries instead of genes. The same statistical approach was used to determine significance.

Relative Abundance of Antibiotic Resistance Genes and Taxa

Antibiotic resistance genes were annotated with their Type, Class, Group and Mechanism from the MEGARES v2 database, each representing a different level of their functional characterization. TPM expression values, which are normalized by sequencing depth and gene length, were scaled to a (0,1) interval to represent their relative abundance in each sample. Scaling was performed

by dividing each TPM value by the sum of the TPM values of the corresponding sample. Relative abundances from replicates of the same condition (i.e., timepoint + group) were averaged. The procedure was performed at the class, group and mechanism annotation levels. Given the large number of classes, groups and mechanisms, the top 10 classes (or groups or mechanisms) were represented independently, and the remaining classes were grouped together under the "Other" label. The top 10 entries were selected by averaging the relative abundance of each entry across all conditions and sorting the means decreasingly. All these operations were performed with a custom python (v3.6.4) script using the pandas (v1.0.1) and plotnine (v0.6.0) modules.

The relative abundance of taxa was determined similarly. Given the large number of unclassified reads, only classified reads were retained to improve further data visualization. Taxonomic abundance was assessed using the normalized counts produced by bracken at the genus and phylum levels. Unrelated counts belonging to the "Arthropoda," "Chordata" or "Mollusca" phyla were discarded. The relative abundances were then rescaled to a (0,1) interval.

Alpha and Beta Diversity

Principal coordinate analysis (PCoA), richness, diversity, dissimilarity and non-metric multidimensional scaling (NMDS) ordinations were calculated for ARG expression and for taxa (in both cases using read counts). The operations were performed in a custom python (v3.6.4) code using the following modules: pandas (v1.0.1), numpy (v1.18.1), de_toolkit (v0.9.12), sklearn (v0.23.0), and skbio (v0.5.6). Principal coordinates (skbio.stats.ordination.pcoa, method = "eigh") were computed from a matrix containing Euclidean distances between samples (scipy.spatial.distance.pdist, metric = "braycurtis"). Richness ("observed_otus") and diversity ("shannon") were computed in both subsets for each condition (i.e., timepoint + treatment), using the "alpha_diversity" function of the skbio python module. Significance levels ($p < 0.05$) in comparisons between richness and diversity values among treatments were assessed in an R script with a Mann–Whitney *U* test using the R function wilcox.test. Dissimilarity ("braycurtis") was calculated with the "beta_diversity" function of skbio. Multidimensional scaling was performed with the "manifold.MDS" function of the sklearn python module (n_components = 2, dissimilarity = "precomputed," metric = False) (alpha = 0.05). Significant differences ($p < 0.05$) between NMDS ordinations were calculated pairwise between different groups of samples using a permanova test performed within a python script using the permanova function contained in the skbio.stats.distance module. Plots were generated with the plotnine python module and the ggplot2 R library (Wickham, 2016).

RESULTS

Sequencing Data Overview

The sequencing generated approximately 1.3 billion Illumina single-end transcript reads, ranging from 8 to 18 million reads per sample (100 bp read length). On average, 82% of the raw reads passed the quality control. In detail, approx. eight percent of the reads were removed due to low quality (Phred score < 33), approx. six percent of the reads were classified as rRNA, and ∼ 4% of reads were classified as host reads (*Gallus gallus*) or PhiX bacteriophage reads. Filtered reads were then assigned to antibiotic resistance genes (ARGs) based on sequence identity to known resistance genes contained in the MegaRES2 database. Assigned reads were also screened for the presence or absence of single-nucleotide polymorphisms (SNPs) that could remove the resistance power of a certain ARG (see section "Materials and Methods").

Gut Resistome Diversity and Composition

The reads were assigned to 506 different ARGs out of the 7,868 ones contained in the MEGARes2 database. Considering all chicken samples together, 271 of the detected ARGs belonged to type "Drugs," 120 to type "Metals," 75 to type "Multicompound" and 40 to type "Biocides." For the sake of this analysis, we focused only on ARGs assigned to the "Drugs" type, which encompass 11 classes of resistance and are involved in 25 mechanisms. From the raw read counts, we obtained normalized expression values in terms of transcripts per million (TPM) (**Supplementary Data File 1**). We measured alpha diversity metrics within each treatment in terms of ARG richness (i.e., number of ARGs represented) and diversity (Shannon index, i.e., evenness of the expression levels among ARGs). The results are summarized in **Supplementary Data File 1** - ARG_RICHNESS, ARG_DIVERSITY and **Figure 1**.

The overall size (i.e., richness) of the resistome was not affected by treatments when compared to the control (CON). However, AGP + PFA-treated chicken samples exhibited a significantly higher richness ($p < 0.05$) than the AB + PFA combination at Day 15 (**Figure 1A**). In general, ARG richness had a heterogeneous distribution across replicates, which likely affected the significance testing Overall, the richness ranged from 25 ARGs in AB + PFA at Day 14 to 76.5 ARGs in samples of chickens treated with AGP + PFA on day 35. In terms of Shannon diversity, there was no statistically significant difference among the treatments (**Figure 1B**), although, numerical difference in diversity was observed in samples of chickens treated with AB + PFA at Day 35 (mean: 4.8 ± 0.50), with respect to the samples of chickens treated with CON at Day 14 (mean: 4.0 ± 0.68).

We performed non-metric multidimensional scaling (NMDS) ordinations based on Bray–Curtis dissimilarities at gene level to assess the differences in composition between the treatments and timepoints, which did not show any specific clustering of the analyzed factors (**Figure 2**, **Supplementary Data File 1** and **Supplementary Data File 3** – see **Supplementary Figures 1–3** for further details).

We then set out to determine whether certain ARGs were uniquely expressed in a certain treatment when compared to other treatments at any given timepoint. TPM values determined in previous experiments were used. The results are summarized in **Figure 3** and in **Supplementary Data File 1** –

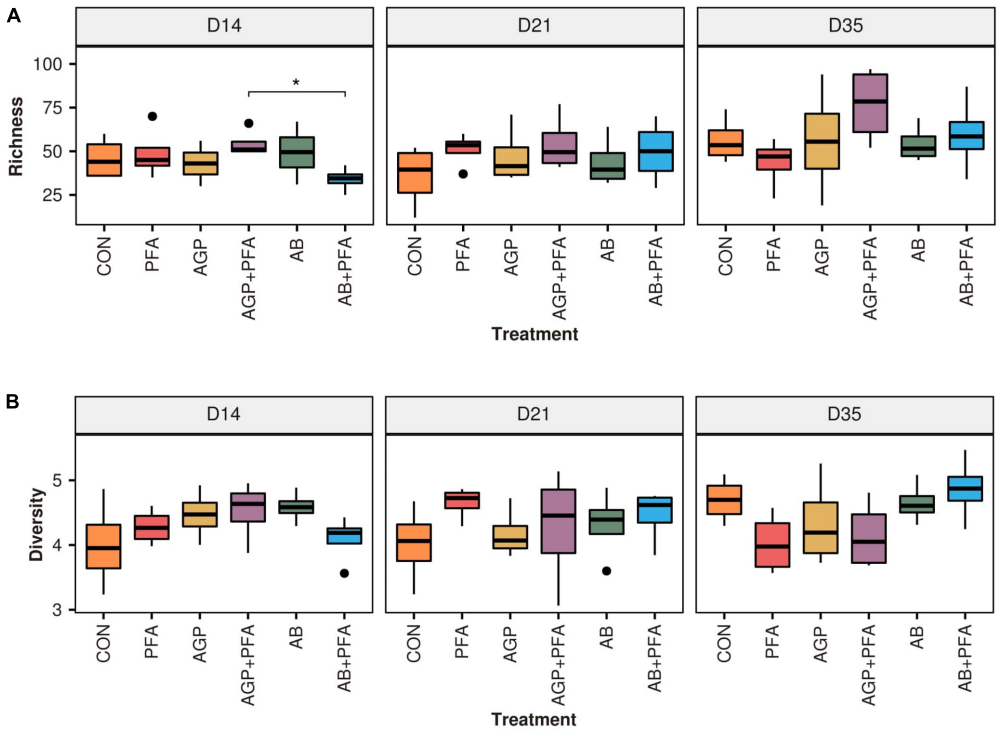

FIGURE 1 | (A) Richness and **(B)** diversity (Shannon) of ARGs across feeding treatments (CON, PFA, AGP, AGP + PFA, AB, AB + PFA) and sampling points (D14, D21, D35). Bars in the boxplot represent interquartile ranges (25th to 75th percentile). The horizontal black line represents the median. Whiskers show intervals going from –1.5 to + 1.5 of the interquartile range. Dots indicate values falling outside of the interquartile range. Significance was tested with a Mann–Whitney *U* test ("*" = 0.05). Colors indicate different treatments.

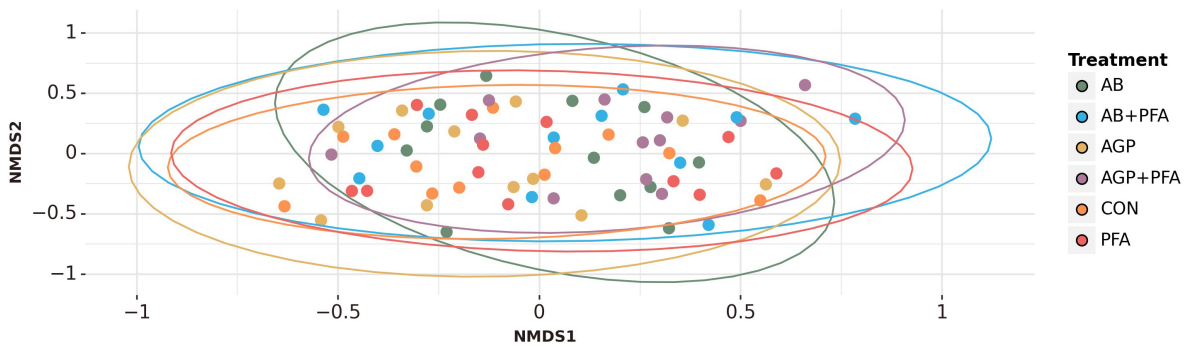

FIGURE 2 | NMDS ordination based on Bray-Curtis dissimilarity metric represents bacterial compositional differences between the treatments.

ARG_UNIQUE_CLASS. At Day 14, samples of chickens treated with PFA showed 21 unique ARGs that were not found in the other treatment groups. Of these 21 were 14 unique ARGs belonging mostly to aminoglycosides. Samples derived from chickens that were fed AGP or AB harbored four unique ARGs, three of which belong to the tetracycline class. The control samples showed five unique ARGs, most of which belong to the tetracycline class (**Figure 3**).

At Day 21, 23 unique ARGs was found in the samples from chickens treated with AGP, and these unique ARGs belong to the tetracycline, macrolide-lincosamide-streptogramin (MLS), and multidrug classes. Samples from chickens treated only with AB contained six unique ARGs belonging to the MLS and aminoglycoside classes. The other treatments showed three or fewer unique ARGs (**Figure 3**).

At Day 35, a very high number of unique ARGs (28) was found for samples of chickens treated with bacitracin given as AGP. These ARGs belong mostly to the aminoglycosides, sulfonamides or MLS classes. CON samples showed 10 unique ARGs. Other treatments showed two or fewer unique ARGs (**Figure 3**). Samples of chickens treated with the combinations AGP + PFA or AB + PFA contained no unique ARGs (0) at

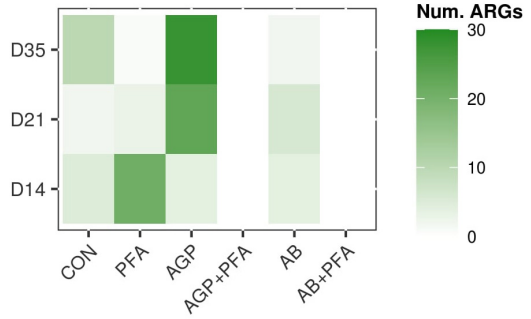

FIGURE 3 | Heatmap representing the number of unique ARGs found in each treatment that were not found in any other treatment at any given timepoint.

Days 14, 21, and 35 (**Figure 3**; **Supplementary Data File 1** – ARG_UNIQUE_CLASS).

The ARGs detected in the read dataset were then analyzed in terms of relative transcript expression based on their expression level calculated in TPM (transcripts per million). Overall, tetracycline resistance was the predominant class to which reads aligned (71 ARGs), followed by aminoglycoside and MLS resistance (64 ARGs and 52 ARGs, respectively) (**Supplementary Data File 1** – ARG_RELATIVE_ABUNDANCE_CLASS and **Figure 4A**). In the tetracycline class, the predominant mechanism of resistance observed was resistance through ribosomal protection proteins (RPPs), represented by 64 ARGs. Other mechanisms were aminoglycoside O-nucleotidyltransferases, aminoglycoside O-phosphotransferases, lincosamide nucleotidyltransferases and MLS resistance AB efflux pumps, all of which were found at high levels (**Supplementary Data File 1** –ARG_RELATIVE_ABUNDANCE_MECHANISM and **Figure 4B**). Overall, only a few differences were observed between the treatments and sampling points in terms of relative transcript abundance of ARG classes and mechanisms. Bacitracin resistance genes were present throughout the entire period in almost all the samples from chickens at very low abundance (<0.5% for the majority of samples). Bacitracin supplementation given as antibiotic intervention at a high dose, however, revealed a relative abundance of 2% on Day 21. In fact, regardless of the bacitracin application, all the treatments harbored a diverse range of ARGs at all sampling points (**Figure 4**).

We then determined differentially expressed ARGs between each treatment and the control sample from the same sample day (CON) at any given timepoint (**Supplementary Data File 1** – ARG_DEGS and **Figure 5**).

All the treatments were first compared against the control (CON) at given any timepoint. We identified a total of 10 differentially expressed ARGs in all the treatments (**Figure 5** and **Supplementary Data File 1**). These 10 ARGs produced 20 instances of differential expression, as certain genes (MEG1004_ANT9 – aminoglycosides and MEG1558_CAT-Phenicol) were found to be differentially expressed in multiple comparisons. Considering that each comparison was independent from the others, we treated them as 20 independent differentially expressed genes. Of these 20 instances of differential expression, two included increases in differential abundance (**Figure 5**, red tiles). These included MEG 3271, a gene of interest belonging to the Resistance-Nodulation-Division (RND) multidrug resistance class [Histone-like Nucleoid Structuring (HNS) proteins]. This gene showed a significant increase in gene expression [Log2foldchange (LFC) $\sim$ 3.5, $p < 0.05$] after AGP + PFA administration at Day 35. The second gene with increased expression was MEG 7220 (LFC $\sim$ 3.2, $p < 0.05$), belonging to the tetracycline resistance class, after AB treatment at Day 21 (**Figure 5** and **Supplementary Data File 1** – ARG_DEGS). The remaining 18 instances of differential expression included decreases in abundance. AGP + PFA-treated samples showed a higher number of differentially expressed ARGs ($p < 0.05$) (for more details refer **Supplementary Data File 1** – ARG_DEGS and **Figure 5**) at Day 14 than at Day 21 and Day 35 in all treatments. Interestingly, MEG_7055-TETB (tetracycline) and MEG_1588-CAT (phenicol) ARGs had significantly decreased expression after PFA administration at Day 35. In detail, MEG 7055-TETB showed an LFC $\sim$ −19.3, while MEG 1588-CAT showed an LFC $\sim$ −17 (both genes with $p < 0.05$).

All treatments were then compared to each other over timepoints. A richer collection of instances of differential expression (168) that corresponded to 20 different ARGs was found. For example, MEG_3271 (RND multidrug resistance class) was increased in abundance when comparing chicken treated with AGP + PFA against the PFA treatment alone (LFC $\sim$ 3.6, $p < 0.05$, **Supplementary Data File 1** – ARG_DEGS). We did not find any changes in transcript abundance at the ARG class or gene level that directly corresponded to bacitracin administration at low or high doses. Instead, we observed that many of the ARGs belonging to the tetracycline class were significantly increased in abundance and that many of the aminoglycoside classes were significantly decreased in abundance in response to high-dose bacitracin administration at Day 21 (**Supplementary Data File 1** – ARG_DEGS).

Microbiome Diversity and Gut Composition

We then assigned the quality-trimmed RNA-Seq reads to their most likely taxonomic origin. With the read counts per taxon, we assessed the relative abundance, richness, and diversity of taxa in each sample (**Supplementary Data File 2**).

The results showed that the total number of identified genera (richness) and the evenness of their abundance (Shannon diversity) were different (only at numerical level) in samples of chickens that received antibiotics alone or in combination with phytogenics (AGP, AGP + PFA, AB, AB + PFA) than in those treated with PFA only or the control (CON) (**Figure 6A**). In fact, chickens treated with AB or AB + PFA showed a significantly higher ARG richness in the feces than CON (control) and PFA treated chickens at Day 21 ($p < 0.05$; **Figure 6A**). Additionally, chickens treated with AGP + PFA showed a significantly higher

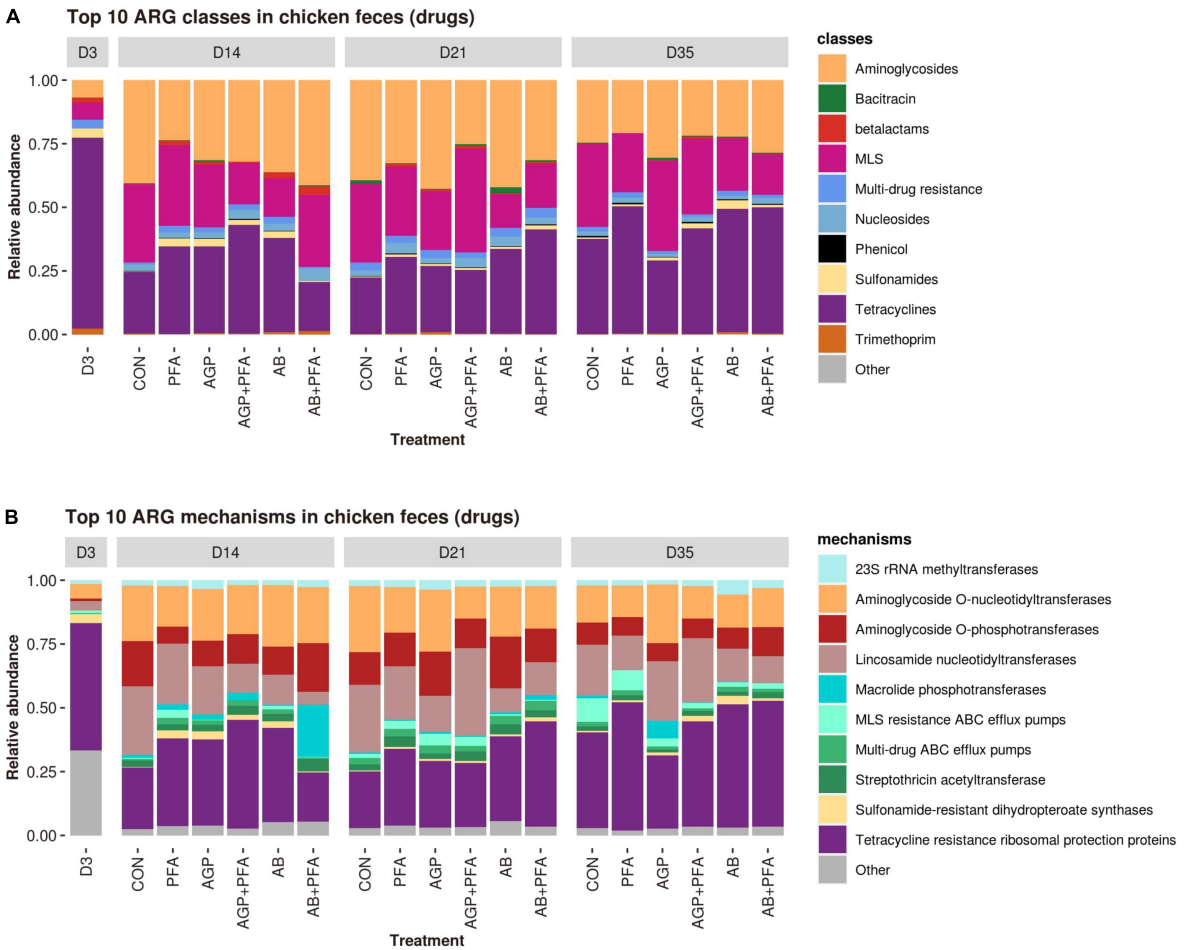

FIGURE 4 | Relative transcript abundances of the top 10 ARG classes **(A)** and mechanisms **(B)** in chicken fecal samples from all feeding treatments (CON, PFA, AGP, AGP + PFA, AB, AB + PFA) and sampling points (D3, D14, D21, D35). The ARG classes and mechanisms with a relative abundance of <1% of the total reads were grouped into "Other". To facilitate comparisons, the D3 timepoint was represented as a single feeding treatment alongside the other six because all samples at D3 could be considered replicates.

ARG richness in the feces than those that received PFA at Day 21 ($p < 0.05$; **Figure 6A**).

When looking at the diversity (**Figure 6B**), samples derived from chickens treated with CON and PFA showed numerically different median value (Shannon) than those from bacitracin-treated chickens (AGP, AGP + PFA, AB, AB + PFA), this difference was not statistically significant though. However, high-dose bacitracin-treated chickens (AB and AB + PFA) had a significantly higher diversity in their feces than those treated with PFA at Day 21.

Further assessment of the microbiome composition and diversity across the treatments and timepoints after NMDS ordinations based on the Bray–Curtis dissimilarity displayed no clear separation between treatments and timepoints (**Figure 2**, **Supplementary Data File 2** and **Supplementary Data File 3** – see **Supplementary Figures 4**, **5**). However, a permanova test revealed that six comparisons between control and non-control samples were significantly different ($p < 0.05$) at Day 21: AGP + PFA vs. CON; AGP + PFA vs. PFA; AB vs. CON; AB vs. PFA; AB + PFA vs. CON; AB + PFA vs. PFA. This indicates that there were significant compositional differences of the microbes in the feces of bacitracin-treated animals (AGP, AGP + PFA, AB, AB + PFA), control (CON), and PFA-treated animals at Day 21 (**Supplementary Data File 2**).

Taxonomic profiling was carried out to determine whether the temporal changes in ARG profiles were related to the changes in the fecal microbial communities in response to PFA, AGP, and AB administration. **Figure 7** shows the distribution of the most prevalent phyla and genera in the fecal samples over the feeding trial (**Supplementary Data File 2** – TAXA _RELATIVE_ABUNDANCE_PHYLUM and TAXA_RELATIVE_ABUNDANCE_GENUS). Firmicutes was by far the most predominant phylum, followed by *Proteobacteria, Actinobacteria*, and *Bacteroidetes*. At Day 35, *Bacteroidetes* and *Proteobacteria* were found at high relative abundance in broiler chickens treated with AGP and AGP + PFA, respectively.

At the genus level, samples from chickens treated with PFA (Digestarom®) exhibited a high relative abundance of

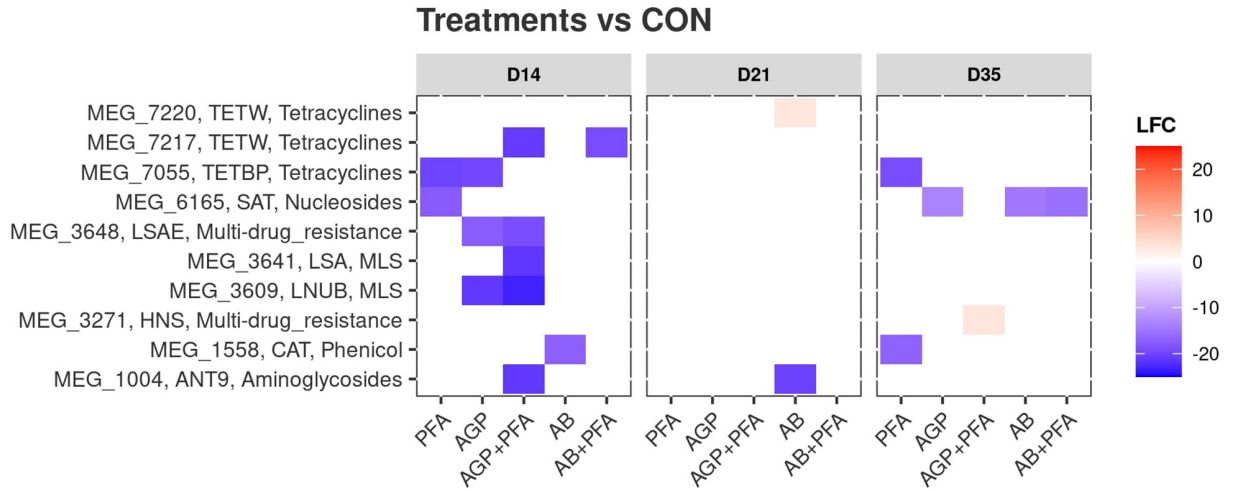

FIGURE 5 | Differential expression of antibiotic resistance genes after administration of treatments and compared against the control (CON). *X*-axis: treatments by timepoint; "CON" represents the control sample. *Y*-axis: gene IDs as per the MEGARes2 database, together with their group and their class. The color reflects the detected log2foldChange (LFC) value. Only significantly ($p < 0.05$) differentially expressed genes are shown.

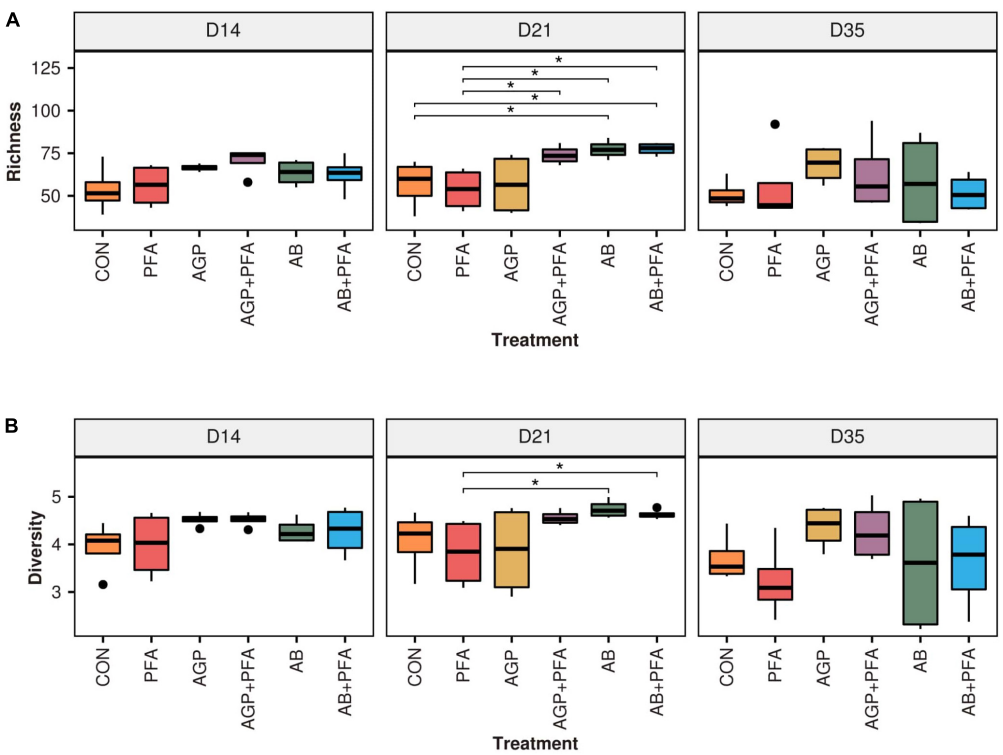

FIGURE 6 | (A) Richness and **(B)** diversity (Shannon) of taxa across treatments and over sampling points. Bars in the boxplot represent interquartile ranges (25th to 75th percentile). The horizontal black line represents the median. Whiskers show intervals going from −1.5 to + 1.5 of the interquartile range. Dots indicate values falling outside of the interquartile range. Significance was tested with a Mann–Whitney *U* test ("*" = 0.05). Colors indicate different treatments.

Lactobacillus (probiotic), and AGP-treated animals also displayed an increased abundance of *Escherichia* throughout the feeding trial (from Day 14 to 35). At Day 21, AGP + PFA (low-dose bacitracin + digestarom), AB (high-dose bacitracin) and AB + PFA (high-dose bacitracin + digestarom)-treated chickens showed a steep decrease in the abundance of the *Lactobacillus* genus, and AB and AB + PFA samples also showed a low abundance of *Streptococcus*. At Day 35, the genus *Lactobacillus* was at low relative abundance, while the *Escherichia* genus displayed high abundance in the samples of chickens treated with

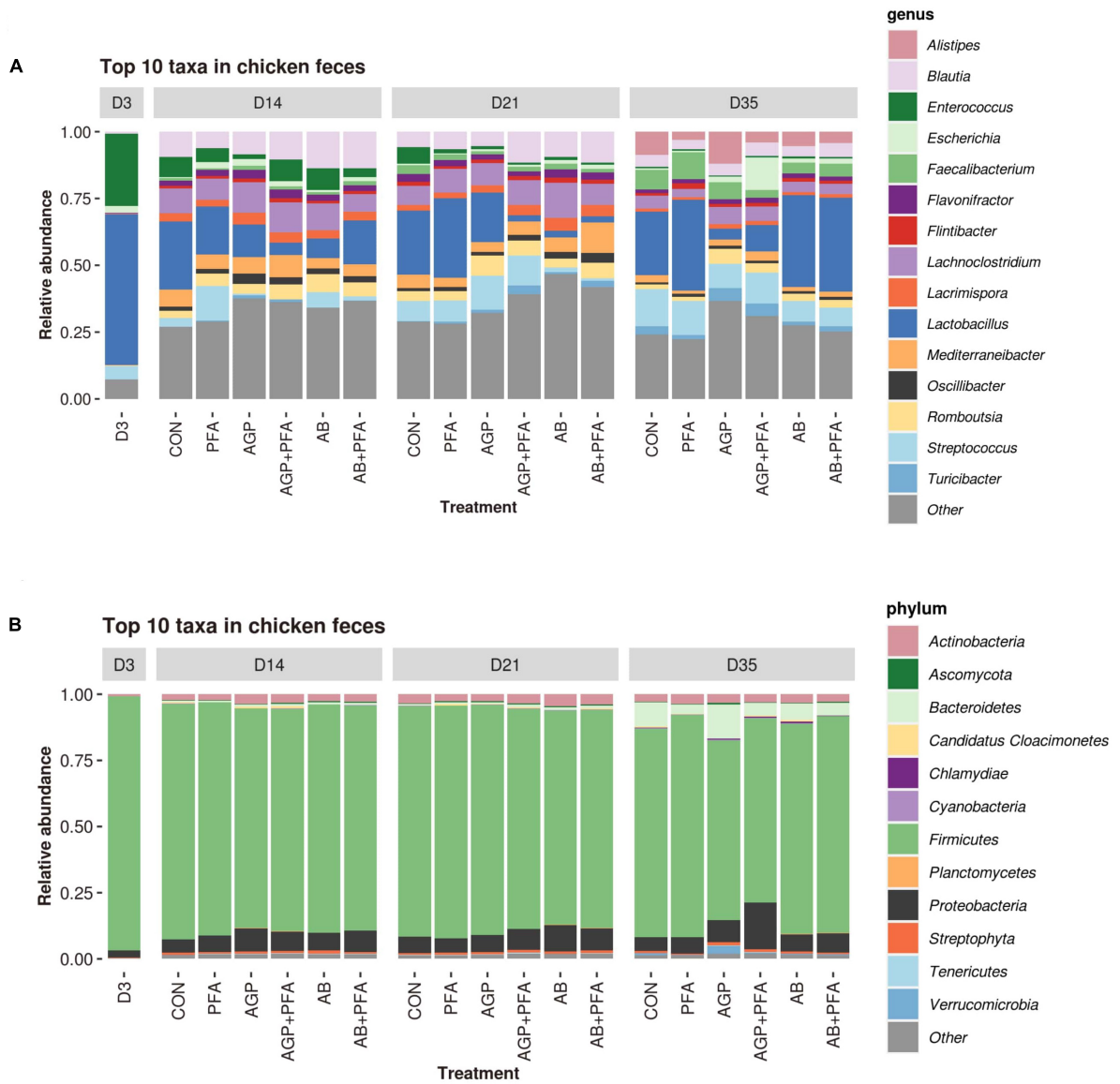

FIGURE 7 | Relative abundance of the most abundant taxa (≥1% of the total reads) in each treatment at each time point at the genus **(A)** and phylum **(B)** levels; taxa representing < 1% of the total reads were grouped together under the label "Other".

AGP and AB + PFA (**Figure 7A**). Interestingly, the abundance of the *Lactobacillus* and *Streptococcus* genera in samples of chickens derived from the AB or AB + PFA treatments recovered at Day 35, 2 weeks after antibiotic (high-dose bacitracin) withdrawal (**Figure 7A**).

We then calculated the differential abundance of each detected taxon in each treatment against the control (CON; **Figure 8**). The results are summarized in **Supplementary Data File 2** – TAXA_DEGS. The analysis at the genus level showed 85 instances of significant differential abundance across all comparisons (e.g., PFA vs. AGP, etc.), which all referred to six genera (*Lactobacillus, Enterococcus, Escherichia, Streptococcus, Turicibacter*, and *Pseudoflavonifractor*). The majority of these instances regarded *Lactobacillus* and *Pseudoflavonifractor* (24 and 27 instances, respectively). At Day 14, all treated samples showed a significantly higher abundance of *Turicibacter* than that of the control (CON). Moreover, chickens treated with AGP + PFA also exhibited a decrease in the abundance of the genera *Pseudoflavonifractor* and *Streptococcus*. At Day 21, chickens treated with AGP + PFA, AB and AB + PFA showed a general decrease in the *Enterococcus, Lactobacillus* and *Pseudoflavonifractor* genera when compared to the control. At Day 35, an increase in *Escherichia* was found in samples of chickens treated with AGP + PFA compared to CON chickens (LFC > 10, $p < 0.05$).

When comparing treatments against each other (and not against CON), at Day 21, the *Lactobacillus* genus was significantly ($p < 0.05$) more abundant in chickens treated with PFA

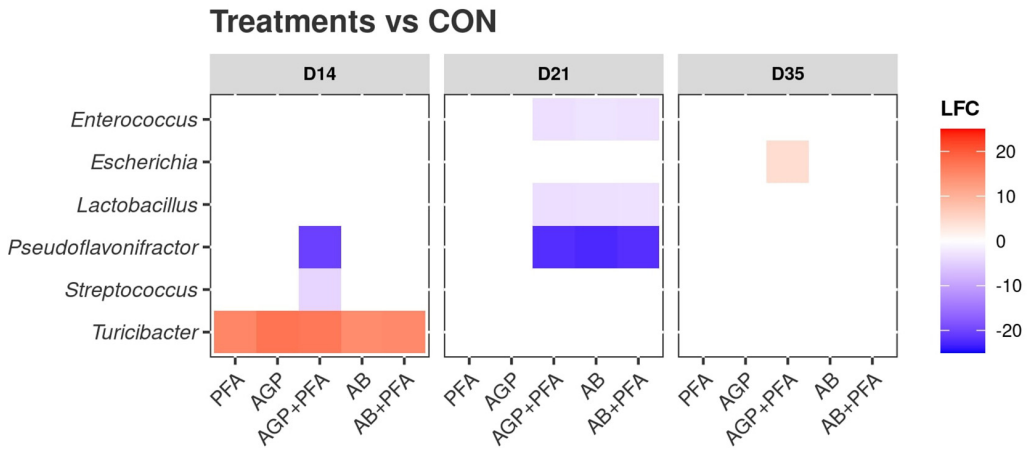

FIGURE 8 | Differential abundance of bacterial genera compared against the control (CON). *X*-axis: treatments by timepoint; "CON" represents the control sample. *Y*-axis: genera. The color reflects the detected log2foldChange (LFC) value. Only significant ($p < 0.05$) differences in taxa abundance are shown.

(Digestarom®) than in those treated with AGP + PFA, AB or AB + PFA (**Supplementary Data File 2** – TAXA_DEGS).

DISCUSSION

Antimicrobial resistance gene spread in livestock has reached alarming levels in most parts of the world and has now been recognized as a significant emerging threat to global public health and food security (Hawkey, 2008; Van Boeckel et al., 2017). Resistance patterns among bacteria have traditionally been studied using culture on media selecting for resistant bacteria. However, when we move away from the most well-studied pathogens, the vast majority of microorganisms cannot be cultured, at least not by standard methods (Browne et al., 2016; Lau et al., 2016). The recent advances in culturomics (Lagier et al., 2018; Nowrotek et al., 2019) and next-generation sequencing techniques (Crofts et al., 2017; Lanza et al., 2018), have made it possible to investigate the resistome in specific bacteria or in bacterial populations at an unprecedented depth. Shotgun whole-metagenome sequencing (WMS) is a reliable tool that can provide a comprehensive and high-resolution analysis of the microbiome and resistome (Schmieder and Edwards, 2011; Nesme et al., 2014; Ghanbari et al., 2019; Ma et al., 2021), and it has been applied to quantify the abundance of many resistance genes in parallel in poultry (Wang et al., 2017; Kumar et al., 2020), cattle (Thomas et al., 2017), pig (Ghanbari et al., 2019; Mencía-Ares et al., 2020) and the human gut (Feng et al., 2018). Other metagenomic studies have found multiple ARGs in chicken gut as well (Tong et al., 2017; Xiong et al., 2018; Eckstrom and Barlow, 2019; Wang Y. et al., 2021; De Cesare et al., 2022). However, WMS provides only limited information regarding ARG activity or the overall functional profile of the active microbial community. Shotgun whole-metatranscriptome sequencing (WMTS) is therefore needed at the population level to determine whether the predicted ARGs are partially or fully expressed. For example, one study that used combined metagenomics and metatranscriptomics on human, pig, and chicken gut resistomes by Wang et al. (2020) observed that ARG transcripts have different abundances when compared to their ARG gene abundance. Interestingly, a study by Franzosa et al. (2014) showed that across the subjects, metatranscriptomic functional profiles were more individualized than metagenomic data. In the current study, we focused on the expression of antibiotic resistance genes in microbial communities of the chicken gut receiving AGP, therapeutic agents (ABs), and/or a phytogenic feed additive (PFA) using WMTS.

Our diversity results revealed that in all treatments, including the control, a diverse range of antibiotic resistance genes was expressed, even in the absence of antibiotic pressure and regardless of the antibiotic choice. The common ARG classes, encoding tetracycline and aminoglycoside resistance, as well as MLS resistance, were the most prevalent ARGs in all treatments, including the control (**Figure 4**). The expressed ARGs found in this study were similar to what was found in chicken feces in previous metagenomics studies by Xiong et al. (2018) and Wang et al. (2020) and in chicken cecum by Juricova et al. (2021). This result supports the theory that ARGs are not spread randomly in different environments (Xiong et al., 2018) but rather that there exists a high background level of the gut resistome in chickens because antibiotics have been used for five decades in poultry, both at the subtherapeutic and therapeutic levels (Tong et al., 2017).

We found that bacitracin administration as an antibiotic growth promoter (AGP) or therapeutic agent (AB) and a phytogenic feed additive (PFA) did not show any significant impact on the alpha diversity of the resistome. We speculate that this is due to general differences in the level of expression of ARGs, which would have only marginally affected common diversity indices or could have been a result of limited statistical power due to the low sample size ($n = 4$; **Figure 1**). However, on Day 21, bacitracin administration at a high dose (AB) resulted in a detectable increase in the relative expression of the bacitracin ARG class, which was even higher than the high

background resistance, although the gut resistome diversity had mostly recovered after 2 weeks of antibiotic withdrawal. A study from Gupta et al. (Gupta et al., 2021) found an increase in the relative abundance of bacitracin resistance in hens given bacitracin, which is consistent with our findings.

Interestingly, we found that AGP-treated chicken samples showed a continuous increase in the number of unique ARGs over the course of the feeding trial. In contrast, PFA-treated chickens showed a decrease in the number of unique ARG transcripts over time. Additionally, antibiotic combination with phytogenics (AGP + PFA; AB + PFA) showed no unique ARG transcripts over the feeding trial. These findings are supported by those from previous studies and indicate that administration of AGP (low-dose antibiotics) in feed causes an accumulation of ARGs in complex ecosystems (Butaye et al., 2003; You and Silbergeld, 2014; Salaheen et al., 2017; Gupta et al., 2021). Overall, the most expressed ARG classes in our study (aminoglycosides, MLS, tetracyclines) are known to be prevalent in the chicken gut resistome (Li B. et al., 2015; Wang et al., 2020; Wang Y. et al., 2021). However, the results from another study by Gupta et al. (2021) indicated that multidrug and beta-lactam ARGs were most abundant. In our study we did not observe high expression of these ARG classes. The differential abundance analysis revealed increased expression of the MEG_3271 gene in samples from chickens treated with AGP + PFA (**Figure 5**). This gene belongs to the multidrug resistance class of the RND multidrug resistance efflux pump mechanism. This change may be attributed to the detected significant increase in the transcript abundance of *Escherichia* (**Figure 7**) after AGP + PFA administration at Day 35. In fact, in a previous study, the *Escherichia* genus was found to be the most common host for multidrug resistance ARGs (Li B. et al., 2015; Xiong et al., 2018; Afridi et al., 2020). While interesting, we note that this may very well be also due to the fact that Escherichia coli is a popular model organism. Interestingly, at Day 21 and Day 35, we found that samples of chickens treated with PFA showed more ARGs decreased in expression when compared to the control group and to other antibiotic treatment groups (**Supplementary Data File 1** – ARG_DEGS). At Day 35, the transcript abundance of the tetracycline-TETBP and phenicol-CAT ARG class genes decreased significantly in PFA-treated animals compared to those in CON- or AB + PFA- and AB-treated animals, respectively.

Taxonomically, *Firmicutes* was the most prevalent phylum, accounting for more than 90% of the bacterial population in all treatments throughout the feeding trial (**Figure 7**). Other abundant phyla were *Proteobacteria, Actinobacteria*, and *Bacteroidetes.* Similar findings were reported in other studies (Videnska et al., 2013; Becker et al., 2014). Moreover, *Bacteroidetes* and *Proteobacteria* showed increased relative abundance in the feces of bacitracin-treated chickens. Compositional shifts in the bacterial communities were mainly observed at Day 21 (after 7 days of antibiotic administration) in all the treated chicken samples, including the control. It may be possible that these changes are the result of AGP or AB administration, as found by previous studies that showed that AGP or AB administration alters the composition of chicken gut microbiota (Díaz Carrasco et al., 2018; Kumar et al., 2018; Proctor and Phillips, 2019). The microbial diversity analysis revealed that a high-dose bacitracin treatment increased both the bacterial community richness and diversity at Day 21. A significant increase in richness was also observed in samples of chickens treated with AGP + PFA (**Figure 6**). These results align with those obtained by Crisol-Martínez et al. (2017) and suggest that a marked reduction in predominant taxa such as *Lactobacillus* in chickens treated with bacitracin correlates with increased bacterial community richness and diversity. On the other hand, these results differ from those observed in the microbial community of the chicken cecum when treated with bacitracin, where an increase of *Lactobacillus* was detected (Díaz Carrasco et al., 2018). The antimicrobial activity of phytogenic feed additives (PFAs) has been studied using metagenomics (Dorman and Deans, 2000; Mitsch et al., 2004), but only a few studies have examined how they could aid the proliferation of beneficial bacteria (Jamroz et al., 2005; Mountzouris et al., 2011). The results of our study revealed that animals treated with PFA showed an increased abundance of active bacteria associated with probiotic properties such as those belonging to the *Lactobacillus* genus over the course of the trial (**Figure 7A**). Interestingly, the abundance of the genus *Escherichia* increased significantly in the feces of chickens receiving AB + PFA at Day 35. In a previous study (Murugesan et al., 2015), it was shown that PFA (i.e., Digestarom®) promoted the development of beneficial gut microbiota with higher numbers of *Lactobacillus* than those in low-dose bacitracin (AGP)-treated chickens. Multiple studies have documented that the *Lactobacillus* genus is an outstanding probiotic, preventing enteric diseases by selectively excluding pathogens from adhering and promoting poultry health by stimulating the immune system (Lutful Kabir, 2009; Mountzouris et al., 2011; Díaz Carrasco et al., 2018).

CONCLUSION

Over the course of the trial, the phytogenic feed additive (Digestarom®) increased the abundance of genera from the *Firmicutes* phylum such as *Lactobacillus* and *Faecalibacterium.* It also resulted in lower abundance of *Escherichia*, whereas low-dose bacitracin treatment administered together with digestarom increased the abundance of the *Escherichia* genus. We speculate that this could be connected to the observed increase in the abundance of multidrug resistance genes such as efflux pumps because *Escherichia* is known to have a high prevalence of multidrug resistance ARGs (Li H. L. et al., 2015; Xiong et al., 2018). In addition, *Alistipes* was significantly increased in the feces of the chickens which received either AGP (low-dose bacitracin) and AB (high-dose bacitracin) or AB + PFA (high-dose bacitracin + digestarom). Of note, administration of the phytogenic feed additive (PFA) significantly decreased the gene expression of ARGs in the feces of the chickens compared to those in the control group and other antibiotic treatment groups.

To the best of our knowledge, this is the first chicken gut meta-transcriptomic study that focused on the impact of different diets containing a phytogenic feed additive and bacitracin at different dosages and combinations. Our study highlighted the

trends in resistome gene expression and the active microbiota composition that resulted from each treatment, showing that treatment with PFA (Digestarom®) could be a good candidate alternative to low-dose bacitracin treatments (AGPs) in poultry, which are banned in the EU.

DATA AVAILABILITY STATEMENT

The datasets presented in this study can be found in online repositories. The names of the repository/repositories and accession number(s) can be found in the article/**Supplementary Material**.

ETHICS STATEMENT

The animal study was reviewed and approved by the animal trial was carried out at the Center of Animal Nutrition (Tulln, Austria) under a protocol approved by the office of the Lower Austrian Region Government, Group of Agriculture and Forestry, Department of Agricultural Law (approval code LF1-TVG-57/005-2018) according to European Guidelines for the Care and Use of Animals for Research Purposes (European Council, 2010). Written informed consent was obtained from the owners for the participation of their animals in this study.

AUTHOR CONTRIBUTIONS

MG and KD contributed to the conception and design of the project. RK performed the experiments. MS and RK performed the data analysis, interpreted the data, and wrote the manuscript. MS conducted the statistical analysis. NG and AK supported the experiments. MG, GW, JD, and KD supervised the development of the work and helped in data interpretation. GW, AK, VK, JD, MG, and KD reviewed the manuscript and provided critical suggestion and comments. All authors have read and approved the final manuscript.

FUNDING

This research was funded by the Austrian Research Promotion Agency (FFG) through the projects "Frontrunner: Omics technologies and natural feed additives-solving challenges of the livestock industry in the area of digitalization" (Project Number 866384) and COMET-K1 Competence Centre for Feed and Food Quality, Safety and Innovation (FFoQSI GmbH, Project Number 854182). The COMET-K1 Competence Center FFoQSI was funded by the Austrian ministries BMVIT and BMDW and the Austrian provinces Niederoesterreich, Upper Austria, and Vienna within the scope of COMET – Competence Centers for Excellent Technologies. The program COMET is handled by the Austrian Research Promotion Agency FFG.

ACKNOWLEDGMENTS

We thank Benjamin Zwirzitz, University of Natural Resources and Life Sciences, Vienna (BOKU), Department of Food Science and Technology, Institute of Food Science, Vienna, Austria, for his helpful feedback, suggestions, and comments on the manuscript. We thank the Core Facility Bioinformatics of the University of Natural Resources and Life Sciences, Vienna for their assistance in data handling and analysis. The computational results presented have been achieved using the Vienna Scientific Cluster (VSC).

SUPPLEMENTARY MATERIAL

The Supplementary Material for this article can be found online at: https://www.frontiersin.org/articles/10.3389/fmicb.2022.833790/full#supplementary-material

REFERENCES

Afridi, O. K., Ali, J., and Chang, J. H. (2020). Next-Generation Sequencing Based Gut Resistome Profiling of Broiler Chickens Infected with Multidrug-Resistant *Escherichia coli*. *Animals* 10:2350. doi: 10.3390/ani10122350

Bampidis, V., Azimonti, G., Bastos, M., Christensen, H., Dusemund, B., Kouba, M., et al. (2019). Safety and efficacy of Biomin®DC-P as a zootechnical feed additive for chickens for fattening, chickens reared for laying and minor avian species to the point of lay. *EFSA J.* 17:5724. doi: 10.2903/j.efsa.2019.5724

Becker, A. A. M. J., Hesta, M., Hollants, J., Janssens, G. P. J., and Huys, G. (2014). Phylogenetic analysis of faecal microbiota from captive cheetahs reveals underrepresentation of Bacteroidetes and Bifidobacteriaceae. *BMC Microbiol.* 14:43. doi: 10.1186/1471-2180-14-43

Bolger, A. M., Lohse, M., and Usadel, B. (2014). Trimmomatic: a flexible trimmer for Illumina sequence data. *Bioinformatics* 30, 2114–2120. doi: 10.1093/bioinformatics/btu170

Browne, H. P., Forster, S. C., Anonye, B. O., Kumar, N., Neville, B. A., Stares, M. D., et al. (2016). Culturing of 'unculturable' human microbiota reveals novel taxa and extensive sporulation. *Nature* 533, 543–546. doi: 10.1038/nature17645

Butaye, P., Devriese, L. A., and Haesebrouck, F. (2003). Antimicrobial Growth Promoters Used in Animal Feed: Effects of Less Well Known Antibiotics on Gram-Positive Bacteria. *Clin. Microbiol. Rev.* 16, 175–188. doi: 10.1128/cmr.16.2.175-188.2003

Castanon, J. I. R. (2007). History of the Use of Antibiotic as Growth Promoters in European Poultry Feeds. *Poult. Sci.* 86, 2466–2471. doi: 10.3382/ps.2007-00249

Costa, M. C., Bessegatto, J. A., Alfieri, A. A., Weese, J. S., Filho, J. A. B., and Oba, A. (2017). Different antibiotic growth promoters induce specific changes in the cecal microbiota membership of broiler chicken. *PLoS One* 12:e0171642. doi: 10.1371/journal.pone.0171642

Crisol-Martínez, E., Stanley, D., Geier, M. S., Hughes, R. J., and Moore, R. J. (2017). Understanding the mechanisms of zinc bacitracin and avilamycin on animal production: linking gut microbiota and growth performance in chickens. *Appl. Microbiol. Biotechnol.* 101, 4547–4559. doi: 10.1007/s00253-017-8193-9

Crofts, T. S., Gasparrini, A. J., and Dantas, G. (2017). Next-generation approaches to understand and combat the antibiotic resistome. *Nat. Rev. Microbiol.* 15, 422–434. doi: 10.1038/nrmicro.2017.28

Danzeisen, J. L., Kim, H. B., Isaacson, R. E., Tu, Z. J., and Johnson, T. J. (2011). Modulations of the Chicken Cecal Microbiome and Metagenome in Response to Anticoccidial and Growth Promoter Treatment. *PLoS One* 6:e27949. doi: 10.1371/journal.pone.0027949

De Cesare, A., Oliveri, C., Lucchi, A., Savini, F., Manfreda, G., and Sala, C. (2022). Pilot Study on Poultry Meat from Antibiotic Free and Conventional Farms: Can Metagenomics Detect Any Difference?. *Foods* 11:249. doi: 10.3390/foods11030249

Diarra, M. S., and Malouin, F. (2014). Antibiotics in Canadian poultry productions and anticipated alternatives. *Front. Microbiol.* 5:282. doi: 10.3389/fmicb.2014.00282

Díaz Carrasco, J. M., Redondo, E. A., Pin Viso, N. D., Redondo, L. M., Farber, M. D., and Fernández Miyakawa, M. E. (2018). Tannins and Bacitracin Differentially Modulate Gut Microbiota of Broiler Chickens. *BioMed. Res. Int.* 2018:1879168. doi: 10.1155/2018/1879168

Dorman, H. J. D., and Deans, S. G. (2000). Antimicrobial agents from plants: antibacterial activity of plant volatile oils. *J. Appl. Microbiol.* 88, 308–316. doi: 10.1046/j.1365-2672.2000.00969.x

Doster, E., Lakin, S. M., Dean, C. J., Wolfe, C., Young, J. G., Boucher, C., et al. (2019). MEGARes 2.0: a database for classification of antimicrobial drug, biocide and metal resistance determinants in metagenomic sequence data. *Nucleic Acids Res.* 48, D561–D569. doi: 10.1093/nar/gkz1010

Doyle, M. P., and Erickson, M. C. (2012). Opportunities for mitigating pathogen contamination during on-farm food production. *Int. J. Food Microbiol.* 152, 54–74. doi: 10.1016/j.ijfoodmicro.2011.02.037

Eckstrom, K., and Barlow, J. W. (2019). Resistome metagenomics from plate to farm: The resistome and microbial composition during food waste feeding and composting on a Vermont poultry farm. *PLoS One* 14:e0219807. doi: 10.1371/journal.pone.0219807

European Council (2010). *Directive 2010/63/EU of the European Parliament and of the Council of 22 September 2010 on the Protection of Animals Used for Scientific Purposes Text with EEA Relevance*. Available online at: https://eur-lex.europa.eu/eli/dir/2010/63/oj

Feng, J., Li, B., Jiang, X., Yang, Y., Wells, G. F., Zhang, T., et al. (2018). Antibiotic resistome in a large-scale healthy human gut microbiota deciphered by metagenomic and network analyses. *Environ. Microbiol.* 20, 355–368. doi: 10.1111/1462-2920.14009

Franzosa, E. A., Morgan, X. C., Segata, N., Waldron, L., Reyes, J., Earl, A. M., et al. (2014). Relating the metatranscriptome and metagenome of the human gut. *Proc. Natl. Acad. Sci. U. S. A.* 111, E2329–E2338. doi: 10.1073/pnas.1319284111

Ghanbari, M., Klose, V., Crispie, F., and Cotter, P. D. (2019). The dynamics of the antibiotic resistome in the feces of freshly weaned pigs following therapeutic administration of oxytetracycline. *Sci. Rep.* 9:4062. doi: 10.1038/s41598-019-40496-8

Gupta, C. L., Blum, S. E., Kattusamy, K., Daniel, T., Druyan, S., Shapira, R., et al. (2021). Longitudinal study on the effects of growth-promoting and therapeutic antibiotics on the dynamics of chicken cloacal and litter microbiomes and resistomes. *Microbiome* 9:178. doi: 10.1186/s40168-021-01136-4

Hawkey, P. M. (2008). The growing burden of antimicrobial resistance. *J. Antimicrob. Chemother* 62, i1–9. doi: 10.1093/jac/dkn241

Inglis, G. D., McAllister, T. A., Busz, H. W., Yanke, L. J., Morck, D. W., Olson, M. E., et al. (2005). Effects of subtherapeutic administration of antimicrobial agents to beef cattle on the prevalence of antimicrobial resistance in Campylobacter jejuni and Campylobacter hyointestinalis. *Appl. Environ. Microbiol.* 71, 3872–3881. doi: 10.1128/AEM.71.7.3872-3881.2005

Jamroz, D., Wiliczkiewicz, A., Wertelecki, T., Orda, J., and Skorupińska, J. (2005). Use of active substances of plant origin in chicken diets based on maize and locally grown cereals. *Br. Poult. Sci.* 46, 485–493. doi: 10.1080/00071660500191056

Juricova, H., Matiasovicova, J., Matiasovicova, J., Kubasova, T., Cejkova, D., and Rychlik, I. (2021). The distribution of antibiotic resistance genes in chicken gut microbiota commensals. *Sci. Rep.* 11:3290. doi: 10.1038/s41598-021-82640-3

Kaschubek, T., Mayer, E., Rzesnik, S., Grenier, B., Bachinger, D., Schieder, C., et al. (2018). Effects of phytogenic feed additives on cellular oxidative stress and inflammatory reactions in intestinal porcine epithelial cells1. *J. Anim. Sci.* 96, 3657–3669. doi: 10.1093/jas/sky263

Kopylova, E., Noé, L., and Touzet, H. (2012). SortMeRNA: Fast and accurate filtering of ribosomal RNAs in metatranscriptomic data. *Bioinformatics* 28, 3211–3217. doi: 10.1093/bioinformatics/bts611

Kumar, H., Park, W., Lim, D., Srikanth, K., Kim, J.-M., Jia, X.-Z., et al. (2020). Whole metagenome sequencing of cecum microbiomes in Ethiopian indigenous chickens from two different altitudes reveals antibiotic resistance genes. *Genomics* 112, 1988–1999. doi: 10.1016/j.ygeno.2019.11.011

Kumar, S., Chen, C., Indugu, N., Werlang, G. O., Singh, M., Kim, W. K., et al. (2018). Effect of antibiotic withdrawal in feed on chicken gut microbial dynamics, immunity, growth performance and prevalence of foodborne pathogens. *PLoS One* 13:e0192450. doi: 10.1371/journal.pone.0192450

Lagier, J.-C., Dubourg, G., Million, M., Cadoret, F., Bilen, M., Fenollar, F., et al. (2018). Culturing the human microbiota and culturomics. *Nat. Rev. Microbiol.* 16, 540–550. doi: 10.1038/s41579-018-0041-0

Langmead, B., and Salzberg, S. L. (2012). Fast gapped-read alignment with Bowtie 2. *Nat. Methods* 9, 357–359. doi: 10.1038/nmeth.1923

Lanza, V. F., Baquero, F., Martínez, J. L., Ramos-Ruíz, R., González-Zorn, B., Andremont, A., et al. (2018). In-depth resistome analysis by targeted metagenomics. *Microbiome* 6:11. doi: 10.1186/s40168-017-0387-y

Lau, J. T., Whelan, F. J., Herath, I., Lee, C. H., Collins, S. M., Bercik, P., et al. (2016). Capturing the diversity of the human gut microbiota through culture-enriched molecular profiling. *Genom. Med.* 8:72. doi: 10.1186/s13073-016-0327-7

Lawley, B., Sims, I. M., and Tannock, G. W. (2013). Whole-Transcriptome Shotgun Sequencing (RNA-seq) Screen Reveals Upregulation of Cellobiose and Motility Operons of Lactobacillus ruminis L5 during Growth on Tetrasaccharides Derived from Barley β-Glucan. *Appl. Environ. Microbiol.* 79, 5661–5669. doi: 10.1128/AEM.01887-13

Li, B., Yang, Y., Ma, L., Ju, F., Guo, F., Tiedje, J. M., et al. (2015). Metagenomic and network analysis reveal wide distribution and co-occurrence of environmental antibiotic resistance genes. *ISME J.* 9, 2490–2502. doi: 10.1038/ismej.2015.59

Li, H. L., Zhao, P. Y., Lei, Y., Hossain, M. M., and Kim, I. H. (2015). Phytoncide, phytogenic feed additive as an alternative to conventional antibiotics, improved growth performance and decreased excreta gas emission without adverse effect on meat quality in broiler chickens. *Livest. Sci.* 181, 1–6. doi: 10.1016/j.livsci.2015.10.001

Looft, T., Allen, H. K., Casey, T. A., Alt, D. P., and Stanton, T. B. (2014). Carbadox has both temporary and lasting effects on the swine gut microbiota. *Front. Microbiol.* 5:276. doi: 10.3389/fmicb.2014.00276

Love, M. I., Huber, W., and Anders, S. (2014). Moderated estimation of fold change and dispersion for RNA-seq data with DESeq2. *Genom. Biol.* 15:550. doi: 10.1186/s13059-014-0550-8

Lu, J., Breitwieser, F. P., Thielen, P., and Salzberg, S. L. (2017). Bracken: Estimating species abundance in metagenomics data. *PeerJ Comput. Sci.* 3:e104. doi: 10.7717/peerj-cs.104

Lutful Kabir, S. M. (2009). The role of probiotics in the poultry industry. *Int. J. Mol. Sci.* 10, 3531–3546. doi: 10.3390/ijms10083531

Ma, T., McAllister, T. A., and Guan, L. L. (2021). A review of the resistome within the digestive tract of livestock. *J. Anim. Sci. Biotechnol.* 12:121. doi: 10.1186/s40104-021-00643-6

Marshall, B. M., and Levy, S. B. (2011). Food animals and antimicrobials: impacts on human health. *Clin. Microbiol. Rev.* 24, 718–733. doi: 10.1128/cmr.00002-11

Mehdi, Y., Létourneau-Montminy, M.-P., Gaucher, M.-L., Chorfi, Y., Suresh, G., Rouissi, T., et al. (2018). Use of antibiotics in broiler production: Global impacts and alternatives. *Anim. Nutrit.* 4, 170–178. doi: 10.1016/j.aninu.2018.03.002

Mencía-Ares, O., Cabrera-Rubio, R., Cobo-Díaz, J. F., Álvarez-Ordóñez, A., Gómez-García, M., Puente, H., et al. (2020). Antimicrobial use and production system shape the fecal, environmental, and slurry resistomes of pig farms. *Microbiome* 8:164. doi: 10.1186/s40168-020-00941-7

Miles, R. D., Butcher, G. D., Henry, P. R., and Littell, R. C. (2006). Effect of antibiotic growth promoters on broiler performance, intestinal growth parameters, and quantitative morphology. *Poult. Sci.* 85, 476–485. doi: 10.1093/ps/85.3.476

Mitsch, P., Zitterl-Eglseer, K., Köhler, B., Gabler, C., Losa, R., and Zimpernik, I. (2004). The effect of two different blends of essential oil components on the proliferation of Clostridium perfringens in the intestines of broiler chickens. *Poult. Sci.* 83, 669–675. doi: 10.1093/ps/83.4.669

Mountzouris, K. C., Paraskevas, V., Tsirtsikos, P., Palamidi, I., Steiner, T., Schatzmayr, G., et al. (2011). Assessment of a phytogenic feed additive effect on broiler growth performance, nutrient digestibility and caecal microflora composition. *Anim. Feed Sci. Technol.* 168, 223–231. doi: 10.1016/j.anifeedsci.2011.03.020

Murugesan, G. R., Syed, B., Haldar, S., and Pender, C. (2015). Phytogenic Feed Additives as an Alternative to Antibiotic Growth Promoters in Broiler Chickens. *Front. Veterinary Sci.* 2:21. doi: 10.3389/fvets.2015.00021

Nesme, J., Cécillon, S., Delmont, Tom, O., Monier, J.-M., Vogel, et al. (2014). Large-Scale Metagenomic-Based Study of Antibiotic Resistance in the Environment. *Curr. Biol.* 24, 1096–1100. doi: 10.1016/j.cub.2014.03.036

Nowrotek, M., Jałowiecki, Ł, Harnisz, M., and Płaza, G. A. (2019). Culturomics and metagenomics: In understanding of environmental resistome. *Front. Environ. Sci. Eng.* 13:40. doi: 10.1007/s11783-019-1121-8

Pachter, L. (2011). Models for transcript quantification from RNA-Se. *Arxiv* [Preprint], arXiv:1104.3889.

Page, S. W., and Gautier, P. (2012). Use of antimicrobial agents in livestock. *Rev. Sci. Tech.* 31, 145–188. doi: 10.20506/rst.31.1.2106

Peimbert, M., and Alcaraz, L. D. (2016). "A Hitchhiker's guide to metatranscriptomics," in *Field Guidelines for Genetic Experimental Designs in High-Throughput Sequencing*, eds A. Aransay and J. Lavín Trueba (Cham: Springer). doi: 10.1007/978-3-319-31350-4_13

Phillips, I. (1999). The use of bacitracin as a growth promoter in animals produces no risk to human health. *J. Antimicrob. Chemother.* 44, 725–728. doi: 10.1093/jac/44.6.725

Proctor, A., and Phillips, G. J. (2019). Differential Effects of Bacitracin Methylene Disalicylate (BMD) on the Distal Colon and Cecal Microbiota of Young Broiler Chickens. *Front. Veterin. Sci.* 6:114. doi: 10.3389/fvets.2019.00114

Sabino, Y. N. V., Santana, M. F., Oyama, L. B., Santos, F. G., Moreira, A. J. S., Huws, S. A., (2019). Characterization of antibiotic resistance genes in the species of the rumen microbiota. *Nat. Commun.* 10:5252. doi: 10.1038/s41467-019-13118-0

Salaheen, S., Kim, S.-W., Haley, B. J., Van Kessel, J. A. S., and Biswas, D. (2017). Alternative Growth Promoters Modulate Broiler Gut Microbiome and Enhance Body Weight Gain. *Front. Microbiol.* 8:2088. doi: 10.3389/fmicb.2017.02088

Sarmah, A. K., Meyer, M. T., and Boxall, A. B. (2006). A global perspective on the use, sales, exposure pathways, occurrence, fate and effects of veterinary antibiotics (VAs) in the environment. *Chemosphere* 65, 725–759. doi: 10.1016/j.chemosphere.2006.03.026

Schmieder, R., and Edwards, R. (2011). Insights into antibiotic resistance through metagenomic approaches. *Futu. Microbiol.* 7, 73–89. doi: 10.2217/fmb.11.135

Song, S. J., Amir, A., Metcalf, J. L., Amato, K. R., Xu, Z. Z., Humphrey, G., et al. (2016). Preservation methods differ in fecal microbiome stability, affecting suitability for field studies. *mSystems* 1:e00021-16. doi: 10.1128/mSystems.00021-16

Stephens, M. (2016). False discovery rates: a new deal. *Biostatistics* 18, 275–294. doi: 10.1093/biostatistics/kxw041

Sun, J., Zhong, H., Du, L., Li, X., Ding, Y., Cao, H., et al. (2018). Gene expression profiles of germ-free and conventional piglets from the same litter. *Sci. Rep.* 8:10745. doi: 10.1038/s41598-018-29093-3

Thomas, M., Webb, M., Ghimire, S., Blair, A., Olson, K., Fenske, G. J., et al. (2017). Metagenomic characterization of the effect of feed additives on the gut microbiome and antibiotic resistome of feedlot cattle. *Sci. Rep.* 7:12257. doi: 10.1038/s41598-017-12481-6

Tong, P., Ji, X., Chen, L., Liu, J., Xu, L., Zhu, L., et al. (2017). Metagenome analysis of antibiotic resistance genes in fecal microbiota of chickens. *Agri. Gene.* 5, 1–6. doi: 10.1016/j.aggene.2017.06.001

Van Boeckel, T. P., Brower, C., Gilbert, M., Grenfell, B. T., Levin, S. A., Robinson, T. P., et al. (2015). Global trends in antimicrobial use in food animals. *Proc. Natl. Acad. Sci. U.S.A.* 112, 5649–5654. doi: 10.1073/pnas.1503141112

Van Boeckel, T. P., Glennon, E. E., Chen, D., Gilbert, M., Robinson, T. P., Grenfell, B. T., et al. (2017). Reducing antimicrobial use in food animals. *Science* 357, 1350–1352. doi: 10.1126/science.aao1495

Videnska, P., Faldynova, M., Juricova, H., Babak, V., Sisak, F., Havlickova, H., et al. (2013). Chicken faecal microbiota and disturbances induced by single or repeated therapy with tetracycline and streptomycin. *BMC Veterin. Res.* 9:30. doi: 10.1186/1746-6148-9-30

von Wintersdorff, C. J. H., Penders, J., van Niekerk, J. M., Mills, N. D., Majumder, S., van Alphen, L. B., et al. (2016). Dissemination of Antimicrobial Resistance in Microbial Ecosystems through Horizontal Gene Transfer. *Front. Microbiol.* 7:173. doi: 10.3389/fmicb.2016.00173

Wang, C., Dong, D., Strong, P. J., Zhu, W., Ma, Z., Qin, Y., et al. (2017). Microbial phylogeny determines transcriptional response of resistome to dynamic composting processes. *Microbiome* 5:103. doi: 10.1186/s40168-017-0324-0

Wang, J., Su, S., Pender, C., Murugesan, R., Syed, B., and Kim, W. K. (2021). Effect of a Phytogenic Feed Additive on Growth Performance, Nutrient Digestion, and Immune Response in Broiler-Fed Diets with Two Different Levels of Crude Protein. *Animals* 11:775. doi: 10.3390/ani11030775

Wang, Y., Hu, Y., Liu, F., Cao, J., Lv, N., Zhu, B., et al. (2020). Integrated metagenomic and metatranscriptomic profiling reveals differentially expressed resistomes in human, chicken, and pig gut microbiomes. *Environ. Int.* 138:105649. doi: 10.1016/j.envint.2020.105649

Wang, Y., Lyu, N., Liu, F., Liu, W. J., Bi, Y., Zhang, Z., et al. (2021). More diversified antibiotic resistance genes in chickens and workers of the live poultry markets. *Environ. Int.* 153:106534. doi: 10.1016/j.envint.2021.106534

Wei, S., Gutek, A., Lilburn, M., and Yu, Z. (2013). Abundance of pathogens in the gut and litter of broiler chickens as affected by bacitracin and litter management. *Vet. Microbiol.* 166, 595–601. doi: 10.1016/j.vetmic.2013.06.006

Wickham, H. (2016). *ggplot2: Elegant Graphics for Data Analysis*. (New York, NY: Springer-Verlag).

Wood, D. E., Lu, J., and Langmead, B. (2019). Improved metagenomic analysis with Kraken 2. *Genom. Biol.* 20:257. doi: 10.1186/s13059-019-1891-0

Xiong, W., Wang, Y., Sun, Y., Ma, L., Zeng, Q., Jiang, X., et al. (2018). Antibiotic-mediated changes in the fecal microbiome of broiler chickens define the incidence of antibiotic resistance genes. *Microbiome* 6:34. doi: 10.1186/s40168-018-0419-2

You, Y., and Silbergeld, E. K. (2014). Learning from agriculture: understanding low-dose antimicrobials as drivers of resistome expansion. *Front. Microbiol.* 5:284. doi: 10.3389/fmicb.2014.00284

Conflict of Interest: MG, GW, NG, AK, and VK are employed by DSM Animal Nutrition & Health, which provided support in the form of salaries for the authors but did not have the main role in the experimental design, data collection and analysis, decision to publish, or preparation of the manuscript. DSM Animal Nutrition & Health is involved in natural feed additive development and research in natural alternatives to in-feed medication in livestock production.

The remaining authors declare that the research was conducted in the absence of any commercial or financial relationships that could be construed as a potential conflict of interest.

Publisher's Note: All claims expressed in this article are solely those of the authors and do not necessarily represent those of their affiliated organizations, or those of the publisher, the editors and the reviewers. Any product that may be evaluated in this article, or claim that may be made by its manufacturer, is not guaranteed or endorsed by the publisher.

frontiers | Frontiers in Microbiology

ORIGINAL RESEARCH
published: 28 April 2022
doi: 10.3389/fmicb.2022.865768

Toxicological Effects of Microplastics and Sulfadiazine on the Microalgae *Chlamydomonas reinhardtii*

*Ze Li[1,2], Sheng Dong[1], Fei Huang[1], Langli Lin[1], Zhangli Hu[1] and Yihong Zheng[1]**

[1] Guangdong Provincial Key Laboratory for Plant Epigenetics, Guangdong Engineering Research Center for Marine Algal Biotechnology, College of Life Sciences and Oceanography, Shenzhen University, Shenzhen, China, [2] Shenzhen Engineering Laboratory of Microalgal Bioenergy, Harbin Institute of Technology Shenzhen, Shenzhen, China

Despite the fact that microplastics (MPs) facilitate the adsorption of environmental organic pollutants and influence their toxicity for organisms, more study is needed on the combination of MPs and antibiotics pollutant effects. In this study, polystyrene MPs (1 and 5 μm) and sulfadiazine (SDZ) were examined separately and in combination on freshwater microalga, *Chlamydomonas reinhardtii*. The results suggest that both the MPs and SDZ alone and in combination inhibited the growth of microalgae with an increasing concentration of MPs and SDZ (5–200 mg l^{-1}); however, the inhibition rate was reduced by combination. Upon exposure for 7 days, both the MPs and SDZ inhibited algal growth, reduced chlorophyll content, and enhanced superoxide dismutase (SOD) activities, whereas glutathione peroxidase (GSH-Px) activity was elevated only with the exposure of 1 μm MPs. Fluorescence microscopy and scanning electron microscopy also indicated that particle size contributed to the combined toxicity by aggregating MPs with periphery pollutants. Further, the amount of extracellular secretory protein increased in the presence of MPs and SDZ removal ratio decreased when MPs and SDZ coexisted, suggesting that MPs affected SDZ metabolism by microalgae. The particle size of microplastics affected the toxicity of MPs on microalgae and the combined effect of MPs and SDZ could be mitigated by MPs adsorption. These findings provide insight into microalgae responses to the combination of MPs and antibiotics in water ecosystems.

Keywords: microplastics size, antibiotics, algae, combined toxicity, oxidative stress

OPEN ACCESS

Edited by:
Wang Jiajun,
Northeast Agricultural University, China

Reviewed by:
Pengzhi Qi,
Zhejiang Ocean University, China
Marko D. Prokic,
University of Belgrade, Serbia

***Correspondence:**
Yihong Zheng
zhengy@szu.edu.cn

Specialty section:
This article was submitted to Antimicrobials, Resistance and Chemotherapy, a section of the journal Frontiers in Microbiology

Received: *30 January 2022*
Accepted: *08 March 2022*
Published: *28 April 2022*

Citation:
Li Z, Dong S, Huang F, Lin L, Hu Z and Zheng Y (2022) Toxicological Effects of Microplastics and Sulfadiazine on the Microalgae Chlamydomonas reinhardtii. Front. Microbiol. 13:865768. doi: 10.3389/fmicb.2022.865768

INTRODUCTION

The invention and use of plastic products have made human life more convenient; in spite of all these good feathers, plastic pollution has become a serious major global environmental threat because of its physicochemical stability and difficulty in degrading naturally in the environment, especially in the aquatic ecosystems (Barboza et al., 2018; Zhu et al., 2019). The effects of plastic pollution in the aquatic environment are being continually discovered, with the presence of plastic components has been detected in the ocean even at depths of 7,000–11,000 m and the discharge of plastic waste is increasing every year (Zhu et al., 2019). The toxic chemical additives are leaching in aqueous environment due to the plastic contaminants; furthermore, they also provide adsorption capacity for the enrichment of antibiotic-resistant bacteria and pesticide residues, which resulting in severe effects on marine ecosystems (Chae et al., 2019; Zhang et al., 2020),

riverine ecosystems (Zhang et al., 2018), and lake ecosystems (Beiras et al., 2021). Known as microplastics (MPs), these plastic pellets with a diameter ranging from 0.1 and 5 mm are long-term environmental contaminants (Sun et al., 2020). These MPs accumulate in aquatic animal through the food chain lead to affect their growth and development, reducing their nutritional status and harmful to the ecosystems and posing a health threat to humans (Coyle et al., 2020; Elizalde-Velázquez and Gómez-Oliván, 2021). In addition, the mixing of multiple pollutants further exacerbates the contamination of MPs due to its roughness, porosity, polarity, and hydrophobicity (Brandon et al., 2016; Nava and Leoni, 2021); it enables MPs to adsorb more contaminants in the environment—heavy metals, antibiotics, persistent organic pollutants, and other contaminants (Holmes et al., 2012; Wright et al., 2013; Coyle et al., 2020). As primary producers of aquatic ecosystems, microalgae may be affected by the toxicity of MPs pollution. In addition to the effects on microalgal growth, studies show that MPs affect algal photosynthesis, as chlorophyll content and photosynthesis efficiency decrease with exposure to MPs and that smaller sizes are considered more toxic. However, study into the effects of mixing microplastics with different pollutants is scarce (Nava and Leoni, 2021). A joint toxicity study of 0.3 mg l^{-1} triclosan and four kinds of 50 mg l^{-1} MPs was conducted with the microalgae *Skeletonema costatum* and it suggests that aggregation affected their combined effect by reducing the total superoxide dismutase (SOD) enzyme activity (Zhu et al., 2019). In another study, combined effects of MPs and mercury (ppb scale) caused neurotoxicity and lipid oxidative damage of *Dicentrarchus labrax* (Barboza et al., 2018). Hence, it is essential to study the combined toxicity of MPs and other pollutants.

Antibiotics are important pharmaceutical and personal care products (PPCPs) and some of them are relatively stable and can persist in surface water and even drinking water, raising concerns about their potential dangers (Chaturvedi et al., 2021). Among them, sulfonamides are the earliest category of synthetic drugs with a broad antibacterial spectrum, definite efficacy, convenience, and safety and are widely used in aquaculture; however, the removal rate of sulfonamides is low in the conventional wastewater treatment process (Zhang et al., 2019). Moreover, as a heavily used group of veterinary antibiotics, sulfonamides have high mobility and low sorption affinity in soil, making them more likely to leach into groundwater (Rath et al., 2019). This has led to a rise in the level of this contaminant in the water. A recent study shown that the growth of *Chlorella vulgaris* (*C. vulgaris*) was inhibited with an increasing SDZ concentrations (10–270 mg l^{-1}), which may be related to reactive oxygen species (ROS) damage to the algal photosynthetic system and chlorophyll biosynthesis. Furthermore, oxidative stress increases the activity of SOD and glutathione reductase, while decreases the activity of catalase. This made the antioxidant response inadequate to cope with the rising ROS and prevent oxidative damage (Chen et al., 2020a). Studies have shown that the co-occurrence of MPs and antibiotics decreases microbial activity and diversity in natural environments such as soil and nitrifying sludge, resulting in combined pollution (Wang et al., 2020a,b).

As a primary producer, microalgae affect the structure and function of an aquatic ecosystem. Microalgae are sensitive to toxic substances, so they are a promising indicator of microplastic pollution threats to freshwater ecosystems (Zhang et al., 2017). Microalgae have been considered to be sensitive to the ubiquitous MPs and antibiotics and studies have been focused on the effects of single pollutants (Prata et al., 2018; Machado and Soares, 2019). The studies on the combined toxicity of these two types of pollutants are still limited. For instance, polystyrene (PS)-MPs affected the removal of levofloxacin by altering the adsorption, enrichment, and enzymatic degradation of antibiotics by *Chlorella vulgaris*; the levofloxacin (initial concentration of 93.8 $\mu g\, l^{-1}$) removal rates for the microplastics group (35 items·L^{-1}) and the control group were 23.34 and 46.71%, respectively, on the third day, but the combined toxicity on microalgae was not extensively studied (Wu et al., 2022).

As a typical phytoplankton, *Chlamydomonas reinhardtii* (*C. reinhardtii*) has a great prospective to easy cultivation, considered as highly susceptible to environmental pollution, used as potential candidate for aquatic contamination assessments, and demonstrated high biosorption and removal efficiency of PPCPs (Xie et al., 2020). In this study, we evaluated the potential toxicity of MPs and sulfonamide antibiotics to *C. reinhardtii*, according to the effects on cell growth of the microalgae and the physiological and biochemical responses, as well as investigating whether microalgae secrete extracellular substances that defend against MPs and antibiotics by adhesion.

MATERIALS AND METHODS

Materials

Virgin PS-MPs microspheres (1 and 5-μm diameter, Cat. No. 7-3-0100 and 7-3-0500, respectively), labeled with green fluorescence (excitation wavelength: 470 nm and emission wavelength: 526 nm), were purchased from BaseLine ChromTech Research Centre (Tianjin, China) and IR absorption spectra confirmed the chemical composition of the microspheres. The diameters of PS-MPs particle were detected using the scanning electron microscope (SCM). Sulfadiazine (SDZ) sodium salt was purchased from Sigma-Aldrich (Cat. No. S6387-25G and purity 99.9%).

Algal Culture

Chlamydomonas reinhardtii CC124 strain was obtained from the *Chlamydomonas* Genetic Center of Duke University (Durham, North Carolina, United States) and cultured in a tris-acetate-phosphate (TAP) medium. Algal cells were cultivated in a constant temperature light incubator at 22 ± 2°C and 20 μmol photon $m^{-2}s^{-1}$ illumination. Algae were grown in 250 ml Erlenmeyer flasks and were shaken daily and randomly arranged to reduce any minor differences in photon irradiance (Huang et al., 2022).

Toxicology of Algal Growth Rate Inhibition

To assess the acute effects, a 24–96 h period is the ideal time (Schuwirth, 2020). In order to evaluate temporary exposure toxicity of single and combined effects of PS-MPs and SDZ, algae

were exposed to SDZ, PS-MPs, and combined SDZ with PS-MPs for 96 h. Since PPCPs were detected in a broad range of 0.1–50 mg l^{-1} in wastewater and *Chlamydomonas* was capable of removal of SDZ by photolysis (Xie et al., 2020), six concentrations of SDZ (5, 10, 20, 50, 100, and 200 mg l^{-1}) and six concentrations of PS-MPs (5, 10, 20, 50, 100, and 200 mg l^{-1}) were selected in this study and then the combination of fixed 50 mg l^{-1} PS-MPs and six concentrations of SDZ (5, 10, 20, 50, 100, and 200 mg l^{-1}) to analysis their conjoint effects based on the results of individual toxicity experiments. *C. reinhardtii* cells were cultured in a 12-well plate (Thermo Fisher Scientific, Cat. No. 150628) and seeded in the concentration of 10^5 cells ml^{-1}; the cell concentration was counted using a hemocytometer for inhibition rate estimation.

It is known that *C. reinhardtii* generally reached stationary stage after 5–6 days of incubation. According to the results of 96 h inhibition tests, the microalgae were subjected to a 7-day toxicity test with 50 mg l^{-1} SDZ, 50 mg l^{-1} PS-MPs, and combined 50 mg l^{-1} SDZ with 50 mg l^{-1} PS-MPs. The microalgae were cultured in 250 ml flasks and kept the other culture conditions consistent with the previous conditions. After exposure, cell concentration and biomass were calculated. A 50-ml culture was collected in order to determine the concentration of extracellular secretory protein and the rest of the culture was centrifugated at 4,500 *g* and 20°C for 10 min to collect algal cells. The total protein was extracted to measure biochemical activities.

Analysis of Chlorophyll Contents and Photosynthetic Activity Parameters

The contents of chlorophyll (Chl) were determined according to a modified method of the previous study (Zheng et al., 2017). The culture of algae (1 ml) was centrifuged at 12,000 rpm (Thermo Scientific Heraeus Pico 17 microcentrifuge) for 30 s at 20°C; then, the pellet was resuspended in 1 ml of 95% ethanol and incubated for 20 min at room temperature under shade condition and centrifuged again. The absorbance of the supernatant was measured at 630, 647, 664, and 750 nm using the Synergy Neo2 Plate Reader (BioTek, United States) and the contents of chlorophyll extract were calculated according to the following equations:

$$\begin{aligned}\text{Chla} &= [11.85(OD_{664} - OD_{750}) - 1.54(OD_{647} - OD_{750}) \\ &\quad -0.08(OD_{630} - OD_{750})]\end{aligned}$$

$$\begin{aligned}\text{Chlb} &= [-5.43(OD_{664} - OD_{750}) + 21.03(OD_{647} - OD_{750}) \\ &\quad -2.66(OD_{630} - OD_{750})]\end{aligned}$$

$$\begin{aligned}\text{Chlc} &= [-1.67(OD_{664} - OD_{750}) - 7.6(OD_{647} - OD_{750}) \\ &\quad +24.52(OD_{630} - OD_{750})]\end{aligned}$$

The parameters of photosynthetic activity of algae were measured using a pulse amplitude modulated (PAM) fluorometer water-PAM (Walz, Germany; (Zheng et al., 2017). Fv/Fm (Fv, variable fluorescence; Fm, maximum fluorescence) is the largest photochemical quantum yield of photosystem II (PSII), which reflects the quantum yield when all the PSII reaction centers are in an open state. Yield (YII) is the actual photochemical efficiency of PSII in light.

Measurement of Antioxidant Activity of Enzyme

The activities of total antioxidant enzyme SOD and glutathione peroxidase (GSH-Px) were measured by using and following the recommended instructions of the colorimetric commercial kits (Cat. No. A001-3-2 and A005-1-2, respectively, Nanjing Jiancheng Bioengineering Research Institute). The activity of SOD was assayed with the reaction based on its inhibition on the scale of superoxide anion generated by xanthine and xanthine oxidase reaction system. A SOD unit was measured as the amount of enzyme that led to a half inhibition of the nitroblue tetrazolium reduction rate using the plate reader at 550 nm. GSH-Px was measured according to the manufacturer's protocol. Based on the reaction ability of dithodinitrobenzoic acid with sulfhydryl compounds at 405 nm absorption peak in producing a relatively stable yellow color, GSH activity was measured. GSH-Px is preferably represented by catalyzed GSH reaction rate by measuring absorbance at 412 nm for 5 min. In this study, the activities of SOD and GSH-Px were expressed as units per milligram of protein (U mg^{-1}). The concentration of protein was determined using a protein quantification kit (C503061-1250, Sangon Biotech, China).

Confocal Laser Microscope and Scanning Electron Microscope Observation

After 96 h exposure, MPs and microalgae in culture were observed using a confocal laser scanning microscope (CLSM; Leica TCS SP8, Germany) and analyzed by image analysis system with HCX PL APO 40X 0.85 dry objective lens. Fluorescence images were recorded for MPs particles with excitation and emission wavelengths of 554 and 586 nm, respectively, and 649/670 nm for the determination of fluorescence for microalgal cells, respectively. MPs particles are shown in green color and microalgal cells are shown in red color. After 96 h of exposure under toxicity assay, the microalgal cells were collected by centrifugation (5,000 rpm, 10 min, and 20°C). Samples were initially fixed overnight at 4°C with 2.50% glutaraldehyde and then washed three times with phosphate-buffered saline (PBS; pH 7.4). Afterward, the samples were dehydrated for 15 min through a series of 30, 50, 70, 80, 90, 95, and 100% alcohol solutions. The dehydrated samples were placed in an oven at 40°C and dried for 24–48 h. After gold spraying, the samples were observed by scanning electron microscopy (SEM; Phenom Pro).

Extracellular Secretory Protein and Sulfadiazine Removal Rate Measurement

The protein, which was extracted from extracellular polymeric substances (EPSs), was quantified and analyzed as follows: by 10,000 *g* centrifugation at 20°C for 15 min, supernatant solution was pipetted and filtered through a 0.45-μm glass fiber (GF) membrane (GF, 25 mm, mesh size 0.45 μm, Munktell). Colorimetric analysis of EPS protein content was carried out

using the protein quantification kit (Sangon Biotech, China). The absorbance of the samples was read at 595 nm using the Synergy Neo2 Plate Reader (BioTek, United States) and protein concentration was calculated by comparison with the standard curve (Bellingeri et al., 2019).

The quantum yield is a critical factor that employs to quantify the efficiency of sulfonamides photodegradation reaction and an absorption peak at 254 nm indicates the photolysis products from SDZ degradation (Liu et al., 2018). Therefore, concentration of SDZ in algal culture was measured for antibiotics removal ratio assessment. A 50-ml of algal culture was centrifuged at 4,500 *g* and 20°C for 15 min; the supernatant was collected and SDZ concentration was measured at 254 nm using the plate reader and calculated by comparison with the standard curve.

Statistical Analysis

Each experiment was performed in triplicate and graphs were plotted by the Prism 8 (GraphPad Software Incorporation). For statistical analysis, data were subjected to IBM SPSS version 25.0 (IBM SPSS) with the Shapiro–Wilk's and Levene's tests ($p > 0.05$) to confirm normal distribution and homoscedasticity, respectively. The differences among the treatments were analyzed by single-factor ANOVA and taking a level of $p < 0.05$ as significant to Duncan's multiple range test. The difference and interactive effects between antibiotics and MPs were examined using the two-way ANOVA followed by the Student–Newman–Keuls (SNK) tests for multiple comparisons (with significant level of $p < 0.05$).

RESULTS AND DISCUSSION

Inhibition Effect of Polystyrene-Microplastics and Sulfadiazine on Microalgae Growth

The toxicity of SDZ and PS-MPs on the growth of microalgae was evaluated by the growth inhibition effect. The results showed that the exposure of PS-MPs and SDZ treatment alone inhibited the growth of algal cells and the inhibition effect was gradually increased at higher concentration. For instance, at the highest tested concentration of 200 mg l^{-1}, the PS-MPs alone inhibited the algal growth rate of 70.41 and 50.41% by using 1 and 5 μm, respectively, while SDZ alone inhibited only 42.40% (**Figure 1A**). It indicates that individual PS-MPs exposure inhibited the growth of *C. reinhardtii* cells. Under the same concentration, for different particle size of MPs, smaller size of particle had a higher inhibition rate of microalgae growth and the inhibition effect was also enhanced with an increasing concentration for 1 and 5 μm PS-MPs. This is similar to the findings, which have been already reported in other organisms (e.g., rotifers, shrimps, fungus), also showed that MPs with smaller sizes of particles were more toxic than those with larger sizes of particles (Varó et al., 2019; Wang et al., 2019a,b). There may probably three main reasons, which are associated to this phenomenon: first, smaller diameter of MPs may be able to enter the cell and affect the microalgae directly (Chen et al., 2020b). Besides, smaller diameter of MPs is more likely to adsorb to the surface of the algal cell and ultimately affect the uptake of external nutrients (Bhattacharya et al., 2010). Finally, the presence of MPs can have a shading effect on microalgae, thereby affecting the photosynthesis of algal cells and causing toxicity. Under the same concentration of MPs, the number of small size of MPs particles is much higher than that of large size of MPs particles, leading to a lower light transmission rate for small size MPs cultures, thus affecting algal cell growth (Zhang et al., 2017). However, microalgal cells are highly resistant to SDZ antibiotics and the inhibition rate was remained below 50% at SDZ concentrations up to 200 mg l^{-1}, suggesting that algal cells can remove antibiotics from the environment. It was shown that microalgae could remove antibiotics by photolysis and biodegradation (Xie et al., 2020).

As the analysis showed that there was no significant difference in inhibition rate of single treatment PS-MPs concentration between 10 and 50 mg l^{-1}, the result of algal cell inhibition rates at fixed concentrations (50 mg l^{-1}) of PS-MPs combined with different concentrations of antibiotics was subsequently analyzed (**Figure 1B**). With contents of SDZ below 50 mg l^{-1}, the joint inhibition rate seems consistently lower than SDZ presence alone. When concentration of SDZ was above 50 mg l^{-1}, the rate of inhibition of PS-MPs with smaller sizes of particle was lower than that of larger sizes of particle. For instance, the combined inhibition of SDZ with 1 μm PS-MPs decreased by 5.43% ($p < 0.05$) at SDZ concentration of 100 mg l^{-1} compared to SDZ alone, while this value decreased by 11.0% ($p < 0.05$) at SDZ concentration of 200 mg l^{-1}. In contrast, there was no significant difference between SDZ alone and in combination with SDZ with 5 μm PS-MPs at SDZ concentrations of 100 and 200 mg l^{-1}. This evidence is suggesting that the presence of MPs may reduce the inhibition of algal growth by excessive antibiotics. This effect is notable for MPs with smaller sizes of particle. The two-way ANOVA results indicated significant effects of MPs and SDZ for growth inhibition of *C. reinhardtii* and the interaction between SDZ and 5 μm PS-MPs (**Supplementary Table 1**). MPs have a strong adsorption capacity for heavy metals, organic pollutants, etc. (Barboza et al., 2018), which could reduce the concentrations of antibiotics in the medium. At the same concentration and with a larger specific surface area, small size of MPs is more powerful in adsorption and, thus, more effective in reducing the inhibition rate (Sjollema et al., 2016). In the control group exposed only to SDZ, the toxicity of SDZ may be reflected in an increased oxidative stress and chlorophyll inhibition in algal cells, thereby reducing photosynthetic efficiency and affecting algal growth. The secretion of EPS by algal cells makes it easier for MPs of small sizes to accumulate around algal cells, potentially forming a barrier and reducing SDZ exposure. Consequently, the two particle sizes of MPs interact differently with SDZ. As MPs compete with SDZ for toxicity, the combined action of SDZ and MPs reduced the rate of growth inhibition of *C. reinhardtii*.

Analysis of morphology of microalgal cell can provide more clues to the health status of microalgae, as well as indications of the effects of combining MPs and antibiotics on microalgae. According to the confocal microscopic image (**Figure 2**), it was observed that the MPs were not uniformly distributed and

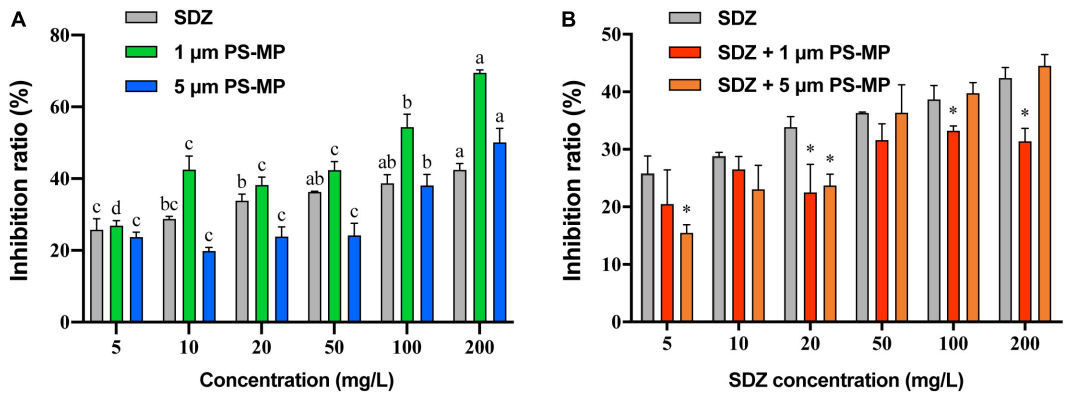

FIGURE 1 | The average growth inhibition ratio of microalgae exposed 96 h to sulfadiazine (SDZ) and polystyrene-microplastics (PS-MPs) in the different groups. **(A)** Single treatment of SDZ and MPs and **(B)** 50 mg l^{-1} of different particle size MPs + SDZ in comparison with SDZ only. Values are the mean ± SEM of three replicates. Significant differences ($p < 0.05$) are denoted with different letters **(A)** and an asterisk for MPs + SDZ vs. SDZ only **(B)**.

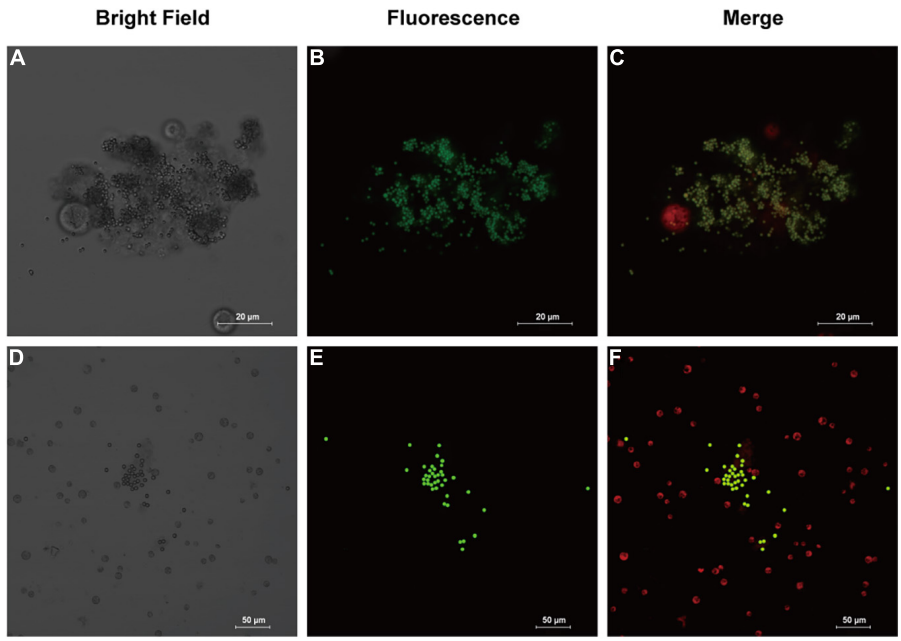

FIGURE 2 | Images of fluorescently labeled PS-MPs in microalgal culture (96 h). **(A–C)**: 1 μm MPs in culture with *Chlamydomonas reinhardtii* (*C. reinhardtii*), bright field **(A)** the fluorescence of MPs distribution **(B)** and merged fluorescence of microalgae (red) and MPs (green) **(C)**. **(D–F)**: 5 μm MPs in culture with *C. reinhardtii*, bright field **(D)** the fluorescence of MPs **(E)** and merged fluorescence **(F)**.

aggregation occurred. The aggregation was evident in microalgae treated with 1 μm PS-MPs, which was likely due to the fact that the algal cells secreted a large amount of extracellular organic matter, which caused the MPs to stick, leading to the deposition and aggregation of MPs at the bottom. Therefore, the concentration of MPs in the medium is decreased and may reduce the toxicity of MPs to algal cells. Stimulation by different excitation light can discriminate between the fluorescence of chlorophyll and MPs; it was found that most of the algal cells did not directly contact with MPs and only a small amount of MPs would be contacted with the surface of algal cells, but no MPs were found to enter the algal cells, which may indicate that the inhibitory effect on algal cells is not caused by internalization of the small-diameter MPs, but possibly by influencing the external environment such as nutrient uptake and light radiation to algal cells. However, another study provided evidence that 1–2 μm MPs could enter cells of two species of microalgae at extremely low rates, but the detailed mechanisms remain undiscovered (Yang et al., 2020).

The morphological characteristics of *C. reinhardtii* under different treatments were observed by scanning electron microscopy. PS-MPs at the concentration of 1 μm could attach to the surface of *C. reinhardtii* (**Figure 3A**) and PS-MPs at the concentration of 5 μm could not attach to the surface of

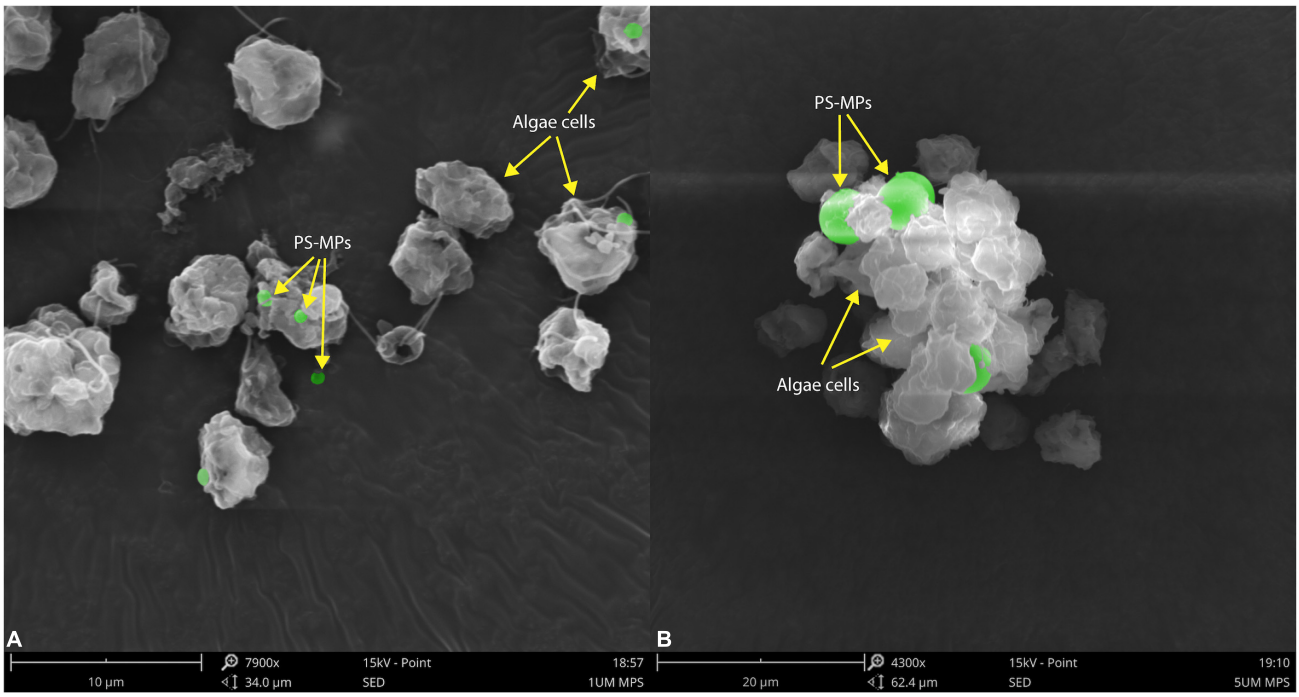

FIGURE 3 | Scanning electron microscopic images of *C. reinhardtii* exposed to different particle size of PS-MPs **(A)** 1 μm MPs; **(B)** 5 μm MPs. The identified MPs are green colored.

microalgae due to their large size, but would aggregate with microalgae to form a cluster (**Figure 3B**). The aggregation of MPs and microalgae may cause physical damage to the algae, such as changes in structure of cell wall (Wang et al., 2016), furthermore inhibiting the growth of the algae. In addition, this aggregation can increase the sedimentation coefficient of microalgae, consequently leading to settling of microalgae and aggregation at the bottom of the flask in the later stages of culture.

Antioxidant Enzymes and Photosynthesis Performance Under Microplastics and Sulfadiazine Toxicity

When the external environment is unfavorable to the growth of microalgae, it causes conducive changes to the growth of algae for their survival and this process is mainly regulated by the activity of some enzymes in algal cells (Li et al., 2020a). The existence of MPs and antibiotics in the external environment is involved in affecting the enzymatic activity of algal cells, but to significantly different extents. Comparison of enzyme activity (**Figure 4**) showed that the intracellular GSH-Px activity was basically same as the control under the condition of individual treatment of SDZ at the concentration of 50 mg l^{-1}, which indicated that antibiotics at this concentration did not affect the intracellular GSH-Px enzyme activity, but when MPs were present in the medium, the intracellular GSH-Px activity was significantly increased in all the cases. The enzyme activity was peaked at the diameter of 1 μm PS-MPs and 50 mg l^{-1} SDZ in combined treatment (**Figure 4B**), suggesting that particle size of MPs affects the growth of algal cell, which is consistent with other previously described studies (Wu et al., 2021). The SOD enzyme activity assay revealed that the results were consistent with GSH-Px, but the highest SOD activity was observed in the presence of 5 μm PS-MPs and SDZ (**Figure 4A**). The two-way ANOVAs revealed significant main effects of MPs, but not SDZ for GSH-Px activity and the effects of MPs on GSH-Px were independent of SDZ. The SOD activity was significantly responsive to MPs and SDZ and the interactions between MPs and SDZ (**Supplementary Table 2**). Studies have suggested that stress from external environmental factors, including heavy metals, organic acids, and salt stress, can induce significant production of ROS inside the plant cells (Cheng et al., 2017). It was found in previous study of the toxicity of aging microplastic polyvinyl chloride and copper to microalgae *Chlorella vulgaris* that both the mPVC (10 mg l^{-1}) and copper (0.5 mg l^{-1}) caused severe cellular damage and increased the concentrations of intracellular SOD and malondialdehyde (MDA; Fu et al., 2019). Excess ROS could damage the cell membrane system of the organism and eventually inhibited their growth. Mitochondria are a major source of free radicals and MPs can interact with their outer membranes (reducing mitochondrial membrane potential) or indirectly affect their function, thus resulting in ROS production. As frontline defense enzymes that directly eliminate ROS, both the SOD and GSH-Px are potentially effective markers of early oxidative damage induced by MPs and antibiotics. The SOD catalyzes the dismutation of O_2^- to molecular oxygen and hydrogen peroxide (H_2O_2), which is subsequently removed by catalase and GSH-Px. These enzymes catalyze the reduction of H_2O_2 to harmless

products and the intracellular antioxidative system scavenges excess oxygen radicals, leading to avoiding or reducing oxidative damage (Cheng et al., 2017; Prokić et al., 2019).

The chlorophyll content of microalgae in the presence of both the MPs and SDZ was measured in this study and the results (**Figure 5A**) showed a higher chlorophyll content in the control group and both the presence of SDZ and MPs alone and in combination resulted in a significant reduction of chlorophyll a, b, and c in algal cells, with inhibition rates of roughly 15–23%. This is following the results of other studies, except for the difference in the inhibition effect, e.g., it was found that the pigment content within microalgae was significantly reduced after 48 h of MPs exposure, with a maximum inhibition rate of 62.86% (Yang et al., 2021). This may be related to the tolerance of different species of microalgae and the material of MPs (Zhu et al., 2019). It appears that *C. vulgaris* was less sensitive to SDZ and the chlorophyll a content decreased significantly in the 10 and 270 mg l^{-1} groups following 7-day exposure, but only slightly reduced in the 30 and 90 mg l^{-1} groups (Chen et al., 2020a). In contrast, *C. reinhardtii* was more sensitive in this experiment and the chlorophyll contents were all significantly decreased after treatment. The two-way ANOVAs revealed that chlorophyll a and c contents were not significantly affected by SDZ, but all the chlorophyll contents were significantly responsive to MPs exposure and their interaction between MPs and SDZ (**Supplementary Table 3**). Chlorophyll fluorescence is sensitive parameter to environmental stress; the decrease in contents of chlorophyll may be related to the accumulation of intracellular ROS that disrupts the cell structure and hinders the synthesis of chlorophyll. In addition, it may be due to the high adsorption capacity of MPs, which adsorb on microalgae to form aggregates during the culture process, rendering some algae inactive (Lagarde et al., 2016). We have observed in this study that there was no significant difference in the contents of chlorophyll in combined treatments (MPs and SDZ) compared to their individual treatments, suggesting that the combined effect of MPs and SDZ on chlorophyll in *C. reinhardtii* is consistent with their presence alone.

Photosynthetic efficiency of microalgae was measured using the PHYTO-PAM fluorometer to examine whether MPs and SDZ affect the photosynthesis of microalgae. Fv/Fm and YII represent the ability of PSII to absorb photon energy and use it for photochemistry under dark-adapted and light-adapted conditions, respectively, when damage or inhibition of protein complexes in the photosystem and reduced viability of algal cells may result in the declined photosynthetic capacity of microalgal cells (Schwab et al., 2011). The results, which are shown in **Figure 5B**, indicated the photosynthetic efficiency of microalgae, despite a slight variance was not statistically different, suggesting that the photosynthetic efficiency of microalgae was not affected by PS-MPs and antibiotics. According to the two-way ANOVA analysis, photosynthetic efficiency was significantly affected by SDZ, but not significantly responsive to MPs and interaction between MPs and SDZ (**Supplementary Table 4**). In a previous study, the results were similar, which indicated that MPs (25 mg l^{-1}, sizes 0.05, 0.5, and 6 μm) did not affect the photosynthesis of various microalgae, including diatoms, *Dunaliella salina*, and freshwater *Chlorella* (Sjollema et al., 2016). However, another study revealed that a unicellular flagellate alga *Karenia mikimotoi* showed decreasing trend in photosynthesis about 25.3 and 17.1% in YII and Fv/Fm, respectively, when exposed it under 0–100 mg l^{-1} 1.0 μm PVC-MPs (Zhao et al., 2019). We have inferred from these findings that the sensitivity of different microalgae to MPs differs and may also be associated with the food web and phytoplankton community in aquatic ecosystems.

Extracellular Secretory Proteins and Removal of Sulfadiazine Antibiotics by Microalgae

In response to diverse environmental stresses, microalgal cells secrete the natural EPS, which provides functions as a barrier to prevent the entry of toxic substances into the cell, triggers the induction of protective mechanisms in response to unfavorable growth conditions from the external environment, and then secretes extracellular proteins to protect the cell (Bellingeri et al., 2019). Thus, the presence of MPs may stimulate the secretion of EPS by microalgae, leading to high protein contents in the culture medium. To test this hypothesis, extracellular secretory proteins were measured after 7 days of PS-MPs and SDZ treatment and the results (**Figure 6A**) showed that individual treatment of SDZ did not increase the amount of secreted extracellular protein. MPs alone and in combination with SDZ increased the amount of extracellular protein secreted by microalgal cells. The amount of extracellular protein, which is secreted by microalgal cells, reached at its maximum stage upon combined treatments of 5 μm PS-MPs and antibiotics. The results of two-way ANOVA showed that SDZ and MPs had a significant effect on EPS production and the interaction analysis of SDZ and MPS revealed a correlation between them (**Supplementary Table 5**). The variation in the quantity and composition of EPS secretion can be influenced by environmental conditions and the discrepancies in the combined effects of MPs and antibiotics of different sizes of particle may be the primary factor, which are contributing to the amount of secreted extracellular proteins (Adeleye and Keller, 2016). After 9 h of 2 μm PS-MPs exposure, the bound and soluble EPS of microalgae *Scenedesmus abundans* significantly increased (Cheng and Wang, 2022). In another study, *C. reinhardtii* was exposed to 50 mg l^{-1} of PS-MPs (300–600 nm) for 6 days and EPS decreased slightly compared to the control group, but remained much higher than the level at the start of this study (Li et al., 2020b). Therefore, stimulus of MPs to microalgae may show different features (e.g., biomass, growth inhibition, and quantity of EPS) depending on species, size, and treatment modality.

The most antibiotics are difficult to biodegrade due to their pharmacological stability (Martin-Laurent et al., 2019) or resistance (Li et al., 2020a), causing the residues of antibiotics in the environment, which are notable for their harmful effects on the ecology and human health. In previous studies, microorganisms were isolated, which have potential capacity to biodegrade the effect of antibiotic, such as SDZ. It was noticed that strain of *Arthrobacter* D2 degrades the effects of SDZ more than 50% at an initial concentration of 50 mg l^{-1} (Deng et al., 2016). The studies have been demonstrated that microalgae

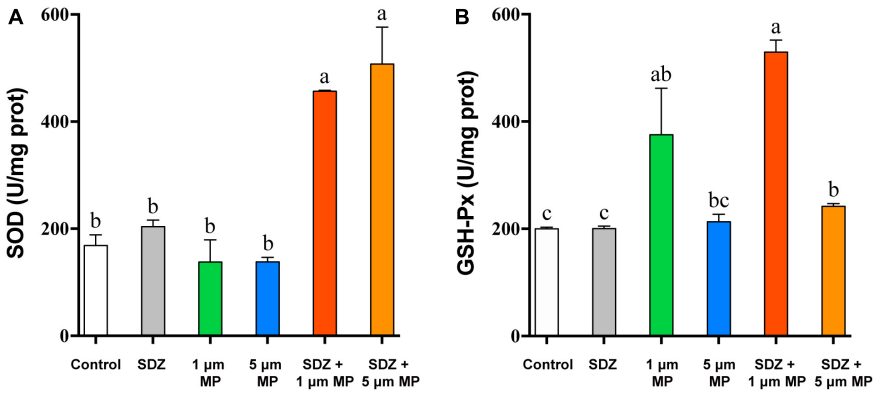

FIGURE 4 | The superoxide dismutase (SOD) **(A)** and glutathione peroxidase (GSH-Px) **(B)** enzyme activities of *C. reinhardtii* exposed to PS-MPs (1 and 5 μm) and/or SDZ (50 mg l^{-1}). Values are means ± SEM of three replicates and significant differences ($p < 0.05$) are denoted with different letters.

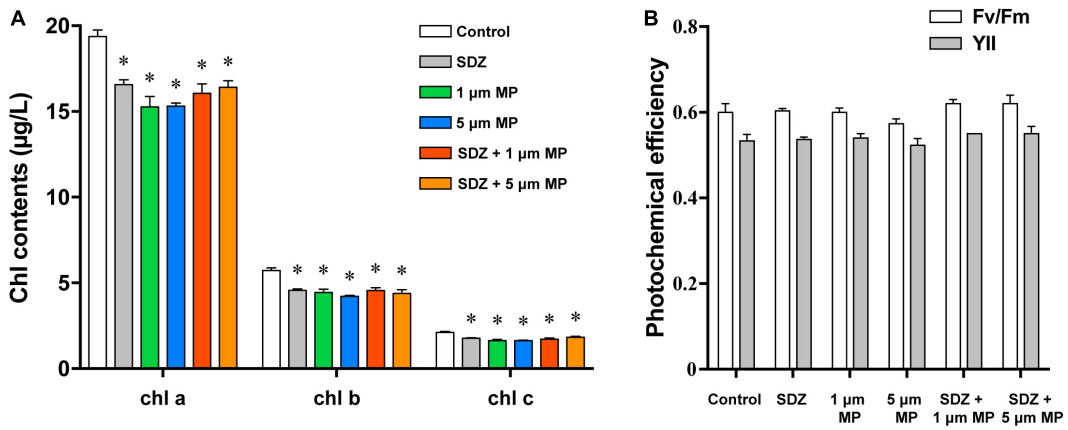

FIGURE 5 | The chlorophyll contents **(A)** and photochemical efficiency **(B)** of *C. reinhardtii* exposed to PS-MPs (1 and 5 μm) and/or SDZ (50 mg l^{-1}). Data are shown as means ± SEM of three replicates and an asterisk note for significant difference between treatments and the control group ($p < 0.05$).

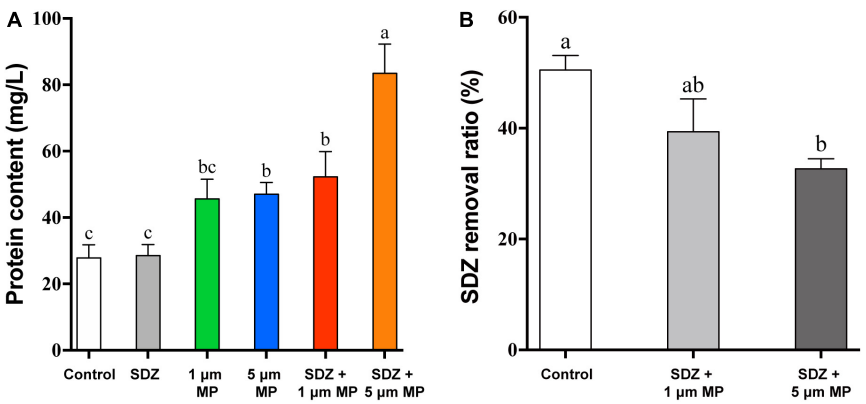

FIGURE 6 | The extracellular cellular protein content of *C. reinhardtii* exposed to PS-MPs (1 and 5 μm) and/or SDZ (50 mg l^{-1}) **(A)** and SDZ removal ratio with different particle sizes PS-MPs coexistence **(B)**. Values are means ± SEM of three replicates and significant differences ($p < 0.05$) are denoted with different letters.

have great prospective to eliminate antibiotics from the aqueous environment through multiple differential mechanisms. The most effective pathways, which are involving in the removal of organic pollutants by microalgae, are performed through enzymatic reactions, mainly including oxidation and hydrolysis (Foflonker et al., 2016; Xiong et al., 2017). There are also

studies showing biosorption of antibiotics by microalgae cells (Angulo et al., 2018), while compounds with the cationic groups tend to adsorb on the surface of microalgae through electrostatic interactions (Xiong et al., 2019). In addition, abiotic reactions, including hydrolysis and photolysis, also contribute to the removal of antibiotics (Norvill et al., 2017; Song et al., 2019). A study revealed that removal efficiency of SDZ by *Chlamydomonas* spp. exceeded 50% at an initial concentration of 10 mg l^{-1}. In PPCPs removal, adsorption played an essential role, ciprofloxacin and SDZ are mainly adsorbed on EPS by binding with the carbonyl and amine groups in tryptophan protein-like substances, and EPS on the microalgae is limited, making it easier for PPCPs to pass through and diffuse into the cells for biodegradation. However, due to the negative zeta potential, SDZ has lower adsorption efficiency with EPS (Xie et al., 2020). To study whether MPs affect the bioremoval of SDZ by microalgae, after 7 days of culture, SDZ concentration in the medium was measured. The removal rate of SDZ reached up to 51% in microalgae medium, which are treated with only 50 mg l^{-1} SDZ (control), while the removal rate decreased by 11 and 18% in the medium supplemented with 1 μm PS-MPs and 5 μm PS-MPs, respectively (**Figure 6B**). The increase of EPS, particularly in the 5 μm MPs group and the relatively low adsorption of SDZ onto microalgal EPS, could affect algal internalization of SDZ, which in conjunction with the cytotoxicity of PS-MPs may reduce SDZ removal efficiency. The results showed that bioremoval of SDZ by microalgae was inhibited in the presence of PS-MPs; this is consistent with a recent study showing that levofloxacin removal by *C. vulgaris* was significantly inhibited when PS-MPs co-exposed (Wu et al., 2022); even though the antibiotic species and MPs have different effects on their degradation mechanisms, understanding the scavenging of antibiotics from the environment by microalgae and the mechanisms is important.

CONCLUSION

In this study, we examined the single and combined effects of PS-MPs and SDZ on freshwater alga *C. reinhardtii*. SDZ exposure and the attachment of MPs to microalgae increased antioxidant enzyme activity, resulting in an increase in extracellular secretory proteins and a decrease in chlorophyll content. This was accompanied by a reduction in the growth rate of microalgae and noticeable aggregation of MPs. Exposure toxicity increased with the concentration and interaction of PS-MPs and SDZ, but different particle sizes and their interactions with SDZ had differential effects and when co-exposed with 5 μm PS-MPs, SDZ removal rates by algae were compromised. Therefore, considering the increasing trend of global antibiotics and microplastics production in response to the demand of the human population growing rapidly and the fundamental role of microalgae as primary producers in aquatic ecosystems, more studies on the combined effects of microplastics and emerging contaminants are required.

DATA AVAILABILITY STATEMENT

The original contributions presented in the study are included in the article/**Supplementary Material**, further inquiries can be directed to the corresponding author/s.

AUTHOR CONTRIBUTIONS

ZL, YZ, and ZH conceived and designed the experiments. ZL and LL performed the experiments. ZL, SD, and FH analyzed the data. ZL and YZ contributed reagents, materials, analysis tools, and wrote the manuscript. All authors contributed to the article and approved the submitted version.

FUNDING

This study was financially supported by the Guangdong Natural Science Foundation (2020A1515010873), the Shenzhen Special Program for Development of Emerging Strategic Industries (JSGG20180130103422600), the National Natural Science Foundation of China (31870343), the Innovation-Driven Development Special Fund Project of Guangxi (Guike AA18242047), and the Grant Plan for Demonstration City Project for Marine Economic Development in Shenzhen (No. 86) to ZH.

SUPPLEMENTARY MATERIAL

The Supplementary Material for this article can be found online at: https://www.frontiersin.org/articles/10.3389/fmicb.2022.865768/full#supplementary-material

REFERENCES

Adeleye, A. S., and Keller, A. A. (2016). Interactions between algal extracellular polymeric substances and commercial TiO2 nanoparticles in aqueous media. *Environ. Sci. Technol.* 50, 12258–12265. doi: 10.1021/acs.est.6b03684

Angulo, E., Bula, L., Mercado, I., Montano, A., and Cubillan, N. (2018). Bioremediation of cephalexin with non-living *Chlorella* sp., biomass after lipid extraction. *Bioresour. Technol.* 257, 17–22. doi: 10.1016/j.biortech.2018.02.079

Barboza, L. G. A., Vieira, L. R., Branco, V., Figueiredo, N., Carvalho, F., Carvalho, C., et al. (2018). Microplastics cause neurotoxicity, oxidative damage and energy-related changes and interact with the bioaccumulation of mercury in the European seabass, *Dicentrarchus labrax* (Linnaeus, 1758). *Aquat. Toxicol.* 195, 49–57. doi: 10.1016/j.aquatox.2017.12.008

Beiras, R., Verdejo, E., Campoy-López, P., and Vidal-Liñán, L. (2021). Aquatic toxicity of chemically defined microplastics can be explained by functional additives. *J. Hazard. Mater.* 406:124338. doi: 10.1016/j.jhazmat.2020.124338

Bellingeri, A., Bergami, E., Grassi, G., Faleri, C., Redondo-Hasselerharm, P., Koelmans, A. A., et al. (2019). Combined effects of nanoplastics and copper on the freshwater alga *Raphidocelis subcapitata*. *Aquat. Toxicol.* 210, 179–187. doi: 10.1016/j.aquatox.2019.02.022

Bhattacharya, P., Lin, S., Turner, J., and Ke, P. (2010). Physical adsorption of charged plastic nanoparticles affects algal photosynthesis. *J. Phys. Chem. C* 114:16556. doi: 10.1021/jp1054759

Brandon, J., Goldstein, M., and Ohman, M. D. (2016). Long-term aging and degradation of microplastic particles: comparing *in situ* oceanic and experimental weathering patterns. *Mar. Pollut. Bull.* 110, 299–308. doi: 10.1016/j.marpolbul.2016.06.048

Chae, Y., Kim, D., and An, Y.-J. (2019). Effects of micro-sized polyethylene spheres on the marine microalga *Dunaliella salina*: focusing on the algal cell to plastic particle size ratio. *Aquat. Toxicol.* 216:105296. doi: 10.1016/j.aquatox.2019.105296

Chaturvedi, P., Shukla, P., Giri, B. S., Chowdhary, P., Chandra, R., Gupta, P., et al. (2021). Prevalence and hazardous impact of pharmaceutical and personal care products and antibiotics in environment: a review on emerging contaminants. *Environ. Res.* 194:110664. doi: 10.1016/j.envres.2020.110664

Chen, S., Wang, L., Feng, W., Yuan, M., Li, J., Xu, H., et al. (2020a). Sulfonamides-induced oxidative stress in freshwater microalga *Chlorella vulgaris*: evaluation of growth, photosynthesis, antioxidants, ultrastructure, and nucleic acids. *Sci. Rep.* 10:8243. doi: 10.1038/s41598-020-65219-2

Chen, Y., Ling, Y., Li, X., Hu, J., Cao, C., and He, D. (2020b). Size-dependent cellular internalization and effects of polystyrene microplastics in microalgae *P. helgolandica* var. *tsingtaoensis* and *S. quadricauda*. *J. Hazard. Mater.* 399:123092. doi: 10.1016/j.jhazmat.2020.123092

Cheng, J., Ye, Q., Yang, Z., Yang, W., Zhou, J., and Cen, K. (2017). Microstructure and antioxidative capacity of the microalgae mutant *Chlorella* PY-ZU1 during tilmicosin removal from wastewater under 15% CO2. *J. Hazard. Mater.* 324, 414–419. doi: 10.1016/j.jhazmat.2016.11.006

Cheng, Y.-R., and Wang, H.-Y. (2022). Highly effective removal of microplastics by microalgae *Scenedesmus abundans*. *Chem. Eng. J.* 435:135079. doi: 10.1016/j.cej.2022.135079

Coyle, R., Hardiman, G., and Driscoll, K. O. (2020). Microplastics in the marine environment: a review of their sources, distribution processes, uptake and exchange in ecosystems. *Case Stud. Chem. Environ. Eng.* 2:100010. doi: 10.1016/j.cscee.2020.100010

Deng, Y., Mao, Y., Li, B., Yang, C., and Zhang, T. (2016). Aerobic degradation of sulfadiazine by *Arthrobacter* spp.: kinetics, pathways, and genomic characterization. *Environ. Sci. Technol.* 50, 9566–9575. doi: 10.1021/acs.est.6b02231

Elizalde-Velázquez, G. A., and Gómez-Oliván, L. M. (2021). Microplastics in aquatic environments: a review on occurrence, distribution, toxic effects, and implications for human health. *Sci. Total Environ.* 780:146551. doi: 10.1016/j.scitotenv.2021.146551

Foflonker, F., Ananyev, G., Qiu, H., Morrison, A., Palenik, B., Dismukes, G. C., et al. (2016). The unexpected extremophile: tolerance to fluctuating salinity in the green alga Picochlorum. *Algal Res.* 16, 465–472. doi: 10.1016/j.algal.2016.04.003

Fu, D. D., Zhang, Q. J., Fan, Z. Q., Qi, H. Y., Wang, Z. Z., and Peng, L. C. (2019). Aged microplastics polyvinyl chloride interact with copper and cause oxidative stress towards microalgae *Chlorella vulgaris*. *Aquat. Toxicol.* 216:105319. doi: 10.1016/j.aquatox.2019.105319

Holmes, L. A., Turner, A., and Thompson, R. C. (2012). Adsorption of trace metals to plastic resin pellets in the marine environment. *Environ. Pollut.* 160, 42–48. doi: 10.1016/j.envpol.2011.08.052

Huang, G., Zhao, D., Lan, C., Wu, B., Li, X., Lou, S., et al. (2022). Glucose-assisted trophic conversion of *Chlamydomonas reinhardtii* by expression of glucose transporter GLUT1. *Algal Res.* 62:102626. doi: 10.1016/j.algal.2021.102626

Lagarde, F., Olivier, O., Zanella, M., Daniel, P., Hiard, S., and Caruso, A. (2016). Microplastic interactions with freshwater microalgae: hetero-aggregation and changes in plastic density appear strongly dependent on polymer type. *Environ. Pollut.* 215, 331–339. doi: 10.1016/j.envpol.2016.05.006

Li, H., Wei, L., and Lu, J. (2020a). Algae-induced photodegradation of antibiotics: a review. *Environ. Pollut.* 272:115589. doi: 10.1016/j.envpol.2020.115589

Li, S., Wang, P., Zhang, C., Zhou, X., Yin, Z., Hu, T., et al. (2020b). Influence of polystyrene microplastics on the growth, photosynthetic efficiency and aggregation of freshwater microalgae *Chlamydomonas reinhardtii*. *Sci. Total Environ.* 714:136767. doi: 10.1016/j.scitotenv.2020.136767

Liu, X., Liu, Y., Lu, S., Guo, W., and Xi, B. (2018). Performance and mechanism into TiO2/Zeolite composites for sulfadiazine adsorption and photodegradation. *Chem. Eng. J.* 350, 131–147. doi: 10.1016/j.cej.2018.05.141

Machado, M. D., and Soares, E. V. (2019). Impact of erythromycin on a non-target organism: cellular effects on the freshwater microalga *Pseudokirchneriella subcapitata*. *Aquat. Toxicol.* 208, 179–186. doi: 10.1016/j.aquatox.2019.01.014

Martin-Laurent, F., Topp, E., Billet, L., Batisson, I., Malandain, C., Besse-Hoggan, P., et al. (2019). Environmental risk assessment of antibiotics in agroecosystems: ecotoxicological effects on aquatic microbial communities and dissemination of antimicrobial resistances and antibiotic biodegradation potential along the soil-water continuum. *Environ. Sci. Pollut. Res.* 26, 18930–18937. doi: 10.1007/s11356-019-05122-0

Nava, V., and Leoni, B. (2021). A critical review of interactions between microplastics, microalgae and aquatic ecosystem function. *Water Res.* 188:116476. doi: 10.1016/j.watres.2020.116476

Norvill, Z. N., Toledo-Cervantes, A., Blanco, S., Shilton, A., Guieysse, B., and Muñoz, R. (2017). Photodegradation and sorption govern tetracycline removal during wastewater treatment in algal ponds. *Bioresour. Technol.* 232, 35–43. doi: 10.1016/j.biortech.2017.02.011

Prata, J. C., Lavorante, B. R. B. O., Montenegro, M. C. B. S. M., and Guilhermino, L. (2018). Influence of microplastics on the toxicity of the pharmaceuticals procainamide and doxycycline on the marine microalgae *Tetraselmis chuii*. *Aquat. Toxicol.* 197, 143–152. doi: 10.1016/j.aquatox.2018.02.015

Prokić, M. D., Radovanović, T. B., Gavrić, J. P., and Faggio, C. (2019). Ecotoxicological effects of microplastics: examination of biomarkers, current state and future perspectives. *TrAC Trends Anal. Chem.* 111, 37–46. doi: 10.1016/j.trac.2018.12.001

Rath, S., Fostier, A. H., Pereira, L. A., Dioniso, A. C., de Oliveira Ferreira, F., Doretto, K. M., et al. (2019). Sorption behaviors of antimicrobial and antiparasitic veterinary drugs on subtropical soils. *Chemosphere* 214, 111–122. doi: 10.1016/j.chemosphere.2018.09.083

Schuwirth, N. (2020). Towards an integrated surface water quality assessment: aggregation over multiple pollutants and time. *Water Res.* 186:116330. doi: 10.1016/j.watres.2020.116330

Schwab, F., Bucheli, T. D., Lukhele, L. P., Magrez, A., Nowack, B., Sigg, L., et al. (2011). Are carbon nanotube effects on green algae caused by shading and agglomeration? *Environ. Sci. Technol.* 45, 6136–6144. doi: 10.1021/es200506b

Sjollema, S. B., Redondo-Hasselerharm, P., Leslie, H. A., Kraak, M. H. S., and Vethaak, A. D. (2016). Do plastic particles affect microalgal photosynthesis and growth? *Aquat. Toxicol.* 170, 259–261. doi: 10.1016/j.aquatox.2015.12.002

Song, C., Wei, Y., Qiu, Y., Qi, Y., Li, Y., and Kitamura, Y. (2019). Biodegradability and mechanism of florfenicol *via Chlorella* sp. UTEX1602 and L38: experimental study. *Bioresour. Technol.* 272, 529–534. doi: 10.1016/j.biortech.2018.10.080

Sun, Q., Ren, S. Y., and Ni, H. G. (2020). Incidence of microplastics in personal care products: an appreciable part of plastic pollution. *Sci. Total Environ.* 742:140218. doi: 10.1016/j.scitotenv.2020.140218

Varó, I., Perini, A., Torreblanca, A., Garcia, Y., Bergami, E., Vannuccini, M. L., et al. (2019). Time-dependent effects of polystyrene nanoparticles in brine shrimp *Artemia franciscana* at physiological, biochemical and molecular levels. *Sci. Total Environ.* 675, 570–580. doi: 10.1016/j.scitotenv.2019.04.157

Wang, J., Liu, X., Dai, Y., Ren, J., Li, Y., Wang, X., et al. (2020a). Effects of co-loading of polyethylene microplastics and ciprofloxacin on the antibiotic degradation efficiency and microbial community structure in soil. *Sci. Total Environ.* 741:140463. doi: 10.1016/j.scitotenv.2020.140463

Wang, Z., Gao, J., Li, D., Dai, H., and Zhao, Y. (2020b). Co-occurrence of microplastics and triclosan inhibited nitrification function and enriched antibiotic resistance genes in nitrifying sludge. *J. Hazard. Mater.* 399:123049. doi: 10.1016/j.jhazmat.2020.123049

Wang, Y., Mao, Z., Zhang, M., Ding, G., Sun, J., Du, M., et al. (2019a). The uptake and elimination of polystyrene microplastics by the brine shrimp, *Artemia parthenogenetica*, and its impact on its feeding behavior and intestinal histology. *Chemosphere* 234, 123–131. doi: 10.1016/j.chemosphere.2019.05.267

Wang, Y., Zhang, D., Zhang, M., Mu, J., Ding, G., Mao, Z., et al. (2019b). Effects of ingested polystyrene microplastics on brine shrimp, *Artemia parthenogenetica*. *Environ. Pollut.* 244, 715–722. doi: 10.1016/j.envpol.2018.10.024

Wang, Y., Zhu, X., Lao, Y., Lv, X., Tao, Y., Huang, B., et al. (2016). TiO2 nanoparticles in the marine environment: physical effects responsible for the toxicity on algae *Phaeodactylum tricornutum*. *Sci. Total Environ.* 565, 818–826. doi: 10.1016/j.scitotenv.2016.03.164

Wright, S. L., Thompson, R. C., and Galloway, T. S. (2013). The physical impacts of microplastics on marine organisms: a review. *Environ. Pollut.* 178, 483–492. doi: 10.1016/j.envpol.2013.02.031

Wu, D., Wang, T., Wang, J., Jiang, L., Yin, Y., and Guo, H. (2021). Size-dependent toxic effects of polystyrene microplastic exposure on *Microcystis aeruginosa* growth and microcystin production. *Sci. Total Environ.* 761:143265. doi: 10.1016/j.scitotenv.2020.143265

Wu, X., Wu, H., Zhang, A., Sekou, K., Li, Z., and Ye, J. (2022). Influence of polystyrene microplastics on levofloxacin removal by microalgae from freshwater aquaculture wastewater. *J. Environ. Manag.* 301:113865. doi: 10.1016/j.jenvman.2021.113865

Xie, P., Chen, C., Zhang, C., Su, G., Ren, N., and Ho, S.-H. (2020). Revealing the role of adsorption in ciprofloxacin and sulfadiazine elimination routes in microalgae. *Water Res.* 172:115475. doi: 10.1016/j.watres.2020.115475

Xiong, J.-Q., Govindwar, S., Kurade, M. B., Paeng, K.-J., Roh, H.-S., Khan, M. A., et al. (2019). Toxicity of sulfamethazine and sulfamethoxazole and their removal by a green microalga, *Scenedesmus obliquus*. *Chemosphere* 218, 551–558. doi: 10.1016/j.chemosphere.2018.11.146

Xiong, J.-Q., Kurade, M. B., and Jeon, B.-H. (2017). Ecotoxicological effects of enrofloxacin and its removal by monoculture of microalgal species and their consortium. *Environ. Pollut.* 226, 486–493. doi: 10.1016/j.envpol.2017.04.044

Yang, S., Li, Y., De Boevre, M., De Saeger, S., Zhou, J., Li, Y., et al. (2020). Toxicokinetics of α-zearalenol and its masked form in rats and the comparative biotransformation in liver microsomes from different livestock and humans. *J. Hazard. Mater.* 393:121403. doi: 10.1016/j.jhazmat.2019.121403

Yang, W., Gao, P., Li, H., Huang, J., Zhang, Y., Ding, H., et al. (2021). Mechanism of the inhibition and detoxification effects of the interaction between nanoplastics and microalgae *Chlorella pyrenoidosa*. *Sci. Total Environ.* 783:146919. doi: 10.1016/j.scitotenv.2021.146919

Zhang, C., Chen, X., Wang, J., and Tan, L. (2017). Toxic effects of microplastic on marine microalgae *Skeletonema costatum*: interactions between microplastic and algae. *Environ. Pollut.* 220, 1282–1288. doi: 10.1016/j.envpol.2016.11.005

Zhang, Q., Qu, Q., Lu, T., Ke, M., Zhu, Y., Zhang, M., et al. (2018). The combined toxicity effect of nanoplastics and glyphosate on *Microcystis aeruginosa* growth. *Environ. Pollut.* 243, 1106–1112. doi: 10.1016/j.envpol.2018.09.073

Zhang, S., Song, H. L., Cao, X., Li, H., Guo, J. H., Yang, X. L., et al. (2019). Inhibition of methanogens decreased sulfadiazine removal and increased antibiotic resistance gene development in microbial fuel cells. *Bioresour. Technol.* 281, 188–194. doi: 10.1016/j.biortech.2019.02.089

Zhang, Y., Lu, J., Wu, J., Wang, J., and Luo, Y. (2020). Potential risks of microplastics combined with superbugs: enrichment of antibiotic resistant bacteria on the surface of microplastics in mariculture system. *Ecotoxicol. Environ. Saf.* 187:109852. doi: 10.1016/j.ecoenv.2019.109852

Zhao, T., Tan, L., Huang, W., and Wang, J. (2019). The interactions between micro polyvinyl chloride (mPVC) and marine dinoflagellate *Karenia mikimotoi*: the inhibition of growth, chlorophyll and photosynthetic efficiency. *Environ. Pollut.* 247, 883–889. doi: 10.1016/j.envpol.2019.01.114

Zheng, Y., Li, Z., Tao, M., Li, J., and Hu, Z. (2017). Effects of selenite on green microalga *Haematococcus pluvialis*: bioaccumulation of selenium and enhancement of astaxanthin production. *Aquat. Toxicol.* 183, 21–27. doi: 10.1016/j.aquatox.2016.12.008

Zhu, Z.-L., Wang, S.-C., Zhao, F.-F., Wang, S.-G., Liu, F.-F., and Liu, G.-Z. (2019). Joint toxicity of microplastics with triclosan to marine microalgae *Skeletonema costatum*. *Environ. Pollut.* 246, 509–517. doi: 10.1016/j.envpol.2018.12.044

Conflict of Interest: The authors declare that the research was conducted in the absence of any commercial or financial relationships that could be construed as a potential conflict of interest.

Publisher's Note: All claims expressed in this article are solely those of the authors and do not necessarily represent those of their affiliated organizations, or those of the publisher, the editors and the reviewers. Any product that may be evaluated in this article, or claim that may be made by its manufacturer, is not guaranteed or endorsed by the publisher.

frontiers | Frontiers in Microbiology

TYPE Original Research
PUBLISHED 28 July 2022
DOI 10.3389/fmicb.2022.886206

OPEN ACCESS

EDITED BY
Wang Jiajun,
Northeast Agricultural University, China

REVIEWED BY
Gautam Kao,
University of Gothenburg, Sweden
Paola Scano,
University of Cagliari, Italy

*CORRESPONDENCE
Anders Olsen
ao@bio.aau.dk

SPECIALTY SECTION
This article was submitted to Antimicrobials, Resistance and Chemotherapy, a section of the journal Frontiers in Microbiology

RECEIVED 28 February 2022
ACCEPTED 30 June 2022
PUBLISHED 28 July 2022

CITATION
Møller KV, Nguyen HTT, Mørch MGM, Hesselager MO, Mulder FAA, Fuursted K and Olsen A (2022) A *Lactobacilli* diet that confers MRSA resistance causes amino acid depletion and increased antioxidant levels in the *C. elegans* host. *Front. Microbiol.* 13:886206. doi: 10.3389/fmicb.2022.886206

A *Lactobacilli* diet that confers MRSA resistance causes amino acid depletion and increased antioxidant levels in the *C. elegans* host

Katrine Vogt Møller[1], Hien Thi Thu Nguyen[2], Maria Grymer Metz Mørch[1], Marianne Overgaard Hesselager[1], Frans A. A. Mulder[3], Kurt Fuursted[4] and Anders Olsen[1]*

[1]Department of Chemistry and Bioscience, Aalborg University, Aalborg, Denmark, [2]Department of Molecular Diagnostics, Aalborg University Hospital, Aalborg, Denmark, [3]Interdisciplinary Nanoscience Center iNANO and Department of Chemistry, Aarhus University, Aarhus, Denmark, [4]Statens Serum Institute, Copenhagen, Denmark

Probiotic bacteria are increasingly popular as dietary supplements and have the potential as alternatives to traditional antibiotics. We have recently shown that pretreatment with *Lactobacillus* spp. Lb21 increases the life span of *C. elegans* and results in resistance toward pathogenic methicillin-resistant *Staphylococcus aureus* (MRSA). The Lb21-mediated MRSA resistance is dependent on the DBL-1 ligand of the TGF-β signaling pathway. However, the underlying changes at the metabolite level are not understood which limits the application of probiotic bacteria as timely alternatives to traditional antibiotics. In this study, we have performed untargeted nuclear magnetic resonance-based metabolic profiling. We report the metabolomes of *Lactobacillus* spp. Lb21 and control *E. coli* OP50 bacteria as well as the nematode-host metabolomes after feeding with these diets. We identify 48 metabolites in the bacteria samples and 51 metabolites in the nematode samples and 63 across all samples. Compared to the control diet, the *Lactobacilli* pretreatment significantly alters the metabolic profile of the worms. Through sparse Partial Least Squares discriminant analyses, we identify the 20 most important metabolites distinguishing probiotics from the regular OP50 food and worms fed the two different bacterial diets, respectively. Among the changed metabolites, we find lower levels of essential amino acids as well as increased levels of the antioxidants, ascorbate, and glutathione. Since the probiotic diet offers significant protection against MRSA, these metabolites could provide novel ways of combatting MRSA infections.

KEYWORDS

***Caenorhabditis elegans*, *Lactobacillus*, MRSA, NMR, metabolomics, amino acids, probiotic bacteria**

Introduction

Since the discovery of antibiotic substances, bacteria have shown an incredible ability to overcome the obstacle by developing resistance. In fact, according to the most recent antibiotic resistance threat report, more than 35,000 people die each year in the United States due to infections by multidrug-resistant bacteria (MDR) (CDC, 2019). MDR bacteria carry several resistance genes and they are evolving in line with the extensive use of antibiotics. Methicillin-resistant *Staphylococcus aureus* (MRSA) is an opportunistic pathogen most often residing in the upper respiratory passages without causing symptoms to the host (Lee et al., 2018). MRSA represents a risk to immune compromised individuals, potentially leading to severe illness and mortality, and carriers transmitting the bacteria without knowing that it is a huge clinical threat (Turner et al., 2019). To avoid antibiotic resistance and ameliorate the increasing threat from MDR bacteria, like MRSA, we require alternatives to traditional antibiotics.

Probiotics might offer such an alternative (Markowiak and Slizewska, 2017). They are defined as live microorganisms that confer a beneficial health effect on the host, when administered in adequate amounts (Hill et al., 2014). The use of probiotics specifically against MRSA is not new and has been evaluated in many different model systems and organisms including humans. It is clear that many different probiotic actions can offer protection against MRSA. These include but are not limited to antibacterial, anti-biofilm, anti-virulence, and antidrug resistance, improved intestinal barrier function, and host immune system stimulation (Sikorska and Smoragiewicz, 2013; Johansson et al., 2016; Nataraj and Mallappa, 2021). In addition to these protective mechanisms, probiotic bacteria can also outcompete MRSA by competition of binding sites or displacement. Interestingly, it has been reported that the consumption of probiotic *Bacillus* bacteria abolishes *S. aureus* nasal and intestinal colonization in a rural Thai population (Piewngam et al., 2018). The protective effect is a consequence of *Bacillus* produced fengycins, lipopeptides capable of inhibiting *S. aureus* quorum sensing (Piewngam et al., 2018). Another study in humans found that the daily oral administration of a *Lactobacillus rhamnosus* reduced odds of carriage of *S. aureus* in the GI tract (Eggers et al., 2018). This finding is consistent with a smaller study showing that oral and nasal spray administration of a probiotic *Lactobacilli* mixture displaced MRSA in long-term carriers (Roos et al., 2011).

The underlying molecular mechanisms are not always well-understood and to fully exploit the potential of probiotics as an alternative to traditional antibiotics, a deeper understanding is needed. Metabolomics, the profiling of metabolites, is one way to investigate the consequence of dietary supplementation of probiotics at the most downstream level of the cellular machinery. Metabolomics can thus provide insights to causal biological pathways and lead to identification of novel biomarkers (Johnson et al., 2016).

The rather complex interplay between humans and probiotic, commensal, and pathogenic bacteria makes simple model organisms, such as the small nematode *Caenorhabditis elegans*, attractive alternatives to study host-microorganism interactions. We recently identified *Lactobacillus* spp. Lb21 (a mix of *Lactiplantibacillus plantarum* and *Levilactobacillus brevis*) in a screen aimed at finding novel potentially probiotic bacteria (Mørch et al., 2021). The *Lactobacillus* spp. Lb21 (from now referred to as Lb21) was shown to extend the life span of *C. elegans* and probiotic pretreatment significantly increased the MRSA resistance. Epistasis analysis showed that the protective effect of Lb21 is mediated through the TGF-β related ligand DBL-1. Furthermore, proteomic analysis identified 308 regulated proteins in worms fed Lb21 vs. worms fed standard *E. coli* food (OP50). Interestingly, several studies have observed increased life span and improved resistance toward infections with other pathogenic bacteria when feeding *C. elegans* probiotic bacteria (Ikeda et al., 2007; Kim and Mylonakis, 2012; Park et al., 2014, 2018; Nakagawa et al., 2016; Christensen et al., 2017). Thus, their potential is not limited to MRSA.

Only a few studies have looked at the metabolome of *C. elegans* in relation to different food sources. Two studies compared the metabolic profile of *C. elegans* fed two different *E. coli* strains, namely, OP50 and HT115 (Reinke et al., 2010; Gao et al., 2017). These strains are typically used as standard food sources for the worm in regular and RNAi experiments, respectively. Interestingly, the identified metabolic profiles were different, and the changes were distinct enough to group the strains according to diet. The effect of a probiotic *Bifidobacterium animalis* subsp. *lactis* food source on the *C. elegans* metabolome has also been examined (Martorell et al., 2016). The strain reduces fat content, and the metabolic analysis suggests that it modulates both antioxidant responses and lipid metabolism of the worms.

In this study, we investigate how the metabolome of probiotic Lb21 differs from the regular OP50 bacteria. Furthermore, we characterize the changes in the host metabolome of *C. elegans* following a probiotic Lb21 diet compared to an OP50 diet. We find that worms being fed Lb21 have reduced levels of essential amino acids and contain a higher level of the antioxidant glutathione.

Materials and methods

Nematode and bacterial strains

The *C. elegans* strain used in this study, NL2099 *rrf-3 (pk1426),* was purchased from the *Caenorhabditis* Genetics Center (CGC) at the University of Minnesota. This mutant is

sterile when cultured at 25°C and used to prevent offspring cross-contaminating and prevent bagging.

The following three different bacterial strains were used in this study: the standard *C. elegans* laboratory food strain *Escherichia coli* OP50 (Brenner, 1974); Lb21, a mix of two *Lactobacillus* strains [*L. plantarum* (LX0811-1) and *L. brevis* (LX0811-2)] provided by DuPont Nutrition Biosciences ApS, now IFF: International Flavors & Fragrances (Brabrand Denmark); and a community-acquired isolate MRSA 43484 provided by from Statens Serum Institut, Copenhagen, Denmark.

Culturing conditions

Bacteria were cultured as previously described (Mørch et al., 2021). Briefly, OP50 and MRSA 43484 stocks were kept on Luria-Bertani (LB) and Tryptic Soy (TS) agar plates (Sigma), respectively, grown ON at 37°C and stored at 5°C. Lb21 was made from stock and stored as aliquots at −80°C in 25% glycerol.

Overnight (ON) bacterial cultures were prepared by inoculation of single colonies into 10 ml of LB or 10 ml of TS broth for OP50 and MRSA 43484, respectively. Lb21 was prepared by inoculation of 75 μl of aliquot into 10 ml De Man, Rogosa, and Sharpe (MRS) broth (Sigma). All cultures were grown under aerobic conditions for 18 h at 37°C in 13 ml of bacterial culture tubes under continuous shaking at 190 rpm.

Large bacterial cultures of OP50 and Lb21 were made by inoculating 1L (LB/MRS) broth with 2 ml of ON culture and grown under aerobic conditions for 18 h at 37°C under continuous shaking at 100 rpm. Cultures were concentrated 4:1 and spotted on large nematode growth media (NGM) plates (Brenner, 1974) to be used for both lawn samples and worm samples and for pathogen life span analysis. Bacterial lawns grew on the plates at room temperature for 6 days before being used for *ad libitum* feeding or harvest.

To generate a large population, worms were cultured on 9 cm NGM plates with concentrated OP50 (40X) at 20°C. Gravid adults were washed off with S-basal (10 M NaCl, 0.05 M KPO_4 in H_2O) and the supernatant was removed before the worm pellet was treated with an alkaline hypochlorite solution (0.25 M KOH, ∼2% sodium hypochlorite (10-15%, Acros Organics) to harvest the eggs and get a synchronous population. A total of 500,000 eggs were divided between 225 plates with UV-irradiated OP50 (OP50-UV). OP50-UV plates were irradiated for 30 min on the previous day, and on the day of hypo-treatment in a UV cross-linker (UVP). This was to prevent residual bacteria from dividing when worms were later transferred to Lb21. The worms were allowed to develop at 25°C for 3 days to get sterile adults. Three-day-old worms were washed off from OP50-UV plates, washed three times in S-basal, and transferred to either OP50 or Lb21. The plates were incubated at 25°C for 48 h before a part of the population was shifted to MRSA 43484 plates for life span analysis and the rest was used for metabolite extraction.

Pathogen life span assay

Worms that have been pretreated with OP50 or Lb21 for 48 h were transferred to MRSA plates on day 5. Notably, 50 worms per plate and five plates per group were used. Death events were scored every other day. Worms were incubated at 25°C. The GraphPad PRISM software was used to plot data and perform log-rank tests and the Gehan-Breslow-Wilcoxon tests.

Samples for metabolic studies

A T-shaped spreader was used to scrape off the lawns and transfer the bacteria to ice-cold isotonic saline (0.9%) solution (ISS). A total of 17 large NGM plates were used for each bacterial lawn sample and three samples of each group were made. Tubes were centrifuged for 10 min at 4,000 rpm at 4°C, supernatants were discarded, and pellets were washed two additional times in ice-cold ISS. Pellets were snap-frozen in liquid nitrogen and stored at −80°C. Before extraction, OD_{600} was measured, and all samples were diluted to the same OD.

Five-day-old worms were sampled for NMR. Approximately, 20 large (9 cm) plates were pooled for each sample, containing around 11,500 worms, by washing them off with S-basal. The worms were left to settle and washed three additional times before pellets were snap-frozen in liquid nitrogen and stored at −80°C. Three samples of each group were made.

Extraction of metabolites

Bacteria: 2 ml of 80% methanol was added to each pellet, and then subjected to four freeze-thaw cycles in liquid nitrogen and hot water to open the cells. The samples were vortexed after being thawed. Finally, the tubes were centrifuged for 10 min at 4,000 rpm, 4°C, and the extracts were dried in a speedVac (Thermo Scientific) and then kept at −80°C until analysis.

Worms: Metabolites were extracted following the method described by Geier et al. (2011) using 80% methanol in water and bead-beating. Briefly, pellets in ice-cold 80% methanol were bead-beaten in a Precellys 24 tissue homogenizer (Bertin-instruments) using glass beads of various sizes (100 mg of each; 0.1 mm, 0.45 mm, and 1.0 mm) to break open the cells of the worms. The extracts were dried as described for bacteria.

NMR spectroscopy

Dried pellets were dissolved in 550 μl of NMR buffer [0.1 M phosphate buffer, pH 7.0, 10% D_2O and 0.25 mM 4,4-dimethyl-4-silapentane-1-sulfonic acid (DSS)]. A volume of 500 μl was transferred to NMR tubes suited for use with Bruker SampleJet. ^{1}H spectra were acquired at 295 K using a 1D NOESY pulse sequence with water pre-saturation on a Bruker 500 MHz NMR spectrometer with a room temperature TXI probe head, collecting 8 scans per sample. A relaxation delay of 2 s and a mixing time of 50 ms were used, collecting 32 K data points over a spectral width of 16 ppm, at an acquisition time of 2.04 s. 2D NMR ^{1}H-^{1}H COSY spectra were acquired to annotate peaks in overlapping regions. Here, 64 scans were collected, using a relaxation delay of 1.5 s, acquiring 16 K data points over a spectral width of 13 ppm, at an acquisition time of 0.63 s.

NMR data processing and analysis

For metabolite identification, two-dimensional (2D) experiments were performed. Information obtained from these spectra was used to find matching metabolites with the Human Metabolome Database (Wishart et al., 2007). Further metabolite assignments were performed using the Chenomx NMR Suite 8.1 professional software (Chenomx Inc., Edmonton, AB, Canada). NMR spectra were aligned and normalized to the DSS spectral area for calculating the concentration of each metabolite. Regions containing residual water (δ 4.825–4.725 ppm) were excluded from the dataset to avoid spectral interference.

Statistical analysis

In this study, the modified MetaboAnalystR 2.0 R package (https://github.com/biocyberman/MetaboAnalystR/tree/dev) was applied for all univariate and multivariate statistical analyses.

An overview of the data and a rough ranking of potential important features were first obtained using univariate analysis. Univariate analysis examines each variable separately without considering the effect of multiple comparisons. The results provided by all univariate methods were further examined using a more sophisticated analysis tool.

We performed multivariate statistical analysis with unsupervised Principal Components Analysis (PCA) and sparse Partial Least Squares discriminant analysis (sPLS-DA). These two methods are the most popular unsupervised and supervised methods, respectively, for the multivariate statistical analysis of metabolomics data where the NMR data are projected into a reduced dimensional space for easier interpretation and visualization (Ebbels et al., 2011). In PCA, the model describes the space corresponding to the highest variance of the data, while in sPLS, the space corresponds to that with the highest covariance between the NMR data and the response variable (Puchades-Carrasco et al., 2016). sPLS has been developed to perform simultaneous variable selection in both X and Y data sets, by including least absolute shrinkage and selection operator (LASSO) $\ell 1$ penalizations in PLS on each pair of loading (Lê Cao et al., 2008). sPLS was shown to be effective and biologically meaningful, and it provides a valuable variable selection tool for high dimensional data sets compared to PLS (Lê Cao et al., 2008, 2011). First, the metabolite profile analysis was performed using unsupervised PCA, which displayed the internal structure of datasets in an unbiased way and decreases the dimensionality of data. Then, the sPLS-DA model was employed to identify the metabolites contributing to discrimination between groups. The loading plot indicated the contribution of each metabolite to the model. Notably, 5-fold cross-validation together with the receiver operating characteristic curve (ROC) was chosen for the evaluation of classification performance of the sPLS-DA model. The heat map of significantly different features was generated to identify clustering metabolites.

Results

Metabolic profiling of Lb21

To gain further insight into the underlying probiotic mechanism of Lb21, we decided to characterize the metabolic profiles of both standard OP50 and probiotic bacteria, as well as metabolic profiles from worms fed the two different food sources. To obtain metabolic profiles of both bacteria and worms mimicking the experimental setup showing probiotic effects, the bacteria were spotted onto agar plates and scraped off and worms were cultured on large plates and not in liquid culture (Figure 1A).

To verify a positive effect of Lb21 under these mass culture conditions, a pathogen resistance analysis was performed simultaneously. As expected, significant resistance toward MRSA infection was observed following pretreatment with Lb21 (Figure 1B). This is consistent with our earlier observations using small NGM plates (Mørch et al., 2021).

Endogenous metabolites of both bacteria and worm samples were extracted and measured using ^{1}H NMR spectroscopy. A total of 63 metabolites were assigned, with 48 metabolites for the bacterial samples and 51 for the worm samples. A heat map with hierarchical clustering of the total assigned metabolites that differed significantly between groups demonstrates the ability of the metabolomics approach to differentiate between different groups since the four groups clustered separately (Figure 2).

The endogenous metabolic variances from bacterial lawn samples (L-OP50 and L-Lb21) and from worms fed the two different bacteria (W-OP50 and W-Lb21) were analyzed by the sPLS-DA method. The sPLS-DA models were able

10.3389/fmicb.2022.886206

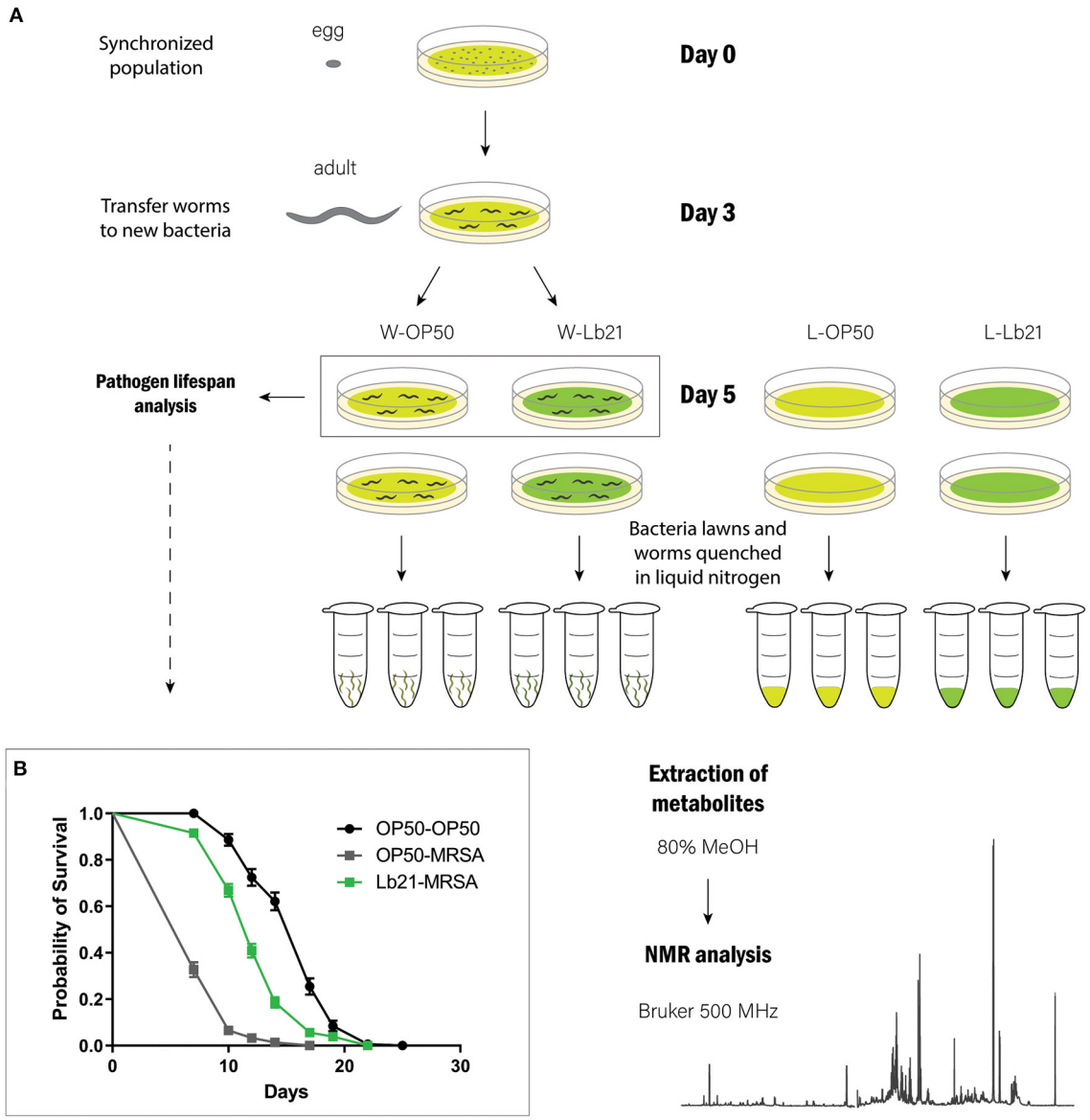

FIGURE 1
Experimental design: **(A)** A synchronized population of rrf-3 worms was obtained by bleaching gravid adults. ~500.000 eggs were distributed onto 225 large agar plates spotted with *E. coli* OP50 (UV irradiated for 30 min) on day 0. On day 3, adult worms were transferred to *E. coli* OP50 or Lb21. On day 5, a subset of the worms was transferred to plates spotted with MRSA for pathogen resistance analysis. The remaining worms and bacterial lawns were prepared in triplicate to extract metabolites. **(B)** MRSA resistance analysis. Worms pretreated with Lb21 lived significantly longer ($p < 0.0001$) than worms fed the standard OP50 bacteria when challenged with MRSA. Mean life span (days) of OP50-MRSA worms was 8.2 ± 2.0 ($n = 214$) compared to 12.7 ± 3.4 ($n = 284$) following Lb21 pretreatment.

to separate the L-OP50 group from the L-Lb21 group (Figure 3A), and the W-OP50 group from the W-Lb21 group (Figure 3B). The sPLS-DA explained 86.3% and 76.1% of variance with the first two components in the samples collected for the two models, respectively. The sPLS-DA model for both shows separation with an overall cross validated accuracy of 100% (data not shown). The loading plots display the top twenty metabolites responsible for the differentiation of the groups in a ranked order (Figures 3C,D). Hierarchical clustering analysis highlighted the significant differences between bacterial lawn groups, L-OP50 vs. L-Lb21 (Figure 3E) and worms fed the two different bacteria, W-OP50 vs. W-Lb21 (Figure 3F).

Several amino acids (AAs) were identified as important factors for the separation of OP50 and Lb21 bacterial lawns and for distinguishing the worms fed the two bacterial diets

10.3389/fmicb.2022.886206

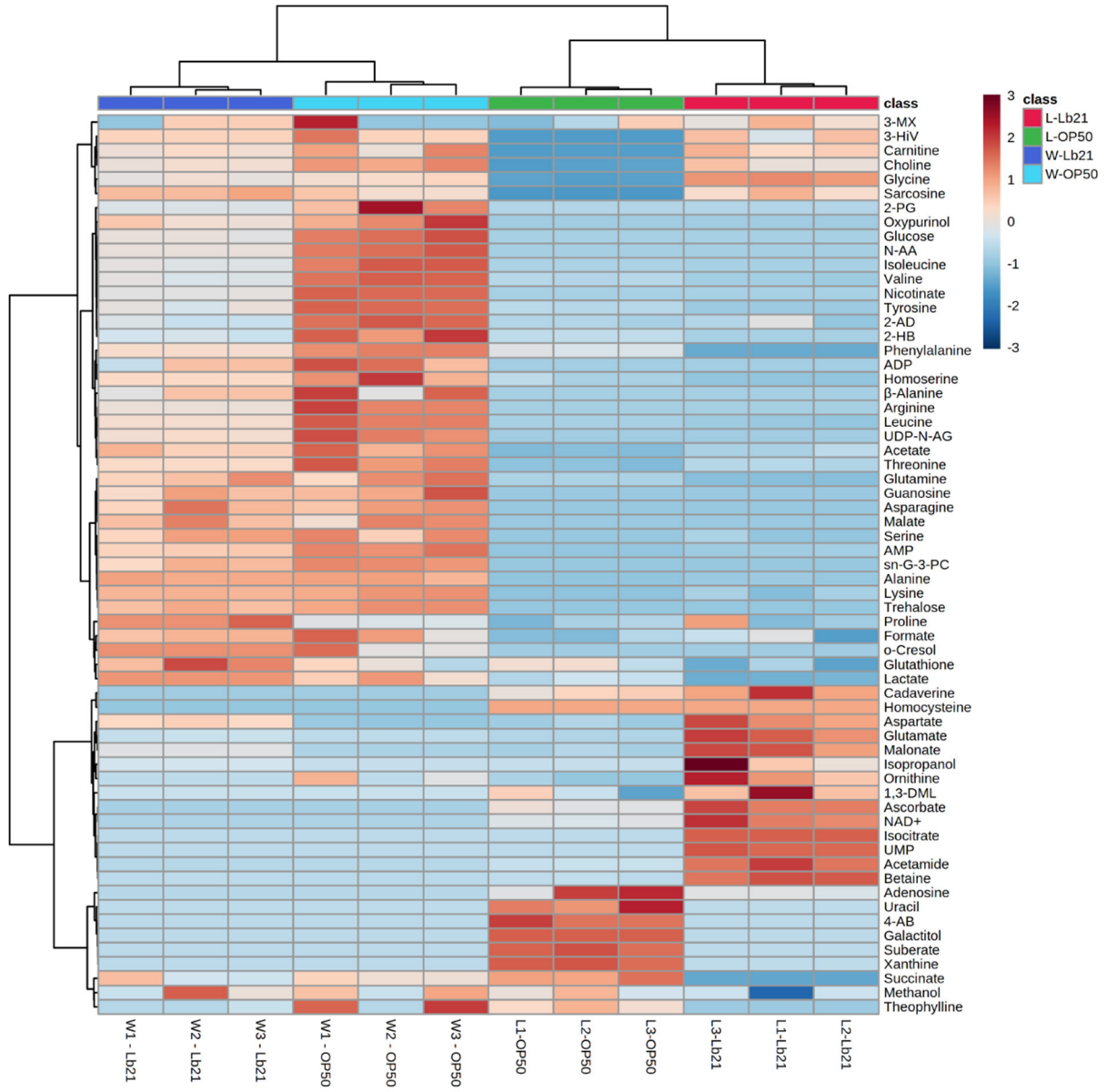

FIGURE 2
Host metabolic profiles do not simply reflect the metabolic profile of the bacterial diets: Heat map representing the hierarchical clustering of all the assigned metabolites in four different sample groups, each made in triplicate. Bacterial lawn samples are shown to the right (L-OP50 and L-Lb21) and worms samples to the left (W-OP50 and W-Lb21). Each row shows data for a specific metabolite, and each column shows data for bacteria and worms. Red and blue denote relatively high and low levels, respectively, compared to the average level.

(Figures 3C,D). Five of these AAs were present in all four groups (i.e., isoleucine, valine, phenylalanine, glutamate, and tyrosine). The levels of the three essential AAs, namely, isoleucine, valine, and phenylalanine, and the non-essential tyrosine were significantly lower in Lb21 and worms fed Lb21 compared to OP50 and worms fed OP50 (Tables 1, 2). In contrast, the non-essential AA glutamate was significantly higher.

A shift was observed for threonine, an essential AA, which was significantly higher in L-Lb21 compared to L-OP50 (Table 1), although the worms fed Lb21 had significantly lower levels of threonine compared to worms fed OP50 (Table 2).

Glutamine was only identified as an important factor for separating L-Lb21 from L-OP50 and the concentration was significantly lower in L-Lb21 (Figure 3C and Table 1). Worms fed Lb21 compared to worms fed standard OP50 food had significantly increased levels of aspartate and proline, and a significantly lower concentration of arginine and leucine (Figure 3D and Table 2).

10.3389/fmicb.2022.886206

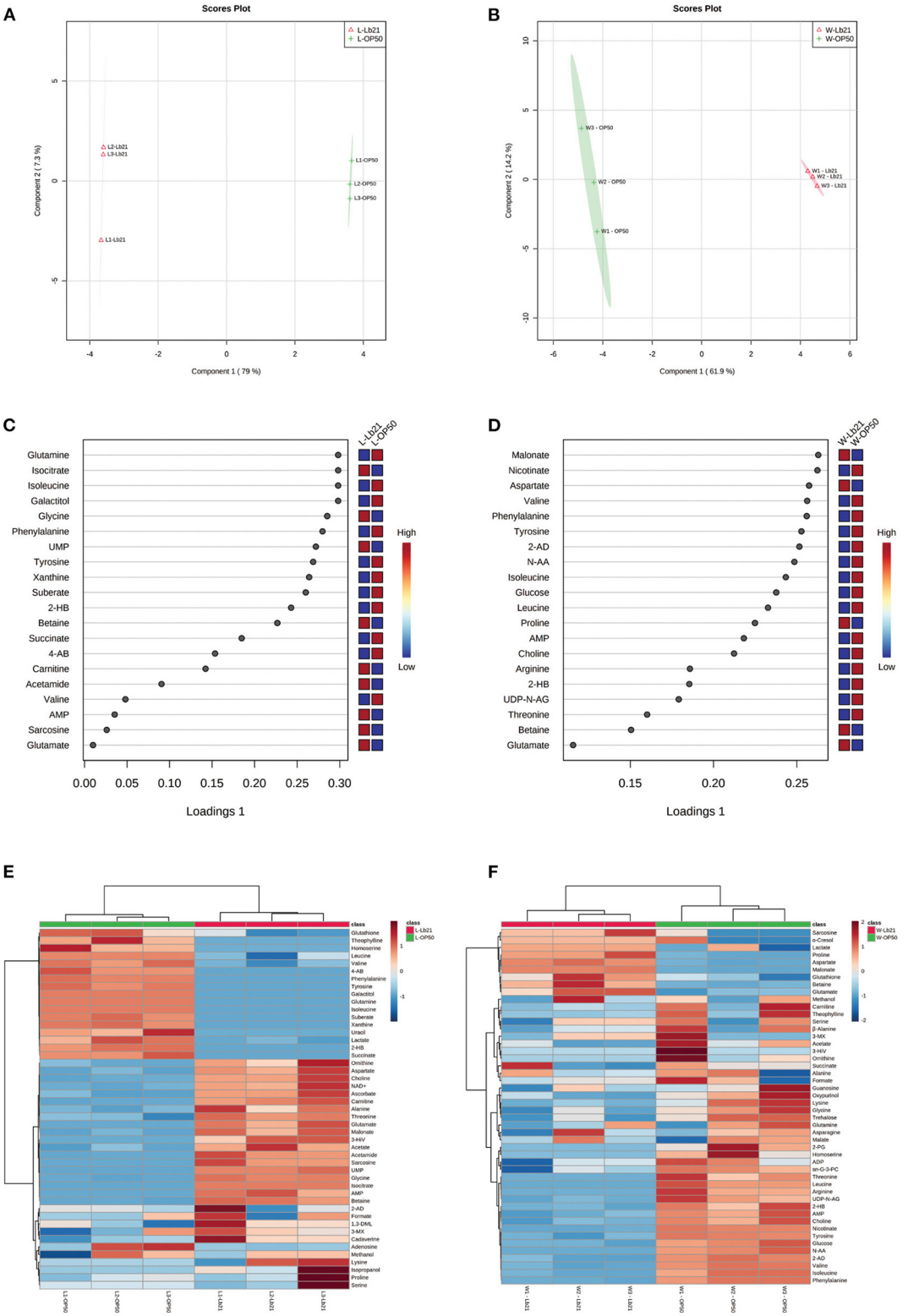

FIGURE 3
sPLS-DA and hierarchical clustering analysis: sPLS-DA score plot and loading plot from bacterial lawn samples and from worms fed the two different bacteria. **(A)** sPLS-DA score plot from *E. coli* strain OP50 (L-OP50, green) vs. *Lactobacillus* spp. Lb21 (L-Lb21, pink). **(B)** sPLS-DA score plot from worms fed different bacteria, *E. coli* strain OP50 (W-OP50, green) vs. Lb21 (W-Lb21, pink). **(C)** Loading plot from the bacterial strains, L-OP50 vs. L-Lb21 **(D)** Loading plot from worms fed OP50 or Lb21 (W-OP50 vs. W-Lb21). Hierarchical clustering analysis highlighted significant differences between bacterial lawn groups, L-OP50 vs. L-Lb21 **(E)**; and worms fed the two different bacteria groups, W-OP50 vs. W-Lb21 **(F)**.

10.3389/fmicb.2022.886206

TABLE 1 Important features selected by *t*-tests for separation of L-OP50 and L-Lb21.

	Compounds	t-stat	*p*-value	−log10(p)	FDR	Description
1	Galactitol	−418	1.9653e-10	9.7066	9.2369e-09	Energy, alcohol form of galactose.
2	Isocitrate	131.2	2.0242e-08	7.6938	4.7568e-07	Energy, intermediate in TCA cycle.
3	Isoleucine	−62	4.0535e-07	6.3922	6.3505e-06	Amino acid (essential).
4	Phenylalanine	−48.204	1.1081e-06	5.9554	1.2071e-05	Amino acid (essential).
5	Glycine	46.457	1.2842e-06	5.8914	1.2071e-07	Amino acid.
6	UMP	40.286	2.2686e-06	5.6442	1.7771e-05	Nucleotide.
7	Tyrosine	−37.812	2.9216e-06	5.5344	1.9616e-05	Amino acid.
8	Xanthine	−34.842	4.0493e-06	5.3926	2.379e-05	Purine base. Degradation of purines.
9	Suberate	−33.272	4.8664e-06	5.3128	2.5414e-05	Organic acid.
10	Glutamine	−30.368	7.0037e-06	5.1547	3.2918e-05	Amino acid.
11	2-Hydroxybutyrate	−22.357	2.3698e-05	4.6253	0.00010126	Ketone body.
12	Betaine	19.648	3.9573e-05	4.4026	0.00015499	Osmoprotectant. Methyl donor to form methionine from homocysteine. Precursor of glycine, serine, and threonine.
13	4-AB (GABA)	−16.857	7.2593e-05	4.1391	0.00026245	Confers resistance toward acidic pH.
14	Succinate	−15.565	9.9465e-05	4.0023	0.00033392	Energy, intermediate in TCA cycle.
15	Carnitine	13.243	0.00018786	3.7262	0.00058863	Osmoprotectant.
16	AMP	12.108	0.0002669	3.5736	0.00076424	Nucleotide.
17	Sarcosine	12	0.00027643	3.5584	0.00076424	Amino acid. N-methyl derivative of glycine.
18	Acetamide	11.442	0.00033292	3.4777	0.00086929	Compound used in the production of plastics.
19	Valine	−10.401	0.00048261	3.3164	0.0011938	Amino acid (essential).
20	Glutamate	9.6687	0.00064022	3.1937	0.0015045	Amino acid.
21	Threonine	9.4997	0.00068531	3.1641	0.0015338	Amino acid (essential).
22	Lactate	−8.8206	0.00091165	3.0402	0.0019476	Energy.
23	Malonate	8.5982	0.0010054	2.9977	0.0020545	Competitive inhibitor of succinate dehydrogenase. Used in fatty acid or β-alanine biosynthesis.
24	Choline	8.2549	0.0011748	2.93	0.0023007	Oxidized to betaine. Cation present in phospholipids. Precursor of neurotransmitter acetylcholine.
25	Ascorbate	8.1536	0.0012314	2.9096	0.0023151	Antioxidant.
26	Aspartate	7.8227	0.0014415	2.8412	0.0026059	Amino acid.
27	Uracil	−7.3321	0.0018417	2.7348	0.0031305	Nucleobase.
28	3-HiV	7.3077	0.001865	2.7293	0.0031305	Organic acid.
29	Theophylline	−6.9322	0.0022735	2.6433	0.0036847	A xanthine alkaloid.
30	NAD+	6.6574	0.0026441	2.5777	0.0041425	Coenzyme.
31	Acetate	6.3614	0.0031302	2.5044	0.0047458	Building block for biosynthesis, such as fatty acids.
32	Homoserine	−6.1418	0.0035635	2.4481	0.0052338	α-amino acid.
33	Alanine	4.9031	0.0080258	2.0955	0.011431	Amino acid.
34	Leucine	−4.818	0.0085357	2.0688	0.011799	Amino acid (essential).
35	Ornithine	4.3704	0.011964	1.9221	0.016066	Non-proteinogenic amino acid. Plays a role in the urea cycle.
36	Glutathione	−3.3966	0.027362	1.5628	0.035723	Antioxidant.

In addition to these AAs, other metabolites were identified as important factors for separating L-Lb21 from L-OP50 (Figure 3C). These include metabolites involved in energy metabolism (isocitrate, succinate, AMP, carnitine and galactitol), and in osmoregulation (carnitine and betaine). The level of 4-aminobutyrate (4-AB), also known as GABA, a metabolite that in bacteria is involved in resistance toward acidic pH, was significantly lower in L-Lb21 compared to L-OP50 (Table 1).

Interestingly, some of the remaining metabolites that are not AAs but identified as important factors discriminating worms fed Lb21 compared to OP50 are also involved in oxidative stress and energy metabolism (Figure 3D). These include higher levels of betaine and malonate, a competitive inhibitor of succinate

TABLE 2 Important features selected by *t*-tests for separation of W-OP50 and W-Lb21.

	Compounds	t-stat	*p*-value	−log10(p)	FDR	Description
1	Malonate	72.458	2.174e-07	6.6627	1.0435e-05	Competitive inhibitor of succinate dehydrogenase. Used in fatty acid or β-alanine biosynthesis.
2	Nicotinate	−56	6.088e-07	6.2155	1.4611e-05	Precursors for coenzymes, NAD^+ and $NADP^+$.
3	Aspartate	24.922	1.5387e-05	4.8128	0.00022291	Amino acid.
4	Valine	−22.858	2.1702e-05	4.6635	0.00022291	Amino acid (essential).
5	Phenylalanine	−22.472	2.3219e-05	4.6342	0.00022291	Amino acid (essential).
6	Tyrosine	−18.882	4.6337e-05	4.3341	0.00037069	Amino acid.
7	2-Aminoadipate	−17.898	5.7278e-05	4.242	0.00039276	Intermediate in lysine biosynthesis/degradation.
8	N-Acetylaspartate	−15.99	8.9428e-05	4.0485	0.00053657	Derivative of aspartic acid.
9	Isoleucine	−13.765	0.00016139	3.7921	0.00086074	Amino acid (essential).
10	Glucose	−12.127	0.00026527	3.5763	0.0012733	Energy.
11	Leucine	−11.088	0.00037625	3.4245	0.0016418	Amino acid (essential).
12	Proline	9.877	0.00058957	3.2295	0.0023583	Amino acid.
13	AMP	−9.0994	0.00080896	3.0921	0.0029869	Nucleotide, energy.
14	Choline	−8.5413	0.0010313	2.9866	0.0035358	Cation present in phospholipids. Oxidized to betaine. Precursor of neurotransmitter acetylcholine.
15	Arginine	−6.8636	0.0023596	2.6272	0.0071505	Amino acid (essential).
16	2-Hydroxybutyrate	−6.8452	0.0023835	2.6228	0.0071505	Ketone body.
17	UDP-N-AG	−3.9973	0.016166	1.7914	0.0078547	Nucleotide sugar and coenzyme.
18	Threonine	−5.8883	0.0041589	2.381	0.011091	Amino acid (essential).
19	Betaine	5.6095	0.0049615	2.3044	0.012534	Methyl donor to form methionine from homocysteine. Precursor of glycine, serine, and threonine.
20	Glutamate	4.8347	0.0084325	2.074	0.020238	Amino acid.
21	Sn-Glycero-3-PC	−3.4429	0.026225	1.5813	0.059943	Nootropic phospholipid, a precursor to choline biosynthesis.
22	2-Phosphoglycerate	−3.166	0.033989	1.4687	0.070993	Substrate in glycolysis.
23	Lysine				0.070993	Amino acid (essential).
24	Trehalose	−3.0823	0.036851	1.4336	0.070993	Sugar.
25	Glutathione				0.070993	Antioxidant.
26	Homoserine	−2.9571	0.041673	1.3801	0.070993	α-amino acid.
27	Sarcosine	2.9492	0.042001	1.3767	0.070993	Amino acid. N-methyl derivative of glycine.
28	Oxypurinol	−2.9446	0.042196	1.3747	0.070993	Purine derivative.
29	Glycine	−2.9282	0.042892	1.3676	0.070993	Amino acid.

dehydrogenase of the TCA cycle (Gupta, 2019). In contrast, the levels of glucose and AMP were significantly lower (Table 2). Interestingly, betaine was one of the metabolites with higher levels in L-Lb21 compared to those in L-OP50 (Tables 1, 2).

Discussion

Probiotic supplementation has been reported by many researchers to prevent and alleviate a wide range of diseases; however, there are also studies reporting no benefit or even negative effects (Suez et al., 2019). The beneficial host-microbiome interaction is complex, as it depends on both the bacterial strains and host genetics. Furthermore, manufacturing and administration protocols can influence the efficacy (Suez et al., 2019; Schifano et al., 2020). In addition, even closely related bacterial strains of the same species may exhibit completely different effects even in the same host (Mørch et al., 2021). Thus, one of the main limitations for fully utilizing probiotics as alternatives to traditional antibiotics is the lack of knowledge about the underlying mechanisms, not least at the metabolite level of both the bacteria and the host.

Well-characterized genetic model organisms, like *C. elegans*, are highly suited for metabolomic studies. In this study, we have performed the mechanistic analysis of the Lb21 probiotic response one step further and investigated changes at the metabolite level due to a probiotic diet.

You are not simply what you eat

Using NMR-based metabolomics, we could identify the top 20 most important metabolites in terms of differentiating probiotics and regular OP50 food as well as the corresponding host metabolomes.

We found that many of the same metabolites identified as important factors in Lb21 bacteria compared to OP50 are also the same identified in the worms fed the two different bacterial diets (Figure 4). When changing the diet of the worms, we expect to find alterations in the metabolome of the host, and some of these will be due to a different nutritional metabolome composition of the new food and other changes will result from alterations of the host metabolism. Indeed, not all metabolites show a proportional relationship between diet and host. For example, the levels of threonine, choline, and glycine were higher in L-Lb21 compared to those in L-OP50, but lower in worms fed Lb21 compared to worms fed OP50 (Tables 1, 2). The opposite was seen for glutathione which had lower levels in Lb21 bacteria compared to OP50 but higher levels in worms fed Lb21 compared to worms fed OP50 (Tables 1, 2). Furthermore, proline and arginine were not significantly different between L-Lb21 and L-OP50, but worms eating Lb21 had significantly higher levels of proline and lower levels of arginine compared to worms eating OP50 (Table 2). The level of the coenzyme nicotinamide adenine dinucleotide (NAD+) was significantly higher in L-Lb21 compared to L-OP50 but not detected in the worms (Table 1). Glutamine is an example of an opposite trend with lower levels in L-Lb21 compared to L-OP50 but similar levels in the worms fed both. These data emphasize the importance of profiling both the bacterial food source and the host response when trying to correlate metabolic changes with specific phenotypes and ultimately identify causal metabolites.

The probiotic effect of Lb21 could be *via* dietary restriction

Our analysis identified 12 AAs with a high impact on the sPLS-DA analysis for both bacteria and nematode samples. Lactic acid bacteria are auxotrophic for many AAs (Deguchi and Morishita, 1992) and require growth media containing these samples. Despite growing Lb21 in MRS media that support the growth of lactic acid bacteria, and being spotted onto NGM plates containing peptone, also a source of AAs, Lb21 was found to have low levels of both essential (isoleucine, phenylalanine, and valine) and non-essential (tyrosine and glutamine) AAs. Interestingly, the levels of non-essential AAs, i.e., glycine and glutamate, and essential threonine were higher compared to those of OP50. This indicates that AA metabolism is considerably altered in the Lb21 compared to OP50, which in turn likely affects the host.

Like humans, *C. elegans* cannot synthesize all AAs *de novo* and thus needs to obtain essential AAs from the diet (Zeči et al., 2019). We noted that the levels of all the identified essential AAs were significantly lower in worms fed Lb21 compared to worms fed the standard OP50 food, including threonine despite its higher level in the Lb21 lawn compared to OP50. Depletion of AAs could cause dietary restriction (DR), which is the reduction of food consumption below *ad libitum* without causing malnutrition. DR is known to increase the life span and stress resistance in many different organisms (Kapahi et al., 2017; Green et al., 2021). Interestingly, iso-caloric modulation of specific AAs affects health and life span. In the fruit fly *Drosophila melanogaster*, a longevity-promoting DR diet supplemented with only the essential AAs restores the life span to the level observed for normal feeding. Thus, a lack of essential AAs was concluded to be the explanation for life span extension of DR (Grandison et al., 2009). If the underlying molecular mechanisms are conserved, a Lb21-diet could perhaps confer a similar DR effect. However, in *C. elegans*, individual supplementation of AAs to an *E. coli* HT115-diet also increases life span, except for phenylalanine and aspartate (Edwards et al., 2015). Both increased and decreased levels of AAs can cause life span extension that demonstrates the complex interplay between AAs and DR-related mechanisms.

There are several DR paradigms established in *C. elegans* including bacterial dilution-mediated dietary restriction and knock down of *eat-2*, a nicotinic acetylcholine receptor subunit (Zhang and Mair, 2017). The *eat-2* mutants have prolonged life span due to DR caused by defective pharyngeal function (Lakowski and Hekimi, 1998). Furthermore, in *eat-2* mutants, the level of the isovaleryl-CoA dehydrogenase PAH-1, a key enzyme in AA metabolism, is reduced (Yuan et al., 2012). Interestingly, we have previously reported lower levels of PAH-1 in worms fed Lb21 compared to OP50 (Mørch et al., 2021). This is in line with AA depletion and DR being part of the Lb21 probiotic response.

In a prior study, the metabolomes of seven day-old *eat-2* mutants were analyzed using 1H high-resolution magic-angle spinning nuclear magnetic resonance analysis of intact worms (Pontoizeau et al., 2014). Compared to wildtype worms, the *eat-2* mutants have increased levels of glutamate, glutamine, lysine, succinate, cystathionine, and arginine. Furthermore, they have decreased levels of glycerophosphocholine, formate, leucine, phosphocholine, and trehalose (Pontoizeau et al., 2014). We observed a similar change for glutamate, leucine, and trehalose but the opposite for lysine and arginine when worms are fed a probiotic Lb21 diet. For the remaining metabolites determined in the *eat-2* study, the levels in our experiment are not significantly different or they have not been identified in our NMR analysis. Thus, the metabolomes of worms fed a Lb21 probiotic diet do not directly reflect those of *eat-2* mutants. However, it should be kept in mind that the protocols differ in the NMR instruments used, the use of 5'-fluorodeoxyuridine,

10.3389/fmicb.2022.886206

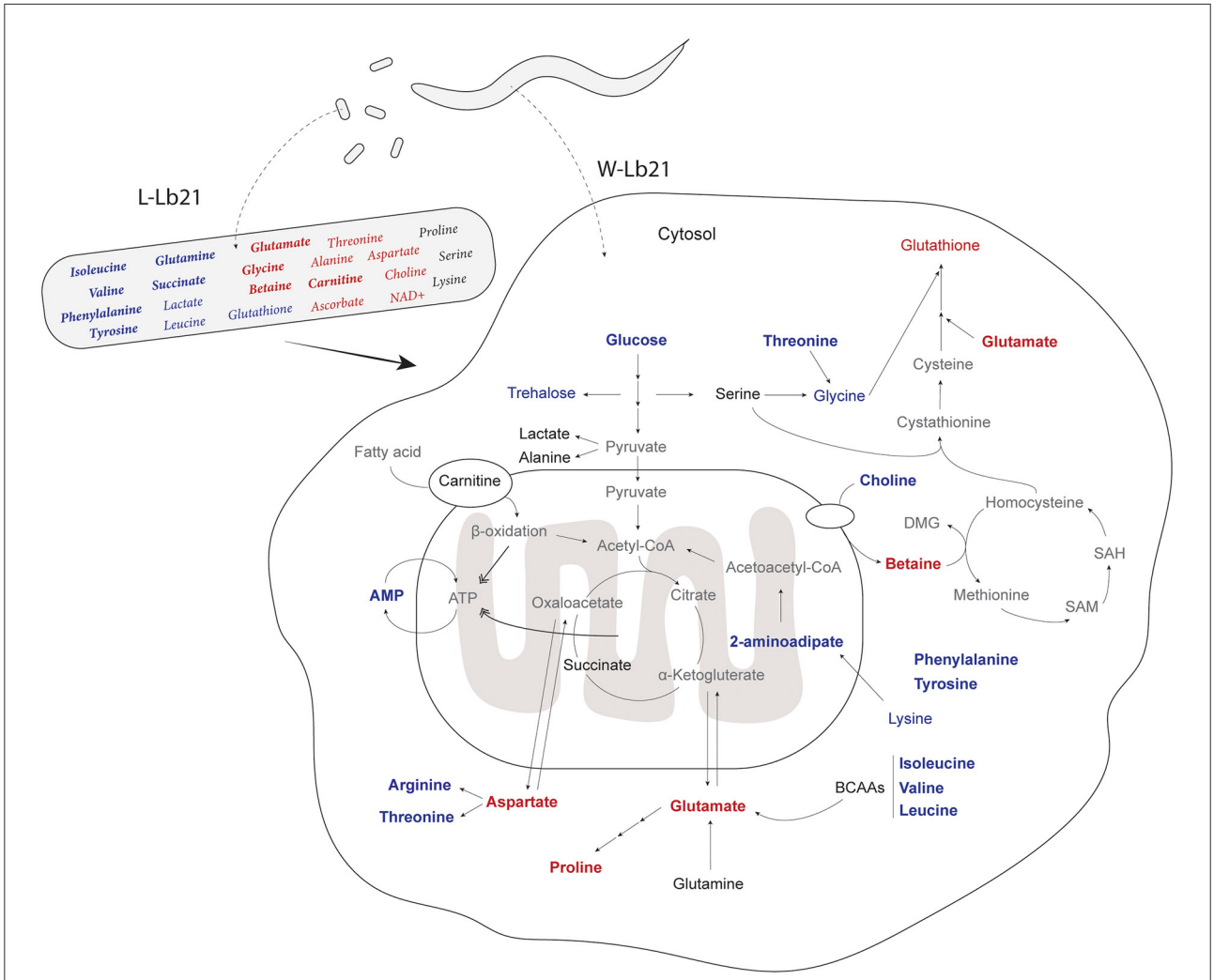

FIGURE 4
Metabolic characterization of *C. elegans* fed Lb21: Metabolites that are significantly differently identified by *t*-test between L-OP50 and L-Lb21 or W-OP50 and W-LB21 are colored; red are increased, blue are decreased, and those without significant changes in black. Metabolites in bold are one of the 20 metabolites identified by the sPLS-DA analysis. Metabolites in gray were not assigned.

and the age of the animals. Age, in particular, has been shown to have a significant influence on the levels of individual AAs (Gao et al., 2017; Liu et al., 2019). Thus, based on the different metabolic profiles, we cannot rule out a Lb21 probiotic mechanism that includes DR.

C. elegans increases the expression of antioxidant genes such as *gst-4* and *gst-10* in response to being starved for 1 day (Tao et al., 2017). Our previously published proteome analysis shows that the protein levels of GST-4 and GST-10 are downregulated in worms fed Lb21 compared to worms fed OP50 (Mørch et al., 2021). This indicates that worms fed Lb21 are not starved, consistent with their better health. In fact, it has been suggested that DR is a low intensity stressor and that the beneficial effect is mediated *via* hormesis (Masoro, 1998). This is supported by the fact that glucose restriction increases life span *via* mitohormesis (Schulz et al., 2007). The latter is particularly interesting because we found that worms fed a probiotic Lb21 diet have reduced the levels of glucose. Thus, it is possible that the Lb21 diet protects against MRSA by inducing a beneficial mild stress.

Lb21-induced metabolic changes do not resemble those of reduced insulin signaling

There are well-documented links between increased stress resistance and longevity and most long-lived mutants are resistant to different types of stress. For example, long-lived mutants in the insulin/IGF-1 signaling pathway are resistant to

heat (Lithgow et al., 1994), oxidative stress (Honda et al., 2008), heavy metals (Barsyte et al., 2001), protein misfolding (Morley et al., 2002; Cohen et al., 2006), and pathogen infection (Garsin et al., 2003; Evans et al., 2008).

The metabolomes of different long-lived mutants (several *daf-2* alleles, *daf-28*, and *ife-2*) are distinctly different from wild type but rather similar to each other (Fuchs et al., 2010). Common longevity signature metabolites include increased levels of trehalose, branched-chain amino acids (BCAAs, leucine, isoleucine, and valine) and glutamine, and decreased levels of choline, betaine, and glutamate (Fuchs et al., 2010). Many of these metabolomic changes have been confirmed by others (Martin et al., 2011; Castro et al., 2013; Davies et al., 2015). Interestingly, in another study, a *sir-2.1* mutant with a slightly shorter life span exhibited the exact opposite change of these metabolites (An et al., 2012). Furthermore, supplementation with trehalose (Honda et al., 2010; Seo et al., 2018) and BCAAs (Mansfeld et al., 2015) increases life span. The mechanism of Lb21-increased life span must be different as we found that Lb21-fed worms show significantly decreased levels of trehalose and BCAAs, and significantly increased levels of betaine and glutamate. The metabolic changes due to a Lb21 diet do not align with those of reduced insulin signaling mutants which is consistent with our observation that MRSA protection by Lb21 is not dependent on the FOXO transcription factor DAF-16 (Mørch et al., 2021).

Putative probiotic metabolites

Prior to this study, others have used *C. elegans* as a screening platform to identify new probiotic bacterial strains (Christensen et al., 2017). However, only a few studies have addressed the metabolome of probiotic bacteria and/or worms feeding on them. A study of three *Lactobacillus delbrueckii* subspecies found them to affect the *C. elegans* life span in opposite directions and only one increased the longevity (Zanni et al., 2017). The metabolomic analysis revealed that the life span extending *L. delbrueckii* subsp. *bulgaricus*, a commercially available strain, contained higher levels of glutamate, aspartate, glycine, asparagine, and serine. Interestingly, Lb21 also has significantly more glutamate, aspartate, and glycine compared to OP50. This suggests that these metabolites could be important for the Lb21 probiotic effect. Previous studies support this result, as glutamate, glycine, and proline supplementation extends life span in worms (Edwards et al., 2015; Liu et al., 2019). As glutamate can be converted to proline, the increased level of proline in Lb21-fed animals is consistent with a high level of glutamate. Glutamate supplementation also increases the life span of yeast (Wu et al., 2013).

Furthermore, glutamate plays a central role in metabolism as it acts as the donor of amino groups for many nitrogen-containing metabolites, and it can feed into the TCA cycle to provide energy (Walker and van der Donk, 2016). Glutamate is also used in the *de novo* synthesis of the antioxidant glutathione, a tripeptide made from glutamate, cysteine, and glycine (Ferguson and Bridge, 2019). The significantly higher levels of glutamate and glycine in L-Lb21 compared to L-OP50 support the synthesis of glutathione, a tripeptide made from glutamate, cysteine, and glycine (Ferguson and Bridge, 2019). In line with this, glutathione was significantly increased in worms fed Lb21. Interestingly, *C. elegans* fed a human fecal microbiota transplantation sample promotes the production of intracellular glutathione, which in turn improves intestinal barrier function and protects against nano-plastics induced toxicity (Chu et al., 2021). Ascorbate was present in a higher level in the Lb21 bacteria compared to OP50. In living organisms, glutathione and ascorbate act as antioxidants and can protect against reactive oxygen species (ROS). Ascorbate also acts as a cofactor in enzymatic reactions (Padayatty et al., 2003). In terms of novel MRSA treatment strategies, antioxidants are receiving increased attention because biofilm development might involve ROS signaling (Cattò et al., 2021). Glutathione is particularly interesting with regards to the Lb21 induced MRSA resistance in *C. elegans*, as it inhibits MRSA growth and biofilm architecture *in vitro* (Das et al., 2019). Thus, glutathione could play a role in the increased resistance toward MRSA observed for Lb21-fed worms.

The levels of glycine are about 10-fold higher in Lb21 bacteria compared to OP50. This is interesting, because glycine supplementation increases the longevity *via* the methionine cycle where it appears to be degraded immediately as it does not accumulate in the animals (Liu et al., 2019). Consistent with this, we found that Lb21-fed worms have slightly reduced levels of glycine despite higher concentrations in the Lb21 diet compared to OP50.

The significant increase in aspartate found in both Lb21 and worms fed Lb21 is intriguing as the restriction of aspartate extends the life span of *C. elegans* and yeast (Wu et al., 2013; Edwards et al., 2015). However, as the levels of several AAs are different in L-Lb21 compared to L-OP50, a higher level of aspartate under these circumstances could be beneficial for the host.

Feeding *C. elegans* with a Lb21 diet increases life span (Mørch et al., 2021). Therefore, the increased level of NAD+ in L-Lb21 compared to L-OP50 is interesting because NAD+ supplementation has been shown to have anti-aging effects and delay the onset of age-related diseases (Fang et al., 2017).

The increased level of betaine found in worms fed Lb21 could play a role in the protective effect against stress as supplementation with betaine reduces protein aggregation induced paralysis in an Alzheimer's disease *C. elegans* model (Leiteritz et al., 2018). The paralysis-reducing effect of betaine was found to be dependent on the enzyme cystathionin-β-synthase (*cbs-1*). Whether *cbs-1* is a target for

betaine in relation to the MRSA-resistant effect of Lb21 remains to be elucidated.

In summary, many of the important metabolites identified in this study, either in the probiotic bacteria Lb21 or in the host following a probiotic diet, have previously been described as health promoting ones. It remains to be shown if there is a single causal metabolite or if MRSA resistance results from the combined effect of multiple metabolites.

Metabolites from probiotic bacteria as novel antibiotic alternatives

Given the global rise in multidrug resistant pathogenic bacteria, alternatives to traditional antibiotics are urgently needed. There is increasing evidence from a range of organisms and model systems that some probiotic bacteria can be as effective as traditional antibiotics. However, using live bacteria for the prevention or treatment of infections is not trivial and requires stringent production methods, storage conditions, and treatment protocols. We have previously shown that the genetic background of the host affects whether the given probiotic bacteria will have a beneficial effect (Mørch et al., 2021). This could be a concern for the shelf products, but this suggests that there is great potential for personalized precision medicine. Many of the inherent limitations of using live organisms could be overcome if the beneficial metabolites could be identified and isolated. This requires a comprehensive characterization of both the bacterial metabolomes and host responses to these across many different probiotic strains and hosts. In this study, we provided a set of metabolites that potentially could lead to strategies for protection against MRSA, as the Lb21 probiotics offer very strong MRSA resistance in *C. elegans*.

Data availability statement

The raw data supporting the conclusions of this article will be made available by the authors, without undue reservation.

Author contributions

AO, FM, and KM contributed to conception and design of the study. KM, MM, and MH performed the experiments. HN and KM analyzed the NMR data. AO, HN, and KM wrote the manuscript. All authors contributed to manuscript revision and approved the submitted version.

Funding

Funding was provided by Innovation Foundation Denmark grant number 4105-00019B. The *C. elegans* NL2099 *rrf-3 (pk1426)* strain was purchased from CGC, which is funded by NIH Office of Research Infrastructure Programs. The authors would like to thank Dr. Arthur Ouwehand (Global Health & Nutrition Sciences, International Flavors and Fragrances, Kantvik, Finland) for providing the Lb21 strain. The community-acquired isolate MRSA 43484 was provided by Statens Serum Institut, Copenhagen, Denmark. Finally, access to the NMR spectrometers at the Danish Center for Ultrahigh-Field NMR Spectroscopy (Ministry of Higher Education and Science grant AU- 2010-612-181) is gratefully acknowledged.

Conflict of interest

The authors declare that the research was conducted in the absence of any commercial or financial relationships that could be construed as a potential conflict of interest.

Publisher's note

All claims expressed in this article are solely those of the authors and do not necessarily represent those of their affiliated organizations, or those of the publisher, the editors and the reviewers. Any product that may be evaluated in this article, or claim that may be made by its manufacturer, is not guaranteed or endorsed by the publisher.

References

An, Y. J., Xu, W. J., Jin, X., Wen, H., Kim, H., Lee, J., et al. (2012). Metabotyping of the *C. elegans sir-2.1* mutant using *in vivo* labeling and (13)C-heteronuclear multidimensional NMR metabolomics. *ACS Chem. Biol.* 7, 2012–2018. doi: 10.1021/cb3004226

Barsyte, D., Lovejoy, D. A., and Lithgow, G. J. (2001). Longevity and heavy metal resistance in *daf-2* and *age-1* long-lived mutants of *Caenorhabditis elegans*. *FASEB J.* 15, 627–634. doi: 10.1096/fj.99-0966com

Brenner, S. (1974). The genetics of *Caenorhabditis elegans*. *Genetics* 77, 71–94. doi: 10.1093/genetics/77.1.71

Castro, C., Krumsiek, J., Lehrbach, N. J., Murfitt, S. A., Miska, E. A., and Griffin, J. L. (2013). A study of *Caenorhabditis elegans* DAF-2 mutants by metabolomics and differential correlation networks. *Mol. Biosyst.* 9, 1632–1642. doi: 10.1039/c3mb25539e

Cattò, C., Villa, F., and Cappitelli, F. (2021). Understanding the role of the antioxidant drug erdosteine and its active metabolite on *Staphylococcus aureus* methicillin resistant biofilm formation. *Antioxidants* 10, e1922. doi: 10.3390/antiox10121922

CDC (2019). *Antibiotic Resistance Threats in the United States, 2019*. Atlanta, GA: U.S. Department of Health and Human Services. Available online at: www.cdc.gov/DrugResistance/Biggest-Threats.html

Christensen, K., Mørch, M., Morthorst, T., Lykkemark, S., and Olsen, A. (2017). "Microbiota, probiotic bacteria and ageing," in *Ageing: Lessons From C. elegans*, eds. A. Olsen and M. Gill. Cham: Springer International Publishing. doi: 10.1007/978-3-319-44703-2_18

Chu, Q., Zhang, S., Yu, X., Wang, Y., Zhang, M., and Zheng, X. (2021). Fecal microbiota transplantation attenuates nano-plastics induced toxicity in *Caenorhabditis elegans*. *Sci. Total Environ.* 779, 146454. doi: 10.1016/j.scitotenv.2021.146454

Cohen, E., Bieschke, J., Perciavalle, R. M., Kelly, J. W., and Dillin, A. (2006). Opposing activities protect against age-onset proteotoxicity. *Science* 313, 1604–1610. doi: 10.1126/science.1124646

Das, T., Paino, D., Manoharan, A., Farrell, J., Whiteley, G., Kriel, F. H., et al. (2019). Conditions under which glutathione disrupts the biofilms and improves antibiotic efficacy of both ESKAPE and non-ESKAPE species. *Front. Microbiol.* 10, 2000. doi: 10.3389/fmicb.2019.02000

Davies, S. K., Bundy, J. G., and Leroi, A. M. (2015). Metabolic youth in middle age: Predicting aging in *Caenorhabditis elegans* using metabolomics. *J. Proteome Res.* 14, 4603–4609. doi: 10.1021/acs.jproteome.5b00442

Deguchi, Y., and Morishita, T. (1992). Nutritional requirements in multiple auxotrophic lactic acid bacteria: Genetic lesions affecting amino acid biosynthetic pathways in *Lactococcus lactis, Enterococcus faecium*, and *Pediococcus acidilactici*. *Biosci. Biotechnol. Biochem.* 56, 913–918. doi: 10.1271/bbb.56.913

Ebbels, T. M. D., Lindon, J. C., and Coen, M. (2011). "Processing and modeling of nuclear magnetic resonance (NMR) metabolic profiles," in *Metabolic Profiling: Methods and Protocols*, ed T. O. Metz (Totowa, NJ: Humana Press). doi: 10.1007/978-1-61737-985-7_21

Edwards, C., Canfield, J., Copes, N., Brito, A., Rehan, M., Lipps, D., et al. (2015). Mechanisms of amino acid-mediated lifespan extension in Caenorhabditis elegans. *BMC Genet.* 16, 8. doi: 10.1186/s12863-015-0167-2

Eggers, S., Barker, A. K., Valentine, S., Hess, T., Duster, M., and Safdar, N. (2018). Effect of *Lactobacillus rhamnosus* HN001 on carriage of *Staphylococcus aureus*: results of the impact of probiotics for reducing infections in veterans (IMPROVE) study. *BMC Infect. Dis.* 18, 3028. doi: 10.1186/s12879-018-3028-6

Evans, E. A., Chen, W. C., and Tan, M. W. (2008). The DAF-2 insulin-like signaling pathway independently regulates aging and immunity in *C. elegans*. *Aging Cell* 7, 879–893. doi: 10.1111/j.1474-9726.2008.00435.x

Fang, E. F., Lautrup, S., Hou, Y., Demarest, T. G., Croteau, D. L., Mattson, M. P., et al. (2017). NAD(+) in Aging: Molecular Mechanisms and Translational Implications. *Trends Mol. Med.* 23, 899–916. doi: 10.1016/j.molmed.2017.08.001

Ferguson, G. D., and Bridge, W. J. (2019). The glutathione system and the related thiol network in *Caenorhabditis elegans*. *Redox Biol.* 24, 101171. doi: 10.1016/j.redox.2019.101171

Fuchs, S., Bundy, J. G., Davies, S. K., Viney, J. M., Swire, J. S., and Leroi, A. M. (2010). A metabolic signature of long life in *Caenorhabditis elegans*. *BMC Biol.* 8, 14. doi: 10.1186/1741-7007-8-14

Gao, A. W., Chatzispyrou, I. A., Kamble, R., Liu, Y. J., Herzog, K., Smith, R. L., et al. (2017). A sensitive mass spectrometry platform identifies metabolic changes of life history traits in *C. elegans*. *Sci. Rep.* 7, 1–14. doi: 10.1038/s41598-017-02539-w

Garsin, D. A., Villanueva, J. M., Begun, J., Kim, D. H., Sifri, C. D., Calderwood, S. B., et al. (2003). Long-lived *C. elegans daf-2* mutants are resistant to bacterial pathogens. *Science* 300, 1921. doi: 10.1126/science.1080147

Geier, F. M., Want, E. J., Leroi, A. M., and Bundy, J. G. (2011). Cross-platform comparison of *Caenorhabditis elegans* tissue extraction strategies for comprehensive metabolome coverage. *Anal. Chem.* 83, 3730–3736. doi: 10.1021/ac2001109

Grandison, R. C., Piper, M. D. W., and Partridge, L. (2009). Amino-acid imbalance explains extension of lifespan by dietary restriction in *Drosophila*. *Nature* 462, 1061–1064. doi: 10.1038/nature08619

Green, C. L., Lamming, D. W., and Fontana, L. (2021). Molecular mechanisms of dietary restriction promoting health and longevity. *Nat. Rev. Mol. Cell Biol.* 23, 56–73. doi: 10.1038/s41580-021-00411-4

Gupta, A. (2019). *Metabolism of Carbohydrates in Comprehensive Biochemistry for Dentistry: Textbook for Dental Students*. Singapore: Springer Singapore. doi: 10.1007/978-981-13-1035-5_15

Hill, C., Guarner, F., Reid, G., Gibson, G. R., Merenstein, D. J., Pot, B., et al. (2014). Expert consensus document. The International Scientific Association for Probiotics and Prebiotics consensus statement on the scope and appropriate use of the term probiotic. *Nat. Rev. Gastroenterol. Hepatol.* 11, 506–514. doi: 10.1038/nrgastro.2014.66

Honda, Y., Tanaka, M., and Honda, S. (2008). Modulation of longevity and diapause by redox regulation mechanisms under the insulin-like signaling control in *Caenorhabditis elegans*. *Exp. Gerontol.* 43, 520–529. doi: 10.1016/j.exger.2008.02.009

Honda, Y., Tanaka, M., and Honda, S. (2010). Trehalose extends longevity in the nematode *Caenorhabditis elegans*. *Aging Cell* 9, 558–569. doi: 10.1111/j.1474-9726.2010.00582.x

Ikeda, T., Yasui, C., Hoshino, K., Arikawa, K., and Nishikawa, Y. (2007). Influence of lactic acid bacteria on longevity of *Caenorhabditis elegans* and host defense against *Salmonella enterica serovar Enteritidis*. *Appl. Environ. Microbiol.* 73, 6404–6409. doi: 10.1128/AEM.00704-07

Johansson, M. A., Björkander, S., Forsberg, M. M., Qazi, K. R., Celades, M. S., Bittmann, J., et al. (2016). Probiotic *Lactobacilli* modulate *staphylococcus aureus*-induced activation of conventional and unconventional T cells and NK Cells. *Front. Immunol.* 7, e0273. doi: 10.3389/fimmu.2016.00273

Johnson, C. H., Ivanisevic, J., and Siuzdak, G. (2016). Metabolomics: beyond biomarkers and towards mechanisms. *Nat. Rev. Mol. Cell Biol.* 17, 451–459. doi: 10.1038/nrm.2016.25

Kapahi, P., Kaeberlein, M., and Hansen, M. (2017). Dietary restriction and lifespan: Lessons from invertebrate models. *Ageing Res. Rev.* 39, 3–14. doi: 10.1016/j.arr.2016.12.005

Kim, Y., and Mylonakis, E. (2012). *Caenorhabditis elegans* immune conditioning with the probiotic bacterium *Lactobacillus acidophilus* strain ncfm enhances gram-positive immune responses. *Infect. Immun.* 80, 2500–2508. doi: 10.1128/IAI.06350-11

Lakowski, B., and Hekimi, S. (1998). The genetics of caloric restriction in *Caenorhabditis elegans*. *Proc. Natl. Acad. Sci. U.S.A.* 95, 13091–13096. doi: 10.1073/pnas.95.22.13091

Lê Cao, K.-A., Boitard, S., and Besse, P. (2011). Sparse PLS discriminant analysis: biologically relevant feature selection and graphical displays for multiclass problems. *BMC Bioinform.* 12:253. doi: 10.1186/1471-2105-12-253

Lê Cao, K.-A., Rossouw, D., Robert-Granié, C., and Besse, P. (2008). A sparse PLS for variable selection when integrating omics data. *Stat. Appl. Genet. Mol. Biol.* 7, e1390. doi: 10.2202/1544-6115.1390

Lee, A. S., De Lencastre, H., Garau, J., Kluytmans, J., Malhotra-Kumar, S., Peschel, A., et al. (2018). Methicillin-resistant *Staphylococcus aureus*. *Nat. Rev. Dis. Prim.* 4, 1–23. doi: 10.1038/nrdp.2018.33

Leiteritz, A., Dilberger, B., Wenzel, U., and Fitzenberger, E. (2018). Betaine reduces β-amyloid-induced paralysis through activation of cystathionine-β-synthase in an Alzheimer model of *Caenorhabditis elegans*. *Genes Nutr.* 13, 21. doi: 10.1186/s12263-018-0611-9

Lithgow, G. J., White, T. M., Hinerfeld, D. A., and Johnson, T. E. (1994). Thermotolerance of a long-lived mutant of *Caenorhabditis elegans*. *J. Gerontol.* 49, B270–B276. doi: 10.1093/geronj/49.6.B270

Liu, Y. J., Janssens, G. E., McIntyre, R. L., Molenaars, M., Kamble, R., Gao, A. W., et al. (2019). Glycine promotes longevity in *Caenorhabditis elegans* in a methionine cycle-dependent fashion. *PLoS Genet.* 15, e1007633. doi: 10.1371/journal.pgen.1007633

Mansfeld, J., Urban, N., Priebe, S., Groth, M., Frahm, C., Hartmann, N., et al. (2015). Branched-chain amino acid catabolism is a conserved regulator of physiological ageing. *Nat. Commun.* 6, 10043. doi: 10.1038/ncomms10043

Markowiak, P., and Slizewska, K. (2017). Effects of probiotics, prebiotics, and synbiotics on human health. *Nutrients* 9, 1021. doi: 10.3390/nu9091021

Martin, F.-P. J., Spanier, B., Collino, S., Montoliu, I., Kolmeder, C., Giesbertz, P., et al. (2011). Metabotyping of *Caenorhabditis elegans* and their culture media revealed unique metabolic phenotypes associated to amino acid deficiency and insulin-like signaling. *J. Proteome Res.* 10, 990–1003. doi: 10.1021/pr100703a

Martorell, P., Llopis, S., González, N., Chenoll, E., López-Carreras, N., Aleixandre, A., et al. (2016). Probiotic strain *Bifidobacterium animalis* subsp. *lactis* CECT 8145 reduces fat content and modulates lipid metabolism and antioxidant response in *Caenorhabditis elegans*. *J. Agric. Food Chem.* 64, 3462–3472. doi: 10.1021/acs.jafc.5b05934

Masoro, E. J. (1998). Hormesis and the antiaging action of dietary restriction. *Exp. Gerontol.* 33, 61–66. doi: 10.1016/S0531-5565(97)00071-5

Mørch, M. G. M., Møller, K. V., Hesselager, M. O., Harders, R. H., Kidmose, C. L., Buhl, T., et al. (2021). The TGF-β ligand DBL-1 is a key player in a multifaceted probiotic protection against MRSA in *C. elegans*. *Sci. Rep.* 11, 10717. doi: 10.1038/s41598-021-89831-y

Morley, J. F., Brignull, H. R., Weyers, J. J., and Morimoto, R. I. (2002). The threshold for polyglutamine-expansion protein aggregation and cellular toxicity is dynamic and influenced by aging in *Caenorhabditis elegans*. *Proc. Natl. Acad. Sci. U.S.A.* 99, 10417–10422. doi: 10.1073/pnas.152161099

Nakagawa, H., Shiozaki, T., Kobatake, E., Hosoya, T., Moriya, T., Sakai, F., et al. (2016). Effects and mechanisms of prolongevity induced by *Lactobacillus gasseri* SBT2055 in *Caenorhabditis elegans*. *Aging Cell* 15, 227–236. doi: 10.1111/acel.12431

Nataraj, B. H., and Mallappa, R. H. (2021). Antibiotic resistance crisis: an update on antagonistic interactions between probiotics and methicillin-resistant *Staphylococcus aureus* (MRSA). *Curr. Microbiol.* 78, 2194–2211. doi: 10.1007/s00284-021-02442-8

Padayatty, S. J., Katz, A., Wang, Y., Eck, P., Kwon, O., Lee, J.-H., et al. (2003). Vitamin C as an antioxidant: evaluation of its role in disease prevention. *J. Am. Coll. Nutr.* 22, 18–35. doi: 10.1080/07315724.2003.10719272

Park, M. R., Ryu, S., Maburutse, B. E., Oh, N. S., Kim, S. H., Oh, S., et al. (2018). Probiotic *Lactobacillus fermentum* strain JDFM216 stimulates the longevity and immune response of *Caenorhabditis elegans* through a nuclear hormone receptor. *Sci. Rep.* 8, 1–10. doi: 10.1038/s41598-018-25333-8

Park, M. R., Yun, H. S., Son, S. J., Oh, S., and Kim, Y. (2014). Short communication: Development of a direct *in vivo* screening model to identify potential probiotic bacteria using *Caenorhabditis elegans*. *J. Dairy Sci.* 97, 6828–6834. doi: 10.3168/jds.2014-8561

Piewngam, P., Zheng, Y., Nguyen, T. H., Dickey, S. W., Joo, H. S., Villaruz, A. E., et al. (2018). Pathogen elimination by probiotic *Bacillus* via signalling interference. *Nature* 562, 532–537. doi: 10.1038/s41586-018-0616-y

Pontoizeau, C., Mouchiroud, L., Molin, L., Mergoud-Dit-Lamarche, A., Dallière, N., Toulhoat, P., et al. (2014). Metabolomics analysis uncovers that dietary restriction buffers metabolic changes associated with aging in *Caenorhabditis elegans*. *J. Proteome Res.* 13, 2910–2919. doi: 10.1021/pr5000686

Puchades-Carrasco, L., Palomino-Schätzlein, M., Pérez-Rambla, C., and Pineda-Lucena, A. (2016). Bioinformatics tools for the analysis of NMR metabolomics studies focused on the identification of clinically relevant biomarkers. *Brief. Bioinform.* 17, 541–552. doi: 10.1093/bib/bbv077

Reinke, S. N., Hu, X., Sykes, B. D., and Lemire, B. D. (2010). *Caenorhabditis elegans* diet significantly affects metabolic profile, mitochondrial DNA levels, lifespan and brood size. *Mol. Genet. Metab.* 100, 274–282. doi: 10.1016/j.ymgme.2010.03.013

Roos, K., Simark-Mattsson, C., Grahn Håkansson, E., Larsson, L., Sandberg, T., and Åhrén, C. (2011). Can probiotic *lactobacilli* eradicate persistent carriage of meticillin-resistant *Staphylococcus aureus*? *J. Hosp. Infect.* 78, 77–78. doi: 10.1016/j.jhin.2011.01.010

Schifano, E., Cicalini, I., Pieragostino, D., Heipieper, H. J., Del Boccio, P., and Uccelletti, D. (2020). *In vitro* and *in vivo* lipidomics as a tool for probiotics evaluation. *Appl. Microbiol. Biotechnol.* 104, 8937–8948. doi: 10.1007/s00253-020-10864-w

Schulz, T. J., Zarse, K., Voigt, A., Urban, N., Birringer, M., and Ristow, M. (2007). Glucose restriction extends *Caenorhabditis elegans* life span by inducing mitochondrial respiration and increasing oxidative stress. *Cell Metab.* 6, 280–293. doi: 10.1016/j.cmet.2007.08.011

Seo, Y., Kingsley, S., Walker, G., Mondoux, M. A., and Tissenbaum, H. A. (2018). Metabolic shift from glycogen to trehalose promotes lifespan and healthspan in *Caenorhabditis elegans*. *Proc. Natl. Acad. Sci. U.S.A.* 115, E2791–E2800. doi: 10.1073/pnas.1714178115

Sikorska, H., and Smoragiewicz, W. (2013). Role of probiotics in the prevention and treatment of meticillin-resistant *Staphylococcus aureus* infections. *Int. J. Antimicrob. Agents* 42, 475–481. doi: 10.1016/j.ijantimicag.2013.08.003

Suez, J., Zmora, N., Segal, E., and Elinav, E. (2019). The pros, cons, and many unknowns of probiotics. *Nat. Med.* 25, 716–729. doi: 10.1038/s41591-019-0439-x

Tao, J., Wu, Q.-Y., Ma, Y.-C., Chen, Y.-L., and Zou, C.-G. (2017). Antioxidant response is a protective mechanism against nutrient deprivation in *C. elegans*. *Sci. Rep.* 7, 43547. doi: 10.1038/srep43547

Turner, N. A., Sharma-Kuinkel, B. K., Maskarinec, S. A., Eichenberger, E. M., Shah, P. P., Carugati, M., et al. (2019). Methicillin-resistant *Staphylococcus aureus*: an overview of basic and clinical research. *Nat. Rev. Microbiol.* 17, 203–218. doi: 10.1038/s41579-018-0147-4

Walker, M. C., and van der Donk, W. A. (2016). The many roles of glutamate in metabolism. *J. Ind. Microbiol. Biotechnol.* 43, 419–430. doi: 10.1007/s10295-015-1665-y

Wishart, D. S., Tzur, D., Knox, C., Eisner, R., Guo, A. C., Young, N., et al. (2007). HMDB: the human metabolome database. *Nucleic Acids Res.* 35, D521–D526. doi: 10.1093/nar/gkl923

Wu, Z., Song, L., Liu, S. Q., and Huang, D. (2013). Independent and additive effects of glutamic acid and methionine on yeast longevity. *PLoS ONE* 8, e079319. doi: 10.1371/journal.pone.0079319

Yuan, Y., Kadiyala, C. S., Ching, T.-T., Hakimi, P., Saha, S., Xu, H., et al. (2012). Enhanced energy metabolism contributes to the extended life span of calorie-restricted *Caenorhabditis elegans*. *J. Biol. Chem.* 287, 31414–31426. doi: 10.1074/jbc.M112.377275

Zanni, E., Schifano, E., Motta, S., Sciubba, F., Palleschi, C., Mauri, P., et al. (2017). Combination of metabolomic and proteomic analysis revealed different features among *Lactobacillus delbrueckii* subspecies *bulgaricus* and lactis strains while *in vivo* testing in the model organism *Caenorhabditis elegans* highlighted probiotic properties. *Front. Microbiol.* 8, e01206. doi: 10.3389/fmicb.2017.01206

Zeči,ć, A., Dhondt, I., and Braeckman, B. P. (2019). The nutritional requirements of *Caenorhabditis elegans*. *Genes Nutr.* 14, 15. doi: 10.1186/s12263-019-0637-7

Zhang, Y., and Mair, W. B. (2017). "Dietary restriction in *C. elegans*," in: *Ageing: Lessons from C. elegans*, eds A. Olsen and M. S. Gill (Cham: Springer International Publishing). doi: 10.1007/978-3-319-44703-2_16

Advantages of publishing in Frontiers

OPEN ACCESS
Articles are free to read for greatest visibility and readership

FAST PUBLICATION
Around 90 days from submission to decision

HIGH QUALITY PEER-REVIEW
Rigorous, collaborative, and constructive peer-review

TRANSPARENT PEER-REVIEW
Editors and reviewers acknowledged by name on published articles

Frontiers
Avenue du Tribunal-Fédéral 34
1005 Lausanne | Switzerland

Visit us: www.frontiersin.org
Contact us: frontiersin.org/about/contact

REPRODUCIBILITY OF RESEARCH
Support open data and methods to enhance research reproducibility

DIGITAL PUBLISHING
Articles designed for optimal readership across devices

FOLLOW US
@frontiersin

IMPACT METRICS
Advanced article metrics track visibility across digital media

EXTENSIVE PROMOTION
Marketing and promotion of impactful research

LOOP RESEARCH NETWORK
Our network increases your article's readership